UNIWERSYTET
IM. ADAMA MICKIEWICZA
W POZNANIU

WYDZIAŁ CHEMII

ROZPRAWA DOKTORSKA

„Wpływ funkcjonalizowanych silseskwioksanów na właściwości fizykochemiczne i mechaniczne niektórych materiałów polimerowych”

„The influence of functionalized silsesquioxanes on physicochemical and mechanical properties of selected polymer materials”

Dariusz Brząkalski

Promotor:
Prof. dr hab. Bogdan Marciniec
Promotor pomocniczy:
Dr hab. Robert Przekop

Praca przygotowana w Zakładzie Chemii Metaloorganicznej Wydziału Chemii oraz Laboratorium Procesów Technologicznych Centrum Zaawansowanych Technologii Uniwersytetu im. Adama Mickiewicza w Poznaniu, z wykorzystaniem infrastruktury Wielkopolskiego Centrum Zaawansowanych Technologii

Poznań, 2022

Składam serdeczne podziękowania mojemu promotorowi, **Profesorowi Bogdanowi Marcińcowi**, za wieloletnią opiekę i powierzanie mi tematyki badawczej, której realizacja zaowocowała tą rozprawą doktorską.

Składam serdeczne podziękowania mojemu promotorowi, **Profesorowi Robertowi Edwardowi Przekopowi**, za pouczającą współpracę, która rozwinęła mnie naukowo oraz prywatnie, oraz za stworzenie warunków umożliwiających realizację założeń tej rozprawy doktorskiej.

Serdecznie dziękuję Koleżankom i Kolegom z Centrum Zaawansowanych Technologii UAM oraz Zespołu Hal Technologicznych, za cenne porady i pomysły, okazaną pomoc oraz tworzenie dobrej atmosfery do wspólnej pracy.

Szczególnie dziękuję **dr Bognie Sztorch**, **mgr Darii Pakule** i **mgr Miłoszowi Frydrychowi** za udaną współpracę i pomoc, bez której ukończenie tej rozprawy nie byłoby możliwe.

Najbardziej dziękuję **Rodzinie** i **Przyjaciołom** za wsparcie bez względu na wszystko, w chwilach lepszych i tych najtrudniejszych. Bez Was nie zdołałbym tu dotrzeć.

1. Spis treści

2. Streszczenie

A. w języku polskim

Niniejsza praca doktorska stanowi krytyczne spojrzenie na problematykę wytwarzania układów polimerowych zawierających w swoim składzie dodatki funkcjonalne w postaci silseskwioksanów oraz ich bliskich pochodnych, sferokrzemianów, które ze strukturalnego punktu widzenia uważać można za podtyp silseskwioksanów. Modyfikatory krzemoorganiczne przebadano zarówno pod kątem dodatków do masy tworzywa, jak i czynników modyfikacji powierzchniowej (środków sprzęgających) pigmentu mineralnego TiO_2. Analizie poddano zasadność aplikacji badanych typów związków krzemoorganicznych w różnych technologiach przetwórczych, mianowicie wtrysku, wytłaczaniu folii, druku 3D techniką FDM oraz odlewaniu pigmentowanych żywic epoksydowych. Pozwoliło to na wskazanie obszarów, w których dalszy rozwój materiałów z modyfikatorami silseskwioksanowymi i sferokrzemianowymi uznano za perspektywiczne oraz zakresów stężeń racjonalnych z ekonomicznego punktu widzenia. Omówiono także koncepcję napełniaczy i nanonapełniaczy, jak i środków pomocniczych, celem właściwego zaklasyfikowania omawianych związków jako dodatków do tworzyw, z uwagi na rozbieżności występujące w literaturze naukowej.

B. w języku angielskim

The presented doctoral thesis gives a critical view on the issues of the production of polymer systems containing in their composition various functional additives in the form of silsesquioxanes and their close derivatives, spherosilicates, which from a structural point of view can be considered a sub-type of silsesquioxanes. Organosilicon modifiers were tested both as additives used in the mass of the material and as surface modifiers (coupling agents) for an inorganic pigment, TiO_2. The validity of the application of the tested types of organosilicon compounds in different processing technologies, namely injection moulding, foil extrusion, FDM type 3D printing and casting of pigmented epoxy resins was subjected to an analysis. This allowed to identify areas where the further development of materials with silsesquioxane and spherosilicate modifiers is considered prospective, and the ranges of additives loading rational from an economic point of view. The concept of fillers and nanofillers, as well as processing aids, was also discussed in order to properly classify these compounds as modifiers for plastics, due to the discrepancies in the scientific literature.

3. Wykaz publikacji wchodzących w skład rozprawy doktorskiej

Zgodnie z art. 13 ust. 1 ustawy z dn. 14 marca 2003 r. o stopniach i tytule naukowym oraz o stopniach i tytule w zakresie sztuki (tekst jednolity Dz. U. z 2017 r. poz. 1789) oraz § 5 ust. 1 Rozporządzenia Ministra Nauki i Szkolnictwa Wyższego z dn. 19 stycznia 2018 r. w sprawie szczegółowego trybu i warunków przeprowadzania czynności w przewodzie doktorskim, w postępowaniu habilitacyjnym o raz w postępowaniu o nadanie tytułu profesora (Dz. U. z 2018 r. poz. 261); na podstawie art. 179 ust. 1 ustawy z dn. 3 lipca 2018 r. Przepisy wprowadzające ustawę – Prawo o szkolnictwie wyższym i nauce (Dz. U. z 2018 r. poz. 1669).

P1

Dariusz Brząkalski, Robert E. Przekop, Marta Dobrosielska, Bogna Sztorch, Piotr Marciniak, Bogdan Marciniec

"Highly bulky spherosilicates as functional additives for polyethylene processing – influence on mechanical and thermal properties",

Polymer Composites, 2020, 41(8), 3389-2302

IF 2020: 3.171 IF-5 2020: 2.877

P2

Dariusz Brząkalski, Robert E. Przekop, Bogna Sztorch, Paulina Jakubowska, Marek Jałbrzykowski, Bogdan Marciniec

„Silsesquioxane Derivatives as Functional Additives for Preparation of Polyethylene-Based Composites: a Case of Trisilanol Melt-Condensation"

Polymers, 2020, 12(10), 2269

IF 2020: 4.329 IF-5 2020: 4.493

P3

Dariusz Brząkalski, Bogna Sztorch, Miłosz Frydrych, Daria Pakuła, Kamil Dydek, Rafał Kozera, Anna Boczkowska, Bogdan Marciniec, Robert E. Przekop

„Limonene Derivative of Spherosilicate as a Polylactide Modifier for Applications in 3D Printing Technology"

Molecules, 2020, 25(24), 5882.

IF 2020: 4.412 IF-5 2020: 4.588

P4

Dariusz Brząkalski, Robert E. Przekop, Bogna Sztorch, Miłosz Frydrych, Daria Pakuła, Marek Jałbrzykowski, Grzegorz Markiewicz, Bogdan Marciniec

„Why POSS-Type Compounds Should Be Considered Nanomodifiers, Not Nanofillers — A Polypropylene Blends Case Study"

Polymers, 2021, 13(13), 2124.

IF 2020: 4.329 IF-5 2020: 4.493

P5

Dariusz Brząkalski, Robert E. Przekop, Miłosz Frydrych, Daria Pakuła, Marta Dobrosielska, Bogna Sztorch, Bogdan Marciniec

„Where ppm Quantities of Silsesquioxanes Make a Difference—Silanes and Cage Siloxanes as TiO_2 Dispersants and Stabilizers for Pigmented Epoxy Resins"

Materials, 2022, 15(2), 494.

	IF 2020: 3.623	IF-5 2020: 3.920
	IF2020	IF-5-2020
SUMA:	19.864	20.371
ŚREDNIA:	3.973	4.074

Wartości IF na podstawie bazy Journal Citation Reports.

4. Wprowadzenie

4.1 Silseskwioksany

Silseskwioksany to związki krzemoorganiczne o wzorze ogólnym $[RSiO_{3/2}]_n$, gdzie „R" stanowi atom wodoru, grupę alkilową, arylową lub inny podstawnik zawierający heteroatom bądź grupę funkcyjną, np. eterową, estrową, epoksydową, a „n" oznacza liczbę merów stanowiących jednostki budulcowe związku. Istnieje szereg struktur silseskwioksanowych o różnym stopniu uporządkowania przestrzennego, od całkowicie przypadkowych (żywice silseskwioksanowe, żywice „T", ang. *„T" resins*), przez układy drabinkowe i hybrydowe zawierające podjednostki o niedomkniętych lub zdeformowanych klatkach [1-3], aż po różnorodne układy klatkowe (Rys. 1) [4,5].

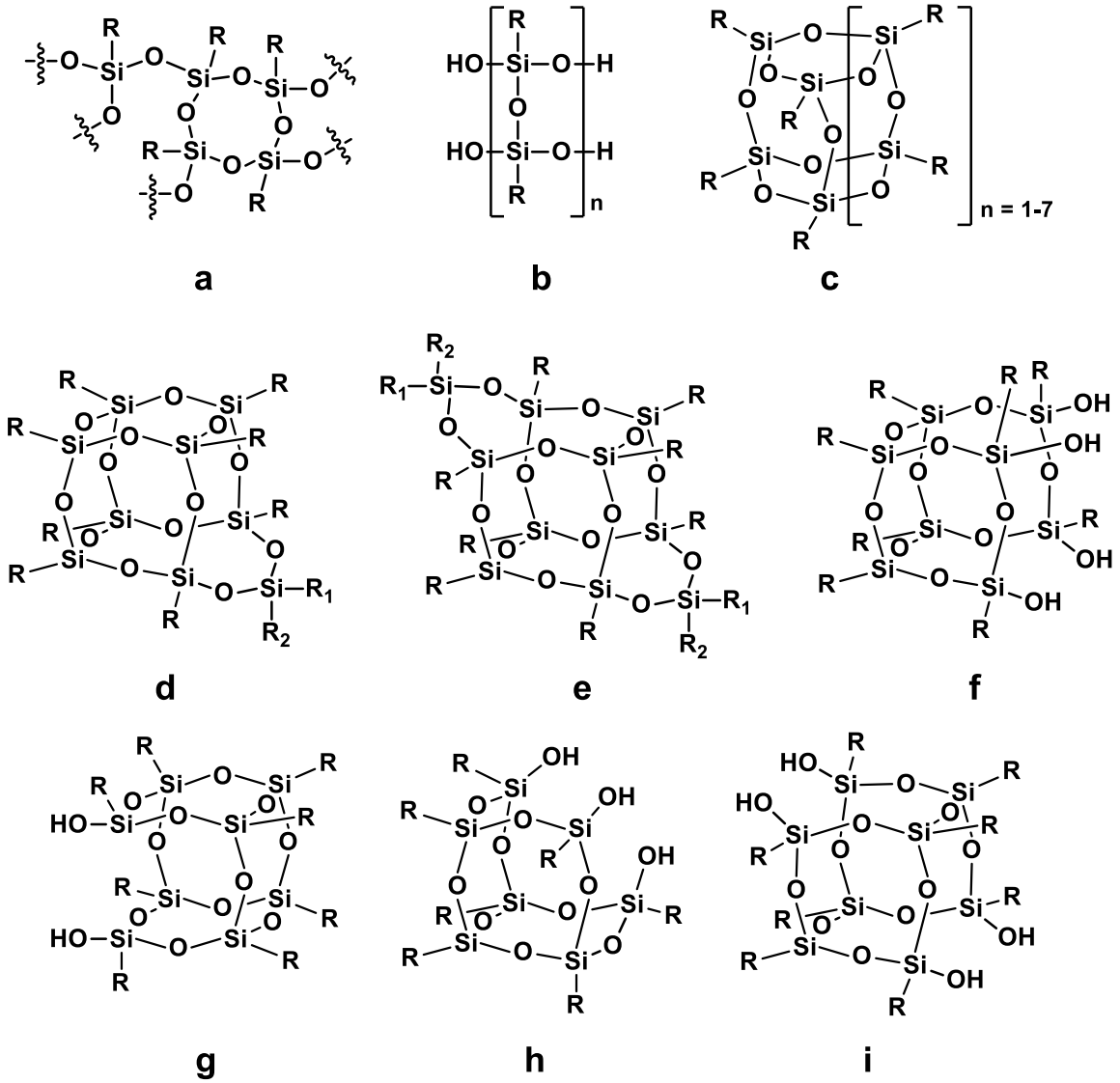

Rysunek 1: Struktury wybranych silseskwioksanów o dobrze zdefiniowanej budowie: a – przypadkowe; b – drabinkowe; c-i – klatkowe, w tym: c – zamknięte; d – o powiększonym narożu; e – o dwóch przeciwległych powiększonych narożach (Double-Decker); f – tetrasilanol drabinkowy; g – disilanol; h – trisilanol; i – tetrasilanol Double-decker.

Dla molekularnych układów klatkowych „n" mieści się w granicach 4-32, przy czym największą do tej pory strukturą wyizolowaną w postaci czystej były pochodne o n=18 [6]. Wzór ogólny $[RSiO_{3/2}]_n$ jest poprawny jedynie dla prostych struktur (Rys. 1a-c), powstałych w przypadku całkowitej kondensacji hydrolitycznej organotrifunkcyjnych silanów $RSiX_3$ (X = alkoksyl, zwykle MeO, EtO; halogen, zwykle Cl), będących prekursorem jednostek strukturalnych T.

Układ przedstawiony na Rys. 1f to szczególny przypadek, gdzie cząsteczka ma cechy strukturalne zarówno silseskwioksanu drabinkowego, jak i klatkowego. Jest ona układem tricyklicznym, a jej wzór strukturalny można wyrazić w sposób przedstawiony dla struktury 1b, dla n = 4. Obliczenia teoretyczne pozwoliły określić, że cząsteczka taka może przyjmować dwie dynamiczne konformacje i występować zarówno w postaci otwartej struktury drabinkowej (konformacja egzo), jak i stabilizowanej wiązaniami wodorowymi struktury klatkowej (konformacja endo), przy czym ta ostatnia charakteryzuje się niższą energią układu; stabilizacja konformacji klatkowej nie występowała dla porównawczego układu zawierającego grupy funkcyjne Si-H zamiast Si-OH [7]. Przyjmowanie takiej konformacji przez układy drabinkowe o różnej długości (Rys. 1b) stanowi prawdopodobnie jeden z mechanizmów powstawania zamkniętych układów klatkowych (Rys. 1c) podczas syntezy silseskwioksanów, jako, że te dwie grupy związków często powstają równolegle podczas kondensacji hydrolitycznej organotrifunkcyjnych silanów [8-10] oraz jako produkt uboczny reakcji kondensacji silseskwioksanów drabinkowych [11,12].

Układy 1d i 1e to tzw. homosilseskwioksany, czyli układy klatkowe o klatce powiększonej jednostkami D (lub T, jednakże zazwyczaj innym od jednostek T tworzących rdzeń klatki) [13]. Układy typu 1e są znane jako tzw. silseskwioksany Double-Decker [14].

Ze względu na złożoność i różnorodność budowy silseskwioksanów, pewną trudność może przynosić ich nazewnictwo czy zapis struktury. Użyteczną i prostą notację wprowadziło w latach 40. General Electric na potrzeby opisu silikonów, a system został przyjęty zarówno przez przemysł, jak i środowisko naukowe, również w zastosowaniu dla innych związków krzemoorganicznych [5,15,16]. Jednostki strukturalne stanowiące bloki budulcowe nie tylko silseskwioksanów, ale i innych związków krzemoorganicznych (silikonów, olejów, czy żywic silikonowych) są opisywane jako M, D, T i Q, różniące się liczbą atomów tlenu otaczających daną jednostkę, odpowiednio jednym, dwoma, trzema lub czterema (R_3SiO, R_2SiO_2, $RSiO_3$ i SiO_4). Ponadto określa się liczbę wiązań siloksanowych tworzonych przez daną jednostkę z jednostkami sąsiadującymi, umieszczając odpowiednią liczbę w indeksie górnym. Przykładowo, jednostka T^3 to ugrupowanie typu $RSiO_3$, gdzie każdy z trzech atomów tlenu łączy się z kolejnym atomem krzemu [17]. Jednostki T^3 stanowią jedyny mer strukturalny idealnych klatek silseskwioksanowych typu 1c. Dla odmiany, jednostki T^2 tworzą ugrupowania silanolowe niedomkniętych klatek (silanoli silseskwioksanowych, 1f-i), gdzie jeden z atomów tlenu jest terminowany atomem wodoru. w ten sposób można przedstawić strukturę 1g jako $T_6^3T_2^2$, a strukturę 1h jako $T_4^3T_3^2$.

Silseskwioksany klatkowe, zarówno o całkowicie, jak i niecałkowicie domkniętych klatkach, stanowią układy policykliczne, których nazewnictwo podlega konwencji opisanej w ogólnych zasadach IUPAC dotyczących tejże klasy związków. Jako, że nazewnictwo

układów policyklicznych jest dość złożone, a poprawne nazwy silseskwioksanów wygenerowane zgodnie z zasadami IUPAC są długie, w literaturze rzadko spotyka się ich zastosowanie, choćby w sekcji eksperymentalnej, gdzie zainteresowany czytelnik spodziewałby się pełnego opisu i charakterystyki omawianej pochodnej. Zamiast tego, zazwyczaj spotyka się notację General Electric (najczęściej w najbardziej ogólnej postaci, bez dodatkowych wyznaczników w indeksie górnym) lub uproszczone nazwy, szczególnie zawierające jako rdzeń „POSS" oraz opis jego otoczenia chemicznego (POSS® to nazwa zastrzeżona przez Hybrid Plastics), a nawet oznaczenia numeryczne lub kodowe pochodnych, stosowane w połączeniu ze schematycznymi rysunkami strukturalnymi, bez jakiegokolwiek nazewnictwa czy notacji. Rzadkie stosowanie systemu IUPAC może być spowodowane niechęcią autorów artykułów naukowych do adaptowania ustalonych dla niego zasad. Tymczasem zasady nazewnictwa niektórych pochodnych silseskwioksanowych przybliżył pokrótce już Voronkov w znakomitej pracy przeglądowej z 1982r [13]. Opisał on zasady numeracji naroży klatki oraz połączeń policyklicznych dla oktasilseskwioksanu T_8 oraz homosilseskwioksanu T_8D. Na Rysunku 2 przedstawiono przykładową strukturę prostego oktasilseskwioksanu klatkowego typu T_8, 3,5,7,9,11,13,15-heptaizobutylo[9.5.1.1^{3,9}.1^{5,15}.1^{7,13}]oktasiloksan-1-olu, wraz z oznaczeniem tzw. mostka pierwotnego (kolor czerwony) i mostków wtórnych (kolor niebieski), a także ukazanie struktury w postaci płaskiej, dla ułatwienia wizualizacji rozkładu mostków odpowiedzialnych za tworzenie wielopierścieniowej struktury cząsteczki.

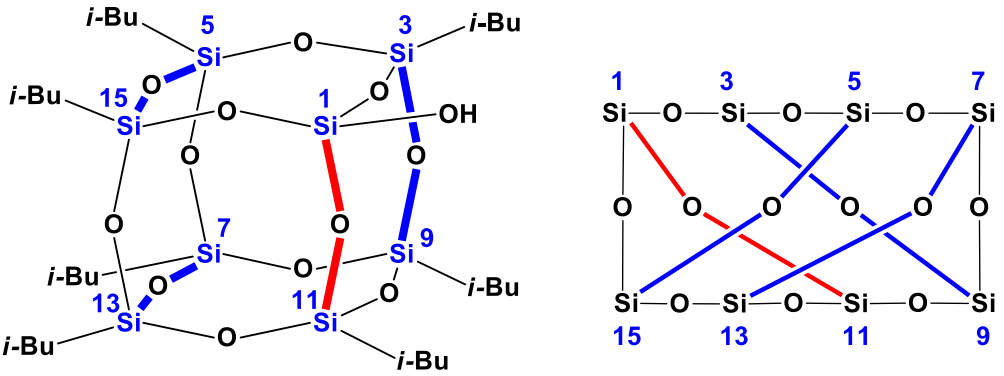

Rysunek 2: Struktura przykładowego oktasilseskwioksanu, 3,5,7,9,11,13,15-heptaizobutylo[9.5.1.1^{3,9}.1^{5,15}.1^{7,13}]oktasiloksan-1-olu, wraz z oznaczeniem numeracji naroży oraz połączeń (mostków) policyklicznych.

Szczególną odmianą silseskwioksanów są sferokrzemiany. Charakterystycznym motywem strukturalnym jest występowanie jednostki typu M, połączonej z rdzeniem klatki, zazwyczaj z jednostką typu Q (Rysunek 3). Sferokrzemiany mogą być uznawane za pochodne mono- lub oktasilanolanu silseskwioksanowego [16], natomiast przez niektórych uważane są za oddzielną grupę związków i razem z silseskwioksanami klasyfikowane wspólnie jako siloksany klatkowe [18]. Pomimo pozornie znacznie bardziej złożonej struktury, z powodzeniem stosować można oba opisane wyżej systemy nazewnictwa.

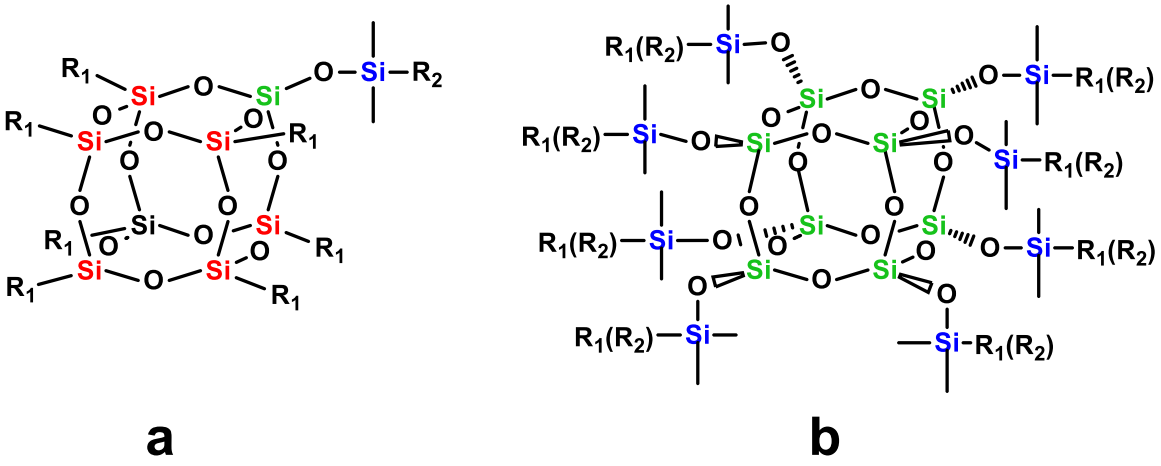

Rysunek 3: Struktury mono- (a) i oktasferokrzemianu (b). Na niebiesko zaznaczono jednostki M połączone z rdzeniem silseskwioksanowym, na czerwono – jednostki T, na zielono – jednostki Q.

Synteza silseskwioksanów oraz sferokrzemianów obejmuje otrzymywanie rdzenia (w przypadku sferokrzemianów również korony) cząsteczki na drodze hydrolitycznej kondensacji (organo)silanów, co decyduje o architekturze struktury klatkowej, oraz modyfikację podstawników organicznych (grup funkcyjnych). Monofunkcyjne silseskwioksany klatkowe otrzymuje się zazwyczaj poprzez hydrolityczną kondensację trichloro- lub trialkoksysilanów, a rodzaj podstawnika decyduje o szybkości reakcji, jej wydajności i selektywności formowanych struktur T (Rys. 1c, Rysunek 4) [4,16].

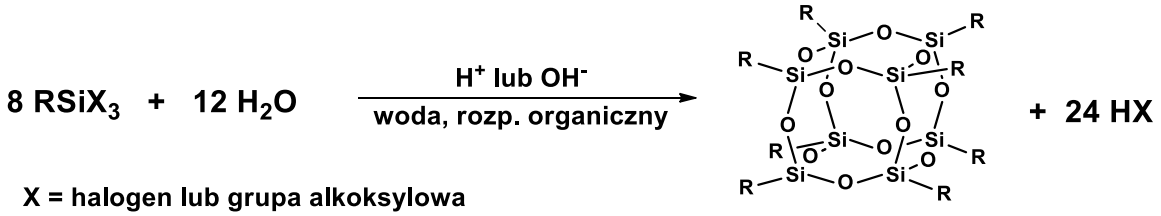

Rysunek 4: Schemat reakcji otrzymywania silseskwioksanów klatkowych (na przykładzie struktury typu T_8) na drodze hydrolitycznej kondensacji organotrifunkcyjnych silanów.

Na szybkość i wydajność reakcji wpływają też warunki syntezy, takie jak dobór rozpuszczalnika, temperatura, kataliza kwasowa lub zasadowa. Dla ograniczonej puli podstawników opracowano także efektywne procedury otrzymywania di-, tri- oraz tetrasilanoli. Silseskwioksany dwufunkcyjne syntezuje się na drodze kondensacji hydrolitycznej poprzez domykanie naroży (ang. *corner capping*) klatek silanolowych silanami o innych rodzajach grup funkcyjnych (Rysunek 5).

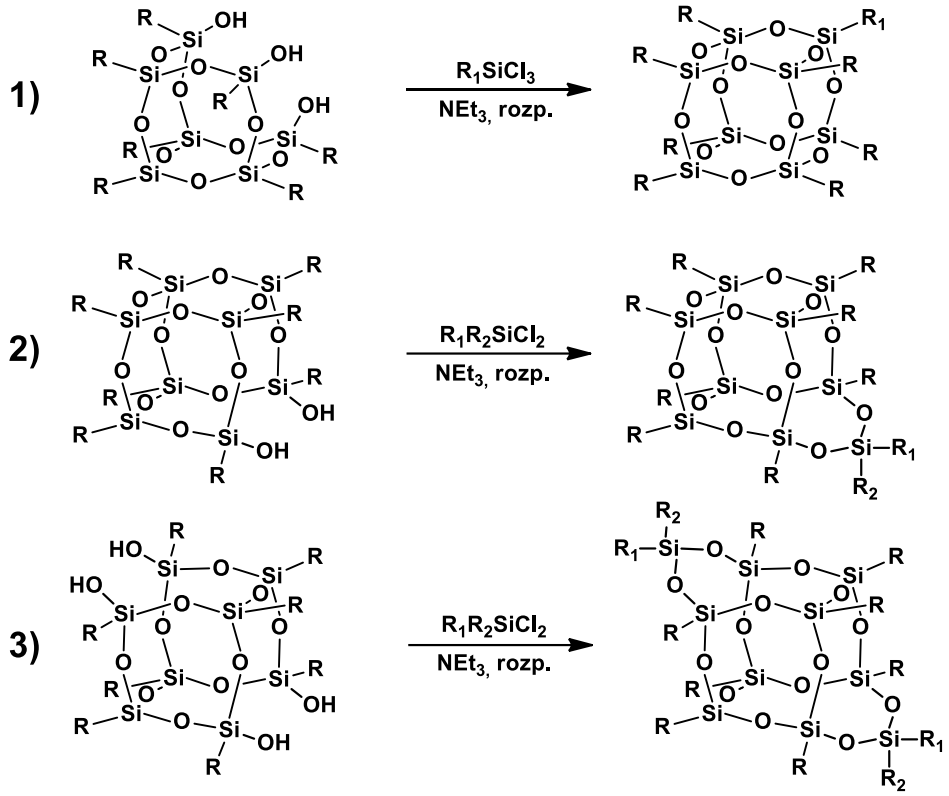

Rysunek 5: Schematy reakcji domykania naroży (corner capping) klatek silanoli silseskwioksanowych silanami: trisilanolu (1), disilanolu (2) oraz tetrasilanolu (3).

W przypadku mono- i oktasferokrzemianów synteza przeprowadzana jest kilkuetapowo, obejmując kolejno syntezę rdzenia, a następnie wprowadzanie podstawników organicznych w jego otoczenie (Rysunek 6).

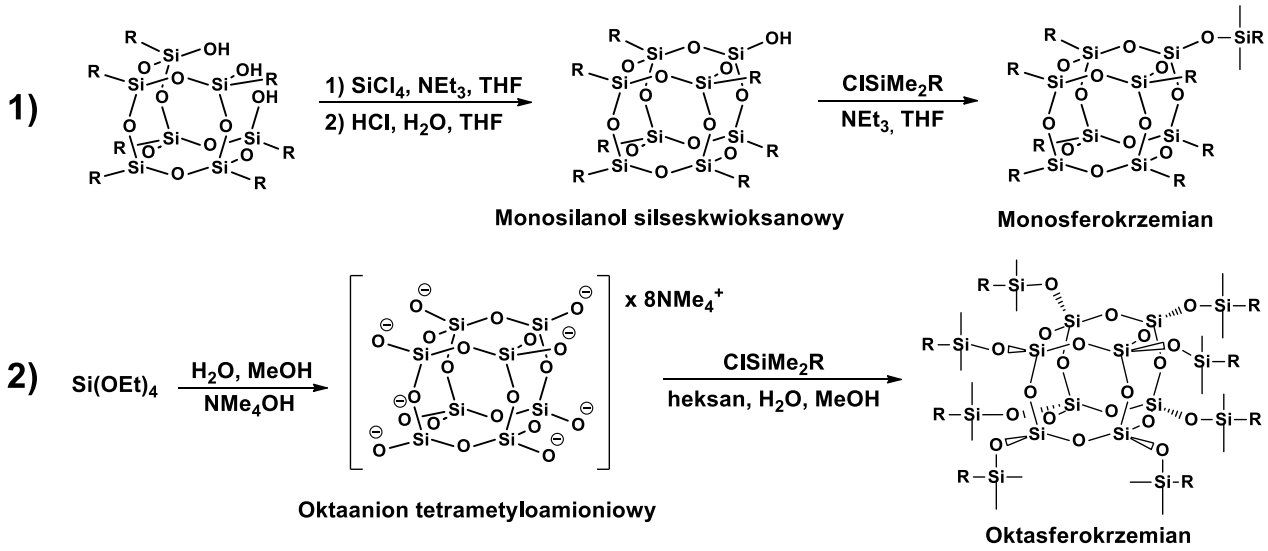

Rysunek 6: Schematy reakcji otrzymywania mono- (1) i oktasferokrzemianów (2).

Metody modyfikacji i wprowadzania podstawników organicznych do rdzenia klatki podzielić można na katalityczne i niekatalityczne. Do metod niekatalitycznych zaliczają się: substytucja nukleofilowa, estryfikacja, amidowanie, utlenianie i redukcja (z zastosowaniem reagenta stechiometrycznego, np. $NaBH_4$), nitrowanie, czy różnego rodzaju reakcje

kondensacji, a dostępne prace syntetyczne dotyczące chemii silseskwioksanów opisują setki wariantów procedur typowych dla tradycyjnej chemii organicznej. Do metod katalitycznych należy w szczególności hydrosililowanie olefin, które ze względu na łatwość prowadzenia oraz ilościową wydajność uzyskiwanych produktów kwalifikuje się do klasy reakcji „click chemistry". Ponadto wymienić należy metatezę krzyżową olefin, sililujące sprzęganie, dehydrogenujące sililowanie terminalnych olefin i alkinów oraz alkoholi, cykloaddycję azydków do olefin i alkinów, redukcję i uwodornienie. Na dzień dzisiejszy najbardziej rzetelne prace przeglądowe zestawiające techniki syntezy i chemicznej modyfikacji silseskwioksanów i sferokrzemianów stanowią opracowania Lickissa [4] i Claire-Thompson [16].

4.2 Reakcja hydrosililowania olefin

Reakcja hydrosililowania stanowi addycję wiązania Si-H do wiązań wielokrotnych węgiel-węgiel alkenów, allenów i alkinów, a także różnego rodzaju nienasyconych ugrupowań heteroatomowych, w tym C≡N, C=N, C=O, C=S [19], N=O [20] bądź homoatomowych N=N [21]. Pierwsze doniesienie literaturowe dotyczące hydrosililowania sięga roku 1947, kiedy to Leo Harry Sommer przeprowadził reakcję okt-1-enu i trichlorosilanu z zastosowaniem nadtlenku acetylu jako inicjatora, obserwując formację n-oktylotrichlorosilanu [22] (Rysunek 7).

Rysunek 7: Schemat reakcji hydrosililowania okt-1-enu trichlorosilanem inicjowanej nadtlenkiem acetylu.

W kontekście stosowanych substratów reakcji, największe, przemysłowe znaczenie ma hydrosililowanie olefin oraz ich funkcyjnych pochodnych, ponieważ stanowi to wydajną metodę syntetyczną otrzymywania monomerów silanowych do produkcji funkcjonalizowanych kopolimerów siloksanowych, a także szerokiej gamy silanowych środków sprzęgających [19]. Ponadto, reakcja hydrosililowania w skali przemysłowej stosowana jest do sieciowania polisiloksanów w produkcji elastomerów silikonowych (Rysunek 8). Rozpuszczalnikami, stanowiącymi równocześnie ligandy stabilizujące katalizator, są dla tej aplikacji oleje winylosiloksanowe, ulegające reakcji sieciowania wraz z substratowymi prepolimerami siloksanowymi, dzięki czemu w usieciowanej masie nie występują lotne pozostałości.

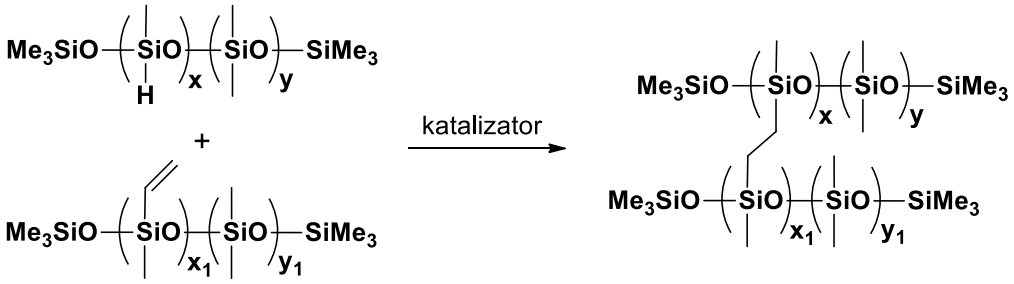

Rysunek 8: Schemat reakcji sieciowania polisiloksanów w produkcji elastomerów silikonowych.

Reakcja przebiegać może na drodze rodnikowej, jak w przykładzie syntezy Sommera, bądź też katalitycznej. Katalizatorami hydrosililowania olefin o najwyższej aktywności w rozumieniu

wartości TON i TOF są kompleksy Pt i Rh, a dalej Ir, Ru i Pd (znane jako pierwiastki z grupy platynowców), przy czym metali tych nie można uszeregować aktywnością w sposób jednoznaczny, ponieważ jest ona zależna od wielu czynników, jak chemiczna postać katalizatora (heterogeniczna lub homogeniczna; sól bądź kompleks), dobór ligandów w przypadku formy kompleksowej, rodzaj substratów (silanu i olefiny), czy też rozpuszczalnika reakcji [19]. Tym samym, dobierając właściwy katalizator hydrosililowania do wybranego procesu, należy kierować się specyfiką stosowanych reagentów, warunkami, w jakich odbywać będzie się reakcja, a także chemo-, regio- czy stereoselektywnością katalizatora, co może mieć decydujące znaczenie o wydajności produktu końcowego. Ponadto, oprócz przedstawicieli grupy platynowców, znane są katalizatory na bazie Ni, Co, Cu, Fe, Mo, Mn, Au, Y, a także lantanowców oraz pierwiastków o charakterze kwasów Lewisa (B, Al, Sn, In, Ga). Na dzień dzisiejszy najpowszechniejszym katalizatorem hydrosililowania, ze względu na wysoką aktywność, stabilność na powietrzu oraz względnie dobrą tolerancję na obecność różnych grup funkcyjnych substratówm, jest kompleks Karstedta, [$Pt_2(dvds)_3$]. Wykazuje on aktywność katalityczną w temperaturze pokojowej lub niższej, a wysokie wartości TON pozwalają na jego stosowanie w ilościach na poziomie pojedynczych ppm Pt w stosunku do masy olefiny. w praktyce przemysłowej przy wytwarzaniu gum i elastomerów silikonowych stosowane są preparaty, gdzie katalizator Karstedta występuje w postaci roztworu w olejach winylosiloksanowych [23,24]. Do samodzielnego przygotowywania formulacji o pożądanym składzie i właściwościach użytkowych kompozycji usieciowanej dostępne są układy o wysokich stężeniach platyny [25]. z kolei oligomery siloksanowe zawierające ugrupowanie Si-H noszą nazwę czynnika sieciującego (ang. *crosslinker*).

4.3 Polimery i tworzywa polimerowe

Syntetyczne materiały polimerowe towarzyszą życiu człowieka i umożliwiają rozwój techniki już od ponad stu lat. w XIX wieku, po odkryciu nitrocelulozy w 1847r. przez Schönbeina, wynalezione zostały pierwsze półsyntetyczne tworzywa termoplastyczne, pod nazwami „Parkesine" (1862r.), „Xylonite" (1869r.), czy najbardziej rozpoznawalny „Celluloid" (celuloid, 1869r.) [26-28]. John Wesley Hyatt, wynalazca celuloidu, opatentował w 1872 r. ze swoim bratem urządzenie do ekstruzji prętów i rurek z celuloidu, co stanowi prawdopodobnie najstarszy udokumentowany przykład wytłaczania tworzyw termoplastycznych w historii [28]. Za moment odkrycia pierwszego w pełni syntetycznego tworzywa polimerowego przyjmuje się rok 1907, kiedy to Leo Hendrik Baekeland złożył wniosek o patent na metodę wytwarzania żywicy fenolowo-formaldehydowej (bakelitu), który to przyznano mu w roku 1909 [29]. Był to trudny w produkcji i względnie kruchy duroplast, wymagający użycia toksycznych i rakotwórczych prekursorów, jednakże w ówczesnym okresie nie miał w skali przemysłowej żadnej znaczącej konkurencji. Następnie, w roku 1912 Fritz Klatte opisał proces wytwarzania PVC, a w 1926 Waldo L. Semon z Goodrich Company opracował metodę jego plastyfikowania, co nadało polimerowi realny potencjał aplikacyjny jako pierwszemu w pełni syntetycznemu tworzywu termoplastycznemu [26].

Jeden ze stosowanych systemów klasyfikacji tworzyw syntetycznych dzieli je według właściwości fizykochemicznych na termoplastyczne i duroplastyczne [30]. Tworzywa termoplastyczne charakteryzują się możliwością swobodnego przetwarzania (prasowania,

walcowania, wytłaczania, wtryskiwania, rozdmuchu i innych) w odpowiedniej dla danego tworzywa temperaturze, zwanej temperaturą przetwórczą. Do tworzyw tej grupy należą m.in. polietylen, polipropylen, polilaktyd, polistyren, czy różne typy poliamidów. Tworzywa duroplastyczne natomiast ulegają w warunkach przetwarzania (np. odlewania, natryskiwania) reakcji sieciowania, co prowadzi do znacznego wzrostu średniej masy cząsteczkowej i utworzenia zwartej sieci polimerowej, a materiał traci zdolność do dalszej obróbki plastycznej pod wpływem ciepła. Wyjątkiem jest stan po przekroczeniu temperatury zeszklenia tworzywa, który dla niektórych materiałów (np. wybranych gatunków żywic epoksydowych) prowadzi do nadania mu w ograniczonym zakresie właściwości plastycznych i umożliwia niewielkie jego odkształcanie.

4.3.1 Żywice epoksydowe

Za początek historii żywic epoksydowych często podaje się 1891r., kiedy Aleksandr Dianin otrzymał po raz pierwszy w historii Bisfenol a (ang. *BPA, Bisphenol A*) [31-34]. z tego względu, jak podaje profesor Rabek, żywice epoksydowe na bazie Bisfenolu a znane są pod ogólną nazwą żywic dianowych [35]. Dopiero jednak w 1936r. Pierre Castan z De Trey Frères Company opracował pierwszą kompozycję utwardzanej żywicy epoksydowej na bazie eteru diglicydylowego bisfenolu a (DGEBA) utwardzanego bezwodnikiem ftalowym, na co uzyskał patent w 1938r., a licencję patentu wykupiło szwajcarskie Ciba AG. Sylvan Greenlee z DeVoe and Raynolds opatentował w 1943r. zbliżoną kompozycję przeznaczoną do wytwarzania powłok ochronnych i różniącą się średnią masą cząsteczkową żywicy [33,34,36]. Żywice epoksydowe znajdują zastosowanie jako powłoki ochronne, kleje dwuskładnikowe, surowce do wytwarzania kompozytów i laminatów, surowce do produkcji płytek drukowanych do elektroniki, czy materiał izolacyjny (np. do uzwojeń silników elektrycznych oraz transformatorów) [35].

Najpowszechniejszymi na rynku masowym żywicami epoksydowymi (tak zwanymi żywicami bazowymi, w odróżnieniu od żywic usieciowanych, stanowiących materiał gotowych wyrobów), zarówno ciekłymi, jak i stałymi, są te oparte na DGEBA i jego oligomerycznych pochodnych [36]. Jego produkcja, przedstawiona na Rysunku 9, w zależności od typu wytwarzanej żywicy, przeprowadzana jest w różnych warunkach, co prowadzi do mieszanin produktów o zmiennej strukturze cząsteczkowej (od zbliżonych do czystego DGEBA do produktów oligomerycznych, gdzie „n" dla wyrobów handlowych wynosi od 1 do ok. 35) i tym samym lepkości. w szczególności rozróżnia się żywice ciekłe i stałe, gdzie „n" wynosi od ~0.1 do ~0.2 dla żywic ciekłych (ang. *LER, Liquid epoxy resins*) i od ok. ~2 w górę dla żywic stałych (ang. *SER, Solid epoxy resins*). Głównym czynnikiem decydującym o średniej masie cząsteczkowej uzyskiwanego produktu jest stosunek molowy epichlorohydryny do bisfenolu A. DGEBA można również przekształcać do żywic o wyższej średniej masie cząsteczkowej w tzw. procesie poliaddycji w stopie bądź tzw. reakcji przedłużania łańcucha (ang. *Fusion proces, Advancement process*), gdzie DGEBA poddaje się działaniu nadmiaru BPA w obecności katalizatora [37].

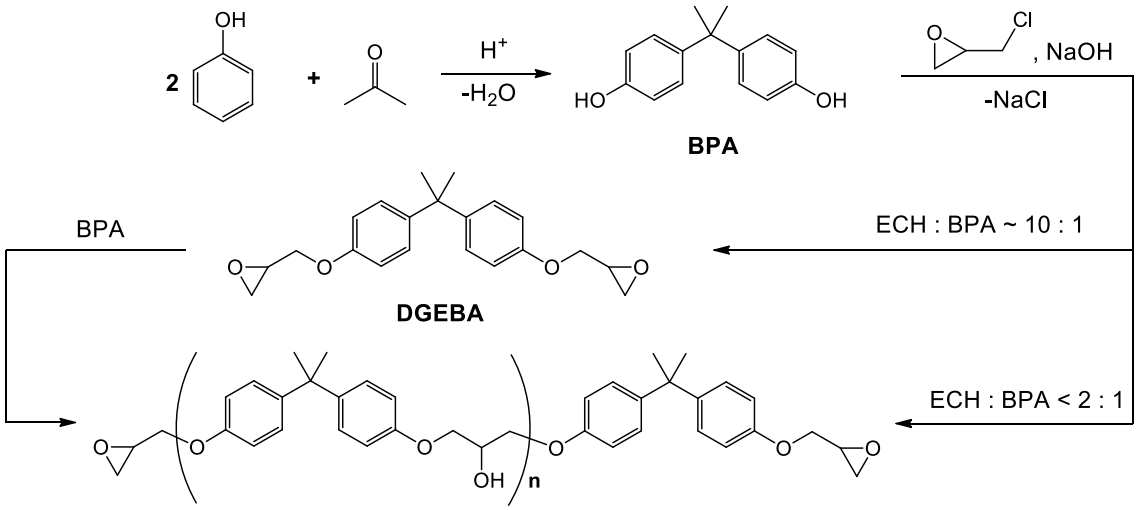

Rysunek 9: Schemat syntezy DGEBA oraz jego oligomerycznych pochodnych.

Żywice epoksydowe nieusieciowane, zwane także żywicami bazowymi, poddawane są działaniu wybranego utwardzacza, co prowadzi do uzyskania żywic usieciowanych. Na rynku dostępne są układy jedno- i dwuskładnikowe [36]. Układy jednoskładnikowe zawierają żywicę bazową wymieszaną w odpowiedniej proporcji z utwardzaczem, a sieciowaniu ulegają powyżej określonej temperatury aktywacji. Charakteryzują się również tzw. okresem trwałości (ang. *shelf life*), czyli okresem zdatności do użycia, powyżej którego kompozycja nabiera lepkości przekraczającej zakres określony w karcie technicznej produktu, co uniemożliwia jej poprawną aplikację w przewidzianym obszarze zastosowań (np. wykonywanie laminatów). Kompozycje dwuskładnikowe zawierają żywicę bazową i utwardzacz w oddzielnych opakowaniach, a ich mieszania w określonej proporcji dokonuje się tuż przed procesem odlewania. Takie układy ulegają sieciowaniu już w temperaturze pokojowej, charakteryzują się tzw. czasem pracy (ang. *pot life*), czyli okresem czasu, po upłynięciu którego kompozycja osiąga lepkość uniemożliwiającą jej odlewanie. w języku polskim parametr ten bywa też nazywany czasem życia lub czasem żelowania kompozycji. w zależności od końcowego zastosowania wyrobu epoksydowego, stosowane są różne typy utwardzaczy, przy czym podzielić je można na trzy zasadnicze grupy:

a) utwardzacze aminowe,
b) utwardzacze karboksylowe,
c) utwardzacze katalityczne.

Utwardzacze aminowe działają poprzez nukleofilowe otwarcie pierścienia oksiranowego żywicy epoksydowej (Rysunek 10, reakcja 1). Cząsteczka utwardzacza, posiadająca dwie lub więcej grup aminowych, powoduje sieciowanie łańcuchów żywicy bazowej poprzez atak nukleofilowy na pierścienie oksiranowe sąsiednich łańcuchów, co powoduje szybki i znaczny wzrost średniej masy cząsteczkowej żywicy oraz stopnia usieciowania układu. Utwardzacze karboksylowe bazują głównie na bezwodnikach kwasowych i poliestrach. Utwardzacze poliestrowe zbudowane są z łańcuchów zakończonych grupami kwasowymi, zdolnymi do tworzenia estrów z żywicą epoksydową poprzez otwarcie pierścienia oksiranowego lub kondensację z grupami -OH żywicy (Rysunek 10, reakcja 2). Utwardzacze bezwodnikowe reagują z grupami -OH żywicy epoksydowej z formacją wiązań estrowych (Rysunek 10,

reakcja 3), a także katalizując formację wiązań eterowych pomiędzy grupami -OH i pierścieniami oksiranowymi (Rysunek 10, reakcja 4). Kompozycje epoksydowe z utwardzaczami bezwodnikowymi zazwyczaj zawierają katalizatory, bez których reakcja sieciowania przebiega efektywnie dopiero powyżej 200°C (np. aminy trzeciorzędowe lub sole fosfoniowe). Utwardzacze katalityczne powodują homopolimeryzację z otwarciem pierścienia epoksydowego i bazują na kwasach (kompleksy trihalogenków boru z aminami, chlorki glinu, cynku, cyny, żelaza) lub zasadach (aminy trzeciorzędowe, pochodne imidazolu, czwartorzędowe sole fosfoniowe) Lewisa (Rysunek 10, reakcja 5) [36].

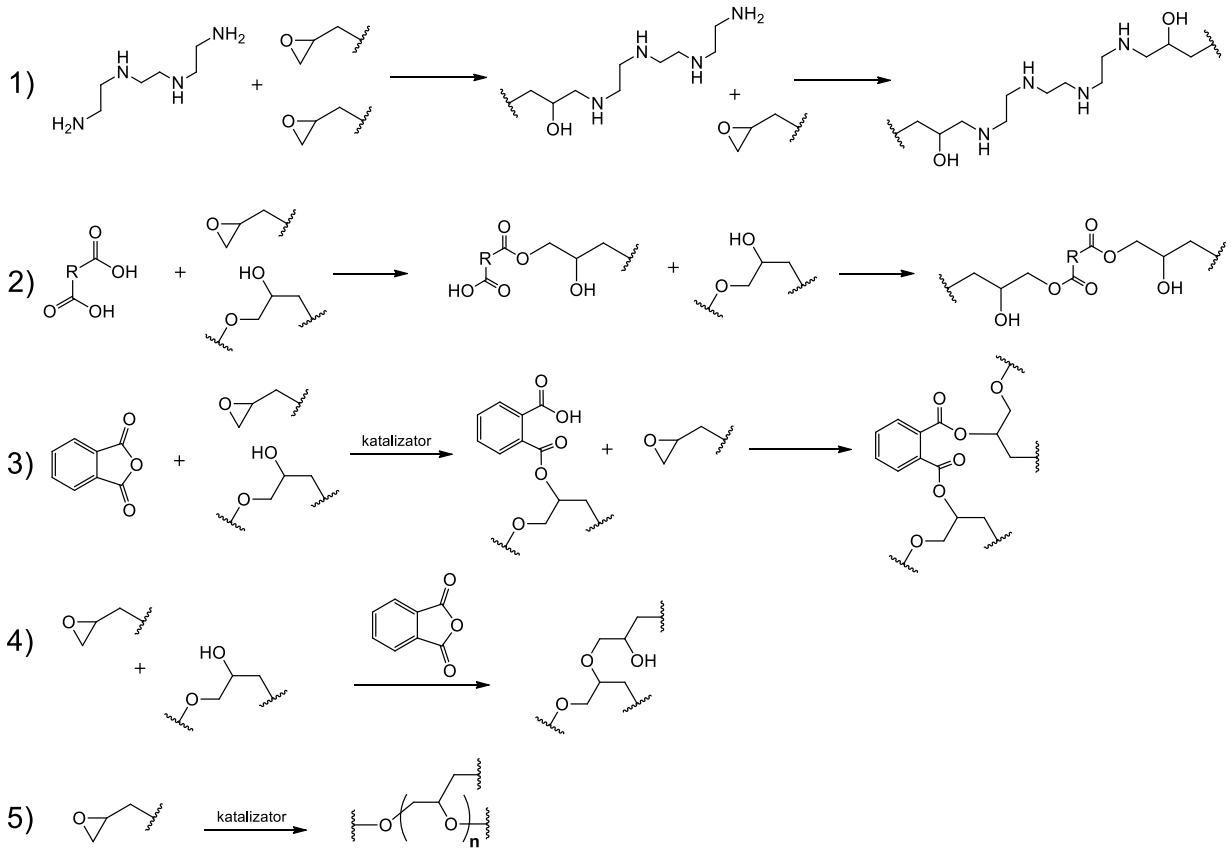

Rysunek 10: Schemat podstawowych mechanizmów utwardzania żywic epoksydowych w zależności od typu zastosowanego utwardzacza. Jako przykładowe utwardzacze zaprezentowano trietylenotetraaminę (reakcja 1) i bezwodnik ftalowy (reakcje 3, 4).

4.3.2 Poliolefiny

Polietylen, najprostszy strukturalnie polimer z grupy poliolefin, ze względu na niski koszt surowca, łatwość przetwórstwa i stosunkową wysoką inertność chemiczną, znajduje liczne zastosowania w masowej produkcji wyrobów użytkowych. Wytwarza się z niego folie, rury, izolacje kablowe, butelki i inne opakowania, powłoki do laminacji, włókna czy obudowy akumulatorów [35]. Jest odporny praktycznie na wszystkie rozpuszczalniki organiczne w temperaturze pokojowej, a także na roztwory zasad i kwasów nieutleniających. Polipropylen (PP), inny powszechnie stosowany polimer, w zależności od metody produkcji, może występować w postaci ataktycznej (aPP), syndiotaktycznej (sPP) lub izotaktycznej (iPP), przy czym na dzień dzisiejszy przeważające znaczenie przemysłowe ma iPP. Charakteryzuje się on mniejszą odpornością chemiczną, za to wyższą temperaturą topnienia czy wyższą

sztywnością od LDPE oraz niższą gęstością i wyższą wytrzymałością na rozciąganie od HDPE. Wytwarza się z niego wyroby cienkościenne, profile, rury, zbiorniki i skrzynie transportowe, włókna czy materiały spienione. Polietylen zaczął być produkowany w Imperial Chemical Industries (ICI) w Wielkiej Brytanii, gdzie w 1939r. opracowano proces wysokociśnieniowej, wolnorodnikowej polimeryzacji etylenu, a uzyskiwany wtedy materiał stanowił według dzisiejszej klasyfikacji LDPE [28].

W roku 1954 Giulio Natta otrzymał izotaktyczny polipropylen, iPP, a badania Karla Zieglera również z początku lat 50. zaowocowały opracowaniem pierwszej technologii produkcji polietylenu wysokiej gęstości (HDPE) [38,39]. Za swoje osiągnięcia zostali oni wspólnie uhonorowani Nagrodą Nobla w 1963r., a odkryte przez nich systemy katalityczne znane są od tamtej pory pod nazwą katalizatorów Zieglera-Natty. Olabisi i Adewale podali w 2016r., że poliolefiny stanowiły ponad 50% światowej produkcji tworzyw [40]. w roku 2018 produkcja globalna PP wynosiła 69 mln ton, HDPE – 44 mln ton, LDPE – 63 mln ton, obok około 180 mln ton innych rodzajów poliolefin [41]. Prognozy Inkwood Research z 2017r. przewidywały osiągnięcie w 2025r. światowej kombinowanej produkcji PE na poziomie 256 mln ton rocznie, a według raportu Transparency Market Research Company z 2016, światowe zapotrzebowanie na PP do 2023r. ma wynieść niemal 130 mln ton rocznie [42].

4.3.3 Polilaktyd

Polilaktyd (PLA) jest tworzywem znanym od pierwszej połowy XX wieku, jednakże zainteresowanie tym polimerem zaczęło wzrastać dopiero w latach 90. [43]. Pierwsze doniesienie historyczne dotyczące syntezy PLA sięga 1845r., kiedy Thèophile-Jules Pelouze zaobserwował zestaloną pozostałość na dnie kolby, w której destylował kwas mlekowy, wydzielając przy tym sublimujący produkt, dimeryczny laktyd [44]. Dokładniejsze eksperymenty przeprowadził uznawany na wynalazcę nylonu i neoprenu Wallace Hume Carothers, opracowując metodę jego polimeryzacji w 1932r., a firma z DuPont, dla której pracował, uzyskała patent na wytwarzanie PLA w 1954r. [43]. Dopiero w latach 90. Cargill Inc. opracowało technologię wytwarzania PLA metodą polimeryzacji z otwarciem pierścienia laktydu, a w 1997r. utworzono we współpracy z The Dow Chemical Company firmę Cargill Dow LLC, która rozpoczęła produkcję polilaktydu pod marką NatureWorks. Wzrost zainteresowania PLA spowodował fakt, że jest to biopolimer, produkowany z kwasu mlekowego, naturalnego produktu procesów fermentacyjnych, a więc monomerem do jego produkcji nie jest żaden surowiec pochodzenia petrochemicznego. Ponadto ze względu na poliestrowy charakter łańcucha polimerowego, ulega on powolnej degradacji w kontakcie ze środowiskiem wodnym, czy enzymami wytwarzanymi przez mikroorganizmy i tkanki żywe. Polilaktyd jest biodegradowalny, co spowodowało, że z jednej strony stał się atrakcyjną opcją jako ekologiczny zamiennik tworzyw sztucznych pochodzenia całkowicie syntetycznego, jak poliolefiny, między innymi w przemyśle opakowaniowym, a z drugiej stanowi jeden z akceptowanych i stosowanych w medycynie materiałów biokompatybilnych, do produkcji szwów chirurgicznych, a także syntetycznych materiałów kościozastępczych ulegających resorpcji [43].

PLA stanowi powszechny wybór jako tworzywo do druku 3D techniką FDM (osadzanie topionego materiału, ang. *Fused Deposition Modeling*). Wynika to z łatwości jego stosowania,

w tym niskiego skurczu przetwórczego, stosunkowo niskiej temperatury przetwórczej, czy niskiego ryzyka wytworzenia toksycznych oraz drażniących oparów w przypadku przegrzania i degradacji materiału. Ostatnie zjawisko jest realnym zagrożeniem podczas stosowania innego popularnego w FDM polimeru, ABS [45,46].

4.4 Techniki addytywne

Druk 3D, czyli technika wytwarzania przyrostowego, składa się z szeregu technologii addytywnych, skategoryzowanych i opisanych ogólnie w normie ISO/ASTM 52900, przy czym ze względu na dynamiczny rozwór branży, zarówno na rynku, jak i w literaturze naukowej spotykać się można z kolejnymi propozycjami lub prototypami rozwiązań, nie zawsze wpasowującymi się w prosty sposób w kategorie w niej ustanowione. Choć pierwszy artykuł opisujący technologię druku z zastosowaniem stereolitografii (SLA) wydał w 1981 r. Hideo Kodama, często mówi się, że druk 3D narodził się w 1986 r., kiedy to Charles Hull uzyskał, po dwóch latach od złożenia wniosku, pierwszy na świecie patent na technologię przyrostową SLA [47,48]. Ze względu na koszt licencji na tę i inne opracowane technologie (SLS, Carl Deckard; FDM, Scott Crump, ten sam rok), techniki druku trójwymiarowego były dostępne przez kolejne lata jedynie dla dużych firm lub jednostek naukowych. Dopiero wygaśnięcie oryginalnych licencji spowodowało otwarcie rynku ekonomicznych rozwiązań dla małych odbiorców, a także publicznego dostępu do darmowego oprogramowania i modeli obiektów 3D, czy schematów urządzeń. Na dzień dzisiejszy nową drukarkę 3D w technologii FDM zakupić można za około tysiąc złotych, a model obiektu do wydruku w postaci pliku .stl pobrać z jednej z kilkudziesięciu dostępnych baz modeli trójwymiarowych lub zaprojektować samodzielnie. Liczba zastosowań druku 3D jest ogromna, przede wszystkim stosuje się go do szybkiego prototypowania oraz produkcji niskoseryjnej i projektów indywidualnych. Natomiast istotna jest mnogość branży korzystających z technologii addytywnych [49]:

a) przemysł maszynowy: najważniejszą funkcją druku 3D w przemyśle maszynowym jest utrzymanie ruchu w zakładach produkcyjnych, polegającym na zachowaniu ciągłości pracy linii produkcyjnej – odbywa się to poprzez szybkie wykonanie zamiennika uszkodzonego elementu (tymczasowego bądź trwałego) z użyciem drukarki 3D. Element taki może pełnić funkcję zastępczą do momentu otrzymania właściwego zamiennika z serwisu lub do momentu kolejnej wymiany;

b) przemysł motoryzacyjny: na potrzeby testowania podzespołów i elementów ozdobnych oraz konstrukcyjnych nowych modeli pojazdów, pozwala to na szybkie testowanie podzespołów bez konieczności drogiego oraz skomplikowanego projektowania i wykonywania form wtryskowych, czy czasochłonnego ręcznego wykonywania elementów lub form do termoformowania próżniowego. Techniki addytywne umożliwiają w ten sposób szybką weryfikację walorów wizualnych projektu pojazdu czy spasowania zaprojektowanych elementów;

c) przemysł lotniczy i kosmiczny: na Międzynarodowej Stacji Kosmicznej znajduje się drukarka 3D, pozwalająca na wydruk niezbędnych części, co jest kluczowe ze względu na trudności logistyczne związane z wysyłaniem tam zaopatrzenia;

d) branża medyczna i protetyka: druk 3D pozwala na drukowanie obiektów stanowiących pomoce naukowe dla studentów medycyny, a także na modelowanie oraz odtwarzanie złożonych struktur anatomicznych. Chirurdzy mają możliwość przeprowadzenia symulacji operacji chirurgicznej na wydrukowanym modelu 3D, a także na zaprojektowanie idealnie dopasowanej protezy dla konkretnego przypadku (np. w traumatologii, chirurgii rekonstrukcyjnej). Na potrzeby rehabilitacji drukować można odpowiednie przyrządy i aparaty dopasowane do konkretnego pacjenta;

e) edukacja, szkolnictwo wyższe: Druk 3D umożliwia wytwarzanie pomocy dydaktycznych, modeli przestrzennych (np. bryły w matematyce, struktury komórkowe czy anatomiczne w biologii);

f) przemysł dekoratorski: możliwość uzyskiwania obiektów o skomplikowanym kształcie, według indywidualnej wizji artysty;

g) hydraulika, pneumatyka: drukowanie złączy, uszczelek, elementów zaworów;

h) elektronika: m.in. do wykonywania obudów i innych elementów urządzeń elektrycznych i elektronicznych, stosowana jest także w badaniach nad elastyczną elektroniką, sensorami naprężenia/rozciągania.

4.5 Składniki dodatkowe do tworzyw

Tworzywa stosowane i produkowane przemysłowo rzadko składają się z czystego polimeru i zazwyczaj zawierają szereg składników dodatkowych. Zgodnie z podziałem przedstawionym przez profesora Koszkula, składniki te dzielimy na napełniacze (wypełniacze) oraz środki pomocnicze (środki modyfikujące, modyfikatory) [50]. Składniki dodatkowe w najszerszym rozumieniu mają na celu poprawę właściwości użytkowych (uzyskanie pożądanych właściwości mechanicznych, nadanie barwy i zachowanie jej stabilności w czasie, zwiększenie odporności na promieniowanie UV i inne czynniki środowiskowe oraz mikroorganizmy, ułatwienie czyszczenia i hydrofobizacja powierzchni oraz inne) lub przetwórczych (reologia przetwórcza, łatwość tworzenia filmu, wyrzut wypraski z formy wtryskowej, kompatybilizacja napełniaczy i składników blend polimerowych). Napełniacze odpowiadają przede wszystkim za zmianę właściwości fizycznych tworzyw, w tym właściwości mechanicznych (sztywność, tj. moduł Younga, moduł zginania; wytrzymałość na rozciąganie, udarność), termicznych (współczynnik przenikania ciepła), elektrycznych (stała dielektryczna, wytrzymałość elektryczna na przebicie), a także obniżenie palności tworzywa. Często stosowane są również dla obniżenia kosztów produkcji wyrobów. Środki modyfikujące pełnią szereg zadań, w tym: przeciwutleniające, kompleksujące śladowe zanieczyszczenia metaliczne po procesie polimeryzacji, pigmentujące, hydrofobizujące, antymikrobiologiczne, czy smarne. Niektóre modyfikatory, tzw. promotory adhezji lub środki sprzęgające, zmieniają charakter powierzchniowy napełniaczy dla poprawy ich dyspersji w osnowie (zmniejszenia efektu aglomeracji cząstek) oraz efektu zwilżania napełniacza polimerem, czyli kontaktu pomiędzy polimerem, a powierzchnią cząstek napełniacza [50].

4.5.1 Pigmenty

Pigmenty to składniki dodatkowe mające na celu nadanie wyrobowi pożądanej barwy, uczynienie go nieprzejrzystym lub zatrzymującym światło, bądź maskującym przebarwienia wynikające ze składu bądź jakości zastosowanego materiału [51,52]. Ponadto, pigmenty mogą spełniać funkcję blokera UV, co zwiększa żywotność tworzywa. Przykładowo, użycie pigmentu w żywicach epoksydowych umożliwia zamaskowanie żółtawej barwy pochodzącej od produktów utleniania utwardzaczy aminowych, która to pogłębia się wraz z czasem przechowywania utwardzacza. Pigmenty, w odróżnieniu od barwników, stanowią materiały praktycznie całkowicie nierozpuszczalne w medium, w którym pełnią funkcję barwiącą, a ich mieszanie z osnową (polimerem, żywicą) polega na rozpraszaniu (dyspersji), a nie rozpuszczaniu pigmentu w materiale. z tego też względu parametry takie jak dystrybucja rozmiaru cząstek pigmentu, czy poziom jego dyspersji w tworzywie stanowią krytyczne czynniki decydujące o sile krycia dodatku, a więc ilości pochłanianego lub odbijanego światła. Bezpośrednio przekłada się to na efektywne stężenie określonego pigmentu w osnowie, a więc jego ilość potrzebną do uzyskania pożądanego stopnia zabarwienia materiału o określonej grubości. Niemal wszystkie dostępne handlowo pigmenty to substancje nieorganiczne z grupy tlenków, soli (m. in. siarczków, węglanów), soli mieszanych oraz układów hybrydowych, gdzie substancja barwna jest strącana lub adsorbowana na powierzchni nośnika o składzie innym od właściwej substancji barwnej. Pigmenty hybrydowe wytwarzane są z zastosowaniem zarówno substancji pigmentujących pochodzenia nieorganicznego, jak i organicznego. Istotną z przemysłowego punktu widzenia klasą materiałów są nieorganiczne formy węgla (czerń węglowa, sadza).

W kontekście światowego zapotrzebowania na wszystkie stosowane pigmenty, na czele znajduje się biel tytanowa (TiO_2), której produkcja w roku 2000 stanowiła 69% rynku światowego [51], a w roku 2009, wraz z tlenkami żelaza i czerniami węglowymi, 90% rynku światowego [52]. Biel tytanowa znajduje zastosowanie w produkcji farb rozpuszczalnikowych i proszkowych, tworzyw termoplastycznych i duroplastycznych (w tym żywic epoksydowych), papieru, leków tabletkowanych oraz innych wyrobów.

4.6 Silseskwioksany jako nowa klasa dodatków do tworzyw

Wśród modyfikatorów tworzyw ważną rolę odgrywają związki krzemoorganiczne, w szczególności dwie ich grupy, tj. silany oraz polisiloksany (oleje silikonowe). Pierwsza grupa pełni rolę silanowych środków sprzęgających, poprawiających efekt zwilżania napełniacza polimerem [53]. Związki z pozostałej grupy mogą pełnić podobną rolę, natomiast dodatkowo służą jako czynniki smarujące (poślizgowe) czy antyspieniające. Od końca lat 90., wyraźnie wzrosło zainteresowanie związkami silseskwioksanowymi jako potencjalnie nową klasą krzemoorganicznych składników dodatkowych do tworzyw polimerowych. z uwagi na charakter tej pracy, w Tabeli 1 sporządzono zestawienie związków silseskwioksanowych i sferokrzemianowych, których kompozycje na osnowie polietylenu były przedmiotem doniesień literaturowych.

Tabela 1: Zestawienie związków silseskwioksanowych oraz sferokrzemianowych stosowanych jako modyfikatory w układach na osnowie polietylenu lub polipropylenu.

L.p.	Wzór	Uwagi	Matryca/ Odnośniki
1	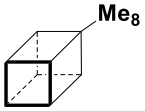	PP: W [54] stosowano metylopolisilseskwiok san. W [55] jako kompatybilizator napełniacza – mączki z łupiny kokosa W [56] w blendzie polimerowej PP/POM W [57,58] jako kompatybilizator SiO_2	PE: [59-70] PP: [54-56,71-78]
2	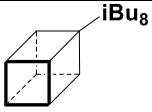	PE: W [79] jako kompatybilizator SiO_2 w kompozytach z UHMWPE W [80] kompozytach z HDPE, EVA oraz blenach HDPE/EVA PP: W [81] w reakcji z PP-g-MA i zwykłym PP W [82] w reakcji z PP-g-MA W [83] w blendzie polimerowej PP/PA6	PE: [59-62,79, 80,84-92] PP: [71,75,77,78, 81-83.93-95]
3	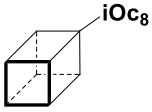		PE: [59-63] PP: [71,75,77]
4	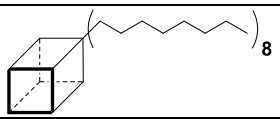		PE: [96]
5	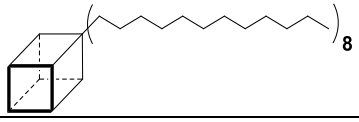		PE: [96]
6	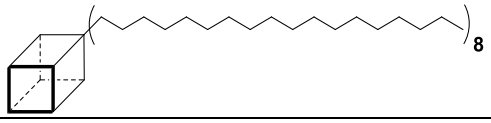		PE: [96]

7	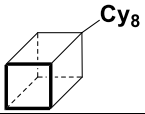		PE: [68]
8	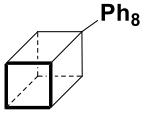	PP: W [84] stosowano fenylopolisilseskwio-ksan	PE: [68-70] PP: [54,72,97,98]
9	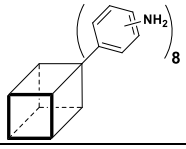	W reakcji z PP-g-MA oraz zwykłym PP	PP: [99]
10	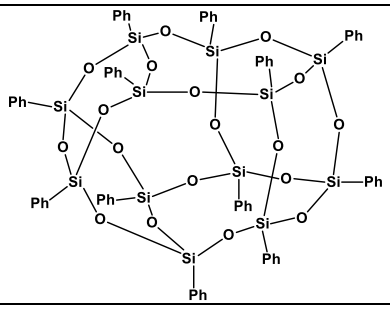		PP: [100]
11	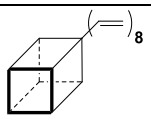	PE: Jako dodatek do EPDM w [101] W przypadku [102] otrzymany silseskwioksan to mieszanina struktur T_8 i T_{10} PP: W [54] stosowano winylopolisilseskwio-ksan	PE: [101-104] PP: [54,105-110]
12	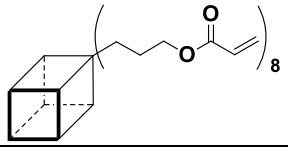		PP: [111]
13	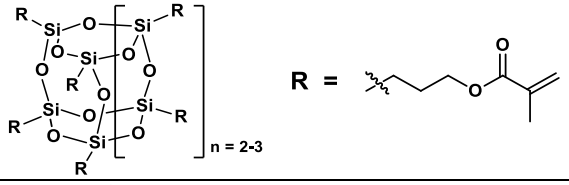		PP: [112]
14	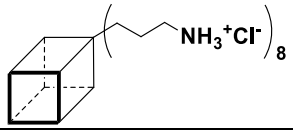		PP: [98,113,114]
15	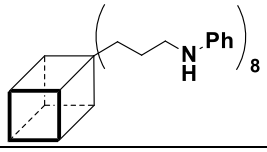		PP: [100]

16	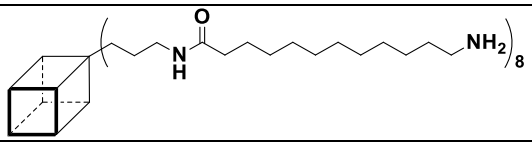		PE: [115]
17	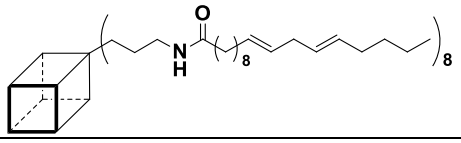		PE: [116]
18	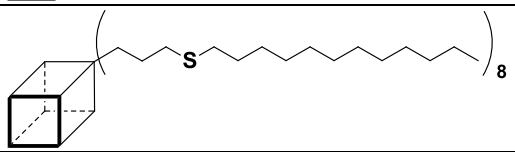		PP: [117]
19	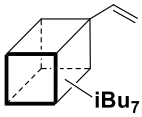	W [118] jako monomer kopolimeryzacji etylenu	PE: [118-119]
20	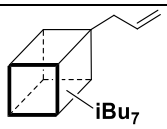	PE: Jako monomer do kopolimeryzacji etylenu w [118,120]	PE: [104,118,120, 121] PP: [122,123]
21	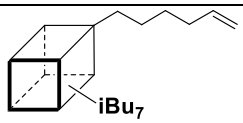	Jako monomer do kopolimeryzacji etylenu w [118,124]	PE: [118,124]
22	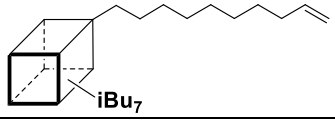	Jako monomer do kopolimeryzacji etylenu w [118,124]	PE: [118,124]
23	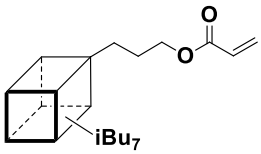	PE: Jako monomer do kopolimeryzacji etylenu w [125-127]	PE: [125-127] PP: [128]
24	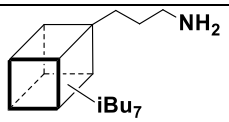	PE: W [129] jako kompatybilizator węgliku krzemu do kompozytów z UHMWPE. W reakcji z HDPE-g-MA oraz zwykłym HDPE w [130,131] PP: W [83] w blendzie polimerowej PP/PA6 W reakcji z PP-g-MA oraz zwykłym PP w [130,132,133] W reakcji z PP-g-MA z dodatkiem uniepalniacza w [134]	PE: [70,129-131] PP: [83,98,130, 132-135]

		W kompozytach warstwowych PP/Nylon 6 w [135]	
25	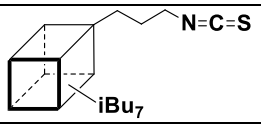		PP: [136]
26	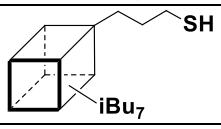		PP: [93,137]
27	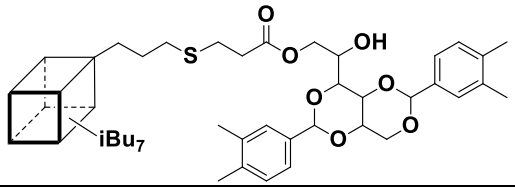		PP: [93]
28	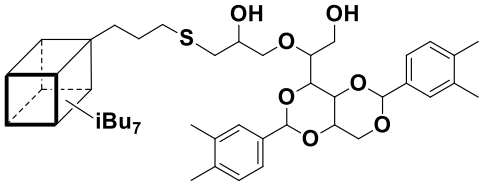		PP: [137]
29	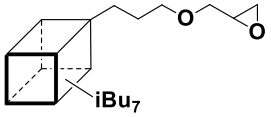	W blendzie polimerowej PP/PA6	PP: [83]
30	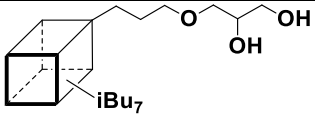		PP: [138]
31	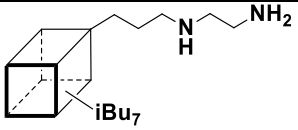	PE: W reakcji z HDPE-g-MA oraz zwykłym HDPE w [121,130,131] PP: W reakcji z PP-g-MA oraz zwykłym PP w [94,130,133]	PE: [121,130, 131] PP: [94,130,133]
32	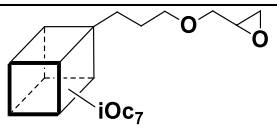		PP: [138]
33	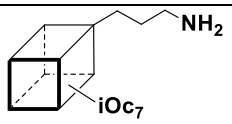	PE: W reakcji z HDPE-g-MA oraz zwykłym HDPE w [130,131] PP: W reakcji z PP-g-MA oraz zwykłym PP w [130,133]	PE: [70,130,131] PP: [130,133]

34	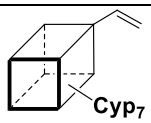	Jako monomer do kopolimeryzacji etylenu	PE: [120,139]
35	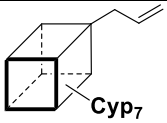	Jako monomer do kopolimeryzacji etylenu	PE: [139]
36	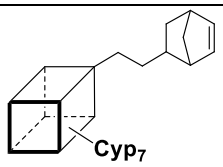	PE: Jako monomer do kopolimeryzacji etylenu PP: Jako monomer do polimeryzacji propylenu	PE: [139-143] PP: [139]
37	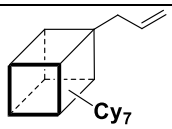	Jako monomer do kopolimeryzacji etylenu	PE: [118]
38	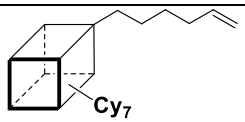	Jako monomer do kopolimeryzacji etylenu	PE: [118,124]
39	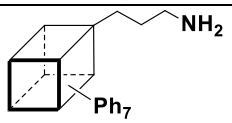		PE: [70]
40	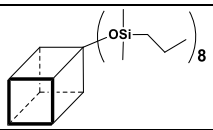		PE: [144]
41	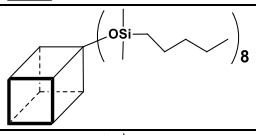		PE: [144,145]
42	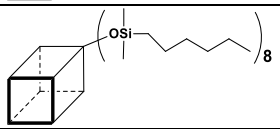		PE: [144]
43	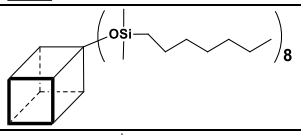		PE: [144]
44	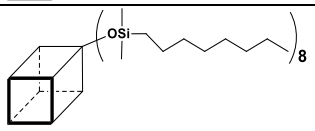		PE: [144,146] PP: [146-148]
45	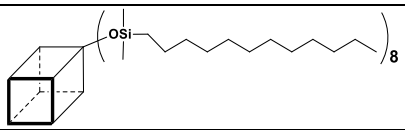		PP: [147]
46	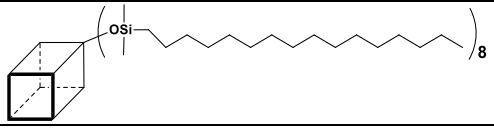		PP: [119]

47	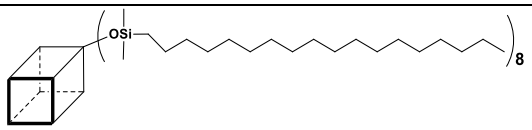		PE: [146,149] PP: [146-148]
48	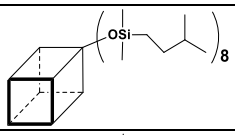		PE: [144,145]
49	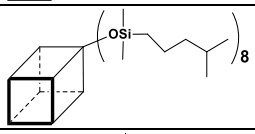		PE: [144]
50	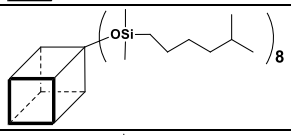		PE: [144]
51	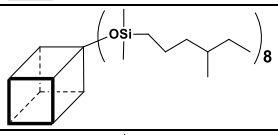		PE: [146]
52	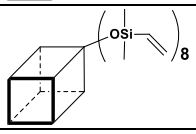		PP: [119]
53	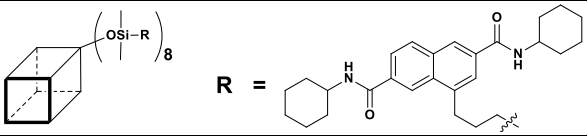		PP: [150]
54	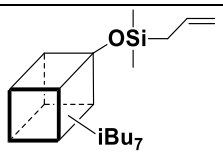	Jako monomer do kopolimeryzacji etylenu	PE: [118,124]
55	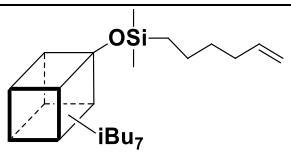	Jako monomer do kopolimeryzacji etylenu	PE: [118,124]
56	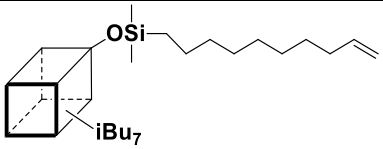	Jako monomer do kopolimeryzacji etylenu	PE: [118,124]
57	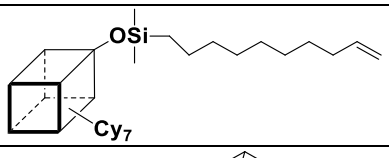	Jako monomer do kopolimeryzacji etylenu	PE: [118,124]
58	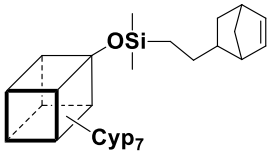	Jako monomer do kopolimeryzacji etylenu	PE: [140]
59	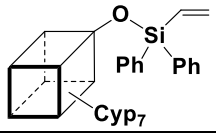	Jako monomer do kopolimeryzacji etylenu	PE: [120]

60	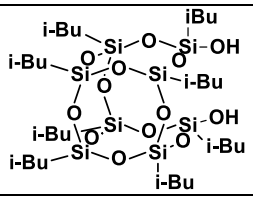	Jako ligand katalizatora w polimeryzacji etylenu	PE: [151-153]
61	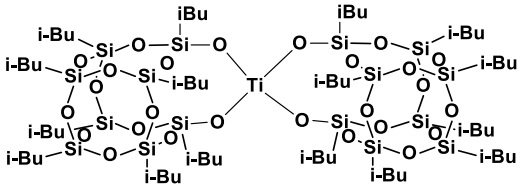	Jako katalizator polimeryzacji etylenu	PE: [154]
62	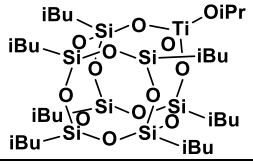		PP: [155]
63	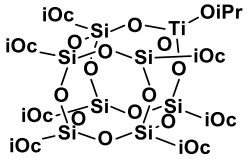	Jako katalizator polimeryzacji etylenu	PE: [154]
64	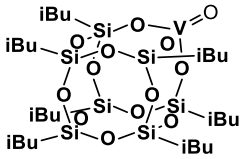		PP: [155]
65	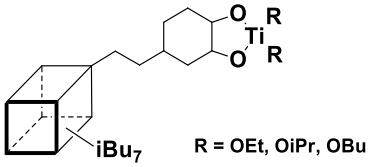	Jako katalizator polimeryzacji etylenu	PE: [156]
66	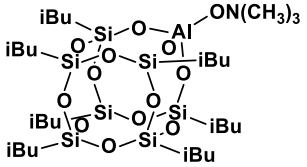		PP: [157]
67	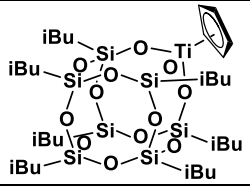		PP: [157]
68	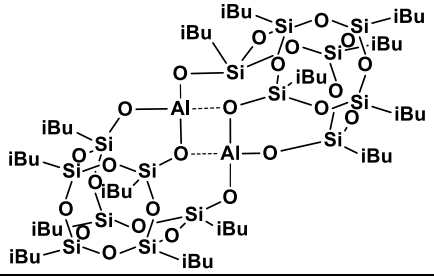		PP: [158]

69	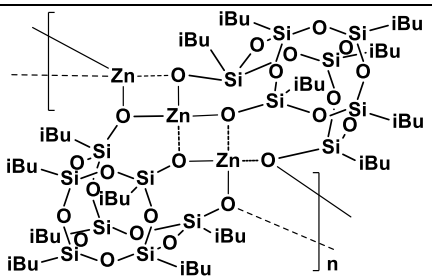		PP: [158]
70	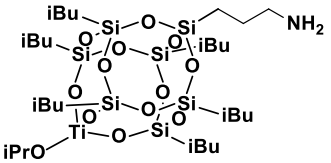	W reakcji z PP-g-MA	PP: [82]
71	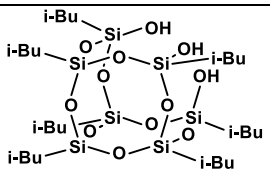	PP: W [83] w blendzie polimerowej PP/PA6 W [159,160] jako kompatybilizator TiO_2	PE: [91] PP: [83,93, 159-161]
72	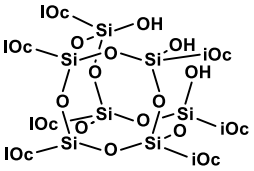	Jako kompatybilizator kaolinitu do kompozytów PP	PP: [162]
73	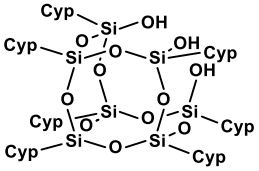		PP: [163,164]
74	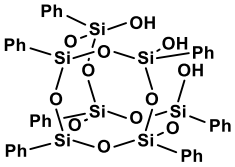	PE: W [165-167] jako kompatybilizator TiO_2 W [168] jako kompatybilizator nanorurek węglowych do kompozytów z UHMWPE PP: W kompozytach warstwowych PP/Nylon 6 w [135]	PE: [165-168] PP: [97,135,163, 164]
75	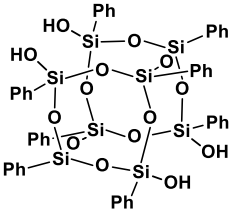		PP: [163,164]

76	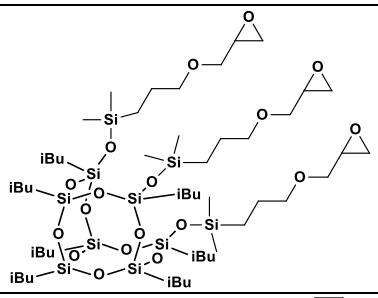		PP: [138]
77	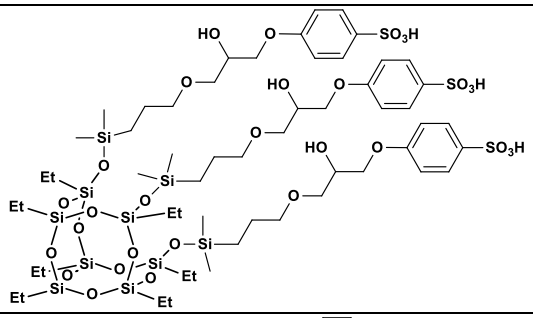		PP: [113]
78	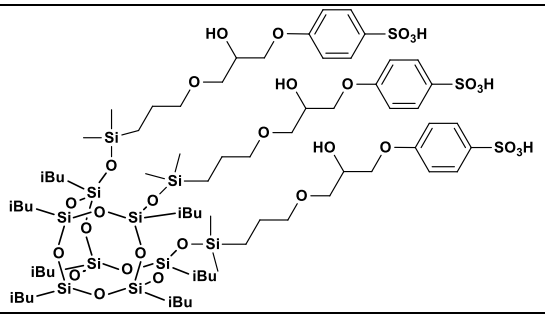		PP: [98]
79	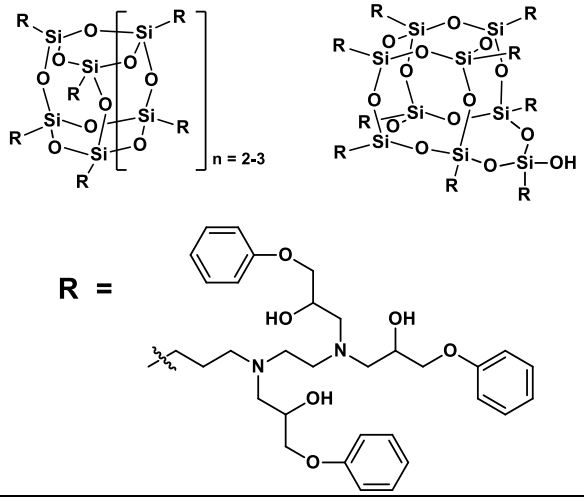	Jako ligandy immobilizowanego katalizatora polimeryzacji etylenu	PE: [169,170]

W kontekście tworzyw termoplastycznych semikrystalicznych, jakimi są PE oraz iPP, obserwowano wpływ dodatków silseskwioksanowych i sferokrzemianowych na parametry takie jak:

a) właściwości mechaniczne (wytrzymałość na rozciąganie i zginanie, moduł Younga, moduł zginania, udarność [71,93,133], moduł zachowawczy i stratności [84]);

b) właściwości termiczne i krystalizacyjne (temperatura topnienia i krzepnięcia, temperatura zeszklenia [146,157], mechanizm i kinetyka krystalizacji [102], poziom krystaliczności [133], profil rozkładu termicznego [145,146,157]);

c) mikro- i nanostruktura tworzywa (morfologia i wielkość sferolitów [146], lokalizacja obszarów koncentracji dodatku [131], uporządkowanie łańcuchów polimeru [145]);

d) właściwości elektroizolacyjne (przenikalność elektryczna, wytrzymałość elektryczna [60]);

e) właściwości reologiczne stopu polimerowego (współczynnik szybkości płynięcia, krzywa lepkości [99,116,119]).

W odniesieniu do analizy tworzyw duroplastycznych, w tym żywic epoksydowych, część parametrów podlegających badaniom pokrywa się z wymienionymi powyżej, np. właściwości mechaniczne, elektroizolacyjne, nanostruktura czy profil rozkładu termicznego. Natomiast szczególnie istotną i swoistą dla tej grupy tworzyw własnością jest charakterystyka procesu sieciowania (kinetyka i ciepło sieciowania, temperatura aktywacji, maksymalna temperatura sieciowania). Dostępne są doniesienia literaturowe, gdzie silseskwioksany pełniły rolę dodatku niereaktywnego [171], katalitycznego [172], jak i sieciującego, zarówno jako składnik epoksydowy (oksiranowy) [173], jak i utwardzający (aminowy [174,175] lub bezwodnikowy [176]).

Ostatnim aspektem poruszanym w pracy jest modyfikacja powierzchni napełniaczy i pigmentów do tworzyw. Napełniacze zarówno mineralne, jak i organiczne, a także pigmenty nieorganiczne charakteryzują się zazwyczaj dużą polarnością powierzchniową (obecność grup -OH lub jonowy charakter napełniacza), co obniża kompatybilność składnika z niskopolarnymi lub niepolarnymi matrycami polimerowymi, w szczególności poliolefinowymi. Jak wspomniano wcześniej, celem poprawy dyspersji napełniaczy, a także pigmentów w osnowie polimerowej stosuje się odpowiednie składniki dodatkowe, często na bazie silanowych środków sprzęgających (silanów) oraz olejów silikonowych, których zadaniem jest zmiana charakteru chemicznego powierzchni materiału, zazwyczaj obniżenie jego polarności [53]. Ze względu na wspólne cechy strukturalne, silseskwioksany były również badane pod kątem zastosowania jako analogi tradycyjnych silanowych środków sprzęgających.

5. Cel badań

Celem badań stanowiących treść rozprawy doktorskiej było określenie wpływu udziału silseskwioksanów oraz sferokrzemianów na układy polimerowe termoplastyczne (polietylenu, polipropylenu i polilaktydu) oraz duroplastyczne (żywicy epoksydowej pigmentowanej TiO_2), z uwzględnieniem struktury stosowanych silseskwioksanów (rdzenia oraz podstawników) oraz natury polimeru. Szczególną uwagę należało przy tym poświęcić aspektom metodyki przetwórczej, stężenia stosowanych silseskwioksanów, charakteru fizykochemicznego składników układu oraz rozproszeniu dodatków w osnowie na zdolność interakcji składników i zmiany we właściwościach przetwórczych oraz użytkowych zmodyfikowanych tworzyw. Polietylen, polipropylen i żywice epoksydowe stanowią powszechnie stosowane polimery o ogromnym znaczeniu przemysłowym, natomiast polilaktyd zyskuje popularność ze względu na pochodzenie z surowców naturalnych, biodegradowalność oraz zastosowanie jako jeden z najczęściej wybieranych materiałów do druku 3D techniką FDM (Fused deposition modeling).

Silseskwioksany i sferokrzemiany stanowią wyspecjalizowane związki krzemoorganiczne, ze względu na szereg właściwości odróżniających je od silanowych środków sprzęgających oraz polisiloksanów mogą stanowić nie tylko alternatywę dla wspomnianych substancji, ale także wypełniać lukę w procesach technologicznych lub zastosowaniach, w których aplikacja powyższych byłaby trudna, niemożliwa lub niebezpieczna. Jednakże, z uwagi na odmienne właściwości fizykochemiczne, a więc i zachowanie w układach polimerowych, a także wysoki koszt produkcji, niezbędne jest dogłębne zbadanie natury oddziaływań silseskwioksanów i sferokrzemianów z osnowami polimerowymi i napełniaczami, ich zdolności dyspersji lub mieszania z tworzywami, czy zmiany charakteru powierzchniowego modyfikowanych nimi napełniaczy bądź pigmentów. Zrozumienie tych oddziaływań wraz z eksperymentalnym odnalezieniem optymalnych stężeń i metodyki przetwórczej, pozwoli na wskazanie realnych obszarów zastosowań tychże związków, gdzie ich aplikacja będzie nie tylko korzystna, ale co istotne, zasadna z ekonomicznego punktu widzenia w aspekcie zastosowań przemysłowych.

Z powyższych względów jednym z kluczowych aspektów pracy jest badanie omawianych zależności w obszarze niskich stężeń (od 50 ppm do 1.5% w/w) stosowanych pochodnych krzemoorganicznych oraz porównanie ich właściwości z komercyjnie dostępnymi silanowymi środkami sprzęgającymi (Rysunek 11).

Wyżej wymieniony problem badawczy stanowił przedmiot grantu PRELUDIUM, którego kierownikiem był autor tejże rozprawy doktorskiej. Realizacja projektu zaowocowała serią publikacji naukowych składających się na dorobek omawiany w dalszej części pracy. Pomimo przeważającego charakteru badań podstawowych, celem głównym była ocena zasadności koncepcji stosowania silseskwioksanów i sferokrzemianów jako modyfikatorów do materiałów polimerowych w kontekście realnego użycia takich układów do zastosowań przemysłowych lub specjalistycznych.

Tezę pracy można ująć następująco: związki w postaci pochodnych silseskwioksanowych oraz sferokrzemianowych mogą być stosowane w roli dodatków przetwórczych do tworzyw syntetycznych i układów polimerowych na bazie tworzyw omawianych w pracy, przy czym z racji kosztów ich otrzymywania, zakres ich stosowania

w realnych aplikacjach przemysłowych ogranicza się do ułamka procenta wagowego w przeliczeniu na masę tworzywa i przy takim ich udziale należy doszukiwać się poprawy cech funkcjonalnych modyfikowanych tworzyw. Najbardziej przyszłościowym kierunkiem zastosowania silseskwioksanów i sferokrzemianów jest możliwość ich aplikacji jako nowej klasy środków sprzęgających, a więc chemicznych modyfikatorów powierzchni, gdzie niewielka ilość czynnika w przeliczeniu na masę tworzywa przekłada się na istotne zmiany fizykochemii układu, a także wykazanie obszarów, w których systemy te oferują przewagę w stosunku do klasycznych preparatów silanowych (Rysunek 11).

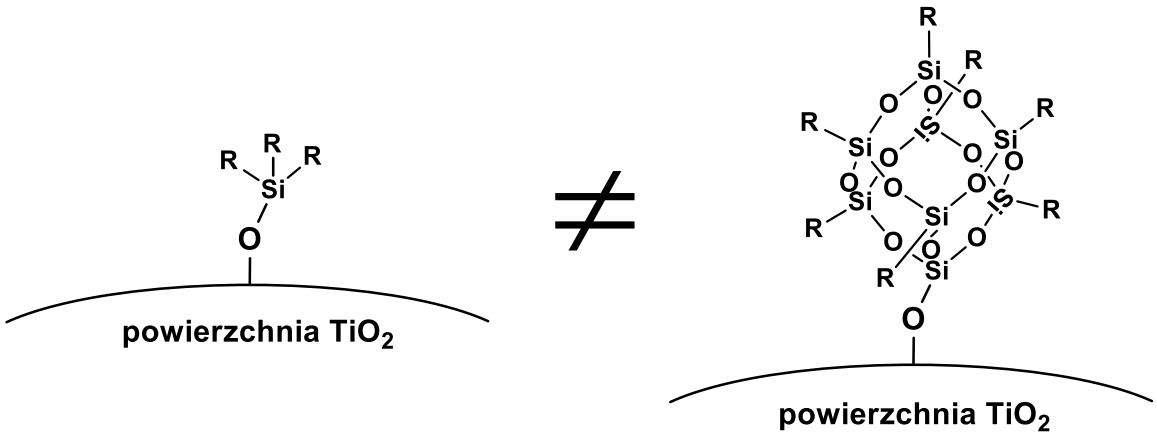

Rysunek 11: Porównanie organofunkcyjnych silanów oraz silseskwioksanów/ sferokrzemianów jako środków sprzęgających do modyfikacji powierzchni pigmentów na bazie bieli tytanowej.

6. Omówienie publikacji składających się na rozprawę doktorską

W ramach realizacji planu badawczego rozprawy doktorskiej otrzymano i scharakteryzowano szereg pochodnych silseskwioksanowych, mono- oraz oktasferokrzemianowych. Dwie z nich (**3** i **5**) stanowiła nowe, wcześniej niepublikowane struktury, pozostałe natomiast nie zostały wcześniej przebadane pod kątem aplikacji jako dodatków w omówionych poniżej osnowach polimerowych, bądź też inny był zakres prowadzonych badań (stosowane stężenia, techniki przetwórcze i pomiarowe, wykorzystane osnowy polimerowe).

W pracy **P1** przedstawiono syntezę oktasferokrzemianów funkcjonalizowanych sterycznie rozbudowanymi grupami funkcyjnymi celem zbadania wpływu podstawnika na kompatybilność dodatku z osnową polimerową oraz właściwości funkcjonalne modyfikowanego tworzywa. Zestawienie otrzymanych pochodnych przedstawiono w Tabeli 2.

Tabela 2: Pochodne oktasferokrzemianowe zastosowane w pracy **P1**.

Rdzeń	Związek	Oznaczenie	Podstawnik R
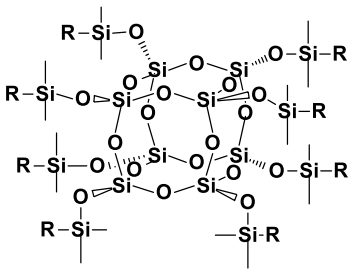	1	SS-H	H
	2	SS-Vi	Vi
	3	SS-Norbornene	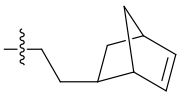 **57%** 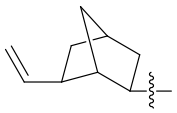 **10%** 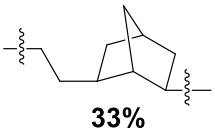 **33%**
	4	SS-Limonene	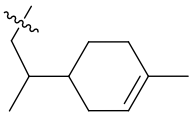
	5	SS-Pinene	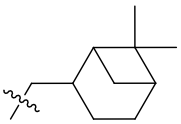

Pochodne **4** i **5** zostały wcześniej omówione jako modyfikatory do membran żelowych PVDF/HFP, jednakże w pracy przedstawiono jedynie analizę FT-IR [177]; synteza pochodnej **3** nie była wcześniej publikowana. w publikacji **P1** omówiono szczegółową analizę NMR, MALDI-TOF-MS, DSC i TG otrzymanych związków. Porównawczo w badaniach wykorzystano również bazowy oktawodorosferokrzemian **1** będący substratem do syntezy pochodnych **3-5** na drodze hydrosililowania oraz oktawinylosferokrzemian **2**. Obydwa związki cechują się niską zawadą steryczną wpływającą na osłanianie polarnego rdzenia cząsteczki.

Otrzymane związki poddawano mieszaniu w stopie z LDPE, a następnie wytłaczano granulat modyfikowanego tworzywa oraz folie i wtryskiwano normalizowane kształtki do badań wytrzymałościowych.

Analiza DSC umożliwiła zaobserwowanie zjawiska polimeryzacji i sieciowania związków SS-Limonene i SS-Norbornene w warunkach przetwórstwa LDPE. Ponadto, analiza TG wykazała dwuetapowy przebieg rozkładu SS-Norbornene, gdzie pierwszy etap rozkładu spowodowany był reakcją retro-Dielsa-Aldera (rDA). Na podstawie NMR potwierdzono również aktywność wewnątrzpierścieniowego wiązania podwójnego winylonorbornenu w reakcji hydrosililowania, co powodowało tworzenie dodatkowych wiązań inter- oraz intramolekularnych i nowych ugrupowań cyklicznych podczas syntezy, a formację policyklicznych produktów ubocznych potwierdzono za pomocą MALDI-TOF-MS (Rysunek 12).

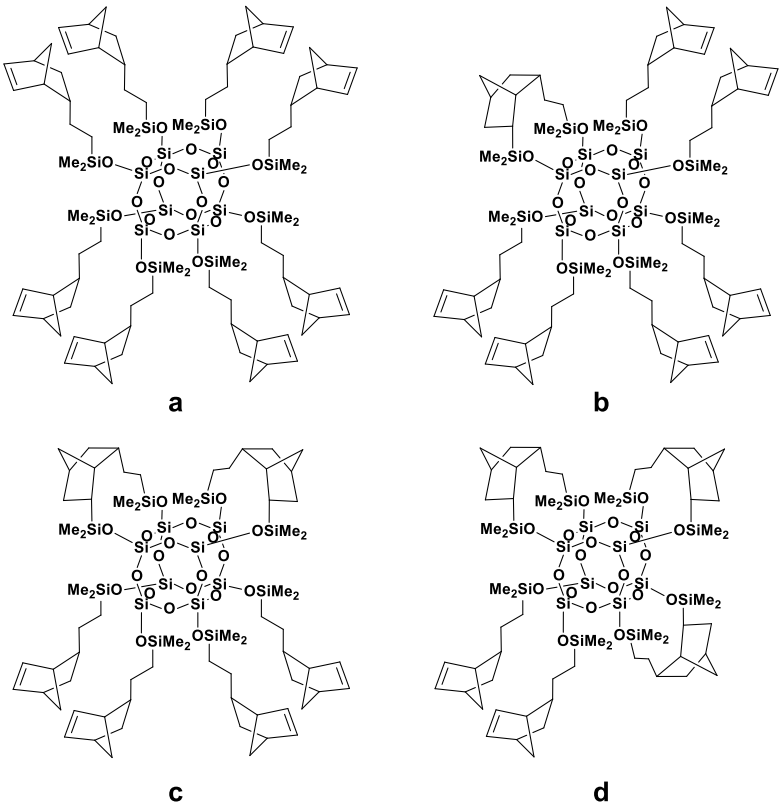

Rysunek 12: Struktury cząsteczki czystego, monomerycznego SS-Norbornene (a) oraz struktur produktów policyklicznych powstałych w wyniku odpowiednio jednej, dwóch oraz trzech (b-d) reakcji intramolekularnej addycji Si-H do wewnątrzpierścieniowego wiązania podwójnego winylonorbornenu.

Omówiono również wpływ dodatków na właściwości termiczne otrzymanych układów polimerowych. Zaobserwowano, że pozytywnie wpływają one na stabilność termiczną tworzywa, podwyższając temperatury początku rozkładu, 5% ubytku masy oraz punktu największej szybkości rozkładu (ang. *DTG peak*), szczególnie w atmosferze utleniającej. Jednocześnie zwrócono uwagę, że efekt ten związany jest najprawdopodobniej z rekombinacją wolnych rodników przez cząsteczki modyfikatora, a nie formowaniem ochronnej warstwy popiołu na powierzchni degradującego tworzywa, co stanowi często powtarzane w literaturze wyjaśnienie. To wytłumaczenie wydaje się niezasadne z dwóch przyczyn: jedną jest

skuteczność otrzymanych dodatków już przy niskim stężeniu na poziomie 0.1% w/w, zbyt niskim do wytworzenia opisywanej warstwy popiołowej; drugim jest fakt, że polietylen, w trakcie rozkładu termicznego, tworzy ruchliwą masę wydzielającą gazy, co dodatkowo utrudnia uformowanie warstwy ochronnej.

Szczególnym osiągnięciem pracy **P1** w aspekcie metodologii badawczej było zastosowanie wtryskarki do tworzyw celem przygotowania wysoce jednorodnych i powtarzalnych wymiarowo próbek do badań wytrzymałościowych, zgodnie z normą EN ISO 527-2. w kontekście kompozytów i nanokompozytów PE zawierających dodatek związków silseskwioksanowych bądź sferokrzemianowych, takie podejście zostało wcześniej opisane w literaturze zaledwie raz [146]. Zazwyczaj wytwarzanie próbek realizowano na drodze wytłaczania lub prasowania na gorąco, bądź też analiza mechaniczna była zupełnie pomijana. Tak przygotowane próbki zostały wykorzystane do obrazowania mikrostruktury wewnętrznej tworzywa.

W pracy udowodniono istotny wpływ otoczenia chemicznego rdzenia siloksanowego (silseskwioksanowego) na zdolności dyspersyjne sferokrzemianów oraz obecności wiązań nienasyconych w cząsteczce modyfikatora na jego zachowanie podczas mieszania w stopie tworzywa, co zostało zbadane z zastosowaniem technik obrazowania SEM oraz SEM-EDS. w porównaniu do krystalicznych, nietopliwych SS-H i SS-Vi, pozostałe pochodne charakteryzowały się podwyższoną mieszalnością z tworzywem, w szczególności SS-Limonen, który to na skutek sieciowania termicznego tworzył najprawdopodobniej blendę polimerową z LDPE. Uzyskane modyfikowane tworzywo charakteryzowało się zauważalnie poprawionymi właściwościami mechanicznymi dla kształtek wtryskiwanych pomimo niskiego udziału dodatku (≤1% w/w). w przypadku folii obserwowano głównie pogorszenie właściwości mechanicznych, co wyjaśniono na podstawie zaburzenia orientacji polimeru w próbkach. Wyjątkiem był SS-Pinene, który dla stężenia 1% w/w podwyższył nieznacznie wartość odkształcenia przy zerwaniu. Istotnym aspektem pracy jest też badanie wpływu omawianych dodatków w zakresie niskich stężeń (0.1%-1% w/w), w odróżnieniu od licznych doniesień literaturowych, w których pochodne silseskwioksanowe czy sferokrzemianowe stosowano w roli napełniaczy w ilościach do 10, a nawet 20% w/w. Pozwoliło to zaobserwować, że optymalne stężenie stosowanych dodatków, w zależności od konkretnego związku czy cechy funkcjonalnej stosowanego tworzywa, znajduje się za każdym razem na pewnym poziomie poniżej 1%., co wiąże się z ograniczoną kompatybilnością tego typu dodatków z LDPE.

W pracy **P2** zbadano wpływ mono- i difunkcyjnych silseskwioksanów na właściwości modyfikowanego nimi LDPE. Zastosowano metodykę badawczą analogiczną do pracy **P1**. w Tabeli 3 zestawiono zastosowane modyfikatory. Podobnie do **P1**, stosowane związki krzemoorganiczne badano w zakresie niskich stężeń (0.1-1.5% w/w), obserwując przy tym optimum stężenia dodatku w granicach 1%.

Zaobserwowano zbliżone właściwości dyspersyjne pochodnych **6-8** w matrycy polimerowej, co związane było z obecnością wspólnego motywu strukturalnego, tj. klatki heptaizobutylosilseskwioksanowej, a także krystalicznym charakterem cząsteczek. Dla odmiany, lepszą dyspersją charakteryzowały się SSQ-8Cl oraz *i*Bu$_7$SSQ-3OH. Efekt wyjaśniono na podstawie amorficznej postaci dodatków. Kod SSQ-8Cl reprezentował

wyidealizowaną strukturę związku, w rzeczywistości stanowiącą mieszaninę oligomerycznych silseskwioksanów (ang. *cage mix, cage mixture*). *i*Bu$_7$SSQ-3OH natomiast w wyniku mieszania w stopie polimeru tworzył serię produktów kondensacji, których obecność potwierdzono za pomocą MALDI-TOF-MS, a wykryte wartości *m/z* były zgodne z przewidywanymi strukturami związków. w obydwu przypadkach amorficzny charakter dodatków wpływał na poprawę ich mieszalności z osnową, ponieważ nie dochodziło do formowania przez nie polikrystalicznych aglomeratów. Równocześnie, produkty kondensacji *i*Bu$_7$SSQ-3OH charakteryzowały się niższą polarnością cząsteczki co dodatkowo tłumaczy dobrą mieszalność z tworzywem.

Tabela 3: Pochodne silseskwioksanowe zastosowane w pracy **P2**.

Rdzeń	Związek	Oznaczenie	Podstawnik R
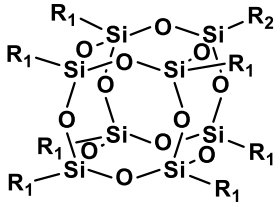	6	*i*Bu$_7$SSQ-Vi	R_1 = *i*Bu, R_2 = Vi
	7	*i*Bu$_7$SSQ-NH_2	R_1 = *i*Bu, R_2 = $(CH_2)_3NH_2$
	8	*i*Bu$_7$SSQ-Cl	R_1 = *i*Bu, R_2 = $(CH_2)_3Cl$
	9	SSQ-8Cl	R_1 = R_2 = $(CH_2)_3Cl$
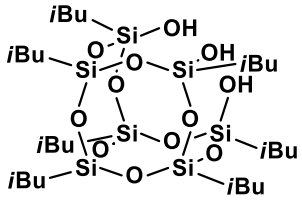	10	*i*Bu$_7$SSQ-3OH	zgodnie z rysunkiem

W pracy **P2** wykazano także pozytywny wpływ techniki wtryskowej na dyspersję dodatków w tworzywie. w wyniku porównania obrazów SEM-EDS próbek wytłaczanych i wtryskiwanych, zaobserwowano spadek udziału aglomeratów modyfikatora w tych ostatnich, co spowodowane było udziałem dużych sił ścinających generowanych w cyklu przetwórczym. Podobnie, jak w **P1**, obserwowano głównie niekorzystny wpływ dodatków na właściwości mechaniczne folii, za wyjątkiem *i*Bu$_7$SSQ-3OH, gdzie dochodziło do podwyższenia wartości wytrzymałości na rozciąganie.

Dodatkowo zaobserwowano, że *i*Bu$_7$SSQ-NH_2 szczególnie skutecznie zwiększał stabilność termiczną LDPE w warunkach utleniających, co przypisano antyoksydacyjnym właściwościom grupy aminowej w strukturze modyfikatora. SSQ-8Cl oraz *i*Bu$_7$SSQ-3OH wykazywały przy wyższych stężeniach niewielki efekt plastyfikujący na tworzywo.

Istotnym efektem naukowym pracy **P2** było wykazanie, że związki typu silseskwioksanów nie powinny być uznawane za napełniacze bądź nanonapełniacze, a za szeroko pojęte modyfikatory. Wynika to z szeregu czynników, mianowicie multifunkcjonalności omawianych dodatków (wpływ na właściwości mechaniczne, krystalizacyjne, przetwórcze, stabilność termiczną/oksydacyjną), ale również ceny tych systemów, co decyduje o konieczności szukania ich skutecznych zastosowań w zakresie niskich stężeń. Dodatkowo jest to spowodowane zjawiskiem aglomeracji obserwowanej przy

wyższych stężeniach modyfikatorów, co zmniejsza efekt ich oddziaływania na osnowę i może wpływać na pogorszenie właściwości uzyskanych tworzyw lub kompozytów.

W pracy **P3** zbadano wpływ opisanej wyżej pochodnej sferokrzemianowej **4**, tj. SS-Limonene, na właściwości PLA stosowanego w technologii addytywnej FDM. Wykazano, że mieszanie dodatku z PLA powoduje sieciowanie **4**, z uformowaniem kompozytu na osnowie polilaktydu (Rys. 13).

Rysunek 13: Drukarka 3D w technologii FDM i wytworzone na niej próbki.

Szczególnym osiągnięciem naukowym pracy jest uzyskanie znacznej poprawy właściwości mechanicznych otrzymanych materiałów. Wzrostowi uległy wytrzymałość na rozciąganie i zginanie oraz wydłużenie przy zerwaniu i udarność. Dwa ostatnie efekty sugerują właściwości plastyfikujące dodatku, co jest szczególnie pożądane ze względu na kruchość PLA, stanowiącą jedną z cech szczególnie ograniczających perspektywy zastosowania tego tworzywa jako materiału konstrukcyjnego. Przy udziale 0.25% **4**, próbki wytwarzane z tworzywa modyfikowanego w technologii FDM charakteryzowały się w granicach odchylenia standardowego wytrzymałością na rozciąganie równą odpowiednikom wykonanym techniką wtrysku, a także próbkom wtryskiwanym z czystego PLA. Wydłużenie przy zerwaniu dla omawianego materiału wzrosło średnio o 73% dla układów drukowanych, co jest znaczącą poprawą w kontekście badanego polimeru. Na podstawie mikroskopii optycznej udowodniono ponadto, że obiekty wytworzone z PLA z dodatkiem 0.25% **4** charakteryzowały się zwiększonym przetopem warstw materiału, co było jedną z głównych przyczyn poprawionych właściwości wytrzymałościowych tworzywa. Kolejną negatywną cechą polilaktydu w aspekcie zastosowań konstrukcyjnych jest podatność na degradację w wyniku działania wilgoci. Tymczasem wytworzone kompozyty charakteryzowały się

zwiększonymi wartościami kąta zwilżania wodą, co stanowi punkt wyjścia do badań stabilności hydrolitycznej tej klasy materiałów w czasie. Ostatecznie zaobserwowano również znaczący wzrost wskaźnika płynięcia tworzywa (ang. *MFR, melt flow rate*), co przekładało się na poprawioną przetwarzalność tworzywa i zmniejszenie współczynnika odpadowości próbek podczas druku 3D próbek. Podwyższenie tego parametru przekłada się też w wymiarze praktycznym na wydajność procesu druku w rozumieniu szybkości drukowania, a więc ilości ekstudatu opuszczającej dyszę w kontrolowany sposób w jednostce czasu, bądź na prowadzenie procesu z zastosowaniem niższych temperatur.

W pracy **P4** zbadano wpływ dodatków mono- i oktasferokrzemianowych oraz silseskwioksanowych na właściwości izotaktycznego polipropylenu (iPP). w Tabeli 4 przedstawiono pochodne krzemoorganiczne wykorzystane w pracy.

Tabela 4: Pochodne sferokrzemianowe i silseskwioksanowe zastosowane w pracy **P4**.

Rdzeń	Związek	Oznaczenie	Podstawnik R
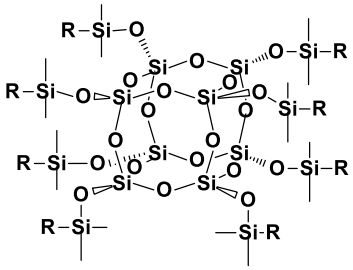	1	SS-H	H
	2	SS-Vi	Vi
	4	SS-Limonene	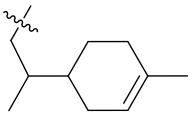
	13	SS-Glycidyl	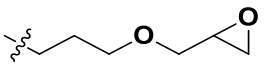
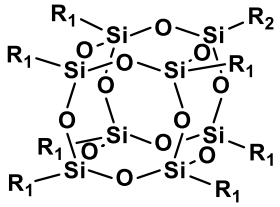	8	*i*Bu$_7$SSQ-Cl	R_1 = *i*Bu, R_2 = $(CH_2)_3Cl$
	11	*i*Bu$_7$SS-H	R_1 = *i*Bu, R_2 = $OSiMe_2H$
	12	*i*Bu$_7$SS-Vi	R_1 = *i*Bu, R_2 = $OSiMe_2Vi$
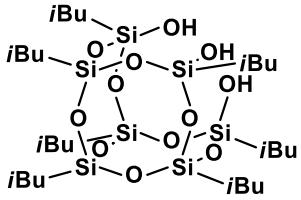	10	*i*Bu$_7$SSQ-3OH	zgodnie z rysunkiem

Podobnie, jak w przypadku pracy **P1**, zaobserwowano, że dodatki będące produktami hydrosililowania oktawodorosferokrzemianu **1**, (pochodne **4** i **13**) charakteryzują się wyższą zdolnością dyspersji w osnowie, niż wyjściowy **1**, czy też oktawinylosferokrzemian **2**. Na podstawie mapowania SEM-EDS potwierdzono też, że spośród pochodnych badanych w pracach **P1** i **P2**, wszystkie zastosowane do przygotowania kompozycji z iPP charakteryzowały się lepszą mieszalnością z osnową, niż dla LDPE. Do analizy porównawczej zastosowano przy tym układy zawierające związki **1**, **2**, **4**, **8** i **10**. Ponadto, SS-Glycidyl ulegał łatwemu mieszaniu w stopie z polipropylenem, w czasie, gdy próby wprowadzenia go do

osnowy LDPE skutkowały widocznym tzw. wypacaniem dodatku (jego migracji do powierzchni) z tworzywa nawet przy stężeniu 0.25% w/w, co skutkowało jego eliminacją z badań. Wszystkie powyższe obserwacje wyjaśniono na podstawie wyższych parametrów polarności iPP w porównaniu do LDPE, wyrażonych jako parametr rozpuszczalności Hildebrandta oraz parametr dyspersyjny Hansena. Efekt lepszej mieszalności z osnową przekładał się na większy wpływ dodatków na właściwości termiczne, mechaniczne i przetwórcze polipropylenu w stosunku do polietylenu.

Amorficzne dodatki SS-Limonene, SS-Glycidyl oraz *i*By$_7$SSQ-3OH pozytywnie wpływały na właściwości mechaniczne, szczególnie wytrzymałość na rozciąganie i zginanie. Dwa ostatnie związki charakteryzowały się również właściwościami smarnymi, co wywnioskowano na podstawie MFI.

Zaobserwowano również, że we wszystkich przypadkach, bez względu na zastosowaną pochodną, dodatki krzemoorganiczne wywoływały spadek stabilności termicznej układów, przeciwnie do wyników uzyskanych dla LDPE. Wnioskować można, że w warunkach degradacji cieplnej, modyfikatory biorą udział w rekombinacji wolnych rodników, przy czym zaobserwowane różnice spowodowane są odmienną charakterystyką procesu rozkładu iPP w odniesieniu do LDPE, w rozumieniu parametrów takich jak kinetyka tworzenia, przenoszenia i terminacji rodników. Tym samym badane pochodne silseskwioksanowe i sferokrzemianowe mogą pełnić rolę katalizatorów recyklingu termicznego polipropylenu. Interesującym efektem była ponadto niewielka, ale zauważalna na podstawie pomiarów DSC zdolność wszystkich pochodnych izobutylowych (**6, 7, 8, 10**), jak i krystalicznej pochodnej sferokrzemianowej **1**, do nukleacji iPP do odmiany polimorficznej β.

Istotnym wnioskiem końcowym płynącym z pracy **P4** jest niepoprawność nazywania związków typu silseskwioksanów nanonapełniaczami. Pierwszą kwestią jest wysoka ich cena, zajmująca pułap o dwa rzędy wielkości wyższy w stosunku do omawianych poliolefin (PE, iPP), co powoduje, że nawet 1% w/w dodatku takiej substancji prowadzić będzie do co najmniej dwukrotnego wzrostu kosztów produkcji modyfikowanego tworzywa. Drugi aspekt stanowi multifunkcjonalność silseskwioksanów i sferokrzemianów, w związku z czym zamiast napełniaczami lub nanonapełniaczami, właściwsze jest określenie ich mianem modyfikatorów, zgodnie z podziałem i definicjami przytaczanymi przez prof. Koszkula. Trzecią kwestią jest poprawność samego określenia „nanonapełniacz", ponieważ zgodnie z normą ISO/TS 80004-2:2015, obiekty mogą być określane przedrostkiem „nano-", gdy ich rozmiary w co najmniej jednym z trzech wymiarów mieszczą się mniej więcej w granicach 1-100 nm [178,179]. Tymczasem wyniki badań z prac **P1-P4** udowodniły, że zazwyczaj nawet przy stężeniach <1% w/w dochodzi do agregacji tych materiałów w matrycy polimerowej powyżej wspomnianego zakresu, a wraz ze wzrostem ich udziału w osnowie, efekt ten ulega nasileniu.

W pracy **P5** zbadano wpływ pochodnych silseskwioksanowych i sferokrzemianowych na stabilność i zdolność dyspersji cząstek pigmentu, bieli tytanowej (TiO_2), w żywicy epoksydowej Epidian 5. Otrzymane związki zestawiono w Tabeli 5.

Tabela 5: Pochodne sferokrzemianowe i silseskwioksanowe zastosowane w pracy **P5**.

Rdzeń	Związek	Oznaczenie	Podstawnik R
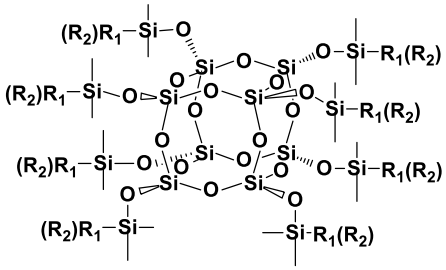	14	SS-6GP-2TMOS	R_1 = 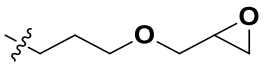 R_2 = 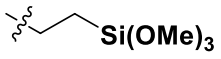
	15	SS-5GP-3TMOS	R_1 = 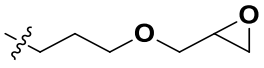 R_2 = 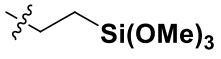
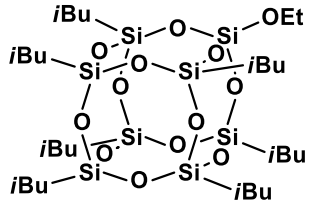	16	*i*Bu$_7$SSQ-OEt	zgodnie z rysunkiem

Jako, że wyżej wymienione pochodne badano w roli krzemoorganicznych modyfikatorów powierzchni, dla porównania zastosowano dwa stosowane przemysłowo i dostępne handlowo silanowe środki sprzęgające o analogicznych grupach funkcyjnych, tj. izobutylotrimetoksysilan (*i*BuTMOS), oraz 3-glicydoksypropylotrietoksysilan (GPTES). Wszystkie otrzymane związki charakteryzowały się obecnością grup funkcyjnych alkoksysililowych (SiOEt lub $Si(OMe)_3$). Ugrupowania te były odpowiedzialne za kowalencyjne wiązanie modyfikatora z powierzchnią cząstek TiO_2.

Istotnym osiągnięciem pracy było opracowanie metodyki ekologicznej funkcjonalizacji powierzchniowej pigmentu w środowisku wodnym poprzez ucieranie go z wybranymi dodatkami krzemoorganicznymi w młynach kulowych. Dotychczasowe prace dotyczące modyfikacji powierzchniowej TiO_2, a także innych materiałów nieorganicznych, jak SiO_2, podobnymi związkami, prezentują metodykę z użyciem rozpuszczalników organicznych, a wykorzystanie mediów na bazie wody ogranicza się do silanowych środków sprzęgających. Analiza FT-IR potwierdziła skuteczną funkcjonalizację bieli tytanowej zastosowanymi czynnikami poprzez reakcję z powierzchniowymi grupami funkcyjnymi -OH, a analiza kąta zwilżania próbek wodą wykazała superhydrofobowy charakter układów modyfikowanych *i*BuTMOS oraz *i*Bu$_7$SSQ-OEt. Należy przy tym zaznaczyć, że bazowy pigment

charakteryzował się silną hydrofilowością. Kolejnym aspektem było opracowanie metodyki dyspergowania bieli tytanowej w pompie zębatej, wytwarzającej wysokie siły oraz szybkości ścinania, co powodowało znaczną poprawę dyspergowania cząstek TiO_2 w żywicy. Zaobserwowano także efekt synergiczny obróbki chemicznej i mieszania mechanicznego, co prowadziło, w zależności od układu, do kilkudziesięciokrotnego wzrostu siły krycia układów, a także do kilkudziesięciokrotnego wzrostu stabilności pigmentowanych żywic w czasie, zapobiegając sedymentacji bieli tytanowej (Rys. 14).

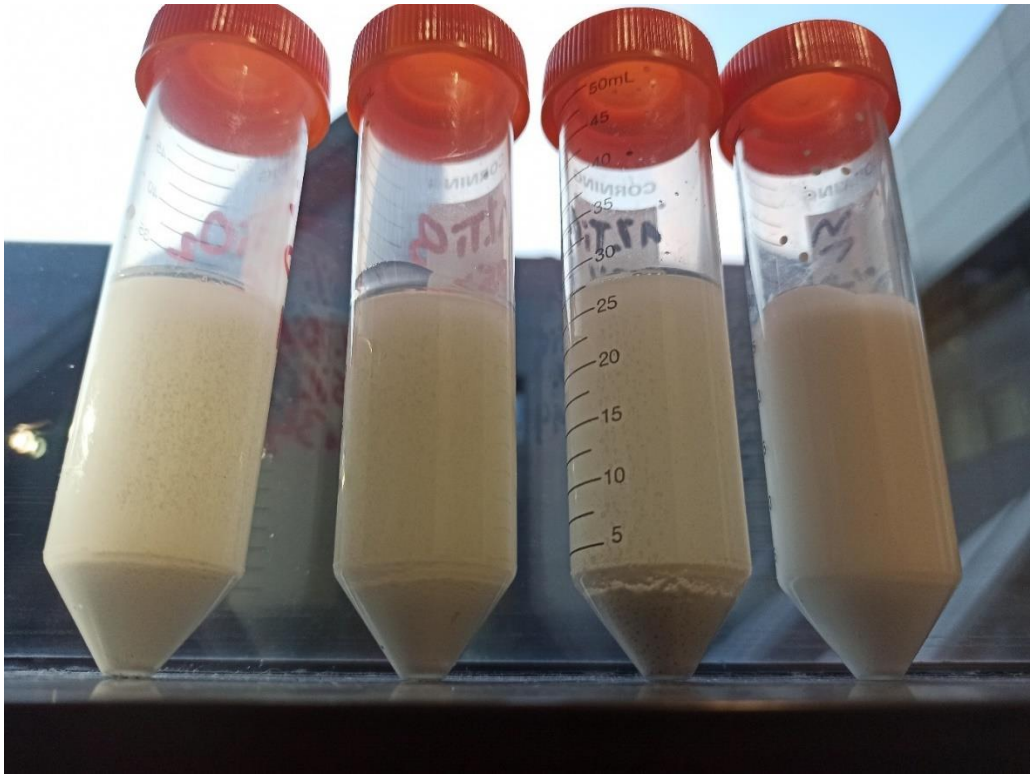

Rysunek 14: Próbki ciekłej (nieusieciowanej) żywicy epoksydowej zawierającej modyfikowaną biel tytanową po 6 miesiącach od przygotowania. Trzy lewe próbki są wyraźnie rozdzielone z dużą ilością sedymentu TiO_2, ostatnia z prawej stabilna.

W kontekście porównania do silanowych środków sprzęgających, istotny był większy efekt stabilizacji TiO_2 oraz siły krycia układów przygotowanych z użyciem *i*Bu$_7$SSQ-OEt. Jednocześnie, pochodne sferokrzemianowe nie wykazywały w tym zakresie przewagi nad analogicznym silanem wykorzystanym w badaniu, oferując bardziej porównywalne wyniki. Siłę krycia układów oceniano na podstawie analizy prześwietleniowej z zastosowaniem specjalnie zaprojektowanej i wykonanej do tego celu przystawki do aparatu spektrofotometrycznego.

Wyniki przeprowadzonych badań pozwalają stwierdzić, że funkcjonalizowane silseskwioksany oraz sferokrzemiany stanowią nową klasę silanowych, a precyzyjniej – silseskwioksanowych/sferokrzemianowych środków sprzęgających (Rysunek 15).

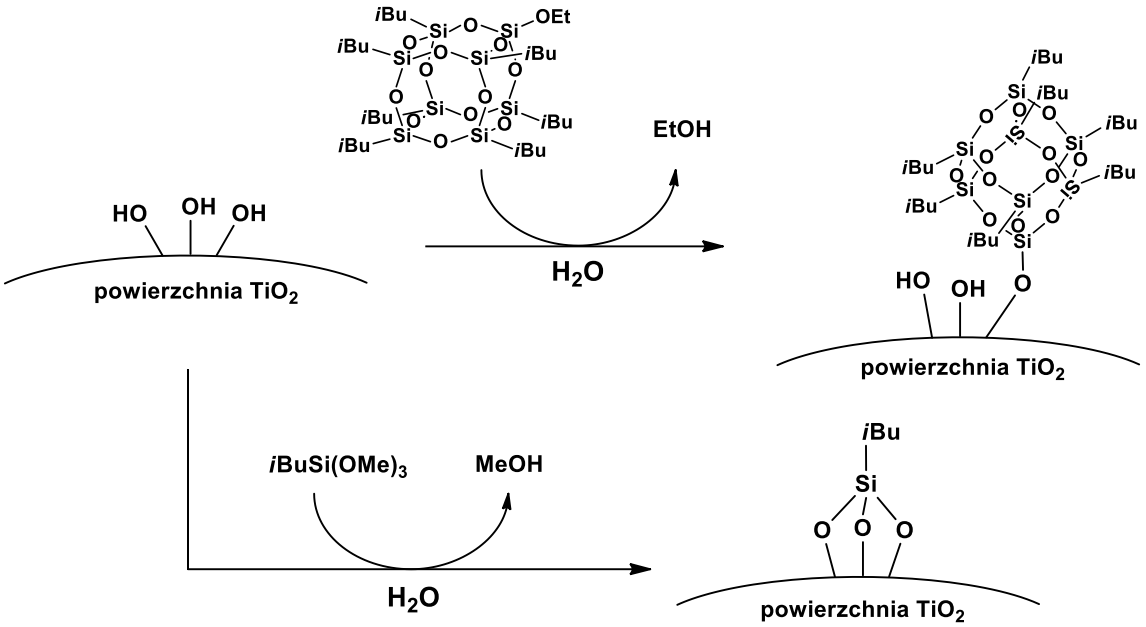

Rysunek 15: Schemat modyfikacji powierzchni TiO_2 z użyciem *i*Bu_7SSQ-OEt oraz *i*BuTMOS.

7. Podsumowanie i wnioski

W wyniku realizacji pracy doktorskiej otrzymano szereg pochodnych silseskwioksanowych, mono- oraz oktasferokrzemianowych. Zbadano wpływ otoczenia chemicznego cząsteczki na kompatybilność dodatków z osnową polimerową i zmiany we właściwościach fizykochemicznych oraz funkcjonalnych tworzyw, a także wpływ metodyki przetwórczej na zdolność mieszania modyfikatorów z polimerami. w badaniach wykorzystano trzy różne metody przetwórcze. w pierwszej z nich skupiono się na przetwórstwie poliolefin (LDPE i iPP), stanowiących materiały wyjściowe do produkcji masowej szerokiej gamy wyrobów użytkowych. Dalej, badano zastosowanie wybranej pochodnej sferokrzemianowej w technologii FDM celem poprawy właściwości PLA, materiału stosowanego do druku 3D oraz obiektów z niego wytwarzanych. w ostatniej metodzie zweryfikowano możliwość wykorzystania silseskwioksanów oraz sferokrzemianów jako środków sprzęgających zmieniających charakter powierzchniowy bieli tytanowej do pigmentowania żywic epoksydowych, celem poprawy dyspersji i stabilności TiO_2 w zawiesinie oraz siły krycia tak uzyskanych układów.

Wyniki przeprowadzonych badań pozwalają stwierdzić, że silseskwioksany i sferokrzemiany charakteryzowały się większą mieszalnością z iPP w porównaniu do LDPE, co wyjaśniono na podstawie wyższego parametru rozpuszczalności Hildebrandta oraz dyspersyjnego Hansena. Ponadto, na kompatybilność, a zarazem poziom interakcji z osnową i wpływ na jej właściwości pozytywnie wpływały dwa rodzaje motywów strukturalnych. Jednym z nich było otoczenie chemiczne osłaniające polarny rdzeń klatki (przede wszystkim sterycznie rozbudowane, alkilowe podstawniki, ale również obecność identycznych grup znoszących lokalne momenty dipolowe). Drugim natomiast była struktura amorficzna pochodnych, niewykazująca tendencji do krystalizacji w tworzywie. Taki charakter wykazywały SSQ-8Cl typu polisilseskwioksanowego i produkty kondensacji termicznej *i*Bu_7SSQ-3OH z uwagi na nieuporządkowaną strukturę rdzenia, ale również SS-Limonene, SS-Pinene, SS-Norbornene czy SS-Glycidyl, mające w temperaturze pokojowej postać cieczy o różnej lepkości. Charakter krystaliczny zwiększał efekt agregacji pochodnych w tworzywie. Praktycznie bez względu na rodzaj wybranej pochodnej, wzrost stężenia dodatku w osnowie przyczyniał się do efektu aglomeracji, który zmniejszał oddziaływanie pomiędzy modyfikatorem, a polimerem.

Powyższe wnioski, w połączeniu z analizą cen poliolefin oraz handlowo dostępnych silseskwioksanów i sferokrzemianów, pozwoliły ocenić, że górna granica stosowania tych związków w charakterze modyfikatorów do PE i iPP wynosi 1% w/w. Wskazane jest przy tym operowanie w zakresie możliwie najniższych stężeń, zależnych od końcowego zastosowania wybranego tworzywa oraz jego cechy przetwórczej czy użytkowej będącej przedmiotem modyfikacji. Alternatywnie, kierunki aplikacji omawianych pochodnych powinny skupiać się na wyrobach o stosunkowo małej masie, gdzie na jednostkę wyrobu przypada wagowo niewielka ilość dodatku, a także na wyrobach specjalistycznych, gdzie cena surowca stanowi niewielki ułamek ceny końcowej produktu. Stwierdzenie to prowadzi do kolejnego wniosku, odnoszącego się do badań związanych z technologią przyrostową FDM, gdzie filamenty

termoplastyczne dostępne na rynku charakteryzują się typowo cenami o rząd wielkości wyższymi od bazowych tworzyw, z których są wytwarzane. Zastosowanie dodatku podwyższającego koszt surowca jest w tym przypadku ekonomicznie łatwiejszy do uzasadnienia nie tylko ze względu na mniejszy udział w cenie końcowej materiału handlowego, ale również z uwagi na specyfikę samego procesu druku trójwymiarowego. Po pierwsze, technologia FDM nie tylko ma znacząco mniejszy udział w światowym zużyciu tworzyw termoplastycznych w stosunku do dojrzałych technologii wytwarzania wielkoseryjnego, jak wtrysk i wytłaczanie, co przekłada się na mniejsze zużycie dodatków przetwórczych. Po drugie, z uwagi na niedoskonałość omawianej technologii, przekładającej się na niską wytrzymałość mechaniczną obiektów drukowanych, czy też duży współczynnik odpadowości wyrobów, koniecznym jest jej udoskonalanie czy to na drodze procesowej (aparatura, oprogramowanie), czy też surowcowej (materiał filamentu). W efekcie, nawet przy zastosowaniu droższego tworzywa, możliwe jest obniżenie kosztów produkcji ze względu na mniejszą odpadowość oraz czas pracy urządzenia i obsługi. Poprawa właściwości uzyskanych obiektów drukowanych w odniesieniu do prób referencyjnych, omówiona w pracy **P3**, była znacząco większa od zmian ilościowych obserwowanych dla rezultatów prac **P1**, **P2** i **P4**, gdzie próbki wytwarzano metodą wtryskową. Wiąże się to ze znacznie większą jednorodnością i ciągłością mechaniczną materiału w kształtkach wtryskiwanych.

Kolejnym aspektem jest zastosowanie silseskwioksanów i sferokrzemianów jako modyfikatorów powierzchni materiałów nieorganicznych (praca **P5**). w tym przypadku nie tylko udało się potwierdzić tezę, że związki te stanowią nową klasę środków sprzęgających, obok powszechnie stosowanych silanów i polisiloksanów, ale też mogą stanowić atrakcyjną alternatywę pod kątem poprawy wybranych właściwości. Kluczowa tu jest możliwość stosowania ich w znacznie niższych stężeniach, niż miało to miejsce w pracach **P1-P4**, ponieważ pozytywny wpływ na zmianę właściwości obserwowano przy ilości 50 ppm w przeliczeniu na masę kompozytu, a 150 ppm przyczyniało się do znacznej poprawy parametrów układu (stabilność zawiesiny, siła krycia, dyspersja TiO_2). z tego względu jest to najbardziej obiecujący kierunek zastosowań silseskwioksanów i sferokrzemianów – jako modyfikatorów powierzchni napełniaczy, pigmentów bądź kompatybilizatorów blend polimerowych, a więc tam, gdzie niewielka ilość dodatku znajduje się na granicy faz (ang. *interphase*), prowadząc do istotnych zmian fizykochemii układu na tej granicy.

Ostatnim wnioskiem płynącym z dokładnej analizy literatury dotyczącej układów polimerowych z dodatkiem silseskwioksanów i/lub sferokrzemianów w odniesieniu do rezultatów realizacji pracy doktorskiej jest konieczność zrozumienia różnic strukturalnych i fizykochemicznych pomiędzy napełniaczami i nanonapełniaczami, a wspomnianymi związkami krzemoorganicznymi. Wszystkie napełniacze mają albo budowę nieorganiczną (tlenki, sole, materiały węglowe), gdzie w skali atomowej za wysoką siłę oddziaływań w materiale odpowiada sieć krystaliczna lub kowalencyjna, albo też organiczną (włókna naturalne lub syntetyczne), gdzie materiał jest polimerem kowalencyjnym. Natomiast silseskwioksany i sferokrzemiany to (poza związkami typu polisilseskwioksanów) substancje molekularne, a cząstki widziane podczas obrazowania mikroskopowego (SEM, TEM) pochodzą od kryształów lub krystalitów tego związku w matrycy. o ile standardem dla napełniaczy nieorganicznych jest podawanie dystrybucji rozmiarów cząstek, ponieważ metody przetwórcze obejmujące procesowanie termoplastów nie prowadzą do zmniejszania rozmiaru

cząstek tych napełniaczy ze względu na siłę ich kohezji (wynikających z opisanych oddziaływań), nie można metodyki tej przekładać na omawiane układy krzemoorganiczne. w tym przypadku, w zależności od zastosowanej metodyki przetwórczej, czy też doboru tworzywa, możliwe jest w teorii rozpraszanie dodatku do poziomu molekularnego, a obserwowanie jego kryształów lub agregatów amorficznych w matrycy polimerowej jest dowodem na niekompatybilność składników układu lub ich niską zdolność przetwarzania w wybranym procesie.

8. Ankieta pozostałego dorobku naukowego

A. Publikacje niewchodzące w skład rozprawy doktorskiej

[1] Beata Dudziec, Monika Rzonsowska, Bogdan Marciniec, Dariusz Brząkalski, Bartosz Woźniak, "New Mono-and Diethynylsiloxysilsesquioxanes - Efficient Procedures for their Synthesis", *Dalton Transactions*, 2014, 43(35), 13201-13207
IF2014: 4.197 IF2020: 4.070 Cytowania Scopus: 20(6) Cytowania GS: 25(12)

[2] Katarzyna Mitula, Julia Duszczak, Dariusz Brzakalski, Beata Dudziec, Maciej Kubicki, Bogdan Marciniec, "Tetra-functional double-decker silsesquioxanes as anchors for reactive functional groups and potential synthons for hybrid materials", *Chemical Communications*, 2017, 53(75), 10370-10373
IF2017: 6.290 IF2020: 6.008 Cytowania Scopus: 16(9) Cytowania GS: 17(9)

[3] Dariusz Brząkalski, Monika Rzonsowska, Beata Dudziec, "Regioselective formation of β-(E)- and α-alkenylsilane moiety attached to silsesquioxane core via Pt- and Ru-based hydrosilylation", *Applied Organometallic Chemistry*, 2018, 32(4), e4267
IF2018: 3.259 IF2020: 3.966 Cytowania Scopus: 2(1) Cytowania GS: 2(1)

[4] Dariusz Brząkalski, Marcin Walczak, Julia Duszczak, Beata Dudziec, Bogdan Marciniec, "Chlorine-free catalytic formation of silsesquioxanes with Si-OH and Si-OR functional groups", *Eur. J. Inorg. Chem.*, 2018, 2018(45), 4905-4910
IF2018: 2.578 IF2020: 2.431 Cytowania Scopus: 8(5) Cytowania GS: 6(5)

[5] Paulina Jakubowska, Agnieszka Martyła, Bogna Sztorch, Dariusz Brząkalski, Monika Osińska-Broniarz, Robert E. Przekop, "Application of one-pot sol-gel method to prepare polyolefin fillers", *Composites Theory And Practice*, 2018, 18(3), 167-173
IF2018: - IF2020: - Cytowania Scopus: - Cytowania GS: 0

[6] Daria Pakuła, Marta Dobrosielska, Bogna Sztorch, Maciej Popiół, Bartosz Klonowski, Dariusz Brząkalski, Bogdan Marciniec, Robert E. Przekop, "Microsilica filler for polyurea systems", *Composites Theory And Practice*, 2019, 19(2), 76-82
IF2019: - IF2020: - Cytowania Scopus: - Cytowania GS: 3(3)

[7] Marta Dobrosielska, Daria Pakuła, Bogna Sztorch, Maciej Popiół, Bartosz Klonowski, Dariusz Brząkalski, Bogdan Marciniec, Robert E. Przekop, "The influence of surface physicochemistry of solid fillers on dispersion in polyurea systems", *Composites Theory And Practice*, 2019, 19(2), 83-90
IF2019: - IF2020: - Cytowania Scopus: - Cytowania GS: 2(2)

[8] Marta Dobrosielska, Robert E. Przekop, Bogna Sztorch, Dariusz Brząkalski, Izabela Zgłobicka, Magdalena Łępicka, Romuald Dobosz, Krzysztof J. Kurzydłowski, "Biogenic

Composite Filaments Based on Polylactide and Diatomaceous Earth for 3D Printing", *Materials*, 2020, 13(20), 4632
IF2020: 3.623 IF2020: 3.920 Cytowania Scopus: 4(2) Cytowania GS: 5(2)

[9] Miłosz Frydrych, Bogna Sztorch, Dariusz Brząkalski, Daria Pakuła, Dawid Frąckowiak, Mariusz Majchrzak, Bogdan Marciniec, "New Functionalized Borasilsesquioxanes Obtained via Metathetical Transformation of 4-Vinylphenylborasilsesquioxanes", *Eur. J. Inorg. Chem.*, 2020, 2000(37), 3597-3600
IF2020: 2.431 Cytowania Scopus: 2(1) Cytowania GS: 1(0)

[10] Marta Dobrosielska, Renata Dobrucka, Michał Gloc, Dariusz Brząkalski, Marcin Szymański, Krzysztof J. Kurzydłowski, Robert E. Przekop, "A New Method of Diatomaceous Earth Fractionation—a Bio-Raw Material Source for Epoxy-Based Composites", *Materials*, 2021, 14(7), 1663
IF2020: 3.920 Cytowania Scopus: 3(1) Cytowania GS: 3(1)

[11] Bogna Sztorch, Dariusz Brząkalski, Marek Jałbrzykowski, Robert E. Przekop, "Processing Technologies for Crisis Response on the Example of COVID-19 Pandemic—Injection Molding and FFF Case Study", *Processes*, 2021, 9(5), 791
IF2020: 2.824 Cytowania Scopus: 0 Cytowania GS: 0

[12] Miłosz Frydrych, Daria Pakuła, Bogna Sztorch, Dariusz Brząkalski, Robert E. Przekop, Bogdan Marciniec, "Novel Silsesquioxane-Derived Boronate Esters—Synthesis and Thermal Properties", *Molecules* 2021, 26(14), 4107
IF2020: 4.588 Cytowania Scopus:1(0) Cytowania GS: 1(0)

[13] Marta Dobrosielska, Renata Dobrucka, Dariusz Brząkalski, Michał Gloc, Janusz Rębiś, Julia Głowacka, Krzysztof J. Kurzydłowski, Robert E. Przekop, "Methodological Aspects of Obtaining and Characterizing Composites Based on Biogenic Diatomaceous Silica and Epoxy Resins", *Materials*, 2021, 14(16), 4607
IF2020: 3.920 Cytowania Scopus: 2(1) Cytowania GS: 2(1)

[14] Robert E. Przekop, Paulina Jakubowska, Bogna Sztorch, Rafał Kozera, Kamil Dydek, Marek Jałbrzykowski, Tomasz Osiecki, Piotr Marciniak, Agnieszka Martyła, Arkadiusz Kloziński, Dariusz Brząkalski, "Opoka—Sediment Rock as New Type of Hybrid Mineral Filler for Polymer Composites", *AppliedChem* 2021, 1(2), 90-110
IF2020: N/D IF2022: N/D Cytowania Scopus: N/D Cytowania GS: 2(0)

[15] Paulina Jakubowska, Grzegorz Borkowski, Dariusz Brząkalski, Bogna Sztorch, Arkadiusz Kloziński, Robert E. Przekop, "The Accelerated Aging Impact on Mechanical and Thermal Properties of Polypropylene Composites with Sedimentary Rock Opoka-Hybrid Natural Filler", *Materials*, 2022, 15(1), 338
IF2020: 3.920 Cytowania Scopus: 0 Cytowania GS: 0

[16] Anna Olejnik, Bogna Sztorch, Dariusz Brząkalski, Robert E. Przekop, “Silsesquioxanes in the Cosmetics Industry—Applications and Perspectives”. Materials 2022, 15(3), 1126
IF2020: 3.920 Cytowania Scopus: 0 Cytowania GS: 0

Cytowania na podstawie bazy Scopus oraz Google Scholar (GS). w nawiasie podano wartości z wyłączeniem cytowania przez któregokolwiek z autorów. Wartości IF na podstawie bazy Journal Citation Reports.

B. Rozdziały monografii naukowych

[1] Bogna Sztorch, Daria Pakuła, Miłosz Frydrych, Kamil Dydek, Dariusz Brząkalski, Rafał Kozera, Robert E. Przekop, Krzemoorganiczne pochodne jako modyfikatory właściwości tworzyw termoplastycznych dla przyrostowej techniki FDM, str. 71-85, w: Wybrane zagadnienia z zakresu nanotechnologii, inżynierii materiałowej oraz termodynamiki, red. Konrad Skrzątek, Izabela Mołdoch-Mendoń, Wydawnictwo Naukowe TYGIEL sp. z o.o., 2021.

[2] Bogna Sztorch, Dariusz Brząkalski, Kacper Włodarek, Miłosz Frydrych, Daria Pakuła, Kamil Dydek, Rafał Kozera, Robert Przekop, Wpływ modyfikatorów krzemoorganicznych na własności dyspersyjne bieli tytanowej oraz właściwości kompozytów PLA z jej udziałem stosowanych w przyrostowej technice FDM, str. 86-106, w: Wybrane zagadnienia z zakresu nanotechnologii, inżynierii materiałowej oraz termodynamiki, red. Konrad Skrzątek, Izabela Mołdoch-Mendoń, Wydawnictwo Naukowe TYGIEL sp. z o.o., 2021.

[3] Dariusz Brząkalski, Bogna Sztorch, Miłosz Frydrych, Daria Pakuła, Kamil Dydek, Rafał Kozera, Anna Boczkowska, Bogdan Marciniec, Robert E. Przekop, Limonene Derivative of Spherosilicate as a Polylactide Modifier for Applications in 3D Printing Technology, w: Various Aspects of Silicon Polymer Chemistry a Themed Issue in Honor of Professor Julian Chojnowski on the Occasion of His 85th Birthday, red. Sławomir Rubinsztajn, Marek Cypryk, Włodzimierz Stańczyk, MDPI, 2022 (przedruk pracy **P3**).

Cytowania na podstawie bazy Scopus oraz Google Scholar (GS). w nawiasie podano wartości z wyłączeniem cytowania przez któregokolwiek z autorów. Wartości IF na podstawie bazy Journal Citation Reports.

C. Uczestnictwo w konferencjach naukowych

Międzynarodowe:

1) Beata Dudziec, Monika Rzonsowska, Dariusz Brząkalski, Bartosz Woźniak, Bogdan Marciniec, "Alkynyl Functionalized Silsesqiuoxanes", 2nd International Symposium on C-H Bond Activation, 30.06-03.07, 2014 r., Rennes, Francja, P 101.

2) Beata Dudziec, Monika Rzonsowska, Dariusz Brząkalski, Bogdan Marciniec, "New ethynylsubstituted silsesquioxanes as potential building blocks for POSS/DDSQ based materials", 10th International Workshop on Silicon-Based Polymers, 26-30.04.2015 r., Aussois, Francja (wystąpienie ustne).
3) Beata Dudziec, Dariusz Brząkalski, Monika Rzonsowska, Bogdan Marciniec, "Synthesis and catalytic activity of new ethynylsubstituted silsesquioxanes", 21th EuCheMS Conference on Organometallic Chemistry, 05-09.07.2015 r., Bratysława, Repubika Słowacka, PO46.
4) Beata Dudziec, Dariusz Brząkalski, Monika Rzonsowska, Bogdan Marciniec, "Ethynylsubstituted silsesquioxanes – reactivity and application", International Symposium on Synthesis and Catalysis, 02-04.09.2015 r., Evora, Portugalia, Poster 49.
5) Dariusz Brząkalski, Beata Dudziec, Bogdan Marciniec, "Hydrosilylation of ethynylsiloxysubstituted silsesquioxanes as a method for stereoselective synthesis of POSS-alkenyl systems", Polymat 2016 - Silesian Meetings On Polymer Materials, 27-28.06.2016 r., Zabrze, Polska, Poster 4.
6) Dariusz Brząkalski, Beata Dudziec, Bogdan Marciniec, "Hydrosilylation of ethynylsiloxysubstituted silsesquioxanes as a method for stereoselective synthesis of unsaturated POSS systems", 8th European Silicon Days, 28-31.08.2016 r., Poznań, Polska, P7 (poster).
7) Beata Dudziec, Patrycja Żak, Michał Dutkiewicz, Dariusz Brząkalski, Monika Rzonsowska, Grzegorz Wilkowski, Monika Ludwiczak, Mariusz Majchrzak, Marek Nowicki, Bogdan Marciniec, "New Class of Functional Silsesquioxane Systems as Precursors and Building Blocks of New Materials", 8th European Silicon Days, 28-31.08.2016 r., Poznań, Polska (wystąpienie ustne).
8) Dariusz Brząkalski, Marcin Walczak, Beata Dudziec, Michał Dutkiewicz, Bogdan Marciniec, "A New Procedure For Synthesis Of Si-OH And Si-OR Containing Silsesquioxanes", 17th International Seminar of PhD Students on Organometallic and Coordination Chemistry, 02-06.04.2017 r., Kraskov, Republika Czeska (wystąpienie ustne).
9) Beata Dudziec, Patrycja Żak, Michał Dutkiewicz, Monika Rzonsowska, Dariusz Brząkalski, Marcin Walczak, Grzegorz Wilkowski, Katarzyna Mituła, Julia Duszczak, Bogdan Marciniec, “Perspectives of functional double-decker silsesquioxanes as molecular scaffolds for reactive organic groups”, 18th International Symposium on Silicon Chemistry (ISOS XVIII) in conjunction with the 6th Asian Silicon Symposium, 06-11.08.2017 r., Ji’nan, Chińska Republika Ludowa (wystąpienie ustne).
10) Robert Przekop, Dariusz Brząkalski, Paulina Jakubowska, Bogna Sztorch, Arkadiusz Kloziński, Mariusz Szołyga, Paweł Koch, Joanna Przybylska, Daria Pakuła, Klaudia Jankowska, Bogdan Marciniec, “Mixed functional group-bearing POSS compounds as modifiers for mineral fillers”, 9TH EUROPEAN SILICON DAYS, 09-12.09.2018 r., Saarbrücken, Republika Federalna Niemiec.
11) Dariusz Brząkalski, Robert Przekop, Arkadiusz Kloziński, Bogna Sztorch, Paulina Jakubowska, Mariusz Szołyga, Paweł Koch, Joanna Przybylska, Daria Pakuła, Klaudia Jankowska, Bogdan Marciniec, “Application of functionalized POSS compounds as modifiers for polyolefins processing”, 9TH EUROPEAN SILICON DAYS, 09-12.09.2018 r., Saarbrücken, Republika Federalna Niemiec.

12) Dariusz Brząkalski, Robert Przekop, "Functionalised silsesquioxanes as additives and filler modifiers for polymer composites", Workshop on 2nd bilateral Chinese-Polish Project Cooperation - NCBR, 21.11-02.12, 2019 r, Jinan, Chińska Republika Ludowa (wystąpienie ustne).
13) Bogna Sztorch, Robert E. Przekop, Miłosz Frydrych, Daria Pakuła, Dariusz Brząkalski, Kacper Włodarek, Kamil Dydek, Bogdan Marciniec, "Organosilicon Additives for 3D Printing Materials", 19th International Symposium on Silicon Chemistry, 05-07.07.2021 r., Tuluza, Francja, P156.
14) Miłosz Frydrych, Bogna Sztorch, Daria Pakuła, Dariusz Brząkalski, Robert Przekop, Bogdan Marciniec, "Functionalization of Borasilsesquioxanes by the Hydrosilylation Reaction", 19th International Symposium on Silicon Chemistry, 05-07.07.2021 r., Tuluza, Francja, P090.
15) Daria Pakuła, Bogna Sztorch, Robert Przekop, Miłosz Frydrych, Dariusz Brząkalski, Bogdan Marciniec, "Organosilicon Modifiers of Thermoplastics Properties for 3D Printing", 19th International Symposium on Silicon Chemistry, 05-07.07.2021 r., Tuluza, Francja, P037.
16) Dariusz Brząkalski, Silsesquioxane derivatives as additives for improved dispersion of TiO_2 in epoxy systems, 5th International Symposium on Silsesquioxanes-based Functional Materials (SFM 2021), 24-25.09.2021 r., P-14 (wystąpienie ustne).

Krajowe:

1) Dariusz Brząkalski, Bartosz Woźniak, Beata Dudziec, Patrycja Żak, Bogdan Marciniec, "Katalityczne metody syntezy funkcjonalizowanych silseskwioksanów typu double – decker", 57 Zjazd PTChem i SITPChem, 14-18.09.2014 r., Częstochowa, S05-P02 (Poster nagrodzony).
2) Dariusz Brząkalski, Beata Dudziec, Monika Rzonsowska, Bogdan Marciniec, "Hydrosililowanie Etynylosiloksypodstawionych Silseskwioksanów", II Poznańskie Sympozjum Młodych Naukowców. Nowe Oblicze Nauk Przyrodniczych, 14.11.2015 r., Poznań, Poster 37.
3) Julia Duszczak, Dariusz Brząkalski, Beata Dudziec, Monika Rzonsowska, Bogdan Marciniec, "Etynylopodstawione silseskwioksany jako molekularne prekursory materiałów hybrydowych", XLIV Ogólnopolska Szkoła Chemii „Poznaj naszą chemię!", 30.04-04.05, 2016 r., Koszuty, Poster.
4) Dariusz Brząkalski, Beata Dudziec, Bogdan Marciniec, „Etynylosiloksy podstawione silseskwioksany – zastosowanie w syntezie nienasyconych układów krzemoorganicznych", 59 Zjazd naukowy polskiego towarzystwa chemicznego, 19-23.09.2016 r., Poznań, S03P04.
5) Dariusz Brząkalski, Marcin Walczak, Beata Dudziec, Michał Dutkiewicz, Bogdan Marciniec, "Nowa procedura syntez silseskwioksanów z funkcyjnymi grupami Si-OR i Si-OH", III Poznańskie Sympozjum Młodych Naukowców, 05.11.2016 r., Poznań, Poster.
6) Dariusz Brząkalski, Beata Dudziec, Bogdan Marciniec, "Stereoselektywna synteza nienasyconych układów krzemoorganicznych na drodze hydrosililowania etynylosiloksypodstawionych silseskwioksanów", XLVI Ogólnopolska Szkoła Chemii "Potęga Pierwiastków", 29.04-03.05, 2017 r., Jachranka (wystąpienie ustne).

7) Piotr Marciniak, Dariusz Brząkalski, Bogna Sztorch, Marta Dobrosielska, Robert Przekop, Miłosz Frydrych, Bogdan Marciniec, „Synteza wielkolaboratoryjna organofunkcyjnych silseskwioksanów na drodze reakcji hydrosililowania", X Poznańska Konferencja Naukowa "Chemia – Nauka i Przemysł", 30.11.2018 r., Poznań.
8) Dariusz Brząkalski, Bogna Sztorch, Miłosz Frydrych, Marta Dobrosielska, Robert Przekop, Bogdan Marciniec, „Potencjał aplikacyjny związków typu POSS z mieszanymi grupami funkcyjnymi", X Poznańska Konferencja Naukowa "Chemia – Nauka i Przemysł", 30.11.2018 r., Poznań.
9) Dariusz Brząkalski, Robert Przekop, Bogna Sztorch, Marta Dobrosielska, Miłosz Frydrych, Agnieszka Martyła, Bogdan Marciniec, "Zastosowanie organofunkcyjnych silseskwioksanów jako modyfikatorów poliolefin", VII Konferencja Naukowa Materiały Polimerowe „Pomerania-Plast 2019", 05-07.06.2019 r., Międzyzdroje (wystąpienie ustne).
10) Dariusz Brząkalski, Robert Przekop, Bogna Sztorch, Marta Dobrosielska, Bogdan Marciniec, 62. Zjazd Naukowy PTChem, 02-06.09.2019 r., Warszawa, "Zastosowanie funkcjonalizowanych sferokrzemianów jako modyfikatorów kompozytów polimerowych" (S14P56).
11) Dariusz Brząkalski, Bogna Sztorch, Miłosz Frydrych, Robert Przekop, "Wpływ modyfikatorów krzemoorganicznych na własności dyspersyjne bieli tytanowej oraz właściwości kompozytów PLA z jej udziałem stosowanych w przyrostowej technice FDM", XIII Interdyscyplinarna Konferencja Naukowa TYGIEL 2021, 25-28.03.2021 r., spotkanie online, Fundacja TYGIEL (wystąpienie ustne).

D. Udział w projektach badawczych

1) 2011-2014: UDA-POIG 01.03.01-30-173/09: "Silseskwioksany jako nanonapełniacze i modyfikatory w kompozytach polimerowych", w roli wykonawcy. Projekt finansowany ze środków Europejskiego Funduszu Rozwoju Regionalnego w ramach Programu Operacyjnego Innowacyjna Gospodarka.
2) 2012-2016: MAESTRO 2, UMO-2011/02/A/ST5/00472: "Kataliza metalonieorganiczna - nowa strategia syntezy metaloorganicznych reagentów, polimerów i nanomateriałów", w roli wykonawcy. Projekt finansowany przez NCN.
3) 2013-2016: PRELUDIUM 3, UMO-2012/05/N/ST5/00759: "Synteza i zastosowanie nowych nienasyconych związków germano- i germanokrzemoorganicznych", w roli wykonawcy. Projekt finansowany przez NCN.
4) 2013-2016: SONATA 3, UMO - 2012/05/D/ST5/03348: "Synteza nienasyconych pochodnych silseskwioksanów typu double-decker (DDSQ) jako prekursorów nowych organiczno - nieorganicznych materiałów hybrydowych", w roli wykonawcy. Projekt finansowany przez NCN.
5) 2015-2018: PBS3/A1/16/2015: "Zaawansowane technologie syntezy funkcjonalizowanych silseskwioksanów do zastosowań w materiałach specjalnych", w roli wykonawcy. Projekt finansowany przez NCBR.
6) 2018-2021: UMO/2017/27/B/ST5/00149: „Nowe funkcjonalizowane heterosilseskwioksany jako prekursory materiałów hybrydowych - synteza i charakterystyka", w roli wykonawcy. Projekt finansowany przez NCN.

7) Od 2019: LIDER/01/0001/L-10/18/NCBR/2019: „Krzemoorganiczne modyfikatory właściwości tworzyw termoplastycznych dla przyrostowej techniki FDM", w roli wykonawcy. Projekt finansowany przez NCBR.
8) 2019-2021: UMO-2018/29/N/ST5/00868: „Funkcjonalizowane układy POSS jako modyfikatory napełniaczy do polimerów termoplastycznych i żywic epoksydowych", w roli kierownika. Projekt finansowany przez NCN.
9) 2020: POIR.02.03.02-IP.03-00-001/18 „Opracowanie innowacyjnego biopreparatu do ochrony nasion zbóż przed żerującymi zwierzętami" w roli wykonawcy. Projekt finansowany ze środków Europejskiego Funduszu Rozwoju Regionalnego w ramach Programu Operacyjnego Inteligentnego Rozwoju.
10) od 2020: POIR, JG-09/2020-UCITT: „Fotel przeznaczony do pojazdów komunikacji miejskiej, o zwiększonej odporności na zabrudzenia spowodowane aktami wandalizmu", w roli wykonawcy. Projekt finansowany ze środków Europejskiego Funduszu Rozwoju Regionalnego w ramach Programu Operacyjnego Inteligentnego Rozwoju.
11) 2021: JG-222/2021-UCITT: „Badania wybranych poliuretanów termoplastycznych do druku 3D metodą FDM", literaturowe badanie stanu techniki.
12) 2021: JG-335/2021-UCITT: „Przegląd patentowy, przegląd literatury oraz przegląd stanu techniki w obszarze katalizatorów stosowanych do rozkładu amoniaku do wodoru".
13) Od 2021: POIR.01.01.01-00-0288/21: „Opracowanie znacząco lepszej mieszanki kompozytowej oraz optymalizacja form do zastosowań w produktach konglomeratowych dla gospodarstw domowych". Projekt finansowany ze środków Europejskiego Funduszu Rozwoju Regionalnego w ramach Programu Operacyjnego Inteligentnego Rozwoju.
14) Od 2021: LIDER/46/0185/L-11/2019: „Kompozyty polimerowe o podwyższonych właściwościach mechanicznych i elektrycznych na bazie innowacyjnej żywicy termoplastycznej" , w roli wykonawcy. Projekt finansowany przez NCBR.

E. Pozostałe osiągnięcia, w tym staże naukowe

[1] Ukończenie studiów magisterskich na Wydziale Chemii UAM w Poznaniu z wyróżnieniem Maxima Cum Laude oraz Medalem UAM, 24.06.2015 r.
[2] Udział w organizacji konferencji 8th European Silicon Days, organizowanych na WCh i w CZT UAM w Poznaniu, 28-31.08.2016 r.
[3] Uzyskanie dofinansowania NCN oraz kierownictwa w projekcie „Funkcjonalizowane układy POSS jako modyfikatory napełniaczy do polimerów termoplastycznych i żywic epoksydowych", 24.01.2019 r.
[4] Udział w organizacji seminarium i warsztatów: **„**Technologie przyrostowe, w poszukiwaniu wspólnych kierunków rozwoju", organizowanych w CZT UAM w Poznaniu, 27-28.06.2019 r.
[5] Współorganizacja seminarium "Silseskwioksany podstawą innowacyjnych materiałów", organizowanych w CZT UAM w Poznaniu, 16.12.2019 r.
[6] Czynny udział w organizacji akcji uruchomienia oraz utrzymania produkcji przyłbic ochronnych produkowanych dla służb medycznych i mundurowych oraz studentów i pracowników UAM na terenie Centrum Zaawansowanych Technologii UAM w Poznaniu w ramach walki z epidemią COVID-19, 2020 r.

9. Literatura

(1) Liu, W. C.; Yu, Y. Y.; Chen, W. C. Structural Control and Properties of Low-Dielectric-Constant Poly(Hydrogen Silsesquioxane) Precursors and Their Thin Films. *J. Appl. Polym. Sci.* **2004**, *91* (4), 2653–2660. DOI:10.1002/app.13446.

(2) Han, X.; Zhang, X.; Guo, Y.; Liu, X.; Zhao, X.; Zhou, H.; Zhang, S.; Zhao, T. Synergistic Effects of Ladder and Cage Structured Phosphorus-Containing Poss with Tetrabutyl Titanate on Flame Retardancy of Vinyl Epoxy Resins. *Polymers* **2021**, *13* (9). DOI:10.3390/polym13091363.

(3) Šurca Vuk, A.; Jovanovski, V.; Pollet-Villard, A.; Jerman, I.; Orel, B. Imidazolium-Based Ionic Liquid Derivatives for Application in Electrochromic Devices. *Sol. Energy Mater. Sol. Cells* **2008**, *92* (2), 126–135. DOI:10.1016/j.solmat.2007.01.023.

(4) Cordes, D. B.; Lickiss, P. D.; Rataboul, F. Recent Developments in the Chemistry of Cubic Polyhedral Oligosilsesquioxanes. *Chem. Rev.* **2010**, *110* (4), 2081–2173. DOI:10.1021/cr900201r.

(5) Baney, R. H.; Itoh, M.; Sakakibara, A.; Suzuki, T. Silsesquioxanes. *Chem. Rev.* **1995**, *95* (5), 1409–1430. DOI:10.1021/cr00037a012.

(6) Laird, M.; Herrmann, N.; Ramsahye, N.; Totée, C.; Carcel, C.; Unno, M.; Bartlett, J. R.; Wong Chi Man, M. Large Polyhedral Oligomeric Silsesquioxane Cages: The Isolation of Functionalized POSS with an Unprecedented Si18O27 Core. *Angew. Chemie - Int. Ed.* **2021**, *60* (6), 3022–3027. DOI:10.1002/anie.202010458.

(7) Hillson, S. D.; Smith, E.; Zeldin, M.; Parish, C. A. Cages, Baskets, Ladders, and Tubes: Conformational Studies of Polyhedral Oligomeric Silsesquioxanes. *J. Phys. Chem. a* **2005**, *109* (37), 8371–8378. DOI:10.1021/jp052949j.

(8) Dirè, S.; Borovin, E.; Ribot, F. *Handbook of Sol-Gel Science and Technology*; **2017**. DOI:10.1007/978-3-319-19454-7.

(9) Lee, A. S. S.; Choi, S. S.; Lee, H. S.; Jeon, H. Y.; Baek, K. Y.; Hwang, S. S. Synthesis and Characterization of Organic-Inorganic Hybrid Block Copolymers Containing a Fully Condensed Ladder-like Polyphenylsilsesquioxane. *J. Polym. Sci. Part a Polym. Chem.* **2012**, *50* (21), 4563–4570. DOI:10.1002/pola.26269.

(10) Brown, John F., J.; Vogt, Lester H., J.; Katchman, A.; Eustace, J. W.; Kiser, K. M.; Krantz, K. W. Double Chain Polymers of Phenylsilsesquioxane. *J. Am. Chem. Soc.* **1960**, *82* (23), 6194–6195. DOI: 10.1021/ja01508a054.

(11) Unno, M.; Matsumoto, T.; Matsumoto, H. Nonacyclic Ladder Silsesquioxanes and Spectral Features of Ladder Polysilsesquioxanes. *Int. J. Polym. Sci.* **2012**, *2012*, 1–5. DOI:10.1155/2012/723892.

(12) Unno, M.; Suto, A.; Takada, K.; Matsumoto, H. Synthesis of Ladder and Cage Silsesquioxanes from 1,2,3,4- Tetrahydroxycyclotetrasiloxane. *Bull. Chem. Soc. Jpn.* **2000**, pp 215–220. DOI:10.1246/bcsj.73.215.

(13) Voronkov, M. G.; Lavrent'yev, V. I. Polyhedral Oligosilsesquioxanes and Their Homo Derivatives. *Inorg. Ring Syst.* **1982**, *102*, 199–236. DOI:10.1007/3-540-11345-2_12.

(14) Yoshida, K.; Hattori, T.; Ootake, N.; Tanaka, R.; Matsumoto, H. Silsesquioxane-Based Polymers: Synthesis of Phenylsilsesquioxanes with Double-Decker Structure and Their Polymers. In *Silicon Based Polymers: Advances in Synthesis and Supramolecular Organization*; Ganachaud, F., Boileau, S., Bury, B., Eds.; Dordrecht, **2008**; pp 205–212.

(15) Hurd, C. B. Studies on Siloxanes. I. The Specific Volume and Viscosity in Relation to Temperature and Constitution. *J. Am. Chem. Soc.* **1946**, *68* (3), 364–370. DOI:10.1021/ja01207a005.

(16) Hartmann-Thompson, C. *Applications of Polyhedral Oligomeric Silsesquioxanes*; Springer: Heidelberg, 2011.

(17) Choi, S. S.; Lee, A. S.; Hwang, S. S.; Baek, K. Y. Structural Control of Fully Condensed Polysilsesquioxanes: Ladderlike *vs* Cage Structured Polyphenylsilsesquioxanes. *Macromolecules* **2015**, *48* (17), 6063–6070. DOI:10.1021/acs.macromol.5b01539.
(18) Liu, H.; Kondo, S. I.; Takeda, N.; Unno, M. Synthesis of Octacarboxy Spherosilicate. *J. Am. Chem. Soc.* **2008**, *130*, 10074–10075. DOI:10.1021/ja803513n.
(19) Marciniec, B.; Maciejewski, H.; Pietraszuk, C.; Pawluć, P. *Hydrosilylation: a Comprehensive Review on Recent Advances*; Springer, **2009**.
(20) Bartz, J.; Guliński, J.; Kornetka, Z. W.; Marciniec, B.; Gulińska, H.; Malcher, E.; Nowicka, T.; Siekierczak, K.; Urbaniak, W. *Hydrosililowanie*; Marciniec, B., Ed.; PWN: Poznań, **1981**.
(21) Yamamura, M.; Kano, N.; Kawashima, T. Photoswitching of the Reactivity Involving Hydrosilylation of a 1,1,3,3-Tetrahydrodisiloxane Bearing Two Azo Groups. *Tetrahedron Lett.* **2007**, *48* (23), 4033–4036. DOI:10.1016/j.tetlet.2007.04.020.
(22) Sommer, L. H.; Pietrusza, E. W.; Whithmore, F. Peroxide-catalyzed addition of trichloro- silane to 1-octene. *J. Am. Chem. Soc.* **1947**, *69* (1), 188. DOI: 10.1021/ja01193a508.
(23) Liao, M.; Chen, Y.; Brook, M. A. Spatially Controlled Highly Branched Vinylsilicones. *Polymers.* **2021**, *13* (6), 859. DOI:10.3390/polym13060859.
(24) Moretto, H.-H.; Schulze, M.; Wagner, G. Silicones. W: *Ullmann's Encyclopedia of Industrial Chemistry 7th ed.*; Elvers, B., Ed.; Wiley-VCH: Weinheim, **2011**; pp 1–40. DOI: 10.1002/14356007.a24 057.
(25) "BRB International B.V." Silicone solutions for RTV Formulations https://www.brb-international.com/clients/asset_854EB699-0F42-4F14-AFF3-345C27039448/contentms/img/Silicone/pdf/product/silicone-intermediates/solutions-for-silicone-rtv-2-formulator.pdf (accessed Apr 12, 2022).
(26) Knot, M.; Mulder, K. PVC Plastic: a History of Systems Development and Entrenchment. *Technol. Soc.* **2001**, *23* (2), 265–286. DOI: 10.1016/s0160-791x(01)00013-6.
(27) Brinson, H. F., Brinson, L. C. *Polymer Engineering Science and Viscoelasticity Polymer Engineering Science and Viscoelasticity An Introduction*; **2008**. DOI:10.1007/978-0-387-73861-1.
(28) Fried, J. R. Polymer Science and Technology. *Polymer Science and Technology*. Prentice Hall PTR: New Jersey **1995**.
(29) Chanda, M.; Roy, S. K. *Industrial Polymers, Specialty Polymers, and Their Applications*; Boca Raton, **2009**. DOI:10.1017/CBO9781107415324.004.
(30) Rabek, J. F. *Współczesna Wiedza o Polimerach Tom 1*, Wydanie I.; Wydawnictwo Naukowe PWN: Warszawa, **2017**.
(31) Jalal, N.; Surendranath, A. R.; Pathak, J. L.; Yu, S.; Chung, C. Y. Bisphenol a (BPA) the Mighty and the Mutagenic. *Toxicol. Reports* **2018**, *5*, 76–84. DOI:10.1016/j.toxrep.2017.12.013.
(32) Allard, P.; Colaiacovo, M. P. Bisphenol A. In *Reproductive and Develompental Toxicology*; Gupta, R. C., Ed.; Academic Press (Elsevier): London, **2011**; pp 673–686.
(33) Dodiuk, H.; Goodman, S. H. *Handbook of Thermoset Plastics*; Wiiliam Andrew, **2014**.
(34) Bilyeu, B.; Brostow, W.; Menard, K. P. Epoxy Thermosets and Their Applications I: Chemical Structures and Applications. *J. Mater. Educ.* **1999**, *21*, 281–286.
(35) Rabek, J. F. *Polimery: Otrzymywanie, Metody Badawcze, Zastosowanie*, Wydanie I.; Wydawnictwo Naukowe PWN: Warszawa, **2013**.
(36) Pham, H. Q.; Marks, M. J. Epoxy Resins. W: *Ullmann's Encyclopedia of Industrial Chemistry 7th ed.*; Elvers, B., Ed.; Wiley-VCH: Weinheim, **2011**; pp 1–94. DOI:10.1002/14356007.a09 547.pub2.

(37) Górczyk, J.; Bogdał, D.; Dworakowska, S. Stałe Żywice Epoksydowe z Bisfenolu a i Binaftolu – Synteza i Charakterystyka. *Czas. Tech. Chem.* **2012**, *109* (16), 19–27.
(38) Malpass, D. B. Industrial Metal Alkyls and Their Use in Polyolefin Catalysts. In *Handbook of Transition Metal Polymerization Catalysts*; Hoff, R., Ed.; Wiley: Hoboken, **2018**; pp 1–30. DOI:10.1021/ja102842d.
(39) Natta, G.; Danusso, F. *Stereoregular Polymers and Stereospecific Polymerizations: The Contributions of Giulio Natta and His School to Polymer Chemistry*; Pergamon Press: Oxford, **1967**.
(40) Olabisi, O. Polyolefins. In *Handbook of Thermoplastics*; Olabisi, O., Adewale, K., Eds.; CRC Press: Boca Raton, **2016**; pp 1–52. DOI:10.1201/b19190.
(41) Jubinville, D.; Esmizadeh, E.; Saikrishnan, S.; Tzoganakis, C.; Mekonnen, T. a Comprehensive Review of Global Production and Recycling Methods of Polyolefin (PO) Based Products and Their Post-Recycling Applications. *Sustain. Mater. Technol.* **2020**, *25*, e00188. DOI:10.1016/j.susmat.2020.e00188.
(42) Makaryan, I. A.; Sedov, I. V. Analysis of the State and Development Prospects of the Industrial Catalysts Market for Polyolefins Production. *Russ. J. Gen. Chem.* **2020**, *90* (6), 1141–1162. DOI:10.1134/S1070363220060304.
(43) Auras, R.; Lim, L.-T.; Selke, S. E. M.; Tsuji, H. *Poly(Lactic Acid): Synthesis, Structures, Properties, Processing, and Applications*; Johm Wiley & Sons: Hoboken, **2010**.
(44) Benninga, H. a *History of Lactic Acid Making*; Springer: Dordrecht, **1990**.
(45) Xinhua, L.; Shengpeng, L.; Zhou, L.; Xianhua, Z.; Xiaohu, C.; Zhongbin, W. An Investigation on Distortion of PLA Thin-Plate Part in the FDM Process. *Int. J. Adv. Manuf. Technol.* **2015**, *79* (5–8), 1117–1126. DOI:10.1007/s00170-015-6893-9.
(46) Rodríguez-Panes, A.; Claver, J.; Camacho, A. M. The Influence of Manufacturing Parameters on the Mechanical Behaviour of PLA and ABS Pieces Manufactured by FDM: a Comparative Analysis. *Materials.* **2018**, *11* (8), 1333. DOI:10.3390/ma11081333.
(47) Jakus, A. E. *An Introduction to 3D Printing-Past, Present, and Future Promise*; Elsevier Inc., **2018.** DOI:10.1016/B978-0-323-58118-9.00001-4.
(48) Hull, C. W. Apparatus for Production of Three-Dimensional Objects by Stereolithography. US4575330A, **1984.**
(49) Shahrubudin, N.; Lee, T. C.; Ramlan, R. An Overview on 3D Printing Technology: Technological, Materials, and Applications. *Procedia Manuf.* **2019**, *35*, 1286–1296. DOI:10.1016/j.promfg.2019.06.089.
(50) Koszkul, J. *Materiały Polimerowe*; Wydawnictwo Politechniki Częstochowskiej: Częstochowa, **1999**.
(51) Buxbaum, G.; Hempelmann, U.; Volz, H. G. Introduction. In *Industrial Inroganic Pigments*; Buxbaum, G., Pfaff, G., Eds.; Wiley-VCH: Weinheim, **2005**; pp 1–50.
(52) Buxbaum, G. Introduction to Inorganic High Performance Pigments. In *High performance pigments*; Faulkner, E. B., Schwartz, R. J., Eds.; Wiley-VCH: Weinheim, **2009**; pp 3–6.
(53) Plueddemann, E. P. *Silane Coupling Agents*; Springer Science+Business Media: New York, **1982**.
(54) Fina, A.; Tabuani, D.; Camino, G. Polypropylene – Polysilsesquioxane Blends. *Eur. Polym. J.* **2010**, *46* (1), 14–23. DOI:10.1016/j.eurpolymj.2009.07.019.
(55) Mohaiyiddin, M. S.; Lin, O. H.; Akil, H. M.; Yee, T. G.; Adik, N. N. A. N.; Villagracia, A. R. Effects of Polypropylene Methyl Polyhedral Oligomeric Silsesquioxanes and Polypropylene-Grafted Maleic Anhydride Compatibilizers on the Properties of Palm Kernel Shell Reinforced Polypropylene Biocomposites. *Polimeros* **2016**, *26* (3), 228–235. DOI:10.1590/0104-1428.2038.

(56) Durmus, A.; Kasgoz, A.; Ercan, N.; Ak, D.; Selen, S. Effect of Polyhedral Oligomeric Silsesquioxane (POSS) Reinforced Polypropylene (PP) Nanocomposite on the Microstructure and Isothermal Crystallization Kinetics of Polyoxymethylene (POM). *Polymer.* **2012**, *53* (23), 5347–5357. DOI:10.1016/j.polymer.2012.09.026.

(57) Lin, O. H.; Ishak, Z. A. M.; Akil, H. Preparation and Properties of Nanosilica-Filled Polypropylene Composites with PP-Methyl POSS as Compatibiliser. *Mater. Des.* **2009**, *30* (3), 748–751. DOI:10.1016/j.matdes.2008.05.007.

(58) Sofiah, M. K. A.; Lin, H.; Akil, H.; Ishak, Z. A. M. Effect of Polypropylene-Methyl Polyhedral Oligomeric Silsesquioxane Compatibilizer in Polypropylene/Silica Nanocomposites : Mechanical , Morphological and Thermal Studies. *Mater. Sci. Forum* **2014**, *803*, 265–268. DOI:10.4028/www.scientific.net/MSF.803.265.

(59) Fréchette, M.; Guo, M.; David, É.; Min, D.; Li, S. The Dielectric Response of Polyethylene/Polyhedral Oligomeric Silsesquioxanes Composites at Various Temperatures. In *2017 IEEE Conference on Electrical Insulation and Dielectric Phenomenon (CEIDP)*; **2017**; pp 501–504

(60) Guo, M.; David, É.; Fréchette, M.; Demarquette, N. R. Polyethylene/Polyhedral Oligomeric Silsesquioxanes Composites: Dielectric, Thermal and Rheological Properties. *Polymer.* **2017**, *115*, 60–69. DOI:10.1016/j.polymer.2017.03.015.

(61) Guo, M.; Frechette, M.; David, É.; Demarquette, N. R.; Daigle, J. Polyethylene/Polyhedral Oligomeric Silsesquioxanes Composites: Electrical Insulation for High Voltage Power Cables. In *IEEE Transactions on Dielectrics and Electrical Insulation*; **2017**; *24*, pp 798–807. DOI:10.1109/TDEI.2017.006144.

(62) Xu, Z.; Guo, M.; Fréchette, M.; David, É.; Chen, G. Space Charge Properties of LDPE-Based Composites with Three Types of POSS. In *2016 IEEE Conference on Electrical Insulation and Dielectric Phenomena (CEIDP)*; **2016**; pp 679–682.

(63) Guo, M.; David, É.; Fréchette, M.; Demarquette, N. R. Low-Density Polyethylene / Polyhedral Oligomeric Silsesquioxanes Composites Obtained by Extrusion. In *2016 IEEE Conference on Electrical Insulation and Dielectric Phenomena (CEIDP)*; **2016**; pp 647–650.

(64) Hato, M. J.; Ray, S. S.; Luyt, A. S. Nanocomposites Based on Polyethylene and Polyhedral Oligomeric Silsesquioxanes, 1 – Microstructure, Thermal and Thermomechanical Properties. *Mol. Mater. Eng.* **2008**, *293* (9), 752–762. DOI:10.1002/mame.200800146.

(65) Hato, M. J.; Ray, S. S.; Africa, S.; Luyt, A. S. Melt-State Viscoelastic Properties of POSS-Containing Polyethylene Melt-State Viscoelastic Properties of POSS-Containing Polyethylene Nanocomposites. *Adv. Sci. Lett.* **2011**, *4* (11–12), 3585–3589. DOI:10.1166/asl.2011.1911.

(66) Joshi, M.; Butola, B. S. Studies on Nonisothermal Crystallization of HDPE/POSS Nanocomposites. *Polymer.* **2004**, *45* (14), 4953–4968. DOI:10.1016/j.polymer.2004.04.057.

(67) Joshi, M.; Butola, B. S.; Simon, G.; Kukaleva, N. Rheological and Viscoelastic Behavior of HDPE/Octamethyl-POSS. *Macromolecules.* **2006**, *39* (5), 1839–1849. DOI:10.1021/ma051357w.

(68) Li, W.; Chen, T.; Guan, C.; Gong, D.; Mu, J.; Chen, Z.; Zhou, Q. Influence of Polyhedral Oligomeric Silsesquioxane Structure on the Disentangled State of Ultrahigh Molecular Weight Polyethylene Nanocomposites during Ethylene in Situ Polymerization. *Ind. Eng. Chem. Res.* **2015**, *54* (5), 1478–1486. DOI:10.1021/ie504273r.

(69) Lim, S.; Hong, E.; Choi, H. J.; Chin, I. Polyhedral Oligomeric Silsesquioxane and Polyethylene Nanocomposites and Their Physical Characteristics. *J. Ind. Eng. Chem.* **2010**, *16* (2), 189–192. DOI:10.1016/j.jiec.2010.01.049.

(70) Lim, S.; Lee, J. Y.; Choi, H. J.; Chin, I. On Interaction Characteristics of Polyhedral Oligomeric Silsesquioxane Containing Polymer. *Polym. Bull.* **2015**, *72* (9), 2331–2352. DOI:10.1007/s00289-015-1405-5.
(71) Baldi, F.; Bignotti, F.; Fina, A.; Tabuani, D.; Ricco, T.; Valotti, V. Mechanical Characterization of Polyhedral Oligomeric Silsesquioxane/Polypropylene Blends. *J. Appl. Polym. Sci.* **2007**, *105* (2), 935–943. DOI:10.1002/app.26142.
(72) Butola, B. S.; Joshi, M.; Kumar, S. Hybrid Organic-Inorganic POSS (Polyhedral Oligomeric Silsesquioxane)/Polypropylene Nanocomposite Filaments. **2010**, *11* (8), 1137–1145. DOI:10.1007/s12221-010-1137-y.
(73) Chen, J.; Chiou, Y. Crystallization Behavior and Morphological Development of Isotactic Polypropylene Blended with Nanostructured Polyhedral Oligomeric Silsesquioxane Molecules. *J. Polym. Sci. Part B Polym. Phys.* **2006**, *44* (15), 2122–2134. DOI: 10.1002/polb.20878.
(74) Chen, J.; Yao, B.; Su, W.; Yang, Y. Isothermal Crystallization Behavior of Isotactic Polypropylene Blended with Small Loading of Polyhedral Oligomeric Silsesquioxane. *Polymer.* **2007**, *48* (6), 1756–1769. DOI:10.1016/j.polymer.2007.01.010.
(75) Fina, A.; Tabuani, D.; Frache, A.; Camino, G. Polypropylene – Polyhedral Oligomeric Silsesquioxanes. *Polymer.* **2005**, *46* (19), 7855–7866. DOI:10.1016/j.polymer.2005.06.121.
(76) Fu, B. X.; Yang, L.; Somani, R. H.; Zong, S. X.; Hsiao, B. S.; Phillips, S.; Blanski, R.; Ruth, P. Crystallization Studies of Isotactic Polypropylene Containing Nanostructured Polyhedral Oligomeric Silsesquioxane Molecules under Quiescent and Shear Conditions. *J. Polym. Sci. Part B Polym. Phys.* **2001**, *39* (22), 2727–2739. DOI: 10.1002/polb.10028.
(77) Pracella, M.; Chionna, D.; Fina, A.; Tabuani, D.; Frache, A.; Camino, G. Polypropylene-POSS Nanocomposites: Morphology and Crystallization Behaviour. *Macromol. Symp.* **2006**, *234* (1), 59–67. DOI:10.1002/masy.200650209.
(78) Takala, M.; Karttunen, M.; Salovaara, P.; Kortet, S.; Kannus, K.; Kalliohaka, T. Dielectric Properties of Nanostructured Polypropylene - Polyhedral Oligomeric Silsesquioxane Compounds. *Trans. Dielectr. Electr. Insul.* **2008**, *15* (1), 40–51. DOI: DOI: 10.1109/T-DEI.2008.4446735.
(79) Fréchette, M. F.; Guo, M.; Savoie, S.; Vanga-Bouanga, C.; David, E. POSS Dispersion in Polyethylene Microcomposites Containing Quartz and Dielectric Responses. In *2013 Annual Report - Conference on Electrical Insulation and Dielectric Phenomena, CEIDP*; **2013**; pp 742–745. DOI:10.1109/CEIDP.2013.6748169.
(80) Scapini, P.; Figueroa, C. A.; Amorim, C. L. G.; Machado, G.; Mauler, R. S.; Crespo, J. S.; Oliviera, R. V. Thermal and Morphological Properties of High-Density Polyethylene/Ethylene – Vinyl Acetate Copolymer Composites with Polyhedral Oligomeric Silsesquioxane Nanostructure. *Polym. Int.* **2010**, *59* (2), 175–180. DOI:10.1002/pi.2704.
(81) Tang, Y.; Lewin, M. Migration and Surface Modification in Polypropylene (PP)/Polyhedral Oligomeric Silsequioxane (POSS) Nanocomposites. *Polym. Adv. Technol.* **2009**, *20* (1), 1–15. DOI:10.1002/pat.1229.
(82) Hoyos, M.; Fina, A.; Carniato, F.; Prato, M.; Monticelli, O. Novel Hybrid Systems Based on Poly(Propylene-g-Maleic Anhydride) and Ti-POSS by Direct Reactive Blending. *Polym. Degrad. Stab.* **2011**, *96* (10), 1793–1798. DOI:10.1016/j.polymdegradstab.2011.07.018.
(83) Kodal, M. Polypropylene/Polyamide 6/POSS Ternary Nanocomposites: Effects of POSS Nanoparticles on the Compatibility. *Polymer.* **2016**, *105*, 43–50. DOI:10.1016/j.polymer.2016.10.021.

(84) Lim, S.; Lee, J. Y.; Choi, H. J.; Chin, I. On Interaction Characteristics of Polyhedral Oligomeric Silsesquioxane Containing Polymer Nanohybrids. *Polym. Bull.* **2015**, *72* (9), 2331–2352. DOI:10.1007/s00289-015-1405-5.

(85) Xu, Z.; Chen, G.; Guo, M.; David, É.; Fréchette, M. Space Charge Properties of UHMWPE/OibPOSS Composites. In *2015 Annual Report Conference on Electrical Insulation and Dielectric Phenomena*; **2015**; pp 543–546. DOI: 10.1109/CEIDP.2015.7352152.

(86) Guo, M.; Frechette, M. F.; David, E.; Couderc, H.; Savoie, S.; Vanga Bouanga, C.; Demarquette, N. R. Characterization of UHMWPE/POSS Composite Prepared by Ball Milling. In *2013 IEEE Electrical Insulation Conference, EIC 2013*; **2013**; pp 444–448. DOI:10.1109/EIC.2013.6554285.

(87) Guo, M.; Fréchette, M.; David, É.; Demarquette, N. R. Influence of Fabrication Techniques on the Dielectric Properties of PE/POSS Polymeric Composites. In *2016 Electrical Insulation Conference (EIC)*; **2016**; pp 297–300. DOI: 10.1109/EIC.2016.7548605

(88) Guo, M.; Fréchette, M.; David, É.; Demarquette, N. R.; Daigle, J. Polyethylene-Based Nanodielectrics Containing Octaisobutyl Polyhedral Oligomeric SilSesquioxanes Obtained by Solution Blending in Xylene. In *2014 Annual Report Conference on Electrical Insulation and Dielectric Phenomena Polyethylene-based*; **2014**; pp 731–734. DOI: 10.1109/CEIDP.2014.6995752.

(89) Guo, M.; Frechette, M.; Demarquette, N. R.; David, E. Polyethylene-Based Nanodielectric Containing Octaisobutyl Polyhedral Oligomeric SilSesquioxanes Obtained by Hexane Slurry Blending. In *Proceedings of 2014 International Symposium on Electrical Insulating Materials*; **2014**; pp 61–64. DOI: 10.1109/ISEIM.2014.6870720.

(90) Guo, M.; Fréchette, M. F.; David, E.; Couderc, H.; Demarquette, N. R. Effects of Stearic Acid and Thermal Treatment on Morphology and Dielectric Properties of UHMWPE/POSS Composites Prepared by Ball Milling. In *2013 Annual Report Conference on Electrical Insulation and Dielectric Phenomena Effects*; **2013**; pp 760–763. DOI: 10.1109/CEIDP.2013.6748299.

(91) Safarikova, B.; Kalendova, A.; Habrova, V.; Zatloukalova, S.; Machovsky, M. Synergistic Effect between Polyhedral Oligomeric Silsesquioxane and Flame Retardants. In *AIP Conference Proceedings*; **2014**; *1599*, pp 106–109. DOI:10.1063/1.4876789.

(92) Fréchette, M. F.; Ghafarizadeh, S. B.; Ahn, T. T.; Vadeboncoeur, S.; Guo, M.; David, E. LDPE Nanocomposites Containing Functionalized SiO2 Molecular Structures: Properties Associated with a Ball-Milled Preparation. In *1st International Conference on Electrical Materials and Power Equipment - Xi'an - China*; **2017**; pp 221–224. DOI:10.1109/ICEMPE.2017.7982067.

(93) Guanyun, C.; Baixuan, F.; Kongying, Z.; Yunhui, Z.; Xiaoyan, Y. Effect of Polyhedral Oligomeric Silsesquioxane and Sorbitol on Properties of Isotactic Polypropylene. *Chem. Res. Chinese Univ.* **2015**, *31* (2), 303–307. DOI:10.1007/s40242-015-4394-x.

(94) Fina, A.; Tabuani, D.; Peijs, T.; Camino, G. POSS Grafting on PPgMA by One-Step Reactive Blending. *Polymer.* **2009**, *50* (1), 218–226. DOI:10.1016/j.polymer.2008.11.002.

(95) Misra, R.; Fu, B. X.; Morgan, S. E. Surface Energetics, Dispersion, and Nanotribomechanical Behavior of POSS/PP Hybrid Nanocomposites. *J. Polym. Sci. Part B Polym. Phys.* **2007**, *45* (17), 2441–2455. DOI:10.1002/polb.

(96) Heeley, E. L.; Hughes, D. J.; El, Y.; Taylor, P. G.; Bassindale, A. R. Morphology and Crystallization Kinetics of Polyethylene/Long Alkyl-Chain Substituted Polyhedral Oligomeric Silsesquioxanes (POSS) Nanocomposite Blends : a SAXS/WAXS Study.

Eur. Polym. J. **2014**, *51*, 45–56. DOI:10.1016/j.eurpolymj.2013.11.020.
(97) Perilla, J. E.; Lee, B.; Jana, S. C. Rheological Investigation of Interactions between Sorbitol and Polyhedral Oligomeric Silsesquioxane in Development of Nanocomposites of Isotactic Polypropylene. *J. Rheol. (N.Y.N.Y).* **2010**, *54* (4), 761–778. DOI:10.1122/1.3439695.
(98) Turgut, G.; Dogan, M.; Tayfun, U.; Ozkoc, G. The Effects of POSS Particles on the Flame Retardancy of Intumescent Polypropylene Composites and the Structure-Property Relationship. *Polym. Degrad. Stab.* **2018**, *149*, 96–111. DOI:10.1016/j.polymdegradstab.2018.01.025.
(99) Zhou, Z.; Ouyang, C.; Zhang, Y.; Zhang, Y.; Yin, N. Crystallization and Rheological Behavior of POSS Filled Polypropylene. *e-Polymers.* **2013**, *9* (1), 1–12. DOI: 10.1515/epoly.2009.9.1.438.
(100) Davulcu, A.; Dogan, M. Production of Dyeable Polypropylene Fiber Using Polyhedral Oligomeric Silsesquioxanes via Melt Spinning. *Fibers Polym.* **2014**, *15* (11), 2370–2375. DOI:10.1007/s12221-014-2370-6.
(101) Du, B.; Su, J.; Tian, M.; Han, T.; Li, J. Understanding Trap Effects on Electrical Treeing Phenomena in EPDM/POSS Composites. *Sci. Rep.* **2018**, *8* (8481), 1–11. DOI:10.1038/s41598-018-26773-y.
(102) Gao, J.; Hua, D.; Du, Y.; Li, X. Rheology, Crystallization Kinetics and Mechanical Properties of HDPE/Vinyl-POSS Nanocomposites. *Polym. Plast. Technol. Eng.* **2011**, *50* (14), 1429–1437. DOI:10.1080/03602559.2011.593074.
(103) Huang, X.; Xie, L.; Jiang, P.; Wang, G.; Yin, Y. Morphology Studies and Ac Electrical Property of Low Density Polyethylene/Octavinyl Polyhedral Oligomeric Silsesquioxane Composite Dielectrics. *Eur. Polym. J.* **2009**, *45* (8), 2172–2183. DOI:10.1016/j.eurpolymj.2009.05.019.
(104) Morici, E.; Di, A. Double Bond-Functionalized POSS: Dispersion and Crosslinking in Polyethylene-Based Hybrid Obtained by Reactive Processing. *Polym. Bull.* **2016**, *73* (12), 3385–3400. DOI:10.1007/s00289-016-1662-y.
(105) Song, X.; Zhou, S.; Wang, Y.; Kang, W.; Cheng, B. Mechanical and Electret Properties of Polypropylene Unwoven Fabrics Reinforced with POSS for Electret Filter Materials. *J. Polym. Res.* **2012**, *19* (1), 1–8. DOI:10.1007/s10965-011-9812-2.
(106) Song, X.; Zhou, S.; Wang, Y.; Kang, W.; Cheng, B. Mechanical Properties and Crystallization Behavior of Polypropylene Non-Woven Fabrics Reinforced with POSS and SiO_2 Nanoparticles. *Fibers Polym.* **2012**, *13* (8), 1015–1022. DOI:10.1007/s12221-012-1015-x.
(107) Zhou, Z.; Zhang, Y.; Zeng, Z.; Zhang, Y. Properties of POSS-Filled Polypropylene: Comparison of Physical Blending and Reactive Blending. *J. Appl. Polym. Sci.* **2008**, *110* (6), 3745–3751. DOI:10.1002/app.29007
(108) Zhou, Z.; Cui, L.; Zhang, Y.; Zhang, Y.; Yin, N. Preparation and Properties of POSS Grafted Polypropylene by Reactive Blending. *Eur. Polym. J.* **2008**, *44* (10), 3057–3066. DOI:10.1016/j.eurpolymj.2008.05.036.
(109) Zhou, Z.; Cui, L.; Zhang, Y.; Zhang, Y.; Yin, N. Isothermal Crystallization Kinetics of Polypropylene/POSS Composites. *J. Polym. Sci. Part B Polym. Phys.* **2008**, *46* (17), 1762–1772. DOI:10.1002/polb.21509.
(110) Zhou, Z.; Zhang, Y.; Zhang, Y.; Yin, N. Rheological Behavior of Polypropylene/Octavinyl Polyhedral Oligomeric Silsesquioxane Composites. *J. Polym. Sci. Part B Polym. Phys.* **2008**, *46* (5), 526–533. DOI:10.1002/polb.21386.
(111) Choi, J.; Jung, C.; Kim, D.; Suh, D.; Nho, Y.; Kang, P.; Ganesan, R. Preparation of Polymer/POSS Nanocomposites by Radiation Processing. *Radiat. Phys. Chem.* **2009**, *78* (7–8), 517–520. DOI:10.1016/j.radphyschem.2009.03.037.

(112) Gao, J.; Cao, X.; Zhang, C.; Hu, W. Non-Isothermal Crystallization Kinetics of Polypropylene/MAP-POSS Nanocomposites. *Polym. Bull.* **2013**, 1977–1990. DOI:10.1007/s00289-013-0907-2.
(113) Davulcu, A. Production of POSS Nanoparticle Containing Polypropylene Fibres Dyeable with Acid and Basic Dyes. *Indian J. Fibre Text. Res.* **2017**, *42* (2), 209–214.
(114) Nanoparticles, Q.; Tutak, M.; Dogan, M. Development of Bio-Active Polypropylene Fiber Containing QA-POSS Nanoparticles. *Fibers Polym.* **2015**, *16* (11), 2337–2342. DOI:10.1007/s12221-015-5213-1.
(115) Nguyen, T.; Gregersen, Ø. W.; Männle, F. Thermal Oxidation of Polyolefins by Mild Pro-Oxidant Additives Based on Iron Carboxylates and Lipophilic Amines: Degradability in the Absence of Light and Effect on the Adhesion to Paperboard. *Polymers.* **2015**, *7*, 1522–1540. DOI:10.3390/polym7081468.
(116) Nguyen, T.-A.; Mannle, F.; Gregersen, Ø. W. Polyethylene/Octa-(Ethyl Octadeca-10,13 Dienoamide) Silsesquioxane Blends and the Adhesion Strength to Paperboard. *Int. J. Adhes. Adhes.* **2012**, *38*, 117–124. DOI:10.1016/j.ijadhadh.2012.05.002.
(117) Wang, X.; Xing, W.; Tang, G.; Hong, N.; Hu, W. Synthesis of a Novel Sulfur-Bearing Secondary Antioxidant with a High Molecular Weight and Its Comparative Study on Antioxidant Behavior in Polypropylene with Two Commercial Sulfur-Bearing Secondary Antioxidants Having Relatively Low Molecular Weight. *Polym. Degrad. Stab.* **2013**, *98* (11), 2391–2398. DOI:10.1016/j.polymdegradstab.2013.08.030.
(118) Groch, P.; Dziubek, K.; Czaja, K.; Dudziec, B.; Marciniec, B. Copolymers of Ethylene with Monoalkenyl- and Monoalkenyl (Siloxy)Silsesquioxane (POSS) Comonomers – Synthesis and Characterization. *Eur. Polym. J.* **2017**, *90*, 368–382. DOI:10.1016/j.eurpolymj.2017.03.038.
(119) Barczewski, M.; Czarnecka-Komorowska, D.; Andrzejewski, J.; Sterzyński, T.; Dutkiewicz, M.; Dudziec, B. Właściwości Przetwórcze Termoplastycznych Tworzyw Polimerowych Modyfikowanych Silseskwioksanami (POSS). *Polimery* **2013**, *58* (10), 805–815. DOI: 10.14314/polimery.2013.805.
(120) Zhang, H.; Jung, M.; Shin, Y.; Yoon, K.; Lee, D. Preparation and Properties of Ethylene/POSS Copolymer with Rac-Et(Ind)2ZrCl2 Catalyst. *J. Appl. Polym. Sci.* **2009**, *111*, 2697–2702. DOI: 10.1002/app.29284.
(121) Morici, E.; Di Bartolo, A.; Arrigo, R.; Tzankova Dintcheva, N. POSS Grafting on Polyethylene and Maleic Anhydride-Grafted Polyethylene by One-Step Reactive Melt Mixing. *Adv. Polym. Technol.* **2016**, *37* (2), 349–357. DOI:10.1002/adv.21673.
(122) Kumar, S.; Butola, B. S.; Joshi, M. POSS/Polypropylene Hybrid Nanocomposite Monofilaments by Reactive Extrusion. *Fibers Polym.* **2013**, *14* (3), 428–435. DOI:10.1007/s12221-013-0428-5.
(123) Kumar, S.; Butola, B. S.; Joshi, M. Preparation of Hybrid AHO-POSS/Polypropylene Nanocomposite Monofilaments by Radiation Induced Grafting. *Fibers Polym.* **2013**, *14* (4), 550–555. DOI:10.1007/s12221-013-0550-4.
(124) Groch, P.; Dziubek, K.; Czaja, K.; Grzymek, M. Investigation of Thermal Stability of Ethylene Copolymers with POSS - Study under Static and Dynamic Conditions. *Polym. Degrad. Stab.* **2018**, *156*, 218–227. DOI:10.1016/j.polymdegradstab.2018.09.010.
(125) Wang, J.; Ye, Z.; Joly, H. Synthesis and Characterization of Hyperbranched Polyethylenes Tethered with Polyhedral Oligomeric Silsesquioxane (POSS) Nanoparticles by Chain Walking Ethylene Copolymerization With. *Macromolecules* **2007**, *40* (17), 6150–6163. DOI:10.1021/ma0706733.
(126) Ye, Z.; Li, S. Hyperbranched Polyethylenes and Functionalized Polymers by Chain Walking Polymerization with Pd-Diimine Catalysis. *Mol. React. Eng.* **2010**, *4*, 319–

332. DOI:10.1002/mren.200900068.
(127) Zhang, Y.; Ye, Z. Homogeneous Polyhedral Oligomeric Silsesquioxane (POSS)-Supported Pd–Diimine Complex and Synthesis of Polyethylenes End-Tethered with a POSS Nanoparticle via Ethylene '"Living"' Polymerization. *Chem. Commun.* **2008**, *14* (10), 1178–1180. DOI:10.1039/b716900k.
(128) Choi, J.; Jung, C.; Kim, D.; Ganesan, R. Radiation-Induced Grafting of Inorganic Particles onto Polymer Backbone: a New Method to Design Polymer-Based Nanocomposite. *Nucl. Instruments Methods Phys. Res. B* **2008**, *266* (1), 203–206. DOI:10.1016/j.nimb.2007.11.012.
(129) Gu, J.; Guo, Y.; Lv, Z.; Geng, W.; Zhang, Q. Highly Thermally Conductive POSS-g-SiCp/UHMWPE Composites with Excellent Dielectric Properties and Thermal Stabilities. *Compos. Part a* **2015**, *78*, 95–101. DOI:10.1016/j.compositesa.2015.08.004.
(130) Grala, M.; Bartczak, Z.; Gadzinowska, K. Polyolefins – polyhedral oligomeric silsesquioxanes (POSS) nanocomposites : mechanical properties , morphology and thermal behaviour. In *ECCM15 - 15TH EUROPEANEUROPEAN CONFERENCE ON COMPOSITE MATERIALS*; 2012; pp 1–2.
(131) Grala, M.; Bartczak, Z. Morphology and Mechanical Properties of High Density Polyethylene-POSS Hybrid Nanocomposites Obtained by Reactive Blending. *Polym. Eng. Sci.* **2014**, *55* (9), 2058–2072. DOI:10.1002/pen.24048.
(132) Bouza, R.; Barral, L.; Díez, F. J.; López, J.; Montero, B.; Rico, M.; Ramírez, C. Study of Thermal and Morphological Properties of a Hybrid System, IPP/POSS. Effect of Flame Retardance. *Compos. Part B Eng.* **2014**, *58*, 566–572. DOI:10.1016/j.compositesb.2013.11.010.
(133) Grala, M.; Bartczak, Z.; Pracella, M. Morphology and Mechanical Properties of Polypropylene-POSS Hybrid Nanocomposites Obtained by Reactive Blending. *Polym. Compos.* **2013**, *34* (6), 929–941. DOI:10.1002/pc.22499.
(134) Du, B.; Ma, H.; Fang, Z. How Nano-Fillers Affect Thermal Stability and Flame Retardancy of Intumescent Flame Retarded Polypropylene. *Polym. Adv. Technol.* **2011**, *22* (7), 1139–1146. DOI:10.1002/pat.1914.
(135) Herbert, M. M.; Andrade, R.; Ishida, H.; Maia, J.; Schiraldi, D. A. Multilayered Confinement of IPP/TPOSS and Nylon 6/APOSS Blends. *Polymer.* **2013**, *54* (26), 6992–7003. DOI:10.1016/j.polymer.2013.11.001.
(136) Wanke, C. H.; Feijo, J. L.; Barbosa, L. G.; Campo, L. F.; Oliveira, R. V. B.; Horowitz, F. Tuning of Polypropylene Wettability by Plasma and Polyhedral Oligomeric Silsesquioxane Modi Fi Cations. *Polymer.* **2011**, *52* (8), 1797–1802. DOI:10.1016/j.polymer.2011.01.064.
(137) Feng, B.; Li, Z.; Chen, G.; Zhu, K.; Zhao, Y.; Yuan, X.; Materials, F. Improving Crystallization Behaviors of Isotactic Polypropylene via a New POSS-Sorbitol Compound. *Polym. Eng. Sci.* **2016**, *57* (4), 357–364. DOI:10.1002/pen.24430.
(138) Smith, E. R.; Howlin, B. J.; Hamerton, I. Using POSS Reagents to Reduce Hydrophobic Character in Polypropylene Nanocomposites. *J. Mater. Chem. a* **2013**, *1* (41), 12971–12980. DOI:10.1039/c3ta80001f.
(139) Zheng, L.; Farris, R. J.; Coughlin, E. B. Novel Polyolefin Nanocomposites: Synthesis and Characterizations of Metallocene-Catalyzed Polyolefin Polyhedral Oligomeric Silsesquioxane Copolymers. *Macromolecules* **2001**, *34* (23), 8034–8039. DOI:10.1021/ma0110094.
(140) Lee, D.; Yoon, K.; Jung, M.; Sung, J. Preparation of Ethylene/Polyhedral Oligomeric Silsesquioxane(POSS) Copolymers with Rac-Et(Ind)2ZrCl2/MMAO Catalyst System. In *Progress in Olefin Polymerization Catalysts and Polyolefin Materials*; **2006**; pp 53–

58. DOI:10.1016/S0167-2991(06)80434-9.
(141) Waddon, A. J.; Zheng, L.; Farris, R. J.; Coughlin, E. B. Nanostructured Polyethylene-POSS Copolymers: Control of Crystallization and Aggregation. *Nano Lett.* **2002**, *2* (10), 1149–1155. DOI:10.1021/nl020208d.
(142) Zheng, L. E. I.; Farris, R. J.; Coughlin, E. B. Synthesis of Polyethylene Hybrid Copolymers Containing Polyhedral Oligomeric Silsesquioxane Prepared with Ring-Opening Metathesis Copolymerization. *J. Polym. Sci. Part a Polym. Chem.* **2001**, *39*, 2920–2928.
(143) Zheng, L.; Waddon, A. J.; Farris, R. J.; Coughlin, E. B. X-Ray Characterizations of Polyethylene Polyhedral Oligomeric Silsesquioxane Copolymers. *Macromolecules* **2002**, *35* (6), 2375–2379. DOI:10.1021/ma011855e.
(144) Xavier, F.; Mihaela, D.; Nicoleta, A.; Radovici, C.; Nicolae, C. The Influence of Alkyl Substituents of POSS in Polyethylene Nanocomposites. *Polymer.* **2013**, *54* (9), 2347–2354. DOI:10.1016/j.polymer.2013.02.035.
(145) Nicoleta, A.; Xavier, F.; Radovici, C.; Mihaela, D. Influence of Branched or Un-Branched Alkyl Substitutes of POSS on Morphology , Thermal and Mechanical Properties of Polyethylene. *Compos. Part B* **2013**, *50*, 98–106. DOI:10.1016/j.compositesb.2013.01.028.
(146) Niemczyk, A.; Dziubek, K.; Sacher-Majewska, B.; Czaja, K.; Dutkiewicz, M.; Marciniec, B. Study of Thermal Properties of Polyethylene and Polypropylene Nanocomposites with Long Alkyl Chain-Substituted POSS Fillers. *J. Therm. Anal. Calorim.* **2016**, *125* (3), 1287–1299. DOI:10.1007/s10973-016-5497-4.
(147) Niemczyk, A.; Dziubek, K.; Czaja, K.; Szatanik, R. Polypropylene / Polyhedral Oligomeric Silsesquioxane Nanocomposites – Study of Free Volumes , Crystallinity Degree and Mass Flow Rate. *Polimery* **2016**, *61* (9), 610–615.
(148) Niemczyk, A.; Dziubek, K.; Czaja, K.; Fra, D.; Piasecki, R.; Rabiej, S.; Dutkiewicz, M. Study and Evaluation of Dispersion of Polyhedral Oligomeric Silsesquioxane and Silica Filler in Polypropylene Composites. *Polym. Compos.* **2018**, *40* (4), 1354–1364. DOI:10.1002/pc.24866.
(149) Heeley, E. L.; Hughes, D. J.; Taylor, P. G.; Bassindale, A. R. Crystallization and Morphology Development in Polyethylene–Octakis(n-Octadecyldimethylsiloxy)-Octasilsesquioxane Nanocomposite Blends. *RSC Adv.* **2015**, *5*, 34709–34719. DOI:10.1039/C5RA03267A.
(150) Barczewski, M.; Dobrzyńska-Mizera, M.; Dutkiweicz, M.; Szołyga, M. Novel Polypropylene β-Nucleating Agent with Polyhedral Oligomeric Silsesquioxane Core: Synthesis and Application. *Polym. Int.* **2016**, *65* (9), 1080–1088. DOI:10.1002/pi.5158.
(151) Chen, T.; Yang, H.; Li, W. Phase Structure and Mechanical Properties of Disentangled Ultra-High Molecular Weight Polyethylene / Polyhedral Oligomeric Silsesquioxane Nanocomposites in a Solid State. *J. Polym. Res.* **2015**, *22* (11), 1–8. DOI:10.1007/s10965-015-0867-3.
(152) Guan, C.; Yang, H.; Li, W.; Zhou, D.; Xu, J.; Chen, Z. Crystallization Behavior of Ultrahigh-Molecular-Weight Polyethylene / Polyhedral Oligomeric Silsesquioxane Nanocomposites Prepared by Ethylene In Situ Polymerization. *J. Appl. Polym. Sci.* **2014**, *131* (19), 40847. DOI:10.1002/app.40847.
(153) Li, W.; Guan, C.; Xu, J.; Mu, J.; Gong, D.; Chen, Z. Disentangled UHMWPE/POSS Nanocomposites Prepared by Ethylene in Situ Polymerization. *Polymer.* **2014**, *55* (7), 1792–1798. DOI:10.1016/j.polymer.2014.02.023.
(154) Mehta, A. M.; Tembe, G. L.; Parikh, P. A.; Mehta, G. N. Catalytic Ethylene Polymerization by the Titanium- Polyhedral Oligomeric Silsesquioxane-Et 3 Al 2 Cl 3 System. *React. Kinet. Mech. Catal.* **2011**, *104*, 369–375. DOI:10.1007/s11144-011-

0356-6.
(155) Carniato, F.; Boccaleri, E.; Marchese, L.; Fina, A.; Tabuani, D.; Camino, G. Synthesis and Characterisation of Metal Isobutylsilsesquioxanes and Their Role as Inorganic – Organic Nanoadditives for Enhancing Polymer Thermal Stability. *Eur. J. Inorg. Chem.* **2007**, *2007* (4), 585–591. DOI:10.1002/ejic.200600683.
(156) Mehta, A.; Tembe, G.; Parikh, P.; Mehta, G. a Study of Ethylene Polymerization Catalyzed by Homogeneous and Silsesquioxane Supported Titanium (IV) Complexes. *Polimery* **2013**, *58* (11–12), 875–882.
(157) Carniato, F.; Fina, A.; Tabuani, D.; Boccaleri, E. Polypropylene Containing Ti- and Al-Polyhedral Oligomeric Silsesquioxanes : Crystallization Process and Thermal Properties. *Nanotechnology* **2008**, *19* (47), 1–9. DOI:10.1088/0957-4484/19/47/475701.
(158) Fina, A.; Abbenhuis, H. C. L.; Tabuani, D.; Frache, A.; Camino, G. Polypropylene Metal Functionalised POSS Nanocomposites : a Study by Thermogravimetric Analysis. *Polym. Degrad. Stab.* **2006**, *91* (5), 1064–1070. DOI:10.1016/j.polymdegradstab.2005.07.013.
(159) Li, X.; Mao, H.; Liu, Y.; Nie, M.; Wang, Q. Compatibilization of Polyhedral Oligomeric Silsesquioxane for Polypropylene – Titanium Dioxide Composites and Effect of the Processing Temperature. *J. Appl. Polym. Sci.* **2017**, *134* (18), 44766. DOI:10.1002/app.44766.
(160) Wheeler, P. A.; Misra, R.; Cook, R. D.; Morgan, S. E. Polyhedral Oligomeric Silsesquioxane Trisilanols as Dispersants for Titanium Oxide Nanopowder. *J. Appl. Polym. Sci.* **2008**, *108* (4), 2503–2508. DOI:10.1002/app.27910
(161) Mao, H.; Liu, Y.; Liu, W.; Nie, M.; Wang, Q. Investigation of Crystallisation and Interfacial Nature of Polyhedral Oligomeric Silsesquioxane / Polypropylene Composites in the Presence of β - Nucleating Agent. *Plast. Rubber Compos.* **2017**, *46* (7), 322–328. DOI:10.1080/14658011.2017.1350793.
(162) Batistella, M.; Otazaghine, B.; Sonnier, R.; Petter, C. Fire Retardancy of Polypropylene / Kaolinite Composites. *Polym. Degrad. Stab.* **2016**, *129*, 260–267. DOI:10.1016/j.polymdegradstab.2016.05.003.
(163) Roy, S.; Scionti, V.; Jana, S. C.; Wesdemiotis, C.; Pischera, A. M.; Espe, M. P. Sorbitol-POSS Interactions on Development of Isotactic Polypropylene Composites. *Macromolecules* **2011**, *44* (20), 8064–8079. DOI:10.1021/ma201595j.
(164) Roy, S.; Lee, B. J.; Kakish, Z. M.; Jana, S. C. Exploiting POSS − Sorbitol Interactions: Issues of Reinforcement of Isotactic Polypropylene Spun Fibers. *Macromolecules* **2012**, *45* (5), 2420–2433. DOI:10.1021/ma202783p.
(165) Anh, T. T.; Vanga-Bouanga, C.; David, E.; Frechette, M. Dielectric Response and Breakdown Strength Improvement of LDPE/TiO2 Nanocomposites by Using POSS as Compatibilizing Agent. In *2016 Electrical Insulation Conference (EIC)*; **2016**; pp 65–68.
(166) Zazoum, B.; Fréchette, M.; David, E. Effect of POSS as Compatibilizing Agent on Structure and Dielectric Response of LDPE / TiO 2 Nanocomposites. In *2015 IEEE Conference on Electrical Insulation and Dielectric Phenomena (CEIDP)*; Ann Arbor, **2015**; pp 523–526.
(167) Zazoum, B.; Frechette, M.; David, E. LDPE/TiO2 Nanocomposites: Effect of POSS on Structure and Dielectric Properties. In *IEEE Transactions on Dielectrics and Electrical Insulation*; **2016**; Vol. 23, pp 2505–2507. DOI:10.1109/TDEI.2016.005973.
(168) Dintcheva, N. T.; Arrigo, R.; Carroccio, S.; Curcuruto, G.; Guenzi, M.; Gambarotti, C.; Filippone, G. Multi-Functional Polyhedral Oligomeric Silsesquioxane-Functionalized Carbon Nanotubes for Photo-Oxidative Stable Ultra-High Molecular Weight

Polyethylene-Based Nanocomposites. *Eur. Polym. J.* **2016**, *75*, 525–537. DOI:10.1016/j.eurpolymj.2016.01.002.
(169) Bianchini, D.; Galland, G. B.; Santos, J. H. Z.; Williams, R. J. .; Fasce, D. P.; Dell'erba, I. E.; Quijada, R.; Perez, M. Metallocene Supported on a Polyhedral Oligomeric Silsesquioxane-Modified Silica with High Catalytic Activity for Ethylene Polymerization. *J. Polym. Sci. Part a Polym. Chem.* **2005**, *43* (22), 5465–5476. DOI:10.1002/pola.21049.
(170) Investigacio, C. C. De; Gonc, A. B. Metallocene Supported on a Polyhedral Oligomeric Silsesquioxane- Modified Silica : Structural Characterization and Catalytic Activity for Ethylene Polymerization. *J. Polym. Sci. Part a Polym. Chem.* **2010**, *48* (24), 5938–5944. DOI:10.1002/pola.24407.
(171) Nmr, S.; Brus, J.; Urbanova, M.; Strachota, A. Epoxy Networks Reinforced with Polyhedral Oligomeric Silsesquioxanes : Structure and Segmental Dynamics as Studied by Solid-State NMR. *Macromolecules* **2008**, *41* (2), 372–386. DOI:10.1021/ma702140g.
(172) Fu, B. X.; Namani, M.; Lee, A. Influence of Phenyl-Trisilanol Polyhedral Silsesquioxane on Properties of Epoxy Network Glasses. **2003**, *44*, 7739–7747. DOI:10.1016/j.polymer.2003.09.033.
(173) Suliga, A.; Hamerton, I.; Viquerat, A. Cycloaliphatic Epoxy-Based Hybrid Nanocomposites Reinforced with POSS or Nanosilica for Improved Environmental Stability in Low Earth Orbit. *Compos. Part B Eng.* **2018**, *138*, 66–76. DOI:10.1016/j.compositesb.2017.11.010.
(174) Misasi, J. M.; Jin, Q.; Knauer, K. M.; Morgan, S. E.; Wiggins, J. S. Hybrid POSS-Hyperbranched Polymer Additives for Simultaneous Reinforcement and Toughness Improvements in Epoxy Networks. *Polymer* **2017**, *117*, 54–63. DOI:10.1016/j.polymer.2017.04.007.
(175) Huang, X.; Li, Y.; Liu, F.; Jiang, P.; Iizuka, T.; Tatsumi, K.; Tanaka, T. Electrical Properties of Epoxy/POSS Composites with Homogeneous Nanostructure. *IEEE Trans. Dielectr. Electr. Insul.* **2014**, *21* (4), 1516–1528. DOI:10.1109/TDEI.2014.004314.
(176) Xu, Y.; Ma, Y.; Deng, Y.; Yang, C.; Chen, J.; Dai, L. Morphology and Thermal Properties of Organic-Inorganic Hybrid Material Involving Monofunctional-Anhydride POSS and Epoxy Resin. *Mater. Chem. Phys.* **2011**, *125* (1–2), 174–183. DOI:10.1016/j.matchemphys.2010.09.003.
(177) Osińska-Broniarz, M.; Sierczyńska, A.; Marciniec, B.; Przekop, R. Wpływ Dodatku Silseskwioksanów o Budowie Klatkowej Na Elektrochemiczne Właściwości Membran Opartych Na Kopolimerze Poli(Fluorek Winylidenu)/Heksafluoropropylen. *Przem. Chem.* **2017**, *96* (6), 1250–1254. DOI:10.15199/62.2017.6.11.
(178) ISO/TS 80004-2:2015 Nanotechnologies — Vocabulary — Part 2: Nano-Objects. **2015**.
(179) Thakur, V. K.; Thakur, M. K.; Pappu, A. *Hybrid Polymer Composite Materials: Properties and Characterisation*; Woodhead Publishing (Elsevier): Cambridge, **2017**.

10. Kopie oświadczeń współautorów

UNIWERSYTET IM. ADAMA MICKIEWICZA W POZNANIU
Wydział Chemii

Poznań, 13.04.2022

Mgr Dariusz Brząkalski
Wydział Chemii
Ul. Uniwersytetu Poznańskiego 8
61-614 Poznań

Oświadczenie o współautorstwie

Potwierdzam swój wkład w następujące publikacje:

1. Dariusz Brząkalski, Robert E. Przekop, Marta Dobrosielska, Bogna Sztorch, Piotr Marciniak, Bogdan Marciniec, "Highly bulky spherosilicates as functional additives for polyethylene processing – influence on mechanical and thermal properties", Polymer Composites, 2020, 41(8), 3389-2302
   Mój udział polegał na syntezie wykorzystywanych pochodnych krzemoorganicznych na drodze hydrosililowania, ich analizie NMR, FT-IR i MALDI-TOF-MS, określeniu struktury otrzymanych pochodnych, przygotowaniu próbek materiałów, interpretacji danych DSC, TG, SEM i SEM-EDS, XRD, MFI, analizy mechanicznej, obliczeniu stopnia krystaliczności próbek, dyskusji wyników w manuskrypcie, przeglądzie literaturowym, przygotowaniu manuskryptu i odpowiedzi na recenzje.

2. Dariusz Brząkalski, Robert E. Przekop, Bogna Sztorch, Paulina Jakubowska, Marek Jałbrzykowski, Bogdan Marciniec, „Silsesquioxane Derivatives as Functional Additives for Preparation of Polyethylene-Based Composites: A Case of Trisilanol Melt-Condensation", Polymers, 2020, 12(10), 2269
   Mój udział polegał na syntezie wykorzystywanych pochodnych krzemoorganicznych, ich analizie NMR, FT-IR i MALDI-TOF-MS, badaniu produktów degradacji termicznej pochodnych, interpretacji danych SEM i SEM-EDS, HDT, MFI, analizy mechanicznej, obliczeniu stopnia krystaliczności próbek, dyskusji wyników w manuskrypcie, przeglądzie literaturowym, przygotowaniu manuskryptu i odpowiedzi na recenzje.

3. Dariusz Brząkalski, Bogna Sztorch, Miłosz Frydrych, Daria Pakuła, Kamil Dydek, Rafał Kozera, Anna Boczkowska, Bogdan Marciniec, Robert E. Przekop, „Limonene Derivative of Spherosilicate as a Polylactide Modifier for Applications in 3D Printing Technology", Molecules, 2020, 25(24), 5882.

Mój udział polegał na interpretacji danych DSC, TG, SEM i SEM-EDS, mikroskopii optycznej, MFI, reologii kapilarnej, analizy mechanicznej, udział w dyskusji wyników w manuskrypcie, przygotowaniu manuskryptu w zakresie techniki wtrysku i odpowiedzi na recenzje

4. Dariusz Brząkalski, Robert E. Przekop, Bogna Sztorch, Miłosz Frydrych, Daria Pakuła, Marek Jałbrzykowski, Grzegorz Markiewicz, Bogdan Marciniec, „Why POSS-Type Compounds Should Be Considered Nanomodifiers, Not Nanofillers—A Polypropylene Blends Case Study", *Polymers*, 2021, 13(13), 2124.
   Mój udział polegał na syntezie wykorzystywanych pochodnych krzemoorganicznych (poza SS-H), ich analizie NMR i FT-IR, interpretacji danych DSC, TG, SEM i SEM-EDS, Vicat, MFI, analizy mechanicznej, dyskusji wyników w manuskrypcie, przeglądzie literaturowym, przygotowaniu manuskryptu i odpowiedzi na recenzje

5. Dariusz Brząkalski, Robert E. Przekop, Miłosz Frydrych, Daria Pakuła, Marta Dobrosielska, Bogna Sztorch, Bogdan Marciniec, „Where ppm Quantities of Silsesquioxanes Make a Difference—Silanes and Cage Siloxanes as TiO_2 Dispersants and Stabilizers for Pigmented Epoxy Resins", Materials, 2022, 15(2), 494.
   Mój udział polegał na syntezie wykorzystywanych pochodnych krzemoorganicznych, ich analizie NMR, FT-IR i MALDI-TOF-MS, przygotowaniu modyfikowanych bieli tytanowych i ich dyspersji w żywicy epoksydowej, interpretacji danych DSC, TG, SEM i SEM-EDS, analizy mechanicznej, dyskusji wyników w manuskrypcie, przeglądzie literaturowym, przygotowaniu manuskryptu i odpowiedzi na recenzje.

UNIWERSYTET IM. ADAMA MICKIEWICZA W POZNANIU
Centrum Zaawansowanych Technologii

Poznań, 12.04.2022

Prof. zw. dr hab. Bogdan Marciniec
Centrum Zaawansowanych Technologii UAM w Poznaniu
Ul. Uniwersytetu Poznańskiego 10
61-614 Poznań

Oświadczenie o współautorstwie

Potwierdzam swój wkład w następujące publikacje:

1. Dariusz Brząkalski, Robert E. Przekop, Marta Dobrosielska, Bogna Sztorch, Piotr Marciniak, Bogdan Marciniec, "Highly bulky spherosilicates as functional additives for polyethylene processing – influence on mechanical and thermal properties", Polymer Composites, 2020, 41(8), 3389-2302
2. Dariusz Brząkalski, Robert E. Przekop, Bogna Sztorch, Paulina Jakubowska, Marek Jałbrzykowski, Bogdan Marciniec, „Silsesquioxane Derivatives as Functional Additives for Preparation of Polyethylene-Based Composites: A Case of Trisilanol Melt-Condensation", Polymers, 2020, 12(10), 2269
3. Dariusz Brząkalski, Bogna Sztorch, Miłosz Frydrych, Daria Pakuła, Kamil Dydek, Rafał Kozera, Anna Boczkowska, Bogdan Marciniec, Robert E. Przekop, „Limonene Derivative of Spherosilicate as a Polylactide Modifier for Applications in 3D Printing Technology", Molecules, 2020, 25(24), 5882.
4. Dariusz Brząkalski, Robert E. Przekop, Bogna Sztorch, Miłosz Frydrych, Daria Pakuła, Marek Jałbrzykowski, Grzegorz Markiewicz, Bogdan Marciniec, „Why POSS-Type Compounds Should Be Considered Nanomodifiers, Not Nanofillers—A Polypropylene Blends Case Study", *Polymers*, 2021, 13(13), 2124.
5. Dariusz Brząkalski, Robert E. Przekop, Miłosz Frydrych, Daria Pakuła, Marta Dobrosielska, Bogna Sztorch, Bogdan Marciniec, „Where ppm Quantities of Silsesquioxanes Make a Difference—Silanes and Cage Siloxanes as TiO_2 Dispersants and Stabilizers for Pigmented Epoxy Resins", Materials, 2022, 15(2), 494.

Mój udział w przygotowaniu niniejszych publikacji obejmował sprawdzenie prac pod kątem poprawności merytorycznej i naniesienie niezbędnych poprawek.

ul. Uniwersytetu Poznańskiego 10, 61-614 Poznań
tel.: 61 829 19 00
bogdan.marciniec@amu.edu.pl
www.amu.edu.pl

UNIWERSYTET IM. ADAMA MICKIEWICZA W POZNANIU
Centrum Zaawansowanych Technologii

Poznań, 12.04.2022

Dr hab. Robert Przekop
Centrum Zaawansowanych Technologii UAM w Poznaniu
Ul. Uniwersytetu Poznańskiego 10
61-614 Poznań

Oświadczenie o współautorstwie

Potwierdzam swój wkład w następujące publikacje:

1. Dariusz Brząkalski, Robert E. Przekop, Marta Dobrosielska, Bogna Sztorch, Piotr Marciniak, Bogdan Marciniec, "Highly bulky spherosilicates as functional additives for polyethylene processing – influence on mechanical and thermal properties", Polymer Composites, 2020, 41(8), 3389-2302
2. Dariusz Brząkalski, Robert E. Przekop, Bogna Sztorch, Paulina Jakubowska, Marek Jałbrzykowski, Bogdan Marciniec, „Silsesquioxane Derivatives as Functional Additives for Preparation of Polyethylene-Based Composites: A Case of Trisilanol Melt-Condensation", Polymers, 2020, 12(10), 2269
3. Dariusz Brząkalski, Bogna Sztorch, Miłosz Frydrych, Daria Pakuła, Kamil Dydek, Rafał Kozera, Anna Boczkowska, Bogdan Marciniec, Robert E. Przekop, „Limonene Derivative of Spherosilicate as a Polylactide Modifier for Applications in 3D Printing Technology", Molecules, 2020, 25(24), 5882.
4. Dariusz Brząkalski, Robert E. Przekop, Bogna Sztorch, Miłosz Frydrych, Daria Pakuła, Marek Jałbrzykowski, Grzegorz Markiewicz, Bogdan Marciniec, „Why POSS-Type Compounds Should Be Considered Nanomodifiers, Not Nanofillers—A Polypropylene Blends Case Study", *Polymers*, 2021, 13(13), 2124.
5. Dariusz Brząkalski, Robert E. Przekop, Miłosz Frydrych, Daria Pakuła, Marta Dobrosielska, Bogna Sztorch, Bogdan Marciniec, „Where ppm Quantities of Silsesquioxanes Make a Difference—Silanes and Cage Siloxanes as TiO_2 Dispersants and Stabilizers for Pigmented Epoxy Resins", Materials, 2022, 15(2), 494.

Mój udział w przygotowaniu niniejszych publikacji obejmował udział w opracowaniu metodologii eksperymentalnej obejmującej wytwarzanie próbek materiałów, a także w interpretacji wyników badań mikroskopowych (mikroskopia elektronowa SEM i SEM-EDS oraz świetlna) i termicznych (TG, DSC) wraz z interpretacją wyników i

dyskusją merytoryczną. We wszystkich pracach brałem udział w przygotowaniu manuskryptów i odpowiedzi do recenzentów oraz sprawowałem czynny nadzór merytoryczny nad pracami mgra Dariusza Brząkalskiego.

Poznań, 12.04.2022

Dr Bogna Sztorch
Centrum Zaawansowanych Technologii UAM w Poznaniu
Ul. Uniwersytetu Poznańskiego 10
61-614 Poznań

Oświadczenie o współautorstwie

Potwierdzam swój wkład w następujące publikacje:

1. Dariusz Brząkalski, Robert E. Przekop, Marta Dobrosielska, Bogna Sztorch, Piotr Marciniak, Bogdan Marciniec, "Highly bulky spherosilicates as functional additives for polyethylene processing – influence on mechanical and thermal properties", Polymer Composites, 2020, 41(8), 3389-2302

   Mój udział polegał na wielkolaboratoryjnej syntezie prekursora krzemoorganicznego – oktawodorosferokrzemianu oraz syntezie sferokrzemianowej pochodnej limonenu na drodze hydrosililowania. Udział w przygotowaniu kompozytów na osnowie PE do następczych badań.

2. Dariusz Brząkalski, Robert E. Przekop, Bogna Sztorch, Paulina Jakubowska, Marek Jałbrzykowski, Bogdan Marciniec, „Silsesquioxane Derivatives as Functional Additives for Preparation of Polyethylene-Based Composites: A Case of Trisilanol Melt-Condensation", Polymers, 2020, 12(10), 2269

   Mój udział polegał na wielkolaboratoryjnej syntezie trisilanolu POSS oraz interpretacji danych w zakresie analizy termograwimetrycznej TG i DSC.

3. Dariusz Brząkalski, Bogna Sztorch, Miłosz Frydrych, Daria Pakuła, Kamil Dydek, Rafał Kozera, Anna Boczkowska, Bogdan Marciniec, Robert E. Przekop, „Limonene Derivative of Spherosilicate as a Polylactide Modifier for Applications in 3D Printing Technology", Molecules, 2020, 25(24), 5882.

   Mój udział polegał na syntezie prekursora (oktawodorosferokrzemianu) oraz pochodnej limonenu – głównego modyfikatora, opracowaniu metodologii otrzymywania próbek w technologii FDM, oraz na interpretacji danych DSC, TG, SEM i SEM-EDS, mikroskopii optycznej, MFI, reologii kapilarnej, analizy

mechanicznej, dyskusji wyników w manuskrypcie, przygotowaniu manuskryptu w zakresie granulatu i wykorzystania go w technologii FDM

4. Dariusz Brząkalski, Robert E. Przekop, Bogna Sztorch, Miłosz Frydrych, Daria Pakuła, Marek Jałbrzykowski, Grzegorz Markiewicz, Bogdan Marciniec, „Why POSS-Type Compounds Should Be Considered Nanomodifiers, Not Nanofillers—A Polypropylene Blends Case Study", *Polymers*, 2021, 13(13), 2124.
5. Dariusz Brząkalski, Robert E. Przekop, Miłosz Frydrych, Daria Pakuła, Marta Dobrosielska, Bogna Sztorch, Bogdan Marciniec, „Where ppm Quantities of Silsesquioxanes Make a Difference—Silanes and Cage Siloxanes as TiO_2 Dispersants and Stabilizers for Pigmented Epoxy Resins", Materials, 2022, 15(2), 494.

W pracach 4 i 5 byłam odpowiedzialna za syntezę prekursora krzemoorganicznego (oktawodorosferokrzemian), przeprowadzenie pomiarów reologicznych MFI, DMTA

Bogna Sztorch

UNIWERSYTET IM. ADAMA MICKIEWICZA W POZNANIU
Centrum Zaawansowanych Technologii

Poznań, 12.04.2022

Dr Piotr Marciniak
Centrum Zaawansowanych Technologii UAM w Poznaniu
Ul. Uniwersytetu Poznańskiego 10
61-614 Poznań

Oświadczenie o współautorstwie

Potwierdzam swój wkład w następujące publikacje:

1. Dariusz Brząkalski, Robert E. Przekop, Marta Dobrosielska, Bogna Sztorch, Piotr Marciniak, Bogdan Marciniec, "Highly bulky spherosilicates as functional additives for polyethylene processing – influence on mechanical and thermal properties", Polymer Composites, 2020, 41(8), 3389-2302

Mój udział w przygotowaniu niniejszej publikacji obejmował korektę artykułu pod kątem językowym i stylistycznym.

Piotr Marciniak

ul. Uniwersytetu Poznańskiego 10, 61-614 Poznań
tel.: 61 829 19 77
piomar@amu.edu.pl
www.amu.edu.pl

UNIWERSYTET IM. ADAMA MICKIEWICZA W POZNANIU
Wydział Chemii

Poznań, 12.04.2022

Mgr Daria Pakuła
Wydział Chemii UAM w Poznaniu
Ul. Uniwersytetu Poznańskiego 8
61-614 Poznań

Oświadczenie o współautorstwie

Potwierdzam swój wkład w następujące publikacje:

1. Dariusz Brząkalski, Bogna Sztorch, Miłosz Frydrych, Daria Pakuła, Kamil Dydek, Rafał Kozera, Anna Boczkowska, Bogdan Marciniec, Robert E. Przekop, „Limonene Derivative of Spherosilicate as a Polylactide Modifier for Applications in 3D Printing Technology", Molecules, 2020, 25(24), 5882.
2. Dariusz Brząkalski, Robert E. Przekop, Bogna Sztorch, Miłosz Frydrych, Daria Pakuła, Marek Jałbrzykowski, Grzegorz Markiewicz, Bogdan Marciniec, „Why POSS-Type Compounds Should Be Considered Nanomodifiers, Not Nanofillers—A Polypropylene Blends Case Study", *Polymers*, 2021, 13(13), 2124.
3. Dariusz Brząkalski, Robert E. Przekop, Miłosz Frydrych, Daria Pakuła, Marta Dobrosielska, Bogna Sztorch, Bogdan Marciniec, „Where ppm Quantities of Silsesquioxanes Make a Difference—Silanes and Cage Siloxanes as TiO_2 Dispersants and Stabilizers for Pigmented Epoxy Resins", Materials, 2022, 15(2), 494.

Mój udział w przygotowaniu niniejszych publikacji obejmował wykonanie pomiarów skaningowej kalorymetrii różnicowej wraz z obróbką danych i wykonaniem wykresów, a także udział w przygotowaniu manuskryptów (przegląd literatury pod kątem najnowszych prac, udział w pisaniu wstępów literaturowych).

Daria Pakuła

ul. Uniwersytetu Poznańskiego 8, 61-614 Poznań
tel.: 61 829 19 77
darpak@amu.edu.pl
www.amu.edu.pl

UNIWERSYTET IM. ADAMA MICKIEWICZA W POZNANIU
Wydział Chemii

Poznań, 12.04.2022

Mgr Miłosz Frydrych
Wydział Chemii UAM w Poznaniu
Ul. Uniwersytetu Poznańskiego 8
61-614 Poznań

Oświadczenie o współautorstwie

Potwierdzam swój wkład w następujące publikacje:

1. Dariusz Brząkalski, Bogna Sztorch, Miłosz Frydrych, Daria Pakuła, Kamil Dydek, Rafał Kozera, Anna Boczkowska, Bogdan Marciniec, Robert E. Przekop, „Limonene Derivative of Spherosilicate as a Polylactide Modifier for Applications in 3D Printing Technology", Molecules, 2020, 25(24), 5882.
2. Dariusz Brząkalski, Robert E. Przekop, Bogna Sztorch, Miłosz Frydrych, Daria Pakuła, Marek Jałbrzykowski, Grzegorz Markiewicz, Bogdan Marciniec, „Why POSS-Type Compounds Should Be Considered Nanomodifiers, Not Nanofillers—A Polypropylene Blends Case Study", *Polymers*, 2021, 13(13), 2124.

Mój udział w przygotowaniu niniejszych publikacji obejmował wykonanie pomiarów termograwimetrycznych wraz z obróbką danych i wykonaniem wykresów, a także udział w przygotowaniu manuskryptu (korekty i formatowanie).

3. Dariusz Brząkalski, Robert E. Przekop, Miłosz Frydrych, Daria Pakuła, Marta Dobrosielska, Bogna Sztorch, Bogdan Marciniec, „Where ppm Quantities of Silsesquioxanes Make a Difference—Silanes and Cage Siloxanes as TiO_2 Dispersants and Stabilizers for Pigmented Epoxy Resins", Materials, 2022, 15(2), 494.

Mój udział w przygotowaniu niniejszej publikacji obejmował wykonanie pomiarów kąta zwilżania wodą wraz z obróbką danych oraz wykonanie widm FT-IR z przygotowaniem wykresów, a także udział w przygotowaniu manuskryptu (korekty i formatowanie).

Miłosz Frydrych

ul. Uniwersytetu Poznańskiego 8, 61-614 Poznań
tel.: 61 829 19 13
frydrych@amu.edu.pl
www.amu.edu.pl

Wydział Inżynierii
Materiałowej

Warszawa, 12.04.2022

Mgr Marta Dobrosielska
Wydział Inżynierii Materiałowej Politechniki Warszawskiej
Ul. Wołoska 141
02-507 Warszawa

OŚWIADCZENIE O WSPÓŁAUTORSTWIE

POTWIERDZAM SWÓJ WKŁAD W NASTĘPUJĄCE PUBLIKACJE:

1. Dariusz Brząkalski, Robert E. Przekop, Marta Dobrosielska, Bogna Sztorch, Piotr Marciniak, Bogdan Marciniec, "Highly bulky spherosilicates as functional additives for polyethylene processing – influence on mechanical and thermal properties", Polymer Composites, 2020, 41(8), 3389-2302
2. Dariusz Brząkalski, Robert E. Przekop, Miłosz Frydrych, Daria Pakuła, Marta Dobrosielska, Bogna Sztorch, Bogdan Marciniec, „Where ppm Quantities of Silsesquioxanes Make a Difference—Silanes and Cage Siloxanes as TiO_2 Dispersants and Stabilizers for Pigmented Epoxy Resins", Materials, 2022, 15(2), 494.

Mój udział w przygotowaniu niniejszych publikacji obejmował przeprowadzenie pomiarów wytrzymałościowych (statyczne rozciąganie dla pracy 1 i 2, testy udarności dla pracy 2) wraz z opracowaniem danych i wykonaniem wykresów.

Marta Dobrosielska

Politechnika
Warszawska

ul. Wołoska 141
02-507 Warszawa
www.inmat.pw.edu.pl

WYDZIAŁ MECHANICZNY
POLITECHNIKI BIAŁOSTOCKIEJ

15-351 Białystok, ul. Wiejska 45C, tel. +48 85 746 92 00, fax +48 85 746 92 10
e-mail: wm@pb.edu.pl, www.wm.pb.edu.pl

Białystok, 06.04.2022

Dr hab. inż. Marek Jałbrzykowski

Politechnika Białostocka

Wydział Mechaniczny

Katedra Inżynierii Materiałowej i Produkcji

Ul. Wiejska 45C

15-351 Białystok

Oświadczenie o współautorstwie

Potwierdzam swój wkład w następujące publikacje:

1. Dariusz Brząkalski, Robert E. Przekop, Bogna Sztorch, Paulina Jakubowska, Marek Jałbrzykowski, Bogdan Marciniec, „Silsesquioxane Derivatives as Functional Additives for Preparation of Polyethylene-Based Composites: A Case of Trisilanol Melt-Condensation", *Polymers*, 2020, 12(10), 2269

   Mój udział w przygotowaniu niniejszej publikacji obejmował pomoc w zakresie metodologii i wytwarzania próbek techniką wtryskiwania.

2. Dariusz Brząkalski, Robert E. Przekop, Bogna Sztorch, Miłosz Frydrych, Daria Pakuła, Marek Jałbrzykowski, Grzegorz Markiewicz, Bogdan Marciniec, „Why POSS-Type Compounds Should Be Considered Nanomodifiers, Not Nanofillers - A Polypropylene Blends Case Study", *Polymers*, 2021, 13(13), 2124.

   Mój udział w przygotowaniu niniejszej publikacji obejmował przeprowadzenie badań tribologicznych materiałów polimerowych wraz z dyskusją wyników.

WYDZIAŁ MECHANICZNY
POLITECHNIKI BIAŁOSTOCKIEJ

15-351 Białystok, ul. Wiejska 45C, tel. +48 85 746 92 00, fax +48 85 746 92 10
e-mail: wm@pb.edu.pl, www.wm.pb.edu.pl

Białystok, 06.04.2022

Mgr inż. Grzegorz Markiewicz

Politechnika Białostocka

Wydział Mechaniczny

Katedra Inżynierii Materiałowej i Produkcji

Ul. Wiejska 45C

15-351 Białystok

Oświadczenie o współautorstwie

Potwierdzam swój wkład w następujące publikacje:

1. Dariusz Brząkalski, Robert E. Przekop, Bogna Sztorch, Miłosz Frydrych, Daria Pakuła, Marek Jałbrzykowski, Grzegorz Markiewicz, Bogdan Marciniec, „Why POSS-Type Compounds Should Be Considered Nanomodifiers, Not Nanofillers - A Polypropylene Blends Case Study", *Polymers*, 2021, 13(13), 2124.

   Mój udział w przygotowaniu niniejszej publikacji obejmował wytwarzanie próbek do badań mechanicznych techniką wtrysku oraz przeprowadzenie badań mechanicznych w zakresie statycznego rozciągania.

Grzegorz Markiewicz

Wydział Inżynierii
Materiałowej

Warszawa, 12.04.2022

Prof. dr hab. inż. Anna Boczkowska
Wydział Inżynierii Materiałowej Politechniki Warszawskiej
Ul. Wołoska 141
02-507 Warszawa

Oświadczenie o współautorstwie

Potwierdzam swój wkład w następujące publikacje:

1. Dariusz Brząkalski, Bogna Sztorch, Miłosz Frydrych, Daria Pakuła, Kamil Dydek, Rafał Kozera, Anna Boczkowska, Bogdan Marciniec, Robert E. Przekop, „Limonene Derivative of Spherosilicate as a Polylactide Modifier for Applications in 3D Printing Technology", Molecules, 2020, 25(24), 5882.

Mój udział w przygotowaniu niniejszych publikacji obejmował pomoc w interpretacji wyników analizy mechanicznej próbek drukowanych 3D w technologii FDM oraz wtryskiwanych.

Politechnika
Warszawska

ul. Wołoska 141
02-507 Warszawa
www.inmat.pw.edu.pl

Wydział Inżynierii
Materiałowej

Warszawa, 12.04.2022

Dr inż. Rafał Kozera
Wydział Inżynierii Materiałowej Politechniki Warszawskiej
Ul. Wołoska 141
02-507 Warszawa

Oświadczenie o współautorstwie

Potwierdzam swój wkład w następujące publikacje:

1. Dariusz Brząkalski, Bogna Sztorch, Miłosz Frydrych, Daria Pakuła, Kamil Dydek, Rafał Kozera, Anna Boczkowska, Bogdan Marciniec, Robert E. Przekop, „Limonene Derivative of Spherosilicate as a Polylactide Modifier for Applications in 3D Printing Technology", Molecules, 2020, 25(24), 5882.

Mój udział w przygotowaniu niniejszych publikacji obejmował wykonanie obrazowania SEM-EDS.

Politechnika
Warszawska

ul. Wołoska 141
02-507 Warszawa
www.inmat.pw.edu.pl

Wydział Inżynierii
Materiałowej

Warszawa, 12.04.2022

Mgr inż. Kamil Dydek
Wydział Inżynierii Materiałowej Politechniki Warszawskiej
Ul. Wołoska 141
02-507 Warszawa

Oświadczenie o współautorstwie

Potwierdzam swój wkład w następujące publikacje:

1. Dariusz Brząkalski, Bogna Sztorch, Miłosz Frydrych, Daria Pakuła, Kamil Dydek, Rafał Kozera, Anna Boczkowska, Bogdan Marciniec, Robert E. Przekop, „Limonene Derivative of Spherosilicate as a Polylactide Modifier for Applications in 3D Printing Technology”, Molecules, 2020, 25(24), 5882.

Mój udział w przygotowaniu niniejszych publikacji obejmował wykonanie próbek techniką wtryskiwania.

Kamil Dydek

Elektronicznie podpisany przez Kamil Dydek
Data: 2022.04.13 11:50:14 +02'00'

Politechnika
Warszawska

ul. Wołoska 141
02-507 Warszawa
www.inmat.pw.edu.pl

POLITECHNIKA POZNAŃSKA
Wydział Technologii Chemicznej
ul. Berdychowo 4, 60-965 Poznań
tel. +48 61 665 37 84

Poznań, 13.04.2022

Dr inż. Paulina Jakubowska
Wydział Technologii Chemicznej Politechniki Poznańskiej
Ul. Berdychowo 4
60-965 Poznań

Oświadczenie o współautorstwie

Potwierdzam swój wkład w następującą publikację:

1. Dariusz Brząkalski, Robert E. Przekop, Bogna Sztorch, Paulina Jakubowska, Marek Jałbrzykowski, Bogdan Marciniec, „Silsesquioxane Derivatives as Functional Additives for Preparation of Polyethylene-Based Composites: A Case of Trisilanol Melt-Condensation", Polymers, 2020, 12(10), 2269

Mój udział w przygotowaniu niniejszej publikacji obejmował konsultacje w zakresie metodologii pomiarów HDT oraz wyznaczania poziomu krystaliczności na podstawie DSC.

11. Kopie prac wraz z materiałami uzupełniającymi

Received: 17 December 2019 | Revised: 21 April 2020 | Accepted: 26 April 2020

DOI: 10.1002/pc.25628

RESEARCH ARTICLE

Polymer COMPOSITES WILEY

Highly bulky spherosilicates as functional additives for polyethylene processing—Influence on mechanical and thermal properties

Dariusz Brząkalski[1] | **Robert E. Przekop**[2] | **Marta Dobrosielska**[2] | **Bogna Sztorch**[2] | **Piotr Marciniak**[2] | **Bogdan Marciniec**[1,2]

[1]Faculty of Chemistry, Adam Mickiewicz University in Poznań, Poznań, Poland

[2]Centre for Advanced Technologies, Adam Mickiewicz University in Poznań, Poznań, Poland

Correspondence
Dariusz Brząkalski, Faculty of Chemistry, Adam Mickiewicz University in Poznań, ul. Uniwersytetu Poznańskiego 8, 61‐614 Poznań, Poland.
Email: dariusz.brzakalski@amu.edu.pl

Funding information
Narodowe Centrum Badań i Rozwoju, Grant/Award Number: PBS3/A1/16/2015; Narodowe Centrum Nauki, Grant/Award Number: UMO-2018/29/N/ST5/00868

Abstract

In this work, a series of cage siloxanes (spherosilicate [SS] type) was tested as functional additives for preparation of polyethylene (PE)-based nanocomposites. For this purpose, the compounds were prepared by condensation and olefin hydrosilylation reactions. The effect of these products on properties of obtained nanocomposites was analyzed by means of mechanical, microscopic (scanning electron microscopy-energy dispersive spectroscopy), crystallographic (X-ray diffraction), thermal (differential scanning calorimetry, thermogravimetry), rheological Melt flow rate (exchangeable with MFI) (MFR), and thermomechanical (heat deflection temperature) analyses. The results were compared with similar reports on silsesquioxane- and SS-reinforced PE systems. Effects of SS functional group structure on the behavior of the additive and properties of the composite system were discussed. Aspects of thermal decomposition of PE-containing SS were studied and a probable mechanism of these polymer systems degradation was proposed.

KEYWORDS

additives, composites, polyethylene (PE), processing, thermal properties

1 | INTRODUCTION

Polyolefins play a huge role in polymer industry, as they make up a significant fraction of all thermoplastics used for mass production of different goods. Polyethylene (PE) is the most widely used, as it serves for production of foils, packages, furniture films, pipes, containers, battery separators, and more. Polypropylene is typically applied as material for fibers, coatings, tapes, and molded objects, for example, automotive parts, medical equipment, and other products.[1] Some of their properties are especially desirable, like low glass transition temperatures, easy processability, relatively good chemical inertness, wide spectrum of different grades available, or low price. Although cheap and easy in production and processing, these simple polyolefins have a number of limitations, such as low temperature stability, relatively low mechanical strength, or very poor flammability resistance.[2] Most of these issues may be overcome by choosing different thermoplastics, for example, fluorinated hydrocarbons, poly (acrylonitrile-co-butadiene-co-styrene) (ABS) terpolymer or poly(ethylene terephthalate), depending on the intended use of the final product.[1,3] Another strategy is introduction of functional additives and fillers serving different purposes, for example, increasing abrasion resistance, flame resistance, thermal stability, compression strength, Young's modulus, improving rheological properties or crystallization behavior etc.[4]

Cage siloxanes are a subject of potential application as either fillers/nanofillers or functional additives, as they are

known for properties such as good dispersion, low polarity and volatility, or relatively high melting and/or boiling points, as well as high thermal stability and dielectric properties. They can be divided into two main subgroups, namely polyhedral oligomeric silsesquioxanes and spherosilicates (SS), showing some structural similarities, mainly the siloxane core, with SS having an additional siloxane linker between the core and the functional groups.[5] Due to abovementioned properties, their application as additives or building blocks for preparation of special materials has been a subject of extensive studies. A recent review by Du and Liu presents a comprehensive overview of both synthetic and processing strategies concerning preparation of cage siloxane-containing hybrid materials of high variety.[6] There are a number of papers covering application of octasubstituted silsesquioxanes and SS as additives for polyolefins, including PE, where the organosilicon agents contain different functional groups. These substituents include small alkyl groups, branched and nonbranched alkyl chains of different length (up to 18 carbon atoms),[7–34] phenyl[19–21] and cyclohexyl[19] rings, unsaturated groups,[10,35] or heteroatom-containing groups.[10,21,36–39] Most of these compounds were chosen either on the basis of their simplicity of preparation or commercial availability (eg, Me-, iBu-, iOc-, Ph-octasubstituted silsesquioxanes), or designed towards the best obtainable compatibility with polyolefins (eg, long alkyl chain-substituted derivatives). However, the library of up-to-date tested derivatives is poor of examples of silsesquioxanes or SS with bulky functional groups, rendering the inorganic siloxane core sterically hindered.

In this work, new SS derivatives containing highly bulky substituents were compared to simple, well-known compounds (octhydro- and octavinylspherosilicate) as functional additives for PE at different concentrations and their impact on the properties of obtained SS/PE composites, that is, thermal stability, crystallinity index (CI), melting and crystallization temperatures, Young's modulus, tensile strength, and additive dispersion, was examined. The chosen olefins are relatively low-priced and abundantly used in industry, and of which two ((R)-(+)-limonene and β-pinene) are natural products. SS-limonene and SS-pinene were previously tested as modifiers for poly (vinylidene difluoride-co-hexafluoropropylene) (PVDF/HFP) gel membranes, however in terms of synthesis and analysis, only their Fourier transform-infrared (FT-IR) spectra were reported.[40]

2 | EXPERIMENTAL

2.1 | Materials and instrumentation

The chemicals were purchased from the following sources: tetraethoxysilane from Unisil (Poland), chlorodimethylsilane, chlorodimethylvinylsilane, triethylamine, and tetramethylammonium hydroxide 25% methanol solution from ABCR, olefins (5-vinylnorborn-2-ene, (R)-(+)-limonene, and β-pinene), tetrahydrofuran, toluene, chloroform-d, Karstedt's catalyst xylene solution from Aldrich, P_2O_5 from POCH (Poland). 5-Vinylnorbornene was a mixture of endo and exo isomers, which was confirmed by ^1H nuclear magnetic resonance (NMR) to be in 68:32 M ratio. Low-density polyethylene (LDPE) type Malen E FABS 23 D022 from Basell Orlen Polyolefins. Its characteristics are MFR (190; 2.16 kg) = 2 g/10 minutes and density 0.921 g/cm^3. Toluene was degassed and dried by distilling it from P_2O_5 under argon atmosphere.

Octahydro- and octavinylspherosilicates were prepared according to a literature procedure.[41] The detailed synthesis of the derivatives obtained by hydrosilylation is described in a separate section (see Section 2.2).

PE concentrates were prepared on a two-roll mill ZAMAK MERCATOR WG 150/280 operating at the 175°C to 185°C temperature range. The concentrates were ground in SHINI SG-1417 low-speed mill and dried for 6 hours at 90°C. Prepared concentrates were then diluted to final additive concentrations in an extrusion process with cold granulation using Thermo Fisher Scientific HAAKE PolyLAB OS extrusion setup equipped with a single screw (D = 19.05 mm, L/D: 25) working at 60 rpm. The temperature zones for extrusion were set as follows: 120°C, 160°C, 180°C, and 180°C. For foils production, the setup was equipped with foil extrusion die and chill-roll system. The foils prepared were of 0.2 mm thickness. Dumbbells were prepared on ENGEL E-Victory 170/80 injection molding machine equipped with a double socket mold for preparation of normalized testing specimens consistent with the PN-EN ISO 527-2 norm (type 1A). The parameters for injection molding were as follows: temperature profile of plastification unit: 170°C, 180°C, and 190°C, mold temperature: 22°C, injection time: 2 seconds, cooling time: 20 seconds, injection pressure p1: 1200 bar, p2: 500 bar, mold compression profile: 1200 bar/1 s, 1000 bar/4 seconds, 300 bar/5 seconds.

MFR index was measured on INSTRON CEAST MF20 plastometer equipped with 2.16 kg weight at temperature of 190°C.

For tensile strength tests, a universal testing machine Instron 5969 was used, in accordance to the norm EN ISO 527-2:1996. The speed of traverse was set to 50 mm/min for dumbbells and 100 mm/min for foils.

The ^1H, ^{13}C, and ^{29}Si NMR spectra were recorded at 25°C on a Bruker Ascend 400 and Ultra Shield 300 spectrometers using $CDCl_3$ as a solvent. Chemical shifts are reported in ppm with reference to the residual solvent ($CHCl_3$) peaks for ^1H and ^{13}C.

The FT-IR spectra were recorded on a Nicolet iS 50 Fourier transform spectrophotometer (Thermo Fisher Scientific) equipped with a diamond attenuated total reflectance (ATR) unit with a resolution of 0.09/cm.

Scanning electron microscopy-energy dispersive spectroscopy (SEM/EDS) analyses were recorded on a Quanta FEG 250 (FEI) instrument; SEM at 5 kV and EDS at 30 kV, respectively. The samples were frozen in liquid nitrogen and fractured with pliers to reveal satisfactory surface for analysis.

Thermogravimetry (TG) was performed using NETZSCH 209 F1 Libra gravimetric analyzer. Samples of 5.0 ± 0,2 mg were cut from each granulate and placed in Al_2O_3 crucibles. Measurements were done under nitrogen and air in 30°C to 800°C temperature range and at 20°C/min temperature rise. Differential scanning calorimetry (DSC) was performed using NETZSCH 204 F1 Phoenix calorimeter. Samples of 5.0 ± 0,2 mg were cut from each granulate and placed in aluminum crucible with punched lid. Measurements were done under nitrogen in 20°C to 220°C temperature range and at 10°C/min temperature rise. Each sample was treated by three melting-cooling cycles to erase its thermal history and further observe the thermal behavior of the samples. As the third melting-cooling cycle was basically identical to the second one, the data presented were measured for the second melting-cooling cycle.

X-ray diffraction (XRD) measurements were carried out using a Philips PW1050 diffractometer, working in θ to 2θ geometry with Ni-filtered CuK_α radiation. The following measurement conditions were applied: 2θ 3 to 80°, voltage 40 kV, current 30 mA, scan step 0.013°. The raw data were processed with OriginPro software.

2.2 | General procedure for hydrosilylation process of olefins with SS-H

All hydrosilylation syntheses were conducted under argon atmosphere in round-bottom flasks equipped with condensers, gas bubblers, and magnetic stirrers. In a typical procedure, a 500 mL three-neck, round-bottom flask was charged with 25 g of SS-H, 250 mL of toluene and olefin. A thermometer and condenser equipped with an argon inlet and oil bubbler were attached; the flask placed in a heating mantle and the system was purged with argon. The reaction mixture was set on 110°C and before reaching boiling, Karstedt's catalyst solution (10^{-5} eq Pt/mol Si-H) was added, which resulted in quick increase of temperature and the system starting to reflux. The reaction mixture was kept at the boiling temperature and samples were taken for FT-IR control until full Si-H group consumption was observed. Then, the solvent was evaporated under vacuum to dryness to obtain an analytically pure sample. For 5-vinylnorborn-2-ene hydrosilylation, the temperature was maintained at 40°C to prevent polymerization of the olefin, which was observed at reflux temperature.

2.3 | General procedure for composites preparation and characterization

In a typical procedure, about 200 g of PE was rolled on two-roll mill until complete melt, after which the chosen modifier was added in a quantity corresponding to 5% of the final composite content, and the composition was rolled together at temperature range of 175°C to 185°C until it became completely homogeneous or until no more improvement of homogeneity was observed. After that, the composition was taken off the rolls and set to cool down. It was ground in the low-speed mill and the obtained masterbatch granulate was then diluted to a final concentration of SS additive to be either 1% or 0.5% by mixing it with the granulate of neat PE in a proper proportion and extruding it on a single-screw extruder, and the extrudate being simultaneously granulated. 0.1% concentration composites were obtained by diluting 0.5% granulate in the same manner. For octahydrospherosilicate (SS-H) and octavinylspherosilicate (SS-Vi) systems, the concentrations of 0.1% were not prepared, as SEM-EDS showed poor dispersion of the additives at concentrations as low as 0.5% and no significant improvement was expected to be observed. In addition, the SS-H/PE and SS-Vi/PE systems served only as a reference, and more data on such composites are available in literature. For SS-Vi system, only 0.5% concentration was prepared. The obtained granulates were then measured by TG, DSC, and XRD techniques, and processed into standard dumbbell specimens and foils. Foils were cut into proper specimens using a sample cutter, equipped with a knife in a form of a dumbbell. Tensile strength tests for dumbbells and foil specimens were performed to measure stress and elongation at break, as well as Young's modulus.

3 | RESULTS AND DISCUSSION

3.1 | Characterization of obtained modifiers and compositions

All the modifiers obtained were prepared according to the Scheme 1.

They were investigated by NMR and IR spectroscopy to prove their purity and completion of hydrosilylation reactions (~99% for all examples). NMR analysis allowed

for verification of hydrosilylation selectivity, both in terms of reactivity of the particular double bond (methylidene moiety for limonene, vinyl moiety and internal double bond for 5-vinylnorborn-2-ene), as well as regioselectivity of Si-H addition to the specified double bond (see Scheme 1 and Data S1). In addition, SS-limonene and SS-pinene were obtained as mixtures of diastereoisomeric products, as (R)-(+)-limonene and β-pinene are enantiomers and hydrosilylation introduces another stereogenic center, but no stereoselectivity control was maintained under reaction conditions applied in this work. The existence of diastereomeric products can be proved by ^{13}C NMR, where most of the signals are doubled (with different shift depending on the distance from the stereogenic centers). For SS-norbornene, proton integration revealed that both double bonds are reactive towards hydrosilylation reaction, vinyl moiety being more reactive, and the reactivity of ring double bond resulted in formation of side products, which was confirmed by MALDI-TOF-MS. The molecular weights of dimers and further oligomers were exceeding the *m*/*z* limit of the instrument, but the products of intramolecular cross-linking were observed (see Data S1). Such observations could be done even with 2-fold molar excess of the olefin used for the synthesis with only small improvement of selectivity observed. High share of internal double bond hydrosilylation reaction may be explained by the steric hindrance of remaining Si-H moieties due to presence of norbornene groups introduced to the molecule initially (most likely by hydrosilylation of vinyl group) and blocking the remaining Si-H groups from introducing another molecules of the olefin, thus encouraging intramolecular reaction of hydrosilylation of the second (ring) double bond. Due to overlapping signals of all the isomers produced, together with the exo/endo isomers of the commercial 5-vinylnorborn-2-ene starting material, it was difficult to perform a complete resolution of ^{1}H NMR signals even with the aid of correlation spectroscopy (COSY) NMR. On IR, the most important absorbance bands of SS-Vi were at 3068 and 1603 cm^{-1}, corresponding to C—H and CC stretching of vinyl group, respectively, and 1408 cm^{-1}, corresponding to CC—H scissoring. For SS-H, the characteristic signals were at 2141 and 889 cm^{-1}, from stretching and bending of Si-H moiety, respectively, and disappearing upon hydrosilylation reactions. The derivatives obtained by hydrosilylation (SS-limonene, SS-pinene and SS-norbornene) show strong absorptions in C—H stretching regions, typical for alkane compounds, as well as weak absorptions in C—H region of unsaturated hydrocarbons for SS-norbornene and SS-limonene (see Data S1). Moreover, it was observed during synthesis of SS-norbornene that the material polymerized at reflux temperature even when the temperature was raised when the reaction was close to completion, which suggested that not only the parent olefin, 5-vinylnorborn-2-ene may undergo polymerization, but also the final product as well. For this reason, SS-norbornene was analyzed by DSC to reveal exothermic peak with maximum at ~114°C, not appearing during the second heating-cooling cycle (Figure 1), which proved the sample to polymerize at elevated temperatures, including conditions of polyolefins processing. For SS-limonene, a similar observation was made, but the exothermic peak was with maximum at ~162°C, which was too high to observe any polymerization during the synthesis. For SS-pinene, no polymerization was observed in the applied temperature range. Moreover, an interesting observation was made by thermogravimetric

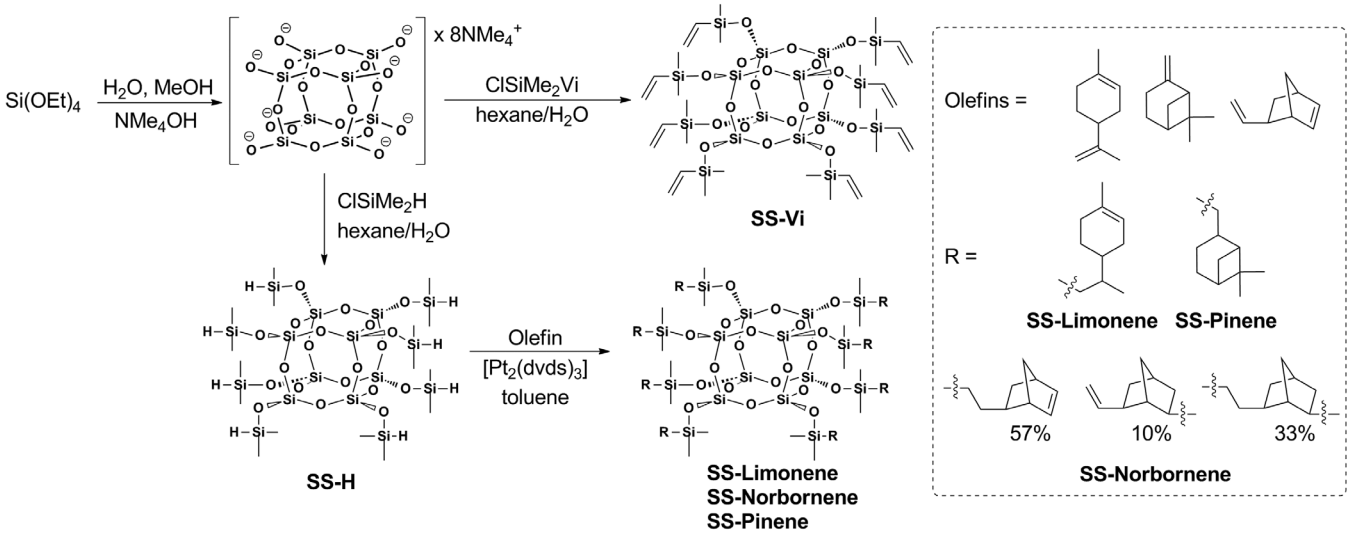

SCHEME 1 The synthetic route to prepare spherosilicate derivatives used in this work

analysis (TGA) of the new additives. SS-pinene and SS-limonene showed only one decomposition event, with derivative thermogravimetry (DTG) peak at 475°C and 460°C accordingly, whereas SS-norbornene showed two distinct events, with DTG peaks at 321°C and 514°C. The first degradation event occurred at relatively low temperature and was most probably due to retro-Diels-Alder reaction (rDA) of the norbonenyl ring (Scheme 2). Such behavior is well-known for norbornene derivatives chemistry.[42] Taking into account the calculated share of the substituents of different hydrosilylation regioselectivity (Scheme 1), total degradation of reactive norbonenyl substituents through rDA reaction would translate into ~15% of SS-norbornene sample mass loss (the saturated rings formed by hydrosilylation of the internal double bond cannot undergo rDA reaction). However, it was observed to be 7.5%. Taking into account the polymerization reaction observed on DSC, it suggests that roughly half of the rings polymerized during sample heating (most likely together with residual vinyl groups), forming cured mass with no further mobility of the substituents, and the remaining rings underwent degradation through the proposed mechanism at above 321°C.

3.2 | SEM-EDS analysis of obtained composites

The SEM was applied to assess dispersion of the additives within PE matrix. EDS was applied to aid the analysis and verify the chemical composition of observed phases on the basis of oxygen and silicon content in the phases, both of these elements building the siloxane core of the SS derivatives. Generally, besides of SS-limonene, all the additives showed a tendency to form two dispersion levels. First, where the additive particles form larger, multimicron-sized agglomerates, easily detected with EDS imaging, and a second, where additive particles are around micron-sized or smaller and form smaller agglomerates. A similar observation was made by Cicala et al. when preparing heptaisobutyl-p-chlorophenyl-modified polyethersulfone soluble veils for epoxy resin composite systems.[43]SS-limonene and SS-pinene showed very good dispersion in the matrix at all concentrations, and all the inconsistencies of silicon concentrations visible on EDS maps (see Data S1) were rather artifacts generated due to nonuniform shapes of the sample surface, as at higher magnifications it was difficult to

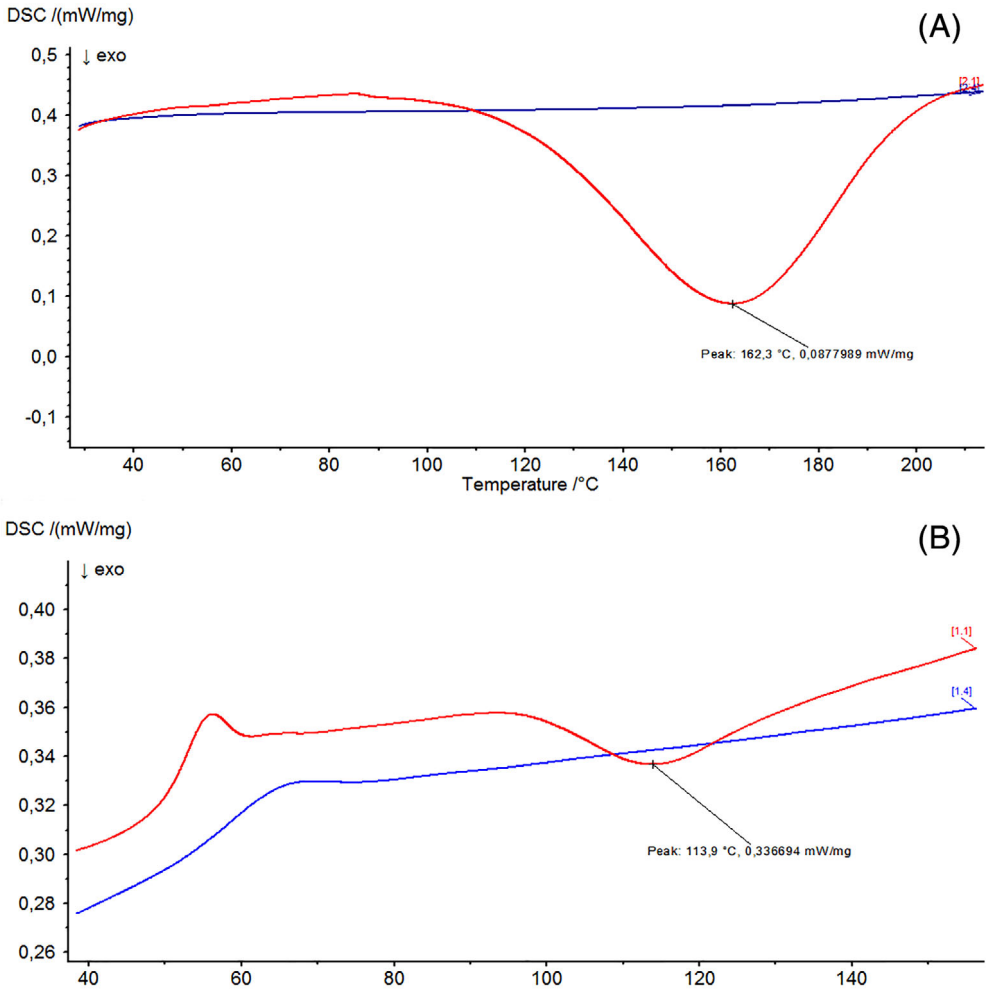

FIGURE 1 DSC plots of spherosilicate additives, SS-limonene, A, and SS-norbornene, B. Red curve presents the first heating cycle, blue one presents the second cycle. SS, spherosilicate [Color figure can be viewed at wileyonlinelibrary.com]

observe particles of the modifiers on SEM images (Figures 2, 3 and Data S1). Both of these additives were observable as amorphous phases, SS-limonene resembling liquid effectively wetting PE surface, while SS-pinene resembled resinous droplets. On the other hand, SS-norbornene was moderately well-dispersed only at 0.1% concentration and at higher loadings it formed agglomerates easily visible on SEM and confirmed by EDS to be particles of the additive. This behavior can be explained on the basis of DSC analysis, as it was proven that the additive polymerized at the temperature much lower than that of PE processing. Polymerization of SS-limonene was not a factor impeding dispersion of the additive in polymer matrix, and the SS-limonene/PE obtained may actually form a polymer blend, as comparison of EDS maps for increasing loading of these two additives suggests. In addition, SS-H and SS-Vi showed poor dispersion properties, forming large agglomerates, however, morphology of large (multimicron) grains observed was different for these two additives, which may explain differences observed for mechanical and rheological analysis. These observations prove that, in general, large alkyl substituents surrounding siloxane core of the SS derivatives improve compatibility with PE matrix, however, for the best compatibility, linear substituents should rather be introduced. Niemczyk et al. reported very good dispersion of long chain-substituted SS increasing together with the chain length, especially for n-octadecyl derivative, as the long chain shows structural similarity to PE.[9] Moreover, Fréchette et al. reported that well-defined octaisobutylsilsesquioxane showed rather poor dispersion properties in ultra-high molecular weight polyethylene (UHMWPE), the additive forming polycrystalline agglomerates varying in

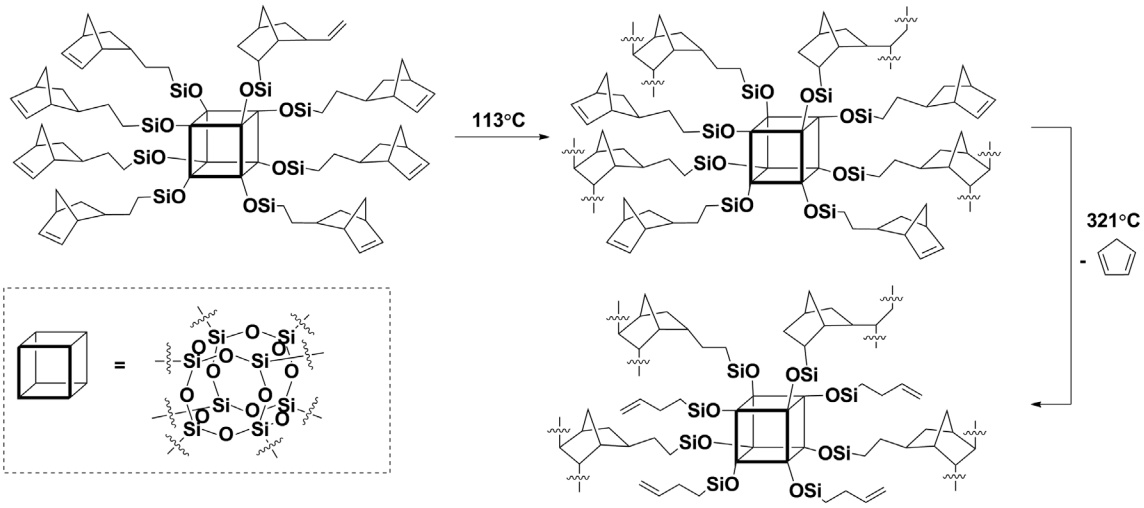

SCHEME 2 The proposed route of SS-norbornene derivative thermal degradation

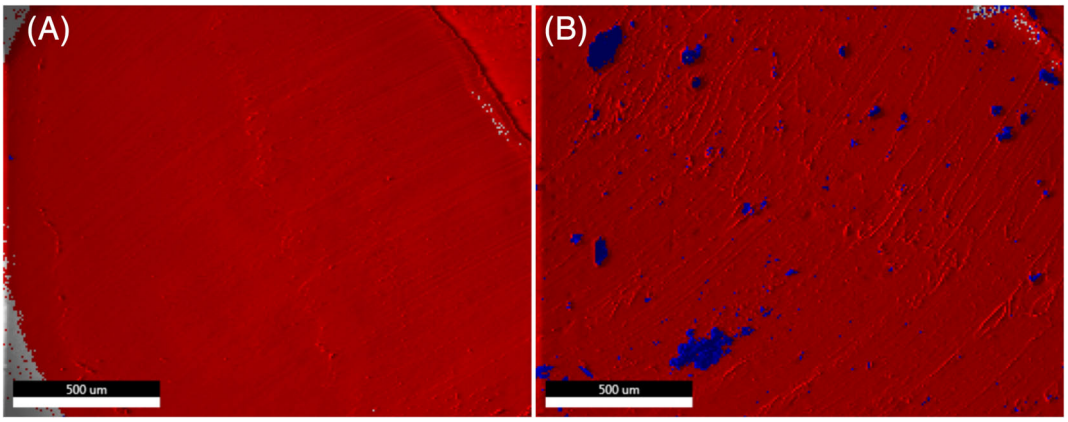

FIGURE 2 SEM-EDS images of 1.0% SS-limonene/PE,A, and 1.0% SS-H/PE, B. Colors added for clarity. Particles of the additive are highlighted in blue. PE, polyethylene; SEM-EDS, scanning electron microscopy-energy dispersive spectroscopy; SS, spherosilicate [Color figure can be viewed at wileyonlinelibrary.com]

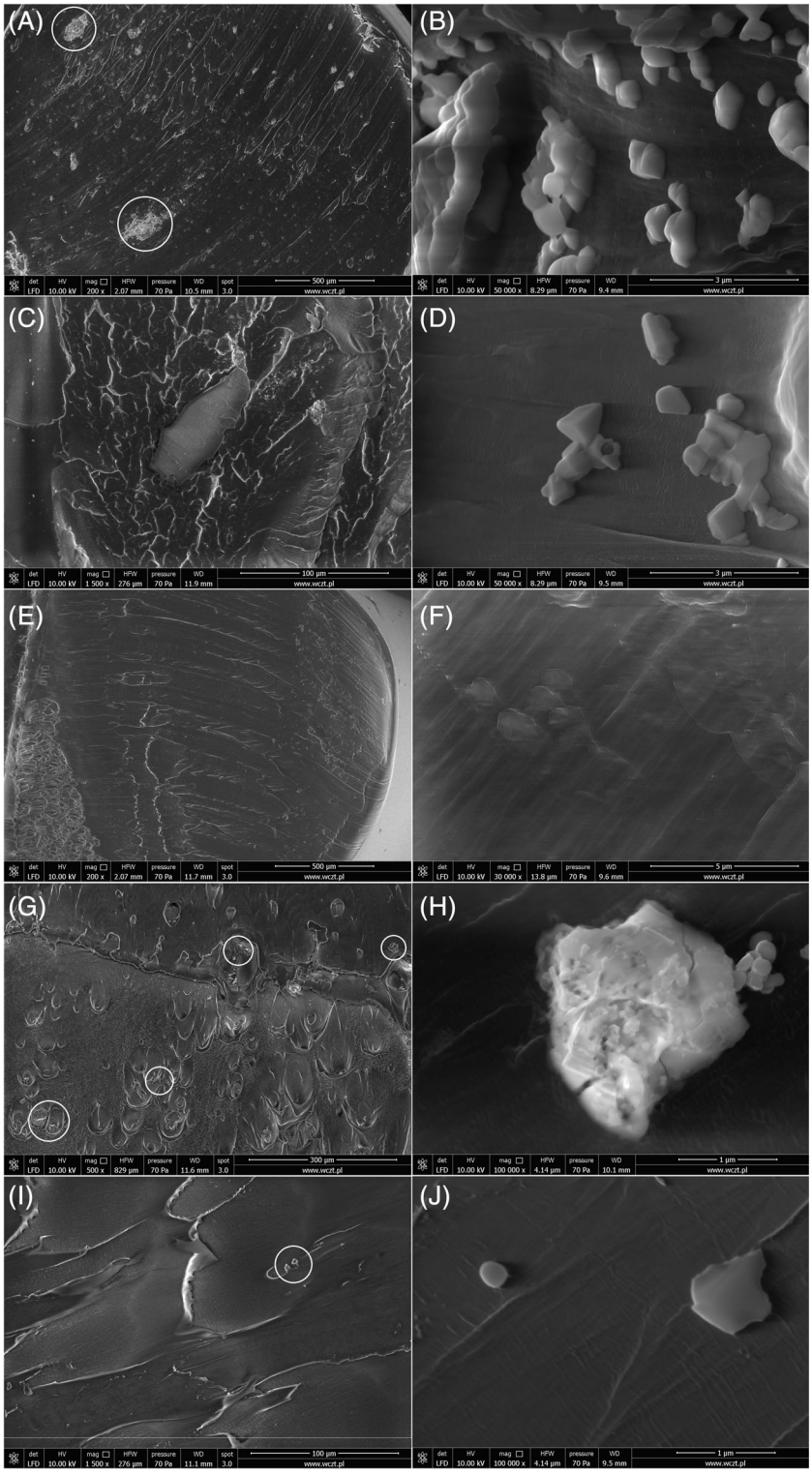

FIGURE 3 SEM images of SS/PE composites at different magnifications, showing visible particles of additives. 1% SS-H/PE, A and B; 0.5% SS-Vi/PE, C and D; 1% SS-limonene/PE, E and F; 1% SS-norbornene/PE, G and H; 1% SS-pinene/PE, I and J. PE, polyethylene; SEM, scanning electron microscopy; SS, spherosilicate

size,[26] however, much better dispersion was obtained for LDPE.[25] Also, the type of substituent surrounding the inorganic core played a huge factor in dispersion properties of the additive in PE matrix and with increasing substituent bulkiness the improvement in dispersion was observed.[22]

3.3 | XRD analysis of obtained composites

The obtained PE/SS composites were analyzed by XRD to assess their crystallinity indices (CI) and verify the impact of organosilicon additives on crystallinity level of

the PE matrix. This should not be confused with crystallization behavior, where the temperature and rate of crystallization are usually measured, instead of CI. The data are collected in Table 1.

For all examples, the CI stayed very close to the base value of 25.49% of neat PE. For PE/SS-pinene system, with the decreasing amount of the additive, crystallinity was increasing slightly, and for 0.1% concentration increased to the level above that of neat PE. A similar observation was made for SS-limonene, suggesting these compounds might serve as weak antiplasticizing agents at such loadings, as well as plasticizing agents at higher concentrations, as for 1.0% loading CI values are lower than that of neat PE. However, for full verification of this thesis, analyses with high additive loadings (eg, ~10%) would be required, which is economically unreasonable, as the proposed SS additives were tested for their effectiveness as PE modifiers at low concentrations (≤1%). Nevertheless, possible antiplasticizing effect was supported later by thermomechanical analysis (see Section 3.7). For SS-norbornene derivative, no clear correlation can be made due to the degradation of the additive and formation of agglomerates of polymerized material. In addition, virtually no change in CI was observed for SS-H/PE and SS-Vi/PE, as due to their poor dispersion in the polymer matrix (especially for SS-H/PE system), very little interaction between the additive and PE crystalline domains may occur. For comparison, Heeley et al. showed that addition of long chain-substituted silsesquioxanes to LDPE increased crystallinity of the samples slightly, but the loading of additives was substantial (10%).[34] Also, for octakis(octadecyl) spherosilicate, for the range of additive concentrations up to 10% the crystallinity change was not either consistent.[11] Joshi et al. made a similar statement for HDPE at the same loading of octamethylsilsesquioxane.[17] Frone et al. reported that for pentyl- and isopentyl-substituted SS CI decreased with increasing loading of the additives.[7]

TABLE 1 Crystallinity indices (CI) of the obtained composites

	Concentration of additive (%)		
	0.1	0.5	1.0
Additive	CI (%)		
Neat PE	25.49		
SS-H	–	25.48	25.21
SS-Vi	–	25.13	–
SS-limonene	26.04	24.80	24.85
SS-norbornene	25.40	26.36	25.45
SS-pinene	26.14	25.17	24.66

Abbreviations: PE, polyethylene; SS, spherosilicate.

3.4 | Mechanical studies

Two groups of specimens were subjected to mechanical analysis, that is, dumbbells and foils, and the results are collected in Tables 2 to 7 (Tables 2–4 in regard to dumbbells, Tables 5–7 to foils). The results for the dumbbells will be discussed first. Different conclusions can be

TABLE 2 Tensile strength of the SS/PE dumbbells

	Concentration of additive (%)		
	0.1	0.5	1.0
Additive	Tensile strength (MPa)		
Neat PE	13.08 ± 0.26		
SS-H	-	12.96 ± 0.42	13.47 ± 0.21
SS-Vi	-	13.37 ± 0.16	-
SS-limonene	13.38 ± 0.21	13.46 ± 0.23	14.34 ± 0.12
SS-norbornene	13.57 ± 0.08	13.03 ± 0.35	12.99 ± 0.31
SS-pinene	13.36 ± 0.23	12.97 ± 0.14	13.23 ± 0.18

Abbreviations: PE, polyethylene; SS, spherosilicate.

TABLE 3 Young's modulus of the SS/PE dumbbells

	Concentration of additive (%)		
	0.1	0.5	1.0
Additive	Young's modulus (MPa)		
Neat PE	91.68 ± 3.46		
SS-H	-	106.13 ± 4.08	94.30 ± 3.75
SS-Vi	-	87.07 ± 3.49	-
SS-limonene	97.40 ± 2.83	92.53 ± 3.53	112.22 ± 1.20
SS-norbornene	89.95 ± 2.92	98.31 ± 3.54	97.91 ± 0.98
SS-pinene	98.21 ± 1.29	89.95 ± 5.77	94.37 ± 6.20

Abbreviations: PE, polyethylene; SS, spherosilicate.

TABLE 4 Plastic elongation of the SS/PE dumbbells

	Concentration of additive (%)		
	0.1	0.5	1.0
Additive	Plastic elongation (%)		
Neat PE	60.38 ± 1.77		
SS-H	-	52.70 ± 2.13	60.12 ± 1.15
SS-Vi	-	63.94 ± 1.99	-
SS-limonene	58.64 ± 0.99	61.59 ± 1.51	56.35 ± 0.60
SS-norbornene	62.73 ± 1.30	56.81 ± 1.88	56.06 ± 1.89
SS-pinene	58.17 ± 0.77	60.06 ± 3.42	59.45 ± 2.97

Abbreviations: PE, polyethylene; SS, spherosilicate.

TABLE 5 Tensile strength of the SS/PE foils

Additive	Concentration of additive (%)		
	0.1	0.5	1.0
	Tensile strength (MPa)		
Neat PE	19.70 ± 0.95		
SS-H	-	15.64 ± 0.73	16.76 ± 1.06
SS-Vi	-	16.38 ± 0.64	-
SS-limonene	14.16 ± 0.48	16.14 ± 0.97	17.30 ± 0.99
SS-norbornene	15.78 ± 0.24	17.45 ± 1.05	19.10 ± 1.07
SS-pinene	17.02 ± 0.54	16.76 ± 0.97	15.05 ± 0.36

Abbreviations: PE, polyethylene; SS, spherosilicate.

TABLE 6 Young's modulus of the SS/PE foils

Additive	Concentration of additive (%)		
	0.1	0.5	1.0
	Young's modulus (MPa)		
Neat PE	213.82 ± 14.59		
SS-H	-	168.24 ± 9.13	169.78 ± 10.96
SS-Vi	-	149.89 ± 7.90	-
SS-limonene	118.69 ± 5.39	161.88 ± 8.68	178.88 ± 10.23
SS-norbornene	169.45 ± 9.03	174.09 ± 10.15	198.41 ± 20.81
SS-pinene	184.21 ± 7.73	176.20 ± 9.40	135.14 ± 8.48

Abbreviations: PE, polyethylene; SS, spherosilicate.

TABLE 7 Plastic elongation of the SS/PE foils

Additive	Concentration of additive (%)		
	0.1	0.5	1.0
	Plastic elongation (%)		
Neat PE	176.69 ± 11.63		
SS-H	-	143.83 ± 8.82	138.45 ± 6.41
SS-Vi	-	127.36 ± 5.43	-
SS-limonene	101.32 ± 4.64	161.25 ± 7.32	129.02 ± 6.95
SS-norbornene	136.65 ± 7.80	144.54 ± 9.13	169.42 ± 7.65
SS-pinene	137.73 ± 4.80	141.32 ± 6.63	193.93 ± 12.06

Abbreviations: PE, polyethylene; SS, spherosilicate.

drawn for these two types of samples, as the mechanical behavior of polymer in bulk and foil form differs, and the processing technology being used should be taken into account, as the dumbbells are produced by injection molding and foils by extrusion, which has an impact on polymer orientation in the finished product. For a number of systems, it was observed that the changes in mechanical properties of the obtained materials were rather small and often next to the level of SD. This may be due to two reasons, one is limited interaction between the additives and PE (PE forming strong internal interactions due to highly linear chain structure), and the second is small loadings of additives. The increased values of Young's modulus can be attributed to three factors. One is physical reinforcement of the polymer with solid additive particles or crystals of proper size with limited ability of dispersing in the PE matrix. Such conclusion can be drawn for dumbbells of PE/SS-H at 0.5% and PE/SS-norbornene at 0.5% and 1.0%. The second mode of reinforcement may be due to interaction (eg, van Der Waals forces, London dispersive forces) between molecules of well-dispersed additive and polymer chains or domains. Such effect may be observed for SS-pinene at 0.1% loading, where very good dispersion was observed, and the synthesized additive was a viscous, resin-like oil instead of crystalline solid, and simple physical reinforcement typical for solid fillers should not be expected. The effect was not linear, however, probably due to the limited amount of the additive able to undergo molecular or submicronic dispersion, and already achieving this critical concentration at the lowest loading tested. It was previously reported that cubic siloxanes have a tendency to form agglomerates or crystals of increasing size with their increasing loading, while some amount of the additive remains dispersed at nanoscopic scale in the polymer matrix.[18,43,44] For SS-pinene, based on SEM-EDS, good compatibilization of the additive may be stated, but at the same time very little change of mechanical parameters stayed was observed, therefore the interaction between the additive and matrix was rather weak. The last factor is the composition forming a polymer blend instead of a typical composite, which may apply for SS-limonene/PE, as it was speculated when discussing SEM-EDS analysis. The additive was proven to polymerize at the temperatures lower than that of PE processing, yet shown very good dispersion properties. SS-limonene at 1.0% loading showed the highest reinforcing effect of all the compositions, increasing Young's modulus of the obtained composite to 112 MPa. The effect of the additive was confirmed by tensile strength value, which was also notably increased at 1% concentration (14.3 MPa), showing improved rigidity of the obtained composite. For the factors decreasing the Young's modulus, the biggest contribution should be accounted for formation of loose particle agglomerates easily deforming under load. Such effect may be observed for SS-Vi/PE composite. Besides of that, the most important effects observed were the reduced plastic elongation for 0.5% SS-H/PE and for higher loadings of SS-norbornene. It may be explained similarly to the effect of increased Young's modulus for these systems, by introduction of poorly dispersed

particles, which resulted in material discontinuity in the bulk material. Such spots become centers of fracture in the sample under load. On the other hand, some improvement of plastic elongation was observed for SS-Vi/PE and 0.1% SS-norbornene/PE, suggesting that at a proper modifier particle size and concentration, the particles may isolate regions of polymer from total load exerted on the bulk material, thus reducing the effect of internal crack propagation.

For the foils, the deterioration of mechanical properties may be attributed to the distortion in polymer orientation, caused by the additive. The trends are clearly visible for SS-limonene and SS-norbornene, where with increasing additive loading, both Young's modulus and tensile strength increased, but in all cases were lower than that of the reference samples. This leads to a conclusion that as much as these modifiers showed some reinforcing character observed better for dumbbell specimens, their addition at any concentration caused distortion in polymer orientation in produced foils, thus reducing their toughness, which was also confirmed by reduced plastic elongation for these materials. For SS-pinene a trend for reducing Young's modulus and tensile strength was observed, together with increasing elongation, the 1% composition being more ductile than the reference. It showed slightly plasticizing effect of the additive at higher concentration, which was consistent with XRD data. For comparison, Nguyen et al. showed that mechanical properties of PE films modified with "bio-POSS" silsesquioxanes were heavily impaired.[35] Gao et al. reported that addition of vinylsilsesquioxane cage mixture (T_8 and T_{10}) initially improved mechanical parameters of HDPE such as Young's modulus or tensile strength, but with higher loadings (>6%) it weakened the material and for all the concentrations tested, elongation at break was reduced, but the work lacked information about the specimens preparation.[45] Grala et al. reported that for HDPE composites with aminopropyl-substituted silsesquioxanes, the mechanical properties degraded both for tensile tests as well as for impact tests, but some improvements were observed for impact strength of samples prepared by reactive blending with high density polyethylene grafted with maleic anhydride (HDPE-*g*-MA).[38]

3.5 | Thermal analysis

The TGA in air and nitrogen atmosphere were performed to assess thermal stability of the obtained composites. The temperatures of 5% mass loss, the onset of the decomposition event, and the temperatures of DTG peak were collected in the Table 8. It was observed that $T_{5\%}$ of all systems was increased, however the improvement was more prominent in air atmosphere, showing stabilizing effect of the additive on polymer matrix under oxidative conditions. The effect, however, was not consistent with increasing concentration of additives in air atmosphere, and in nitrogen, all the compounds showed basically identical effect independent of additive concentration. In addition, T_{onset} and T_{DTG} were increased for all the systems both in air and nitrogen, showing that during degradation event, the modifiers present stabilizing effect on the compositions formed. One needs to keep in mind that at these temperatures, the compositions exist in molten form, no longer meeting the definition of a composite, and rather forming a reactive mixture of molten, cracking polyolefin and the additive, emitting high volumes of gaseous decomposition products (Figure 4). In addition, the loadings of the additives were small; therefore the possibility of an additive forming a protective layer of decomposition products is rather small too. Instead, other factors should be taken into account, for example, molecules of the additive reacting with free radicals of the polymer chains breaking down. It would explain the almost identical $T_{5\%}$ parameter values for all the concentrations of the additives in argon, as only very small, critical concentration of additive is needed to react with such radicals, being usually present in very low concentration in the system. Fina et al. proposed mediating effect of aluminasilsesquioxane on the decomposition mechanism of polypropylene, however the effect was linked to the presence of Al atom in the silsesquioxanes structure.[46] Nonetheless, the authors as well doubted the mechanism of formation of protective layer of the additive decomposition products. It is known that an average Si—C bond is of slightly lower dissociation energy than C—C bond and the resulting silicon radical may take a part in the mechanism of recombination and stabilization of alkyl radicals formed by decomposing polyolefin.[47] This may be the main mechanism of PE thermal stabilization with SS systems, which would explain the almost identical $T_{5\%}$ parameter values for all the additives tested, all of them sharing the same structural feature being the siloxane core. In addition, the cyclic substituents attached to the silsesquioxane core contain secondary and tertiary carbon atoms, which may also take a part in recombination of radicals to more stable intermediates.[47] Such intermediates are also formed during thermal cracking of PE and commonly called naphthene. This mechanism may take place for the experiments in air atmosphere, as each of the tested compounds showed a different thermal profile for the degradation of PE composition, also depending on the additive concentration, which may suggest more complex kinetic relationship between chemical structure of the additive and the course of the degradation event.

TABLE 8 Thermal parameters of SS/PE composites from TGA measurements

Measurements in air atmosphere									
	Concentration of additive (%)								
	0.1			0.5			1.0		
Additive	$T_{5\%}$ (°C)	T_{onset} (°C)	T_{DTG} (°C)	$T_{5\%}$ (°C)	T_{onset} (°C)	T_{DTG} (°C)	$T_{5\%}$ (°C)	T_{onset} (°C)	T_{DTG} (°C)
Neat PE	$T_{5\%}$ (°C) = 348.3			T_{onset} (°C) = 382.4			T_{DTG} (°C) = 418.3		
SS-H	–	–	–	362.2	397.5	441.5	355.2	393.3	435.8
SS-Vi	–	–	–	360.8	395.5	425.5	–	–	–
SS-limonene	359.2	389.7	434.7	370.8	389.2	440.4	363.4	401.4	433.1
SS-norbornene	364.5	396.7	451.3	355.8	390.3	420.1	359.5	397.3	431.0
SS-pinene	362.0	399.4	441.7	370.0	401.0	449.0	360.9	404.8	444.3
Measurements in nitrogen atmosphere									
	Concentration of additive (%)								
	0.1			0.5			1.0		
Additive	$T_{5\%}$ (°C)	T_{onset} (°C)	T_{DTG} (°C)	$T_{5\%}$ (°C)	T_{onset} (°C)	T_{DTG} (°C)	$T_{5\%}$ (°C)	T_{onset} (°C)	T_{DTG} (°C)
Neat PE	$T_{5\%}$ (°C) = 441.8			T_{onset} (°C) = 469.3			T_{DTG} (°C) = 477.9		
SS-H	–	–	–	446.7	475.6	489.0	445.6	482.5	489.5
SS-Vi	–	–	–	446.3	476.3	489.9	–	–	–
SS-limonene	447.7	470.6	487.1	447.4	476.5	489.8	445.5	479.6	486.9
SS-norbornene	445.1	477.8	486.5	445.4	478.7	488.3	446.4	482.7	489.4
SS-pinene	445.5	476.9	485.6	446.0	471.1	486.6	447.8	472.2	488.0

Abbreviations: PE, polyethylene; SS, spherosilicate; TGA, thermogravimetric analysis.

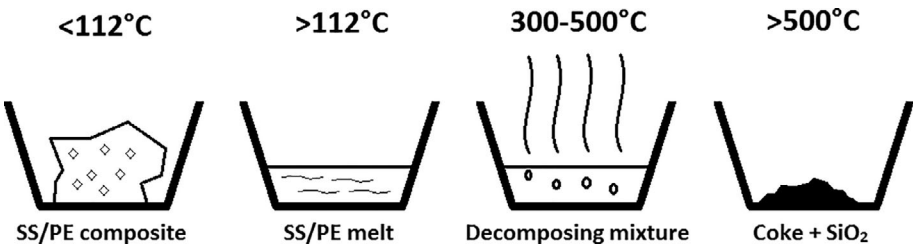

FIGURE 4 Steps of decomposition of SS/PE samples. PE, polyethylene; SS, spherosilicate

Frone et al. reported that pentyl- and isopentyl-substituted SS improved thermal stability of PE composites, however, only on the basis of $T_{5\%}$ parameter.[7] In comparison to SS-H and SS-Vi, the new derivatives were comparable in performance, with the biggest improvement being observed for 1% SS-pinene/PE in air than that of 1% SS-H/PE. However, SS-norbornene at 0.1% in air showed better performance than the other two additives at the same concentration.

The DSC was performed to determine the impact of the additives on melting and crystallization temperatures of the obtained composites. The data are collected in the Table 9. Generally, for most of the systems, increased crystallization temperature was observed, which indicated the nucleating effect of the additives. The strongest nucleating effect was observed for SS-H derivative, as due to poor miscibility with the polymer matrix, it was present in a form of particles and particle agglomerates within PE, providing centers of crystallization. A similar conclusion may be drawn for SS-norbornene and SS-limonene, both compounds forming particles of polymerized additive. SS-pinene showed almost no nucleating activity, as it was verified by DSC to be in a liquid state under the temperature of PE crystallization. Also, with different loading of the additives, no appreciative difference in crystallization temperatures was observed, meaning there is a critical concentration of the modifier, above which the crystallization behavior is not further modified. On the other hand, the small changes of melting temperature of the systems can be associated with the mean size of PE

TABLE 9 Melting and crystallization temperatures of obtained composites

Additive	Concentration of additive (%)			Concentration of additive (%)		
	0.1	0.5	1.0	0.1	0.5	1.0
	Melting temperature (°C)			Crystallization temperature (°C)		
Neat PE	112.4			98.8		
SS-H	–	112.2	112.2	–	99.6	99.7
SS-Vi	–	111.8	–	–	99.2	–
SS-limonene	112.8	112.5	112.4	99.6	99.6	99.6
SS-norbornene	113.9	112.4	112.4	98.8	99.4	99.4
SS-pinene	113.1	113.0	113.6	99.0	98.8	98.8

Abbreviations: PE, polyethylene; SS, spherosilicate.

TABLE 10 MFR values for SS/PE composites

Additive	Concentration of additive (%)		
	0.1	0.5	1.0
	MFR (g/10 min)		
Neat PE	2.02		
SS-H	–	1.85	1.87
SS-Vi	–	2.05	–
SS-limonene	1.88	1.86	1.94
SS-norbornene	1.86	1.86	1.86
SS-pinene	1.86	1.80	1.73

Abbreviations: PE, polyethylene; SS, spherosilicate.

TABLE 11 HDT values for SS/PE composites

Additive	Concentration of additive (%)		
	0.1	0.5	1.0
	HDT (°C)		
Neat PE	36.8		
SS-H	–	36.9	36.9
SS-Vi	–	36.6	–
SS-limonene	38.5	37.0	36.7
SS-norbornene	36.2	36.5	36.9
SS-pinene	36.8	36.9	37.1

Abbreviations: HDT, heat deflection temperature; PE, polyethylene; SS, spherosilicate.

crystallites being slightly modified by the additives. Therefore, SS-H and SS-Vi promoted formation of smaller crystallites, while SS-pinene promoted formation of larger crystallites, thus increasing melting temperature. The other modifiers showed little impact on this property, besides of the samples with 0.1% loading. Generally, the melting temperatures were dependent on the additive concentration, which shows this parameter can be controlled by the additive loading. Joshi et al. concluded that, when octamethylsilsesquioxane was applied as a nucleating agent for HDPE, appreciable nucleation effect was observed only at loading as high as 10%, but the chosen derivative known for rather poor dispersion properties in PE matrix.[17]

3.6 | Rheological analysis

The rheological analysis was performed by measuring the MFR parameter. It presents the ease of molten polymer to flow under static load, which is the basic parameter showing the level of viscosity of a given thermoplastic under the temperature close to the processing parameters. The results are collected in Table 10. In almost all examples, decrease of flow rate was observed. It is common for polymer additives, fillers especially, to have such an impact on the compositions formed, as the introduced particles create additional turbulences in flowing material. For highly dispersed additives such as SS-pinene (possibly dissolving in the molten polyolefin), the entangling effect of bulky SS molecules interacting with polymer chains may occur. It is interesting to note that SS-Vi slightly increased MFR. It may be due to relatively smooth surface and elongated shape of modifier grains as visible by SEM, or further dispersion of the additive in molten matrix, resulting in low shear. Barczewski et al. observed a significant decrease of kinetic viscosity of LDPE modified with heptaisobutylvinylsilsesquioxane at low shear rates, and the effect was improved with increasing amount of the additive used.[10]

3.7 | Thermomechanical analysis

Heat deflection temperature (HDT) analysis was performed to study samples behavior under static load and increasing temperature. The results are collected in

Table 11. For most compositions, the changes are small. However, an interesting observation was made for SS-limonene series, where with the declining concentration of additive, the measured HDT value was increasing, being well above the reference for 0.1% loading composition. This supports the suggestion of the additive working as an antiplasticizing agent at low concentration, as stated during discussion of XRD analysis. For the rest of the systems, the changes are small and increasing HDT values correlate with increasing additive loading, showing small reinforcing action of the additives on the composites being subjected to such type of stress.

4 | CONCLUSIONS

New SS derivatives have been tested as functional additives for PE. Good dispersion properties of SS-limonene and SS-pinene have been observed in comparison to SS-H and SS-Vi derivatives known from literature reports, as well as some silsesquioxanes with small alkyl substituents, like octamethylsilsesquioxane, proving the compatibilizing role of the large alkyl substituents surrounding the siloxane core. On the other hand, as to be expected, bulky SS were not as compatible with PE matrix as long chain-substituted ones reported in the literature. SS-norbornene and SS-limonene showed tendency of polymerization at elevated temperatures, which led to formation of agglomerates of the first additive in PE matrix, but did not disturb dispersion of the latter derivative, thus resulting in a formation of well-mixed polymer blend. An interesting thermal behavior of SS-norbornene thermal degradation was observed and described. The foils prepared from the SS/PE composites showed poor mechanical parameters besides of slight increase of SS-pinene/PE ductility at 1% loading. For injection-molded specimens, little change of properties was found for a number of systems, however some improvements were observed. SS-limonene showed good reinforcing action, increasing both Young's modulus and tensile strength of PE, therefore forming a tougher composite with PE matrix. Crystallinity of PE was slightly affected by the additives, showing the impact of the derivatives on polymer crystal/spherulite formation, which was also confirmed by changed melting and crystallization temperatures measured by DSC and proved weak nucleating effect of the modifiers and their ability to modify the mean crystallite size. The obtained compositions were characterized by improved thermal stability showed by DTG peak of degradation event, as well as the onset temperature of the degradation event and the temperature of 5% mass loss. The SS additives were proven to serve as inhibitors of high temperature decomposition of PE, especially in oxidative atmosphere.

ACKNOWLEDGMENTS

The authors gratefully acknowledge the financial support from National Science Centre, Poland (project no. UMO-2018/29/N/ST5/00868), and National Centre for Research and Development, Poland (project no. PBS3/A1/16/2015).

ORCID

Dariusz Brząkalski https://orcid.org/0000-0003-0773-0041

REFERENCES

[1] M. Chanda, S. K. Roy, *Industrial Polymers, Specialty Polymers, and Their Applications*, CRC Press, Boca Raton, FL **2009**.
[2] P. Cheremisinoff, *Handbook of Engineering Polymeric Materials*, Marcel Dekker, New York, NY **1997**.
[3] A. Kumar, R. K. Gupta, *Fundamentals of Polymer Engineering*, Marcel Dekker, New York, NY **2003**.
[4] M. Xanthos, *Functional Fillers for Plastics*, Wiley-VCH, Weinheim, Germany **2010**.
[5] H. Liu, S. I. Kondo, N. Takeda, M. Unno, *J. Am. Chem. Soc.* **2008**, *130*, 10074.
[6] Y. Du, H. Liu, *Dalton Trans.* **2020**, *49*, 1.
[7] A. Nicoleta, F. Xavier, C. Radovici, D. Mihaela, *Compos. B* **2013**, *50*, 98.
[8] F. Xavier, D. Mihaela, A. Nicoleta, C. Radovici, C. Nicolae, *Polymer* **2013**, *54*, 2347.
[9] A. Niemczyk, K. Dziubek, *J. Therm. Anal. Calorim.* **2016**, *125*, 1287.
[10] M. Barczewski, D. Czarnecka-Komorowska, J. Andrzejewski, T. Sterzyński, M. Dutkiewicz, B. Dudziec, *Polimery/Polymers* **2013**, *58*, 805.
[11] E. L. Heeley, D. J. Hughes, P. G. Taylor, A. R. Bassindale, *RSC Adv.* **2015**, *5*, 34709.
[12] M. Fréchette, M. Guo, É. David, D. Min, S. Li, in *2017 IEEE Conf. on Electrical Insulation and Dielectric Phenomena* **2017**, pp. 501–504.
[13] M. Guo, É. David, M. Fréchette, N. R. Demarquette, *Polymer* **2017**, *115*, 60.
[14] M. Guo, É. David, M. Fréchette, N. R. Demarquette, in *2016 IEEE Conf. on Electrical Insulation and Dielectric Phenomena* **2016**, pp. 647–650.
[15] M. J. Hato, S. S. Ray, A. S. Luyt, *Mol. Mater. Eng.* **2008**, *293*, 752.
[16] M. J. Hato, S. S. Ray, S. Africa, A. S. Luyt, *Adv. Sci. Lett.* **2011**, *4*, 3585.
[17] M. Joshi, B. S. Butola, *Polymer* **2004**, *45*, 4953.
[18] M. Joshi, B. S. Butola, G. Simon, N. Kukaleva, *Macromolecules* **2006**, *39*, 1839.
[19] W. Li, T. Chen, C. Guan, D. Gong, J. Mu, Z. Chen, Q. Zhou, *Ind. Eng. Chem. Res.* **2015**, *54*, 1478.
[20] S. Lim, E. Hong, H. J. Choi, I. Chin, *J. Ind. Eng. Chem.* **2010**, *16*, 189.
[21] S. Lim, J. Y. Lee, H. J. Choi, I. Chin, *Polym. Bull.* **2015**, *72*, 2331.

[22] M. Guo, M. Frechette, É. David, N. R. Demarquette, J. Daigle, in *IEEE Trans. Dielectr. Electr. Insul*. **2017**, pp. 798–807.
[23] Z. Xu, M. Guo, M. Fréchette, É. David, G. Chen, in *2016 IEEE Conf. on Electrical Insulation and Dielectric Phenomena* **2016**, pp. 679–682.
[24] P. Scapini, C. A. Figueroa, C. L. G. Amorim, G. Machado, R. S. Mauler, J. S. Crespo, R. V. Oliviera, *Polym. Int.* **2010**, *59*, 175.
[25] M. F. Fréchette, S. B. Ghafarizadeh, T. T. Ahn, S. Vadeboncoeur, M. Guo, E. David, in *1st Int. Conf. on Electrical Materials and Power Equipment, Xi'an, China* **2017**, pp. 221–224.
[26] M. F. Fréchette, M. Guo, S. Savoie, C. Vanga-Bouanga, E. David, in *Annual Report Conf. on Electrical Insulation and Dielectric Phenomena, CEIDP* **2013**, pp. 742–745.
[27] M. Guo, M. F. Fréchette, E. David, H. Couderc, S. Savoie, C. V. Bouanga, N. R. Demarquette, in *2013 Electrical Insulation Conf*. **2013**, pp. 444–448.
[28] M. Guo, M. Fréchette, É. David, N. R. Demarquette, in *2016 Electrical Insulation Conf*. **2016**, pp. 297–300.
[29] M. Guo, M. Fréchette, É. David, N. R. Demarquette, J. Daigle, in *2014 Annual Report Conf. on Electrical Insulation and Dielectric Phenomena* **2014**, pp. 731–734.
[30] M. Guo, M. Frechette, N. R. Demarquette, E. David, in *Proc. 2014 Int. Symp. on Electrical Insulation and Materials* **2014**, pp. 61–64.
[31] M. Guo, M. F. Fréchette, E. David, H. Couderc, N. R. Demarquette, in *2013 Annual Report Conf. on Electrical Insulation and Dielectric Phenomena Effect* **2013**, pp. 760–763.
[32] B. Safarikova, A. Kalendova, V. Habrova, S. Zatloukalova, M. Machovsky, in *AIP Conf. Proc*. **2014**, pp. 106–109.
[33] Z. Xu, G. Chen, M. Guo, É. David, M. Fréchette, in *2015 Annual Report Conf. on Electrical Insulation and Dielectric Phenomena* **2015**, pp. 543–546.
[34] E. L. Heeley, D. J. Hughes, Y. El, P. G. Taylor, A. R. Bassindale, *Eur. Polym. J.* **2014**, *51*, 45.
[35] T.-A. Nguyen, F. Mannle, Ø. W. Gregersen, *Int. J. Adhes. Adhes.* **2012**, *38*, 117.
[36] T. Nguyen, Ø. W. Gregersen, F. Männle, *Polymers* **2015**, *7*, 1522.
[37] M. Grala, Z. Bartczak, K. Gadzinowska, in *ECCM15-15TH European Conf. on Composite Material* **2012**, pp. 1–2.
[38] M. Grala, Z. Bartczak, *Polym. Eng. Sci.* **2014**, *55*, 2058.
[39] E. Morici, A. Di Bartolo, R. Arrigo, N. Tzankova Dintcheva, *Adv. Polym. Technol.* **2016**, *21673*, 1.
[40] M. Osińska-Broniarz, A. Martyła, A. Sierczyńska, B. Marciniec, R. Przekop, *Przem. Chem.* **2017**, *96*, 1250.
[41] N. L. Dias Filho, H. A. De Aquino, G. Pires, L. Caetano, *J. Braz. Chem. Soc.* **2006**, *17*, 533.
[42] S. Kotha, S. Banerjee, *RSC Adv.* **2013**, *3*, 7642.
[43] G. Cicala, I. Blanco, A. Latteri, G. Ognibene, F. A. Bottino, M. Elena, *Polymers* **2017**, *9*, 281.
[44] A. Fina, D. Tabuani, G. Camino, *Eur. Polym. J.* **2010**, *46*, 14.
[45] J. Gao, D. Hua, Y. Du, X. Li, *Polym. Plast. Technol. Eng.* **2011**, *50*, 1429.
[46] A. Fina, S. Bocchini, G. Camino, *Polym Degrad Stabil.* **2008**, *93*, 1647.
[47] G. Camino, S. M. Lomakin, M. Lageard, *Polymer* **2002**, *43*, 2011.

SUPPORTING INFORMATION

Additional supporting information may be found online in the Supporting Information section at the end of this article.

How to cite this article: Brząkalski D, Przekop RE, Dobrosielska M, Sztorch B, Marciniak P, Marciniec B. Highly bulky spherosilicates as functional additives for polyethylene processing—Influence on mechanical and thermal properties. *Polymer Composites*. 2020; 1–14. https://doi.org/10.1002/pc.25628

Supporting Information for

Highly bulky spherosilicates as functional additives for polyethylene processing – influence on mechanical and thermal properties

Dariusz Brząkalski[a]*, Robert E. Przekop[b], Marta Dobrosielska[b], Bogna Sztorch[b], Piotr Marciniak[b], Bogdan Marciniec[a,b]

[a]*Faculty of Chemistry, Adam Mickiewicz University in Poznań, ul. Uniwersytetu Poznańskiego 8, 61-614 Poznań, Poland*

[b]*Centre for Advanced Technologies, Adam Mickiewicz University in Poznań, ul. Uniwersytetu Poznańskiego 10, 61-614 Poznań, Poland*

Corresponding Author: *D.B.: e-mail: dariusz.brzakalski@amu.edu.pl

Table of contents:

1. Processing of XRD data

The data collected were processed with OriginPro 2016 Suite. To calculate Crystallinity Index (CI), the diffractograms obtained were deconvoluted by Pearson VII deconvolution model, with exponential baseline, which allowed for correction in the low 2θ region, where unwanted small-angle diffraction was observed. Such a method allowed for obtaining $R^2 \geq 0.994$ for all examples. Other deconvolution models (e.g. Gaussian), as well as different methods for baseline correction offered less precise results. CI was calculated from area integrity of such obtained crystalline phase peaks divided by the sum of all crystalline and non-crystalline peaks area (Figure 1).

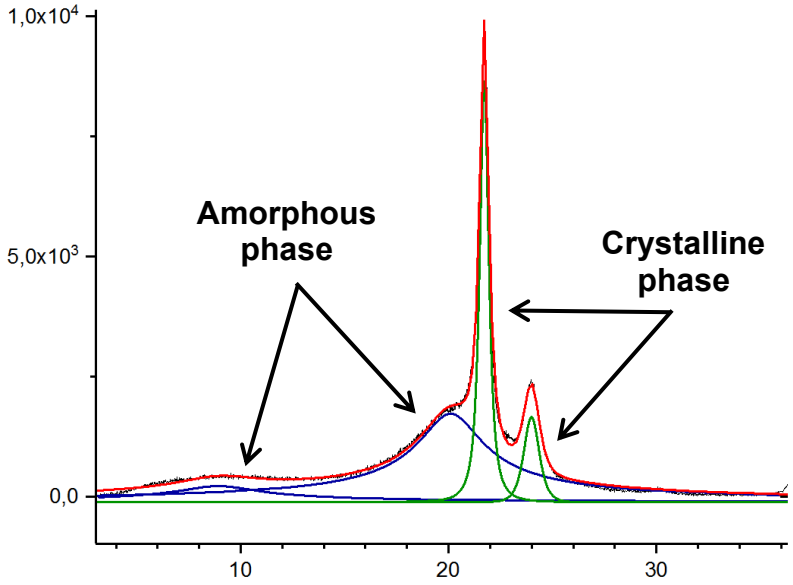

Figure 1: The deconvolution diagram for neat PE. Red – initial diffractogram, blue – deconvoluted amorphous phase, green – deconvoluted crystalline phase.

2. Table of isolated compounds:

Structure	Compound #	Spectra page:
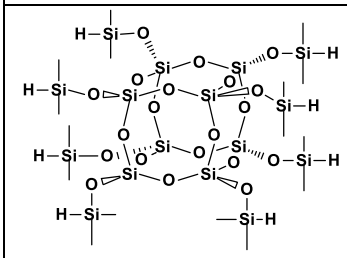 SS-H	1	
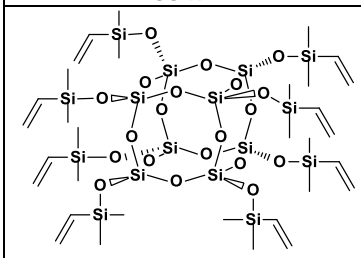 SS-Vi	2	
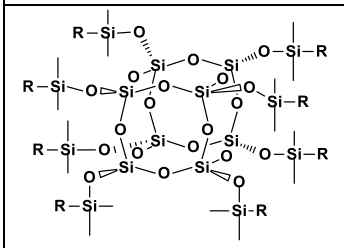 SS-Norbornene R = 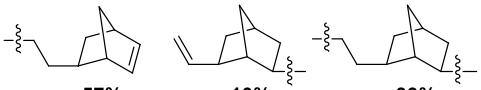 57% 10% 33%	3	
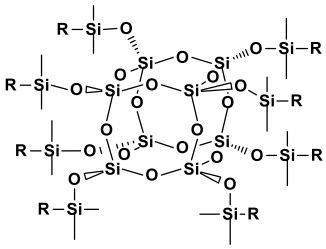 SS-Limonene R = 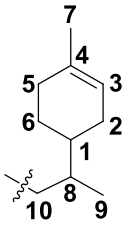	4	
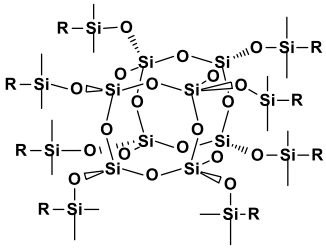 SS-Pinene R = 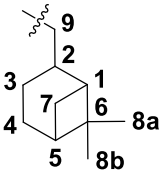	5	

3. Characterization data of the products:
1,3,5,7,9,11,13,15-hepta(dimethylsiloxy)-pentacyclo[9.5.1.1^{3,9}.1^{5,15}.1^{7,13}]octasiloxane (1)

^{1}H NMR (400 MHz, $CDCl_3$): δ (ppm) = 4.73 (sep, J=2.8Hz, 8H, SiH), 0.26 (d, J=2.8Hz, 48H, $SiMe_2$);
^{13}C NMR (101 MHz, $CDCl_3$): δ (ppm) = 0.23 ($SiMe_2$);
^{29}Si NMR (79,5 MHz, $CDCl_3$): δ (ppm) = -1.41 ($SiMe_2$), -108.68 (core).
IR (ATR): 2965, 2905, 2141, 1254, 1069, 889, 834, 769-726, 650, 628, 541.

^{1}H NMR *($CDCl_3$, 400MHz):*

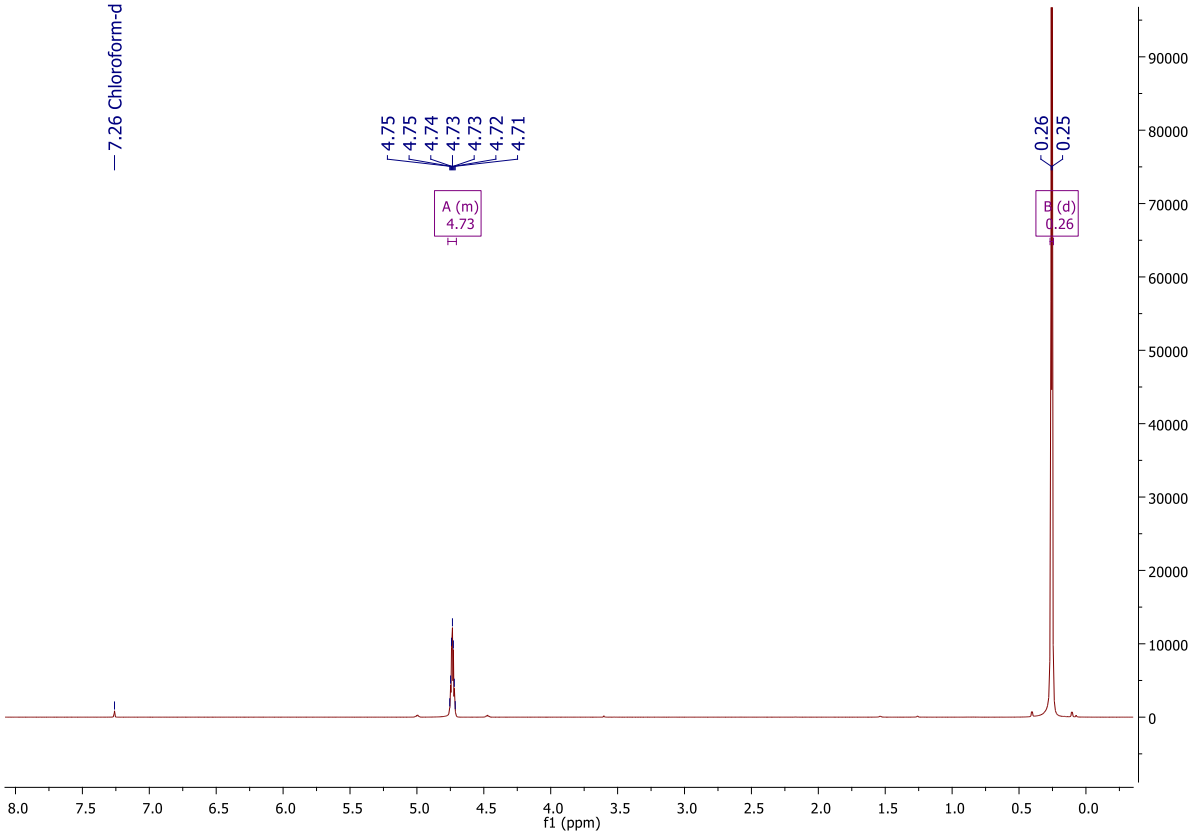

^{13}C NMR (101 MHz, $CDCl_3$)

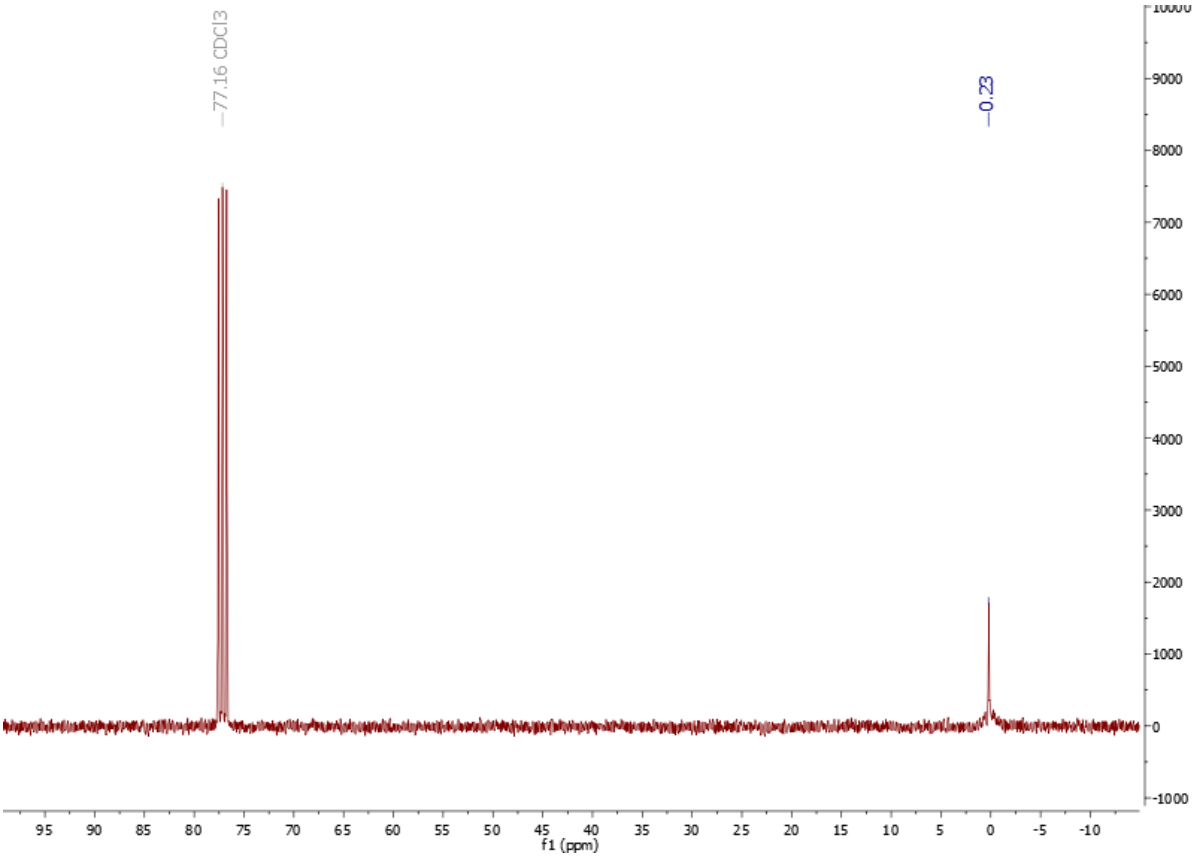

^{29}Si NMR (79,5 MHz, $CDCl_3$)

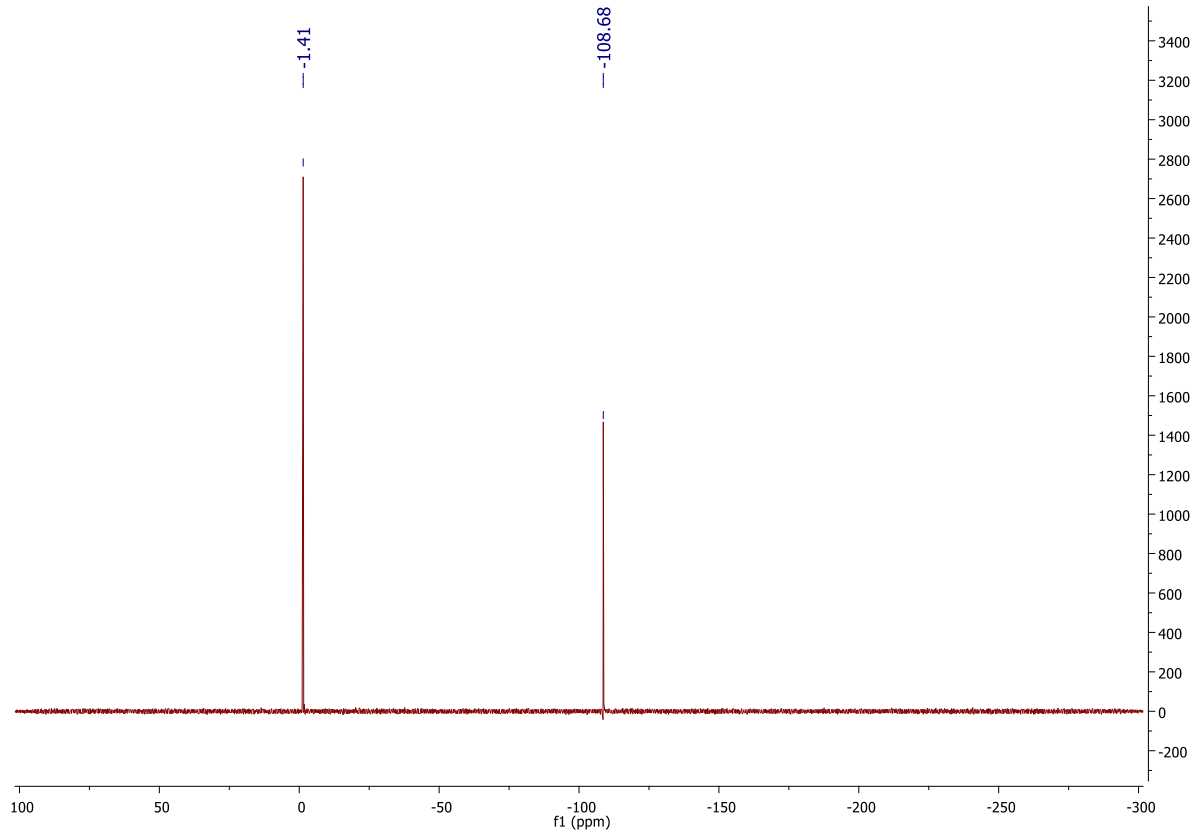

1,3,5,7,9,11,13,15-hepta(dimethylvinylsiloxy)-pentacyclo[9.5.1.1^{3,9}.1^{5,15}.1^{7,13}]octasiloxane (2)

^{1}H NMR (400 MHz, $CDCl_3$): δ (ppm) = 6.13 (dd, J_1=20.2Hz, J_2=14.9Hz, 8H, -C<u>H</u>=CH_2), 5.96 (dd, J_1=14.9Hz, J_2=4.0Hz, 8H, -CH=C<u>H</u>$_2$), 5.79 (dd, J1=20.2Hz, J2=4.0Hz, 8H, -CH=C<u>H</u>$_2$), 0.21 (s, 48H, $SiMe_2$);
^{13}C NMR (101 MHz, $CDCl_3$): δ (ppm) = 138.09, 132.61 (-CH=CH_2), -00.06 ($SiMe_2$);
^{29}Si NMR (79,5 MHz, $CDCl_3$): δ (ppm) = 0.51 ($SiMe_2$), -109.14 (core).
IR (ATR): 3068, 3027, 2988, 2962, 1603, 1408, 1276, 1081, 1002, 967, 775, 568.

^{1}H NMR *($CDCl_3$, 400MHz):*

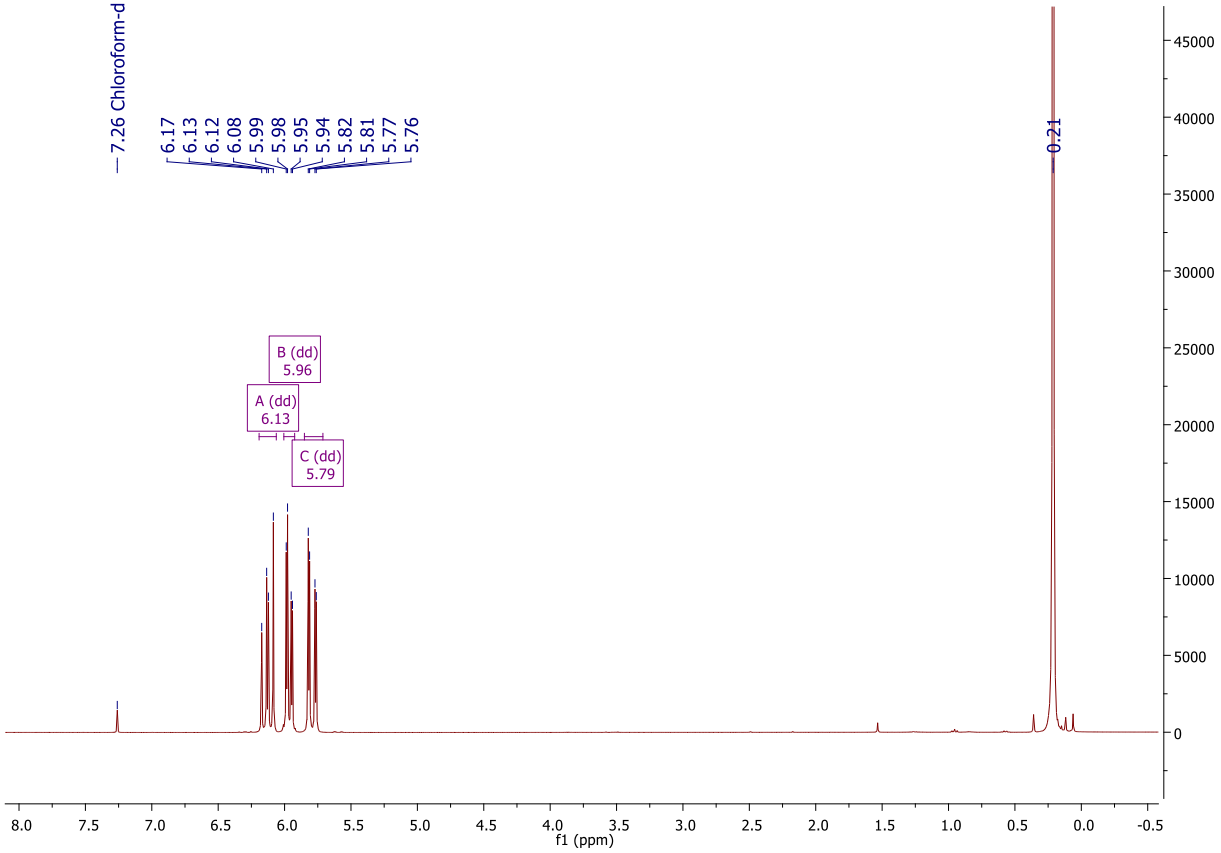

^{13}C NMR *($CDCl_3$, 101 MHz):*

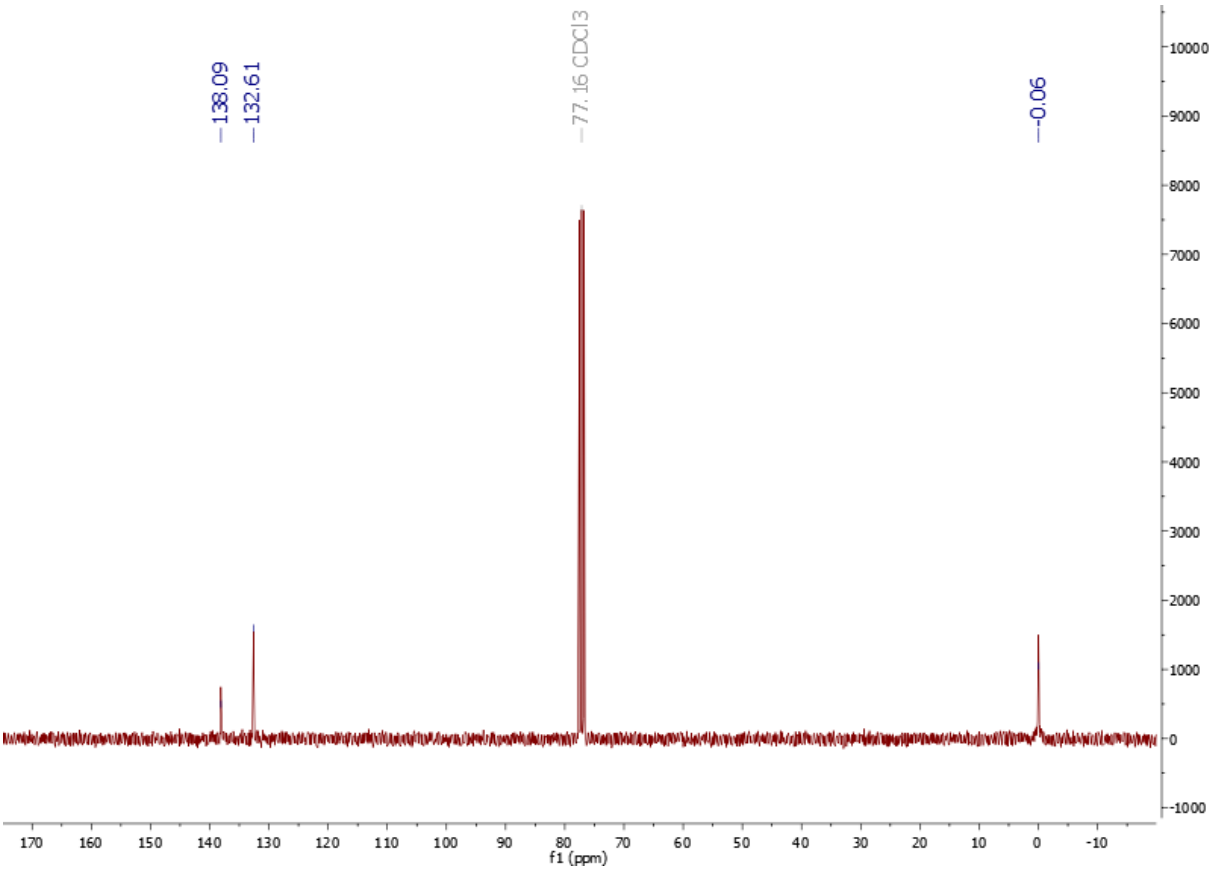

^{29}Si NMR *($CDCl_3$, 79.5 MHz):*

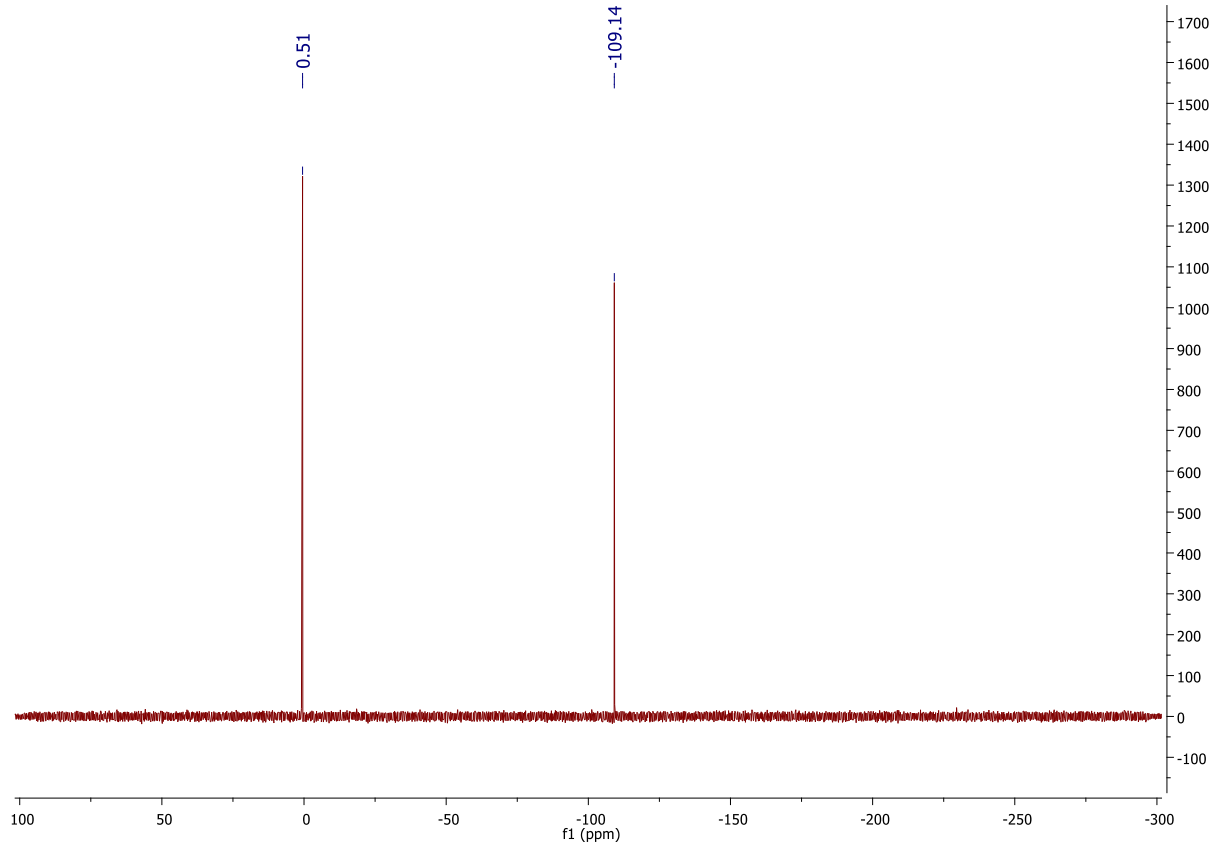

1,3,5,7,9,11,13,15-octa(dimethyl((norbornyl)silyl)-pentacyclo[9.5.1.1^{3,9}.1^{5,15}.1^{7,13}]octasiloxane, isomer mixture (3)

^{1}H NMR (400 MHz, $CDCl_3$): δ (ppm) = 6.10-5.91 (m, ring -C=CH, endo isomer), 6.02-6.00 (m, ring -C=CH, exo isomer), 5.80-5.68 (m, vinyl -CH=C$\underline{H_2}$), 5.04-4.83 (m, vinyl -CH=C$\underline{H_2}$), 2.77 (d, J=18.9Hz), 2.54-2.53, 2.29-2.09, 2.03-1.71 (m, norbornyl ring), 1.54 (s, norbornyl ring), 1.40-1.05 (m, norbornyl ring), 0.68-0.45 ($SiCH_2$, SiCH), 0.13, 0.10 ($SiMe_2$);
^{13}C NMR (101 MHz, $CDCl_3$): δ (ppm) = 137.06, 136.38, 132.44 (C=C), 49.67, 46.10, 45.34, 45.13, 43.19, 42.73, 42.35, 42.23, 41.98, 39.88, 39.15, 38.59, 37.71, 37.01, 33.25, 32.56, 29.69, 27.89, 27.29, 26.75, 17.09, 16.74 (norbornyl substituent), 0.68, -0.19, -1.09, -2.62 ($SiMe_2$);
^{29}Si NMR (79,5 MHz, $CDCl_3$): δ (ppm) = 12.56 ($SiMe_2$), -109.01 (core).
IR (ATR): 3056, 2942-2864, 1251, 1162-1066, 896, 828-718, 544.

^{1}H NMR *($CDCl_3$, 400MHz):*

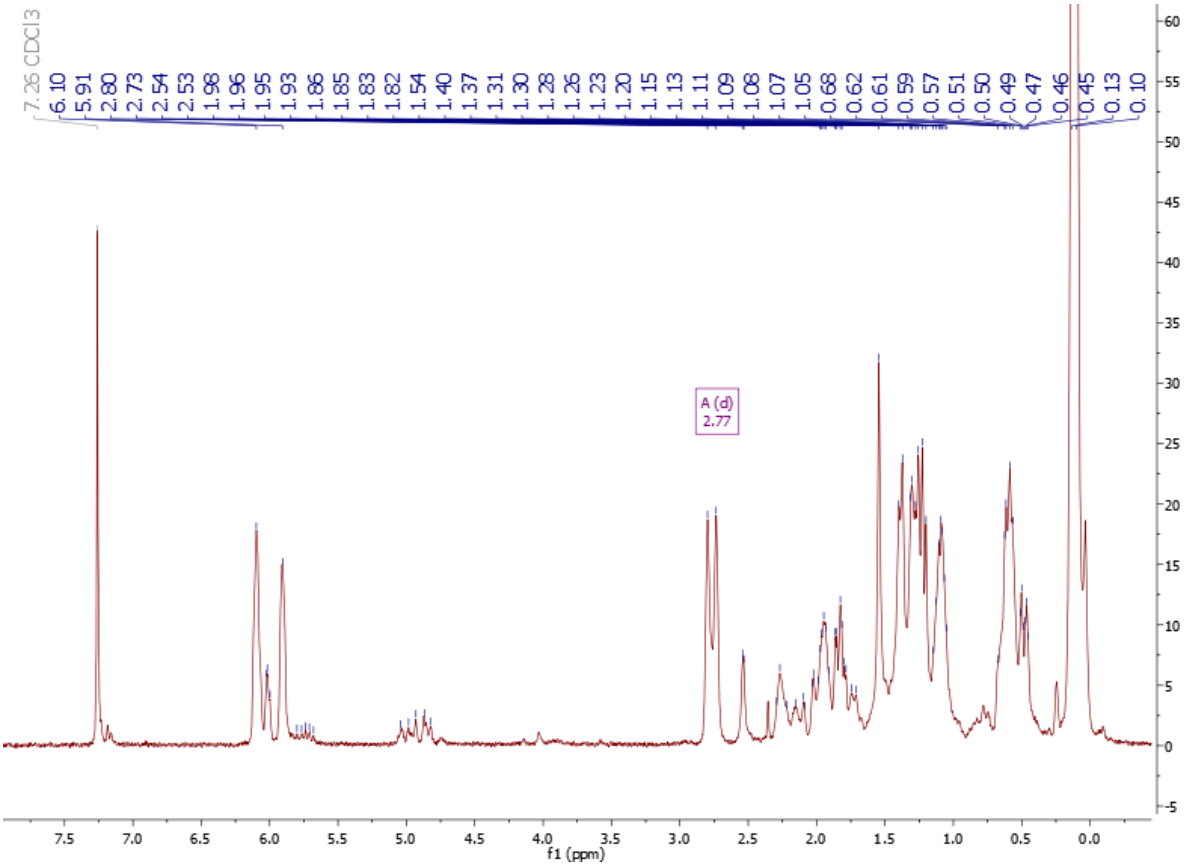

^{13}C NMR *(101 MHz, $CDCl_3$):*

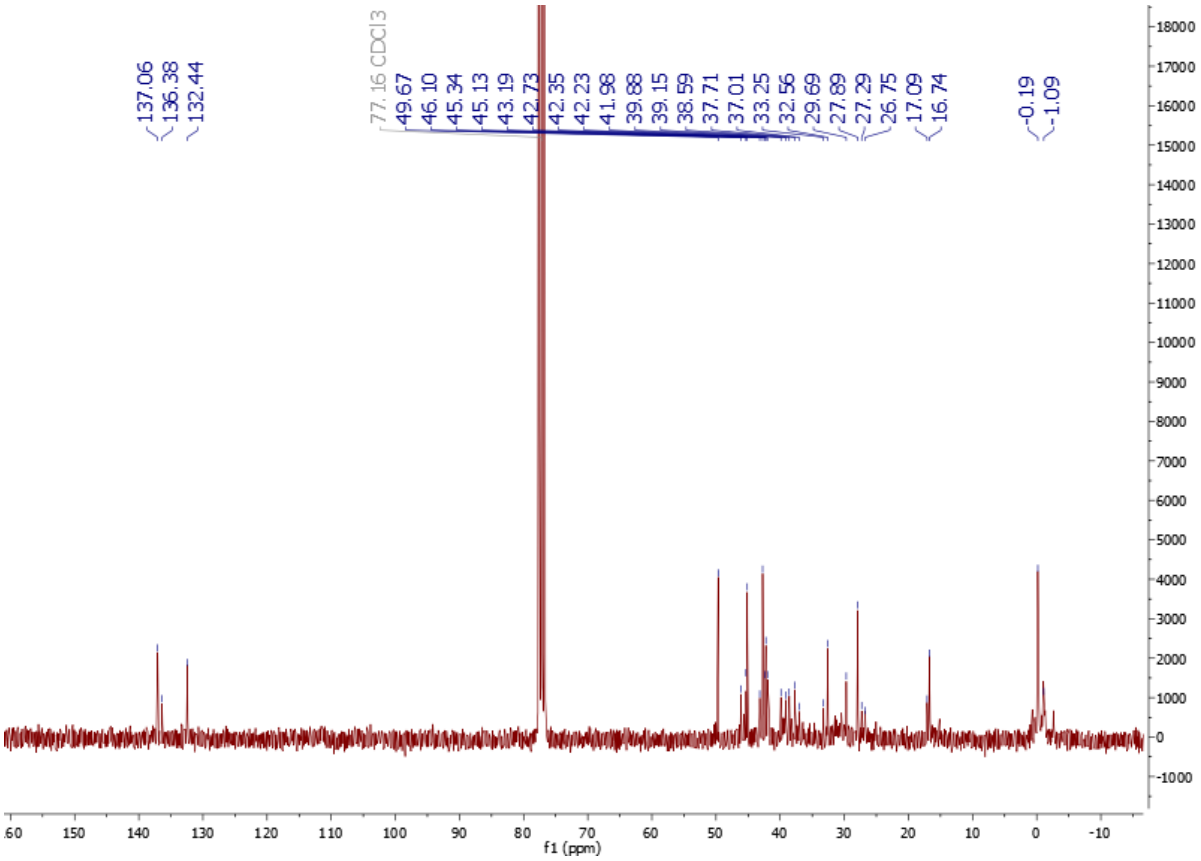

^{29}Si NMR *($CDCl_3$, 79.5 MHz):*

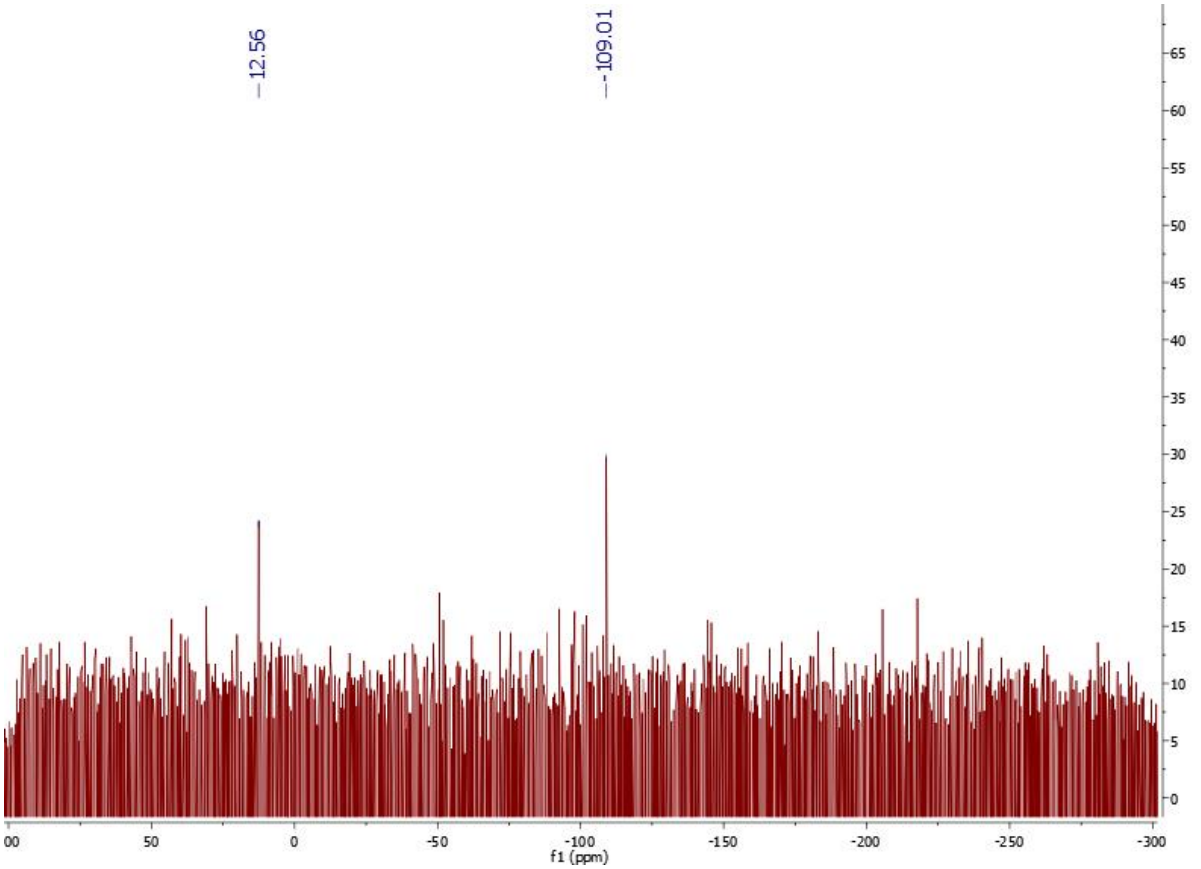

1,3,5,7,9,11,13,15-octa(dimethyl((2-(4-methylcyclohex-3-en-1-yl)propyl)silyl)-pentacyclo[9.5.1.1^{3,9}.1^{5,15}.1^{7,13}]octasiloxane (4)

^{1}H NMR (400 MHz, $CDCl_3$): δ (ppm) = 5.36 (s, 8H, position **3**), 2.00-1.87 (m, 24H, positions **1, 2, 5**), 1.78-1.56 (m, 24H, positions **2, 5, 8**), 1.63 (s, 24H, position **7**), 1.34-1.18 (m, 16H, position **6**), 0.90 (d, 24H, position **9**), 0.75-0.69 (m, 8H, position **10**), 0.52-0.44 (m, 8H, position **10**), 0.15 (s, 48H, $SiMe_2$);
^{13}C NMR (101 MHz, $CDCl_3$): δ (ppm) = 133.96, 121.28, 121.26, 41.48, 41.33, 33.08, 32.93, 31.19, 31.12, 28.80, 28.24, 26.71, 25.71, 23.64, 23.63, 22.87, 22.48, 19.52, 19.22, 0.83, 0.72, 0.66;
^{29}Si NMR (79,5 MHz, $CDCl_3$): δ (ppm) = 12.78 ($SiMe_2$), -109.10 (core).
IR (ATR): 2980-2867, 1252, 1169-1069, 869-734, 549.

^{1}H NMR *($CDCl_3$, 400MHz):*

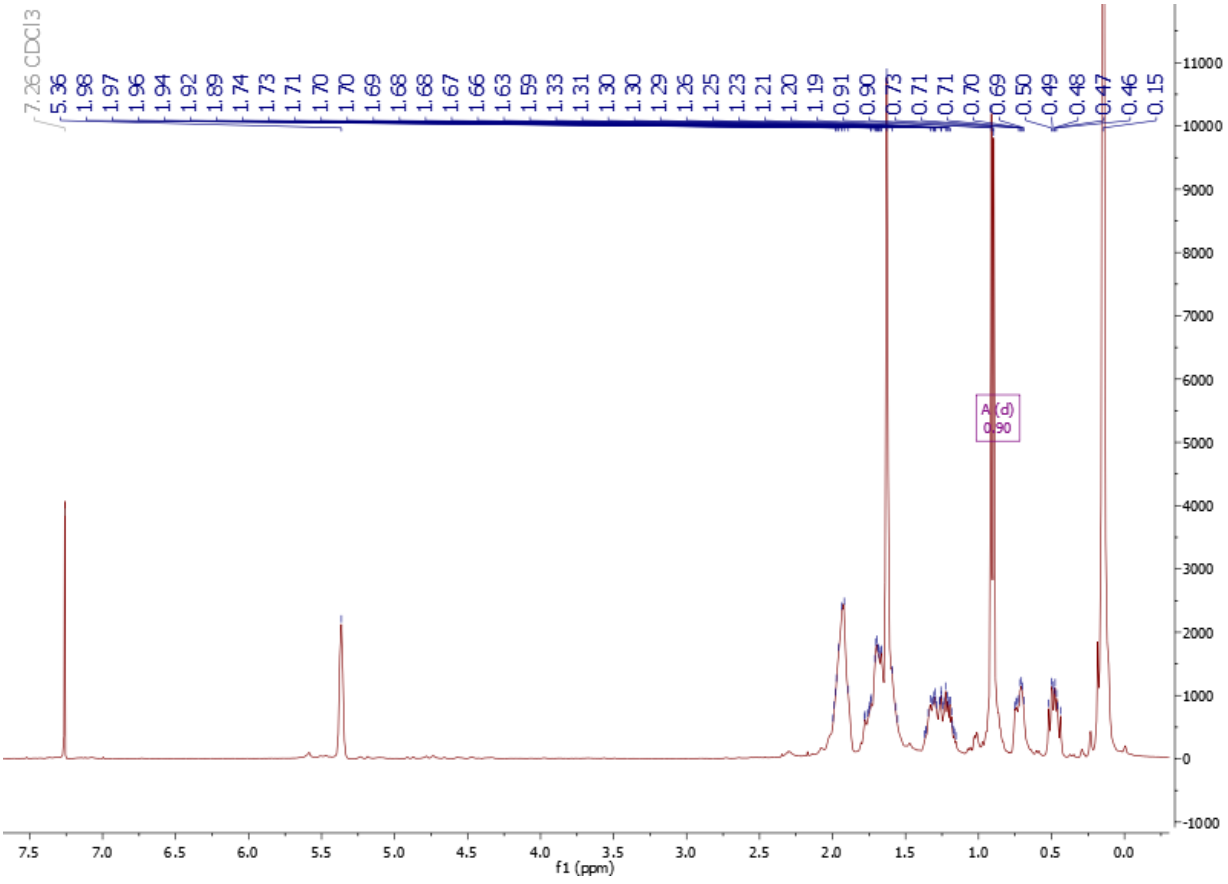

^{13}C NMR *($CDCl_3$, 101 MHz):*

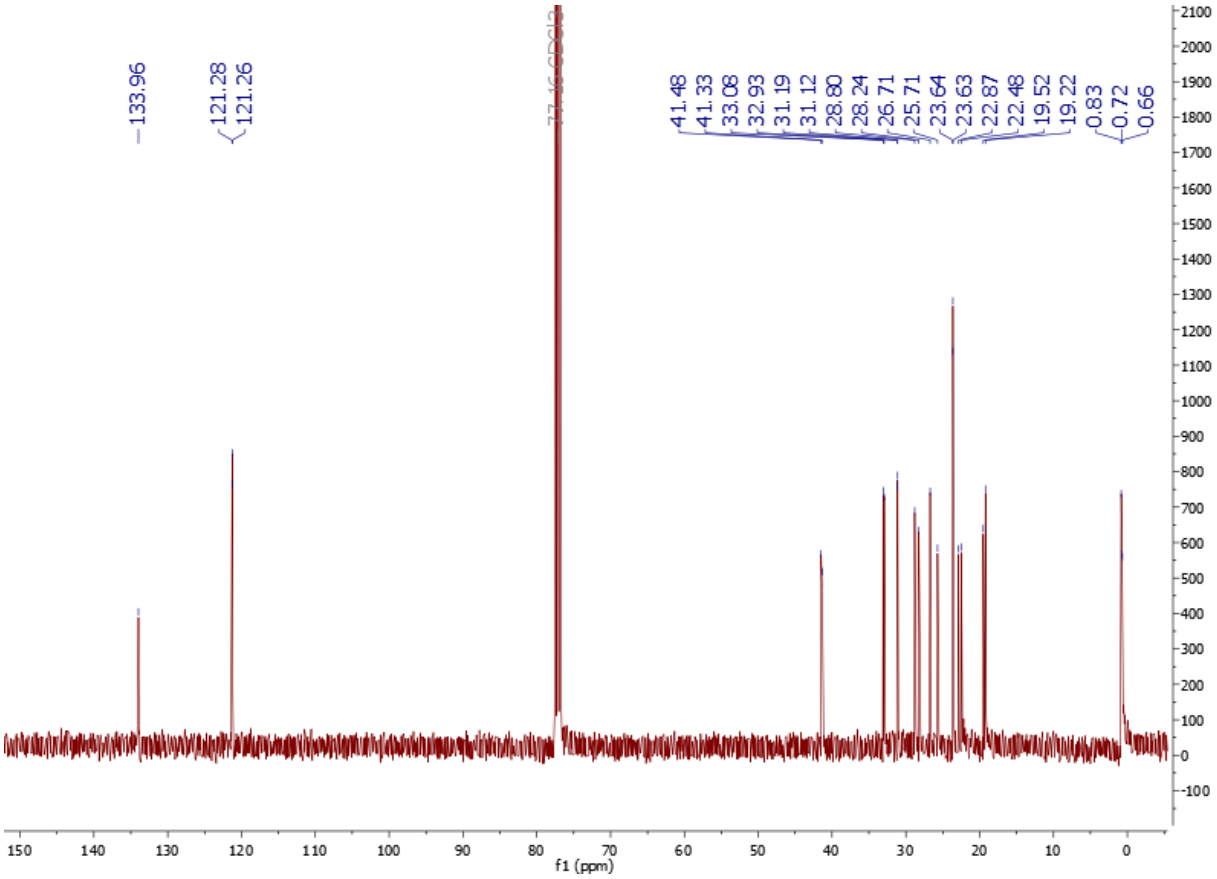

^{29}Si NMR *($CDCl_3$, 79.5 MHz):*

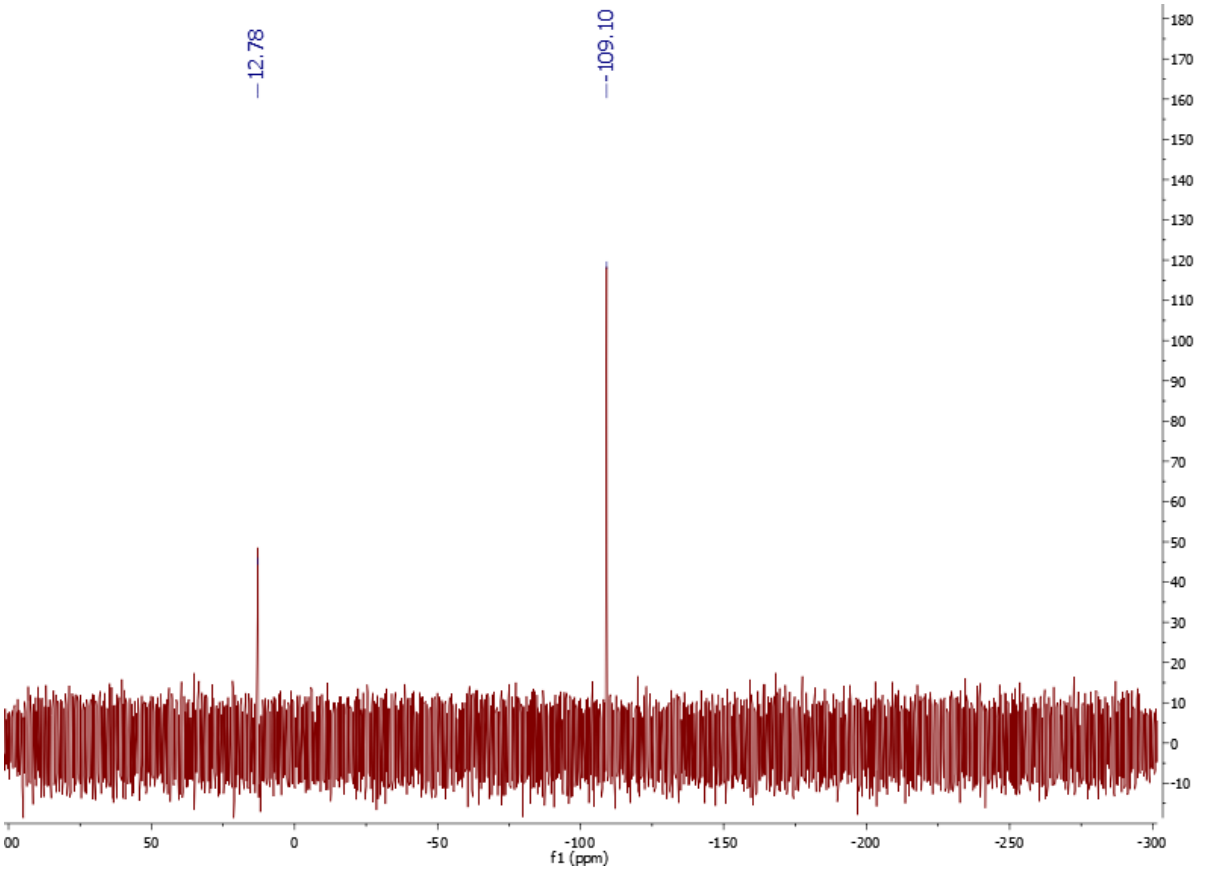

1,3,5,7,9,11,13,15-octa(dimethyl((8,8-dimethylbicyclo[4.1.1]hept-2-yl)methyl)silyl)-pentacyclo[9.5.1.1^{3,9}.1^{5,15}.1^{7,13}]octasiloxane (5)

^{1}H NMR (400 MHz, $CDCl_3$): δ (ppm) = 2.19-2.11 (m, 8H, position **2**), 2.04-1.98 (m, 8H, position **5**), 1.86-1.82 (m, 8H, position **4**), 1.75-1.69 (m, 24H, positions **1**, **3** and **7**), 1.63 (m, 8H, position **4**), 1.36 (d, J=9.8Hz, 8H, position **7**), 1.30-1.23 (m, 8H, position **3**), 1.18 (s, 24H, position **8**), 0.83 (s, 24H, position **8**), 0.70 (dd, J_1=14.8Hz, J_2=9.1Hz, 8H, position **9**), 0.56 (dd, J_1=14.8Hz, J_2=5.6Hz, 8H, position **9**), 0.14 (s, 48H, $SiMe_2$);
^{13}C NMR (101 MHz, $CDCl_3$): δ (ppm) = 49.48, 49.40, 41.42, 40.81, 39.67, 38.91, 36.56, 34.03, 30.54, 28.49, 27.92, 27.13, 26.91, 26.02, 25.29, 25.22, 24.98, 23.45, 23.19, 23.17, 20.26, 1.09, 1.01;
^{29}Si NMR (79,5 MHz, $CDCl_3$): δ (ppm) = 12.34 ($SiMe_2$), -109.13 (core).
IR (ATR): 2980-2867, 1252, 1169-1069, 869-748, 549.

^{1}H NMR *($CDCl_3$, 400MHz):*

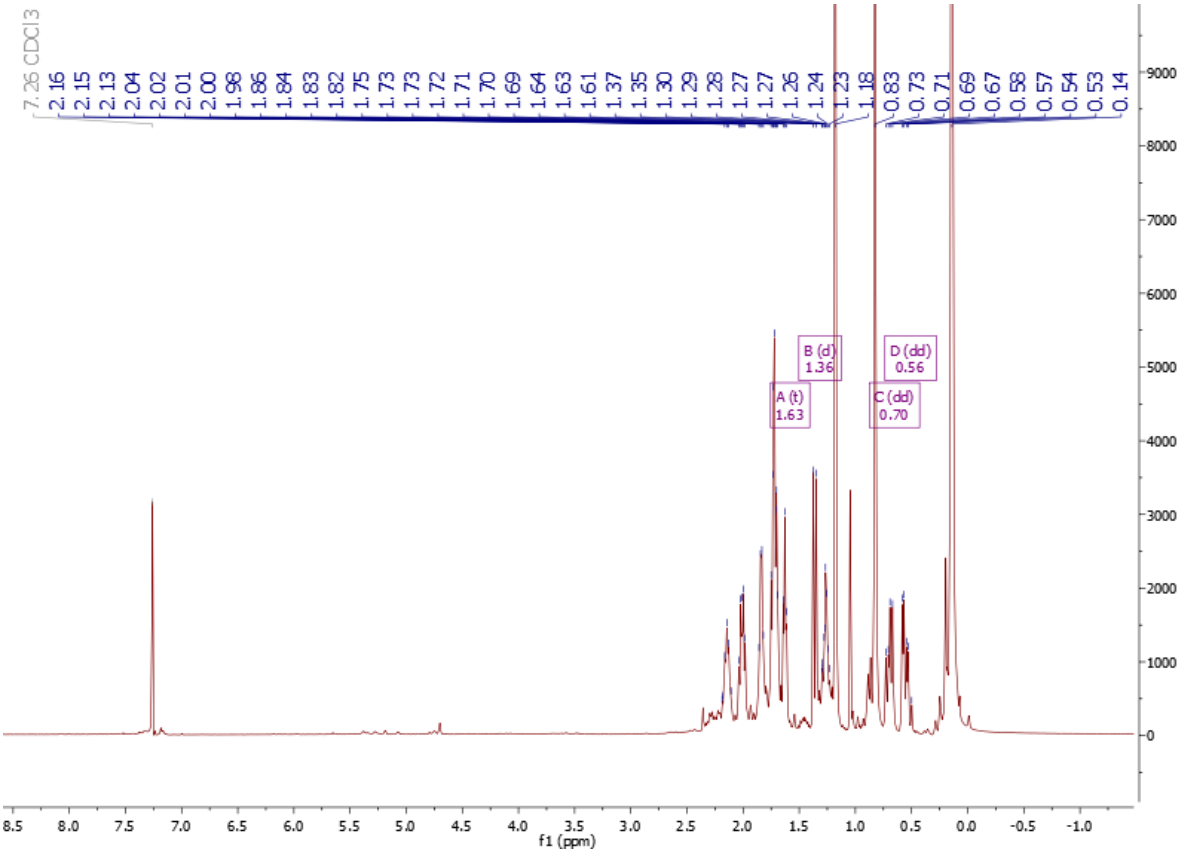

^{13}C NMR *($CDCl_3$, 101 MHz):*

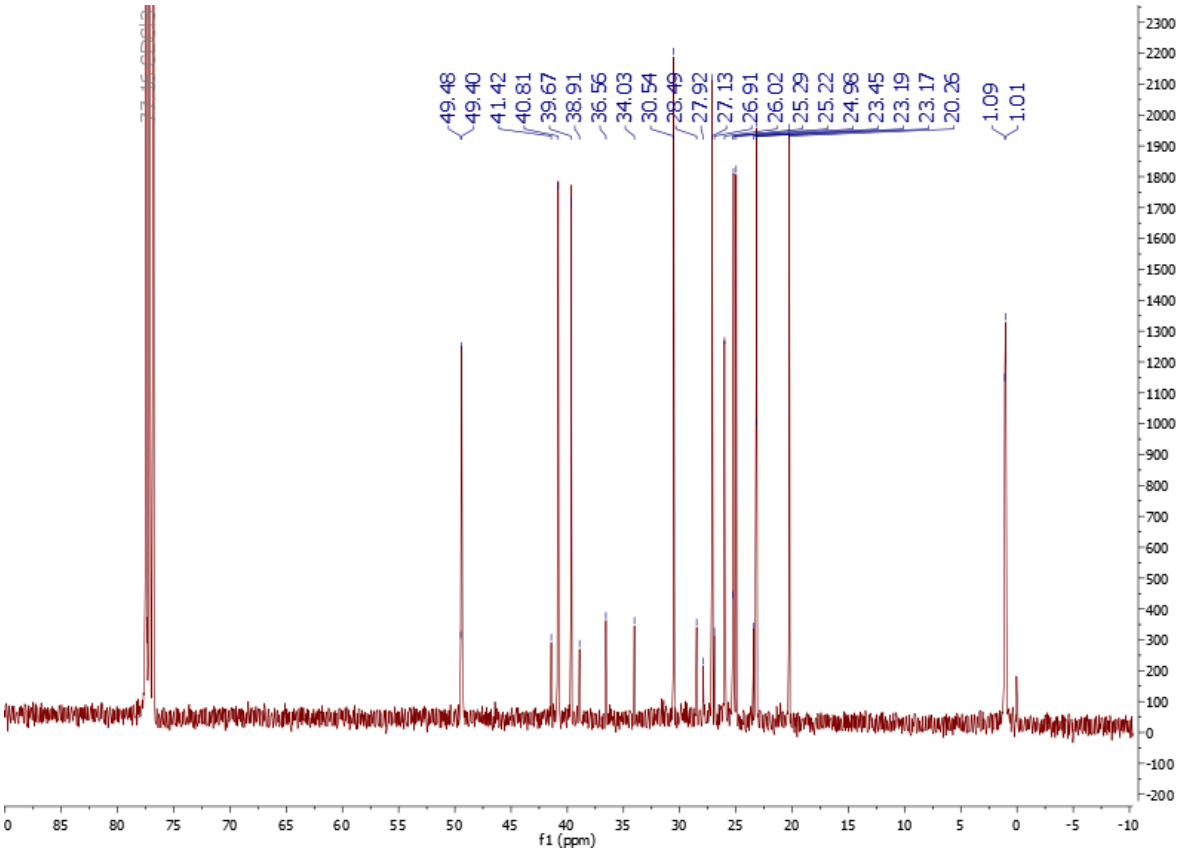

^{29}Si NMR *($CDCl_3$, 79.5 MHz):*

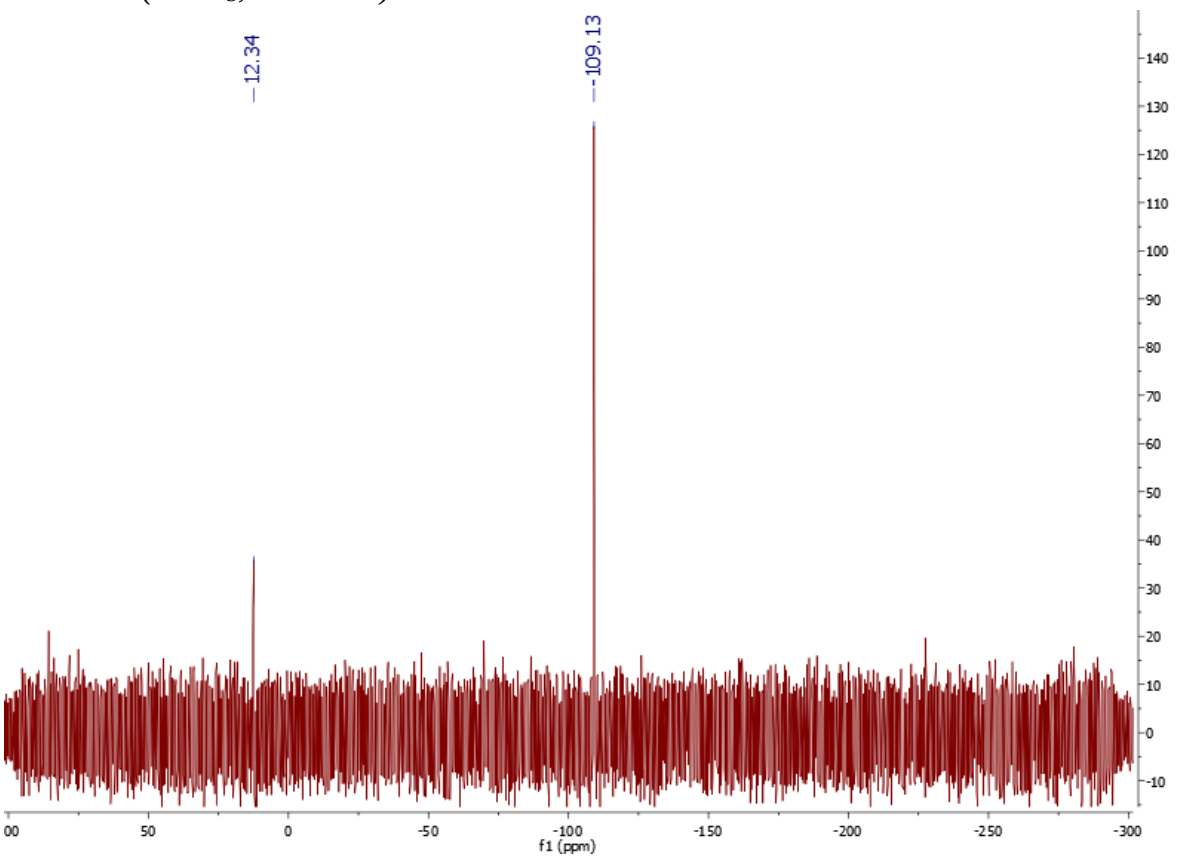

4. MALDI-TOF-MS identification of side products of SS-Norbornene synthesis

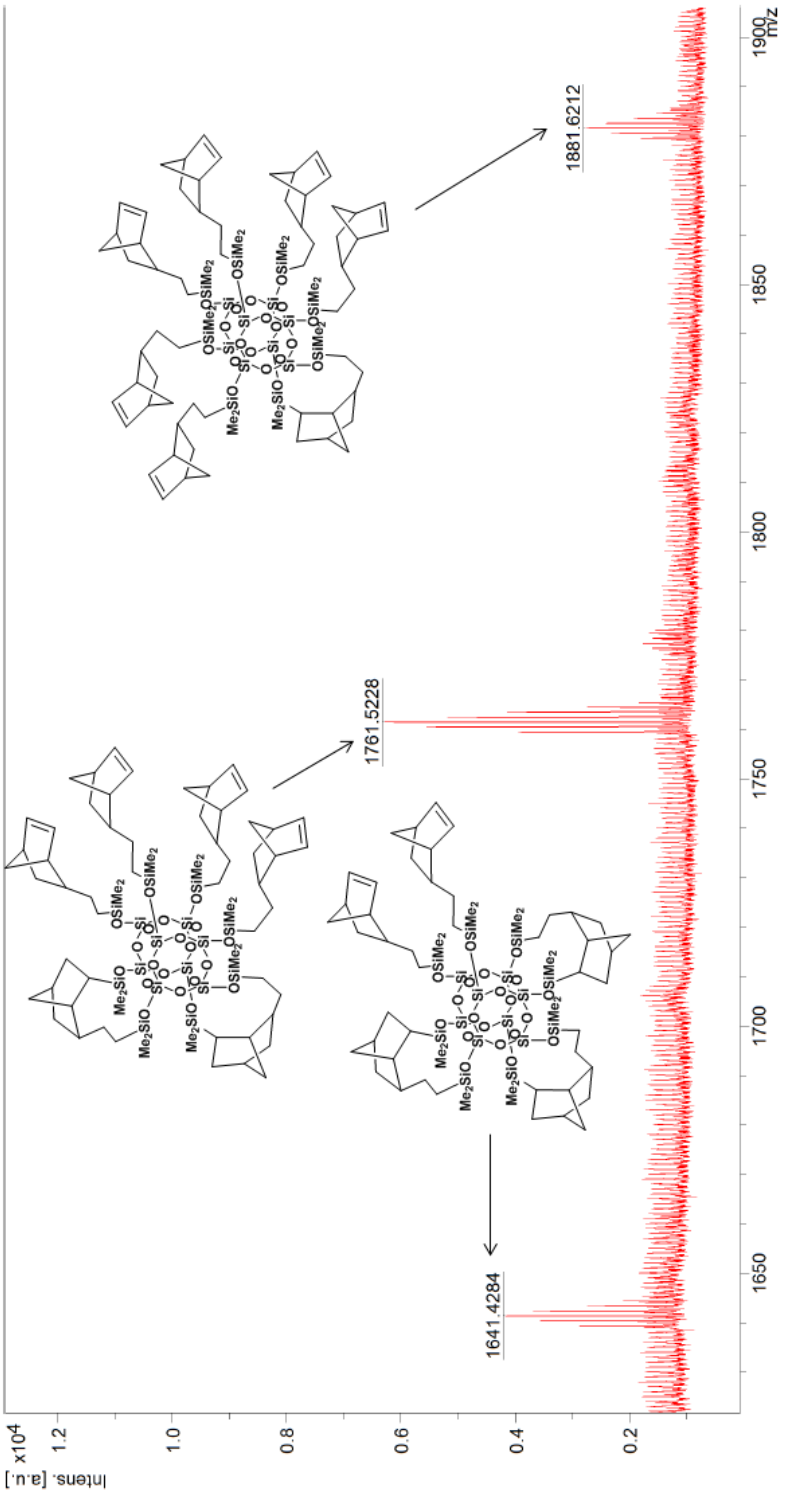

5. SEM and EDS images of the SS/PE composites

0.5% SS-H/PE

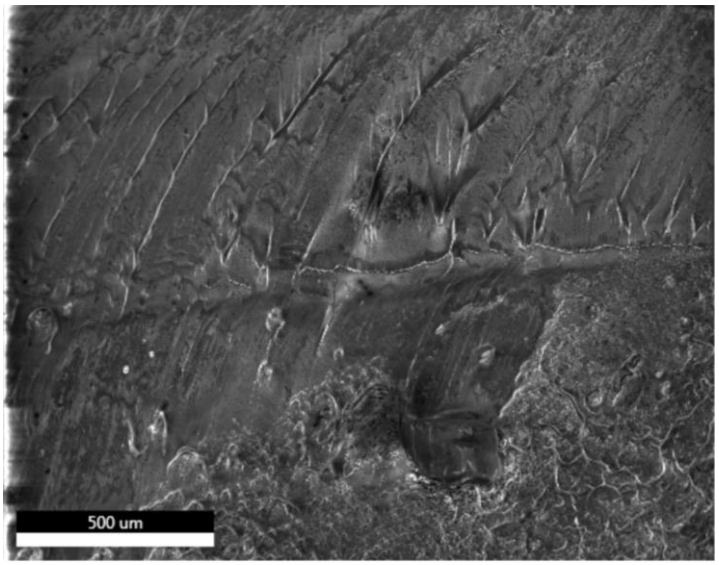

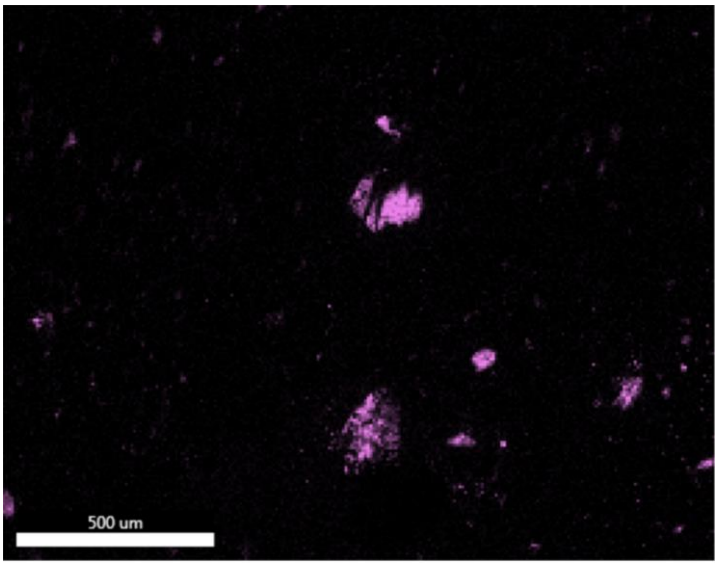

0.5% SS-H/PE (higher magnification)

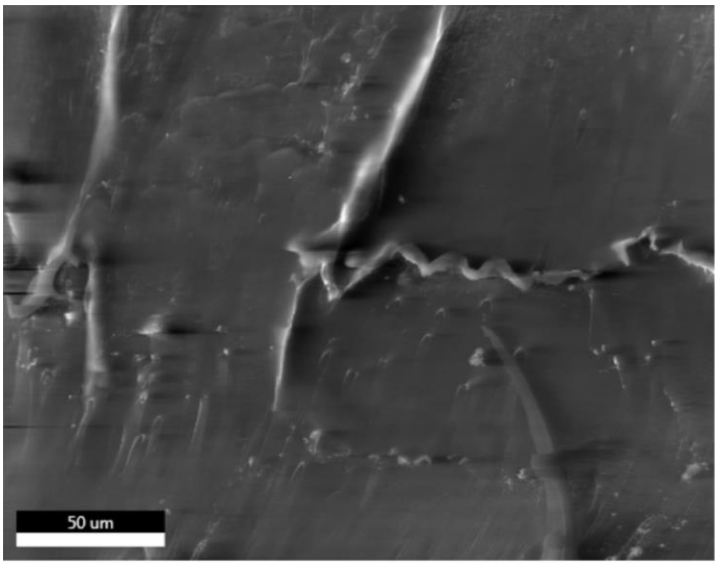

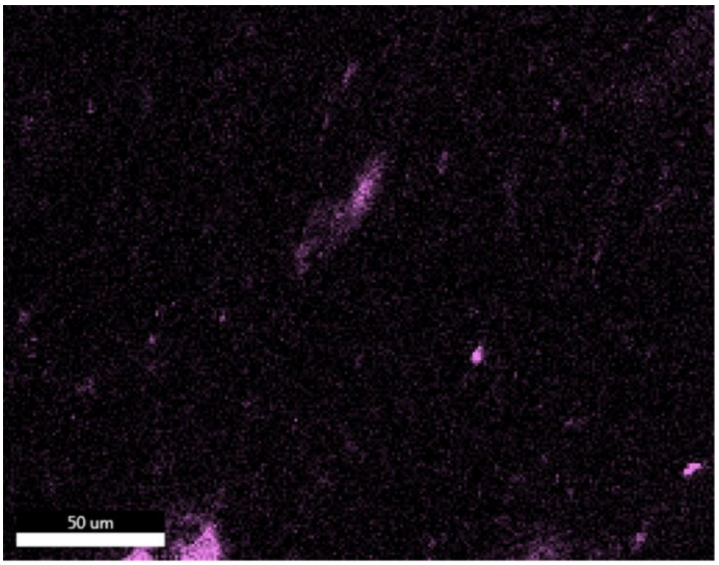

1.0% SS-H/PE

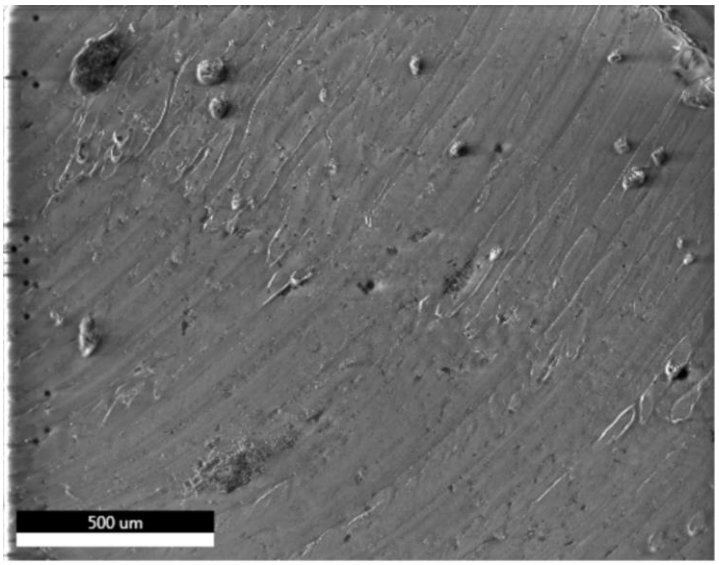

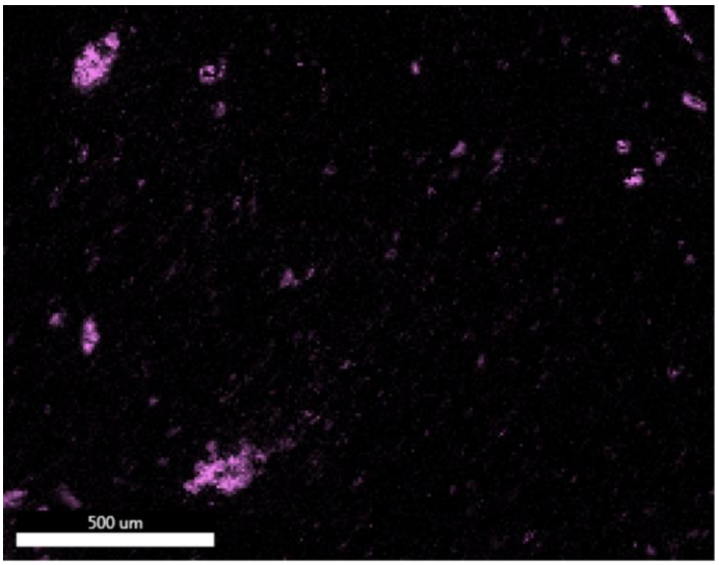

1.0% SS-H/PE (higher magnification)

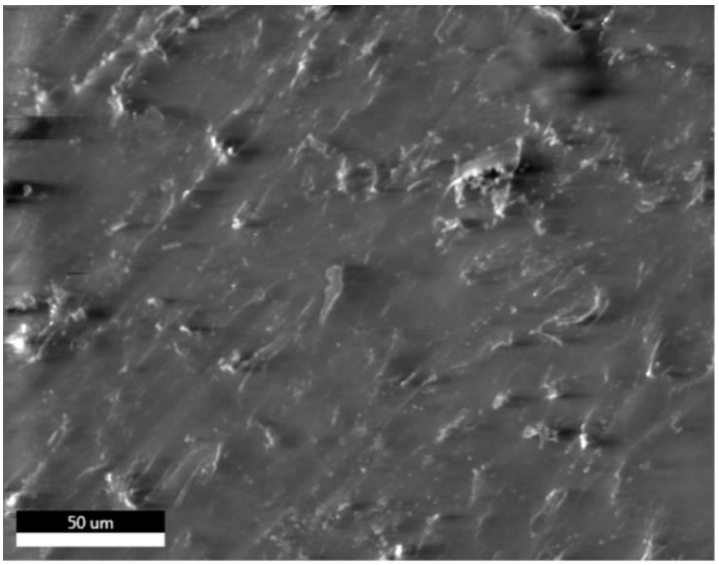

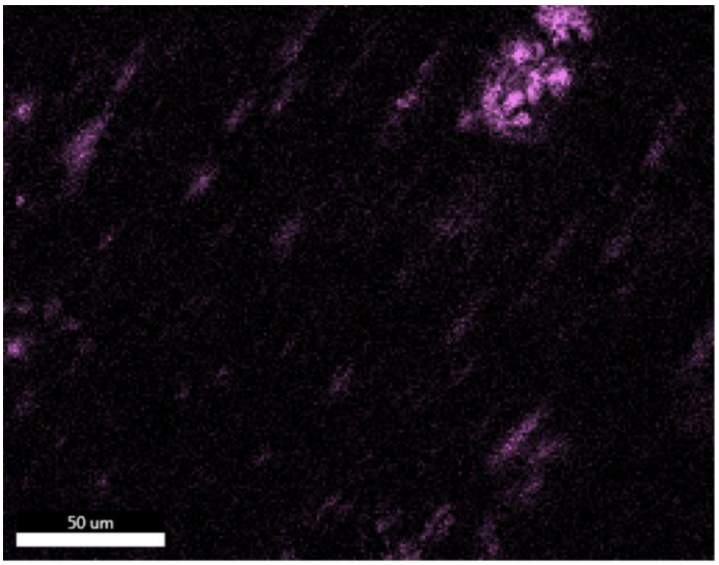

0.5% SS-Vi/PE

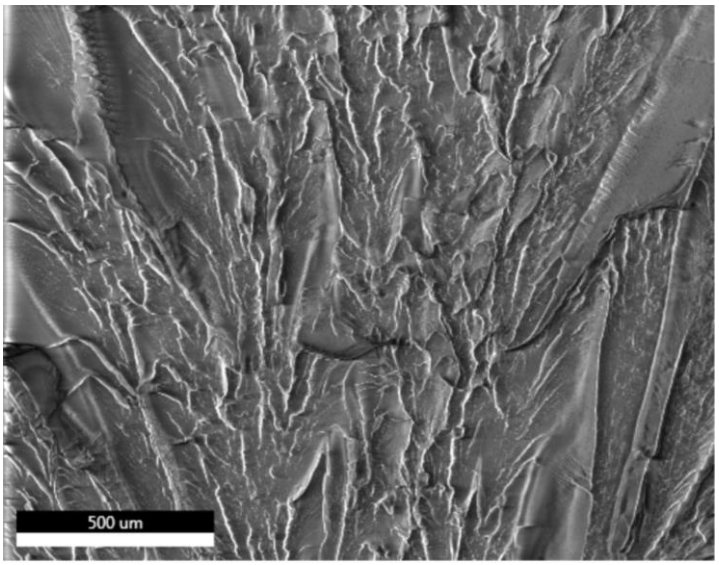

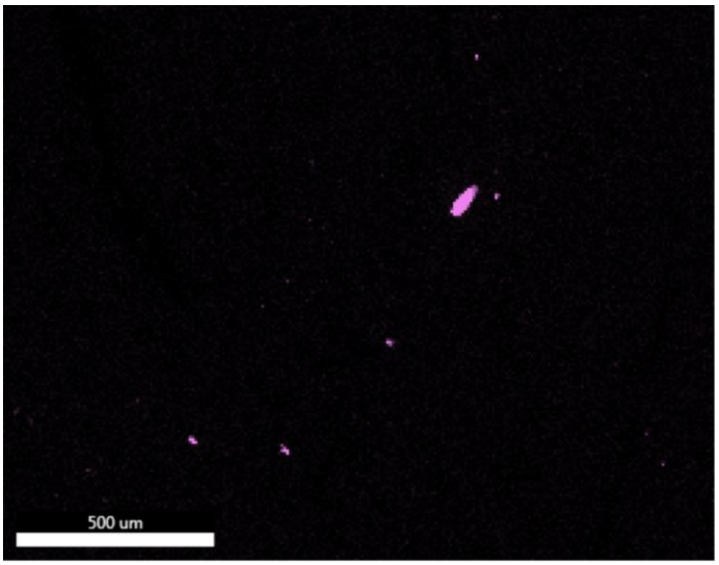

0.5% SS-Vi/PE (higher magnification)

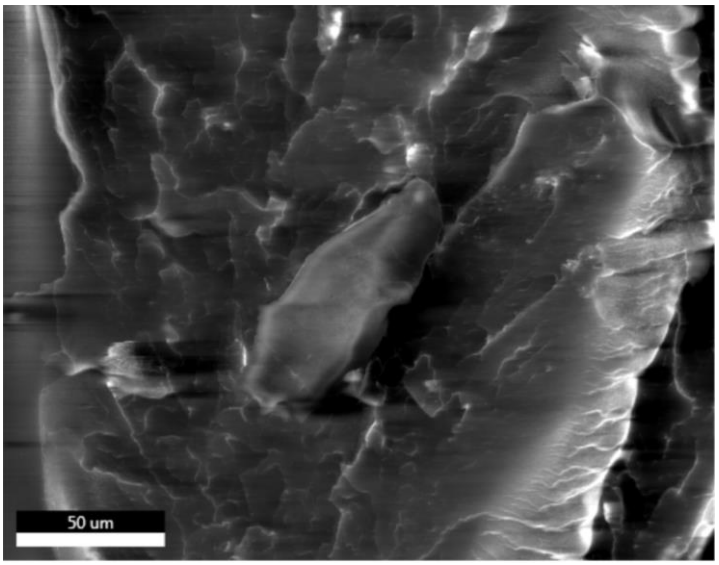

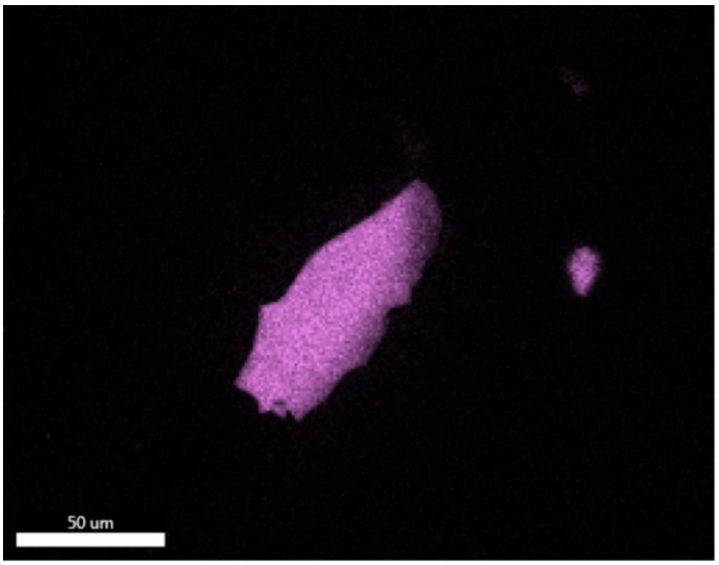

0.1% SS-Pinene/PE

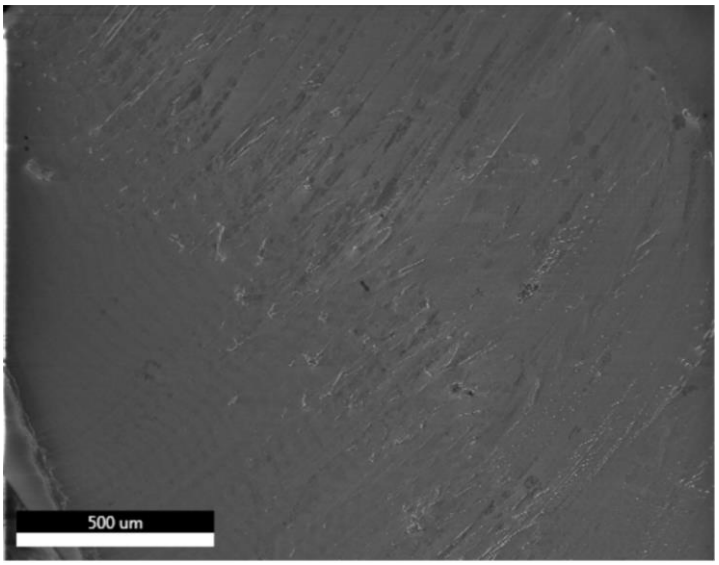

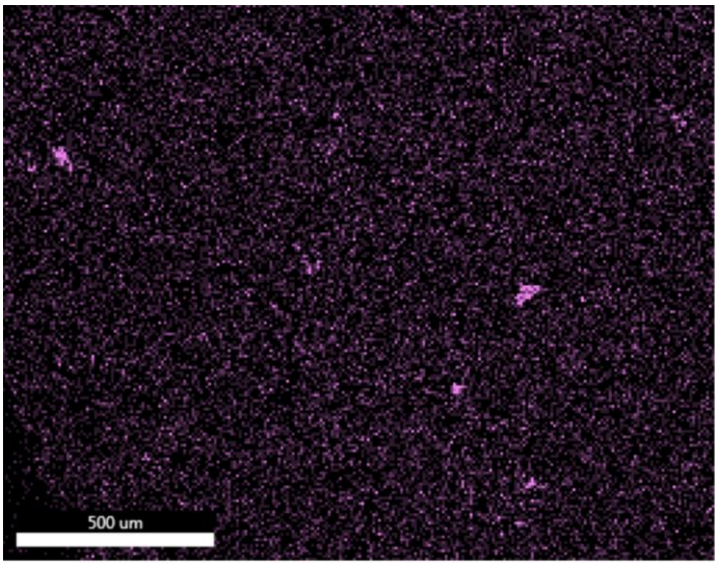

0.1% SS-Pinene/PE (higher magnification)

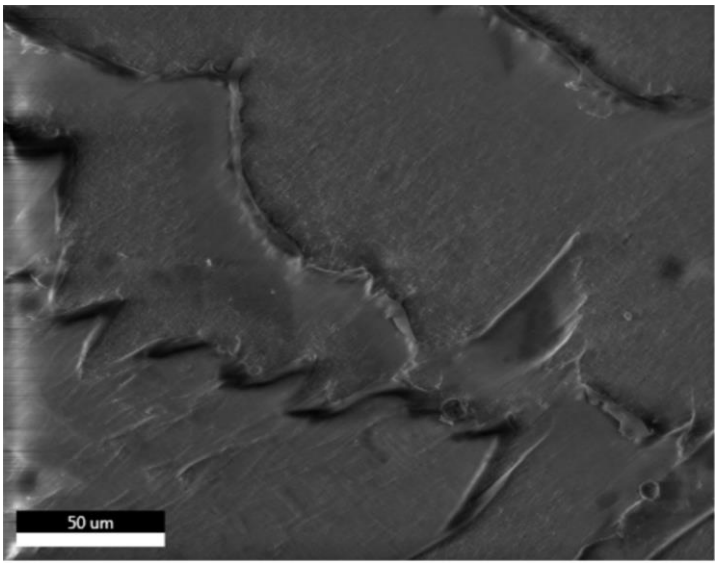

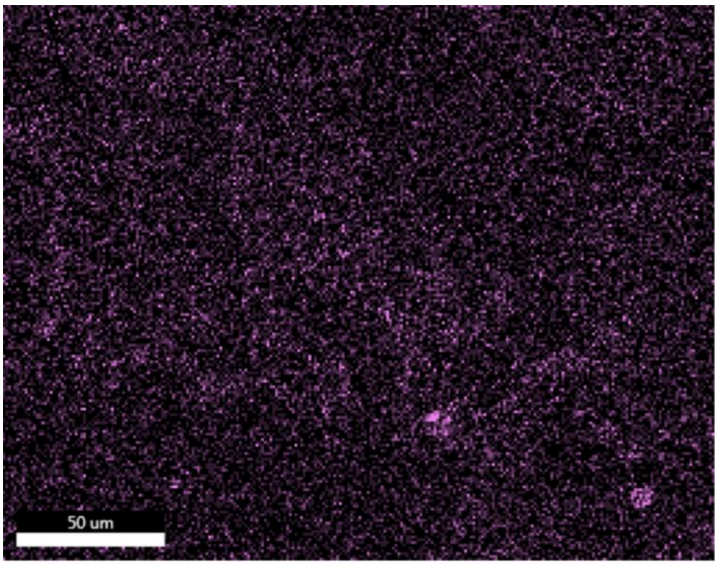

0.5% SS-Pinene/PE

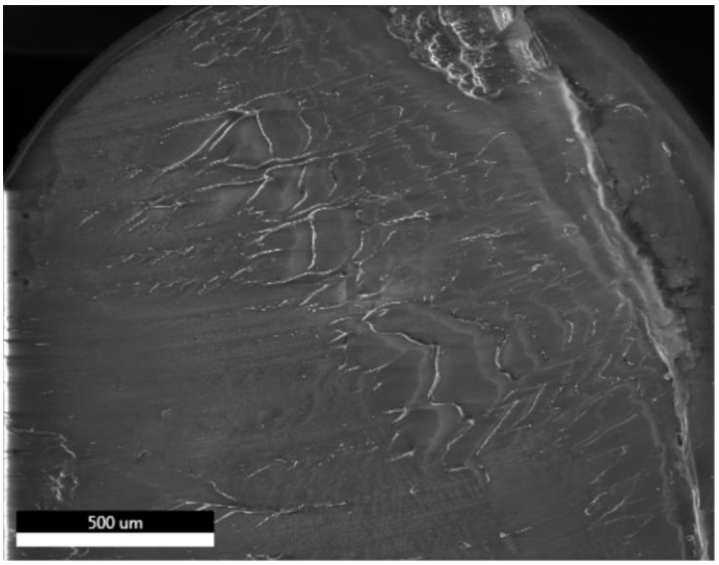

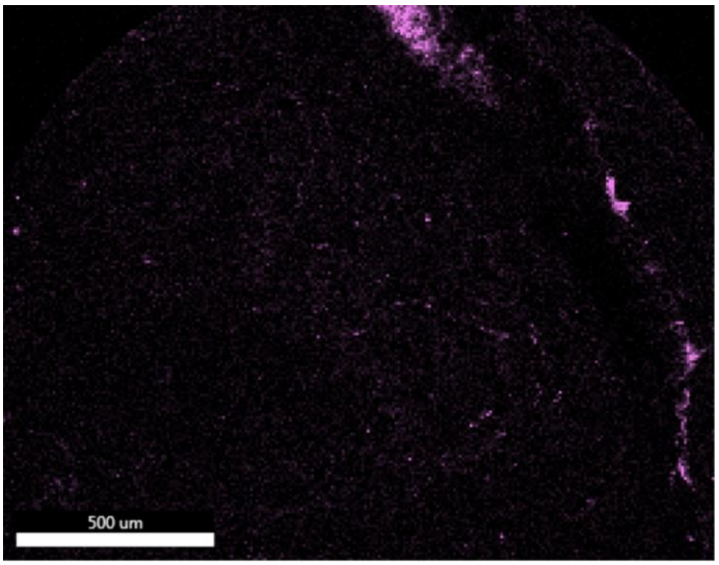

0.5% SS-Pinene/PE (higher magnification)

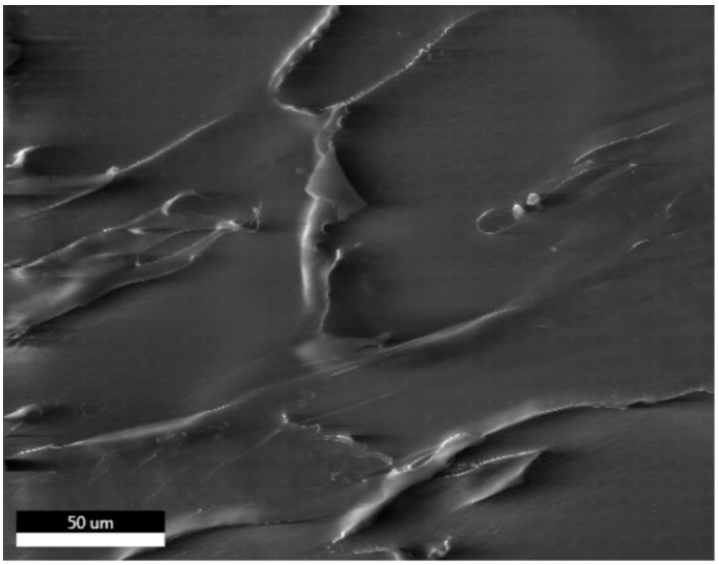

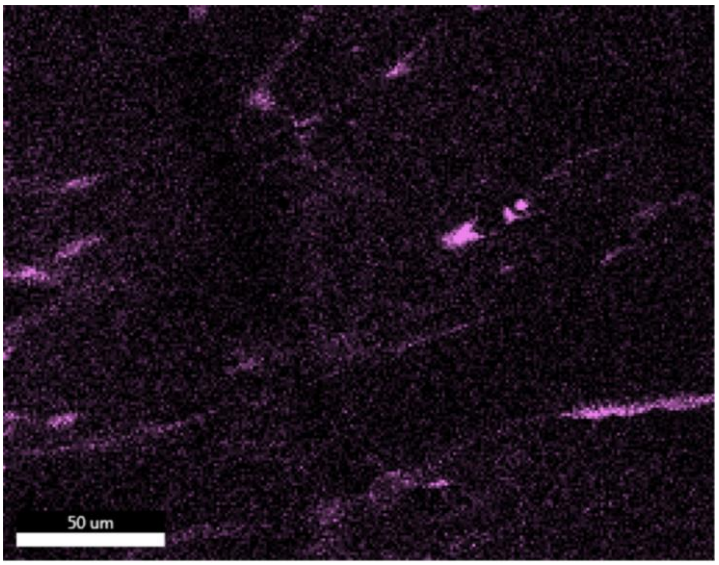

1.0% SS-Pinene/PE

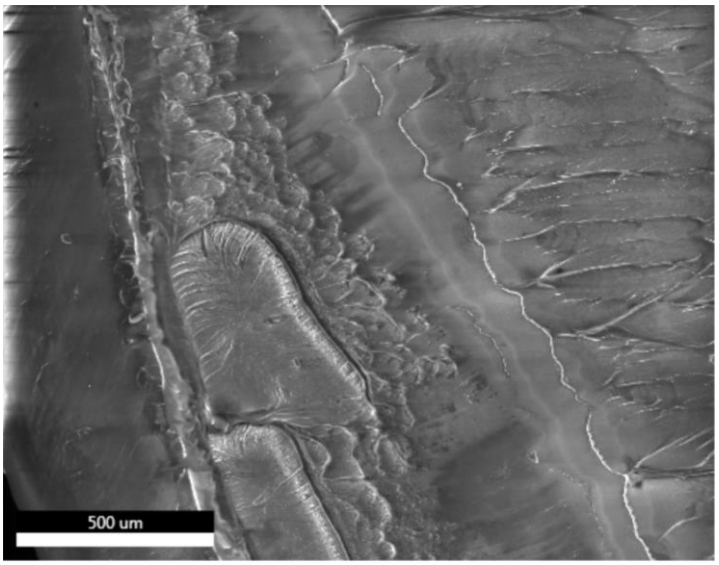

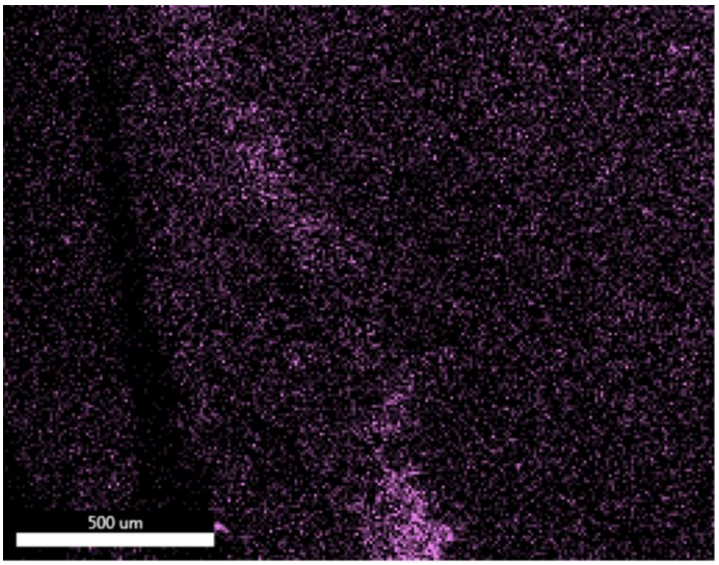

1.0% SS-Pinene/PE (higher magnification)

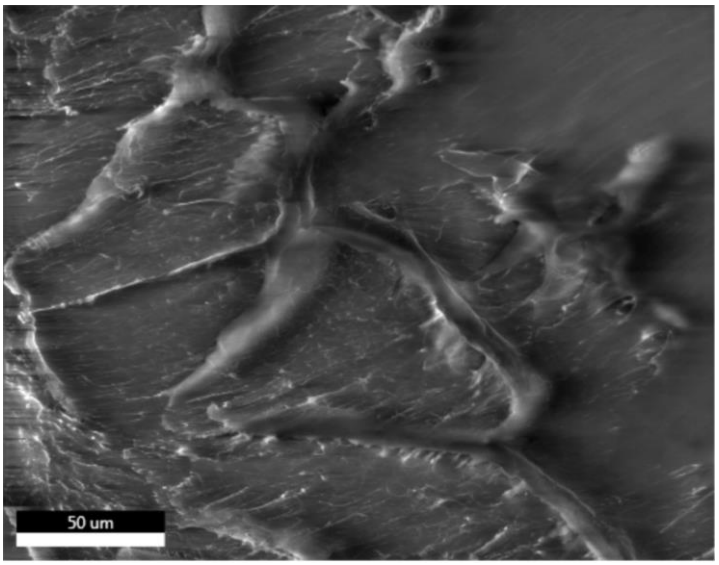

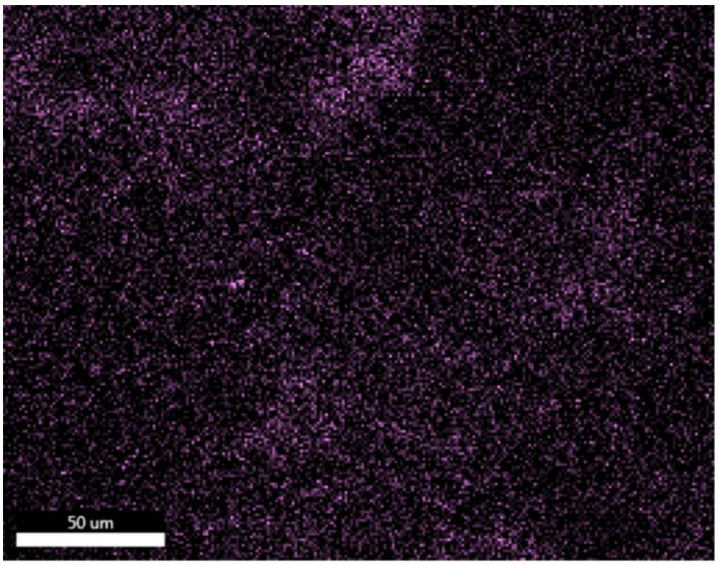

0.1% SS-Limonene/PE

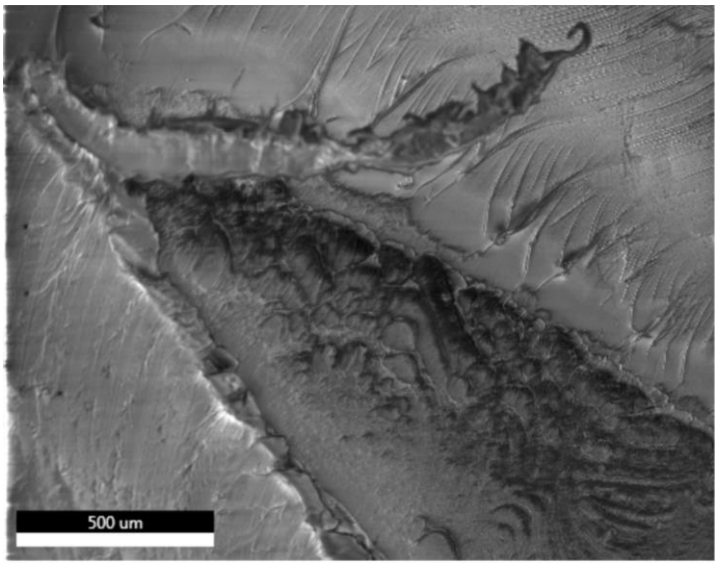

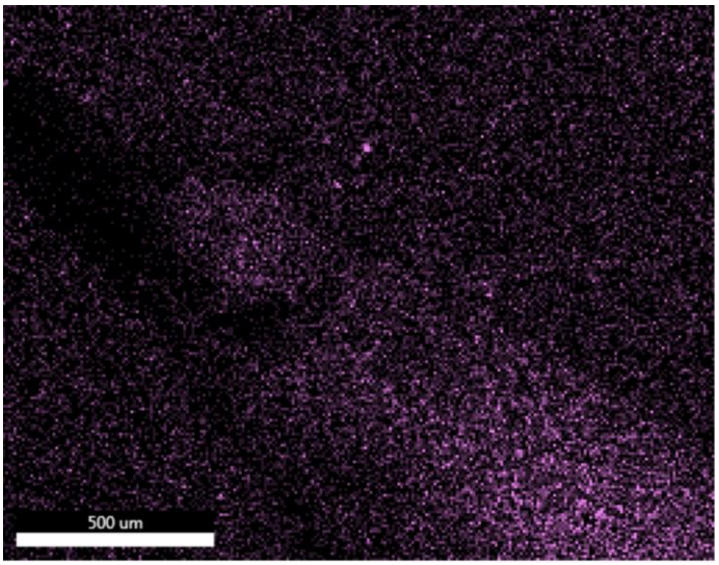

0.1% SS-Limonene/PE (higher magnification)

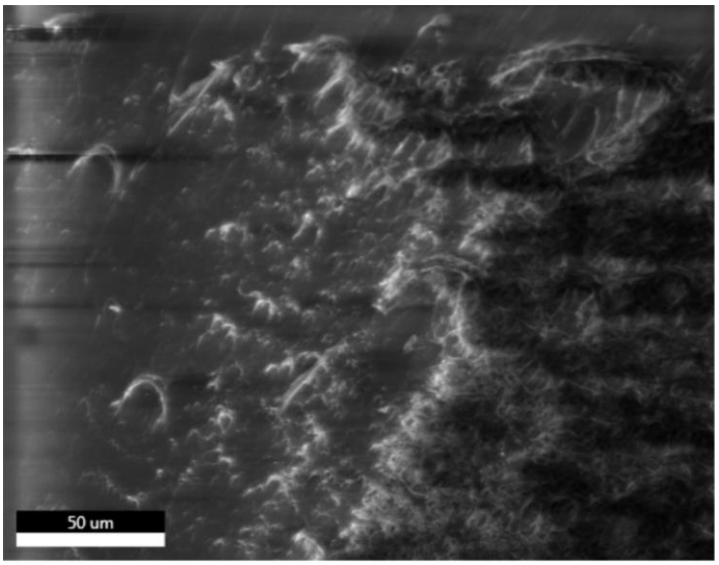

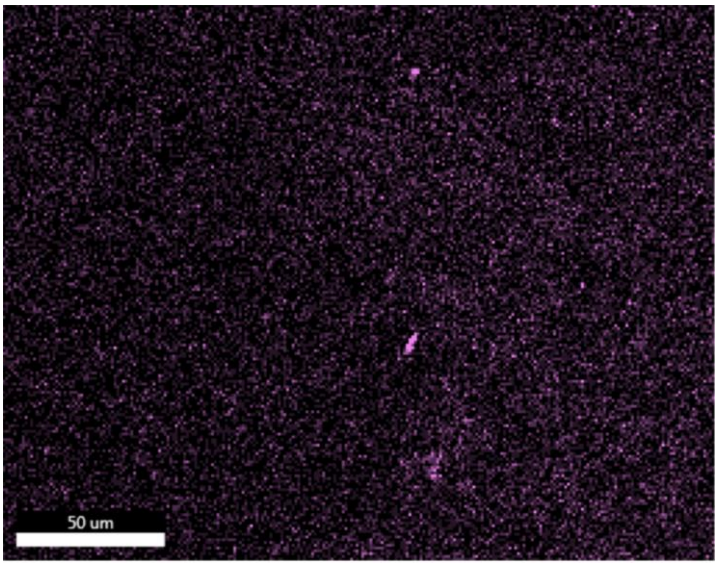

0.5% SS-Limonene/PE

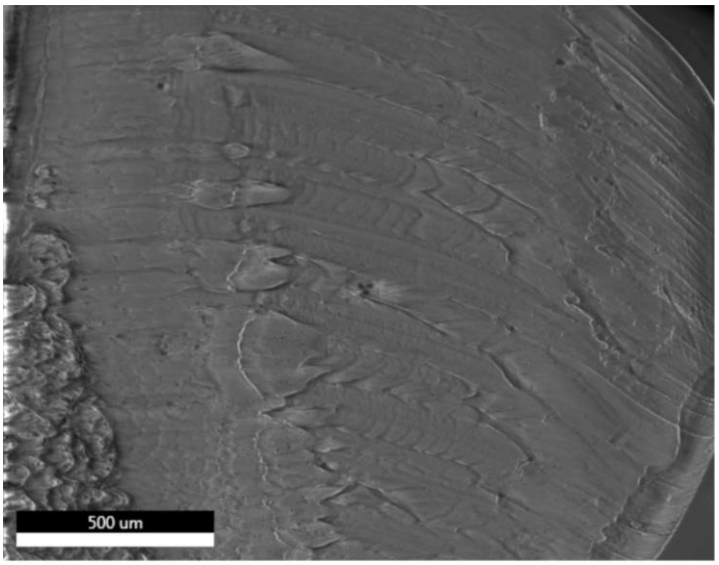

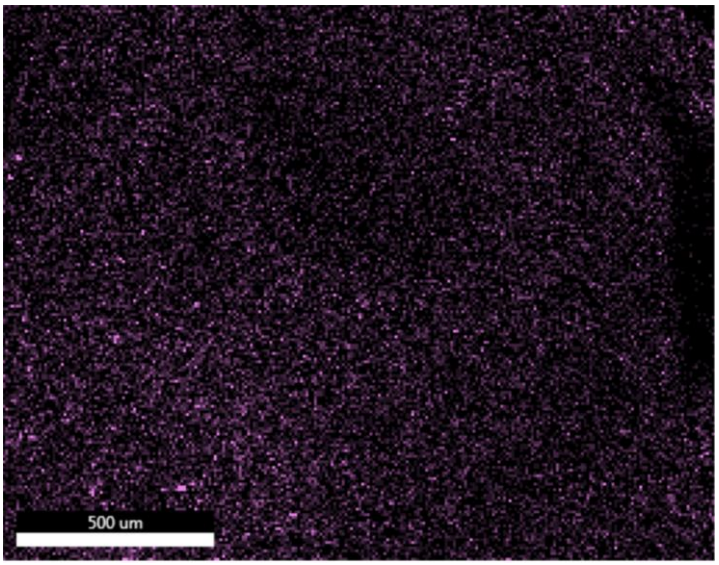

0.5% SS-Limonene/PE (higher magnification)

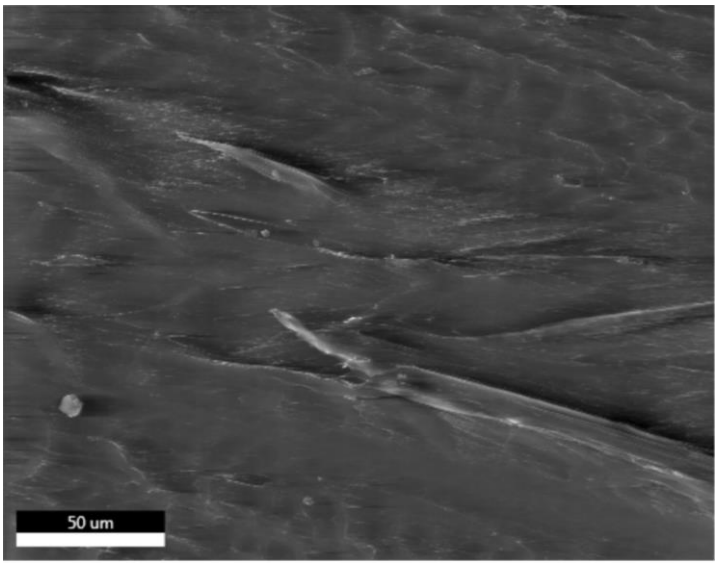

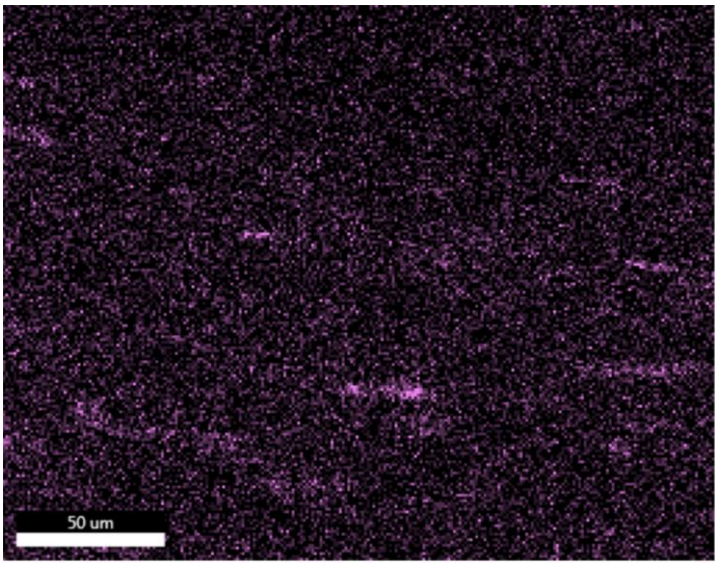

1.0% SS-Limonene/PE

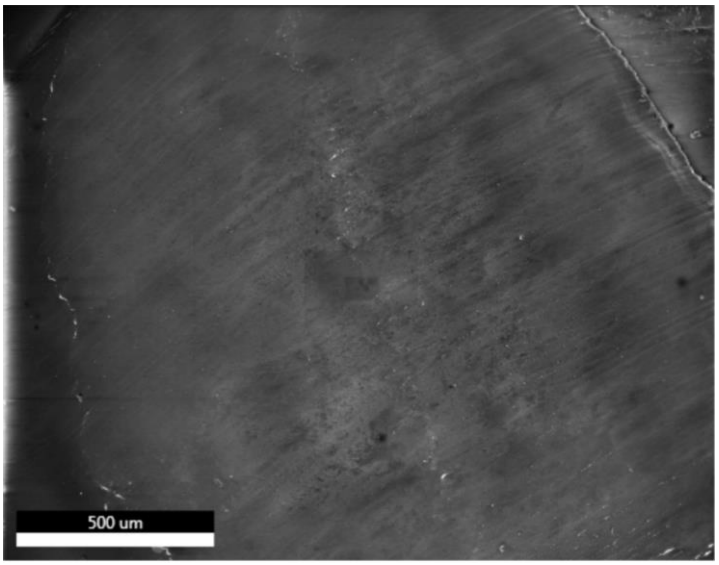

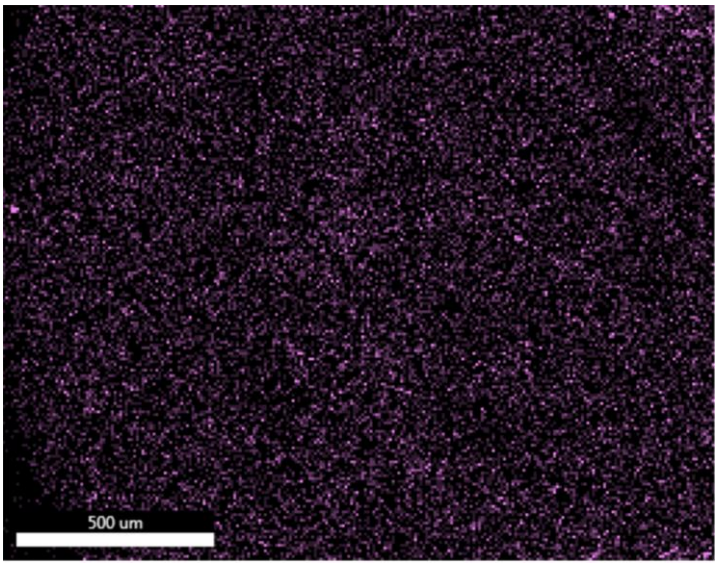

1.0% SS-Limonene/PE (higher magnification)

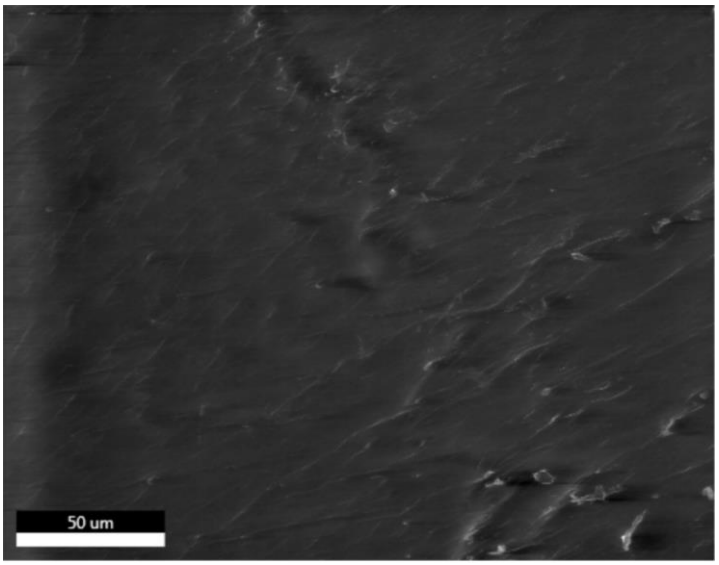

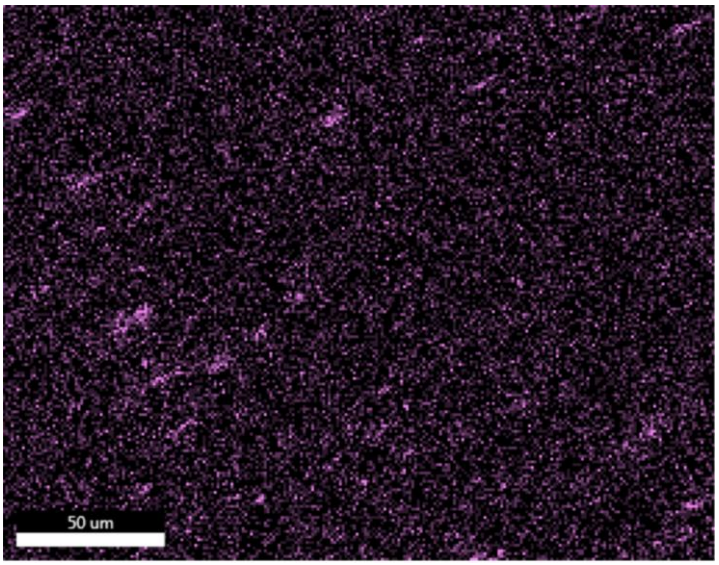

0.1% SS-Norbornene

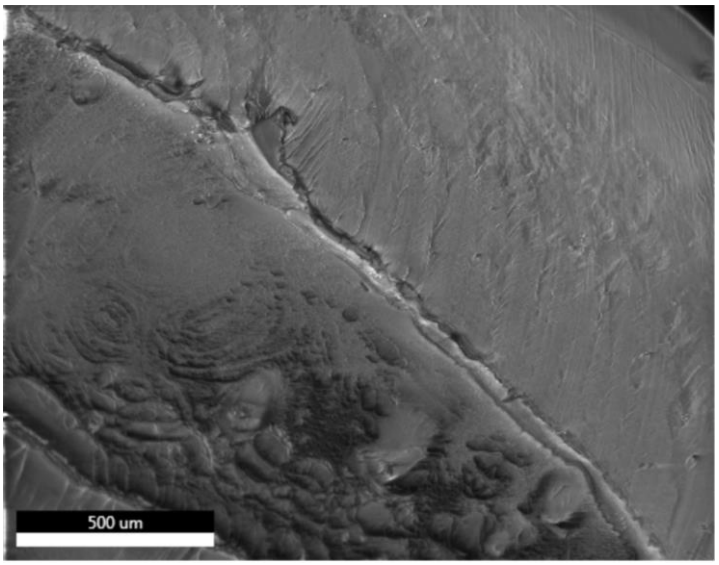

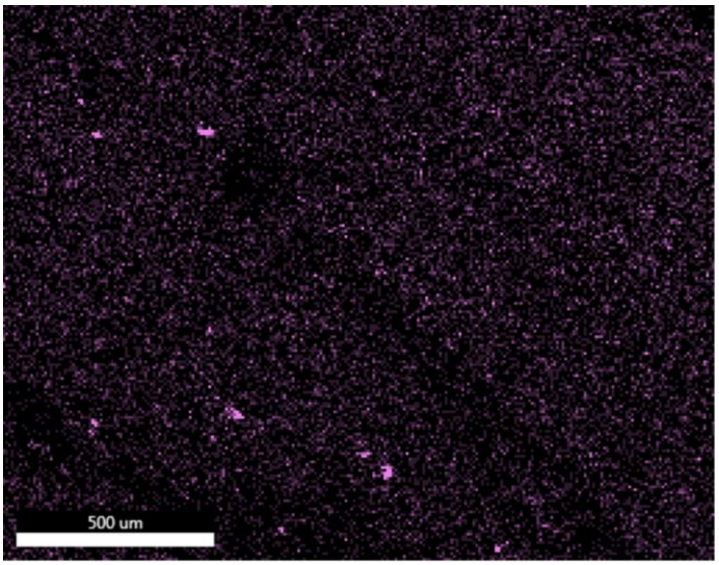

0.1% SS-Norbornene (higher magnification)

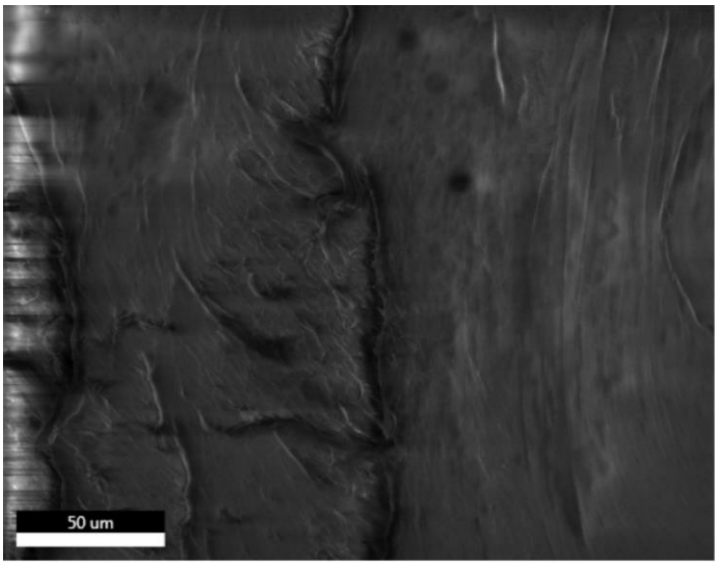

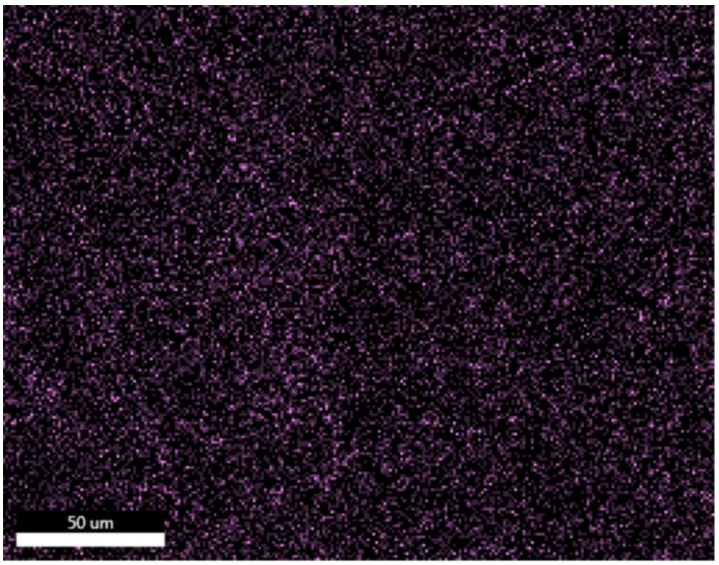

0.5% SS-Norbornene

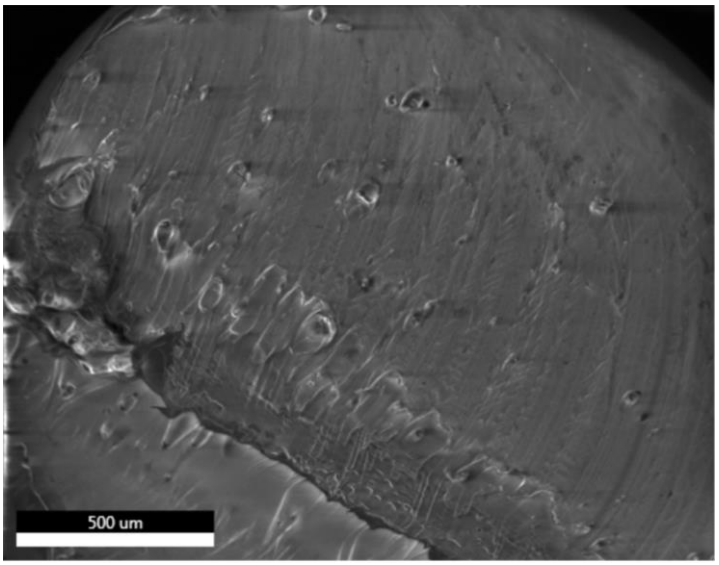

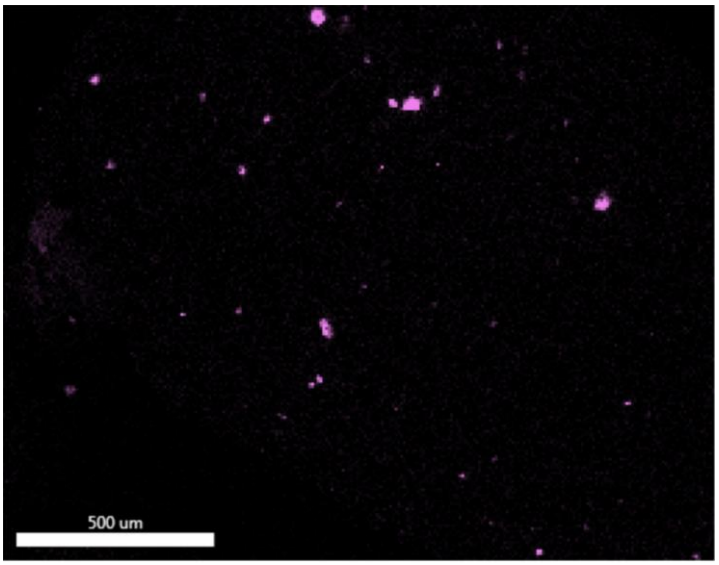

0.5% SS-Norbornene (higher magnification)

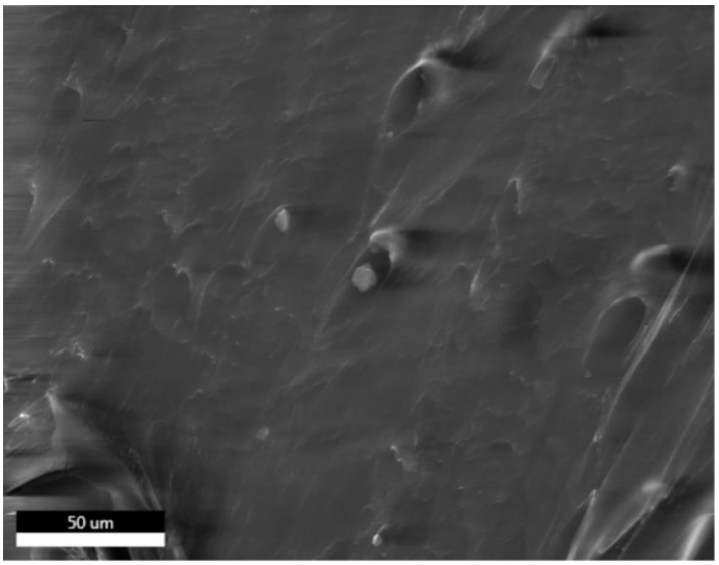

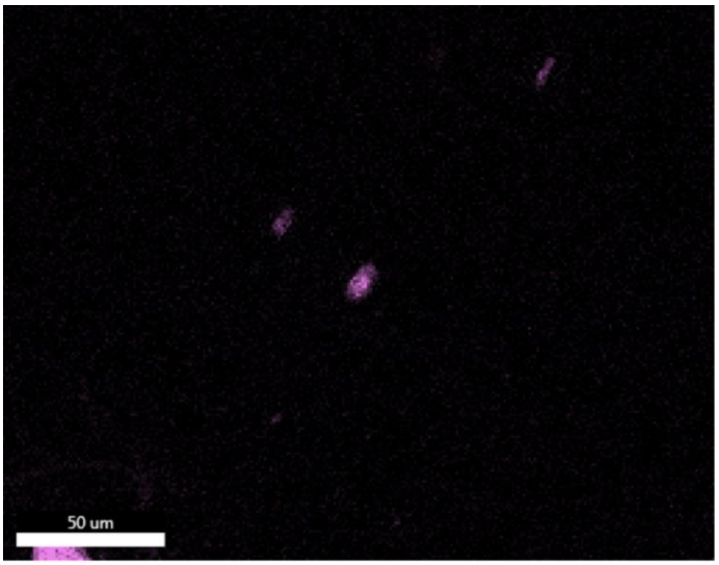

1.0% SS-Norbornene

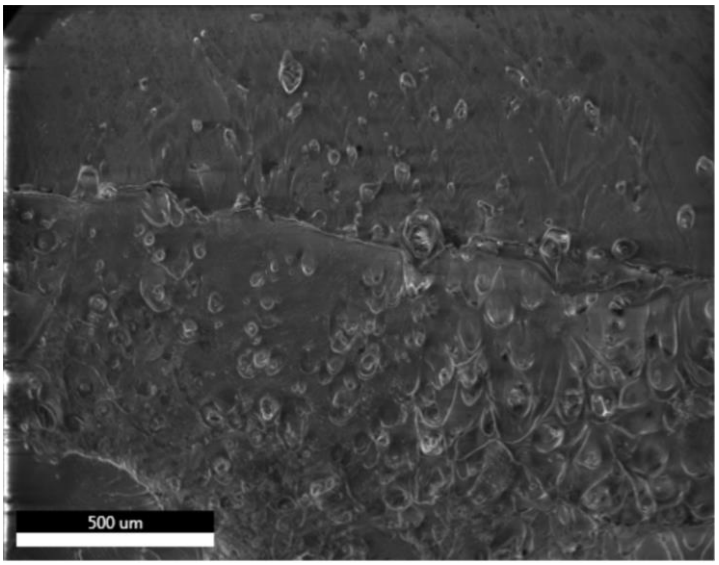

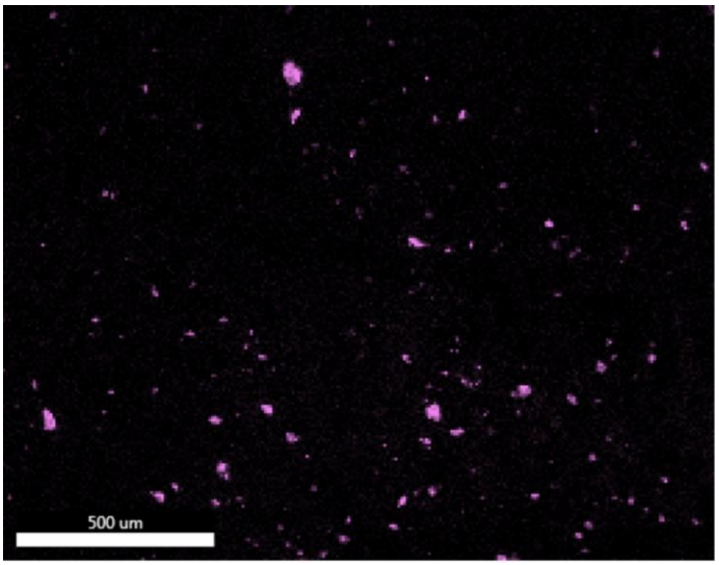

1.0% SS-Norbornene (higher magnification)

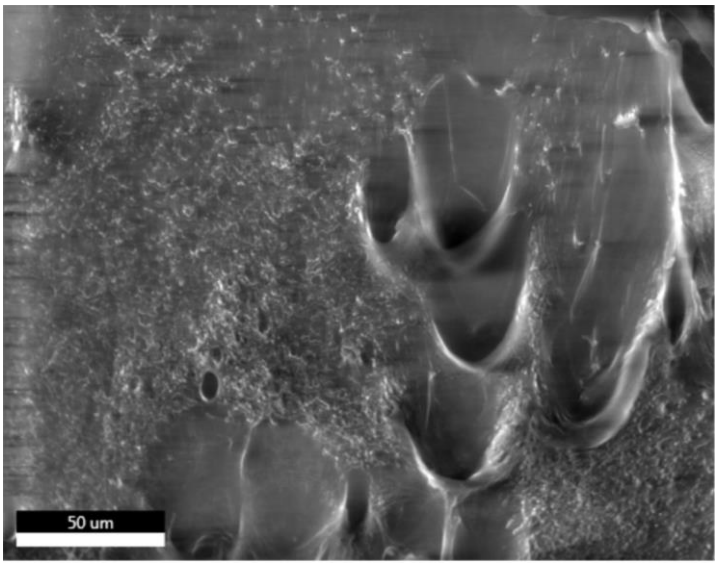

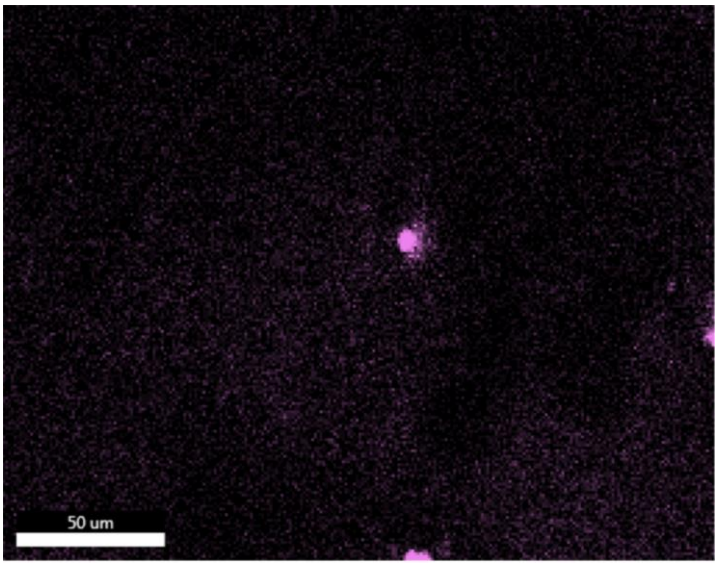

polymers

MDPI

Article

Silsesquioxane Derivatives as Functional Additives for Preparation of Polyethylene-Based Composites: A Case of Trisilanol Melt-Condensation

Dariusz Brząkalski [1,*], Robert E. Przekop [2], Bogna Sztorch [2], Paulina Jakubowska [3], Marek Jałbrzykowski [4] and Bogdan Marciniec [1,2,*]

1 Faculty of Chemistry, Adam Mickiewicz University in Poznań, Uniwersytetu Poznańskiego 8, 61-614 Poznań, Poland
2 Centre for Advanced Technologies, Adam Mickiewicz University in Poznań, Uniwersytetu Poznańskiego 10, 61-614 Poznań, Poland; robert.przekop@amu.edu.pl (R.E.P.); bs33013@amu.edu.pl (B.S.)
3 Faculty of Chemical Technology, Poznan University of Technology, Berdychowo 4, 60-965 Poznań, Poland; paulina.jakubowska@put.poznan.pl
4 Faculty of Mechanical Engineering, Bialystok University of Technology, Wiejska 45 C, 15-351 Bialystok, Poland; m.jalbrzykowski@pb.edu.pl
* Correspondence: dariusz.brzakalski@amu.edu.pl (D.B.); bogdan.marciniec@amu.edu.pl (B.M.)

Received: 25 August 2020; Accepted: 28 September 2020; Published: 2 October 2020

Abstract: In this work, polyethylene (PE) composites were prepared with a series of completely condensed silsesquioxanes (SSQ), as well as with open-cage hepta(*iso*butyl)trisilanol silsesquioxane. The effect of the additives on the thermal, mechanical, rheological, and crystalline properties of the composites obtained was determined. The dispersion of trisilanol derivative within polymer matrix was slightly better than that of the other *iso*butyl compounds, suggesting condensation of the additive to less polar products of different structure, which was confirmed by thermogravimetry (TG) and matrix-assisted laser desorption-ionization time-of-flight (MALDI-TOF) mass spectrometry analysis. The additives improved the thermal stability of polyethylene and formed composites of higher rigidity than the neat polyolefin. The results were compared to the literature data, with aminopropylhepta(*iso*butyl)silsesquioxane and vinylhepta(*iso*butyl)silsesquioxane being used partially as references, as PE composites thereof were reported earlier, but lacked some analytical results and required further investigation. It was proven that the practical upper loading limit for such silsesquioxane compounds as processing and functional additives for polyethylene should be fixed at around 1%.

Keywords: silsesquioxane; polyethylene; composite; nanocomposite; thermal degradation; processing; additive

1. Introduction

Polyolefins are among the most widely applied thermoplastic polymers as their reasonable price and tuneable properties, such as crystallinity level, melt-flow rate, or processing and service temperatures, render them highly versatile. Amongst them, polyethylene (PE) is by far the most commonly used. PE is utilized for production of foils, films, fibers, bags, tubes, containers, battery separators, and many more [1–4]. It is characterized by good thermal and electrical insulating properties, very low glass transition temperature (below −100 °C), high chemical inertness, high stress cracking resistance, and ease of processing. However, it has quite low mechanical properties, such as tensile strength, Young modulus or abrasion resistance, has limited thermal stability, very low heat deflection temperature, and poor flame resistance. To increase the number of possible applications of

this polymer, different blends, copolymers, and grafted polymers thereof have been designed, as well as composites with numerous mineral and organic fillers or compositions with various processing and functional additives [5,6]. Fillers, such as natural fibers [4] or (nano)silica [7–9], have been applied to reinforce PE mechanically. To improve either processing or service properties of PE or composites thereof, additives such as lubricants, compatibilisers, plasticizers, or antioxidants/stabilizers have been extensively used [10]. As a novel type of either processing/functional additives or nanoreinforcing agents for polymer (nano)composites or blends, polyhedral oligomeric silsesquioxanes (SSQ) have been reported several times over the last twenty years, and discussed in detail in reviews by Kausar [11], Du [12], Kuo [13], Ayandele [14], Zhou [15], Shi [16], and Li [17]. Polyhedral oligomeric silsesquioxanes are known for their well-defined, molecular structure, controllable physicochemical properties on the basis of the introduced organic substituents, good solubility and dispersion properties, or simple, reproducible synthetic protocols [18,19]. As organosilicon hybrid compounds, SSQs tend to improve thermal stability of polymer matrices they are introduced into, but also modify materials rheology (e.g., as plasticizers or thixotropic agents) or improve mechanical properties, such as tensile or flexural modulus, tensile strength, heat deflection temperature. Different structures have been tested, including homo-($R_n[SiO_{1.5}]_n$) and heterosubstituted ($R_{n\text{-}m}$ $R'_m[SiO_{1.5}]_n$) systems, bearing either alkyl [20–47], alkenyl [41,48], aryl [24–26], or other functional groups [26,41,49–52], introduced mostly by condensation, hydrosilylation, or substitution reactions. It has been proven that a choice of introduced functional groups plays a major role in miscibility of silsesquioxanes and polymer matrix and the additive tendency towards agglomeration, but also the processing method and parameters have an impact on the obtained additive dispersion in the final composite or nanocomposite [40]. For example, large, linear alkyl chains render silsesquioxanes well-compatible with PE on the basis of similarity to the polyolefin chains, while smaller or branched substituents decrease the additive miscibility with the polymer [40,53]. At the same time, silsesquioxane additives of limited dispersion abilities may form particles serving as a reinforcing phase and improving mechanical properties of the obtained (nano)composite [21,25,40]. Also, it is important to point out that the processing method plays a huge role when discussing the preparation of SSQ/PE compositions. Very good dispersion of the additives has been obtained when high-shearing-forces processes have been applied, such as twin-screw extrusion [22,23,44] or injection moulding [32]. Among other methods, ball milling [30,31,33,37], solution blending [34,35], or reactive melt blending [51,52] have been reported with moderate to good results. The dispersion level plays a huge factor on the properties of the obtained materials, and effective dispersing of the organosilicon additive is crucial to observe effects such as (nano)reinforcing action or thermal stabilization of the composition [11–15]. In the previous work, we showed how a proper choice of organic substituents for spherosilicate compounds, as well as a processing method applied, allowed for effective obtaining of micro-and nanodispersion of the compounds in PE together with limited agglomeration [54]. It is crucial to mention that often two levels of dispersion can be observed and above specific concentration (depending on the compound and polymer matrix) multi-micron agglomerates are formed, together with a fraction of the additive being well-dispersed at a sub-micron scale [55]. In this work, a critical assessment of simple silsesquioxanes application as functional additives for PE was made, including compatibility of the components with the polyolefin matrix and the effects associated with increasing additive loading. For this purpose, a series of silsesquioxanes was applied as such additives, and their dispersion ability and impact on the obtained composite systems were studied. Melting and crystallization, thermal stability, mechanical and basic rheological properties were investigated. Additionally, the behaviour of open-cage hepta(isobutyl)trisilanol silsesquioxane, *i*Bu_7SSQ-3OH, under processing temperature was investigated. To the best of our knowledge, besides of one attempt [38], it was not studied as a direct additive for polyethylene or polypropylene, probably due to concerns about its polarity rendering the compound immiscible with highly apolar polyolefin.

2. Materials and Methods

2.1. Materials and Instrumentation

The chemicals were purchased from the following sources: *iso*butyltrimethoxysilane, trichlorovinylsilane, chloropropyltrichlorosilane, chloropropyltriethoxysilane, aminopropyltrimethoxysilane from ABCR, triethylamine and chloroform-d from Sigma Aldrich, tetrahydrofuran (THF), methanol, hydrochloric acid, acetonitrile and acetone from Avantor Performance Materials (Poland). Low density polyethylene (LDPE) type Malen E FABS 23 D022 from BasellOrlen Polyolefins. Its characteristics are M_w = 66,000, MFR (190 °C; 2.16 kg) = 2 g/10 min, T_m = 112 °C and density 0.921 g/cm^3. Silsesquioxanes were prepared according to the literature procedures [56–59]. *i*Bu$_7$SSQ-Vi was synthesised according to the procedure for the synthesis of *i*Bu$_7$SSQ-Cl. SSQ-8Cl was obtained as a resinous cage mix and was used as such.

Polyethylene concentrates were prepared on a two-roll mill Zamak Mercator WG 150/280. The concentrates were ground in SHINI SG-1417 low-speed mill and dried for 6 h at 90 °C. Prepared concentrates were then diluted to final additive concentrations in an extrusion process with cold granulation using Thermo Fisher Scientific (Waltham, MA, USA) HAAKE PolyLAB OS extrusion setup equipped with a single screw (D = 19.05 mm, *L*/*D*: 25) working at 30 rpm. The temperature zones for extrusion were set, from feed to die, as follows: 120, 160, 180, and 180 °C. For foils production, the setup was equipped with a foil extrusion die and chill-roll system. The foils prepared were of 0.2 mm thickness. Dumbbells were prepared on ENGEL E-Victory 170/80 injection moulding machine equipped with a double socket mould for preparation of normalized testing specimens consistent with the PN-EN ISO 527-2 norm (type 1A). The parameters for injection moulding were as follows: temperature profile of plastification unit, from feed to die: 170, 180 and 190 °C; mould temperature: 22 °C; injection time: 2 s; cooling time: 20 s; injection pressure p1: 1200 bar, p2: 500 bar; holding pressure profile: 1200 bar/1 s, 1000 bar/4 s, 300 bar/5 s.

MFR index was measured on INSTRON CEAST MF20 plastometer equipped with 2.16 kg weight at temperature of 190 °C.

For tensile strength tests, a universal testing machine Instron 5969 was used, in accordance to the norm EN ISO 527-2: 1996. The speed of traverse was set to 50 mm/min for dumbbells and 100 mm/min for foils.

^{1}H, ^{13}C, and ^{29}Si nuclear magnetic resonance (NMR) spectra were recorded at 25 °C on a Bruker Ascend 400 and Ultra Shield 300 spectrometers using $CDCl_3$ as a solvent. Chemical shifts are reported in ppm with reference to the residual solvent ($CHCl_3$) peaks for ^{1}H and ^{13}C.

Fourier transform-infrared (FT-IR) spectra were recorded on a Nicolet is 50 fourier transform spectrophotometer (Thermo Fisher Scientific) equipped with a diamond ATR unit with a resolution of 0.09 cm^{-1}.

SEM/EDS analyses were recorded on a Quanta FEG 250 (FEI) instrument; SEM at 5 kV and EDS at 30 kV, respectively. The samples were frozen in liquid nitrogen and fractured with pliers to reveal a surface satisfactory for an analysis.

Thermogravimetry was performed using NETZSCH 209 F1 Libra gravimetric analyser. Samples of 5.0 ± 0.2 mg were cut from each granulate and placed in Al_2O_3 crucibles. Measurements were performed under nitrogen and air in a 30–800 °C temperature range and at 20 °C/min temperature rise. Differential scanning calorimetry was performed using NETZSCH 204 F1 phoenix calorimeter. Samples of 5.0 ± 0.2 mg were cut from each granulate and placed in aluminium crucible with punched lid. Measurements were done under nitrogen in 20–220 °C temperature range and at 10 °C/min temperature rise. Each sample was treated by two heat-cool cycles to erase its thermal history and the data presented were measured for the second cycle. Crystallinity was determined from the first melting. For determination of materials crystallinity, fusion enthalpy of 100% crystalline PE of 288 J/g was assumed, according to literature reports [60].

2.2. General Procedure for Composites Preparation and Characterization

In a typical procedure, about 200 g of polyethylene was rolled on a two-roll mill until complete melt, after which the chosen modifier was added in a quantity corresponding to 5% of the final composite content, and the composition was rolled together at temperature range of 180–185 °C until it became completely homogeneous or until no more improvement of homogeneity was observed. After that, the composition was taken off the rolls and set to cool down. It was ground in the low-speed mill and the obtained masterbatch granulate was then diluted to 1.5%, 1%, and 0.5% by mixing it with the granulate of neat PE in a proper proportion and extruding it on a single-screw extruder, and the extrudate being simultaneously granulated. 0.1% concentration composites were obtained by diluting 0.5% granulate. For *i*Bu$_7$SSQ-3OH, satisfactory dispersion was observed at 0.5% and therefore 0.1% concentration composite was not prepared. On the other hand, *i*Bu$_7$SSQ-Vi was found to be the most prone to form agglomerates and therefore further diluting it to 0.1% concentration was abandoned. 1.5% concentrations were prepared only with *i*Bu$_7$SSQ-3OH and *i*Bu$_7$SSQ-Vi, to compare the behaviour of two highly different additives at high loading: poorly miscible, crystalline *i*Bu$_7$SSQ-Vi, and well-miscible *i*Bu$_7$SSQ-3OH forming amorphous condensation products. The obtained granulates were then measured by SEM, TG, and DSC techniques, and processed into standard dumbbell specimens and foils. Foils were cut into proper specimens using a sample cutter, equipped with a knife in a form of a dumbbell. Tensile strength tests for dumbbells and foil specimens were performed to measure ultimate tensile strength and elongation at the point of plastic elongation limit, as well as Young's modulus.

3. Results and Discussion

3.1. Characterisation of the Obtained Modifiers

The silsesquioxanes used in this work are presented on Figure 1.

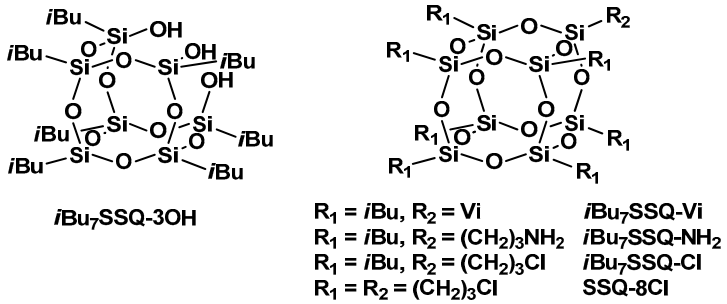

Figure 1. The Silsesquioxane (SSQ) compounds used in this work.

The structure of all the modifiers presented was confirmed spectroscopically (NMR, FT-IR, see Table S1 and Section 2 in the Supplementary Materials). TG analysis of the compounds allowed for verification of thermal stability of most of the additives under the conditions of PE processing, as well as reactivity of *i*Bu$_7$SSQ-3OH, and suggested some of the mechanisms of their thermal degradation at elevated temperatures. For SSQ-8Cl, the product was obtained in two fractions of different form: crystalline, in less than 15% yield, and amorphous in over 65% yield. The crystalline product was found to be pure T_8 cage, but the yields were not satisfactory for further use. The TG of the amorphous product did not show any mass loss under 300 °C, and ^{29}Si NMR did not confirm presence of any free silanol groups (see Figure S4 in the Supplementary Materials), which confirmed full condensation, however the product was an amorphous mixture of different cage hybrids (cage mixture) and Figure 1 represents the idealized structure. The amorphous product was chosen for the composite preparation. For *i*Bu$_7$SSQ-3OH, an unusual two-step mass loss was observed, with the first degradation event occurring at a relatively low temperature. The mass loss of ~3% observed in the 150–210 °C temperature

range, presented in Figure 2 (DTG peak at 180.3 °C), during heating of hepta(isobutyl)trisilanol suggested dehydrative condensation of the compound with the formation of a mixture being a combination of some idealized products presented in Scheme 1, as well as some higher molecular weight products of the cage rearrangement and further condensation.

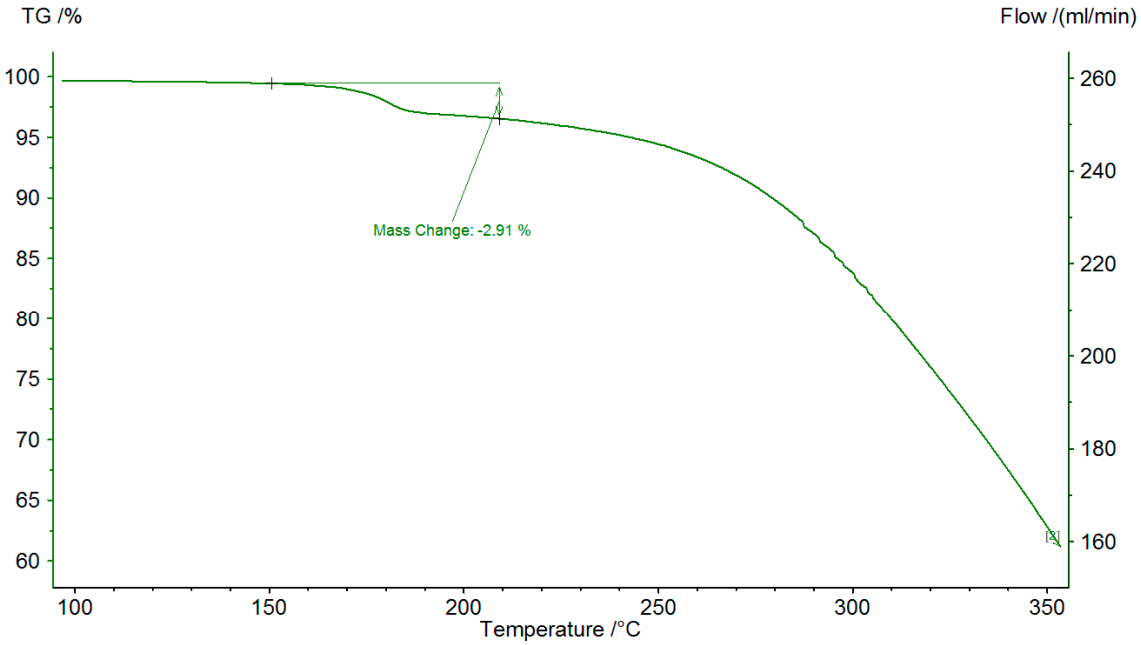

Figure 2. TG analysis of *i*Bu$_7$SSQ-3OH showing initial mass loss (cropped for visibility).

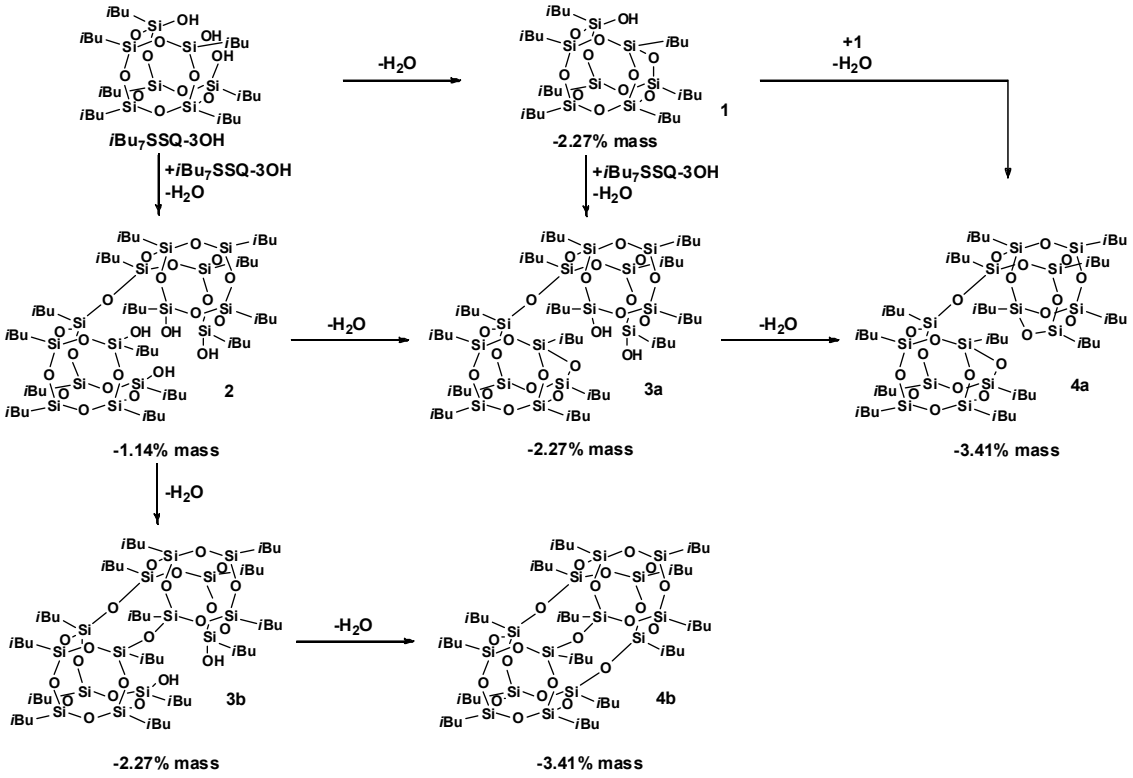

Scheme 1. Possible routes of thermal condensation of hepta(isobutyl)trisilanol silsesquioxane. Depending on the condensation product, mass loss is presented in accordance to either one (1) or two molecules (2, 3a, 3b, 4a, 4b) of the initial trisilanol.

When a sample of *i*Bu$_7$SSQ-3OH was heat-treated in a laboratory dryer for 6 min at 180 °C (the time required for full sample melt), it turned into a glassy, transparent material. MALDI-TOF-MS analysis of heat-treated samples allowed for identification of all the proposed low-molecular products, that is a monomer and dimers (see Scheme 1) according to the molecular weight of the molecule (see Figures S17 and S18 in the Supplementary Materials), but no attempt was made to isolate them and identify their precise molecular structures. Therefore, condensation products bearing the same molecular weight were marked with the same numbers (e.g., Scheme 1. 3a,3b). Similar conclusions on degradation and condensation of trisilanol were drawn by Zeng et al. when heat-treating hepta(*iso*octyl)trisilanol, however MALDI-TOF mass spectra didn't allow for identification of any particular product [61]. It is possible that, during thermal treatment, *i*Bu$_7$SSQ-3OH undergoes condensation to products of higher molecular weight than the ones presented, however those would exceed *m/z* ratio limit available for the instrument used. More findings in the subject of MALDI-TOF-MS analysis of silsesquioxanes and silsesquioxane-derived materials may be found in some recent scientific reports [62–64].

3.2. SEM-EDS Analysis

SEM imaging combined with EDS mapping of silicon allowed for assessment of additives dispersion within PE. For the assessment of silsesquioxane compounds dispersion abilities, the SEM imaging of all the studied materials was first performed on the SSQ/PE extrudates obtained. The dispersion of SSQ-8Cl was satisfactory at all concentrations, showing good compatibility of the non-polar, amorphous additive with the polymer matrix. Also, *i*Bu$_7$SSQ-3OH showed comparably good compatibility with PE, which can be explained on the basis of TG and MALDI-TOF-MS analyses, by the additive forming less polar condensation products upon mixing with molten polymer. Only at 1.5% loading, substantial agglomeration was observed. For 1% *i*Bu$_7$SSQ-3OH/PE, on the basis of SEM and EDS, some agglomerates were observed for the samples prepared by extrusion (Figure 3a,b), but no agglomerates were visible for the injection-moulded specimens in the scale applied for this study (Figure 3c,d). This proves that the additional shearing forces occurring during injection moulding (which is a high temperature, high pressure process) improve the dispersion of the additive. At 1.5%, some agglomeration was observable even in injection-moulded samples, showing the limitation of the additive dispersion abilities. In comparison, the other additives, all bearing *iso*butyl groups, showed dispersion properties similar to each other, but inferior to the ones discussed above. In all cases, at higher loadings agglomerates can be observed forming, which is easily visible on EDS maps (see Figures S18–S35 in the Supplementary Materials). The most significant self-aggregation was observed for *i*Bu$_7$SSQ-Vi, where substantial agglomerates were already observable at 0.5% loading, and at 1.5% very only a small fraction of the additive remains highly dispersed. This presents the limited compatibility of *iso*butyl-substituted and other small alkyl group-substituted silsesquioxanes with polyethylene under different processing techniques, especially with their increasing loading, which was previously presented by Guo and Fréchette [30,31,33–35,43–45]. Additionally, the presence of a different substituent in one corner of hepta(*iso*butylsil)sesquioxanes may introduce dipole moment, increasing polarity of the molecule and reducing the compatibility of the compound with nonpolar PE chains. This may be the reason for better compatibility of products of *i*Bu$_7$SSQ-3OH thermal treatment during composite processing in comparison to the other *i*Bu$_7$SSQ derivatives used in this work. Also, the amorphous state of *i*Bu$_7$SSQ-3OH heat-treated samples, as well as mix-cage SSQ-8Cl, both being mixtures of various condensation products, may play a role in the dispersion mechanism, contrary to *i*Bu$_7$SSQ-Vi, *i*Bu$_7$SSQ-NH$_2$ and *i*Bu$_7$SSQ-Cl, all being crystalline solids, which may promote their self-aggregation, as speculated by Sheen [65] and Perrin [66]. Also, Grala et al. reported on segregation of *i*Bu$_7$SSQ-NH$_2$ additive during crystallization of HDPE composites, as well as two different levels of dispersion, where the size of additive particles varied from less than 100 nm up to several microns [51].

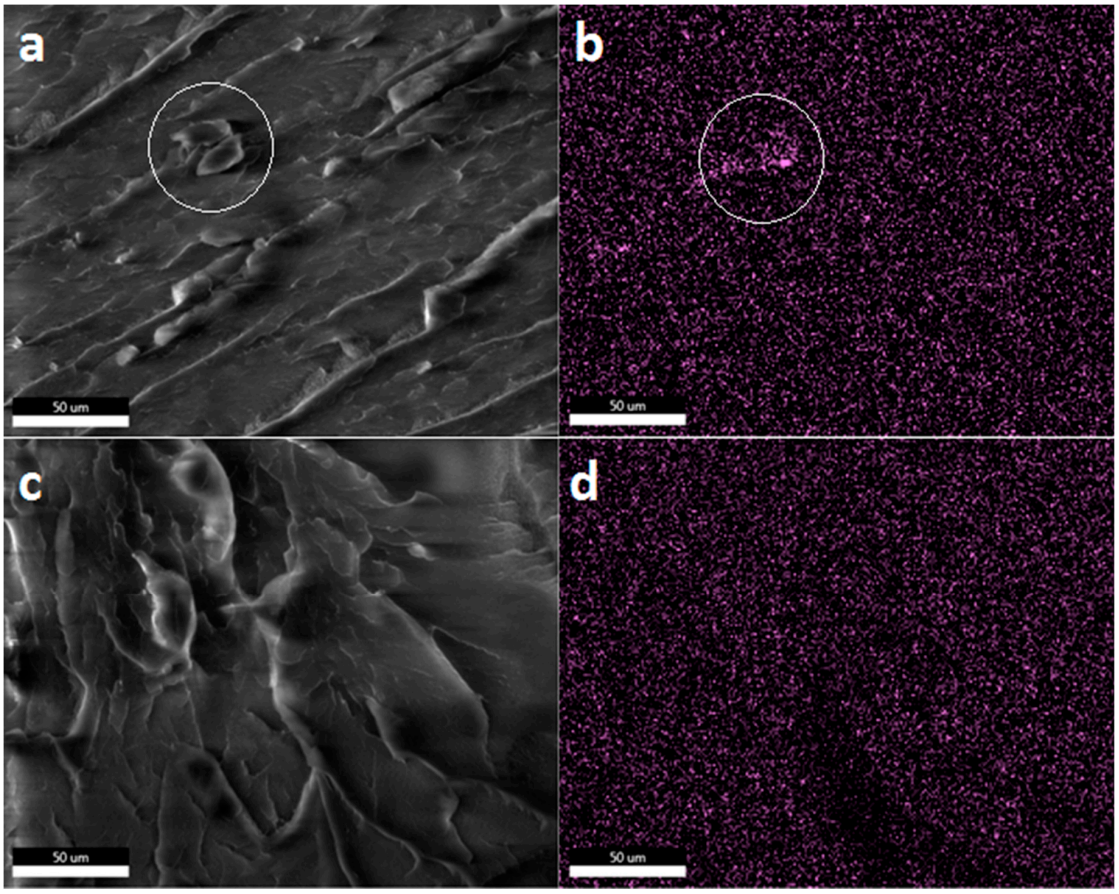

Figure 3. SEM images (**left**) and EDS maps of silicon (**right**) of 1% *i*Bu$_7$SSQ-3OH/PE composite obtained by extrusion (**a**,**b**) and injection moulding (**c**,**d**).

3.3. Mechanical Analysis

Mechanical studies have been performed to evaluate mechanical properties of the obtained materials. The results are collected in Tables 1–3. Some different observations were made upon analysis of two groups of specimens: dumbbells and foils. It was obvious that the form of product the polymer material is made into and especially the processing technology used to obtain the given object have a huge impact on the final properties of the objects and some compounds, as much useful as processing additives for one type of processing technology, may be inappropriate for another one. Very similar observations were made when studying spherosilicate-derived PE processing additives [54]. For dumbbells, in most cases a small increase in tensile strength was observed, with a general trend of strength improvement being smaller for higher concentrations, most likely due to high additive dispersion at lower loadings, as it was proven with SEM-EDS. This small increase can be linked to the presence of silsesquioxane particles in the polymer, forming a reinforcing phase. Agglomerates forming at higher loadings no longer serve reinforcing action, and rather introduce mechanical defects in the materials. Similar observations were made by Lim et al. [25]. However, differences were subtle and often within the limits of standard deviation, probably due to overall low loadings of the additives tested, the silsesquioxane component making up a small fraction of the composition volume. Some higher values of tensile strength were obtained for *i*Bu$_7$SSQ-NH$_2$ and *i*Bu$_7$SSQ-3OH, therefore better compatibility between the PE and particles of mentioned silsesquioxanes may be speculated. All these observations suggest good uniformity of the materials, obtained by high-temperature, high-shearing forces process that injection moulding is. At the same time, it presents limited utility of applied compounds as functional additives when speaking of mechanical properties improvement. Hato et al. showed how the addition of octamethylsilsesquioxane, known for its

tendency of forming agglomerates within PE, decreased mechanical properties, that is tensile strength and elongation at rupture, when applied at 5–10% loadings (lower loadings were not tested) [47]. At such a concentration, the additive only increased Young's modulus, as is typical for a classic solid filler, e.g., silica [7–9]. Grala et al. reported the addition of *i*Bu_7SSQ-NH_2 to generally impart the mechanical parameters of HDPE composites both at static load and on impact, as must have been a result of high additive loading and low additive-polymer interaction [51]. Better results were obtained for HDPE-*g*-MA and *i*Bu_7SSQ-NH_2 reactive blending experiments, however it is difficult to compare such results with those on physical compounding, as reactive blending is chemical modification of the polymer, resulting in changes on the molecular level of the polymer chain. Also, grafted polymers, such as HDPE-*g*-MA, already show properties different than those of neat homopolymers, and are far more expensive, usually intended for use in small quantities as compatibilizing agents for polymer blends or composites with mineral fillers.

Table 1. Tensile strength of the SSQ/PE composites.

Additive	Sample	Concentration of Additive (%)			
		0.1	0.5	1.0	1.5
		Tensile Strength (MPa)			
Neat PE	Dumbbell	13.08 ± 0.26			
	Foil	19.70 ± 0.95			
SSQ-8Cl	Dumbbell	13.11 ± 0.33	13.29 ± 0.19	13.22 ± 0.34	-
	Foil	16.79 ± 0.77	15.99 ± 0.88	15.87 ± 0.81	-
iBu_7SSQ-Cl	Dumbbell	13.41 ± 0.12	13.29 ± 0.21	13.14 ± 0.27	-
	Foil	14.44 ± 0.69	16.44 ± 0.43	15.45 ± 0.71	-
iBu_7SSQ-NH_2	Dumbbell	14.43 ± 0.22	14.20 ± 0.49	14.06 ± 0.19	-
	Foil	18.17 ± 0.39	16.42 ± 0.90	16.62 ± 0.77	-
iBu_7SSQ-Vi	Dumbbell	-	13.00 ± 0.34	12.98 ± 0.32	12.52 ± 0.48
	Foil	-	16.31 ± 0.94	14.49 ± 0.86	14.91 ± 0.80
iBu_7SSQ-3OH	Dumbbell	-	14.41 ± 0.24	14.36 ± 0.18	14.33 ± 0.32
	Foil	-	15.83 ± 0.68	20.81 ± 0.80	19.12 ± 0.70

Table 2. Young's modulus of the SSQ/PE composites.

Additive	Sample	Concentration of Additive (%)			
		0.1	0.5	1.0	1.5
		Young's Modulus (MPa)			
Neat PE	Dumbbell	91.68 ± 3.46			
	Foil	213.82 ± 14.59			
SSQ-8Cl	Dumbbell	92.92 ± 5.31	95.93 ± 4.71	97.71 ± 5.39	-
	Foil	166.08 ± 8.70	155.35 ± 6.13	164.17 ± 9.64	-
iBu_7SSQ-Cl	Dumbbell	94.34 ± 3.08	95.86 ± 4.24	92.73 ± 2.01	-
	Foil	150.74 ± 8.08	168.26 ± 8.74	141.10 ± 7.47	-
iBu_7SSQ-NH_2	Dumbbell	108.92 ± 2.70	101.80 ± 4.87	103.75 ± 4.77	-
	Foil	209.89 ± 11.23	159.42 ± 6.48	166.67 ± 8.39	-
iBu_7SSQ-Vi	Dumbbell	-	92.53 ± 4.84	92.08 ± 3.55	98.63 ± 4.46
	Foil	-	151.69 ± 9.03	166.20 ± 9.40	150.88 ± 11.05
iBu_7SSQ-3OH	Dumbbell	-	109.09 ± 2.08	109.72 ± 3.40	105.67 ± 2.82
	Foil	-	167.58 ± 7.14	194.06 ± 9.79	110.74 ± 6.35

Table 3. Plastic elongation of the SSQ/PE composites.

Additive	Sample	Concentration of Additive (%)			
		0.1	0.5	1.0	1.5
		Elongation at Maximum Load (%)			
Neat PE	Dumbbell	60.38 ± 1.77			
	Foil	176.69 ± 11.63			
SSQ-8Cl	Dumbbell	59.97 ± 2.84	59.25 ± 2.15	57.97 ± 3.41	-
	Foil	166.05 ± 7.83	142.70 ± 6.30	158.96 ± 9.29	-
*i*Bu$_7$SSQ-Cl	Dumbbell	60.29 ± 2.14	59.45 ± 2.06	59.86 ± 1.15	-
	Foil	121.55 ± 6.92	112.41 ± 5.33	101.40 ± 5.23	-
*i*Bu$_7$SSQ-NH$_2$	Dumbbell	57.69 ±1.18	59.28 ± 2.52	58.03 ± 2.02	-
	Foil	161.07 ± 6.13	159.16 ± 7.11	137.63 ± 5.77	-
*i*Bu$_7$SSQ-Vi	Dumbbell	-	59.05 ±2.02	59.28 ± 3.01	53.51 ± 1.32
	Foil	-	158.60 ± 8.02	141.78 ± 8.28	133.73 ± 9.06
*i*Bu$_7$SSQ-3OH	Dumbbell	-	57.13 ± 0.76	56.52 ± 1.28	57.88 ± 0.90
	Foil	-	113.53 ± 5.41	124.40 ± 6.13	76.24 ± 4.12

SSQ-8Cl and *i*Bu$_7$SSQ-3OH showed trends of increasing Young's modulus of the composites, the well-dispersed additives probably increasing chain aggregation in the amorphous phase of the polymer and reducing free volume. For the other additives, the effect of material stiffness increase can also be seen, most likely due to additive particles mechanically reinforcing the composite, but at higher loadings the effect decreased as the particle agglomerates introduced too many discontinuities in the material. As most of the systems showed improved material rigidity, it resulted in small reduction of plastic elongation values for all samples, which is usually expectable in terms of comparison between neat polymers and composites derived thereof (see Table 3).

For the foil samples, for almost all examples, a rather severe reduction of tensile strength was observed, which can be linked to particles of additive disturbing linear flow and orientation of polymer in the foil. Together with reduced Young's modulus and plastic elongation, it represents deterioration of foils properties. *i*Bu$_7$SSQ-3OH/PE system, however, showed similar behaviour of tensile strength change for 0.5% loading, but at 1.0% it surprisingly exceeded tensile strength of the neat polymer, similarly to the dumbbell specimens (Table 1). Together with relatively high Young's modulus (comparable to neat PE foils) and severely decreased value of plastic elongation, it suggests a complex interaction between PE, the highly dispersed products of *i*Bu$_7$SSQ-3OH condensation, and less dispersed particles thereof, acting as a reinforcing phase, despite the general tendency of silsesquioxane particles deteriorating foil properties. Therefore, the *i*Bu$_7$SSQ-3OH composite foils presented satisfactory rigidity, but not exceeding that of neat PE within standard deviation (Table 3). At 1.5% loading, tensile strength of *i*Bu$_7$SSQ-3OH/PE foils remained high, but due to increased additive agglomeration, the material showed heavily decreased values of Young's modulus and plastic elongation. Similar to the dumbbell specimens, all the foils presented decreased plastic elongation, however the change was more severe. The results are, in general, similar to the previously reported observations on spherosilicate/PE composites and prove that such cage siloxane systems are a rather poor choice for additives for PE foils processing [54].

3.4. Thermomechanical Analysis

Heat deflection temperature (HDT) analysis was performed to analyse effect of the SSQ additives on the samples' stiffness under conditions of increasing temperature (Figure 4, Table S3 in the Supplementary Materials). Some interesting trends were observed. SSQ-8Cl and *i*Bu$_7$SSQ-3OH initially caused increase of the HDT values, which corresponds to higher sample stiffness under given temperature. However, with increased loadings, the amorphous additives behaved like plasticizing

agents, decreasing HDT values below that of the neat PE. The effect was especially prominent for SSQ-8Cl at 1.0% loading. *i*Bu$_7$SSQ-Cl also showed plasticizing character, but the effect was visible already at 0.1% loading. It was likely caused by the additive particles causing small disorders of the polymer matrix. On the other hand, *i*Bu$_7$SSQ-NH$_2$ and *i*Bu$_7$SSQ-Vi initially decreased HDT values of the composites thereof, but with increasing loading, the parameter also increased. The initial HDT decrease may be explained the same as for the *i*Bu$_7$SSQ-Cl, by the additive particles introducing disorders of the polymer matrix, however, at higher concentrations, the particles of the crystalline additive most likely provide mechanical reinforcement of the SSQ/PE composite, rendering the composite more stiff, as these compounds do not undergo any softening or melting in the temperature range applied for this study.

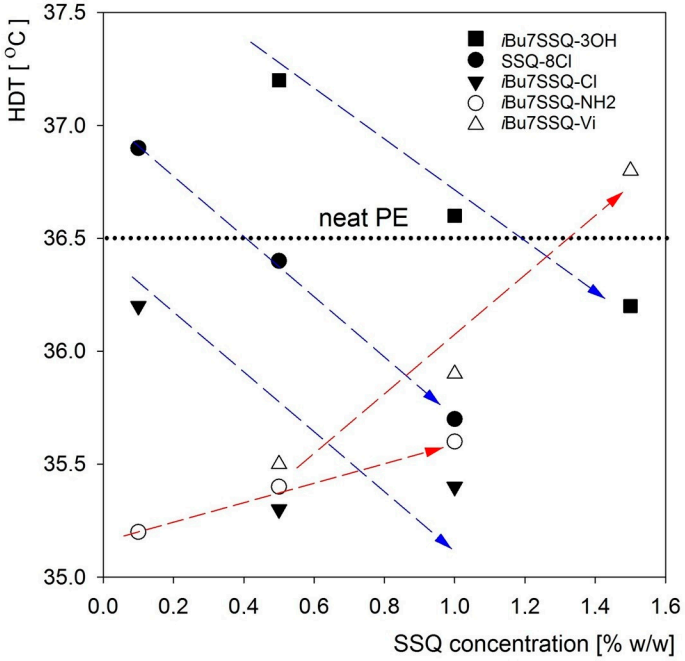

Figure 4. Heat Deflection Temperatures of the obtained composites.

3.5. Thermal Analysis

Thermogravimetric analysis was performed to study the impact of the applied organosilicon additives on the thermal stability of the obtained materials. The results are collected in Table 4. In general, all the obtained compositions showed improved thermal stability, however degradation mechanisms differ in air and ambient atmosphere (nitrogen), and the stabilising effect of silsesquioxanes on the polymer matrix was more significant in air, therefore it will be studied in detail. The nonlinearity of the stabilising action may be linked to two factors, as neither of them allows for full explanation of the observed behaviour on its own. One cause for this effect is the dispersion/agglomeration described above, as it impacts basically all the properties studied for these materials. The second effect is the critical concentration at which the additive moderates a degradation mechanism and above which no further change can be expected (the saturation effect), e.g., free radical reactions of the polymer chain during polyolefin cracking, where only a small concentration of free radicals is present at the time. It should be also noted that even at the polymer melting temperature, simple silsesquioxane additives with small substituents (*i*Bu, Vi, substituted propyl) should not be expected to dissolve or melt, and rather only disperse/agglomerate, besides *i*Bu$_7$SSQ-3OH during the initial compounding process. The above general conclusions are similar to the previous findings on spherosilicate/PE composites [54]. It can be speculated that the siloxane framework of the silsesquioxane molecule plays a role in a recombination or quenching of free radicals, as an average Si–C bond is weaker than a C–C bond, which

results in elimination of an organic group and formation of a silyl radical [67]. Similar conclusions were given by Fina et al. upon studying thermal degradation of various octasilsesquioxanes [68]. For most of the additives, the $T_{5\%}$ parameter decreased upon the increase of additive concentration from 0.5% to 1%, where additive agglomeration was observed, as it translates to decreased concentration of species available towards reaction with free radicals on cracking PE chains. This effect was less severe for T_{onset} and T_{DTG}, probably due to additive further dispersing or reacting with the cracking polyolefin at high temperature, as may be in case of *i*Bu$_7$SSQ-3OH. At 1.5% loading, the additive showed basically the same results to those at 0.5%, as the increased amount of the compound likely compensated for the agglomeration effect. At 0.5% concentration, the SSQ-8Cl/PE composition showed some of the highest thermal parameters, representing good stabilising effect of the additive. The presence of chlorine atom in the structure may play the role in the mechanism of composition stabilization, as it is known that chlorinated compounds are susceptive towards recombination with silyl radicals, as well as other radical species [69]. However, the most prominent thermal stabilising agent was *i*Bu$_7$SSQ-NH$_2$, where together with increasing loading, a rise of all thermal parameters was observed. This effect can be explained by the presence of amino group, which serves as a free radical sweeper and a reducing agent, as well as metal deactivator of polyolefin polymerization catalyst leftovers, which also play a role of a catalyst of high temperature polyolefin degradation in oxidative atmosphere [10,70]. Nguyen et al. described the reactivity of aminoalkylated silsesquioxane towards recombination with peroxyl radicals formed on PE chains, however a more complex composition was described, where together with iron(III) stearate, an amine-mediated catalytic oxidation system was formed [49]. Grala et al. reported a significant increase of $T_{5\%}$ parameter for *i*Bu$_7$SSQ-NH$_2$/HDPE composition, however T_{DTG} parameter was unaffected [51]. Similarities between thermal behaviour of the remaining SSQ additives described in this work are due to their similarities of chemical structure, which was also observed while studying dispersion and crystallinity. Interestingly, Bouza et al. reported a decrease of $T_{5\%}$ and T_{onset} upon the addition of 2% *i*Bu$_7$SSQ-NH$_2$ and a small increase of T_{onset} upon 10% addition, when studying composites thereof with isotactic polypropylene, however the measurements were only done in argon atmosphere [71].

Table 4. Thermal parameters of SSQ/PE composites from TGA measurements.

Measurements in Air Atmosphere							
Additive Conc. [%]	***T* (°C)**	**Additive Type**					
		Neat PE	**SSQ-8Cl**	**iBu$_7$SSQ-Cl**	**iBu$_7$SSQ-NH$_2$**	**iBu$_7$SSQ-Vi**	**iBu$_7$SSQ-3OH**
0.1	$T_{5\%}$	348.3	355.4	355.6	362	-	-
	T_{onset}	382.4	379.4	380.2	400.3	-	-
	T_{DTG}	418.3	422.6	419.8	448.5	-	-
0.5	$T_{5\%}$	348.3	373.3	362.3	365.5	366.6	364.7
	T_{onset}	382.4	399.4	391.7	434.7	398.5	396.9
	T_{DTG}	418.3	455.8	440.8	445.4	443.9	436.5
1.0	$T_{5\%}$	348.3	362.5	354.4	381.4	359.9	369.0
	T_{onset}	382.4	392.1	394.3	448.4	389.7	404.6
	T_{DTG}	418.3	439.1	433.7	458.1	447.2	438.5
1.5	$T_{5\%}$	348.3	-	-	-	364.7	372.8
	T_{onset}	382.4	-	-	-	402.5	404.7
	T_{DTG}	418.3	-	-	-	444.4	441.9

Table 4. *Cont.*

Measurements in Nitrogen Atmosphere							
Additive Conc. [%]	***T* (°C)**	**Additive Type**					
		Neat PE	**SSQ-8Cl**	**iBu$_7$SSQ-Cl**	**iBu$_7$SSQ-NH$_2$**	**iBu$_7$SSQ-Vi**	**iBu$_7$SSQ-3OH**
0.1	$T_{5\%}$	441.8	447.4	446.5	444.9	-	-
	T_{onset}	469.3	479.8	473.8	470.6	-	-
	T_{DTG}	477.9	488.2	487.9	485.2	-	-
0.5	$T_{5\%}$	441.8	444.7	449.1	448.7	445.2	445.7
	T_{onset}	469.3	472.8	462.9	473.2	476.2	470.5
	T_{DTG}	477.9	487.2	489	487.8	489.8	486.6
1.0	$T_{5\%}$	441.8	443.7	445.5	445.3	445.3	445.1
	T_{onset}	469.3	476.2	472.4	460	472.0	471.1
	T_{DTG}	477.9	487.7	489.6	486.3	490.1	487.2
1.5	$T_{5\%}$	441.8	-	-	-	445.1	443.7
	T_{onset}	469.3	-	-	-	476.0	474.4
	T_{DTG}	477.9	-	-	-	490.3	489.2

DSC analysis shows that all the additives affect melting and crystallisation temperatures of the obtained compositions (see Table 5). When discussing crystallisation temperature (T_c), the most important role of the additives to consider is the nucleating effect, observable by increased T_c values. In general, all the additives exhibited nucleating effect. For SSQ-8Cl, a trend for increasing nucleating effect associated with increasing additive loading was visible. For *i*Bu$_7$SSQ-Cl, the nonlinearity was most likely caused by the additive agglomeration at 0.5% loading, and additional nucleating effect of highly abundant agglomerated particles observed by 1% loading. The strongest effect was recorded for *i*Bu$_7$SSQ-NH$_2$, however a similar agglomeration effect was observed by 0.5% concentration. *i*Bu$_7$SSQ-Vi was moderately effective, with nucleating effect decreasing together with increasing loading, and *i*Bu$_7$SSQ-3OH showing an opposite trend. Barczewski et al. reported a significant increase of crystallization temperature of LDPE characterized by low nominal T_c (96.3 °C) and also observed only a minor difference between 0.5% and 1% loading, showing the "saturation effect" of the increasing additive concentration [41].

Table 5. Melting and crystallisation temperatures of obtained composites.

Additive	**Concentration of Additive (%)**				**Concentration of Additive (%)**			
	0.1	**0.5**	**1.0**	**1.5**	**0.1**	**0.5**	**1.0**	**1.5**
	Crystallisation Temperature (°C)				**Melting Temperature (°C)**			
Neat PE	98.8				112.4			
SSQ-8Cl	99.0	99.5	99.8	-	113.4	112.2	111.8	-
*i*Bu$_7$SSQ-Cl	99.3	99.1	99.7	-	112.3	112.5	111.8	-
*i*Bu$_7$SSQ-NH$_2$	99.9	99.4	100.0	-	112.0	111.8	111.5	-
*i*Bu$_7$SSQ-Vi	-	99.5	99.0	98.4	-	112.6	113.1	113.8
*i*Bu$_7$SSQ-3OH	-	98.9	99.2	99.8	-	112.7	113.0	112.0

The changes of the melting temperature can be linked to moderation of mean crystallite size, and larger crystallites being responsible for higher melting temperature [54]. By this principle, all the compounds mediated the PE crystallites size, with a tendency for most additives to reduce the main crystallite size at the highest additive loading. As the amount of additive increases, additional particles of non-melting silsesquioxane compound provide more nucleation sites, and the high number of simultaneously growing spherulites limit their size due to small volume available for growth of each

spherulite. An opposite trend was observed for *i*Bu$_7$SSQ-Vi, most likely due to the additive showing strong agglomeration tendency, therefore providing less nucleation sites together with increasing loading. Also, SSQ-8Cl at 0.1% loading and *i*Bu$_7$SSQ-3OH at 0.5% and 1.0% loadings effectively induced growth of crystallites larger than those of neat PE. This is likely due to low concentration of nucleating species, initiating a non-disturbed spherulite growth. Grala et al. reported little impact of *i*Bu$_7$SSQ-NH$_2$ on melting and crystallization temperatures of HDPE composites at 2.5% and 5% loading, which showed the limited functionality of such additives at higher concentrations, where increased segregation occurs [51].

Additionally, DSC was used to determine the crystallinity indices (CI) of the obtained materials. In general, very small effect of the additives on crystallinity levels of polyethylene in obtained composites was observed (Figure 5, Table S2 in the Supplementary Materials), however, in all cases, the nucleating effect of the additives was confirmed, as the CI values are above those of neat PE. Joshi et al. showed that addition of octamethylsilsesquioxane to HDPE at various loadings had little impact on crystallinity level of the polymer, however it mediated its crystallite size [23]. Guo et al. also suggested that when applying octa(*iso*butyl)silsesquioxane for UHMWPE, the additive segregated on the spherulite interfaces, where most of the polymer amorphous phase is located [37]. The non-linear relationship between the SSQ additive loading and the crystallinity levels of PE can be explained on the basis of two levels of dispersion of the additives, where at higher loadings more agglomerates form and the less numerous, large particles of the additive provide less nucleation sites for the crystallizing polymer [54,55]. For most examples, the highest crystallinity can be observed at 0.5% loading, so it can be speculated that it's the concentration where most of the additive is well dispersed and provides the highest amount of small, nucleation-promoting particles, whereas at 1.0% and 1.5% loadings, multi-micron agglomerates predominate, limiting the number of available nucleation sites. The exact relationship between the additive concentration and the nucleating effect of the additive would be dependent on the type of functional groups present in the compound structure, and a matter of more detailed study, which was not covered in this work.

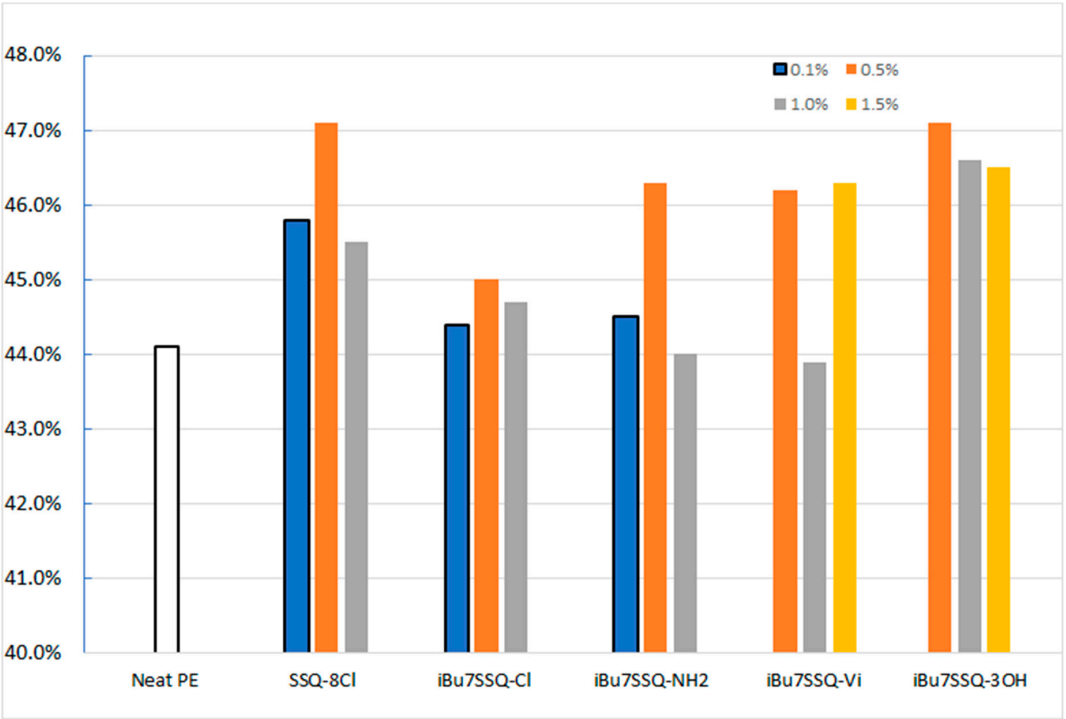

Figure 5. Crystallinity indices (CI) of the obtained composites.

3.6. Rheological Analysis

Basic rheological analysis was performed by assessing the effect of silsesquioxane additives on melt flow rate of the obtained compositions (Table 6). In all cases the additive caused reduction of MFR value, however there was an interesting general trend for this reduction to decline and the MFR values closing to that of the neat polymer together with increasing loading. It suggests that the additives disrupt the flow of composition, either adding thixotropic character to the composition in their particulate form (which is a normal behaviour for molten polymers containing particulate fillers), or by increasing polymer chains interaction, when dispersed on a molecular level. However, with increasing concentration, the additional modifier worked as a lubricating agent, likely by reducing adhesion between the composition and barrel, similarly to silicone additives, which is a positive feature in a perspective of application of such compositions for injection moulding and extrusion technologies. For *i*Bu$_7$SSQ-Vi, an increase of MFR index was observed together with increasing loading, up to 2.03 value at 1.5% concentration, which is comparable to that of the neat PE. Similarly, Barczewski et al. reported that the addition of *i*Bu$_7$SSQ-Vi to LDPE considerably reduced kinetic viscosity of the compositions at low shear rates, with a trend for further viscosity reduction together with an increasing amount of the additive used [41].

Table 6. MFR values for SSQ/PE composites.

Additive	Concentration of Additive (%)			
	0.1	**0.5**	**1.0**	**1.5**
	MFR (g/10 min)			
Neat PE	2.02			
SSQ-8Cl	1.83	1.88	1.90	-
*i*Bu$_7$SSQ-Cl	1.87	1.92	1.99	-
*i*Bu$_7$SSQ-NH$_2$	1.87	1.91	1.98	-
*i*Bu$_7$SSQ-Vi	-	1.91	1.99	2.03
*i*Bu$_7$SSQ-3OH	-	1.86	1.86	1.89

4. Conclusions

Most of the compounds investigated in this work showed tendency for agglomeration at higher loadings, and the most effective concentration was usually such where the additive was highly dispersed without high accompanying agglomeration. The compositions with 1.5% loading were similar in characteristics to those of 0.5% or worse. It is due to limited compatibility between PE and silsesquioxanes bearing small organic substituents. Therefore, for PE processing, it should be considered not to exceed loadings of around 1% of such compounds, especially taking into account the production cost of these compounds. Hepta(isobutyl)trisilanol silsesquioxane was highly reactive at PE processing temperature, resulting in condensation into less polar, amorphous species showing good compatibility with PE, better than that of the investigated close-caged silsesquioxanes, which translated into good mechanical and thermal properties of the obtained compositions. Similar behaviour was observed for SSQ-8Cl/PE composites, the highly symmetrical and apolar, as well as amorphous additive being well-miscible with the polymer matrix. Also, *i*Bu$_7$SSQ-NH$_2$ exhibited very good thermal stabilizing effect in oxidative atmosphere. The processing method type had a great impact on the mechanical properties of the materials obtained, as due to high shear forces applied, the injection moulded SSQ/PE samples were characterised by much better performance than the extruded foils. The method provided better homogenisation of the polymer with the additives, as confirmed by SEM-EDS. Nevertheless, the SSQ compounds had a limited impact on the mechanical properties of the obtained composites, as contrary to different literature reports. However, it was mainly due to low loadings of the additives applied, as the higher concentrations were not considered in this work. All the

investigated compounds showed a limited nucleation effect on PE and moderated the mean crystallite size of the polymer. Also, at higher loadings, SSQ-8Cl and *i*Bu$_7$SSQ-3OH served as plasticizing agents.

In the light of the presented results, as well as other reports, it should be pointed out that the use of the term "nanofiller" to describe polyhedral oligomeric silsesquioxanes is inadequate. Polyhedral oligomeric silsesquioxanes may be applied as functional additives (either thermal, mechanical, anti-oxidative, or processing, e.g., rheological, crystallization-mediating), but due to their multifunctionality, and also relatively high costs, they cannot be considered fillers, as opposed to silica or other affordable mineral or organic materials being applied for this purpose to either reduce production costs or considerably improve mechanical properties of the composite obtained. Probably, this misinterpretation was formed due to the initial fascination over the unique cage structure of polyhedral oligomeric silsesquioxanes, where another inaccurate name for these systems was introduced, i.e., molecular silica. Moreover, for polyethylene systems, at higher loadings, they tend to agglomerate up to a degree where most of the particles or agglomerates cannot be considered nanoscopic anymore.

Supplementary Materials: The following are available online at http://www.mdpi.com/2073-4360/12/10/2269/s1, Table S1: List of isolated compounds; Table S2. Crystallinity indices (CI) of the obtained composites; Table S3. Heat Deflection Temperatures of the obtained composites; Figure S1: ^{1}H NMR of SSQ-8Cl; Figure S2: ^{13}C NMR of SSQ-8Cl; Figure S3: ^{29}Si NMR of SSQ-8Cl; Figure S4: ^{1}H NMR of iBu$_7$SSQ-Cl; Figure S5: ^{13}C NMR of iBu$_7$SSQ-Cl; Figure S6: ^{29}Si NMR of iBu$_7$SSQ-Cl; Figure S7: ^{1}H NMR of iBu$_7$SSQ-NH$_2$; Figure S8: ^{13}C NMR of iBu$_7$SSQ-NH$_2$; Figure S9: ^{29}Si NMR of iBu$_7$SSQ-NH$_2$; Figure S10: ^{1}H NMR of iBu$_7$SSQ-Vi; Figure S11: ^{13}C NMR of iBu$_7$SSQ-Vi; Figure S12: ^{29}Si NMR of iBu7SSQ-Vi; Figure S13: ^{1}H NMR of iBu$_7$SSQ-3OH; Figure S14: ^{13}C NMR of iBu$_7$SSQ-3OH; Figure S15: ^{29}Si NMR of iBu$_7$SSQ-3OH; Figure S16: MALDI-TOF-MS spectrogram of iBu$_7$SSQ-3OH heat treatment products; Figure S17: MALDI-TOF-MS spectrogram of iBu$_7$SSQ-3OH heat treatment products (enhanced); Figure S18: 0.1% SSQ-8Cl/PE; Figure S19: 0.5% SSQ-8Cl/PE; Figure S20: 1% SSQ-8Cl/PE; Figure S21: 0.1% iBu7-SSQ-Cl/PE; Figure S22: 0.5% iBu$_7$-SSQ-Cl/PE; Figure S23: 1% iBu$_7$-SSQ-Cl/PE; Figure S24: 0.1% iBu$_7$-SSQ-NH2/PE; Figure S25: 0.5% iBu$_7$-SSQ-NH2/PE; Figure S26: 1% iBu$_7$-SSQ-NH2/PE; Figure S27: 0.5% iBu$_7$-SSQ-Vi/PE; Figure S28: 1% iBu$_7$-SSQ-Vi/PE; Figure S29: 1.5% iBu$_7$-SSQ-Vi/PE; Figure S30: 0.5% iBu$_7$-SSQ-3OH/PE; Figure S31: 0.5% iBu$_7$-SSQ-3OH/PE (higher magnification); Figure S32: 1% iBu$_7$-SSQ-3OH/PE; Figure S33: 1% iBu$_7$-SSQ-3OH (higher magnification); Figure S34: 1.5% iBu$_7$-SSQ-3OH; Figure S35: 1.5% iBu$_7$-SSQ-3OH (higher magnification).

Author Contributions: Conceptualization, D.B. and R.E.P.; Data curation, B.S. and P.J.; Formal analysis, D.B.; Funding acquisition, D.B.; Investigation, D.B. and R.E.P.; Methodology, R.E.P. and M.J.; Project administration, R.E.P. and B.M.; Resources, R.E.P. and B.S.; Software, D.B.; Supervision, B.M.; Validation, P.J. and M.J.; Writing—original draft, D.B. All authors have read and agreed to the published version of the manuscript.

Funding: This research was funded by National Science Centre, Poland, grant number UMO-2018/29/N/ST5/00868.

Conflicts of Interest: The authors declare no conflict of interest.

References

1. Chanda, M.; Roy, S.K. *Industrial Polymers, Specialty Polymers, and Their Applications*; CRC Press: Boca Raton, FL, USA, 2009. [CrossRef]
2. Brinson, H.F.; Brinson, L.C. *Polymer Engineering Science and Viscoelasticity Polymer Engineering Science and Viscoelasticity an Introduction*; Springer: Heidelberg, Germany, 2008. [CrossRef]
3. Barnes, M.D.; Fukui, K.; Kaji, K.; Kanaya, T.; Noid, D.W.; Otaigbe, J.U.; Pokrovskii, V.N.; Sumpter, B.G. *Polymer Physics and Engineering*; Springer: Heidelberg, Germany, 2001.
4. Manju, V.K.T. *Hybrid. Polymer Composite Materials*; Woodhead Publishing: Cambridge, UK, 2017.
5. Jois, Y.H.R.; Harrison, J.B. Modification of Polyolefins: An Overview. *J. Macromol. Sci. Part C Polym. Rev.* **1996**, *36*, 433–455. [CrossRef]
6. Fink, J.K. *Handbook of Engineering and Specialty Thermoplastics, Volume 1: Polyolefins and Styrenics*, 1st ed.; Wiley-Scrivener: Salem, MA, USA, 2010.
7. Patwary, F.; Mittal, V. Degradable Polyethylene Nanocomposites with Silica, Silicate and Thermally Reduced Graphene Using Oxo-Degradable pro-Oxidant. *Heliyon* **2015**, *1*. [CrossRef]

8. Yang, X.; Shan, Y.; Wei, X.; Zhong, S.; Huang, Y.; Yu, H.; Yang, J. Polyethylene/Silica Nanorod Composites with Reduced Dielectric Constant and Enhanced Mechanical Strength. *J. Appl. Polym. Sci.* **2019**, *136*, 24–28. [CrossRef]
9. Kaczmarek, H.; Chylińska, M.; Królikowski, B.; Klimiec, E.; Bajer, D.; Kowalonek, J. Influence of Glass Beads Filler and Orientation Process on Piezoelectric Properties of Polyethylene Composites. *J. Mater. Sci. Mater. Electron.* **2019**, *30*, 21032–21047. [CrossRef]
10. Cheremisinoff, P. *Handbook of Engineering Polymeric Materials*; Marcel Dekker: New York, NY, USA, 1997.
11. Kausar, A. State-of-the-Art Overview on Polymer/POSS Nanocomposite. *Polym. Plast. Technol. Eng.* **2017**, *56*, 1401–1420. [CrossRef]
12. Du, Y.; Liu, H. Cage-like Silsesquioxanes-Based Hybrid Materials. *Dalt. Trans.* **2020**, *49*, 5396–5405. [CrossRef] [PubMed]
13. Kuo, S.W.; Chang, F.C. POSS Related Polymer Nanocomposites. *Prog. Polym. Sci.* **2011**, *36*, 1649–1696. [CrossRef]
14. Ayandele, E.; Sarkar, B.; Alexandridis, P. Polyhedral Oligomeric Silsesquioxane (POSS)-Containing Polymer Nanocomposites. *Nanomaterials* **2012**, *2*, 445–475. [CrossRef]
15. Zhou, H.; Ye, Q.; Xu, J. Polyhedral Oligomeric Silsesquioxane-Based Hybrid Materials and Their Applications. *Mater. Chem. Front.* **2017**, *1*, 212–230. [CrossRef]
16. Shi, H.; Yang, J.; You, M.; Li, Z.; He, C. Polyhedral Oligomeric Silsesquioxanes (POSS)-Based Hybrid Soft Gels: Molecular Design, Material Advantages, and Emerging Applications. *ACS Mater. Lett.* **2020**, *2*, 296–316. [CrossRef]
17. Li, Z.; Kong, J.; Wang, F.K.; He, C. Polyhedral Oligomeric Silsesquioxanes (POSSs): An Important Building Block for Organic Optoelectronic Materials. *J. Mater. Chem. C* **2017**, *5*, 5283–5298. [CrossRef]
18. Hartmann-Thompson, C. *Applications of Polyhedral Oligomeric Silsesquioxanes*; Springer: Berlin/Heidelberg, Germany, 2011.
19. Cordes, D.B.; Lickiss, P.D.; Rataboul, F. Recent Developments in the Chemistry of Cubic Polyhedral.Pdf. *Chem. Rev.* **2010**, *110*, 2081–2173. [CrossRef] [PubMed]
20. Nicoleta, A.; Xavier, F.; Radovici, C.; Mihaela, D. Influence of Branched or Un-Branched Alkyl Substitutes of POSS on Morphology, Thermal and Mechanical Properties of Polyethylene. *Compos. Part B* **2013**, *50*, 98–106. [CrossRef]
21. Xavier, F.; Mihaela, D.; Nicoleta, A.; Radovici, C.; Nicolae, C. The Influence of Alkyl Substituents of POSS in Polyethylene Nanocomposites. *Polymer* **2013**, *54*, 2347–2354. [CrossRef]
22. Joshi, M.; Butola, B.S. Studies on Nonisothermal Crystallization of HDPE/POSS Nanocomposites. *Polymer* **2004**, *45*, 4953–4968. [CrossRef]
23. Joshi, M.; Butola, B.S.; Simon, G.; Kukaleva, N. Rheological and Viscoelastic Behavior of HDPE/Octamethyl-POSS. *Macromolecules* **2006**, *39*, 1839–1849. [CrossRef]
24. Li, W.; Chen, T.; Guan, C.; Gong, D.; Mu, J.; Chen, Z.; Zhou, Q. Influence of Polyhedral Oligomeric Silsesquioxane Structure on the Disentangled State of Ultrahigh Molecular Weight Polyethylene Nanocomposites during Ethylene in Situ Polymerization. *Ind. Eng. Chem. Res.* **2015**, *54*, 1478–1486. [CrossRef]
25. Lim, S.; Hong, E.; Choi, H.J.; Chin, I. Polyhedral Oligomeric Silsesquioxane and Polyethylene Nanocomposites and Their Physical Characteristics. *J. Ind. Eng. Chem.* **2010**, *16*, 189–192. [CrossRef]
26. Lim, S.; Lee, J.Y.; Choi, H.J.; Chin, I. On Interaction Characteristics of Polyhedral Oligomeric Silsesquioxane Containing Polymer. *Polym. Bull.* **2015**, *72*, 2331–2352. [CrossRef]
27. Guo, M.; Frechette, M.; David, É.; Demarquette, N.R.; Daigle, J. Polyethylene/Polyhedral Oligomeric Silsesquioxanes Composites: Electrical Insulation for High Voltage Power Cables. *IEEE Trans. Dielectr. Electr. Insul.* **2017**, *24*, 798–807. [CrossRef]
28. Xu, Z.; Guo, M.; Fréchette, M.; David, É.; Chen, G. Space Charge Properties of LDPE-Based Composites with Three Types of POSS. In Proceedings of the 2016 IEEE Conference on Electrical Insulation and Dielectric Phenomena (CEIDP), Toronto, ON, Canada, 17–20 October 2016; pp. 679–682.
29. Scapini, P.; Figueroa, C.A.; Amorim, C.L.G.; Machado, G.; Mauler, R.S.; Crespo, J.S.; Oliviera, R.V. Thermal and Morphological Properties of High-Density Polyethylene/Ethylene—Vinyl Acetate Copolymer Composites with Polyhedral Oligomeric Silsesquioxane Nanostructure. *Polym. Int.* **2010**, *59*, 175–180. [CrossRef]

30. Fréchette, M.F.; Ghafarizadeh, S.B.; Ahn, T.T.; Vadeboncoeur, S.; Guo, M.; David, E. LDPE Nanocomposites Containing Functionalized SiO2 Molecular Structures: Properties Associated with a Ball-Milled Preparation. In Proceedings of the 1st International Conference on Electrical Materials and Power Equipment, Xi'an, China, 14–17 May 2017; pp. 221–224. [CrossRef]
31. Fréchette, M.F.; Guo, M.; Savoie, S.; Vanga-Bouanga, C.; David, E. POSS Dispersion in Polyethylene Microcomposites Containing Quartz and Dielectric Responses. In Proceedings of the Annual Report-Conference on Electrical Insulation and Dielectric Phenomena, CEIDP, Shenzhen, China, 20–23 October 2013; pp. 742–745. [CrossRef]
32. Niemczyk, A.; Dziubek, K. Study of Thermal Properties of Polyethylene and Polypropylene Nanocomposites with Long Alkyl Chain-Substituted POSS Fillers. *J. Therm. Anal. Calorim.* **2016**, *125*, 1287–1299. [CrossRef]
33. Guo, M.; Frechette, M.F.; David, E.; Couderc, H.; Savoie, S.; Vanga Bouanga, C.; Demarquette, N.R. Characterization of UHMWPE/POSS Composite Prepared by Ball Milling. In Proceedings of the 2013 IEEE Electrical Insulation Conference, EIC 2013, Ottawa, ON, Canada, 2–5 June 2013; pp. 444–448. [CrossRef]
34. Guo, M.; Fréchette, M.; David, É.; Demarquette, N.R. Influence of Fabrication Techniques on the Dielectric Properties of PE/POSS Polymeric Composites. In Proceedings of the 2016 Electrical Insulation Conference (EIC), Montreal, QC, Canada, 19–22 June 2016; pp. 297–300.
35. Guo, M.; Fréchette, M.; David, É.; Demarquette, N.R.; Daigle, J. Polyethylene-Based Nanodielectrics Containing Octaisobutyl Polyhedral Oligomeric SilSesquioxanes Obtained by Solution Blending in Xylene. In Proceedings of the 2014 Annual Report Conference on Electrical Insulation and Dielectric Phenomena Polyethylene-Based, Des Moines, IA, USA, 19–22 October 2014; pp. 731–734.
36. Guo, M.; Frechette, M.; Demarquette, N.R.; David, E. Polyethylene-Based Nanodielectric Containing Octaisobutyl Polyhedral Oligomeric SilSesquioxanes Obtained by Hexane Slurry Blending. In Proceedings of the 2014 International Symposium on Electrical Insulating Materials, Niigata, Japan, 1–5 June 2014; pp. 61–64.
37. Guo, M.; Fréchette, M.F.; David, E.; Couderc, H.; Demarquette, N.R. Effects of Stearic Acid and Thermal Treatment on Morphology and Dielectric Properties of UHMWPE/POSS Composites Prepared by Ball Milling. In Proceedings of the 2013 Annual Report Conference on Electrical Insulation and Dielectric Phenomena Effects, Shenzhen, China, 20–23 October 2013; pp. 760–763.
38. Safarikova, B.; Kalendova, A.; Habrova, V.; Zatloukalova, S.; Machovsky, M. Synergistic Effect between Polyhedral Oligomeric Silsesquioxane and Flame Retardants. *AIP Conf. Proc.* **2014**, *1599*, 106–109. [CrossRef]
39. Xu, Z.; Chen, G.; Guo, M.; David, É.; Fréchette, M. Space Charge Properties of UHMWPE/OibPOSS Composites. In Proceedings of the 2015 Annual Report Conference on Electrical Insulation and Dielectric Phenomena, Ann Arbor, MI, USA, 18–21 October 2015; pp. 543–546.
40. Heeley, E.L.; Hughes, D.J.; El, Y.; Taylor, P.G.; Bassindale, A.R. Morphology and Crystallization Kinetics of Polyethylene/Long Alkyl-Chain Substituted Polyhedral Oligomeric Silsesquioxanes (POSS) Nanocomposite Blends: A SAXS/WAXS Study. *Eur. Polym. J.* **2014**, *51*, 45–56. [CrossRef]
41. Barczewski, M.; Czarnecka-Komorowska, D.; Andrzejewski, J.; Sterzyński, T.; Dutkiewicz, M.; Dudziec, B. Właściwości Przetwórcze Termoplastycznych Tworzyw Polimerowych Modyfikowanych Silseskwioksanami (POSS). *Polim. Polym.* **2013**, *58*, 805–815. [CrossRef]
42. Heeley, E.L.; Hughes, D.J.; Taylor, P.G.; Bassindale, A.R. Crystallization and Morphology Development in Polyethylene-Octakis(n-Octadecyldimethylsiloxy)-Octasilsesquioxane Nanocomposite Blends. *RSC Adv.* **2015**, *5*, 34709–34719. [CrossRef]
43. Fréchette, M.; Guo, M.; David, É.; Min, D.; Li, S. The Dielectric Response of Polyethylene/Polyhedral Oligomeric Silsesquioxanes Composites at Various Temperatures. In Proceedings of the 2017 IEEE Conference on Electrical Insulation and Dielectric Phenomenon (CEIDP), Fort Worth, TX, USA, 22–25 October 2017; pp. 501–504.
44. Guo, M.; David, É.; Fréchette, M.; Demarquette, N.R. Polyethylene/Polyhedral Oligomeric Silsesquioxanes Composites: Dielectric, Thermal and Rheological Properties. *Polymer* **2017**, *115*, 60–69. [CrossRef]
45. Guo, M.; David, É.; Fréchette, M.; Demarquette, N.R. Low-Density Polyethylene/Polyhedral Oligomeric Silsesquioxanes Composites Obtained by Extrusion. In Proceedings of the 2016 IEEE Conference on Electrical Insulation and Dielectric Phenomena (CEIDP), Eaton Chelsea Hotel, Toronto, ON, Canada, 16–19 October 2016; pp. 647–650.

46. Hato, M.J.; Ray, S.S.; Luyt, A.S. Nanocomposites Based on Polyethylene and Polyhedral Oligomeric Silsesquioxanes, 1 – Microstructure, Thermal and Thermomechanical Properties. *Mol. Mater. Eng.* **2008**, *293*, 752–762. [CrossRef]
47. Hato, M.J.; Ray, S.S.; Africa, S.; Luyt, A.S. Melt-State Viscoelastic Properties of POSS-Containing Polyethylene Melt-State Viscoelastic Properties of POSS-Containing Polyethylene Nanocomposites. *Adv. Sci. Lett.* **2011**, *4*, 3585–3589. [CrossRef]
48. Nguyen, T.-A.; Mannle, F.; Gregersen, Ø.W. Polyethylene/Octa-(Ethyl Octadeca-10,13 Dienoamide) Silsesquioxane Blends and the Adhesion Strength Po Paperboard. *Int. J. Adhes. Adhes.* **2012**, *38*, 117–124. [CrossRef]
49. Nguyen, T.; Gregersen, Ø.W.; Männle, F. Thermal Oxidation of Polyolefins by Mild Pro-Oxidant Additives Based on Iron Carboxylates and Lipophilic Amines: Degradability in the Absence of Light and Effect on the Adhesion to Paperboard. *Polymers* **2015**, *7*, 1522–1540. [CrossRef]
50. Grala, M.; Bartczak, Z.; Gadzinowska, K. Polyolefins—Polyhedral Oligomeric Silsesquioxanes (Poss) Nanocomposites: Mechanical Properties, Morphology and Thermal Behaviour. In Proceedings of the ECCM15—15th European Conference on Composite Materials, Venice, Italy, 24–28 June 2012; pp. 1–2.
51. Grala, M.; Bartczak, Z. Morphology and Mechanical Properties of High Density Polyethylene-POSS Hybrid Nanocomposites Obtained by Reactive Blending. *Polym. Eng. Sci.* **2014**, *55*, 2058–2072. [CrossRef]
52. Morici, E.; Di Bartolo, A.; Arrigo, R.; Tzankova Dintcheva, N. POSS Grafting on Polyethylene and Maleic Anhydride-Grafted Polyethylene by One-Step Reactive Melt Mixing. *Adv. Polym. Technol.* **2016**, *21673*, 1–9. [CrossRef]
53. Panaitescu, D.M.; Frone, A.N.; Radovici, C.; Nicolae, C.; Perrin, F.X. Influence of Octyl Substituted Octakis(Dimethylsiloxy)Octasilsesquioxane on the Morphology and Thermal and Mechanical Properties of Low Density Polyethylene. *Polym. Int.* **2014**, *63*, 228–236. [CrossRef]
54. Brząkalski, D.; Przekop, R.E.; Dobrosielska, M.; Sztorch, B.; Marciniak, P.; Marciniec, B. Highly Bulky Spherosilicates as Functional Additives for Polyethylene Processing—Influence on Mechanical and Thermal Properties. *Polym. Compos.* **2020**, 1–14. [CrossRef]
55. Cicala, G.; Blanco, I.; Latteri, A.; Ognibene, G.; Bottino, F.A.; Elena, M. PES/POS Soluble Veils as Advanced Modifiers for Multifunctional Fiber Reinforced Composites. *Polymers* **2017**, *9*, 281. [CrossRef]
56. Vieira, E.G.; Dal-Bó, A.G.; Frizon, T.E.A.; Dias Filho, N.L. Synthesis of Two New Mo(II) Organometallic Catalysts Immobilized on POSS for Application in Olefin Oxidation Reactions. *J. Organomet. Chem.* **2017**, *834*, 73–82. [CrossRef]
57. Ye, M.; Wu, Y.; Zhang, W.; Yang, R. Synthesis of Incompletely Caged Silsesquioxane (T7-POSS) Compounds via a Versatile Three-Step Approach. *Res. Chem. Intermed.* **2018**, *44*, 4277–4294. [CrossRef]
58. Ervithayasuporn, V.; Wang, X.; Kawakami, Y. Synthesis and Characterization of Highly Pure Azido-Functionalized Polyhedral Oligomeric Silsesquioxanes (POSS). *Chem. Commun.* **2009**, *60*, 5130–5132. [CrossRef]
59. Lee, H.; Hong, S.H. Polyhedral Oligomeric Silsesquioxane-Conjugated Bis(Diphenylphosphino)Amine Ligand for Chromium(III) Catalyzed Ethylene Trimerization and Tetramerization. *Appl. Catal. A Gen.* **2018**, *560*, 21–27. [CrossRef]
60. Mirabella, F.M.; Bafna, A. Determination of the Crystallinity of Polyethylene/α-Olefin Copolymers by Thermal Analysis: Relationship of the Heat of Fusion of 100% Polyethylene Crystal and the Density. *J. Polym. Sci. Part B Polym. Phys.* **2002**, *40*, 1637–1643. [CrossRef]
61. Zeng, J.; Bennett, C.; Jarrett, W.L.; Kumar, S.; Mathias, L.J.; Schiraldi, D.A. Structural Changes in Trisilanol POSS during Nanocomposite Melt Processing Nanocomposite Melt Processing. *Compos. Interfaces* **2005**, *11*, 673–685. [CrossRef]
62. Mao, J.; Zhang, W.; Cheng, S.Z.; Wesdemiotis, C. Analysis of Monodisperse, Sequence-Defined, and POSS-Functionalized Polyester Copolymers by MALDI Tandem Mass Spectrometry. *Eur. J. Mass Spectrom. Chichester Eng.* **2019**, *25*, 164–174. [CrossRef] [PubMed]
63. Qian, Q.; Xu, J.; Zhang, M.; He, J.; Ni, P. Versatile Construction of Single-Tailed Giant Surfactants with Hydrophobic Poly(ε-Caprolactone) Tail and Hydrophilic POSS Head. *Polymers* **2019**, *11*, 311. [CrossRef] [PubMed]

64. Karuppasamy, K.; Prasanna, K.; Vikraman, D.; Kim, H.S.; Kathalingam, A.; Mitu, L.; Rhee, H.W. A Rapid One-Pot Synthesis of Novel High-Purity Methacrylic Phosphonic Acid (PA)-Based Polyhedral Oligomeric Silsesquioxane (POSS) Frameworks via Thiol-Ene Click Reaction. *Polymers* **2017**, *9*, 192. [CrossRef]
65. Sheen, Y.C.; Lu, C.H.; Huang, C.F.; Kuo, S.W.; Chang, F.C. Synthesis and Characterization of Amorphous Octakis-Functionalized Polyhedral Oligomeric Silsesquioxanes for Polymer Nanocomposites. *Polymer* **2008**, *49*, 4017–4024. [CrossRef]
66. Xavier Perrin, F.; Viet Nguyen, T.B.; Margaillan, A. Linear and Branched Alkyl Substituted Octakis(Dimethylsiloxy) Octasilsesquioxanes: WAXS and Thermal Properties. *Eur. Polym. J.* **2011**, *47*, 1370–1382. [CrossRef]
67. Camino, G.; Lomakin, S.M.; Lageard, M. Thermal Polydimethylsiloxane Degradation. Part 2. The Degradation Mechanisms. *Polymer* **2002**, *43*, 2011–2015. [CrossRef]
68. Yang, D.; Zhang, W.; Yao, R.; Jiang, B. Thermal Stability Enhancement Mechanism of Poly(Dimethylsiloxane) Composite by Incorporating Octavinyl Polyhedral Oligomeric Silsesquioxanes. *Polym. Degrad. Stab.* **2013**, *98*, 109–114. [CrossRef]
69. Chatgilialoglu, C. Structural and Chemical Properties of Silyl Radicals. *Chem. Rev.* **1995**, *95*, 1229–1251. [CrossRef]
70. Salamone, J.C. *Concise Polymeric Materials Encyclopedia*, 1st ed.; CRC Press: Boca Raton, FL, USA, 1998.
71. Bouza, R.; Barral, L.; Díez, F.J.; López, J.; Montero, B.; Rico, M.; Ramírez, C. Study of Thermal and Morphological Properties of a Hybrid System, IPP/POSS. Effect of Flame Retardance. *Compos. Part B Eng.* **2014**, *58*, 566–572. [CrossRef]

Supplementary Information for

Silsesquioxane derivatives as functional additives for preparation of polyethylene-based composites: a case of trisilanol melt-condensation

Dariusz Brząkalski [1]*, Robert E. Przekop [2], Bogna Sztorch [2], Paulina Jakubowska [3], Marek Jałbrzykowski [4] and Bogdan Marciniec [1,2]

[1] Faculty of Chemistry, Adam Mickiewicz University in Poznań, Uniwersytetu Poznańskiego 8, 61-614 Poznań, Poland
[2] Centre for Advanced Technologies, Adam Mickiewicz University in Poznań, Uniwersytetu Poznańskiego 10, 61-614 Poznań, Poland
[3] Poznan University of Technology, Faculty of Chemical Technology, Berdychowo 4, 60-695 Poznań, Poland
[4] Bialystok University of Technology, Faculty of Mechanical Engineering, Wiejska 45 C, 15-351 Bialystok, Poland
*Corresponding Author: D.B.: e-mail: dariusz.brzakalski@amu.edu.pl

Table of contents:

1. List of isolated compounds

Table S1: List of isolated compounds:

Structure	Compound #	Code:
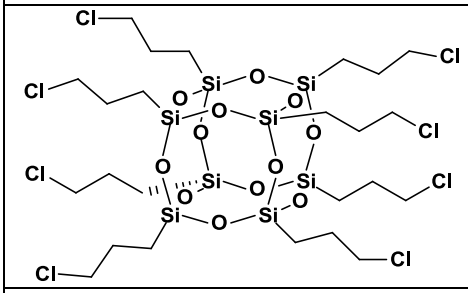	**1**	SSQ-8Cl
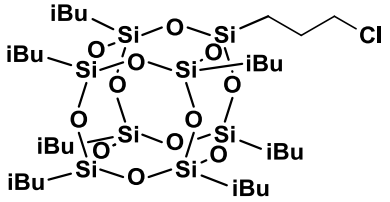	**2**	iBu_7SSQ-Cl
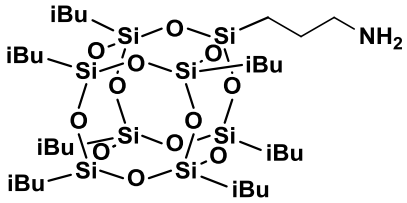	**3**	iBu_7SSQ-NH_2
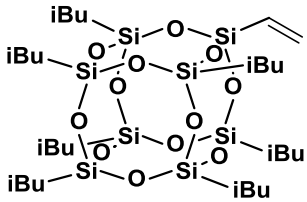	**4**	iBu_7SSQ-Vi
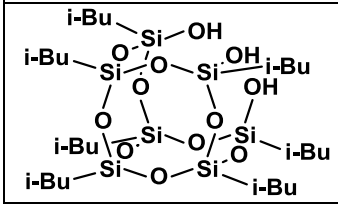	**5**	iBu_7SSQ-3OH

2. Characterization data of the products:

1,3,5,7,9,11,13,15-octakis(3-chloropropyl)-pentacyclo[9.5.1.1^{3,9}.1^{5,15}.1^{7,13}]octasiloxane (2)

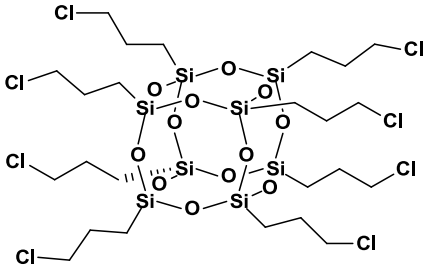

^{1}H NMR (400 MHz, $CDCl_3$): δ (ppm) = 3.54 (t, J = 6.7Hz, 16H, Si-$CH_2CH_2\underline{CH_2}$-Cl), 1.88 (p, J = 6.7Hz, 16H, Si-$CH_2\underline{CH_2}CH_2$-Cl), 0.80 (t, J = 8.2Hz, 16H, Si-$\underline{CH_2}CH_2CH_2$-Cl);
^{13}C NMR (101 MHz, $CDCl_3$): δ (ppm) = 47.17 (Si-$CH_2CH_2\underline{CH_2}$-Cl), 26.39 (Si-$CH_2\underline{CH_2}CH_2$-Cl), 9.48 (Si-$\underline{CH_2}CH_2CH_2$-Cl);
^{29}Si NMR (79,5 MHz, $CDCl_3$): δ (ppm) = -67.07.
FT-IR (ATR) = 2994, 2953-2874, 1456, 1436, 1408, 1349, 1311, 1272, 1240, 1190, 1081, 1000, 914, 867, 811, 778-649, 551, 534.

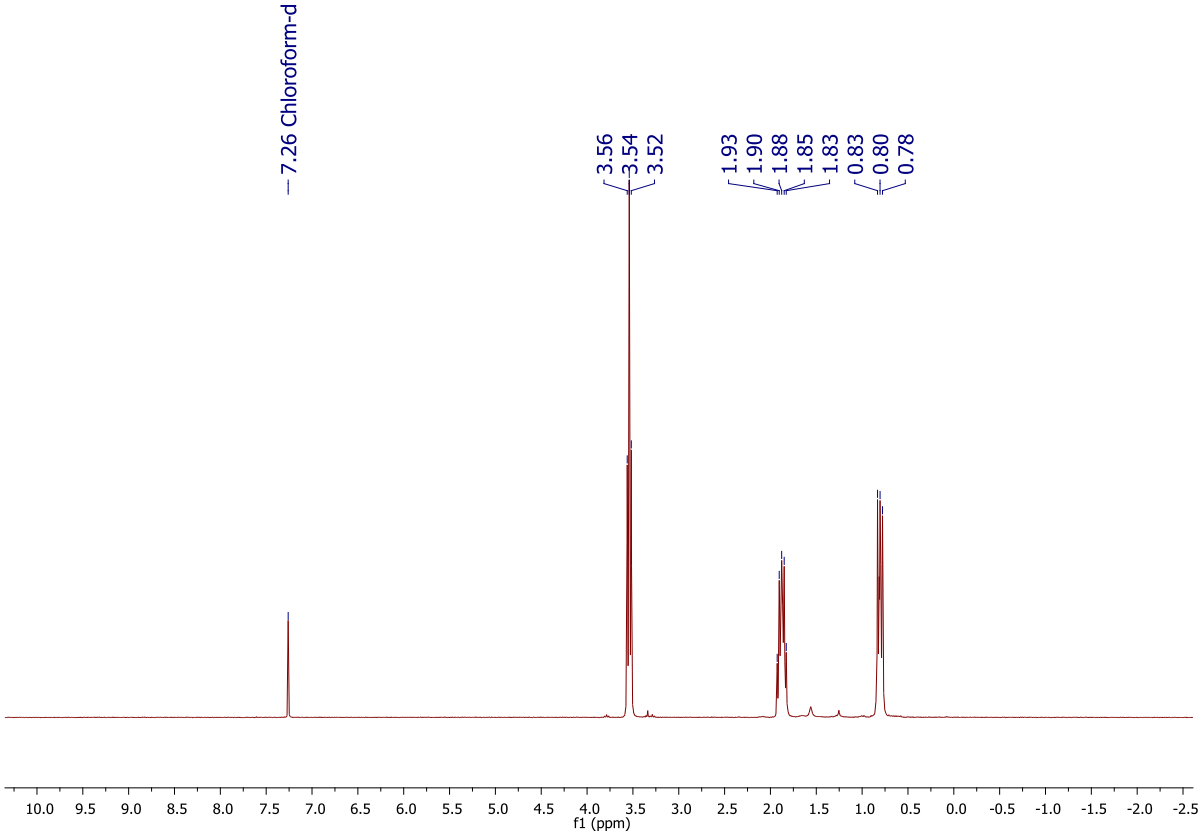

Figure S1: ^{1}H NMR of SSQ-8Cl

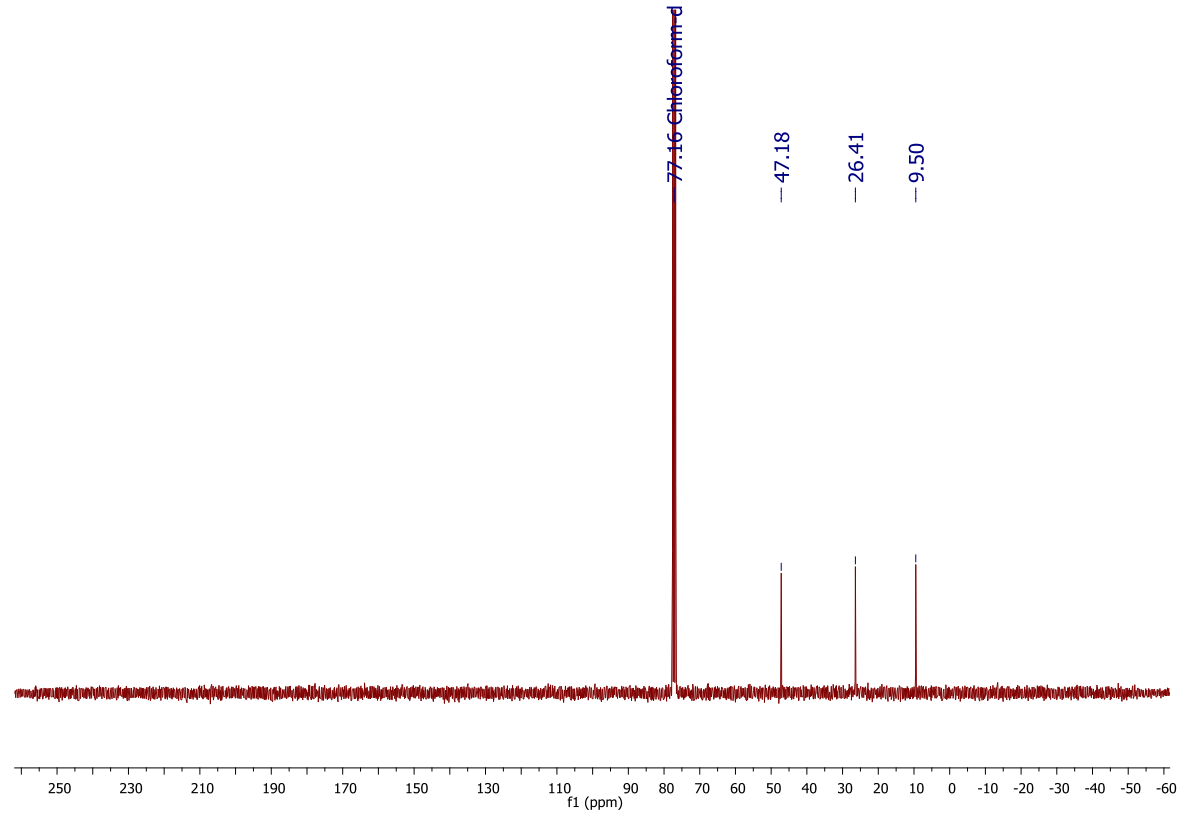

Figure S2: ^{13}C NMR of SSQ-8Cl

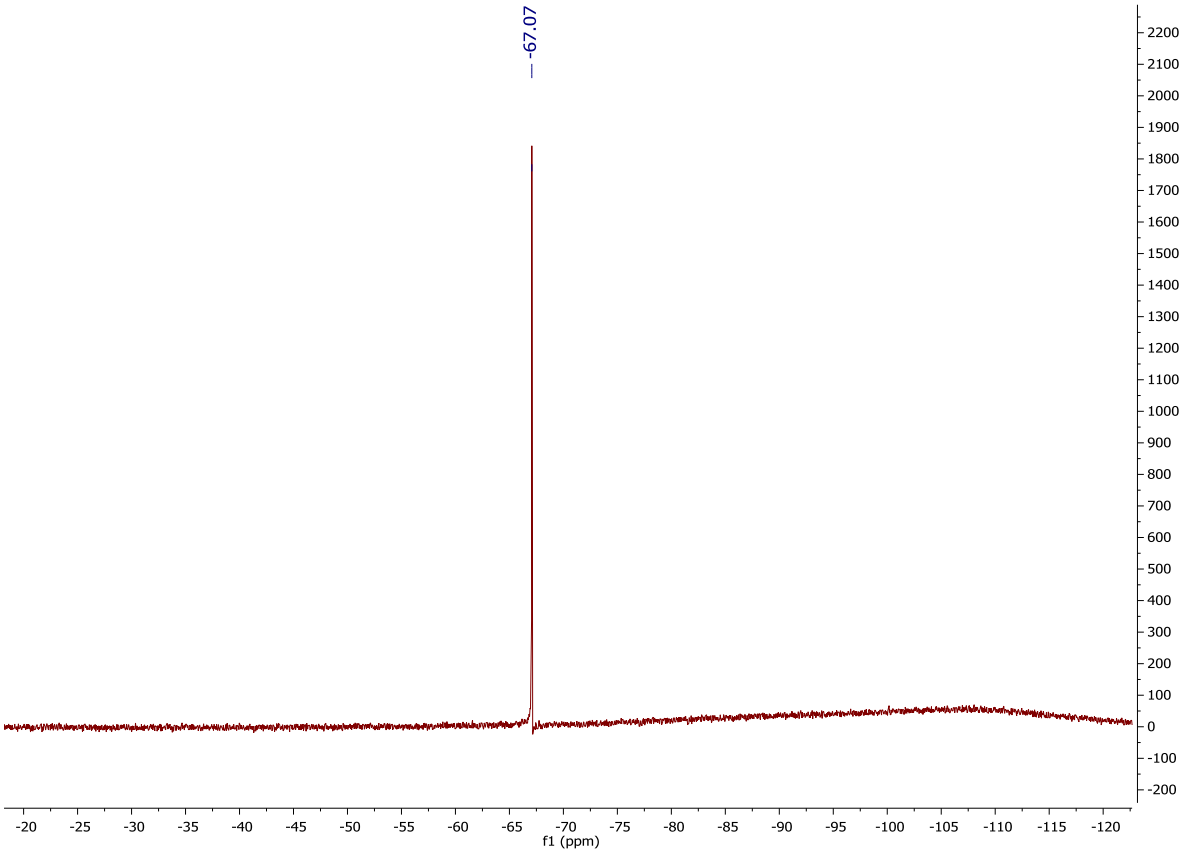

Figure S3: ^{29}Si NMR of SSQ-8Cl

1-(3-chloropropyl)-3,5,7,9,11,13,15-heptaisobutylpentacyclo[9.5.1.1^{3,9}.1^{5,15}.1^{7,13}]octasiloxane (2)

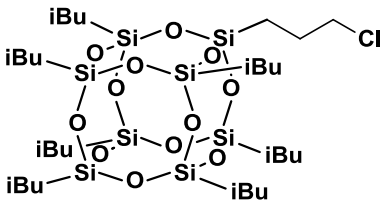

^{1}H NMR (400 MHz, $CDCl_3$): δ (ppm) = 3.52 (t, J = 8.1Hz, 2H, -$CH_2CH_2C\underline{H_2}Cl$), 1.92-1.79 (m, 9H, -$CH_2C\underline{H}(CH_3)_2$, -$CH_2C\underline{H_2}CH_2Cl$), 0.96 (d, J = 6.6Hz, 42H, -$CH_2CH(C\underline{H_3})_2$), 0.74 (t, J = 8.1Hz, 2H, -$C\underline{H_2}CH_2CH_2Cl$), 0.62-0.59 (m, 14H, -$C\underline{H_2}CH(CH_3)_2$);
^{13}C NMR (101 MHz, $CDCl_3$): δ (ppm) = 47.41 (-$CH_2CH_2\underline{CH_2}Cl$), 26.63 -$CH_2\underline{CH_2}CH_2Cl$), 25.85, 24.03, 22.65, 22.59 (iBu), 9.94 (-$C\underline{H_2}CH_2CH_2Cl$);
^{29}Si NMR (79,5 MHz, $CDCl_3$): δ (ppm) = -67.59, -67.87, -68.12.
FT-IR (ATR) = 2953, 2928, 2905, 2871, 1464, 1398, 1383, 1366, 1332, 1229, 1168, 1081, 955, 916, 838, 804, 745, 680, 556.

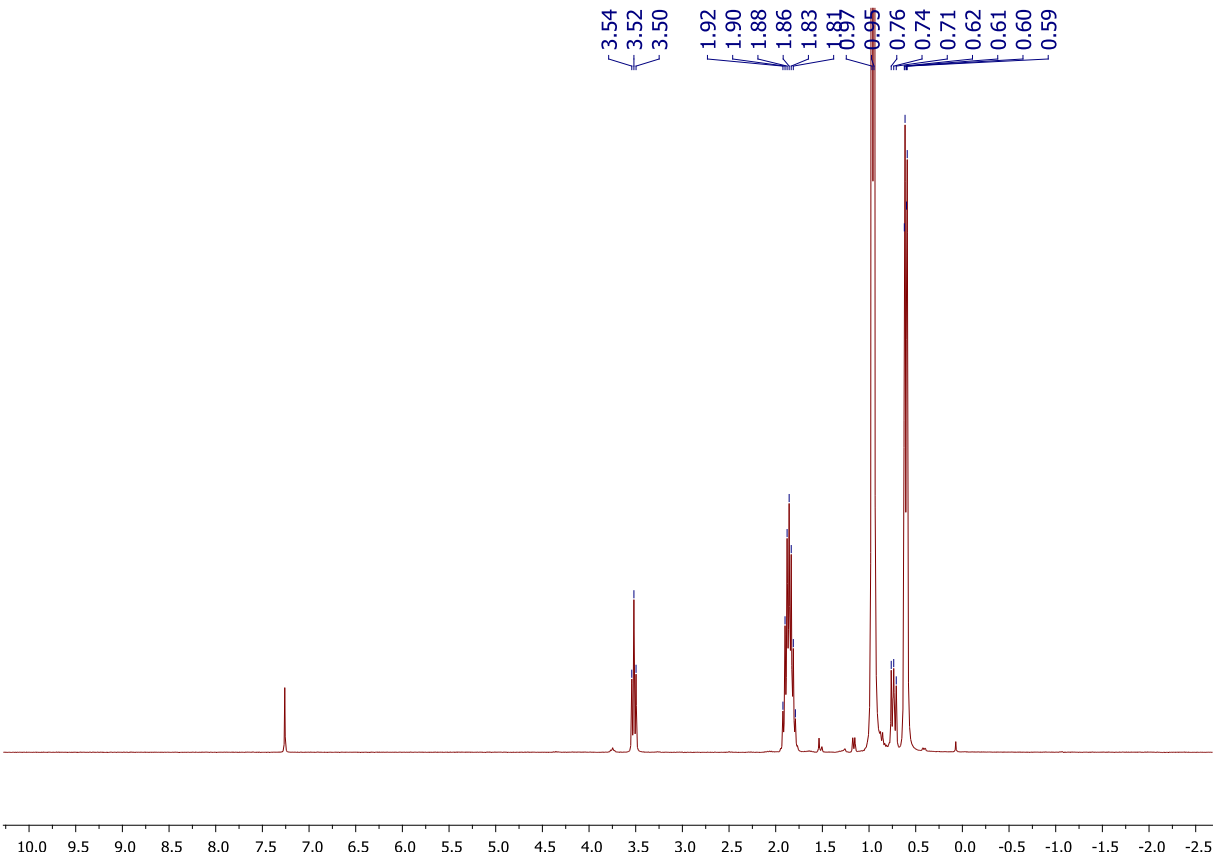

Figure S4: ^{1}H NMR of iBu_7SSQ-Cl

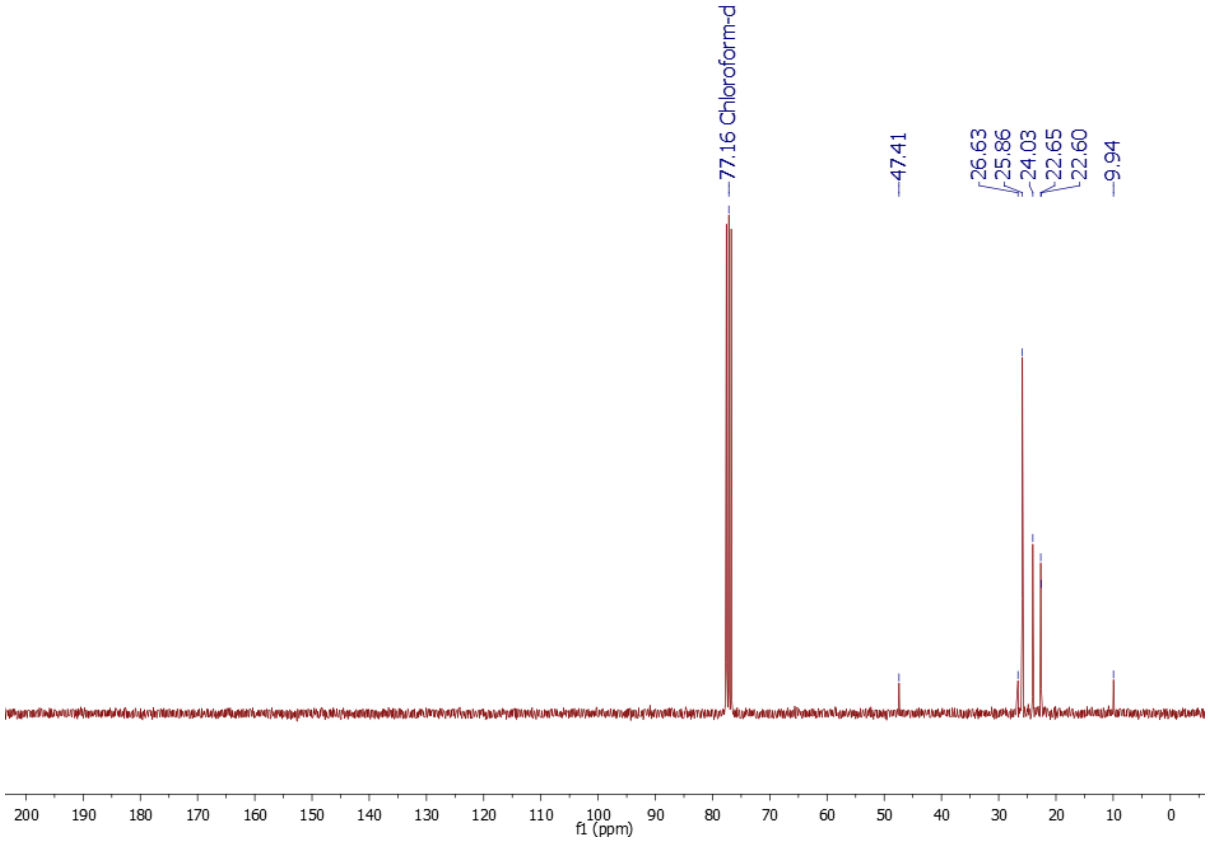

Figure S5: ^{13}C NMR of $iBu_7SSQ\text{-}Cl$

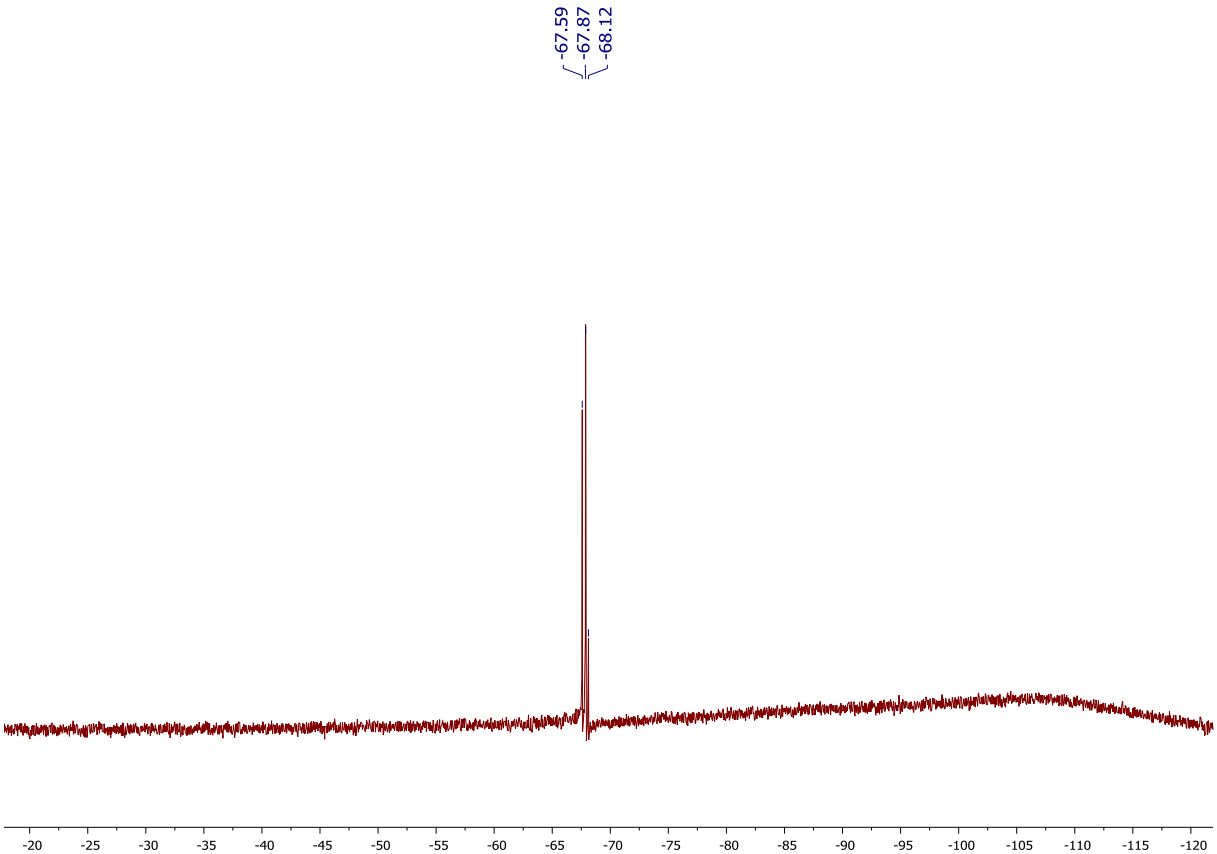

Figure S6: ^{29}Si NMR of $iBu_7SSQ\text{-}Cl$

1-(3-aminopropyl)-3,5,7,9,11,13,15-heptaisobutylpentacyclo[9.5.1.1^{3,9}.1^{5,15}.1^{7,13}]octasiloxane (3)

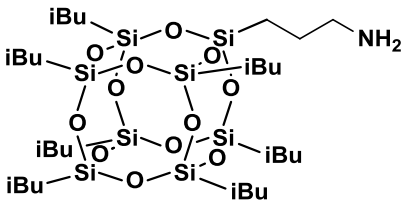

^{1}H NMR (400 MHz, $CDCl_3$): δ (ppm) = 2.67 (t, J = 7.1Hz, 2H, -$CH_2CH_2C\underline{H_2}NH_2$), 1.90-1.80 (m, 7H, -$CH_2C\underline{H}(CH_3)_2$), 1.53 (p, J = 7.1Hz, 2H, -$CH_2C\underline{H_2}CH_2NH_2$), 0.95 (d, J = 6.6Hz, 42H, -$CH_2CH(C\underline{H_3})_2$), 0.61-0.59 (m, 16H, -$C\underline{H_2}CH(CH_3)_2$, -$C\underline{H_2}CH_2CH_2NH_2$);
^{13}C NMR (101 MHz, $CDCl_3$): δ (ppm) = 44.96 (-$CH_2CH_2\underline{CH_2}NH_2$), 27.34 (-$CH_2\underline{CH_2}CH_2NH_2$), 25.85, 25.83, 24.04, 24.01, 22.66, 26.63 (iBu), 9.36 (-$\underline{CH_2}CH_2CH_2NH_2$);
^{29}Si NMR (79,5 MHz, $CDCl_3$): δ (ppm) =.-67.25, -67.70, -67.89;
IR (ATR) = 2953, 2928, 2906, 2871, 1464, 1398, 1383, 1366, 1332, 1228, 1168, 1085, 955, 838, 804, 746, 683, 556.

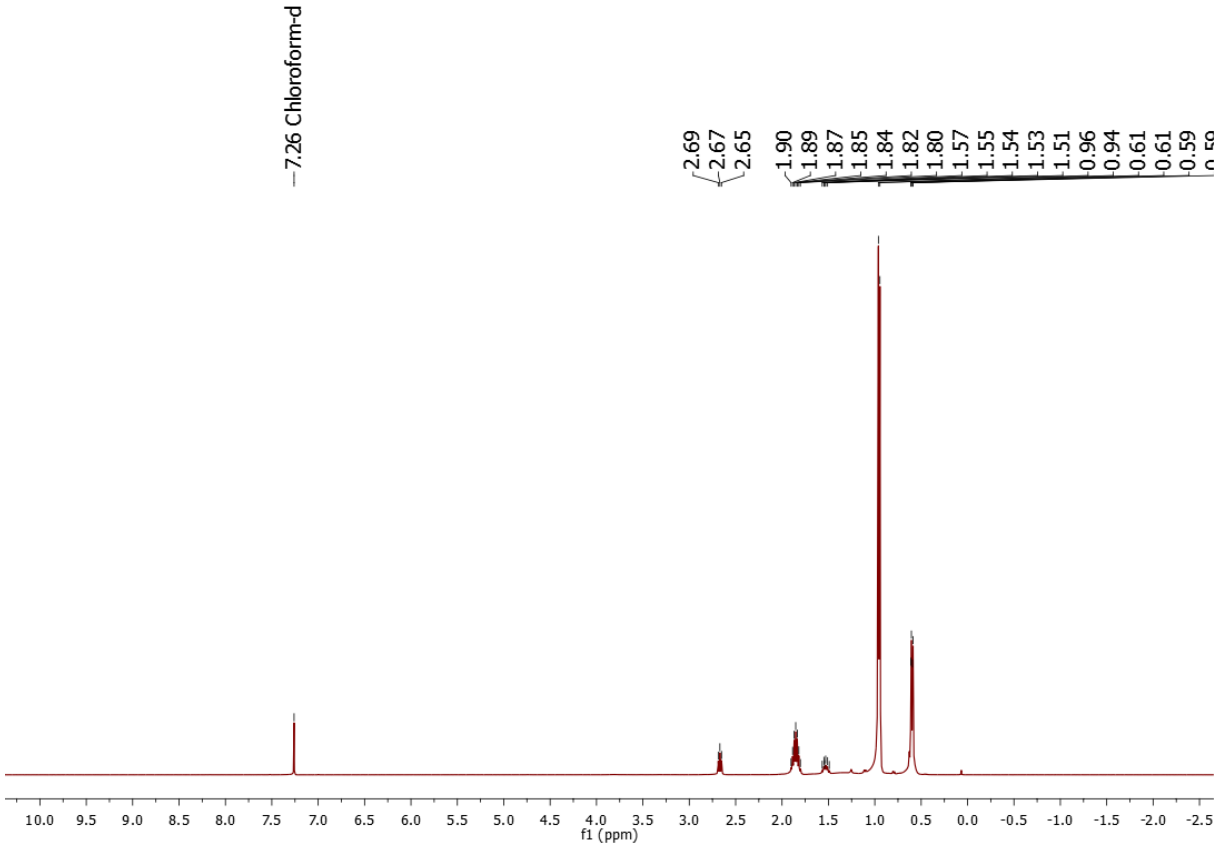

Figure S7: ^{1}H NMR of $iBu_7SSQ\text{-}NH_2$

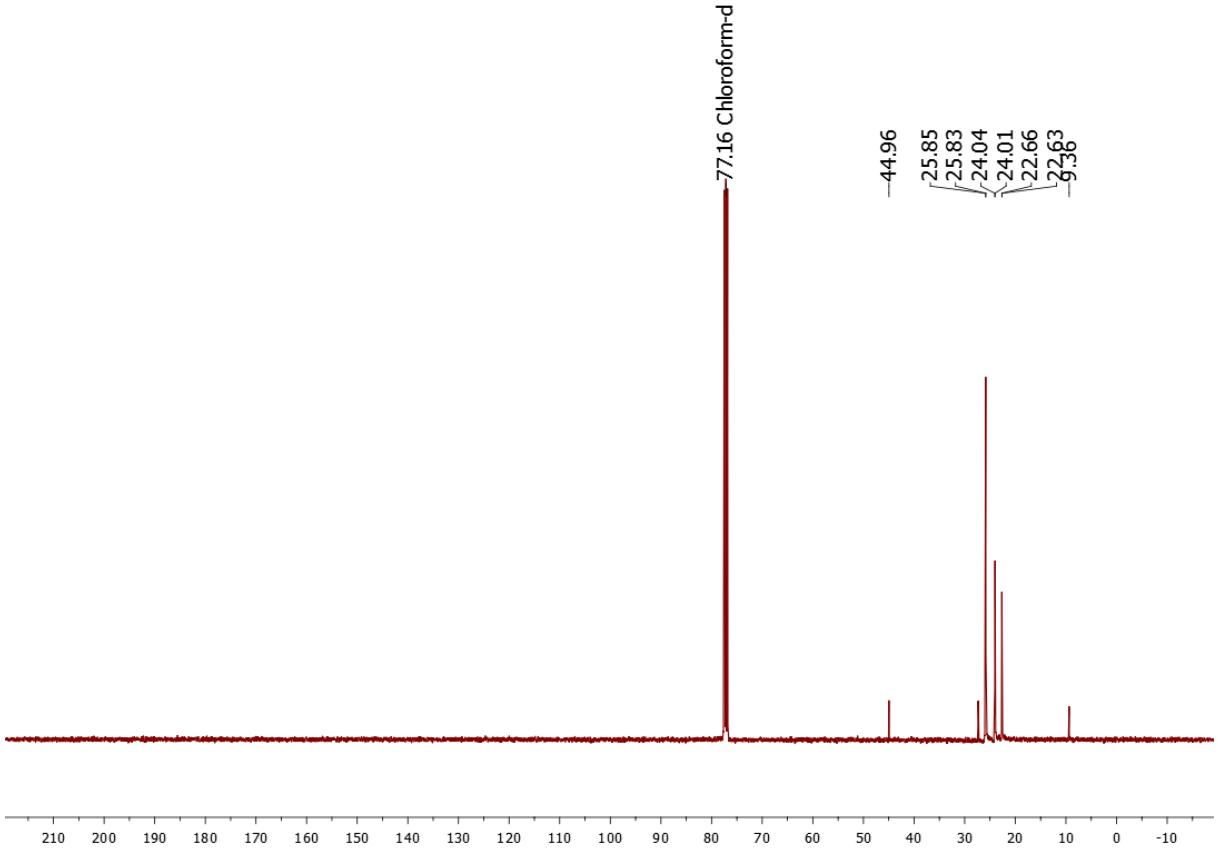

Figure S8: ^{13}C NMR of $iBu_7SSQ\text{-}NH_2$

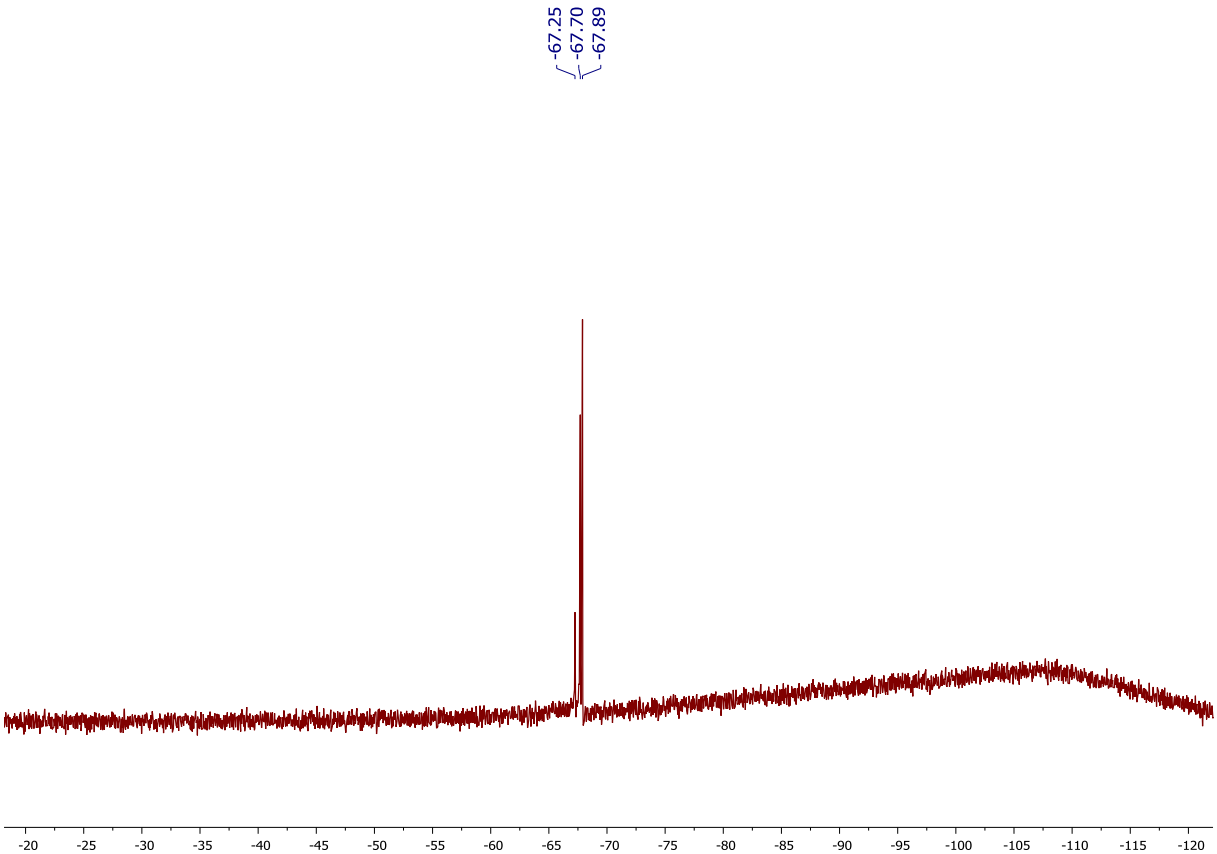

Figure S9: ^{29}Si NMR of $iBu_7SSQ\text{-}NH_2$

1-vinyl-3,5,7,9,11,13,15-heptaisobutylpentacyclo[9.5.1.1^{3,9}.1^{5,15}.1^{7,13}]octasiloxane (4)

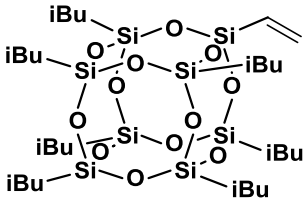

^{1}H NMR (400 MHz, $CDCl_3$): δ (ppm) = 6.08-5.81 (m, 3H, Vi), 1.93-1.79 (m, 7H, -CH_2C<u>H</u>(CH_3)$_2$), 0.96 (d, J = 6.6Hz, 42H, -CH_2CH(C<u>H</u>$_3$)$_2$), 0.63-0.59 (m, 14H, -C<u>H</u>$_2$CH(CH_3)$_2$);
^{13}C NMR (101 MHz, $CDCl_3$): δ (ppm) = 136.00, 130.06 (Vi), 25.87, 25.83, 24.01, 22.64, 22.54 (iBu);
^{29}Si NMR (79,5 MHz, $CDCl_3$): δ (ppm) = -67.40, -67.87, -81.54.
IR (ATR) = 2954, 2928, 2907, 2871, 1464, 1401, 1383, 1366, 1332, 1229, 1168, 1084, 964, 838, 802, 739, 706, 685, 557.

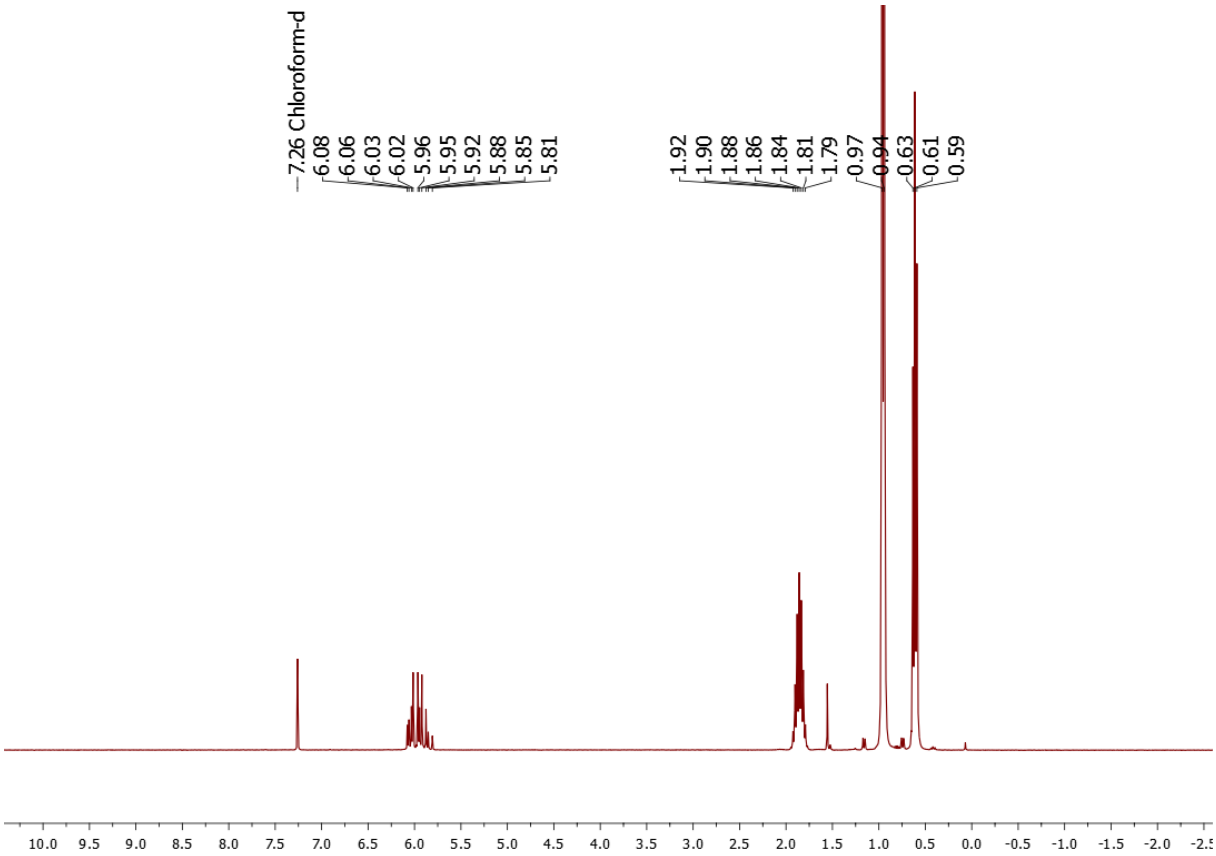

Figure S10: ^{1}H NMR of iBu_7SSQ-Vi

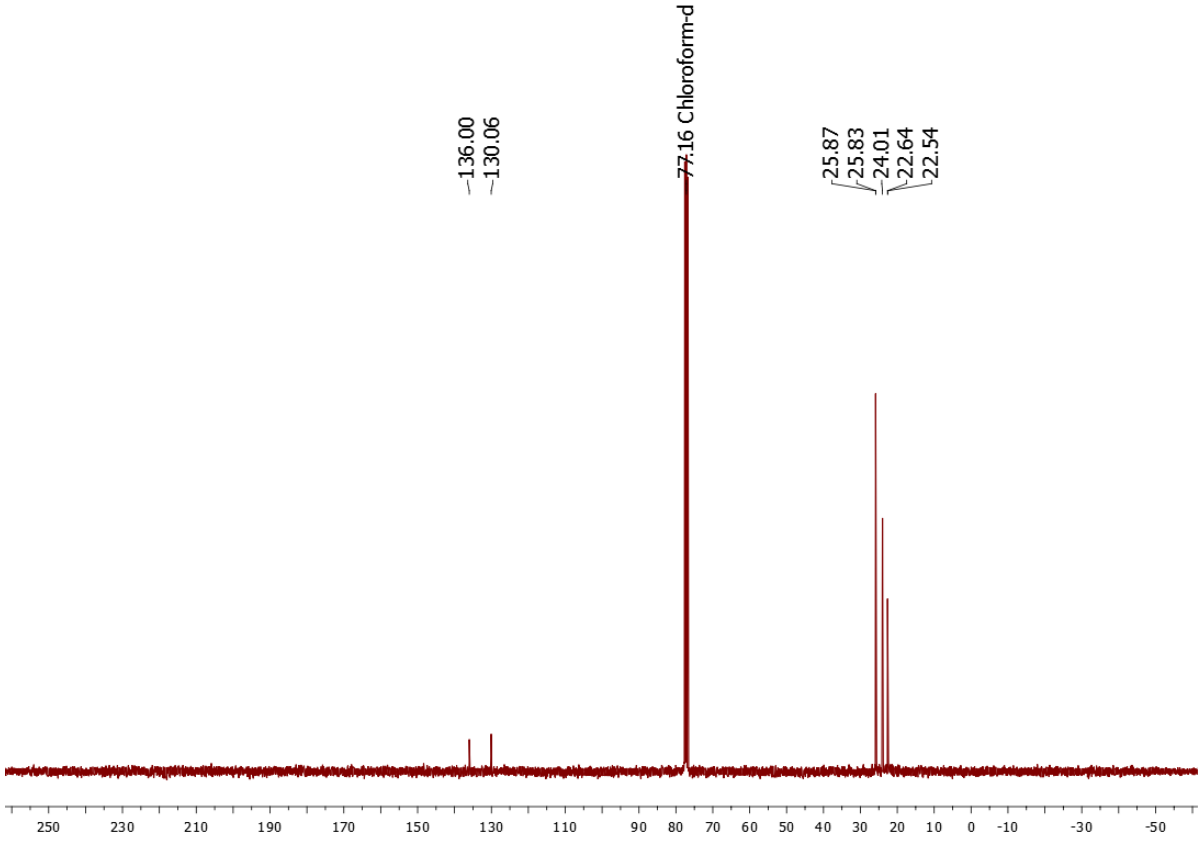

Figure S11: ^{13}C NMR of iBu$_7$SSQ-Vi

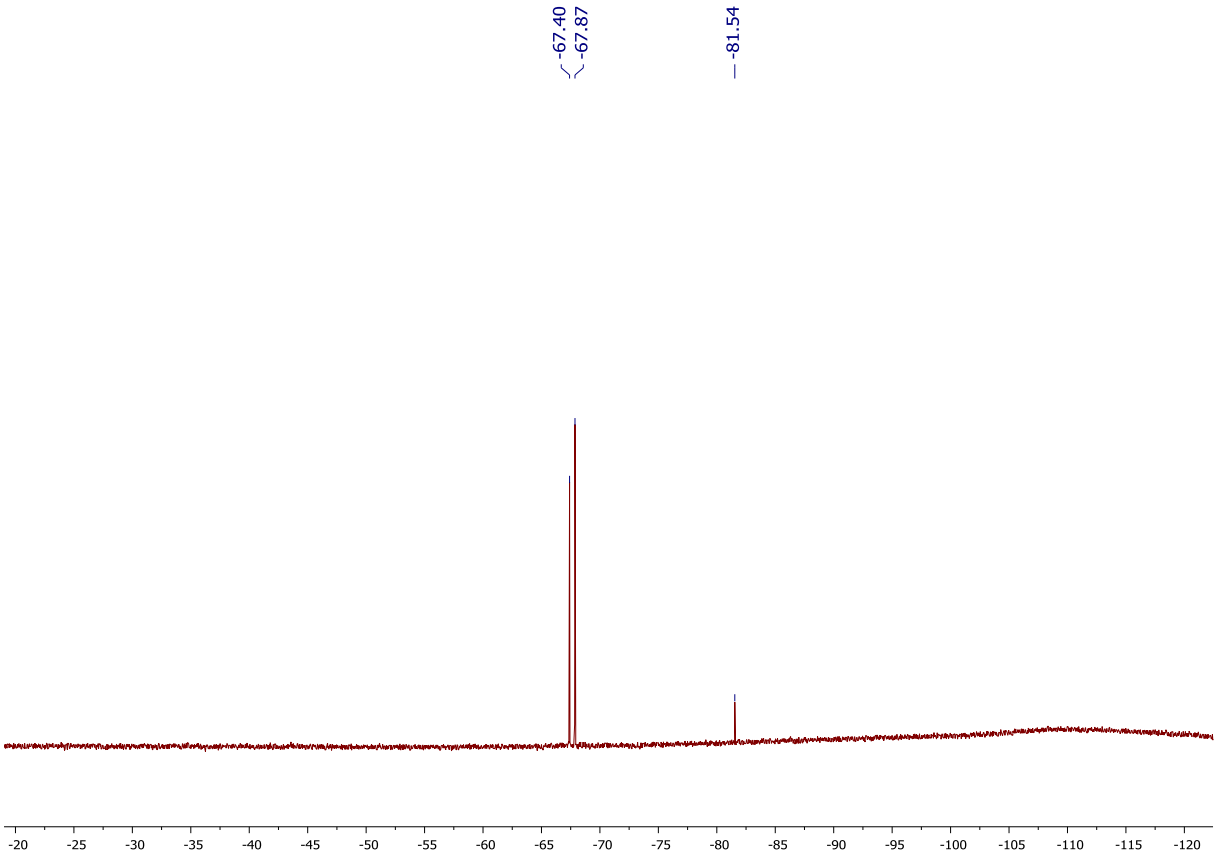

Figure S12: ^{29}Si NMR of iBu$_7$SSQ-Vi

1,3,5,7,9,11,13-heptaisobutyltricyclo[5.5.1.1^{3,9}.1^{7,13}]heptasiloxane-1,5,13-triol (3)

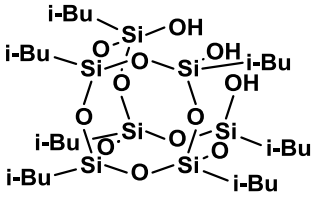

^{1}H NMR (400 MHz, $CDCl_3$): δ (ppm) = 5.71 (s, 3H, -OH), 1.92-1.77 (m, 7H, (-CH_2C<u>H</u>(CH_3)$_2$), 0.97-0.94 (m, 42H, -CH_2CH(C<u>H</u>$_3$)$_2$), 0.61-0.56 (m, 14H, -C<u>H$_2$</u>CH(CH_3)$_2$);
^{13}C NMR (101 MHz, $CDCl_3$): δ (ppm) = 25.94, 25.90, 25.80, 24.10, 24.07, 23.36, 22.98, 22.63;
^{29}Si NMR (79,5 MHz, $CDCl_3$): δ (ppm) = -58.90, -67.41, -68.71.
IR (ATR) = 2953, 2928, 2906, 2871, 1464, 1398, 1383, 1366, 1332, 1228, 1168, 1085, 955, 838, 804, 746, 683, 556.

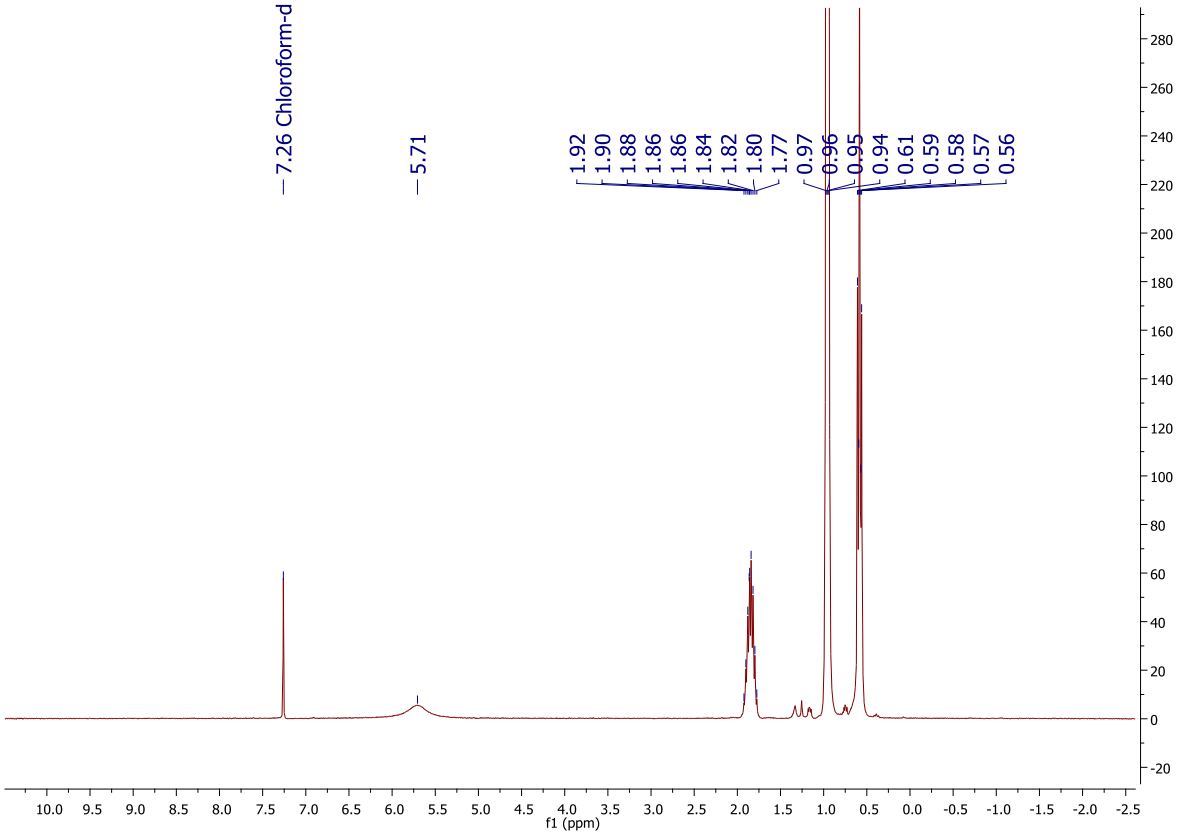

Figure S13: ^{1}H NMR of iBu_7SSQ-3OH

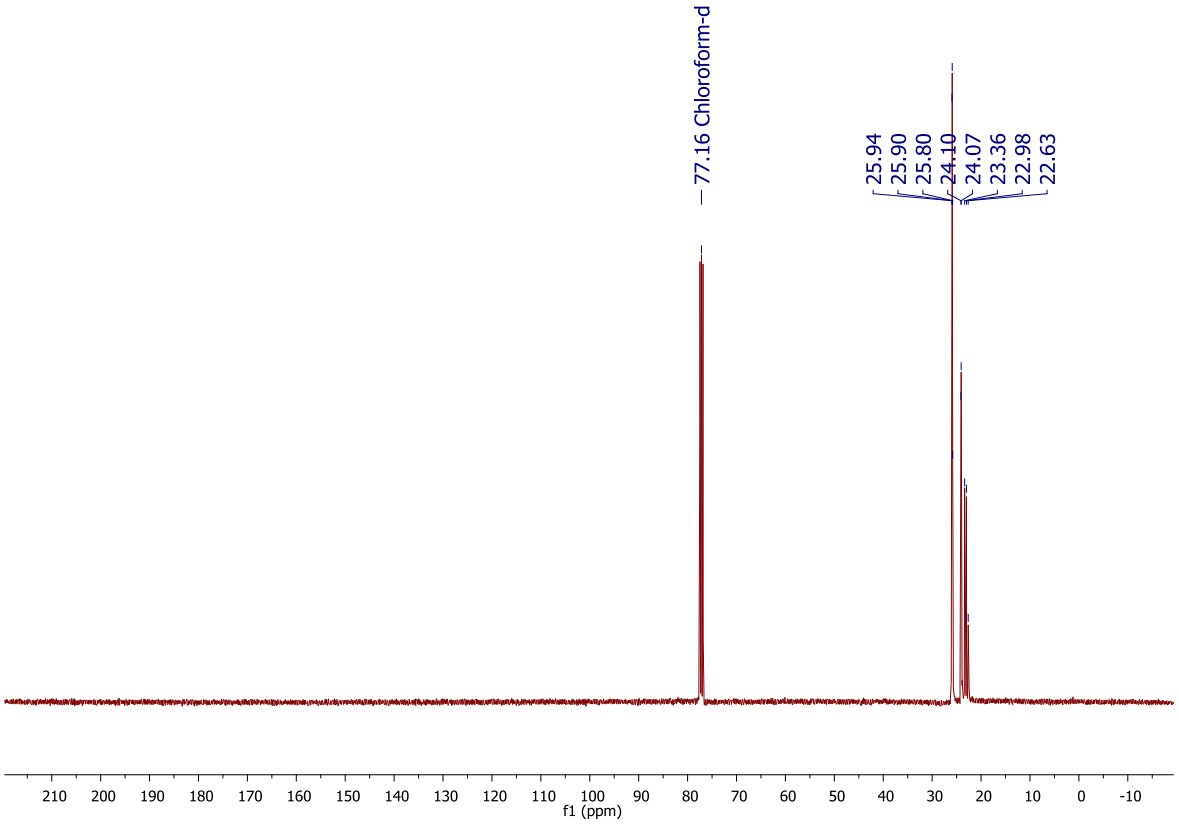

Figure S14: ^{13}C NMR of $iBu_7SSQ\text{-}3OH$

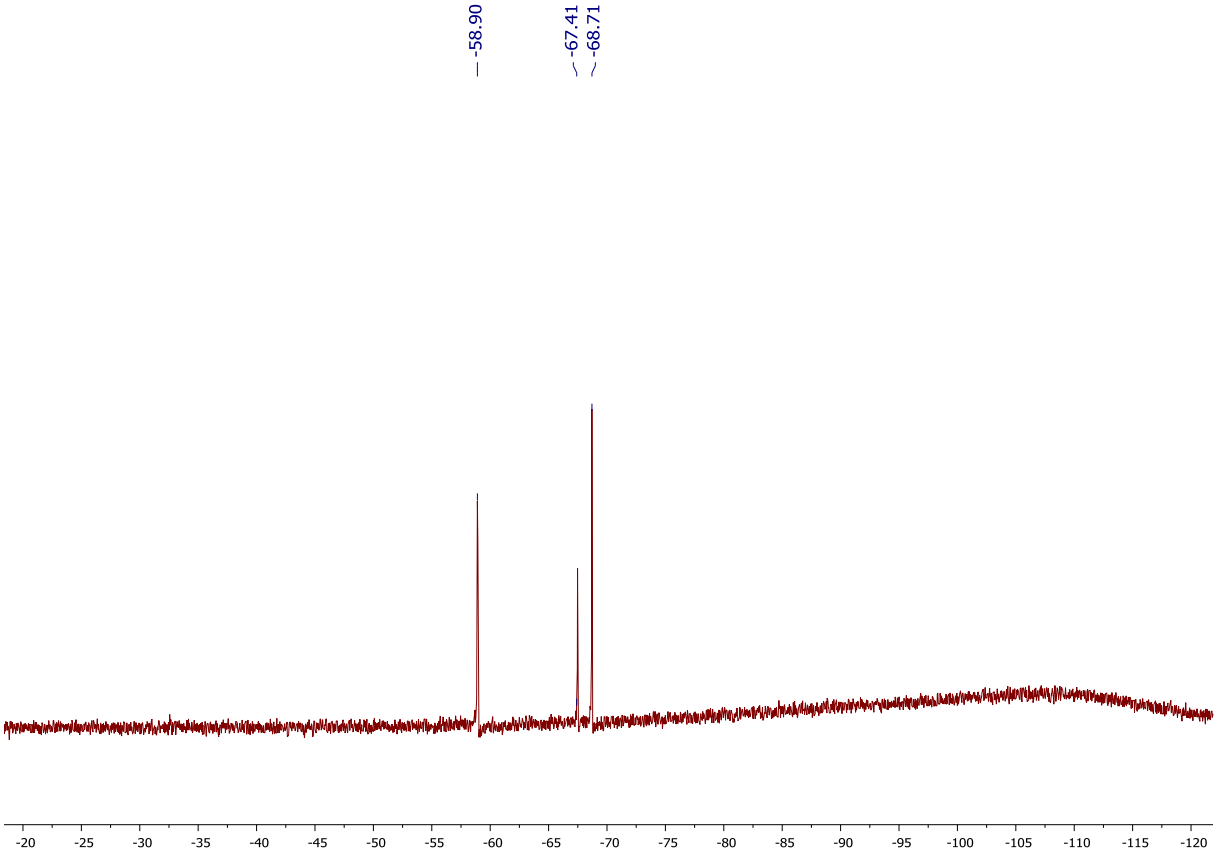

Figure S15: ^{29}Si NMR of $iBu_7SSQ\text{-}3OH$

3. MALDI-TOF-MS analysis of iBu_7SSQ-3OH heat treatment products

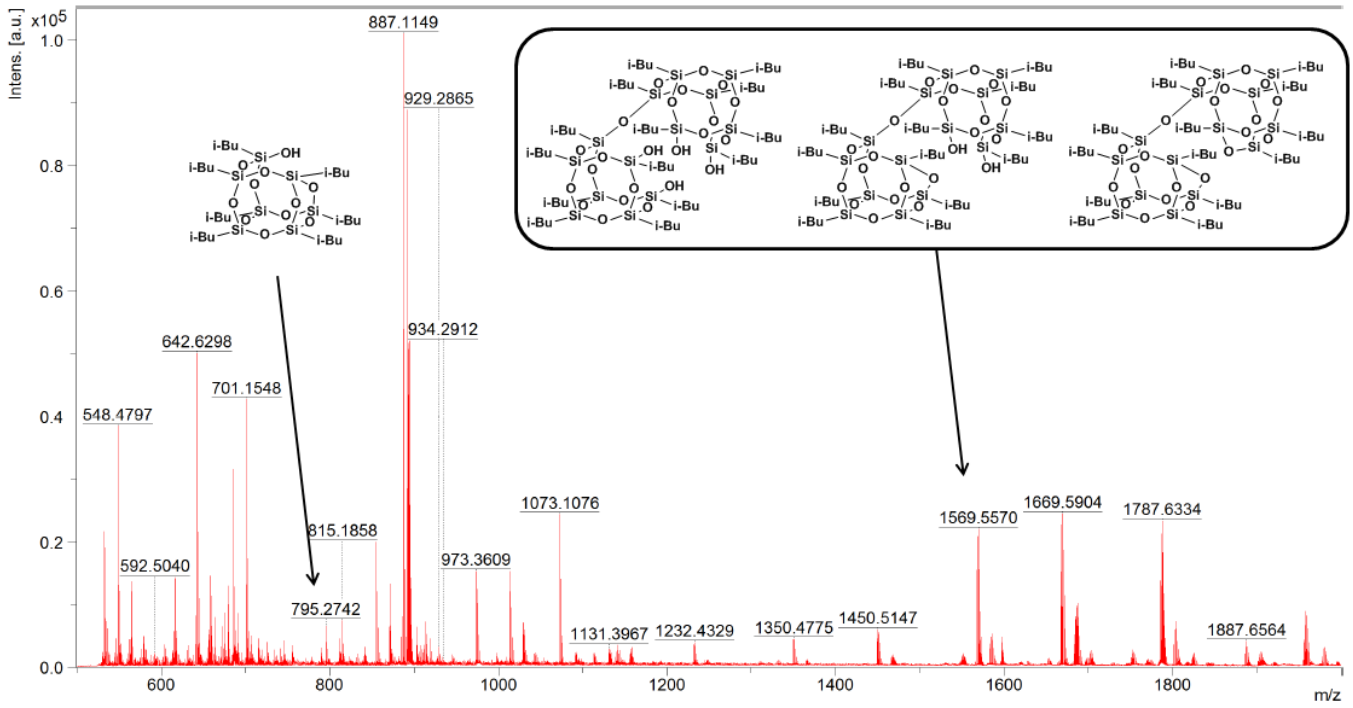

Figure S16: MALDI-TOF-MS spectrogram of iBu_7SSQ-3OH heat treatment products

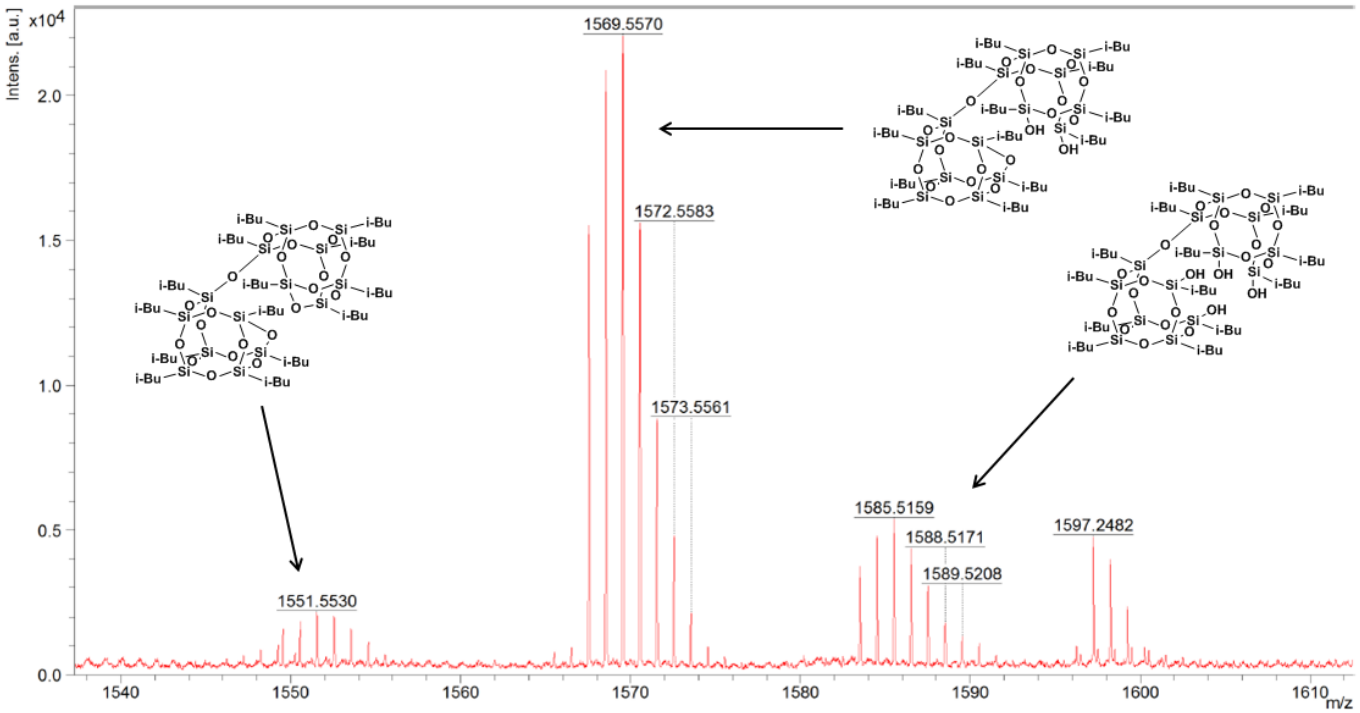

Figure S17: MALDI-TOF-MS spectrogram of iBu_7SSQ-3OH heat treatment products (enhanced)

4. SEM and EDS images of the SSQ/PE composites

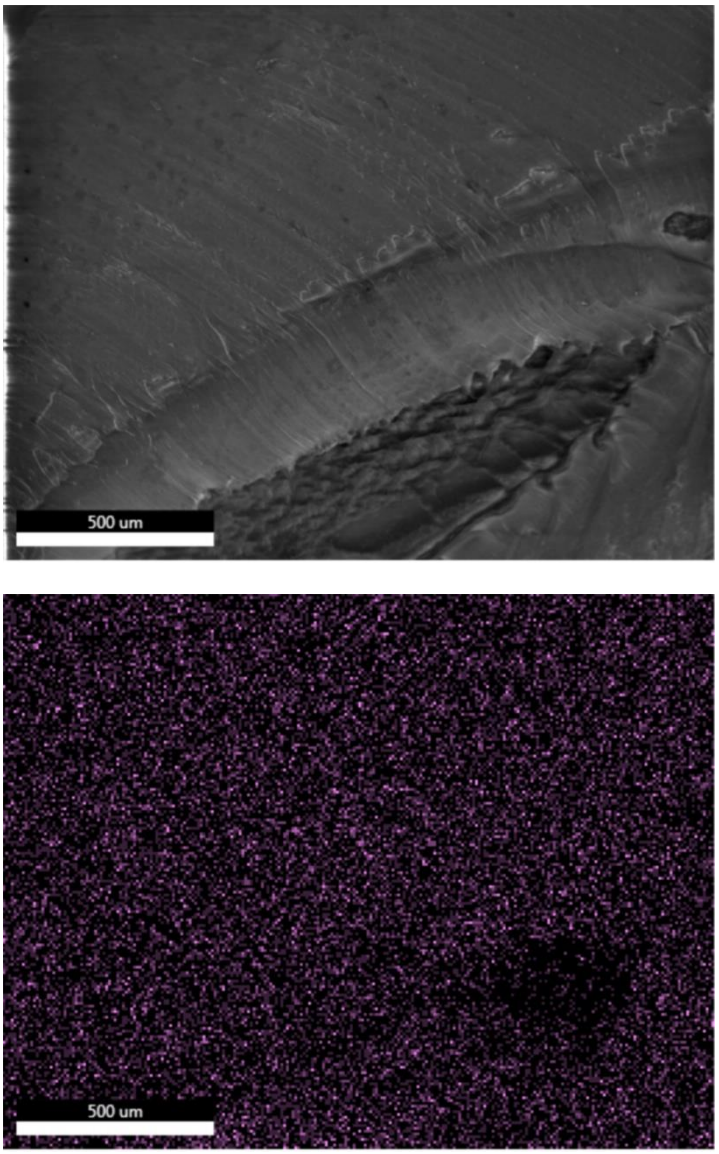

Figure S18: 0.1% SSQ-8Cl/PE

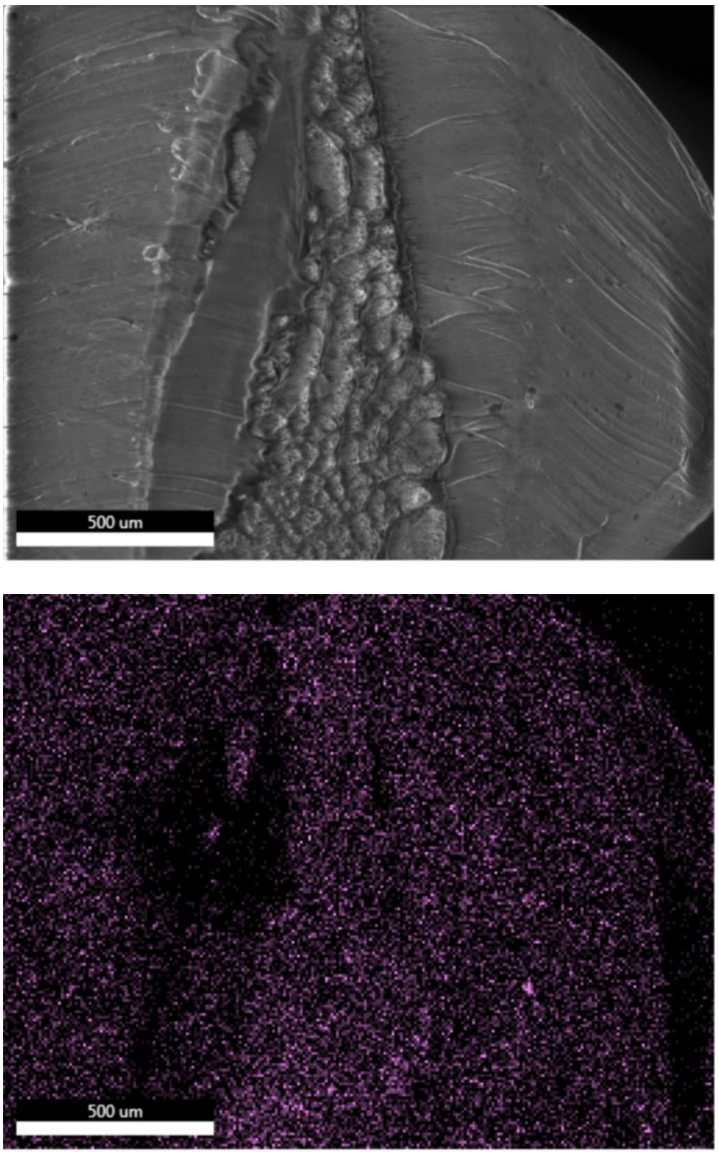

Figure S19: 0.5% SSQ-8Cl/PE

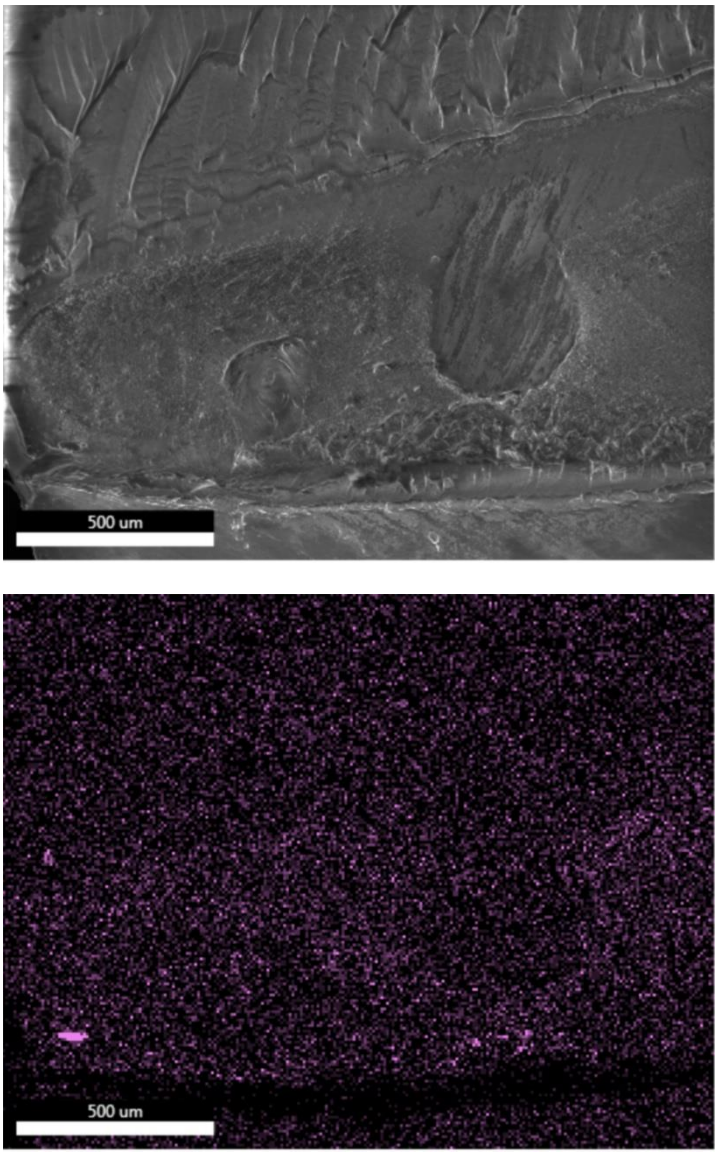

Figure S20: 1% SSQ-8Cl/PE

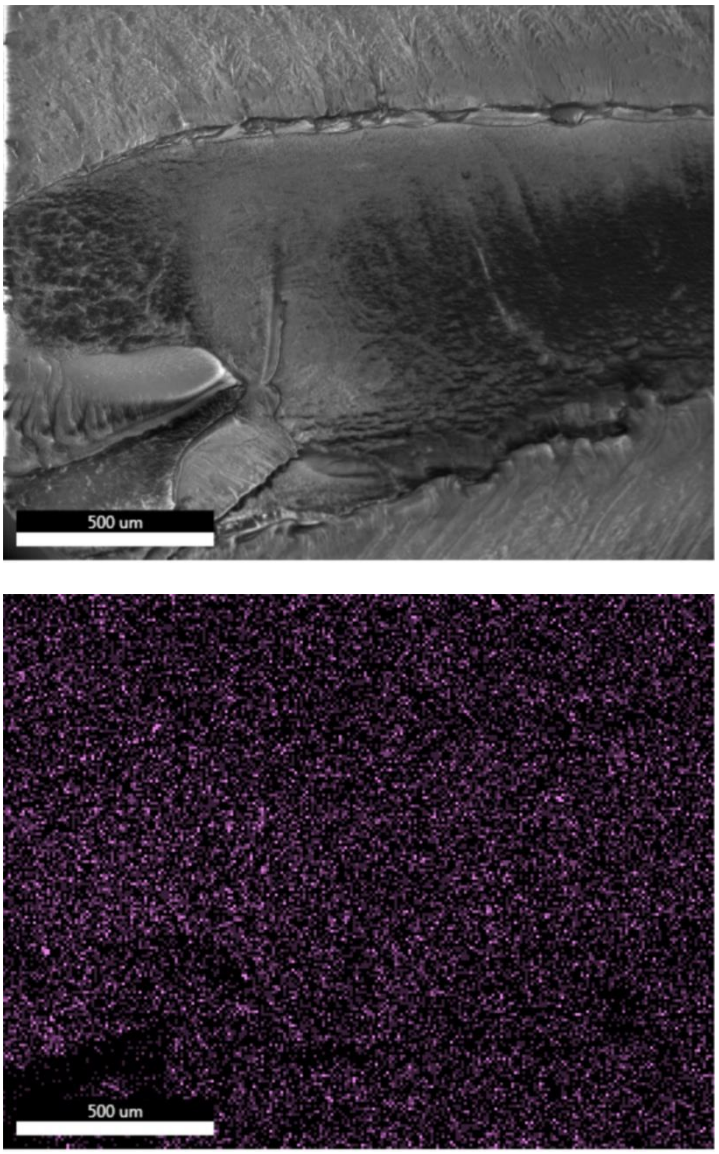

Figure S21: 0.1% iBu_7-SSQ-Cl/PE

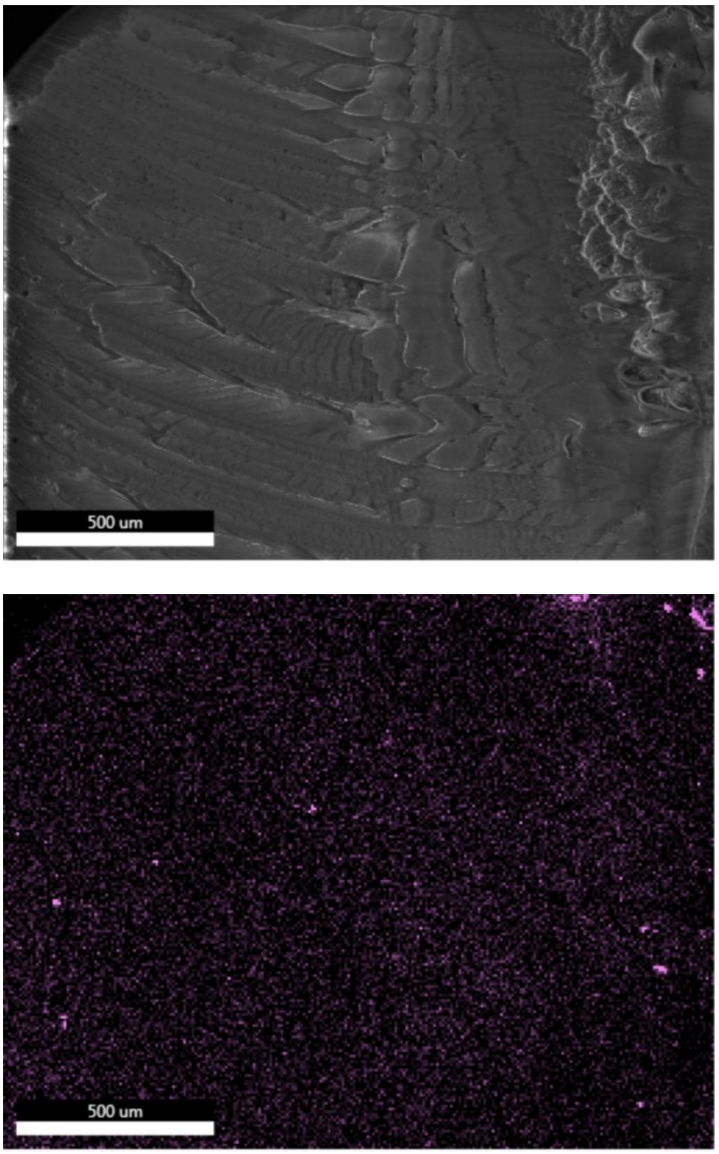

Figure S22: 0.5% iBu_7-SSQ-Cl/PE

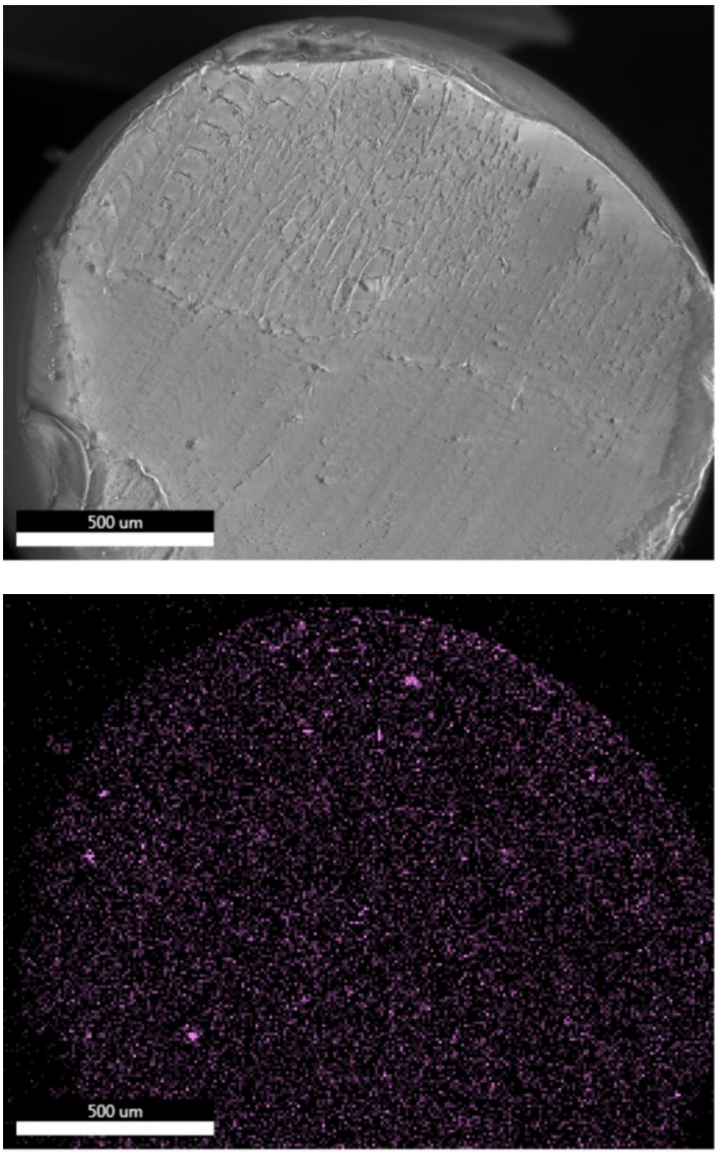

Figure S23: 1% iBu_7-SSQ-Cl/PE

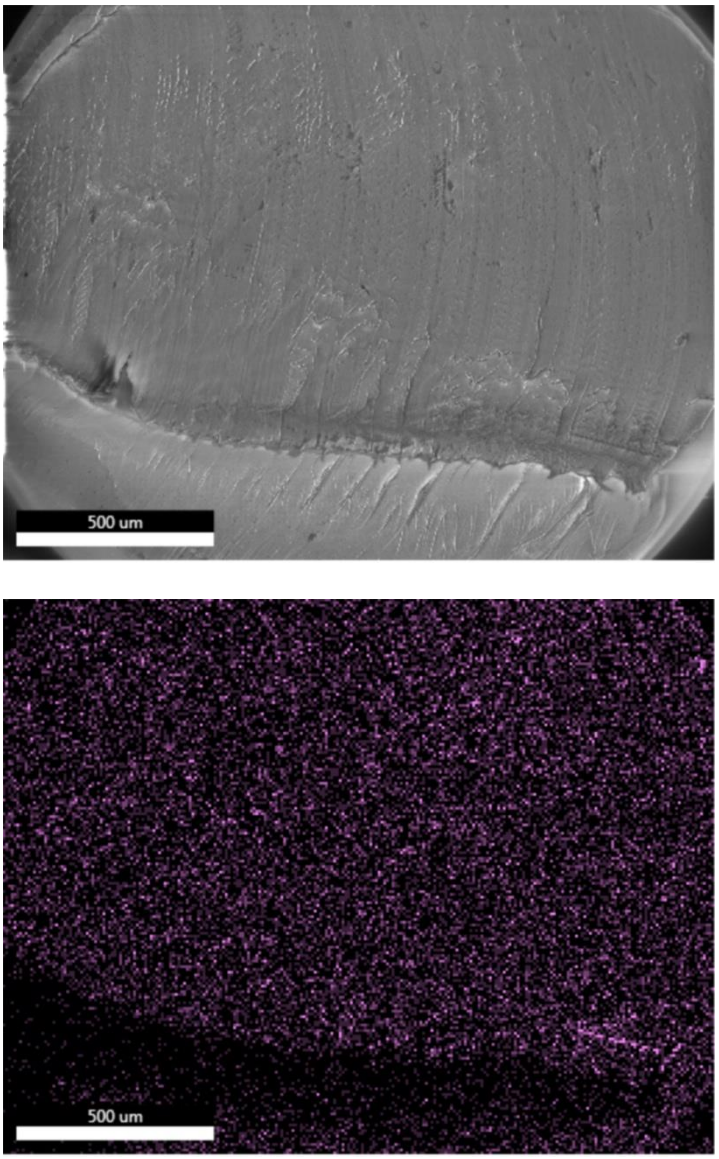

Figure S24: 0.1% iBu_7-SSQ-NH_2/PE

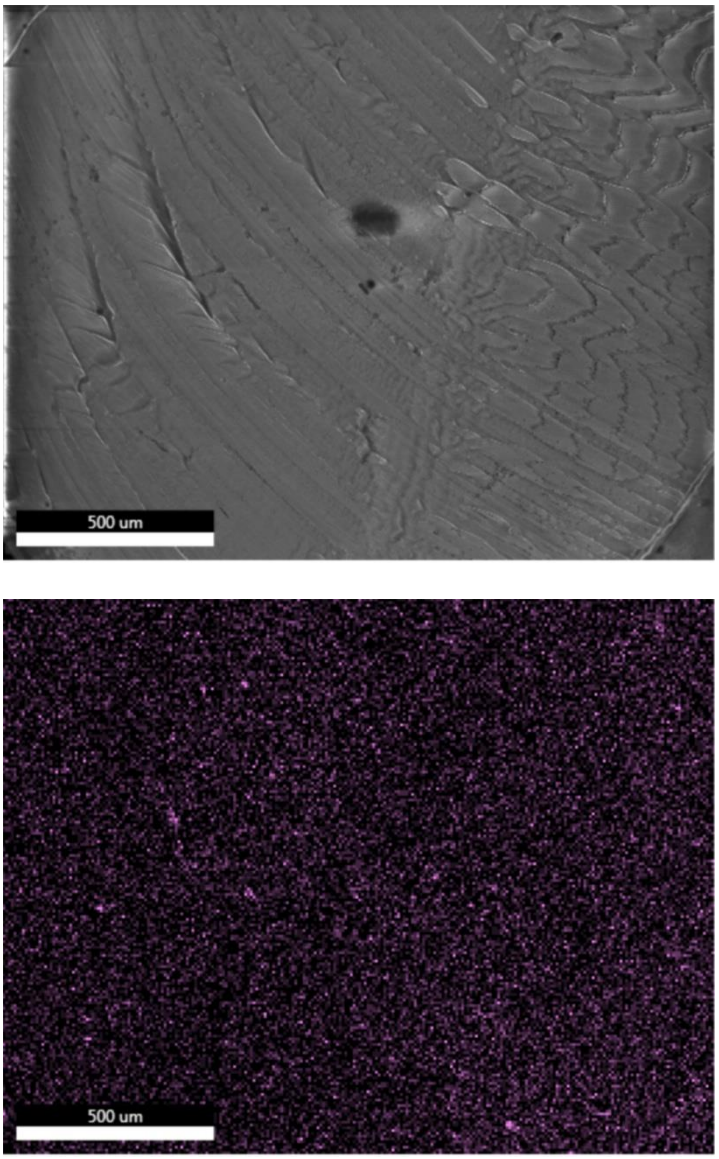

Figure S25: 0.5% iBu_7-SSQ-NH_2/PE

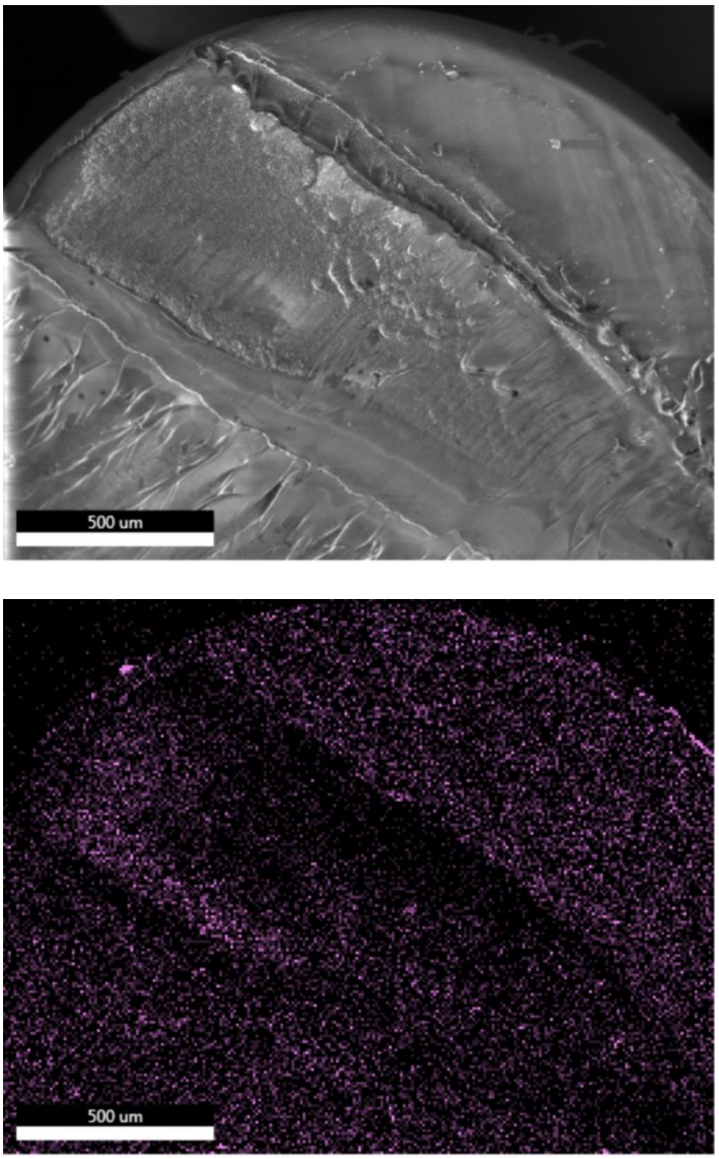

Figure S26: 1% iBu_7-SSQ-NH_2/PE

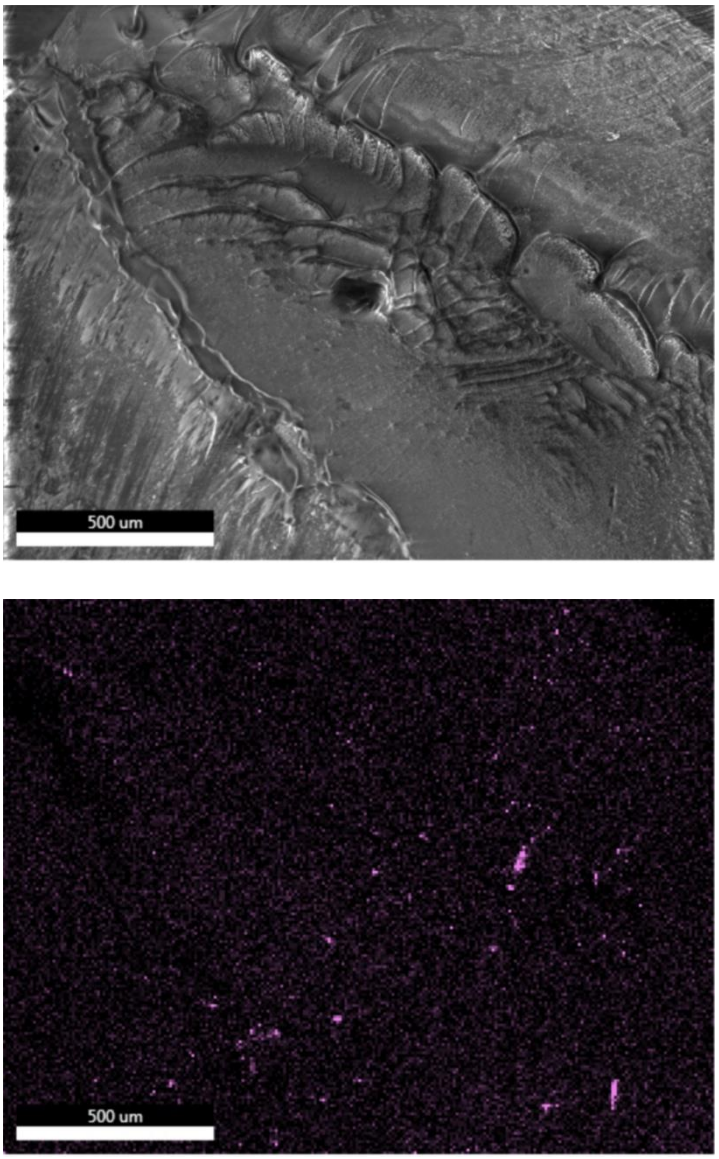

Figure S27: 0.5% iBu_7-SSQ-Vi/PE

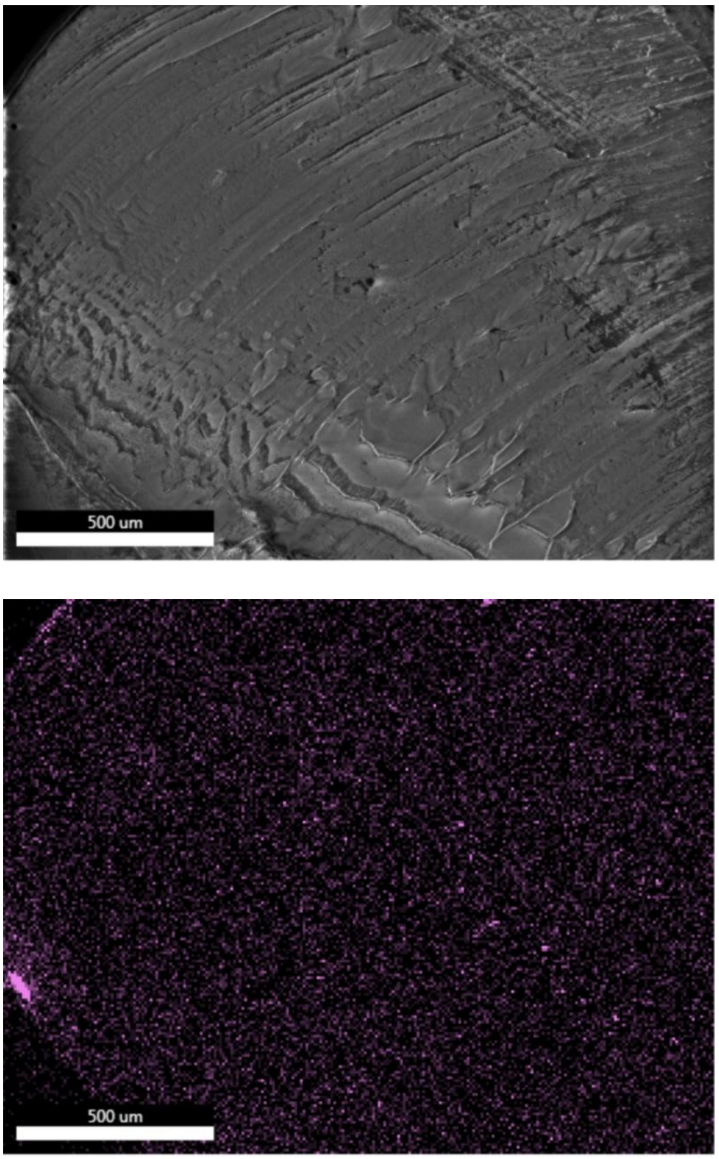

Figure S28: 1% iBu_7-SSQ-Vi/PE

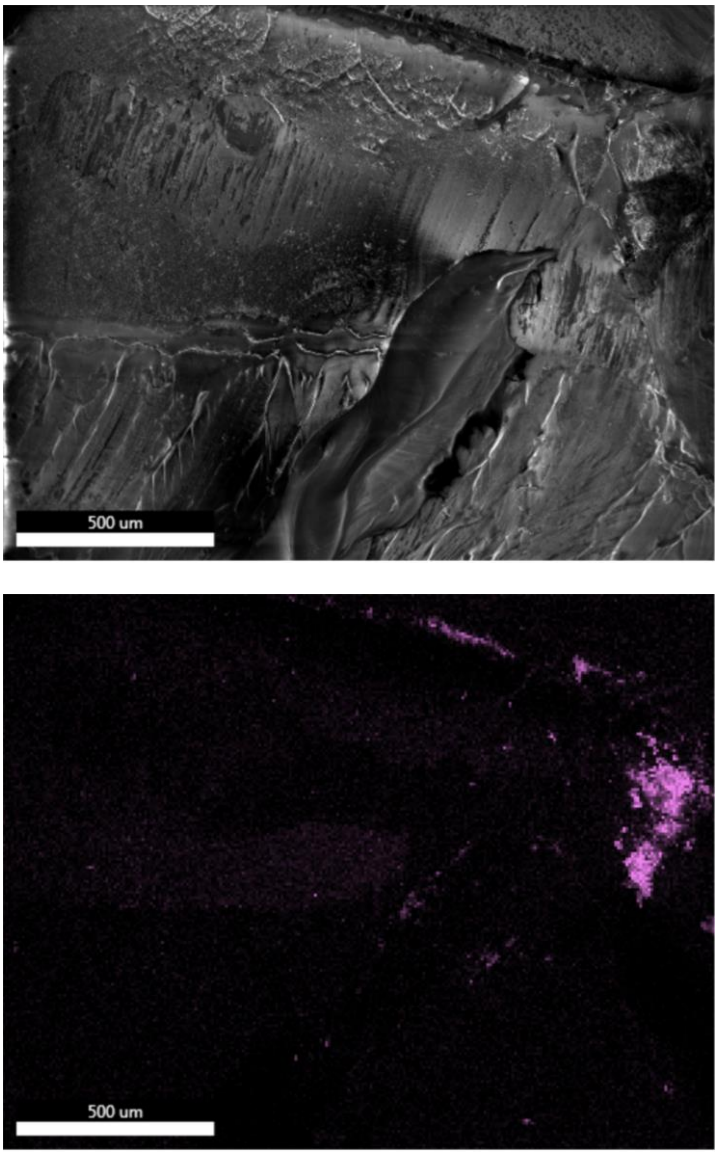

Figure S29: 1.5% iBu_7-SSQ-Vi/PE

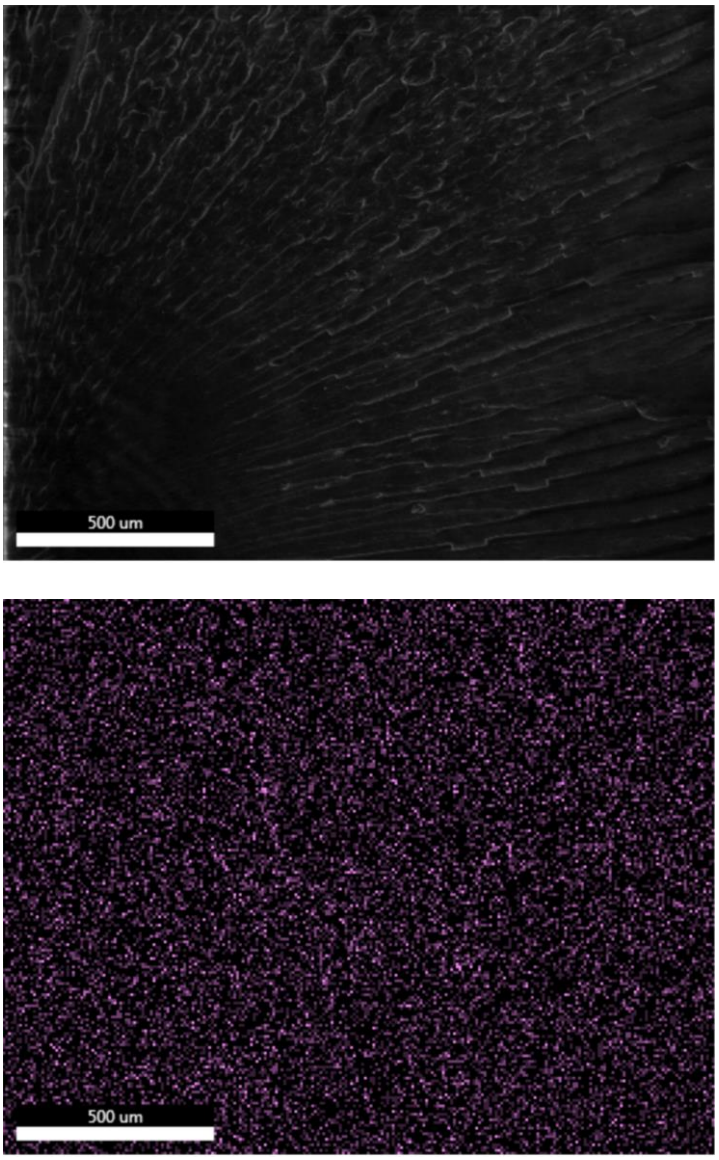

Figure S30: 0.5% iBu_7-SSQ-3OH/PE

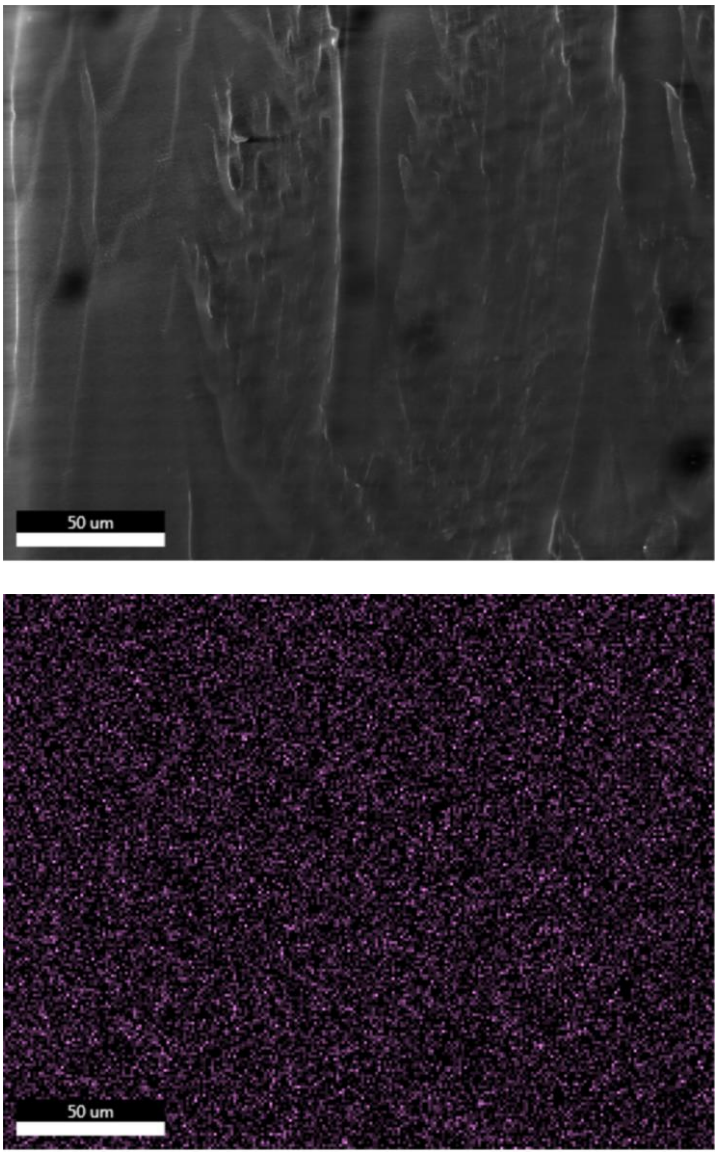

Figure S31: 0.5% iBu_7-SSQ-3OH/PE (higher magnification)

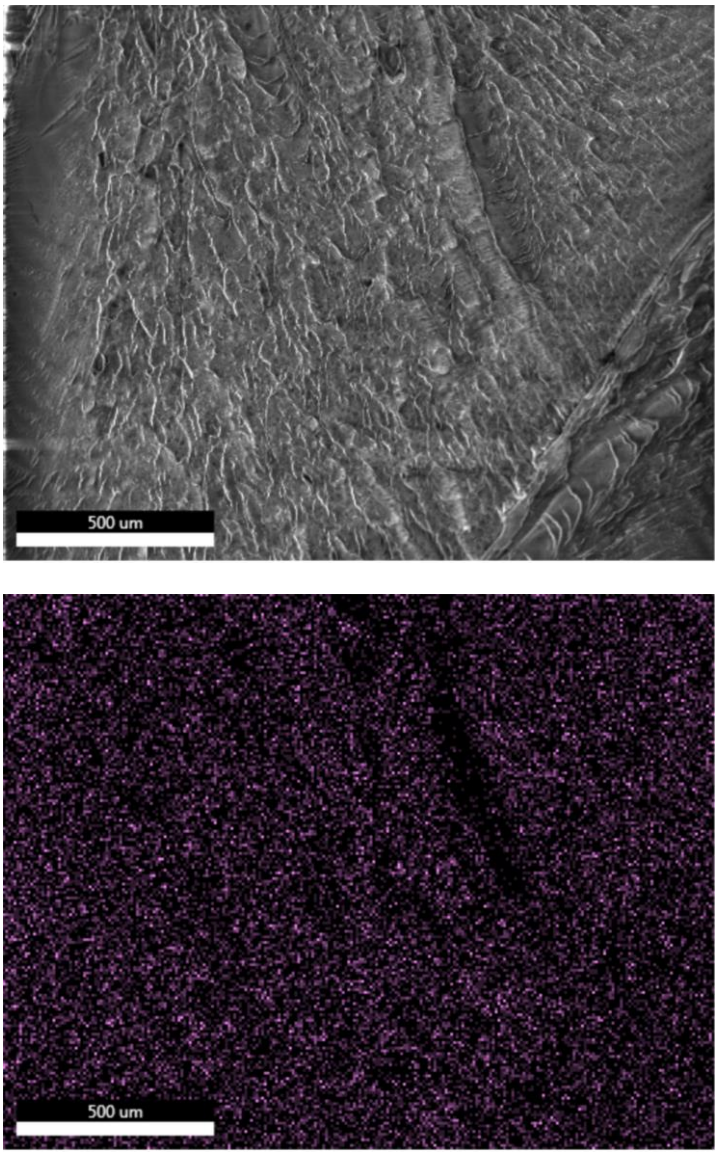

Figure S32: 1% iBu_7-SSQ-3OH/PE

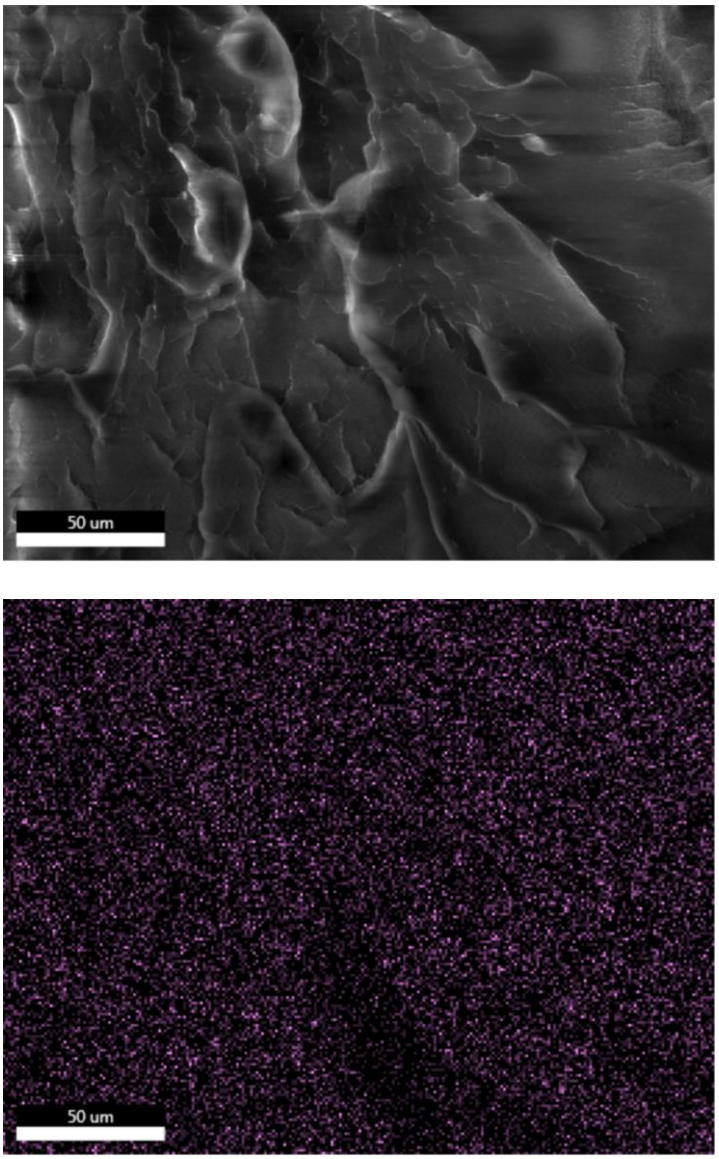

Figure S33: 1% iBu_7-SSQ-3OH (higher magnification)

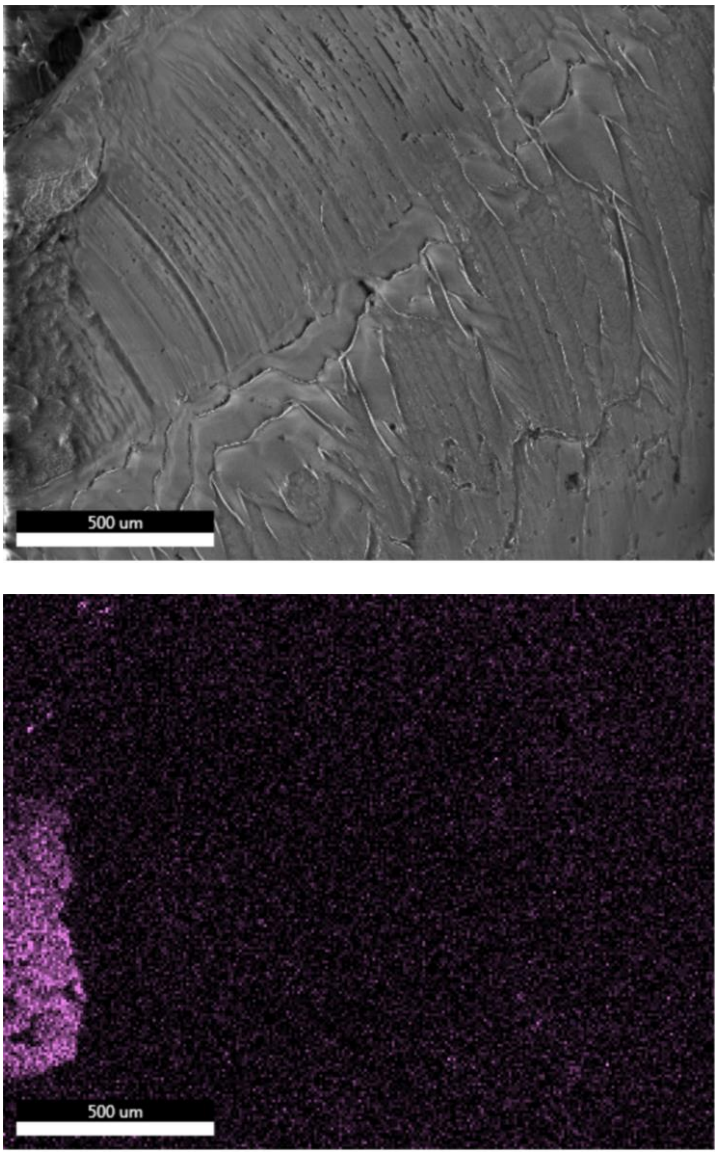

Figure S34: 1.5% iBu_7-SSQ-3OH

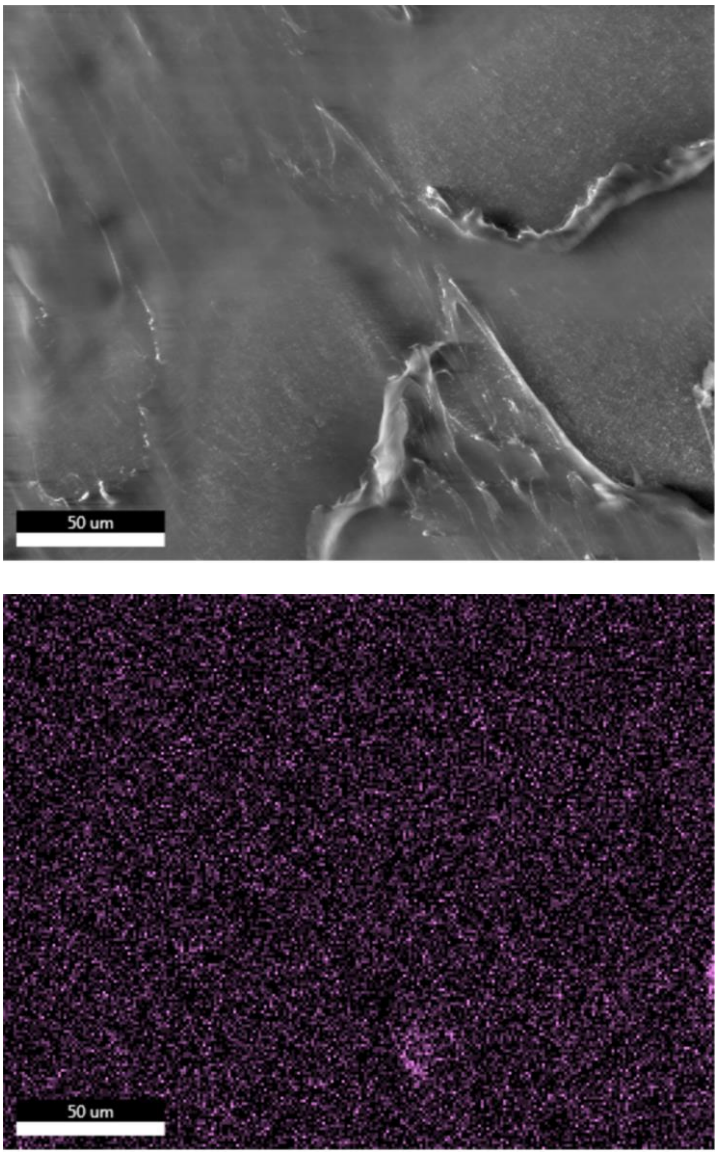

Figure S35: 1.5% iBu_7-SSQ-3OH (higher magnification)

5. Data Tables

Table S2. Crystallinity indices (CI) of the obtained composites measured by DSC.

Additive	Concentration of additive [%]			
	0.1	**0.5**	**1.0**	**1.5**
	Crystallinity Index (CI) [%]			
Neat PE	44.1			
SSQ-8Cl	45.8	47.1	45.5	-
*i*Bu$_7$SSQ-Cl	44.4	45.0	44.7	-
*i*Bu$_7$SSQ-NH$_2$	44.5	46.3	44.0	-
*i*Bu$_7$SSQ-Vi	-	46.2	43.9	46.3
*i*Bu$_7$SSQ-3OH	-	47.1	46.6	46.5

Table S3. Heat Deflection Temperatures of the obtained composites.

Additive	Concentration of additive [%]			
	0.1	**0.5**	**1.0**	**1.5**
	Heat Deflection Temperature [°C]			
Neat PE	36.5			
SSQ-8Cl	36,9	36,4	35,7	-
*i*Bu$_7$SSQ-Cl	36,2	35,3	35,4	-
*i*Bu$_7$SSQ-NH$_2$	35,2	35,4	35,6	-
*i*Bu$_7$SSQ-Vi	-	35,5	35,9	36.8
*i*Bu$_7$SSQ-3OH	-	37,2	36,6	36.2

molecules

MDPI

Article

Limonene Derivative of Spherosilicate as a Polylactide Modifier for Applications in 3D Printing Technology

Dariusz Brząkalski [1], Bogna Sztorch [2], Miłosz Frydrych [1], Daria Pakuła [1], Kamil Dydek [3], Rafał Kozera [4], Anna Boczkowska [3], Bogdan Marciniec [1,2,*] and Robert E. Przekop [2,*]

1 Faculty of Chemistry, Adam Mickiewicz University in Poznań, 8 Uniwersytetu Poznańskiego, 61-614 Poznań, Poland; dariusz.brzakalski@amu.edu.pl (D.B.); frydrych@amu.edu.pl (M.F.); Darpak@amu.edu.pl (D.P.)
2 Centre for Advanced Technologies, Adam Mickiewicz University in Poznań, 10 Uniwersytetu Poznańskiego, 61-614 Poznań, Poland; bogna.sztorch@amu.edu.pl
3 Faculty of Materials Science and Engineering, Warsaw University of Technology, 141 Wołoska, 02-507 Warsaw, Poland; kamil.dydek@pw.edu.pl (K.D.); anna.boczkowska@pw.edu.pl (A.B.)
4 Technology Partners Foundation, 5A Adolfa Pawińskiego, 02-106 Warsaw, Poland; rafal.kozera@technologypartners.pl
* Correspondence: bogdan.marciniec@amu.edu.pl (B.M.); rprzekop@amu.edu.pl (R.E.P.)

Academic Editors: Sławomir Rubinsztajn, Marek Cypryk and Wlodzimierz Stanczyk
Received: 26 November 2020; Accepted: 10 December 2020; Published: 12 December 2020

Abstract: The first report of using limonene derivative of a spherosilicate as a modifier of polylactide used for 3D printing and injection moulding is presented. The paper presents the use of limonene-functionalized spherosilicate derivative as a functional additive. The study compared the material characteristics of polylactide modified with SS-Limonene (0.25–5.0% *w*/*w*) processed with traditional injection moulding and 3D printing (FFF, FDM). A significant improvement in the processing properties concerning rheology, inter-layer adhesion, and mechanical properties was achieved, which translated into the quality of the print and reduction of waste production. Moreover, the paper describes the elementary stages of thermal transformations of the obtained hybrid systems.

Keywords: spherosilicate; limonene; hydrosilylation; polylactide; 3D printing; FDM; FFF; injection moulding; rheology; thermal analysis

1. Introduction

Three-dimensional (3D) printing is one of the most dynamically developing modern technologies. It was discovered and patented in the 1980s by Charles Hull (SLA technique) and was protected by a patent for 20 years [1]. The development and growth of interest in additive technologies has been going on continuously for about 15 years and is mainly caused by the expiration of patents, but also a decrease in printer prices and their increased availability. At that time, technological solutions became commercially available, initially only to the largest enterprises, now it is increasingly used by the sector of small and medium-sized enterprises, but also by individual consumers. Additive technologies are among those of much demand constituting the main pillar of Industry 4.0 [2]. Initially, 3D printing technology did not arouse much interest, and in the Gartner report from 2012 it was included in the area of the so-called 'Trough of Disillusionment' [3]. However, the aforementioned development of new techniques was so rapid that, in 2013, the position of the 3D printing sector changed dramatically and in 2015 Gartner published a separate report dedicated to it [4]. Additive technologies can be divided into: photochemical DLP [5], SLA [6,7], laser SLS [8], thermal FDM [9] or LOM [10].

One of the most popular additive techniques is FDM (fused deposition modelling). The technology originally developed by Stratasys involves extrusion from a die heated above the polymer melting point and then applying it layer by layer in the direction of the Z axis [11]. The extruded material is in the form of a filament with a diameter of usually 1.75 mm. The advantages of the FDM method are its versatility and accessibility [12], as well as the ease of designing and making a model of any shape and geometry [13]. The disadvantages include, first of all, insufficient mechanical strength in the direction of the Z axis due to the appearance of air gaps between successively superimposed layers [14]. This effect does not occur in the case of other traditional methods, such as injection moulding, where solid objects are obtained.

Such air gaps can contribute to the appearance and initiation of cracks and material design defects. Therefore, attempts are continuously made to reduce poor quality of printed materials and improve the interfacial strength of printed models [15]. In addition, when compared to the traditional method such as injection moulding, 3D printing generates a number of technological problems related to insufficient process speed [16] or product quality (often requiring additional post-processing) [17].

Significant disadvantages hampering the future of 3D printing also include high waste generation, higher than in traditional techniques such as extrusion or injection moulding. An attempt to eliminate unfavourable features by improving the processing device, which is the printer, have encountered significant limitations. In the FDM technique, several thermoplastics are usually used with the greatest emphasis on such polymers/copolymers as: PLA, PA, ABS, TPU. The same types of plastics are mostly used in 3D printing and mature processing techniques. FDM is micro-processing and has significant differences when compared to classic thermoplastics processing techniques, such as lower extruder pressure or smaller cross-sections of the canals in which the molten material flows. Therefore, plastics dedicated for 3D printing should be designed to show the properties addressing these differences (e.g., higher MFI/lower viscosity).

In the FDM technique, polylactide is the most commonly used polymer, mainly due to its ease of its processing, low thermal shrinkage [18] and biodegradability. Degradation rate is low enough to make it resistant to mild weather conditions [19] which is why, next to ABS, it is most often used in medicine [20]. The melting point of PLA is around 150–170 °C and is lower than those of many other popular polymers, it also requires much less energy due to low heat of fusion, so it can be widely used in various processing techniques [21]. One of the disadvantages of PLA limiting its application is low mechanical strength, especially the impact resistance [22]. In order to improve these parameters, structural fillers and plasticizers have been used, e.g., glass and carbon fibres, ceramic or metallic fillers, and glycols [23].

Chemical modifiers that improve the functional properties of composites, such as organic and organosilicon compounds, can also be applied. Limonene (4-isopropenyl-1-methylcyclohexene)—is the main component of oils obtained from waste citrus peels (biomass). It can be obtained by natural and synthetic methods, e.g., using pyrolytic processes [24]. Simple distillation or steam distillation of citrus peels makes it possible to recycle the waste citrus peels from food industry and, at the same time, to obtain pure limonene with a small amount of toxic waste. Annually, these methods produce over 70,000 tons of this compound. In 3D printing technology, it is used as a solvent for support materials made of high impact polystyrene [25]. From the point of view of synthetic applications, limonene should be classified as a green olefin that is subjectable to hydrosilylation reaction [26]. The use of limonene as a building block is one of the many necessary steps in creating a chain of products based on raw materials of natural origin with a lower environmental impact. In its pure form, however, it has a low boiling point for PLA processing (176 °C), which may cause its boiling during processing and, as a result, introducing gases into the polymer, as well as emission of vapours to the environment. Nevertheless, attempts have been made to use it in the processing of PLA, when it showed a plasticizing effect on the polymer matrix, which is a great advantage due to the brittleness of the neat polymer [27].

Polyhedral oligomeric silsesquioxanes are well-known organosilicon compounds, mostly recognized for their high symmetry, excellent solubility, or unparalleled simplicity of synthetic

protocols [28]. Among those, a subgroup called spherosilicates may be distinguished, sometimes identified as a different group of compounds, and in such case, both spherosilicates and silsesquioxanes are collectively called cage siloxanes [29]. Due to their high thermal stability and good dispersion properties, they are considered interesting functional additives for polymer processing. In our previous works we have presented approaches towards processing of low-density polyethylene (LDPE) with polyhedral oligomeric silsesquioxanes [30], as well as spherosilicates [31]. These studies allowed determination of the critical level of practical loading in the LDPE matrix, which was much lower than what can be found in numerous literature reports, and was parallelly confirmed by Romo-Uribe et al. [32–34]. One derivative from among the tested ones was found to be particularly interesting, it was SS-Limonene, a product of limonene hydrosilylation with Octahydrospherosilicate. The results suggested its mildly plasticizing effect on the polymer matrix, besides its content improved thermal and mechanical properties of the obtained materials. Therefore, in this study, we decided to assess the applicability of this derivative as a functional and processing additive for PLA for 3D printing.

2. Results and Discussion

2.1. Characterization of SS-Limonene (1,3,5,7,9,11,13,15-octa(Dimethyl((2-(4-methylcyclohex-3-en-1-yl)propyl) silyl)-Pentacyclo [9.5.1.1^{3,9}.1^{5,15}.1^{7,13}]Octasiloxane

SS-Limonene (Figure 1) was prepared according to the synthesis procedure described in Section 3.3 and the reaction completion was determined by FT-IR spectra analysis, the disappearance of the characteristic signals assigned to stretching and bending vibrations of the Si-H group was observed at 2141 and 889 cm^{-1}, respectively). Upon completion of the reaction, the hydrosilylation reached ~99% conversion. The structure and purity of the modifier was confirmed by NMR and MALDI-TOF-MS analyses.

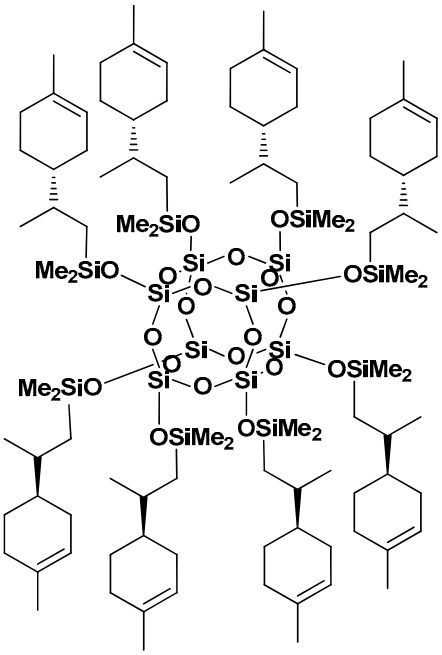

Figure 1. Structure of SS-Limonene.

The purity and chemical structure of the synthesized compound was confirmed by NMR spectroscopy, with the following signals assignment:

^{1}H-NMR (400 MHz, $CDCl_3$): δ (ppm) = 5.36 (s, 8H, ring position 3), 2.00–1.87 (m, 24 H, ring positions 1, 2, 5), 1.78–1.56 (m, 24 H, ring positions 2, 5, =CH- isopropenyl methylidene), 1.63 (s, 24 H,

-CH_3 methyl attached to ring position 4), 1.34–1.18 (m, 16 H, ring position 6), 0.90 (d, 24 H, isopropenyl methyl), 0.75–0.69 (m, 8H, isopropenyl -CH_aH_b-), 0.52–0.44 (m, 8H, isopropenyl -CH_aH_b-), 0.15 (s, 48H, $SiMe_2$); ^{13}C-NMR (101 MHz, $CDCl_3$): δ (ppm) = 133.96, 121.28, 121.26, 41.48, 41.33, 33.08, 32.93, 31.19, 31.12, 28.80, 28.24, 26.71, 25.71, 23.64, 23.63, 22.87, 22.48, 19.52, 19.22, 0.83, 0.72, 0.66; ^{29}Si-NMR (79.5 MHz, $CDCl_3$): δ (ppm) = 12.78 ($SiMe_2$), −109.10 (core). IR (ATR): 2980–2867, 1252, 1169–1069, 869–734, 549. MALDI-TOF-MS: $[M + Na]^+$: 2127.9581 (calc.), 2127.9606 (anal.)

2.2. Density of SS-Limonene/PLA Blends and Mass/Quantity Waste Factor of the Printed Samples

Densities of all samples were measured by the hydrostatic method. Measurements were performed for the samples of 1 cm in length. The average densities of all samples and the base sample of neat PLA were at the same level of around 1.24 g/cm^3. The waste factor of printed samples was also analysed for the bars printed with 100% infill. Data are collected in Table 1. On the basis of the obtained data, the mass and the volume waste factors were determined according to the formula:

$$Wf[m,q] = \frac{mass\ (quantity) of\ corect\ samples \times 100\%}{mass\ (quantity)\ of\ total\ samples} \quad (1)$$

Table 1. Masses and the numbers of models examined in order to establish waste factor values.

Sample	5%	2.5%	1%	0.5%	0.25%
			Total		
Mass [g]	111.11	84.43	91.15	105.52	59.95
Number	38	30	30	34	24
			Correct		
Mass [g]	53.55	51.69	57.44	66.85	44.16
Number	14	12	14	16	11
W_f [m%]	48	61	63	63	74
W_f [q%]	37	40	47	47	46

The calculated waste factors clearly showed that with decreasing content of the SS-Limonene modifier, the amount of 3D printing waste decreases. The issues with printing the samples with high loading of SS-Limonene can be explained on the basis of the additive polymerizing and curing during the polymer processing, which is further explained in Sections 2.4 and 2.5.

2.3. Rheology

The melt flow index (MFI) of pure PLA at 190 °C is 3.7075 g/10 min (Figure 2). For the PLA composites with SS-Limonene the MFI value increased with increasing concentrations of the filler. The composite samples containing 2.5% concentration of the additive are characterized by slightly higher MFR value. On the basis of the data analysis, it can be concluded that SS-Limonene as an additive to the polymer matrix will have a positive effect on its processing.

A capillary rheometer was used to determine the relation between shear rate and viscosity (Figure 3). At low shear rates, the viscosities of all compositions are lower than those of neat PLA, as a consequence of SS-Limonene acting as a plasticizer.

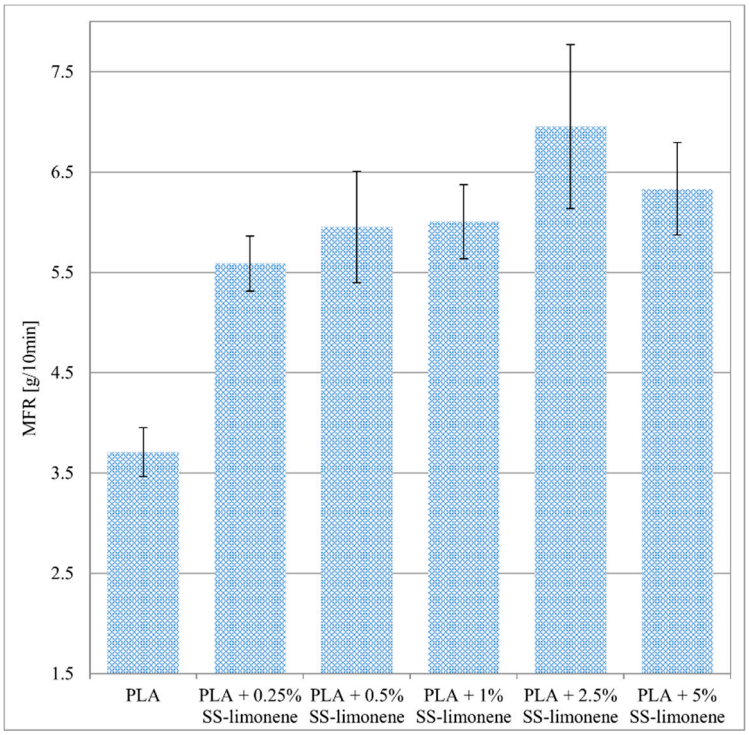

Figure 2. Result of MFR measurements.

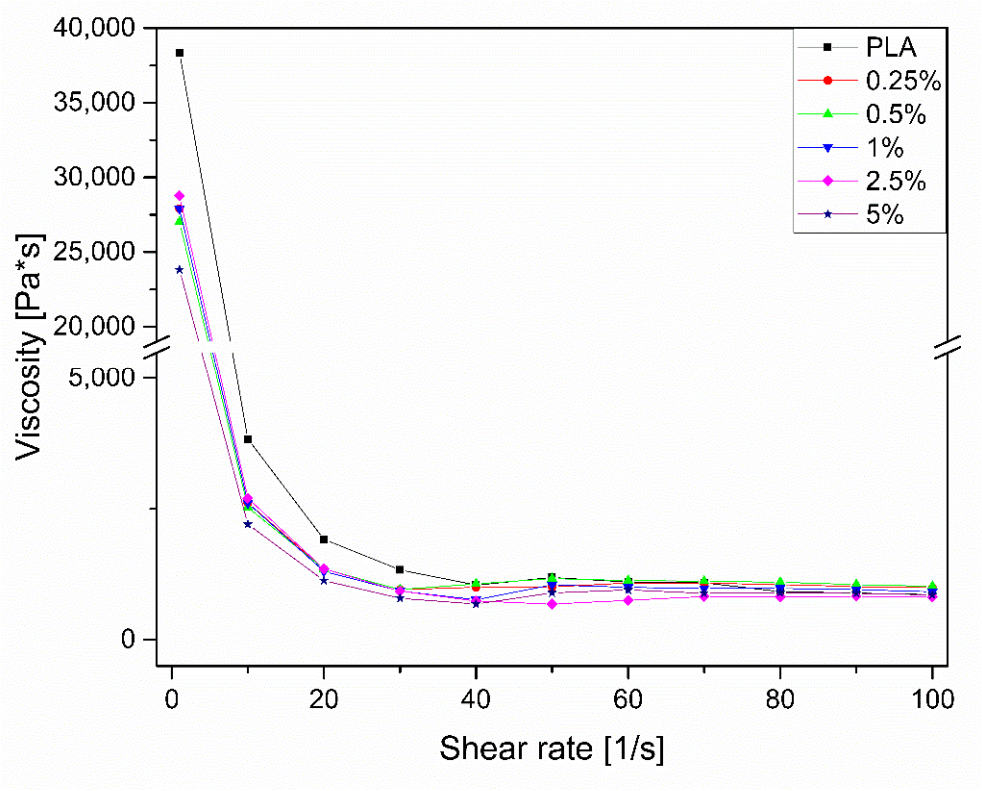

Figure 3. Viscosity measurement results.

2.4. Microscopy

Figures 4 and 5 present the outer and inner texture of 3D-printed (Figure 4) and injection-moulded samples (Figure 5) under a digital light microscope and SEM with an additional EDS analysis (Figure 4e). For the printed samples, different morphologies of the outer and inner regions of the fractured sample (Figure 4b,c) can be seen due to the printing pattern, as the infill has a grid pattern for improved mechanical strength, while the outer layers are made in a rectangular pattern and therefore can be seen as perpendicular to the fracture plane. This is a result of the standard printing process conditions, where the 3D printer outlines the outer shapes of the sample with straight lines first, and then infills the object with a chosen pattern. However, the outline of the outer layers is, in fact, of the highest interest, as it allows observation of the inter-layer interfaces between the individual extrudate strands (and, on this basis, an assessment of the layer-to-layer bonding), as well as the size of the air gaps. In Figure 4b, the inter-layer interfaces between extrudate strands of the neat PLA sample can be clearly seen, which contributes to the low mechanical resistance of the printed PLA objects. On the other hand, for 0.25% SS-Limonene/PLA sample (Figure 4c), this interface is hardly visible, which explains the improved inter-layer adhesion and mechanical rigidity of the samples, which made them mechanically more similar to the injection-moulded ones. However, the formation of air gaps was rather unaffected. Also, on closer inspection, all the samples containing SS-Limonene additive (either 3D printed or injection moulded) contained particles visible both under the light microscope (Figure 4d) and SEM (Figure 4f,g and Figure 5d,e). EDS analysis of silicon allowed identification of the particles to be agglomerates of the polymerized additive (Figure 4e). With increasing loading, more agglomerates of such particles were visible, which contributed to the issues with printing the samples containing high amounts of SS-Limonene. Polymerization of the additive is further discussed in Section 2.5. Additionally, for injection-moulded samples, together with the mentioned particles, small air gaps were observed (Figure 5d,e), which are not present in the sample made from neat PLA (Figure 5b,c). It may be due to difficulties with degassing of the polymer melt, or the generation of gas products either of evaporation or decomposition of SS-Limonene, as the thermogravimetric analysis thereof under the PLA processing temperatures revealed a small mass loss.

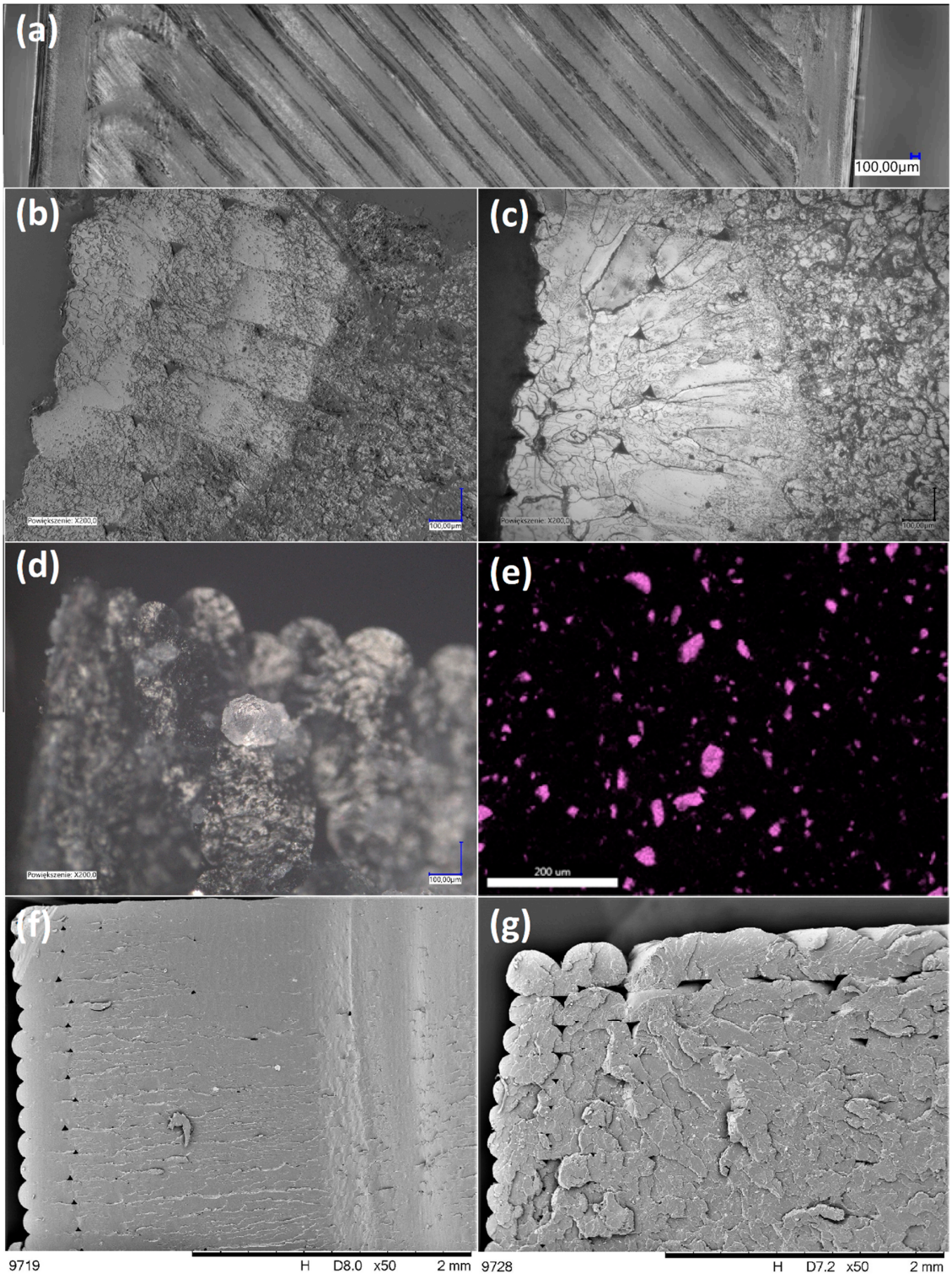

Figure 4. Optical microscopic images (**a**–**d**) and SEM images (**e**–**g**) of printed samples: outer surface (**a**), fractured sample from neat PLA (**b**), fractured sample from 0.25% SS-Limonene/PLA (**c**), a crystal of polymerized SS-Limonene (**d**), silicon EDS image of 0.25% SS-Limonene/PLA fractured sample (**e**), fractured sample from 0.25% SS-Limonene/PLA (**f**), fractured sample from 2.5% SS-Limonene/PLA (**g**).

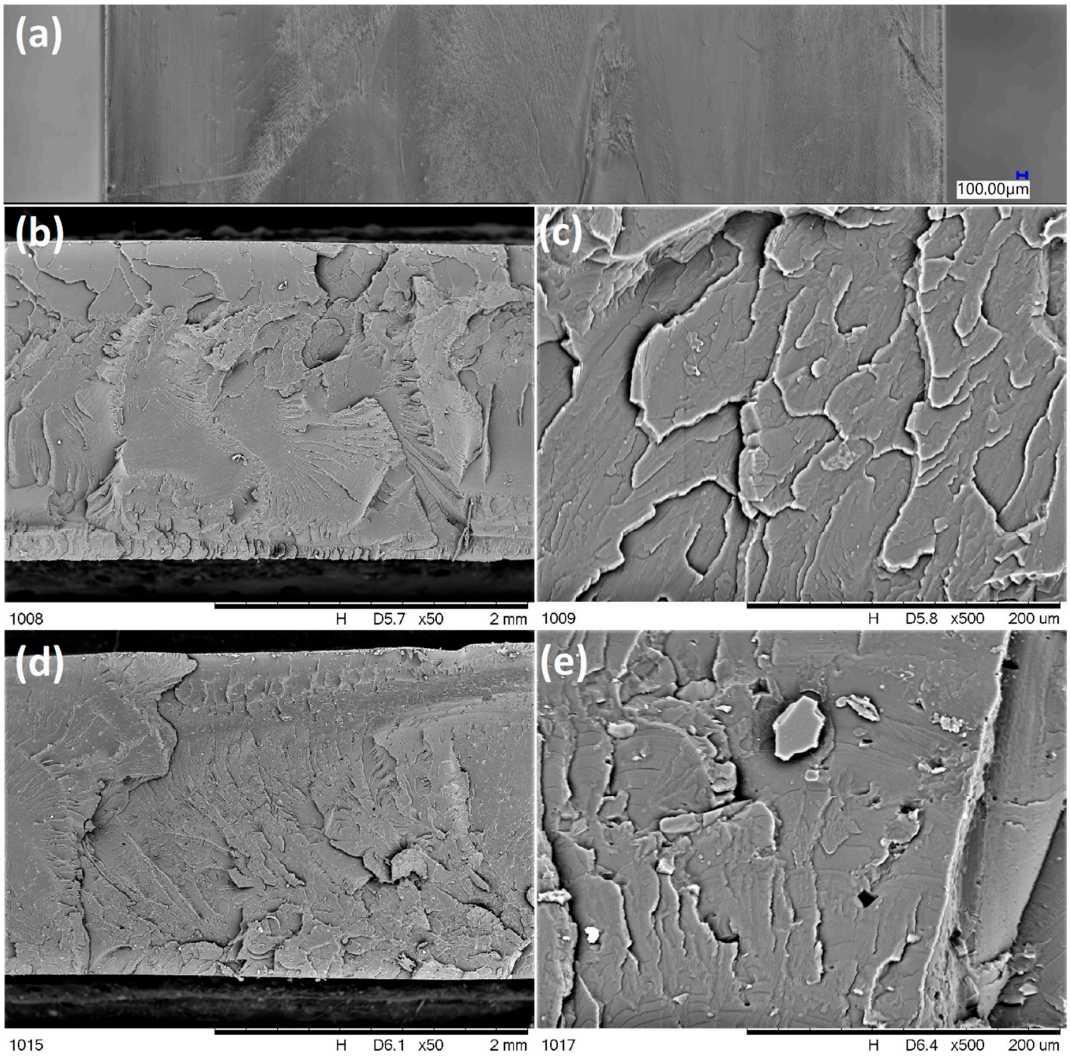

Figure 5. Optical microscopic image (**a**) and SEM images (**b**–**e**) of injection moulded samples: outer surface (**a**), fractured sample from neat PLA (**b**,**c**), fractured sample from 2.5% SS-Limonene/PLA (**d**,**e**).

2.5. Thermal Analysis Results

Thermal effects for SS-Limonene/PLA compositions were measured by differential scanning calorimetry (DSC) and thermogravimetric analysis (TGA).

DSC analysis was performed to determine the effect of SS-Limonene addition on the glass transition (T_g), crystallization (T_c) and melting (T_m) temperatures of the composites. The graphs are shown in Figure 6. In each case, a large peak of glass transition is noticeable at the first heating cycle, which is related to the low crystallinity of the extruded samples (high proportion of the amorphous phase), due to the rapid cooling of the polymer (in air and in a cooling bath during extrusion). The glass transition temperature (T_g) after the second heating cycle of the test samples containing the organosilicon additive is shifted towards lower values relative to that observed for the neat PLA. This is due to the plasticization of the polymer matrix. Similar conclusions can be drawn in the context of T_{cc}, as the presence of the plasticizing phase increases the freedom of the chains in the amorphous phase, accelerating the initiation of crystallization. The change in T_m and T_{cc} values also shows that SS-Limonene is at least partially mixed with PLA and the interaction of these two components occurs, despite the presence of the polymerized additive phase visible in the microscopic photos (SEM-EDS, light microscopy). On the basis of T_g, the strongest plasticizing effect was observed for the system containing 0.25% of the above-mentioned modifier, but the lowest melting point was observed for the

system containing 5% of SS-Limonene. The DSC analysis of the modifier allowed observation of the polymerization of the compound on heating of the sample, which was also confirmed by microscopic analysis as an effect of agglomeration of the polymerized additive in the PLA matrix. A similar effect has been observed in our earlier work, however, most likely due to lower processing temperatures of LDPE, the agglomeration was far less severe [31].

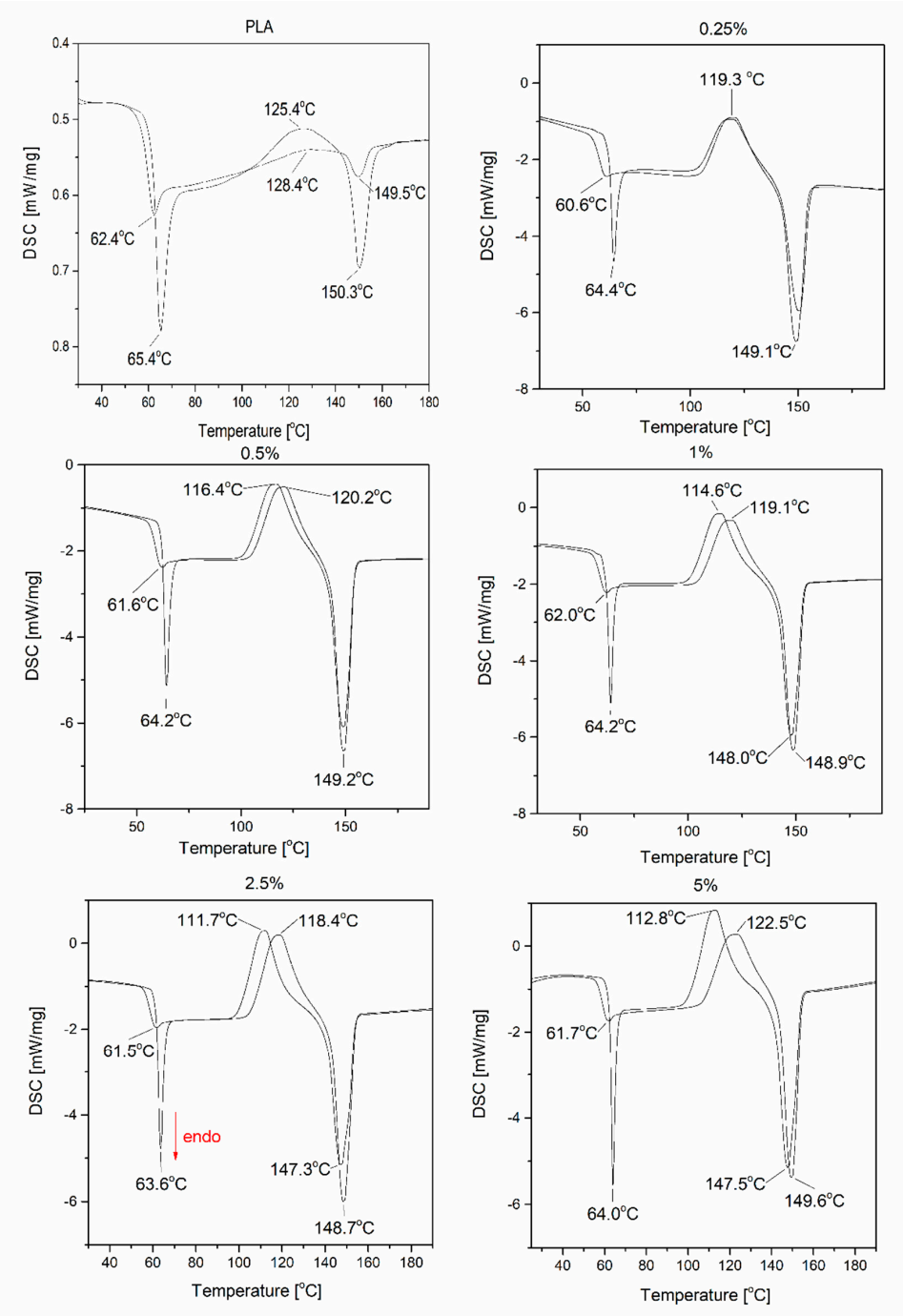

Figure 6. DSC curves recorded for samples of SS-Limonene/PLA composite.

All results of the TGA, DTG and c-DTA measurements are presented in Figure 7. The parameters determined, including the temperature of 1% mass loss, onset, and temperature at the maximum rate of mass loss are collected in Table 2. The process of thermal decomposition of samples was carried out in both nitrogen and air atmosphere. It should be remembered that thermal changes in

thermoplastic systems at temperatures above the melting point of the matrix should not be defined as the 'thermal resistance' or 'thermal strength' of the composite, but refer to the influence of the applied additives on the thermal stability of the polymer system in molten state and the interaction between the system components in the melt. Based on the observation of the complete thermal analysis, i.e., the derivatographic curve, DTG and c-DTA results obtained both in air and nitrogen atmosphere, three stages of thermal transformation can be distinguished. The first step, observed in both air and nitrogen atmosphere, at 140–160 °C is related to the polymerization of SS-Limonene. The second stage, taking place in a nitrogen atmosphere at a temperature above 365.7 °C, is related to the cracking of PLA chains with the simultaneous endothermic distillation of mers, including SS-Limonene degradation products and lactides. According to the c-DTA curve determined in the air atmosphere, the endothermic distillation process overlaps with the exothermic oxidation process of the cracking products. In the last, third stage, in the air atmosphere, one more signal is observed at a temperature of 550–700 °C, which characterizes the process of burning coke, originating mainly from the organosilicon derivative. Stage 1 refers to the functional properties of the composite material, while stages 2 and 3 describe the irreversible processes of thermal decomposition of a mixture of molten PLA and an organosilicon derivative.

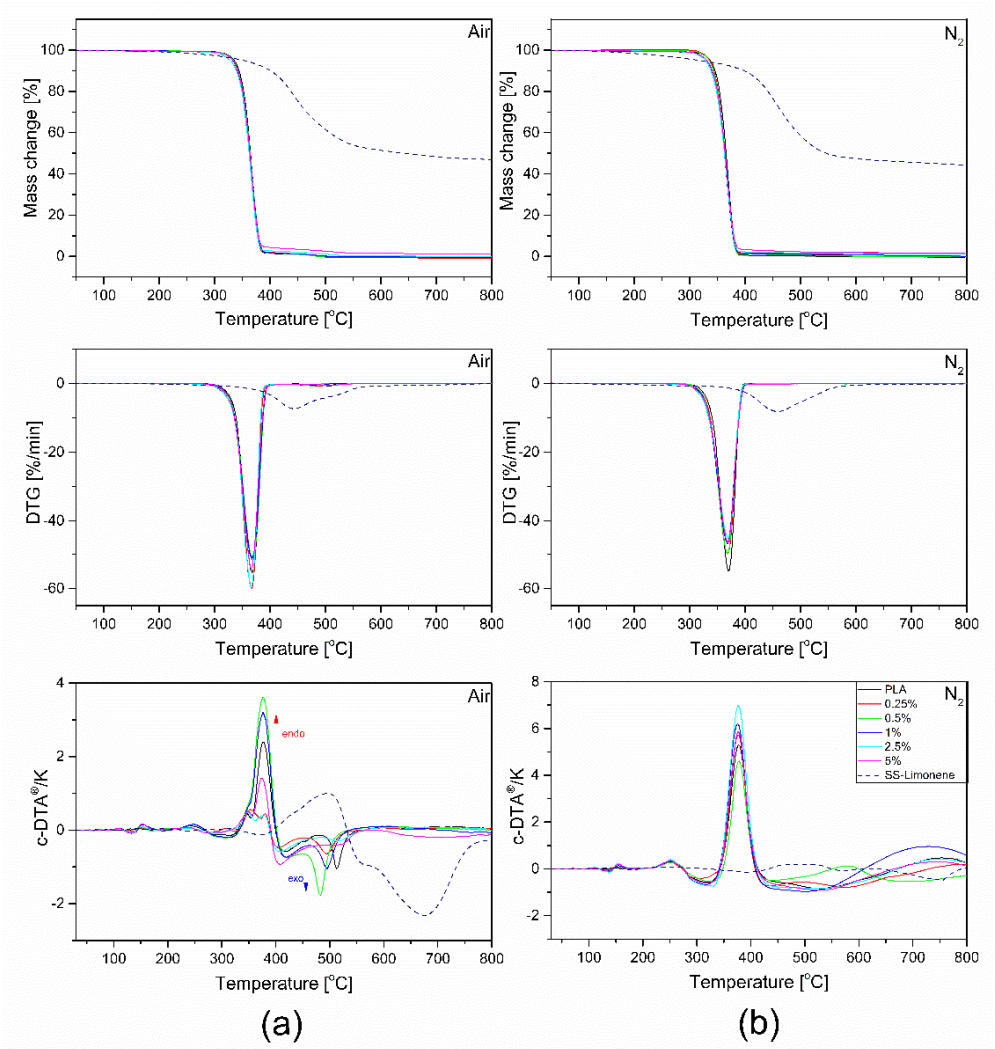

Figure 7. TGA, c-DTA and DTG curves of SS-Limonene/PLA composite in (**a**) air and (**b**) nitrogen atmosphere.

Table 2. Results of thermogravimetric analysis.

	1% Mass Loss [°C]		Onset Temperature [°C]		Temperature at the Maximum Rate of Mass Loss [°C]		Dry Mass Left [%]	
Conditions	**N_2**	**Air**	**N_2**	**Air**	**N_2**	**Air**	**N_2**	**Air**
SS-limonene	166.7	221.0	410.6	397.8	458.6	442.3	44.26	46.99
Neat PLA	304.8	307.9	351.1	348.3	370.1	367.0	0.00	0
PLA + 0.25% SS-Limonene	318.4	287.3	346.3	353.4	367.0	366.5	1.0	0
PLA + 0.5% SS-Limonene	316.3	308.2	348.3	346.1	368.9	366.8	0	0
PLA + 1% SS-Limonene	291.4	307.8	341.4	345.2	368.3	366.3	0.04	0
PLA + 2.5% SS-Limonene	294.9	287.9	342.4	348.5	368.4	365.5	1.03	0
PLA + 5% SS-Limonene	301.4	302.5	343.6	345.9	369.0	366.5	1.54	1.12

2.6. Contact Angle Measurements

The contact angle measurements were performed for SS-Limonene/PLA composites obtained by two different methods—FDM and injection moulding. For the measurements of 3D-printed samples, the samples were placed with the layer-by-layer deposition plane oriented parallelly to the plane of the goniometer stage. The contact angle of the neat PLA was 81.4° for the printed samples and 83.6° for the samples obtained in the injection process, in both cases the surface before modification showed hydrophilic properties. Modification of PLA with SS-Limonene increased the hydrophobicity of all the tested samples (see Table 3). For the printed samples, regardless of the modifier concentration, a hydrophobic surface effect was obtained (the value of the contact angle increased to above 90°). For the samples obtained by injection moulding, the increase in the value of the contact angle was insignificant and it remained at a similar level (max. by 4.3°). The difference in the degree of hydrophobicity of printed and injected samples is due to their surface structure and microstructure. 3D printing allows obtaining microstructures and surface roughness, which results in higher values of the contact angle. This thesis was confirmed by microscopic observations (see Section 2.4). On the other hand, injection moulding produces more smooth surfaces (if no modification of the mould surface is applied), which reduces the microstructure effect on the surface and therefore almost no effect of the organosilicon additive can be observed.

Table 3. Water contact angle [°].

	Injection Moulding [°]	3D Printing [°]
Neat PLA	83.6	81.4
PLA + 0.25% SS-Limonene	87.9	92.4
PLA + 0.5% SS-Limonene	87.8	95.4
PLA + 1% SS-Limonene	84.7	92.3
PLA + 2.5% SS-Limonene	85.7	95.1
PLA + 5% SS-Limonene	85.6	97.5

2.7. Mechanical Properties

2.7.1. Tensile Strength and Flexural Strength

Mechanical tests were carried out for the modified samples obtained by both 3D printing and traditional injection moulding. For the 3D-printed samples, the tensile load was applied parallelly to the plane of layer-by-layer deposition. The basic tensile strength values for neat PLA are 36.5 MPa for the samples obtained by the FDM method and 72.6 MPa for the samples obtained by the injection moulding (Figure 8). This difference is due to the technique of producing the dumbbells for tests. Lower values of mechanical parameters of printed samples are mainly related to low inter-layer adhesion between the extrudate strands and the presence of air gaps between the applied layers. In the caseof injection moulding, the materials are more solid with little to no structural defects. The addition

of the SS-Limonene modifier increased the tensile strength of the printed samples, which brought them closer to the injection moulded ones. The highest value was observed for PLA with the content of 0.25% of the modifier, this value decreased with increasing concentration. This is mainly due to the improved flow of the polymer as shown in the capillary rheometry analysis of the samples (Section 3.1), as well as improved inter-layer adhesion (Section 2.4), which resulted in increased material consistency and improved fusing of the print paths (extrudate strands). For all the tested samples, high values of standard deviation were obtained, which is a characteristic feature of FDM printed objects due to the mentioned structural inconsistencies.

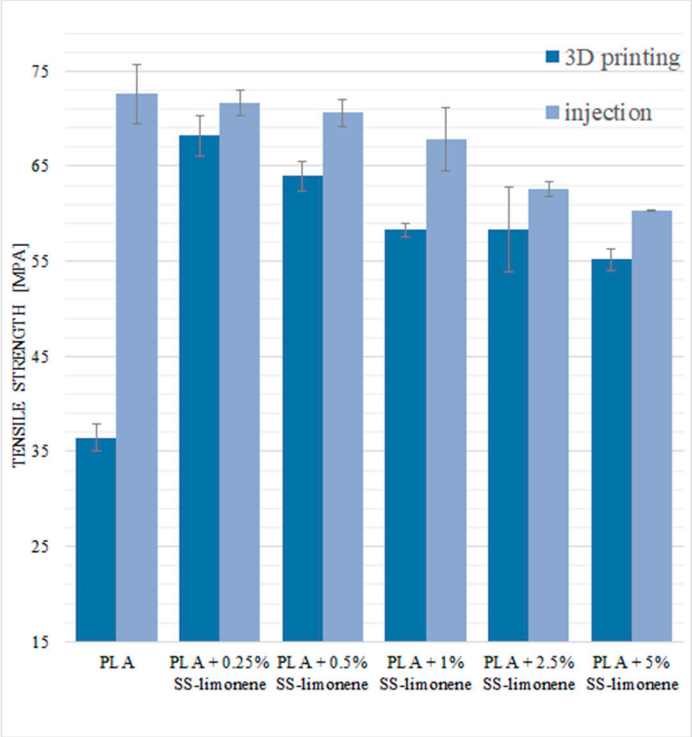

Figure 8. Tensile strength of SS-Limonene/PLA in 3D printing and injection moulding.

For the samples obtained by injection moulding, the tensile stress values are the highest for pure PLA and decrease with increasing loading of the modifier. This result can be explained by two reasons: one is the plasticizing effect of SS-Limonene, and the other is the presence of discontinuities in the polymer phase introduced together with the additive, that is the polymerized SS-Limonene agglomerates and additional air micropockets, as confirmed by the microscopy.

The elongation at maximum load for neat PLA samples obtained by 3D printing and injection moulding is characterized by similar values (2.43% and 2.29%, Figure 9). The addition of SS-Limonene to the samples obtained by the FDM method significantly improves the plasticity of the material. Higher elongation values in the case of modified samples indicate increased "mobility" of the polymer phase as a result of plasticization by SS-Limonene [35]. The plasticizer isolates the chains and spherulites of macromolecules, reducing the interaction between them. The highest value was obtained for PLA + 0.25% SS-Limonene, which was 4.21%. At higher loadings, the effect of the additive polymerization takes over and decreases the plasticizing effect. In the case of injection-moulded samples, the addition of the modifier gave negligible effects.

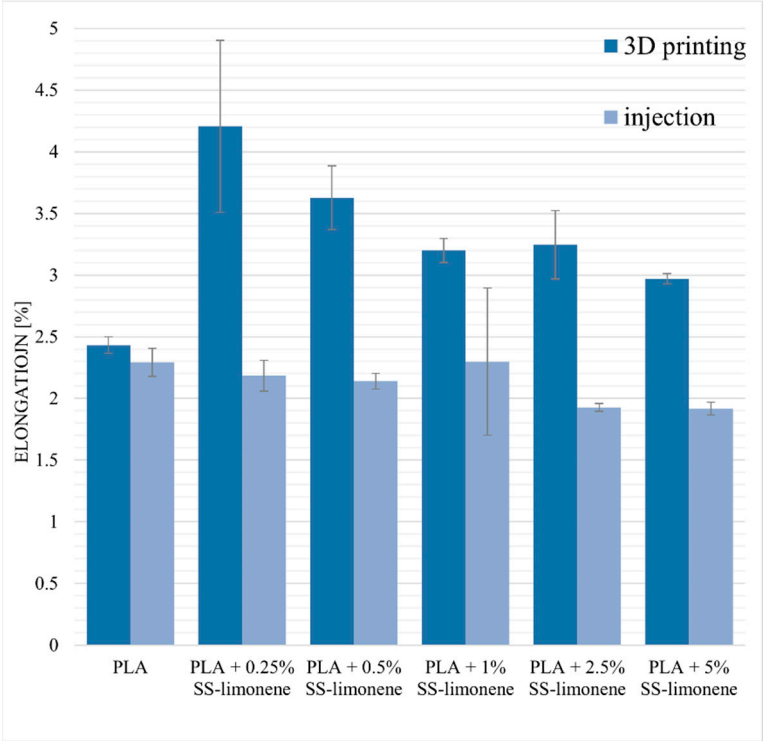

Figure 9. Elongation at maximum load of SS-Limonene/PLA in 3D printing and injection moulding.

2.7.2. Bending Tests

The basic flexural parameters of the samples were determined. For the 3D-printed samples, the bending load was applied perpendicularly to the plane of layer-by-layer deposition. The basic values of flexural strength for pure PLA are 77.98 MPa for the samples obtained by the FDM method and 99.98 MPa for the injection-moulded samples (Figure 10). The flexural strength is also significantly lower for the neat PLA obtained by 3D printing—this is due to the presence of air gaps and limited inter-layer adhesion, the structural discontinuities acting as stress concentration points.

In the case of the 3D printing technique, the addition of the SS-Limonene modifier significantly increased the value of the flexural strength. The samples obtained by printing with the modifier showed similar mechanical properties to those mould-injected. The highest values were obtained for the systems containing 0.25% and 0.5% of SS-Limonene (respectively 97.61 MPa; 98.46 MPa). Higher concentrations of the modifier caused a slight decrease in the strength values in relation to the 0.25% and 0.5% systems, but they were still higher than for the neat PLA samples.

The samples obtained by injection moulding technique were characterized by high values of flexural strength ranging from 88.46 MPa to 100.30 MPa (5% SS-Limonene/PLA and 1% SS-Limonene/PLA, respectively).

The values of flexural modulus for both types of samples were basically unchanged regardless of the additive loading (Figure 11).

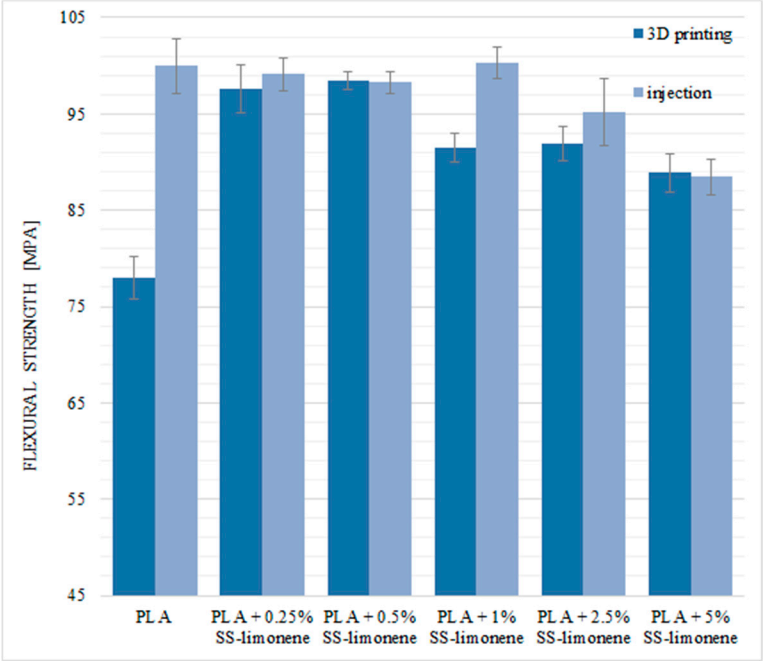

Figure 10. Flexural strength of SS-Limonene/PLA in 3D printing and injection moulding.

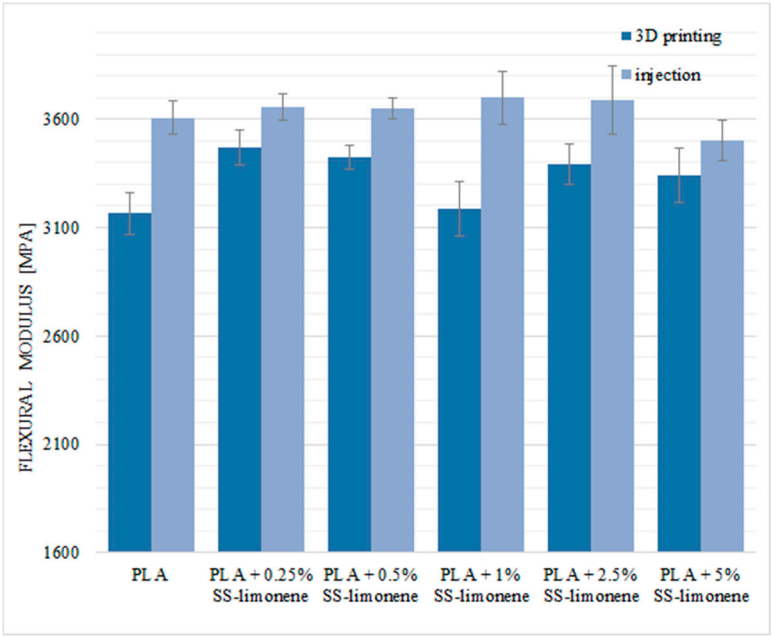

Figure 11. Flexural modulus of SS-Limonene/PLA in 3D printing and injection moulding.

2.7.3. Impact Strength and Hardness

Impact strength of the obtained composite samples was determined. For the 3D-printed samples, the impact direction was perpendicular to the plane of layer-by-layer deposition. Impact resistance tests confirmed the beneficial effect of SS-Limonene (especially at lower loadings) on the tested samples, regardless of the processing technique used (Figure 12). The modifier, as in the case of the previously discussed mechanical tests, acts as a plasticizer, the brittleness of the polymer is reduced therefore, the obtained composite is able to absorb more energy during an impact. High standard deviations are characteristic of the measurement method. The downward tendency along with the increase in the modifier content indicates a limited dispersion of the modifier in the polymer matrix and compatibility

of the system components. Hardness, in Shore D scale, was determined to be virtually unaffected by the additive and on the level of 82–84 for all the samples regardless of the SS-Limonene loading or the processing method.

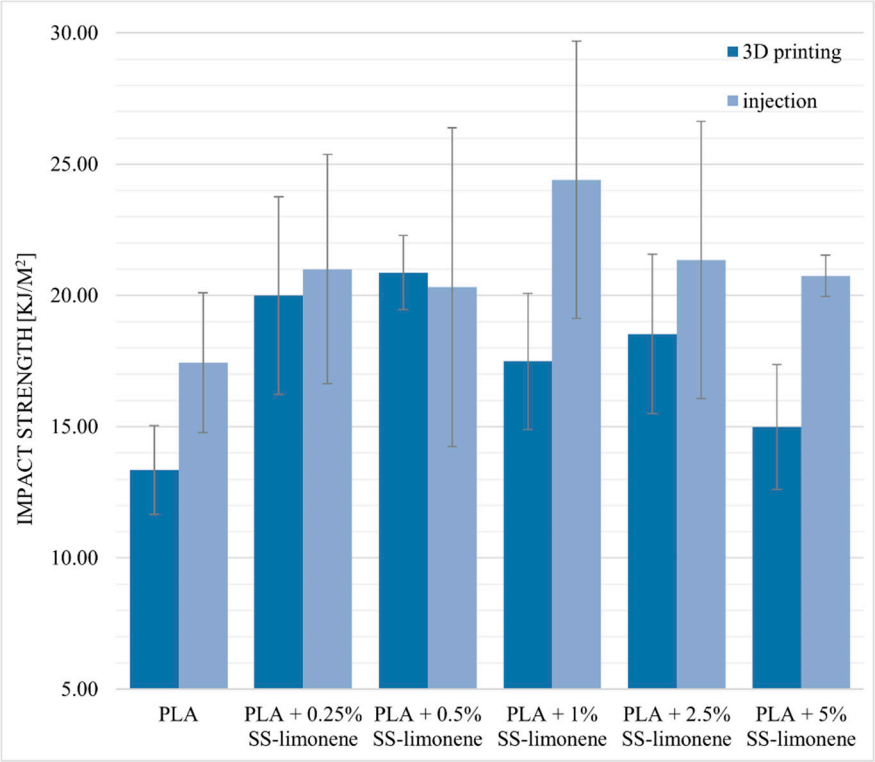

Figure 12. Impact strength of SS-Limonene/PLA in 3D printing and injection moulding.

3. Materials and Methods

3.1. Materials

Polylactide (PLA) type Ingeo 2003D was purchased from NatureWorks (Minnetonka, MN, USA). The chemicals were purchased from the following sources: Tetraethoxysilane (TEOS) from Unisil (Poland), chlorodimethylsilane, tetramethylammonium hydroxide (TMAH) 25% methanol solution from ABCR, (R)-(+)-limonene, toluene, chloroform-d, Karstedt's catalyst xylene solution from Aldrich, P_2O_5 from Avantor Performance Materials Poland S.A. Toluene was degassed and dried by distilling it from P_2O_5 under argon atmosphere.

3.2. Analyses

^{1}H, ^{13}C, and ^{29}Si Nuclear Magnetic Resonance (NMR) spectra were recorded at 25 °C on a Bruker Ascend 400 and Ultra Shield 300 spectrometers using $CDCl_3$ as a solvent. Chemical shifts are reported in ppm with reference to the residual solvent ($CHCl_3$) peaks for ^{1}H and ^{13}C.

MALDI-TOF mass spectra were recorded on a UltrafleXtreme mass spectrometer (Bruker Daltonics), equipped with a SmartBeam II laser (355 nm) in the 500–4000 *m*/*z* range. 2,5-Dihydroxybenzoic acid (DHB, Bruker Daltonics, Bremen, Germany) served as matrix. Mass spectra were measured in reflection mode. The data were analysed using the software provided with the Ultraflex instrument—FlexAnalysis (version 3.4).

Fourier Transform-Infrared (FT-IR) spectra were recorded on a Nicolet iS 50 Fourier transform spectrophotometer (Thermo Fisher Scientific) equipped with a diamond ATR unit with a resolution of 0.09 cm^{-1}.

Contact angle analyses were performed by the sessile drop technique at room temperature and atmospheric pressure, with a Krüss DSA100 goniometer (Hamburg, Germany). Three independent measurements were performed for each sample, each with a 5 μL water drop, and the obtained results were averaged to reduce the impact of surface nonuniformity.

Thermogravimetry (TG) was performed using a NETZSCH 209 F1 Libra gravimetric analyser (Selb, Germany). Samples of 5 ± 0.2 mg were cut from each granulate and placed in Al_2O_3 crucibles. Measurements were conducted under nitrogen (flow of 20 mL/min) in the range of 30–800 °C and a 20 °C/min heating rate. Differential scanning calorimetry (DSC) was performed using a NETZSCH 204 F1 Phoenix calorimeter Samples of 6 ± 0.2 mg were cut from each granulate and placed in an aluminium crucible with a punctured lid. The measurements were performed under nitrogen in the temperature range of −20–290 °C and at a 20 °C/min heating rate, and T_g was measured from the second heating cycle.

The effect of the modifier addition on the mass flow rate (MFR) was also determined. The measurements were made using a Instron plastometer (Norwood, MA, USA), model Ceast MF20 according to the applicable standard ISO 1133. The measurement temperature was 190 ± 0.5 °C, while the piston loading was 2.16 kg.

For flexural and tensile strength tests, the obtained materials were printed into type 1B dumbbell specimens in accordance with EN ISO 527:2012 and EN ISO 178:2006. Tests of the obtained specimens were performed on a universal testing machine INSTRON 5969 with a maximum load force of 50 kN. The traverse speed for tensile strength measurements was set at 2 mm/min, and for flexural strength was also set at 2 mm/min. Charpy impact test (with no notch) was performed on a Instron Ceast 9050 impact-machine according to ISO 179−1. For all the series, 6 measurements were performed.

Hardness of the composite samples was tested by the Shore method using a durometer Bareiss Prüfgerätebau GmbH.

A scanning electron microscope (SEM 3000, Hitachi, Japan) was used to analyse the microstructure and quality of the produced composite samples after 3D printing and injection moulding. Additionally, the effect of SS-Limonene addition on the microstructure of composite materials was investigated. Before the measurement, samples' cross-sections were coated with a thin layer of Au-Pd. The applied voltage for SEM observations was 15 kV.

Surface structure and breakthroughs were analysed under Digital Light Microscope Keyence VHX 7000 with 100× to 1000× VH-Z100T lens (Osaka, Japan). All of the pictures were recorded with a VHX 7020 camera.

3.3. The Procedure for Synthesis of Octaspherosilicate Limonene Derivative (SS-Limonene)

Octahydrospherosilicate was prepared according to a literature procedure [36]. The hydrosilylation reaction was performed accordingly to a previous report [31].

In a typical procedure, a 500 mL three-neck, round-bottom flask was charged with 25 g of Octahydrospherosilicate, 250 mL of toluene and 26.77 g of limonene, and a magnetic stirring bar was added. A thermometer and condenser equipped with an argon inlet and oil bubbler were attached, the flask placed in a heating mantle and the system was purged with argon. The reaction mixture was set on 110 °C and before reaching boiling, 25 μL of Karstedt's catalyst solution was added, which resulted in quick increase of temperature and the system starting to reflux. The reaction mixture was kept at reflux and samples were taken for FT-IR control until full Si-H group consumption was observed. Then, the solvent was evaporated under vacuum to dryness to obtain an analytically pure sample.

3.4. Fabrication of Filaments

3.4.1. Preparation of Granulates

The polymer and the filler were homogenized using a laboratory two-roll mill ZAMAK MERCATOR WG 150/280. A portion of 500 g PLA Ingeo™ 2003 D was mixed with SS-Limonene, until the final concentration of the additive of 5.0% *w*/*w*. The mixing was performed at the rolls temperature of 200 °C for 15 min., getting to full homogeneity of the concentrates. Masterbatch was granulated by a grinding mill WANNER C17.26 sv. The granulates were diluted with pure PLA up to the final filler concentrations of 0.25, 0.5, 1.0, 2.5 and 5.0% *w*/*w* upon extrusion moulding of a stream with consequent cold granulation on the twin-screw extrusion setup line HAAKE Rheomex OS, and then dried for 24 h at 40 °C.

3.4.2. Extrusion of Filaments

The granulates obtained as above were used for moulding of filaments of 1.75 mm in diameter by a single-screw extrusion setup HAAKE Rheomex OS.

3.4.3. 3D Printing (FDM)

Using a 3D printer FlashForge Finder two types of samples were printed by FDM: oars and bars, according to PN-EN-ISO 527-2. Parameters of printing are given in Table 4.

Table 4. Process parameters for sample printing.

Layer height	0.18 mm
Top layer height	0.27 mm
Shells	2
Top and bottom layers number	3
Bottom layers number	3
Infill density	100%
Infill pattern	Grid
Printing speed	60 mm/s
Idle speed	80 mm/s
Extruder temp.	220 °C

3.5. Injection Moulding

To compare the mechanical properties of composite materials made by 3D printing, the samples were produced by the injection moulding method. Specimens for static tensile, three-point bending, and impact tests were in accordance with the dimensions of the following standards: PN-EN ISO 527, PN-EN ISO 178, and PN-EN ISO 179, respectively. HAAKE Minijet Pro Piston Injection Moulding System (ThermoScientific, Bremen, Germany) equipped with a set of moulds was used to produce test samples. Parameters of the injection process are presented in Table 5

Table 5. Injection process parameters.

Cylinder temperature	225 °C
Mould temperature	45 °C
Injection pressure	750 bar
Injection time	10 s
Post-injection pressure	700 bar
Post-injection time	10 s

4. Conclusions

The obtained results confirm the effect of the addition of SS-Limonene on the improvement of rheological and mechanical properties of printed composites based on the PLA matrix. It is especially

important for the FDM-based method for objects manufacturing, as usually objects prepared by such show much lower parameters than their injection-moulded counterparts, which can be explained by poor inter-layer adhesion and the presence of air gaps. On the basis of the obtained data, it can be concluded that the addition of a functionalized spherosilicate significantly improves such parameters as tensile strength, bending strength and impact strength of the samples obtained by 3D printing. SS-Limonene acted as a plasticizing additive for PLA. Additionally, the presence of SS-Limonene was found to increase hydrophobicity of the obtained composites. The addition of this modifier also facilitates the printing process itself, contributes to the improvement of rheological properties (reduces viscosity, increases MFR) and reduces production waste. It should be noted that in the conditions of processing the additive was found to undergo polymerization, leading to its secondary agglomeration observed under the microscope on increasing loading. It seems that the nature of the observed phenomena is complex, and the additive most likely exists in the system in two forms, namely a well-dispersed one and the agglomerated one, as suggested by previous research and the analysis of thermal data. The behaviour of the obtained composites is based on two types of interactions—between PLA and well-dispersed phase, as well as between PLA and the polymerized, agglomerated phase. Nevertheless, this complex interaction scheme should not be considered undesirable as it leads to a final improvement of the printing material system.

Author Contributions: Conceptualization, R.E.P.; Data curation, D.B. and B.S.; Formal analysis, M.F., D.P., and K.D.; Funding acquisition, D.B., B.S., and B.M.; Investigation, D.B. and B.S.; Methodology, B.S. and R.E.P.; Project administration, B.S.; Resources, D.B. and B.S.; Software, M.F., D.P., and K.D.; Supervision, B.M. and R.P.; Validation, R.K. and R.E.P.; Visualization, M.F., D.P., and K.D.; Writing—original draft, D.B., B.S., and R.E.P.; Writing—review & editing, R.K., A.B., and B.M. All authors have read and agreed to the published version of the manuscript.

Funding: This research was funded by the National Centre for Research and Development, Poland, grant number LIDER/01/0001/L-10/18/NCBR/2019, and the National Science Centre, Poland, grant number UMO-2018/29/N/ST5/00868.

Conflicts of Interest: The authors declare no conflict of interest.

References

1. Gibson, I.; Rosen, D.W.; Stucker, B. *Additive Manufacturing Technologies*; Springer: Berlin/Heidelberg, Germany, 2010; pp. 299–332.
2. Fawcett, S.E.; Waller, M.A. Supply chain game changers—Mega, nano, and virtual trends—And forces that impede supply chain design (i.e.; building a winning team). *J. Bus. Logist.* **2014**, *35*, 157–164. [CrossRef]
3. LeHong, H.; Fenn, J. Hype Cycle for Emerging Technologies. 2012. Available online: https://www.gartner.com/en/documents/2100915/hype-cycle-for-emerging-technologies-2012 (accessed on 26 July 2019).
4. Basiliere, P.; Shandler, M. Hype Cycle for 3D Printing. 2015. Available online: https://www.gartner.com/en/documents/3100228/hype-cycle-for-3d-printing-2015 (accessed on 26 July 2019).
5. Varghese, G.; Moral, M.; Castro-García, M.; López-López, J.J.; Marín-Rueda, J.R.; Yagüe-Alcaraz, V.; Hernandez-Afonso, L.; Ruiz-Morales, J.C.; Canales-Vázquez, J. Fabrication and characterisation of ceramics via low-cost DLP 3D printing. *Boletín de la Soc. Española de Cerámica y Vidr.* **2018**, *57*, 9–18. [CrossRef]
6. Schmidleithner, C.; Kalaskar, D.M. Stereolithography. In *3D Printing*; Cvetković, D., Ed.; IntechOpen: Hamilton, NJ, USA, 2018; pp. 1–22.
7. Ma, X.L. Research on Application of SLA Technology in the 3D Printing Technology. *Appl. Mech. Mater.* **2013**, *401*, 938–941. [CrossRef]
8. Fina, F.; Goyanes, A.; Gaisford, S.; Basit, A.W. Selective laser sintering (SLS) 3D printing of medicines. *Int. J. Pharm.* **2017**, *529*, 285–293. [CrossRef]
9. Liu, Z.; Wang, Y.; Wu, B.; Cui, C.; Guo, Y.; Yan, C. A critical review of fused deposition modeling 3D printing technology in manufacturing polylactic acid parts. *Int. J. Adv. Manuf. Technol.* **2019**, *102*, 2877–2889. [CrossRef]
10. Kalmanovich, G. "Curved-Layer" Laminated Object Manufacturing. Available online: https://repositories.lib.utexas.edu/handle/2152/70244 (accessed on 22 October 2020).

11. Grimm, T. *Fused Deposition Modeling: A Technology Evaluation*; T.A. Grimm & Associates Inc.: Atlanta, GA, USA, 2002.
12. Rayna, T.; Striukova, L. From rapid prototyping to home fabrication: How 3D printing is changing business model innovation. *Technol. Forecast. Soc. Chang.* **2016**, *102*, 214–224. [CrossRef]
13. A Third Industrial Revolution. Available online: https://www.economist.com/special-report/2012/04/21/a-third-industrial-revolution (accessed on 22 October 2020).
14. Sood, A.K.; Ohdar, R.K.; Mahapatra, S.S. Parametric appraisal of mechanical property of fused deposition modelling processed parts. *Mater. Des.* **2010**, *31*, 287–295. [CrossRef]
15. Wang, L.; Gardner, D.J. Contribution of printing parameters to the interfacial strength of polylactic acid (PLA) in material extrusion additive manufacturing. *Prog. Addit. Manuf.* **2018**, *3*, 165–171. [CrossRef]
16. Franchetti, M.; Kress, C. An economic analysis comparing the cost feasibility of replacing injection molding processes with emerging additive manufacturing techniques. *Int. J. Adv. Manuf. Technol.* **2017**, *88*, 2573–2579. [CrossRef]
17. Ngo, T.; Kashani, A.; Imbalzano, G.; Nguyen, K.; Hui, D. Additive manufacturing (3D printing): A review of materials, methods, applications and challenges. *Compos. Part B Eng.* **2018**, *143*, 172–196. [CrossRef]
18. Bai, J.; Goodridge, R.D.; Hague, R.J.M.; Okamoto, M. Processing and characterization of a polylactic acid/nanoclay composite for laser sintering. *Polym. Compos.* **2015**, *38*, 2570–2576. [CrossRef]
19. Mochizuki, M. Textile applications. In *Poly (Lactic Acid) Synthesis, Structures, Properties, Processing, and Applications*, 1st ed.; Auras, R.A., Lim, L.T., Selke, S.E., Tsuji, H., Eds.; John Wiley & Sons: Hoboken, NJ, USA, 2010; Volume 10, pp. 469–476. ISBN 978-0-470-29366-9.
20. Mardis, J.N. Emerging Technology and Applications of 3D Printing in the Medical Field. *Mo. Med.* **2018**, *115*, 368–373. [PubMed]
21. King, D.L.; Babasola, A.; Rozario, J.; Pearce, J.M. Mobile Open-Source Solar-Powered 3-D Printers for Distributed Manufacturing in Off-Grid Communities. *Chall. Sustain.* **2014**, *2*, 18–27. [CrossRef]
22. Rasal, R.M.; Hirt, D.E. Toughness decrease of PLA-PHBHHx blend films upon surface-confined photopolymerization. *J. Biomed. Mater. Res. A* **2019**, *88A*, 1079–1086. [CrossRef]
23. Liu, Z.; Lei, Q.; Xing, S. Mechanical characteristics of wood, ceramic, metal and carbon fiber-based PLA composites fabricated by FDM. *Environ. Sci. Technol.* **2019**, *53*, 1527–1535. [CrossRef]
24. Miranda, R.; Bustos-Martinez, D.; Blanco, C.S.; Villarreal, M.H.G.; Rodriguez, M.E.; Cantu, J. Pyrolysis of sweet orange (Citrus sinensis) dry peel. *Anal. Appl. Pyrolysis* **2009**, *86*, 245. [CrossRef]
25. Chae, M.P.; Rozen, W.M.; McMenamin, P.G.; Findlay, M.W.; Spychal, R.T.; Hunter-Smith, D.J. Emerging applications of bedside 3D printing in plastic surgery. *Front. Surg.* **2015**, *2*, 25. [CrossRef]
26. Drozdov, F.V.; Cherkaev, G.V.; Muzafarov, A.M. Synthesis of new functional siloxane derivatives of limonene. Part I: Combination of hydrosilylation and hydrothiolation reactions. *J. Organomet. Chem.* **2019**, *880*, 293–299. [CrossRef]
27. Arrieta, M.P.; López, J.; Ferrándiz, S.; Peltzer, M.A. Characterization of PLA-limonene blends for food packaging applications. *Polym. Test.* **2013**, *32*, 760–768. [CrossRef]
28. Cordes, D.B.; Lickiss, P.D.; Rataboul, F. Recent Developments in the Chemistry of Cubic Polyhedral Oligosilsesquioxanes. *Chem. Rev.* **2010**, *110*, 2081–2173. [CrossRef]
29. Liu, H.; Kondo, S.; Takeda, N.; Unno, M. Synthesis of Octacarboxy Spherosilicate. *J. Am. Chem. Soc.* **2008**, *130*, 10074–10075. [CrossRef] [PubMed]
30. Brząkalski, D.; Przekop, R.E.; Sztorch, B.; Jakubowska, P.; Jałbrzykowski, M.; Marciniec, B. Silsesquioxane Derivatives as Functional Additives for Preparation of Polyethylene-Based Composites: A Case of Trisilanol Melt-Condensation. *Polymers* **2020**, *12*, 2269. [CrossRef] [PubMed]
31. Brząkalski, D.; Przekop, R.; Dobrosielska, M.; Sztorch, B.; Marciniak, P.; Marciniec, B. Highly bulky spherosilicates as functional additives for polyethylene processing—Influence on mechanical and thermal properties. *Polym. Compos.* **2020**, *41*, 3389–3402. [CrossRef]
32. Romo-Uribe, A.; Lichtenhan, J.D. Melt extrusion and blow molding parts-per-million POSS interspersed the macromolecular network and simultaneously enhanced thermomechanical and barrier properties of polyolefin films. *Polym. Eng. Sci.* **2020**. [CrossRef]
33. Romo-Uribe, A.; Lichtenhan, J.D. Polyhedral Oligomeric Silsesquioxane Induced Thermomechanical Reinforcement in Polymer Films Using Only Parts-per-Million Content. *Macromol. Mater. Eng.* **2020**, *305*, 2000354. [CrossRef]

34. Romo-Uribe, A.; Lichtenhan, J.; Reyes-Mayer, A.; Calixto-Rodriguez, M.; Sarmiento-Bustos, E.; Yañez-Lino, M. Parts-per-million polyhedral oligomeric silsesquioxane loading induced mechanical reinforcement in polyethylene nanocomposites. When small and well-dispersed yields big. *Polym. Adv. Technol.* **2020**, *31*, 2453–2465. [CrossRef]
35. Fortunati, E.; Luzi, F.; Puglia, D.; Dominici, F.; Santulli, C.; Kenny, J.M.; Torre, L. Investigation of thermo-mechanical, chemical and degradative properties of PLA-limonene films reinforced with cellulose nanocrystals extracted from Phormium tenax leaves. *Eur. Polym. J.* **2014**, *56*, 77–91. [CrossRef]
36. Filho, N.L.D.; De Aquino, H.A.; Pires, G.; Caetano, L. Relationship between the Dielectric and Mechanical Properties and the Ratio of Epoxy Resin to Hardener of the Hybrid Thermosetting Polymers. *J. Braz. Chem. Soc.* **2006**, *17*, 533–541. [CrossRef]

Sample Availability: Samples of the compounds are available from the authors.

Publisher's Note: MDPI stays neutral with regard to jurisdictional claims in published maps and institutional affiliations.

polymers

MDPI

Article

Why POSS-Type Compounds Should Be Considered Nanomodifiers, Not Nanofillers—A Polypropylene Blends Case Study

Dariusz Brząkalski [1], Robert E. Przekop [2,*], Bogna Sztorch [2], Miłosz Frydrych [1], Daria Pakuła [1], Marek Jałbrzykowski [3], Grzegorz Markiewicz [3] and Bogdan Marciniec [1,2,*]

[1] Faculty of Chemistry, Adam Mickiewicz University in Poznan, 61-614 Poznan, Poland; dariusz.brzakalski@amu.edu.pl (D.B.); frydrych@amu.edu.pl (M.F.); darpak@amu.edu.pl (D.P.)
[2] Centre for Advanced Technologies, Adam Mickiewicz University in Poznan, 61-614 Poznan, Poland; bogna.sztorch@amu.edu.pl
[3] Faculty of Mechanical Engineering, Bialystok University of Technology, Wiejska 45 C, 15-351 Bialystok, Poland; m.jalbrzykowski@pb.edu.pl (M.J.); g.markiewicz@doktoranci.pb.edu.pl (G.M.)
* Correspondence: rprzekop@amu.edu.pl or r.przekop@gmail.com (R.E.P.); bogdan.marciniec@amu.edu.pl (B.M.)

Abstract: In this work, a series of silsesquioxanes (SSQ) and spherosilicates (SS), comprising a group of cage siloxane (CS) compounds, was tested as functional additives for preparation of isotactic polypropylene (iPP)-based nanocomposites and discussed in the aspect of their rationale of applicability as such additives. For this purpose, the compounds were prepared by condensation and olefin hydrosilylation reactions. The effect of these cage siloxane products on properties of obtained CS/iPP nanocomposites was analyzed by means of mechanical, microscopic (scanning electron microscopy-energy dispersive spectroscopy), thermal (differential scanning calorimetry, thermogravimetry), thermomechanical (Vicat softening point) analyses. The results were compared with the previous findings on CS/polyolefin composites. The role of CS compounds was discussed in terms of plastic processing additives.

Keywords: nanomodifiers; additives; composites; polypropylene (PP); processing; thermal properties; low concentration; POSS; silsesquioxanes; spherosilicates

Citation: Brząkalski, D.; Przekop, R.E.; Sztorch, B.; Frydrych, M.; Pakuła, D.; Jałbrzykowski, M.; Markiewicz, G.; Marciniec, B. Why POSS-Type Compounds Should Be Considered Nanomodifiers, Not Nanofillers—A Polypropylene Blends Case Study. *Polymers* **2021**, *13*, 2124. https://doi.org/10.3390/polym13132124

Academic Editor: Markus Gahleitner

Received: 27 May 2021
Accepted: 24 June 2021
Published: 28 June 2021

1. Introduction

In the study of polymer systems with practical application, the cognitive value of the conducted research should be seen on par with the rationality of their use in the light of the final effect. Compounds of the CS type, commonly known under their trade name POSS® (Polyhedral Oligomeric Silsesquioxanes, trademark registered by Hybrid Plastics Inc.), due to the specificity of their structure and methods of obtaining, are not the cheapest modifiers. Their market price ranges from 200 to 3000 USD per 1 kg [1]. Their price is also strongly correlated with the price of simple organosilicon compounds—organofunctional silanes commonly used as adhesion promoters in polymer composite systems [2]. Bearing in mind the above, we would like to discuss the areas in which these compounds can really be modifiers compared to known and existing solutions. Simple and cheap materials such as polyolefins (polyethylene, polypropylene) are very well-studied systems for which changes in mechanical or thermal parameters, and then in processing properties, may be caused by many fillers or modifiers [3,4].

So why try to use POSS compounds as a modifier of the properties of such materials? The study attempts to find convincing thermal and mechanical effects of polypropylene modified with a number of structurally diverse POSS compounds in the low concentration range (0.1–1% *w*/*w*). A very important problem in the use of POSS compounds is their solubility/dispersal under processing conditions (polymer melt); many of the POSS compounds

do not show a sharp melting point, and their basic phase transformation is sublimation at temperatures above 250 °C [5,6]. Such POSS compounds under processing conditions will have considerable difficulty in dispersing in the polymer matrix due to their crystalline form and low solubility/non-fusibility. Therefore, their use will be limited by the concentration limit, above which the role of the nanomodifier will be reduced due to formation of polycrystalline agglomerates, similarly to inorganic nanofillers. An important critical statement was made by Herbert et al. that many studies including silsesquioxane-based composites were concerned around high concentrations of the organosilicon additives used (even exceeding 10% *w*/*w*), while these compounds should be tested at loadings within the limits of their effective dispersion and compatibility with the polymer [7]. From a different point of view, more and more often, the term 'nanofillers' is used in the literature in regard to POSS compounds. According to the definition, fillers are added to plastics to reduce their cost per unit volume and/or to improve such mechanical properties as hardness or Young's/flexural modulus of a given material. Further speaking, a filler may be 'a relatively non-adhesive substance added to an adhesive to improve its working properties, permanence, strength, and other qualities; any compounding ingredient, usually in dry, powder form, added to rubber in substantial amount to improve quality of lower cost' [8]. According to this definition, fillers include china clay, wood flour, silica, silicates, carbon black, fibrous materials, or aluminum powder that markedly enhance the performance of a polymer, and their cost is reasonably low, either lower than that of the neat polymer or close to it. It should be noted that there is a clear difference between additives that cause changes in the material (fillers) and additives that affect the processing properties of the material (modifiers). On the basis of the conducted research, we suggest that in the case of polyolefin systems and other polymer systems in which no unequivocal effects such as permanence, strength, or cost reduction occurred, the term nanofiller in relation to compounds of the POSS type should not be used.

In recent years, there has been a growing interest in the use of polyhedral oligomeric silsesquioxanes (SSQ) or mono- or octa-functional spherosilicates (SS) as modifiers of properties of various classes of materials, especially of organic polymer origin. Silsesquioxanes and their derivatives, which are hybrid compounds of inorganic–organic structure (inorganic core and organic functional groups connected with silicon atoms at the corners of the core) [9] have been introduced into the polymer matrix by several means. The reported methods include reactive processes (copolymerization reaction, chemical grafting, reactive extrusion, irradiation) or traditional processing methods common for thermoplastics, such as injection molding, extrusion, and calendaring [10–12]. Such modification enables the improvement of the physicochemical, rheological, and/or mechanical properties of the resulting (nano)composite, allowing for targeting of a given product to a specific area of (potential) application. The most important feature of silsesquioxanes and spherosilicates is the wide possibility of their functionalization by introducing functional side groups responsible for giving the materials specific properties and allowing the modifier to chemically interact with the polymer matrix, as well as tailoring the physicochemical character of a cage siloxane itself. The use of silsesquioxane or spherosilicate derivatives as modifiers of composite materials can significantly change the properties of the material, e.g., increased corrosion resistance [13], improvement of mechanical properties [14], crystallization behavior [15], surface properties (hydrophilic–hydrophobic character) [16,17], thermal stability [18], flame resistance [19–21], or processability, mainly melt rheology [22]. They may also be used as antioxidants [23] or nanoparticle dispersants for plastics [24,25]. Cage siloxanes have been studied as functional and processing additives for polyolefins, e.g., polyethylene or polypropylene [26], as well as other thermoplastics, including PES [27], PPS [28], PEO [29], or different grades of polyamide (PA) [30]. The effect of these additives on the properties of the base polymer is highly dependent on the level of dispersion of the additive within the polymer matrix and the CS–matrix interactions (either macroscopic or molecular level ones). For this reason, it should be distinguished if the introduction of a given additive to the base polymer results in formation of a composite or a nanocomposite. In our earlier

works, we presented the influence of silsesquioxane- and spherosilicate-based additives on the properties of polyethylene- [31,32] and PLA-based [33] composites. For polypropylene, silsesquioxane-doped composites thereof were studied towards their crystallization behavior, mechanical properties, processing rheology, and thermal stability [34]. Fu presented the crystallization behavior of silsesquioxane-doped PP under different conditions, including shear-induced process [35]. Fina et al. described the influence of octamethyl-, octaisobutyl- and octaisooctyl-SSQs on the thermal and morphological characteristics of the prepared composites [36]. Kamyab et al. applied glycidoxypropylhepta(*iso*butyl)silsesquioxane as a compatibilizer for PCL/PP blends characterized by shape memory properties [37]. Zaharescu et al. reported improved gamma radiation resistance of PP modified with a series of functionalized hepta(*iso*butyl)silsesquioxanes [38]. Zhang et al. presented a synergistic effect of octamethylsilsesquioxane as a support for NA-40 nucleating agent [39]. Polypropylene, due to its satisfactory mechanical strength, moderate hardness and acceptable impact resistance, hydrophobic properties, as well as very good chemical resistance against several agents (including salt solutions, strong non-oxidizing acids, bases, alcohols, fats, oils, esters, ketones) and low production costs, is one of the thermoplastics of high industrial importance [40]. A particularly important feature from the point of view of designing new or improved materials is the ease of processability, either in the injection molding process, or different variants of extrusion process, including extrusion blow molding or blown film/fiber production. Currently, PP, due to its properties, is used as an alternative to materials based on metal, glass, or natural materials such as wood, which allows it to be used in many industries, including transport, construction, electronics, medicine, and the packaging market [41–46]. Despite good physicochemical properties, when compared to numerous other plastics, it has lower Young's modulus, hardness, or softening temperature, which introduces significant limitations in the applications for this material [47]. Therefore, the process of PP modification arouses more and more interest in both the scientific and industrial areas [48].

In this work, the effect of cage siloxanes with different functional groups (including vinyl, alkyl, chloroalkyl, oxirane) as functional additives to iPP is described, including the compatibility of modifiers with the polymer matrix. In order to obtain homogeneous batches, the modifiers were incorporated into the polymer matrix by a melt blending process. The obtained (nano)composites were tested in terms of thermal stability; mechanical properties, rheological properties, and phase transformations (melting and crystallization points) were also determined.

2. Materials and Methods

2.1. Materials

Isotactic polypropylene (iPP), Moplen HP456J grade, was purchased from BaselOrlen Polyolefins (Poland). The chemicals were purchased from the following sources: Tetraethoxysilane (TEOS), chlorodimethylsilane, chlorodimethylvinylsilane, isobutyltrimethoxysilane, tetramethylammonium hydroxide (TMAH) 25% methanol solution from ABCR, (R)-(+)-limonene, allyl-glycidyl ether, toluene, chloroform-d, Karstedt's catalyst xylene solution from Aldrich, P_2O_5 from Avantor Performance Materials Poland S.A. (Gliwice, Poland). Toluene was degassed and dried by distilling it from P_2O_5 under argon atmosphere. Silsesquioxane and spherosilicate compounds were prepared according to literature reports provided in Table 1.

Table 1. Silsesquioxane and spherosilicate derivatives used in this study.

Name	Abbreviation	Literature Report
Octahydrospherosilicate	SS-H	[49]
Octavinylspherosilicate	SS-Vi	[49] (prepared analogically to SS-H)
Octaglycidylspherosilicate	SS-Glycidyl	[50]
Octalimonenespherosilicate	SS-Limonene	[31]
hepta(*iso*butyl)trisilanol silsesquioxane	*i*Bu$_7$SSQ-3OH	[51]
chloropropylhepta(*iso*butyl)silsesquioxane	*i*Bu$_7$SSQ-Cl	[52]
Monovinylhepta(*iso*butyl)spherosilicate	*i*Bu$_7$SS-Vi	[53]
Monohydrohepta(*iso*butyl)spherosilicate	*i*Bu$_7$SS-H	[54]

2.2. Analyses

^{1}H, ^{13}C, and ^{29}Si nuclear magnetic resonance (NMR) spectra were recorded at 25 °C on a Bruker Ascend 400 and Ultra Shield 300 spectrometers using $CDCl_3$ as a solvent. Chemical shifts are reported in ppm with reference to the residual solvent ($CHCl_3$) peak for ^{1}H and ^{13}C. Fourier transform-infrared (FT-IR) spectra were recorded on a Nicolet iS50 Fourier transform spectrophotometer (Thermo Fisher Scientific, Waltham, MA, USA) equipped with a diamond ATR unit with a resolution of 0.09 cm^{-1}. Thermogravimetry (TG) was performed using a NETZSCH 209 F1 Libra gravimetric analyzer. Samples of 5 ± 0.2 mg were placed in Al_2O_3 crucibles. Measurements were conducted under air atmosphere (flow of 20 mL/min) in the range of 30 ÷ 800 °C and a 10 °C/min heating rate. Differential scanning calorimetry (DSC) was performed using a NETZSCH 204 F1 Phoenix calorimeter. Samples of 6 ± 0.2 mg were placed in an aluminum crucible with a punctured lid. The measurements were performed under nitrogen in the temperature range of −30 ÷ 200 °C and at a 5 °C/min heating rate, and T_m was measured from the second heating cycle. SEM/EDS analyses were recorded on a Quanta FEG 250 (FEI) instrument; SEM at 5 kV and EDS at 30 kV, respectively. The samples were frozen in liquid nitrogen and fractured with pliers to reveal a surface satisfactory for an analysis. The samples were taken from the extrudate obtained during preparation of the desired final concentration composites (see Section 2.3). For flexural and tensile strength tests, the obtained materials were printed into type 1B dumbbell specimens in accordance with EN ISO 527:2012 and EN ISO 178:2006. Tests of the obtained specimens were performed on a universal testing machine INSTRON 5969 with a maximum load force of 50 kN. The traverse speed was set at 50 mm/min for tensile strength measurements, at 1 mm/min for the determination of Young's modulus, and at 1 mm/min for flexural strength. For all the series, six measurements were performed. For tribological tests, samples in the shape of mandrels of φ6 × 20 mm dimensions were used. A dial made of 316LV steel was used as a counter-sample. The tests were performed using a pin on a disc tribological tester. The tests were carried out with a unit pressure p = 2 MPa, sliding speed v = 0.25 m/s, and a friction time t = 30 min. The signal was recorded with a Hottinger bridge (Hottinger Baldwin Messtechnik) and processed in QuantumX + CatmanEasy software. The obtained data were processed using the Statistica 13 PL program. Each measurement was repeated three times. Each test was performed on a fresh disc surface (by changing the friction radius) with its initial roughness Ra = 0.3 µm. Due to the variable friction radius, the rotational speed of the disc was controlled so as to obtain the same linear speed v and the same friction path L in each test cycle. Vicat measurements were performed in accordance with ISO 306, B50 method (50 N load, 50 °C/h heating rate). Tests were performed on an Instron CEAST HV3 Vicat tester.

2.3. Preparation of (Nano)Composites

In a typical procedure, about 200 g of iPP was rolled on a two-roll mill until complete melt, after which the chosen modifier was added in a quantity corresponding to 5% of the final masterbatch content, and the composition was rolled together at 190 °C until it became completely homogeneous or until no more improvement of homogeneity was observed.

After that, the composition was taken off the rolls and set to cool down. It was ground in the low-speed mill and the obtained masterbatch granulate was then diluted to 1% by mixing it with the granulate of neat iPP and extruding it on a single-screw extruder at 30 RPM, the extrudate being simultaneously granulated. Temperature zones for extrusion were as follows (from feed to die): 80 °C, 180 °C, 190 °C, 170 °C. Subsequently, 0.1%, 0.25%, and 0.5% concentration composites were obtained by diluting 1% granulate with neat iPP in a proper proportion in a similar fashion. The obtained granulates were then measured by TG, DSC, and SEM-EDS techniques and processed into standard dumbbell specimens by injection molding. For tribological tests, samples were injection molded as mandrels with dimensions of φ6 × 20 mm. For injection molding, the following parameters were applied: temperature zones of the plastifying unit (from feed to die): 190 °C, 200 °C, 190 °C, 180 °C, injection pressure 50 bar, holding pressure 55 bar, holding time 10 s, cooling time 18 s. The parameters of the injection process were developed based on the visual quality of the molded parts and were kept the same for all injection tests.

3. Results and Discussion

3.1. Characterization of the Obtained Modifiers

In Table 1, a series of silsesquioxane and spherosilicate compounds obtained according to the literature procedures and used to prepare iPP-based nanocomposites are collected. SS-H was applied only to prepare SS-Glycidyl and SS-Limonene. The synthesis of the used modifiers was reported elsewhere, which is given in the Table 1. Figure 1 presents their structures together with the compound codes used throughout the whole manuscript.

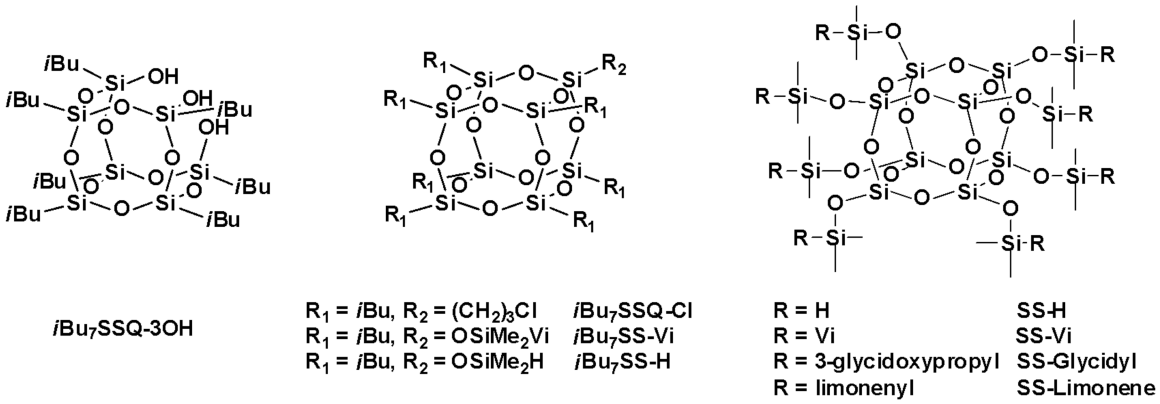

Figure 1. Structures of the cage siloxane compounds studied in this work.

The silsesquioxane and spherosilicate compounds were investigated by ^{1}H, ^{13}C, and ^{29}Si NMR and FT-IR spectroscopy to prove their purity and structure and completion of hydrosilylation reactions (~99% for all examples, see Supplementary Information).

3.2. SEM and EDS Imaging

Scanning electron microscopy combined with energy dispersive spectroscopy was applied to analyze the dispersion/phase separation of the CS additives within the polymer matrix and compatibility of the components. EDS allowed for confirmation of the chemical structure of the observed agglomerates/particles to be of organosilicon origin, as well as detection of agglomerates under the polymer surface. In the study of organosilicon-modified polymer systems, microscopic analysis coupled with X-ray spectroscopy (EDS) shows unique advantages. Very often, during assessment of the homogeneity of the sample, the interpretation of the scanning image alone may be ambiguous, as the morphology of the matrix polymer itself may hinder detection of the particles of the additive. The use of elemental mapping allows us to obtain unambiguity in the interpretation of the observed images and to avoid errors. The oxygen and silicon EDS maps highlight the presence of CS particles in a similar manner, while carbon maps are shadowed in the areas corresponding

to CS presence as these compounds have significantly lower carbon content (as a mass percentage) when compared to iPP (see Figure 2B–D and Figure 3B–D). The conducted research allowed us to unequivocally state which of the modifiers are well-dispersed or even dissolved in the polymer matrix and which, despite mixing and dilution, still do not show satisfactory interaction with the matrix.

The analysis of the obtained materials revealed that for most of the systems prepared, the CS additives exist in both nano- and microdispersed states, with a varying fraction of the latter, depending on the additive structure and loading. On the basis of this observation, the term 'nanocomposite' should be used carefully, especially when CS compounds are used in high concentration (many literature reports show materials with 3% up to 20% loading). Tang et al. reported how, due to limited compatibility with iPP and iPP-g-MA, octaisobutylsilsesquioxane (iBu$_8$SSQ) underwent migration towards the polymer surface and secondary self-aggregation during the composite annealing, despite the use of a high-shear melt-blending method for preparation of the composite [55]. Brabender internal mixer was utilized, which may be considered one of the most effective means for preparation of low amounts of highly dispersed and thoroughly mixed samples of thermoplastic materials and to study the components miscibility. From a practical point of view, it proves that at high loadings, SSQs and iPP may not form stable compositions with CS additives remaining in the state of highly dispersed (nano)particles, even if proper compounding procedures are applied.

In general, the observed dispersion of the CS additives was considerably better than for PE-based composites containing similar additives, as studied in our previous works [31,32]. It can be explained on the basis of a higher Hildebrandt solubility parameter of iPP than that of PE [56] (or the dispersive parameter according to Hansen model [57]), which better matches the slightly polar character of silsesquioxanes and spherosilicates, induced by the presence of an electronegative oxygen atom. An important work on this subject has been reported by Milliman et al. [58]. Also, as expected, when compared to SS-Vi (Figure 3) or SS-Glycidyl (Figure 4A), the alkylated additives (SS-Limonene and isobutyl SS/SSQ compounds, Figure 4B–F) showed much better dispersion when compared to, as the alkyl substituents provide higher compatibility with iPP than the ether-type glycidyl group or the small vinyl group, providing little steric hindrance for the polar Si-O-Si framework. At the highest loading (1%), all the additives showed some tendency towards agglomeration (Figure 4), which was clearly visible at masterbatch concentrations of all compositions, while further dilution facilitated improved dispersion, as less multimicron-sized aggregates are visible (see Supplementary Information). It was unequivocally found that the crystalline derivative SS-Vi does not show the dispersibility in polypropylene, similarly to SS-H/PE system studied earlier (see Figures 2 and 3). The SS-Glycidyl derivative, although under normal conditions a highly viscous liquid, does not tend to disperse, forming vesicle structures inside the matrix (Figure 5). The limited compatibility of this derivative with PP is already visible at the lowest concentration (0.1%).

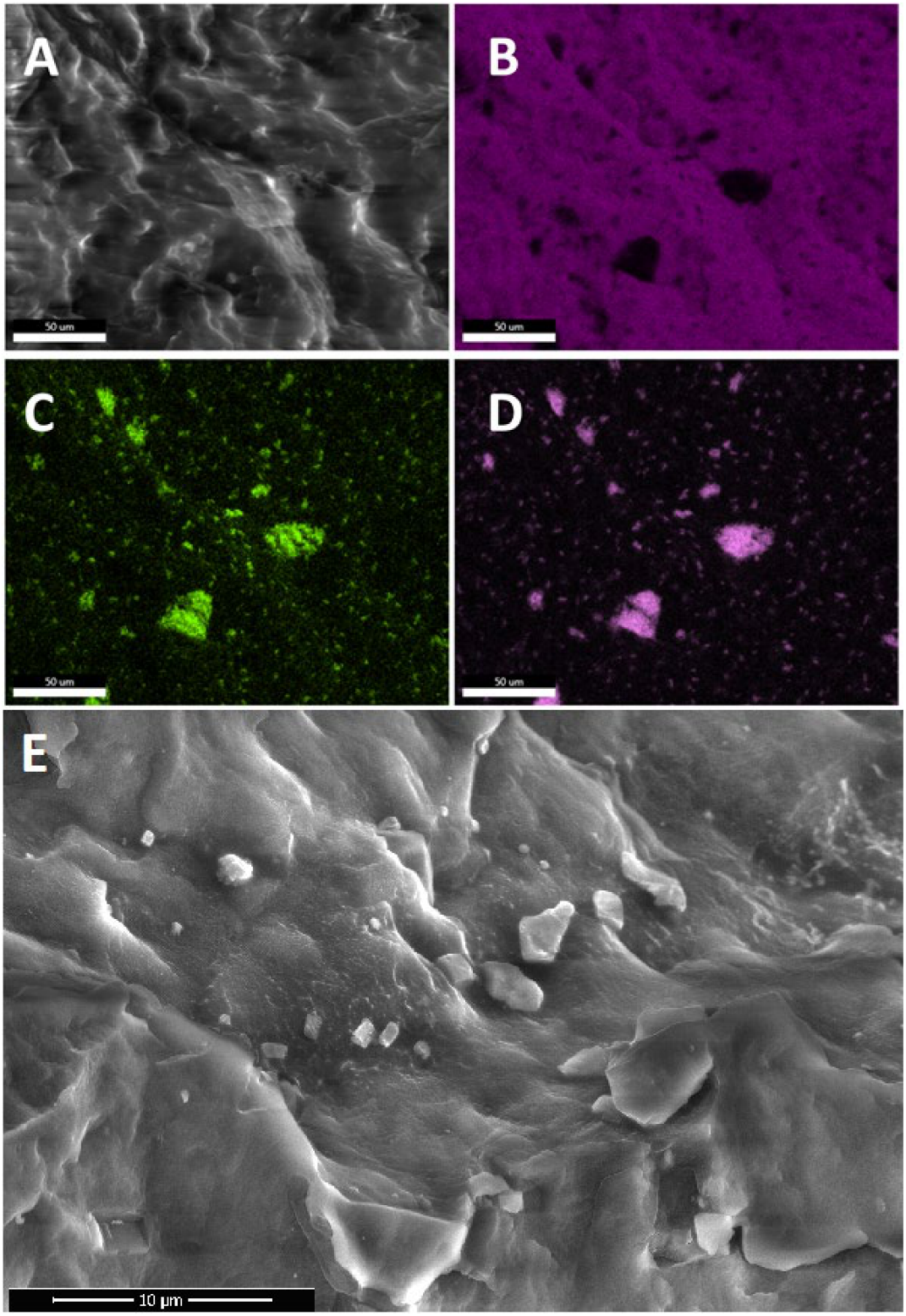

Figure 2. SEM (**A**,**E**) and EDS (**B**–**D**) images of SS-Vi/iPP 5% masterbatch. (**A**)—field of view SEM, (**B**)—carbon EDS, (**C**)—oxygen EDS, (**D**)—Silicon EDS, (**E**)—high resolution SEM.

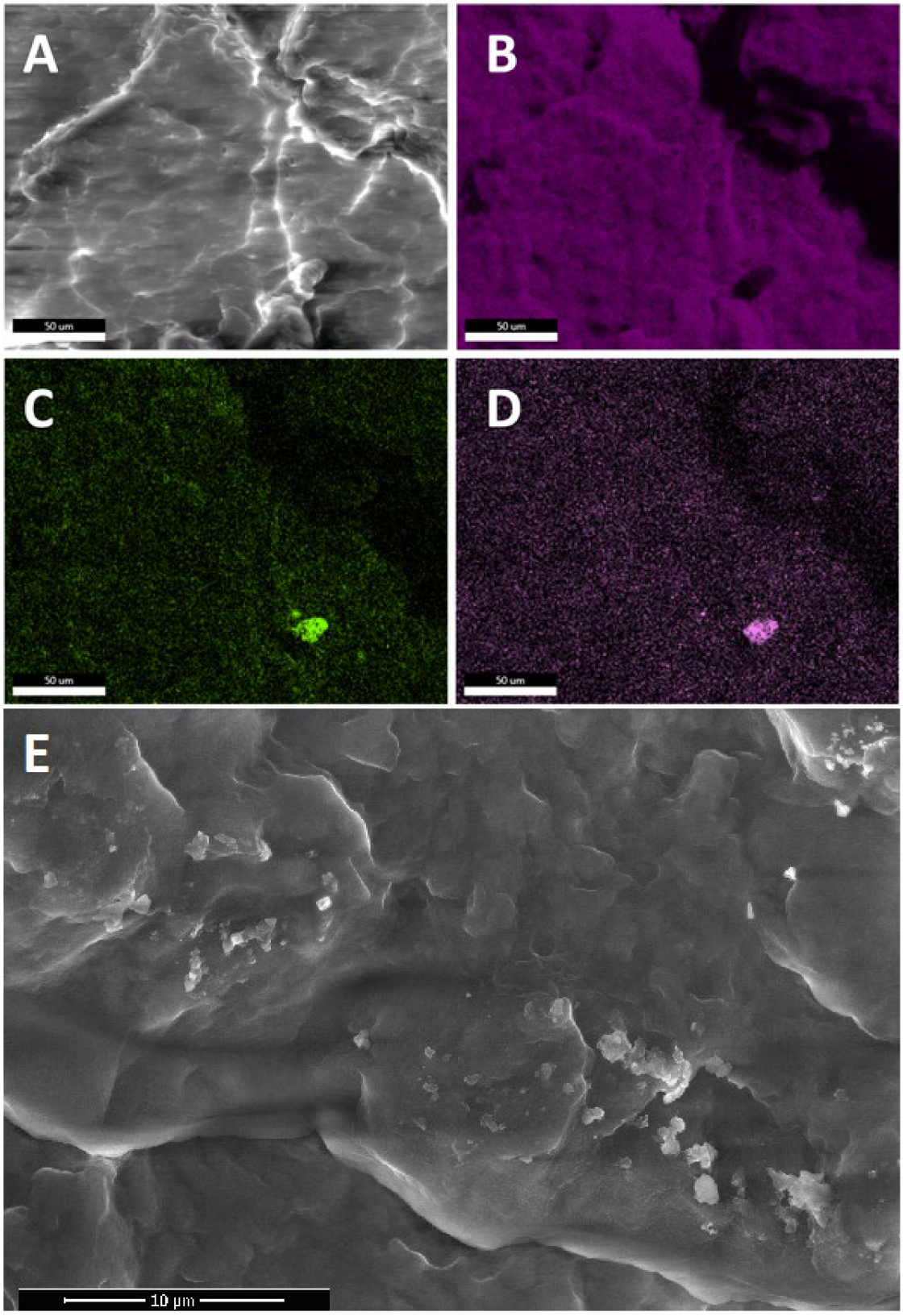

Figure 3. SEM (**A**,**E**) and EDS (**B**–**D**) images of 1% SS-Vi/iPP composite. (**A**)—field of view SEM, (**B**)—carbon EDS, (**C**)—oxygen EDS, (**D**)—Silicon EDS, (**E**)—high resolution SEM.

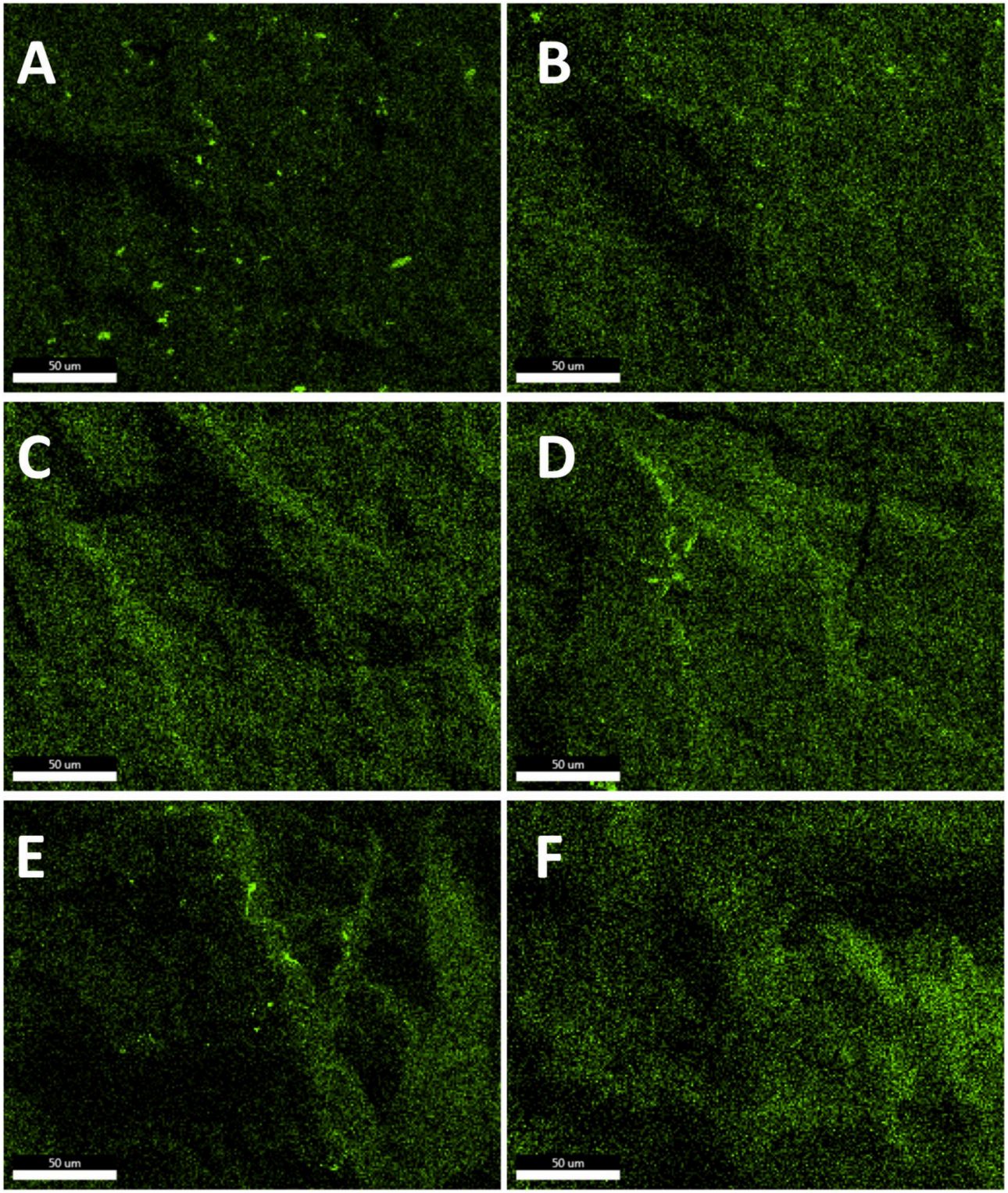

Figure 4. Oxygen EDS images of 1% CS/iPP composites. (**A**)—SS-Glycidyl, (**B**)—SS-Limonene, (**C**)—*i*Bu$_7$SSQ-3OH, (**D**)—*i*Bu$_7$SSQ-Cl, (**E**)—*i*Bu$_7$SS-Vi, (**F**)—*i*Bu$_7$SS-H.

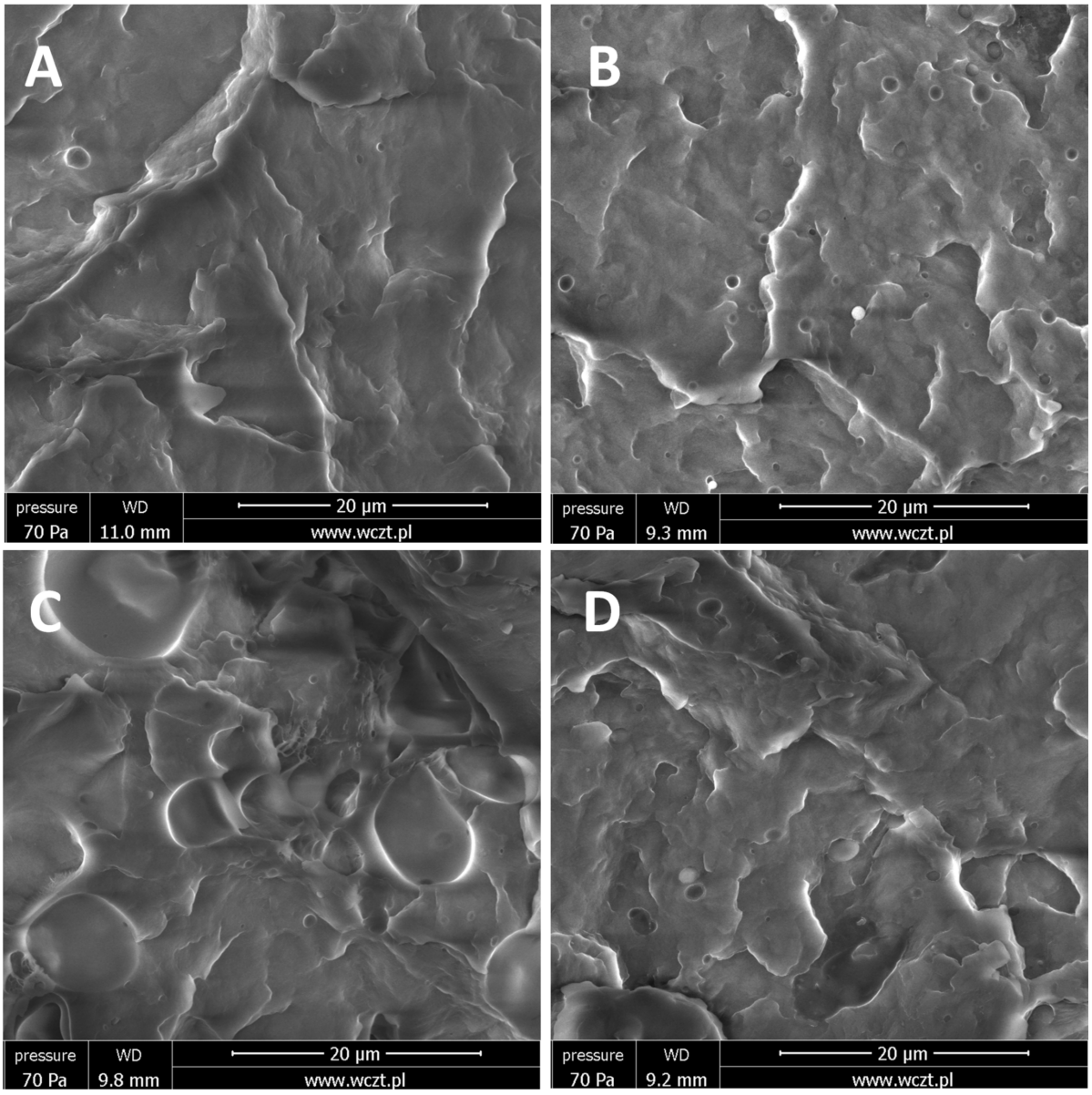

Figure 5. SEM images SS-Glycidyl/iPP composites. (**A**)—0.1%, (**B**)—0.25%, (**C**)—0.5%, (**D**)—1%.

The effect of alkyl substituent bulkiness on the dispersion and compatibility of SSQs with iPP was well-presented by Fina et al. and discussed in the terms of SSQ particles acting as nucleants for the growth of iPP [36]. The loading of CS additives had an impact on the dispersion level; as for the lower loadings, less agglomerates were visible, and the obtained materials were more suitable for the term 'nanocomposites' as the additive was difficult to observe under SEM or visible mostly as sub-micron particles.

3.3. Thermal Analysis Results

Thermal effects for compositions were measured by differential scanning calorimetry (DSC) and thermogravimetric analysis (TGA). The DSC measurements allowed us to determine the effect of the CS additives on the crystallization behavior of the obtained materials, while TG analyses were made to assess the impact of these compounds on the thermal stability of the compositions. For DSC, all the analyzed compositions showed increased crystallization temperatures when compared to neat iPP (see Table 2), which presents their nucleating properties. Interestingly, the highest T_c were recorded for SS-Glycidyl/SS compositions, where the additive did not show any crystallization properties in the temper-

ature range of iPP melting and crystallization. Therefore, the accelerated nucleation must be induced by iPP-chains–SS-additive interaction, possibly by the increased void volume or reduced polymer melt viscosity (see Section 3.7) giving polymer chains more freedom for organizing into spherulites (self-nucleating) [59]. SS-Limonene showed comparably good nucleating properties; however. this additive was proven to polymerize under the temperatures of polymer processing (above 100 °C), and the explanation cannot be based on the solvent-like action of the additive resulting in the viscosity reduction, but rather on the nucleating effect of nanoparticles thereof formed upon heat-induced polymerization. Moreover, all the compositions were characterized by a slightly increased T_m point (by 1–3 °C), which may be linked to formation of larger polymer spherulites. Butola et al. observed that octamethyl- and octaphenylsilsesquioxanes affected the T_m in the range of 1 °C (besides one odd result) over a wide range of loadings (0.1–10% *w*/*w*), and this subtle change may be attributed to poor miscibility of SSQ/iPP systems and poor SSQ–iPP interaction due to low compatibility of the chosen SSQ compounds [60]. The pristine iPP was characterized by a single melting peak of 162.7 °C, rather common for αiPP. On the other hand, samples containing either SS-Vi or any of the *i*Bu$_7$SS/*i*Bu$_7$SSQ additives showed a small, residual endothermic peak at around 150 °C, associated with melting of βiPP and visible only during the first heating. It proves that these additives show a mild β-nucleating character, being revealed during rapid sample cooling; however, during slow cooling (the DSC measurements being recorded at 5 °C/min heating/cooling rate), the β phase either does not form or it recrystallizes into α phase, as β phase is characterized by higher growth rate, but lower stability [61]. This β-nucleating effect, however, was not significant enough to give the CS/iPP composites the traits of typical βiPP materials (see Section 3.4) [62]. For comparison, Pracella et al. also observed formation of βiPP upon addition of octaisobutylsilsesquioxane when studying iPP composites with octaalkyl SSQs, as well as provided micrographs clearly presenting the process of spherulite growth on the surface of SSQ particles [63]. Moreover, Barczewski et al. reported a novel type of β-nucleating silsesquioxane agent derived from NJSTAR NU-100, the addition of which resulted in over 80% selectivity of βiPP crystallites obtained, which was comparable with action of base NJSTAR NU-100 [64]. Also, for most of the additives, the concentration did not play a very significant role, despite SS-Vi being a less effective nucleating agent at 1% loading due to agglomeration (the highest T_c of all SS-Vi/PP compositions), and a similar effect was observed for *i*Bu$_7$SS-Vi, while the nucleating action of *i*Bu$_7$SSQ-3OH was increasing with the concentration of the additive. The other compounds showed a 'saturation effect', where the smallest amount of additive used caused the strongest effect on crystallization temperature, while at higher loadings, the difference was close to negligible. Barczewski et al. observed that addition of SS-Vi and vinylhepta(*iso*butyl)silsesquioxane caused a similar saturation effect, and the increase of T_c was comparable to results discussed here [65]. Bouza et al. observed that aminopropylhepta(*iso*butyl)silsesquioxane acted as a nucleating agent at 2%, but at 10% it actually hindered PP crystallization, probably by disturbing the polymer chain packing or the particles of agglomerated additive physically blocking the spherulite growth [66]. According to the study by Chen et al., isobutyl-substituted SSQs increased the T_c of iPP by up to 1 °C, and a much more common nucleating agent, 1,3:2,4-bis(3,4-dimethylbenzylidene)sorbitol (DMDBS), was proven a superior nucleant, increasing T_c by ~12 °C [67].

Table 2. Results of DSC analysis of CS/iPP composites.

Sample		T_m [°C]	T_c [°C]
Neat PP		**162.7**	**117.2**
SS-Vi	0.1%	164.2 *	119.0
	0.25%	164.1 *	119.3
	0.5%	164.5 *	119.4
	1%	164.2 *	118.6
SS-Glycidyl	0.1%	165.1	122.2
	0.25%	165.5	122.6
	0.5%	164.9	124.0
	1%	165.1	124.9
SS-Limonene	0.1%	165.0	123.1
	0.25%	164.9	123.2
	0.5%	165.1	124.0
	1%	165.3	124.6
***i*Bu$_7$SSQ-3OH**	0.1%	165.2 *	119.9
	0.25%	164.4 *	120.8
	0.5%	164.9 *	121.7
	1%	164.6 *	122.0
***i*Bu$_7$SSQ-Cl**	0.1%	163.5 *	119.3
	0.25%	163.3 *	119.7
	0.5%	165.0 *	119.7
	1%	165.0 *	119.9
***i*Bu$_7$SS-Vi**	0.1%	164.3 *	119.1
	0.25%	164.7 *	119.2
	0.5%	164.8 *	120.5
	1%	164.3 *	119.3
***i*Bu$_7$SS-H**	0.1%	164.6 *	119.4
	0.25%	164.6 *	119.7
	0.5%	165.1 *	119.1
	1%	163.8 *	119.4

* additional, residual β phase melting endotherm observed during the first heating cycle.

For characterization of thermal stability and some mechanisms of thermal degradation of the obtained materials, TGA analysis was performed. The data are collected in Table 3 and presented in Figure S1 (see Supplementary Materials). Interestingly, in all cases, a drop of onset temperature (T_{onset}) was observed, which proved the discussed additives ability to reduce thermal stability of the obtained CS/iPP composites. This is contrary to a report by Carniato et al., where *i*Bu$_7$SSQ-3OH was shown to have a slightly stabilizing effect on the polymer matrix; however, the additive was tested at a loading exceeding the concentration range applied for this study (3%) [18]; or by Fina, where octamethyl-, octaisobutyl-, and octaisooctylsilsesquioxanes induced a slightly stabilizing effect at high loadings (3% and 10% *w*/*w*) [36]. Bouza et al. also observed reduced stability of the SSQ/iPP system containing aminopropylhepta(*iso*butyl)silsesquioxane [66]. On the other hand, Zhou et al. reported a decrease of thermal stability of octavinylsilsesquioxane/PP composites for physically blended samples [68]. A free radical mechanism may be speculated, that is,

formation of free radicals originating from decomposing CS molecules, which undergo intermolecular reactions with iPP chains and accelerate their scission. It may occur on the basis of relatively low Si-C bond energy, resulting in elimination of CS side groups [69]. This is supported by the fact the DTG curves are of a different shape in the onset region (280–300 °C) than that of neat iPP, showing higher decomposition rates than the pristine polymer. The effect was also concentration- and dispersion-dependent for the majority of the studied compounds. For example, SS-Vi (proven to be rather poorly miscible within iPP by SEM-EDS) accelerates iPP degradation the strongest when at 0.1% loading (T_{onset} = 294.4) and then at 1%, (T_{onset} = 290.1). At the lowest loading, the additive is most effectively dispersed, whereas at the higher ones, the saturation effect takes place due to the amount of the additive within the matrix. At the moderate loadings, however, agglomeration tends to slightly lower the effect of the additive, directly lowering the effective contact area between iPP and the CS particles, which are no longer abundant in nanosized form and mostly aggregated. The same observation may be done for SS-Glycidyl forming vesicles of separated additive. At the same time, the other additives tend to accelerate the decomposition of iPP more effectively at higher loadings. Similar conclusions on the correlation between the additive loading and the composite behavior were drawn previously for the CS/PE composites, but on the contrary, a stabilizing effect was observed, which shows a great difference between degradation mechanisms of PE and iPP and the CS composites thereof [31,32]. This suggests that small additions of CS compounds might be helpful for catalysis/promoters of iPP cracking, if pyrolytic recycling of polypropylene-based composites was considered [70].

Table 3. Results of thermogravimetric analysis (air atmosphere).

Sample		$T_{5\%}$ [°C]	T_{onset} [°C]	T_{DTG} [°C]
Neat PP		**283.3**	**312.2**	**341.4**
SS-Vi	0.1%	274.3	294.4	325.5
	0.25%	282.8	306.1	349.9
	0.5%	280.8	302.2	333.7
	1%	274.7	290.1	321.9
SS-Glycidyl	0.1%	279.8	299.3	336.6
	0.25%	283.6	302	351.8
	0.5%	288.6	311.3	360.5
	1%	280.6	304.9	342.7
SS-Limonene	0.1%	274.5	293.6	343.8
	0.25%	271.0	297.3	332.8
	0.5%	274.8	295	328.2
	1%	278.4	299.7	336.0
***i*Bu$_7$SSQ-3OH**	0.1%	283.9	307.4	348.9
	0.25%	276.5	297.6	342.9
	0.5%	274.5	309.6	333.9
	1%	274.6	297.0	334.6

Table 3. *Cont.*

Sample		$T_{5\%}$ [°C]	T_{onset} [°C]	T_{DTG} [°C]
Neat PP		**283.3**	**312.2**	**341.4**
***i*Bu$_7$SSQ-Cl**	0.1%	284.6	306.1	349.1
	0.25%	271.8	289.8	320.5
	0.5%	275.8	294.3	338.8
	1%	279.3	312.2	350.1
***i*Bu$_7$SS-Vi**	0.1%	279.8	300.7	344.0
	0.25%	278.7	301.4	329.7
	0.5%	275.5	291.5	328.4
	1%	274.9	296.2	331.4
***i*Bu$_7$SS-H**	0.1%	279.5	301.4	339.8
	0.25%	277.3	296.4	334.7
	0.5%	271.0	281.9	308.4
	1%	278.2	302.4	341.7

3.4. Mechanical Properties

Mechanical analysis allowed for observation of a reinforcing effect of the additives on the obtained (nano)composites. When studying tensile strength (Figure 6), a general trend was observed for all the additives studied—the results fall into a curve, with the highest values of tensile strength obtained for the composition with lower additive loadings of 0.1–0.5%, the values dropping down for the highest loading (1% *w*/*w*). However, none of the examples showed a drop in tensile strength below that of the reference (neat iPP). When Butola et al. studied SSQ/iPP composites, a similar trend was observed, but for high loadings (up to 5% *w*/*w*), the mechanical parameters were declining below those of the pristine polymer [60]. From this point of view, an optimal loading may be identified for each system where the highest increase of tensile strength was recorded. Additionally, a saturation effect may be observed, especially for SS-Glycidyl, where the maximum increase was obtained already at the 0.1% loading and remained virtually unchanged up to 0.5%. This is due to limited miscibility of the additive with the polymer matrix, which was confirmed by SEM-EDS imaging (critical concentration reached for 0.1% loading). The effect of SS-Limonene may be explained similarly to our previous reports on spherosilicate/polyethylene and spherosilicate/PLA composites, where SS-Limonene was proven to undergo polymerization under high temperatures of polymer processing, which, in case of PE, resulted in formation of a polymer blend of improved mechanical properties [31,33]. For SS-Glycidyl, this explanation is unsuitable as no such polymerization was observed. Rather, molecular level interactions may be considered, where molecules of the additive occupy the polymer void volume and reinforce it on the basis of weak intermolecular interactions between CS and iPP chains, as was speculated for the SS-Pinene/PE system in our previous work. The three isobutyl compounds, i.e., *i*Bu$_7$SSQ-Cl, *i*Bu$_7$SS-Vi, and *i*Bu$_7$SS-H showed very similar patterns due to similarities in their structure. Application of *i*Bu$_7$SSQ-3OH resulted in slightly higher improvement of mechanical properties than the other isobutyl derivatives. This result is similar to our previous findings on polyethylene-based composites, where it was proven that *i*Bu$_7$SSQ-3OH underwent condensation to a series of amorphous products characterized by better dispersion properties than those of well-defined, cage compounds, like the abovementioned *i*Bu$_7$SSQ-Cl, *i*Bu$_7$SS-Vi, and *i*Bu$_7$SS-H [32]. When studying Young's modulus (Figure 7), it can be observed that all octaspherosilicate compounds, as well as *i*Bu$_7$SSQ-3OH, increased stiffness of the samples at loadings up to 0.5%, with a drop at 1%. *i*Bu$_7$SS-Vi showed an improvement of this trait at a concentration up to 0.25%, while *i*Bu$_7$SSQ-Cl and *i*Bu$_7$SS-H

did not impart any statistically relevant change. Reduction of Young's modulus at higher loadings may be caused by self-aggregation of the additives and lowered interaction with iPP. Additionally, SS-Glycidyl may work as a plasticizing agent, as a slight decrease of the coefficient of friction was observed (see Section 3.5).

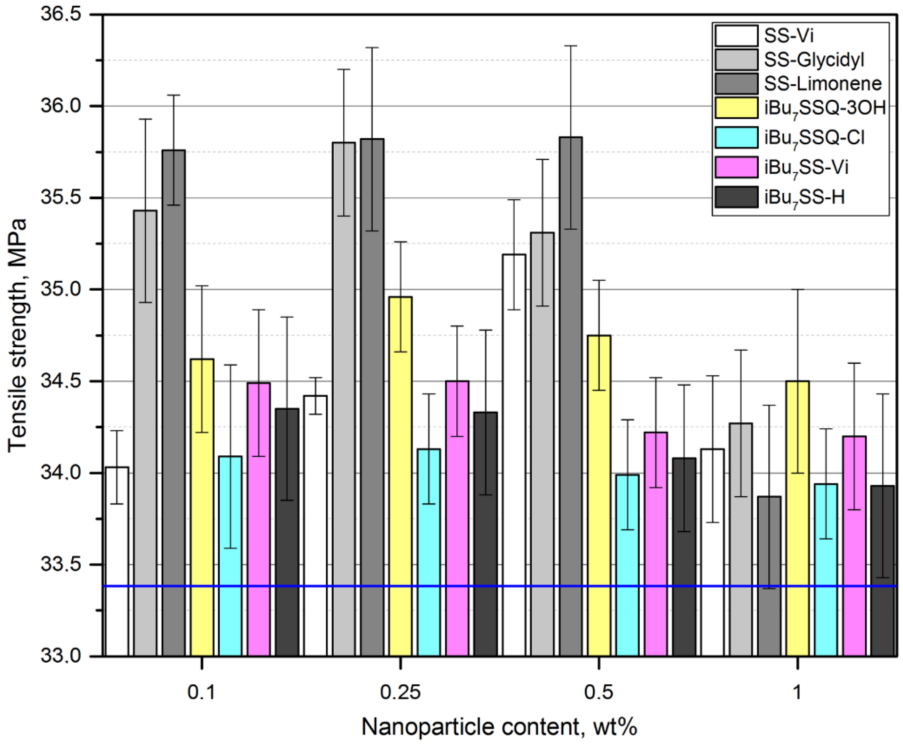

Figure 6. Tensile strength of the CS/iPP composites.

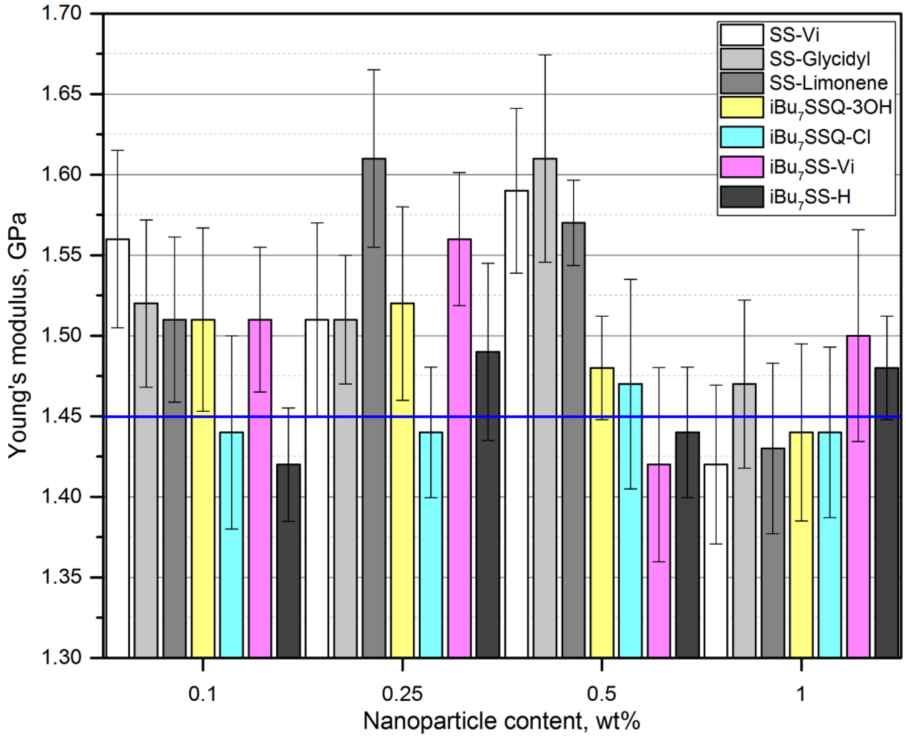

Figure 7. Young's modulus of the CS/iPP composites.

When compared with tensile strength measurements, a similar trend may be observed for flexural strength (Figure 8) when studying iPP composites containing SS-Glycidyl, SS-Limonene, *i*Bu$_7$SSQ-3OH, and *i*Bu$_7$SSQ-Cl. The changes of flexural modulus (Figure 9) confirmed the improved toughness of the nanocomposites thereof. However, for the remaining compounds, as well as the lowest loading of *i*Bu$_7$SSQ-Cl, the values were oscillating around or below that of the reference. As these compounds (that is, SS-Vi, *i*Bu$_7$SSQ-Cl, *i*Bu$_7$SS-H, and *i*Bu$_7$SS-H) are crystalline solids (which was also visible on SEM as microcrystalline phases, see Section 3.2), these additives may serve as microcrack initiators or stress concentrators, which leads to faster failure of the material under flexural stress, which is known behavior for micrometric-sized fillers [71,72]. Also, Milliman et al. presented how mechanical stress exerted on iPP samples caused debonding of silsesquioxane microparticles from the polymer matrix on the example of Ph$_7$SSQ-3OH [59].

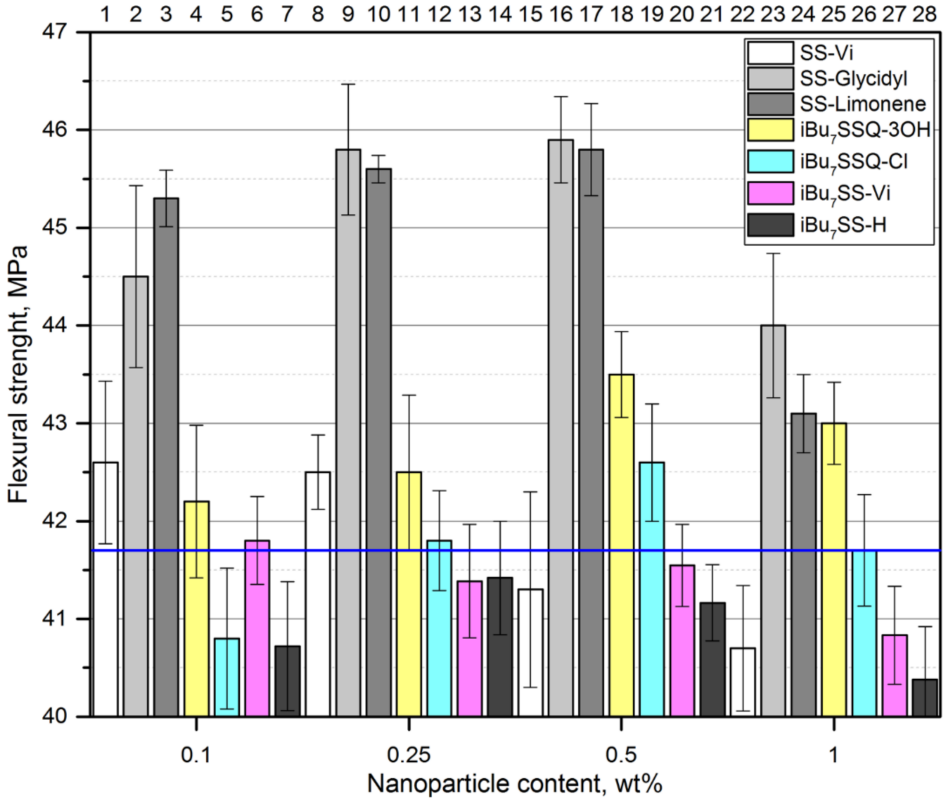

Figure 8. Flexural strength of the CS/iPP composites.

3.5. Tribological Properties

Tribological properties were studied on the basis of the measurements of the coefficient of friction (μ) of the selected SS/iPP compositions. The additives for these tests were chosen on the basis of the mechanical tests' performance (see Section 3.4). Two additives were chosen for this study, SS-Limonene and SS-Glycidyl. Moreover, SS-Limonene was selected due to its heat-polymerizing ability, which, in combination with its great dispersion properties, resulted in the most prominent improvement of the mechanical parameters of the studied CS/iPP composites. On the other hand, SS-Glycidyl, which was found to be an oil partially miscible with iPP (on the basis of SEM, see Figure 5), was chosen to be assessed as a potential slip agent. Such additives tend to form a film on the polymer surface or concentrate in the near-surface region of the polymer, significantly changing its physicochemical behavior, while the bulk material may remain unchanged to a certain degree [73]. It was observed that at lower loadings (0.1% and 0.25%), SS-Limonene did not affect the coefficient of friction, while at higher ones, it caused an increase of its value (Figure S2, Supplementary Materials). It supports the results of the mechanical tests

that SS-Limonene may be considered a functional additive at lower loadings, however at concentration higher than 0.5% it would not be recommended for applications where material friction is occurring. On the other hand, SS-Glycidyl was found to work as a slip agent, as the obtained mean values of the friction coefficient for the tested compositions were about 5–7% lower than in the case of neat PP (Figure S3, Supplementary Materials). Although the mean values of the friction coefficient were only slightly reduced, the notable drop in the standard deviation thereof suggests that at 1% loading, a transition in motion to smoother sliding [74] occurs.

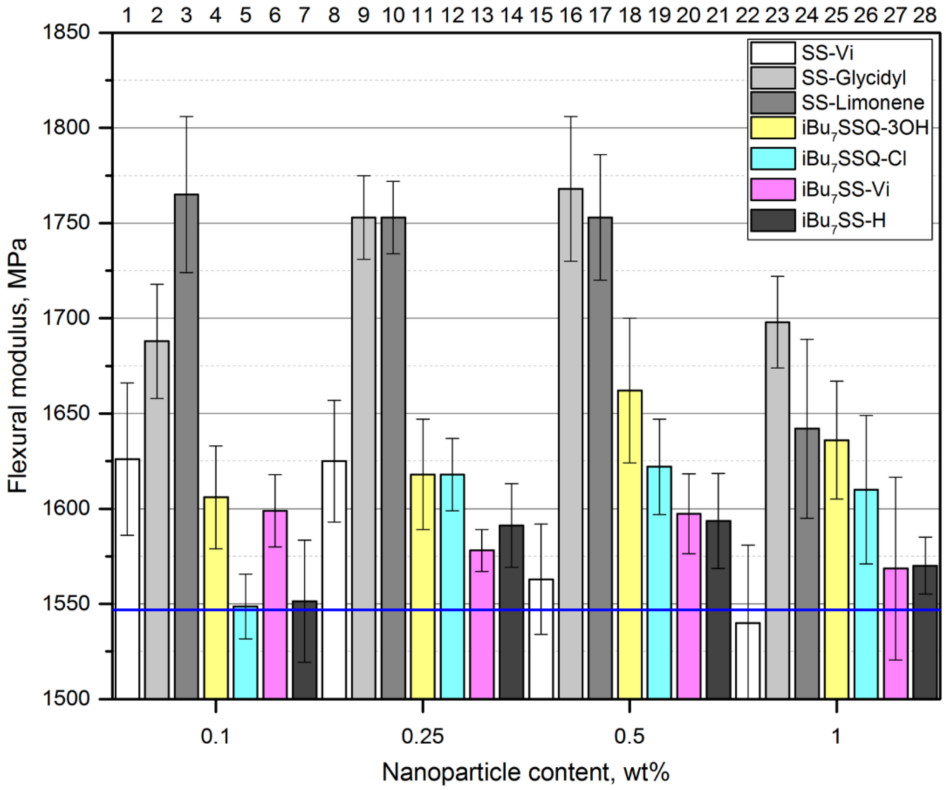

Figure 9. Flexural modulus of the CS/iPP composites.

3.6. Vicat Softening Temperature

Vicat softening temperature measurements were performed to assess the impact of the CS additives on the thermomechanical properties of the obtained iPP composites, that is, the temperature of softening under static load (Figure S4, Supplementary Materials). The SS-Limonene/iPP compositions were virtually unaffected when compared to neat PP, contrary to mechanical analysis at ambient temperature, while the other compounds behaved as plasticizers, either due to increased polymer void volume or due to low adhesion of iPP to the (nano)particles thereof, resulting in CS-iPP debonding and accelerated composite failure. At 0.25% loading, SS-Glycidyl/iPP and *i*Bu$_7$SS-Vi/iPP were characterized by increased VST values due to CS-iPP reinforcing interactions, which proves the importance of the additives being in a highly dispersed form rather than at high concentration.

3.7. Melt Flow Index

Melt flow index (MFI) measurements were performed to assess the flowability of the obtained materials in their molten form under conditions of static load, which is the most basic measure of the polymer melt viscosity, used as a standard in industrial practice of plastics processing. The results are presented in Figure 10. Interestingly, almost all the compositions showed at least a small increase in the MFI value. The effect could be most easily explained for SS-Glycidyl, which, as mentioned above, is an oily liquid partially miscible with iPP, providing additional lubrication to the flowing polymer, quite similarly

to standard lubricants (e.g., silicone oils or synthetic waxes). A notable increase appeared at 0.5% loading, where a possible small phase separation occurred, and at 1% loading, it caused a 40% increase of MFI, which is beneficial for applications such as injection molding, as using a material of correct MFI is crucial for obtaining a product of satisfactory quality. It is a well-known fact that introducing fillers, especially ones of larger aspect ratio (notably reinforcing fibers) causes drastic increase of the flow viscosity [75]. Using proper lubricating additives allows us to minimize this effect. The effect of the other additives may be explained on the basis of intermolecular interactions, where CS molecules diffuse between polymer chains and reduce the polymer chain–chain interaction in favor of chain–CS molecule interaction, which also increases the polymer void volume. This hypothesis has been proposed in a number of other reports on silsesquioxane-containing polymer materials [27,76]. Also, *i*Bu$_7$SSQ-3OH showed a strong lubricating effect at 1% loading, which confirms that the amorphous products of its thermal condensation are more susceptible towards interaction with the polymer matrix. Niemczyk et al. also observed that addition of alkyl-substituted octasilsesquioxanes caused increase of MFI (by up to over 80% at 10% loading). Perilla reported that addition of *i*Bu$_8$SSQ and Ph$_7$SSQ-3OH resulted in reduction of complex viscosity of iPP melt, but the effect was more visible at a very high loading (10% *w*/*w*) [77].

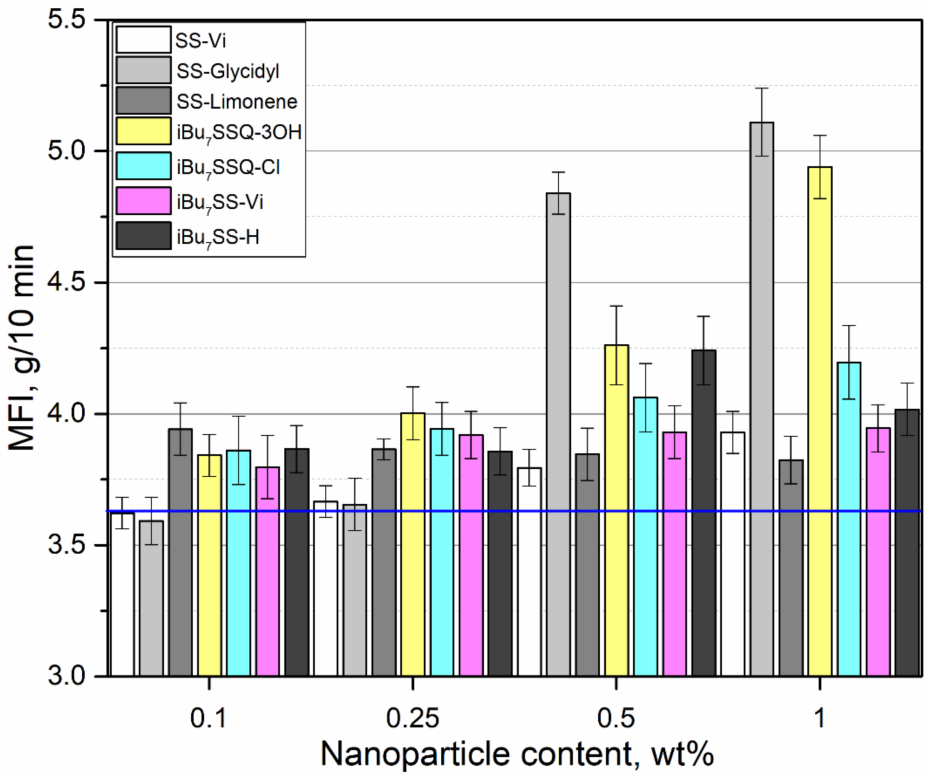

Figure 10. Melt flow index of CS/iPP compositions.

4. Practical Implementation

This study has been conducted to verify the applicability of cage siloxane compounds (often referred to as POSS) as functional additives for iPP. Bearing in mind that one of the most important tasks of a scientist is to care for the practical application of research results, we would like to draw attention to the possibility of practical application of research results by specialists working in this particular field. For this reason, a group of silsesquioxane- and spherosilicate-based compounds was selected and tested in a low concentration range to accommodate their relatively high price. The obtained materials were subjected to a comprehensive study of thermal, mechanical, and rheological properties to reveal the potential of CS compounds as functional or processing additives for polyolefins, which

is a continuation of our previous work on CS/polyethylene composites. Additionally, it was important to clarify the terminology used in accordance with these systems. It should be noted that there is a clear difference between two types of additives, that is, fillers and modifiers. The application of the first one usually reduces the price of the composite and may bring about a secondary effect of changes in the material, while addition of the latter purposely influences the processing properties of the material. This work was meant to explain why the CS compounds should not be referred to as fillers or nanofillers, as it is misleading for the plastics processing/engineering community.

5. Conclusions

A following set of conclusions may be drawn from this study:

1. CS compounds show much better dispersion properties in an iPP matrix when compared to similar compositions prepared in a similar manner with PE serving as a matrix material. It can be explained on the basis of higher Hildebrandt solubility parameter or Hansen dispersive parameter of iPP than that of PE, matching the dipole character of cage siloxanes. It results in better improvement in performance of CS/iPP composites in comparison to similar CS/PE composites.
2. Two factors are critical for obtaining iPP-based nanocomposites containing silsesquioxanes and spherosilicates. One is the chemical structure of the compounds, which should match the character of iPP. The second aspect is dilution of the additive within the polymer-at the highest concentrations tested; most of the studied compounds had a tendency to form aggregates, which reduced their effectiveness as additives.
3. Among the tested CS compounds, functionalized spherosilicate (SS-Glycidyl, SS-Limonene) and silsesquioxane (*i*Bu$_7$SSQ-3OH) additives may be considered valuable agents for improving mechanical properties of iPP, mainly tensile and flexural strength, with optimal loading not exceeding 0.5%. Crystalline CS, mainly the remaining silsesquioxanes, did not present beneficial effects on these properties.
4. SS-Glycidyl and *i*Bu$_7$SSQ-3OH provide lubricating action, according to MFI, which is beneficial from the point of view of selected polymer processing techniques (e.g., injection molding, melt blowing).
5. CS compounds tend to reduce thermal stability of the obtained iPP compositions thereof (degradation promoters), which is contrary to the behavior observed by us for CS/PE composites studied earlier, and to the behavior of iPP composites containing high loadings of CS and reported in other sources (degradation inhibitors). As a result, they may be considered catalysts for pyrolytic decomposition/recycling of iPP-based materials.

On the basis of the conducted research, we suggest that in the case of polyolefin systems and other polymer systems used in bulk quantities, where no unequivocal effects such as permanence, strength, or cost reduction are observed upon addition of a given compound, the use of the term 'nanofiller' in relation to compounds of the CS type should not be considered. Due to agglomeration, the CS additives often do not meet the definition of 'nano' fillers (they form polycrystalline agglomerates). Moreover, due to their high cost, they considerably increase the price of the final composition if used in quantities exceeding a fraction of a single percent by mass. This is contradictory to the definition of a filler, as these are usually applied as a significant mass fraction of the composition. Therefore, these compounds should be used at low concentration and selected or designed in such a way that they indeed play a role of (nano)modifiers in order to be considered viable additives for polymer systems, justifying their cost.

Supplementary Materials: The following are available online at https://www.mdpi.com/article/10.3390/polym13132124/s1, Figure S1: TGA thermograms of CS/iPP compositions, Figure S2: Coefficients of friction for SS-Limonene/iPP composites, Figure S3: Coefficients of friction for SS-Glycidyl/iPP composites, Figure S4: Vicat softening temperatures of the obtained CS/iPP composites,

NMR and FT-IR spectra of the obtained CS compounds; SEM and EDS images of the obtained CS-iPP composites.

Author Contributions: Conceptualization, R.E.P.; Data curation, D.B., B.S., M.F., D.P., M.J. and G.M.; Formal analysis, D.B., M.F., D.P., M.J. and G.M.; Funding acquisition, D.B.; Investigation, D.B., R.E.P., B.S. and M.J.; Methodology, R.E.P.; Project administration, D.B. and R.E.P.; Resources, D.B.; Software, M.F. and D.P.; Supervision, R.E.P. and B.M.; Validation, R.E.P., M.J. and G.M.; Visualization, D.B., M.F., D.P. and M.J.; Writing—original draft, D.B., R.E.P., B.S., M.F. and D.P. All authors have read and agreed to the published version of the manuscript.

Funding: This research was funded by National Science Centre, Poland, grant number UMO-2018/29/N/ST5/00868.

Institutional Review Board Statement: Not applicable.

Informed Consent Statement: Not applicable.

Conflicts of Interest: The authors declare no conflict of interest.

References

1. Available online: https://hybridplastics.com (accessed on 20 May 2021).
2. Furst, K. The Global Silicone Market: Key Trends & Forecasts. In Proceedings of the International Silicone Conference, Cuyahoga Falls, OH, USA, 10–11 April 2018.
3. Hal, F.; Brinson, L. *Catherine Brinson, Polymer Engineering Science and Viscoelasticity: An Introduction*; Springer: Berlin/Heidelberg, Germany, 2008.
4. Chanda, M.; Roy, S.K. *Industrial Polymers, Specialty Polymers, and Their Applications*; CRC Press: Boca Raton, FL, USA, 2009.
5. Fina, A.; Tabuani, D.; Carniato, F.; Frache, A.; Boccaleri, E.; Camino, G. Polyhedral oligomeric silsesquioxanes (POSS) thermal degradation. *Thermochim. Acta* **2006**, *440*, 36–42. [CrossRef]
6. Cordes, D.; Lickiss, P.D.; Rataboul, F. Recent Developments in the Chemistry of Cubic Polyhedral Oligosilsesquioxanes. *Chem. Rev.* **2010**, *110*, 2081–2173. [CrossRef] [PubMed]
7. Herbert, M.M.; Andrade, R.; Ishida, H.; Maia, J.; Schiraldi, D.A. Multilayered confinement of iPP/TPOSS and nylon 6/APOSS blends. *Polymer* **2013**, *54*, 6992–7003. [CrossRef]
8. Gooch, J.W. (Ed.) *Encyclopedic Dictionary of Polymers*; Springer Science & Business Media LLC: Berlin/Heidelberg, Germany, 2007.
9. Zhang, C.; Babonneau, F.; Bonhomme, C.; Laine, R.M.; Soles, C.L.; Hristov, H.A.; Yee, A.F. Highly Porous Polyhedral Silsesquioxane Polymers. Synthesis and Characterization. *J. Am. Chem. Soc.* **1998**, *120*, 8380–8391. [CrossRef]
10. Kuo, S.-W.; Chang, F.-C. POSS related polymer nanocomposites. *Prog. Polym. Sci.* **2011**, *36*, 1649–1696. [CrossRef]
11. Ayandele, E.; Sarkar, B.; Alexandridis, P. Polyhedral Oligomeric Silsesquioxane (POSS)-Containing Polymer Nanocomposites. *Nanomaterials* **2012**, *2*, 445–475. [CrossRef]
12. Du, Y.; Liu, H. Cage-like silsesquioxanes-based hybrid materials. *Dalton Trans.* **2020**, *49*, 5396–5405. [CrossRef]
13. Zhang, X.; Ma, R.; Du, A.; Liu, Q.; Fan, Y.; Zhao, X.; Wu, J.; Cao, X. Corrosion resistance of organic coating based on polyhedral oligomeric silsesquioxane-functionalized graphene oxide. *Appl. Surf. Sci.* **2019**, *484*, 814–824. [CrossRef]
14. Baldi, F.; Bignotti, F.; Fina, A.; Tabuani, D.; Riccò, T. Mechanical characterization of polyhedral oligomeric silsesquioxane/polypropylene blends. *J. Appl. Polym. Sci.* **2007**, *105*, 935–943. [CrossRef]
15. Chen, J.-H.; Chiou, Y.-D. Crystallization behavior and morphological development of isotactic polypropylene blended with nanostructured polyhedral oligomeric silsesquioxane molecules. *J. Polym. Sci. Part B Polym. Phys.* **2006**, *44*, 2122–2134. [CrossRef]
16. Sofiah, M.A.; Ong, H.L.; Akil, H.M.; Ishak, Z.A.M.; Lin, O.H. Effect of Polypropylene-Methyl Polyhedral Oligomeric Silsesquioxane Compatibilizer in Polypropylene/Silica Nanocomposites: Mechanical, Morphological and Thermal Studies. *Mater. Sci. Forum* **2014**, *803*, 265–268. [CrossRef]
17. Misra, R.; Fu, B.X.; Morgan, S.E. Surface energetics, dispersion, and nanotribomechanical behavior of POSS/PP hybrid nanocomposites. *J. Polym. Sci. Part B Polym. Phys.* **2007**, *45*, 2441. [CrossRef]
18. Carniato, F.; Boccaleri, E.; Marchese, L.; Fina, A.; Tabuani, D.; Camino, G. Synthesis and Characterisation of Metal Isobutyl-silsesquioxanes and Their Role as Inorganic–Organic Nanoadditives for Enhancing Polymer Thermal Stability. *Eur. J. Inorg. Chem.* **2007**, *2007*, 585–591. [CrossRef]
19. Bourbigot, S.; Turf, T.; Bellayer, S.; Duquesne, S. Polyhedral oligomeric silsesquioxane as flame retardant for thermoplastic polyurethane. *Polym. Degrad. Stab.* **2009**, *94*, 1230–1237. [CrossRef]
20. Jia, L.; Tong, B.; Li, D.; Zhang, W.; Yang, R. Crystallization and flame-retardant properties of polylactic acid composites with polyhedral octaphenyl silsesquioxane. *Polym. Adv. Technol.* **2018**. [CrossRef]
21. Zhang, W.; Camino, G.; Yang, R. Polymer/polyhedral oligomeric silsesquioxane (POSS) nanocomposites: An overview of fire retardance. *Prog. Polym. Sci.* **2017**, *67*, 77–125. [CrossRef]
22. Zhou, Z.; Cui, L.; Zhang, Y.; Zhang, Y.; Yin, N. Preparation and properties of POSS grafted polypropylene by reactive blending. *Eur. Polym. J.* **2008**, *44*, 3057–3066. [CrossRef]

23. Wang, X.; Xing, W.; Tang, G.; Hong, N.; Hu, W.; Zhan, J.; Song, L.; Yang, W.; Hu, Y. Synthesis of a novel sulfur-bearing secondary antioxidant with a high molecular weight and its comparative study on antioxidant behavior in polypropylene with two commercial sulfur-bearing secondary antioxidants having relatively low molecular weight. *Polym. Degrad. Stab.* **2013**, *98*, 2391–2398. [CrossRef]
24. Wheeler, P.A.; Misra, R.; Cook, R.D.; Morgan, S.E. Polyhedral oligomeric silsesquioxane trisilanols as dispersants for titanium oxide nanopowder. *J. Appl. Polym. Sci.* **2008**, *108*, 2503–2508. [CrossRef]
25. Song, X.; Zhou, S.; Wang, Y.; Kang, W.; Cheng, B. Mechanical properties and crystallization behavior of polypro-pylene non-woven fabrics reinforced with POSS and SiO2 nanoparticles. *Fibers Polym.* **2012**, *13*, 1015–1022. [CrossRef]
26. Pracella, M. Polyolefins with POSS. In *Polymer/POSS Nanocomposites and Hybrid Materials*; Kalia, S., Pielichowski, K., Eds.; Springer Series on Polymer and Composite Materials; Springer Science and Business Media LLC: Cham, Switzerland, 2018; pp. 129–166.
27. Shankar, R.; Kemp, L.K.; Smith, N.A.; Cross, J.A.; Chen, B.; Nazarenko, S.I.; Park, J.G.; Thornell, T.L.; Newman, J.K.; Morgan, S.E. POSS-induced rheological and dielectric modification of polyethersulfone. *J. Appl. Polym. Sci.* **2021**, *138*, 50537. [CrossRef]
28. Knauer, K.M.; Brust, G.; Carr, M.; Cardona, R.J.; Lichtenhan, J.D.; Morgan, S.E. Rheological and crystallization enhancement in polyphenylenesulfide and polyetheretherketone POSS nanocomposites. *J. Appl. Polym. Sci.* **2016**, *134*, 44462. [CrossRef]
29. Zhang, H.; Kulkarni, S.; Wunder, S.L. Blends of POSS−PEO $(n = 4)_8$ and High Molecular Weight Poly(ethylene oxide) as Solid Polymer Electrolytes for Lithium Batteries. *J. Phys. Chem. B* **2007**, *111*, 3583–3590. [CrossRef]
30. Sarkar, B. POSS-Containing Polyamide-Based Nanocomposites. In *Polymer/POSS Nanocomposites and Hybrid Materials*; Kalia, S., Pielichowski, K., Eds.; Springer Series on Polymer and Composite Materials; Springer Science and Business Media LLC: Cham, Switzerland, 2018; pp. 205–231.
31. Brząkalski, D.; Przekop, R.E.; Dobrosielska, M.; Sztorch, B.; Marciniak, P.; Marciniec, B. Highly bulky spherosilicates as functional additives for polyethylene processing—Influence on mechanical and thermal properties. *Polym. Compos.* **2020**, *41*, 3389–3402. [CrossRef]
32. Brząkalski, D.; Przekop, R.E.; Sztorch, B.; Jakubowska, P.; Jałbrzykowski, M.; Marciniec, B. Silsesquioxane Derivatives as Functional Additives for Preparation of Polyethylene-Based Composites: A Case of Trisilanol Melt-Condensation. *Polymers* **2020**, *12*, 2269. [CrossRef]
33. Brząkalski, D.; Sztorch, B.; Frydrych, M.; Pakuła, D.; Dydek, K.; Kozera, R.; Boczkowska, A.; Marciniec, B.; Przekop, R.E. Limonene Derivative of Spherosilicate as a Polylactide Modifier for Applications in 3D Printing Technology. *Molecules* **2020**, *25*, 5882. [CrossRef]
34. Kong, J.; Tan, B.H.; Lu, X.; Li, Z.; He, C. Hybrid POSS Nanocomposites. In *Silicon Containing Hybrid Copolymers*; Wiley: Hoboken, NJ, USA, 2020; pp. 201–237.
35. Fu, B.X.; Yang, L.; Somani, R.H.; Zong, S.X.; Hsiao, B.S.; Phillips, S.; Blanski, R.; Ruth, P. Crystallization studies of isotactic polypropylene containing nanostructured polyhedral oligomeric silsesquioxane molecules under quiescent and shear conditions. *J. Polym. Sci. Part B Polym. Phys.* **2001**, *39*, 2727–2739. [CrossRef]
36. Fina, A.; Tabuani, D.; Frache, A.; Camino, G. Polypropylene–polyhedral oligomeric silsesquioxanes (POSS) nanocomposites. *Polymer* **2005**, *46*, 7855–7866. [CrossRef]
37. Kamyab, A.; Ghasemi-Ghalebahman, A.; Fereidoon, A.; Khonakdar, H.A. Shape memory and mechanical properties of polycaprolactone/polypropylene carbonate nanocomposite blends in the presence of G-POSS nanoparticles. *eXPRESS Polym. Lett.* **2021**, *15*, 473–489.
38. Zaharescu, T.; Blanco, I.; Borbath, T.; Borbath, I.; Mariș, M. Kinetic Analysis on the Stabilization Effects of Substituted POSS Powders Embedded in γ-Radiolyzed Polypropylene. *J. Compos. Sci.* **2021**, *5*, 124. [CrossRef]
39. Zhang, X.; Zhao, S.; Meng, X.; Xin, Z. The mechanical properties, crystallization and rheological behavior of isotactic polypropylene with nucleating agent supported on polyhedral oligomeric silsesquioxanes (POSS). *J. Polym. Res.* **2020**, *27*, 1–10. [CrossRef]
40. Wanke, C.H.; Feijó, J.L.; Barbosa, L.G.; Campo, L.F.; De Oliveira, R.V.B.; Horowitz, F. Tuning of polypropylene wettability by plasma and polyhedral oligomeric silsesquioxane modifications. *Polymer* **2011**, *52*, 1797–1802. [CrossRef]
41. Yang, B.; Chen, Y.; Zhang, M.; Yuan, G. Synergistic and Compatibilizing Effect of Octavinyl Polyhedral Oligomeric Silsesquioxane Nanoparticles in Polypropylene/Intumescent Flame Retardant Composite System. *Compos. Part A Appl. Sci. Manuf.* **2019**. [CrossRef]
42. Yi, J.; Yin, H.; Cai, X. Effects of common synergistic agents on intumescent flame retardant polypropylene with a novel charring agent. *J. Therm. Anal. Calorim.* **2012**, *111*, 725–734. [CrossRef]
43. Xanthos, M. *Functional Fillers for Plastics*, 2nd ed.; Wiley-VCH: Weinheim, Germany, 2010.
44. Adomavičiūtė, E.; Baltušnikaitė-Guzaitienė, J.; Juškaitė, V.; Žilius, M.; Briedis, V.; Stanys, S. Formation and characterization of melt-spun polypropylene fibers with propolis for medical applications. *J. Text. Inst.* **2017**, *109*, 278–284. [CrossRef]
45. Borghetti, A.; Nucci, C.A.; Pasini, G.; Pirani, S.; Rinaldi, M. Tests on self-healing metallized polypropylene capacitors for power applications. *IEEE Trans. Power Deliv.* **1995**, *10*, 556–561. [CrossRef]
46. Karian, H. *Handbook of Polypropylene and Polypropylene Composites, Revised and Expanded*; CRC Press: Boca Raton, FL, USA, 2003.
47. Ellis, B.; Smith, R. *Polymers: A Property Database*, 2nd ed.; CRC Press: Boca Raton, FL, USA, 2020.
48. Zhou, Z.; Cui, L.; Zhang, Y.; Zhang, Y.; Yin, N. Isothermal crystallization kinetics of polypropylene/POSS composites. *J. Polym. Sci. Part B Polym. Phys.* **2008**, *46*, 1762–1772. [CrossRef]

49. Filho, N.L.D.; de Aquino, H.A.; Pires, G.; Caetano, L. Relationship between the Dielectric and Mechanical Properties and the Ratio of Epoxy Resin to Hardener of the Hybrid Thermosetting Polymersrmosetting polymers. *J. Braz. Chem. Soc.* **2006**, *17*, 533–541. [CrossRef]
50. Dutkiewicz, M.; Szołyga, M.; Maciejewski, H.; Marciniec, B. Thiirane functional spherosilicate as epoxy resin modifier. *J. Therm. Anal. Calorim.* **2014**, *117*, 259–264. [CrossRef]
51. Ye, M.; Wu, Y.; Zhang, W.; Yang, R. Synthesis of incompletely caged silsesquioxane (T7-POSS) compounds via a versatile three-step approach. *Res. Chem. Intermed.* **2018**, *44*, 4277–4294. [CrossRef]
52. Ervithayasuporn, V.; Wang, X.; Kawakami, Y. Synthesis and characterization of highly pure azido-functionalized polyhedral oligomeric silsesquioxanes (POSS). *Chem. Commun.* **2009**, *60*, 5130–5132. [CrossRef]
53. Waehner, J.; Marciniec, B.; Pawluc, P. Functionalization of Vinylspherosilicates by Ruthenium-Catalyzed Silylative Coupling Reactions. *Eur. J. Inorg. Chem.* **2007**, *2007*, 2975–2980. [CrossRef]
54. Xu, Y.; Ma, Y.; Deng, Y.; Yang, C.; Chen, J.; Dai, L. Morphology and thermal properties of organic–inorganic hybrid material involving monofunctional-anhydride POSS and epoxy resin. *Mater. Chem. Phys.* **2011**, *125*, 174–183. [CrossRef]
55. Tang, Y.; Lewin, M. Migration and surface modification in polypropylene (PP)/polyhedral oligomeric silsequioxane (POSS) nanocomposites. *Polym. Adv. Technol.* **2009**, *20*, 1–15. [CrossRef]
56. Charles, M. *Hansen Solubility Parameters: A User's Handbook*, 2nd ed.; CRC Press: Boca Raton, FL, USA, 2007.
57. Paseta, L.; Potier, G.; Abbott, S.; Coronas, J. Using Hansen solubility parameters to study the encapsulation of caffeine in MOFs. *Org. Biomol. Chem.* **2014**, *13*, 1724–1731. [CrossRef]
58. Milliman, H.W.; Boris, D.; Schiraldi, D.A. Experimental Determination of Hansen Solubility Parameters for Select POSS and Polymer Compounds as a Guide to POSS–Polymer Interaction Potentials. *Macromolecules* **2012**, *45*, 1931–1936. [CrossRef]
59. Krishnamurthy, S.; Bansil, R. Nucleation and Growth in a Polymer Solution. *Phys. Rev. Lett.* **1983**, *50*, 2010–2013. [CrossRef]
60. Butola, B.S.; Joshi, M.; Kumar, S. Hybrid organic-inorganic POSS (polyhedral oligomeric silsesquioxane)/polypropylene nanocomposite filaments. *Fibers Polym.* **2010**, *11*, 1137–1145. [CrossRef]
61. Lotz, B. α and β phases of isotactic polypropylene: A case of growth kinetics 'phase reentrency' in polymer crystallization. *Polymer* **1998**, *39*, 4561–4567. [CrossRef]
62. Tordjeman, P.; Robert, C.; Marin, G.; Gerard, P. The effect of α, β crystalline structure on the mechanical properties of polypropylene. *Eur. Phys. J. E* **2001**, *4*, 459–465. [CrossRef]
63. Pracella, M.; Chionna, D.; Fina, A.; Tabuani, D.; Frache, A.; Camino, G. Polypropylene-POSS Nanocomposites: Morphology and Crystallization Behaviour. *Macromol. Symp.* **2006**, *234*, 59–67. [CrossRef]
64. Barczewski, M.; Dobrzyńska-Mizera, M.; Dutkiewicz, M.; Szołyga, M. Novel polypropyleneβ-nucleating agent with polyhedral oligomeric silsesquioxane core: Synthesis and application. *Polym. Int.* **2016**, *65*, 1080–1088. [CrossRef]
65. Barczewski, M.; Czarnecka-Komorowska, D.; Andrzejewski, J.; Sterzyński, T.; Dutkiewicz, M.; Dudziec, B. Właściwości Przetwórcze Termoplastycznych Tworzyw Polimerowych Modyfikowanych Silseskwioksanami (POSS). *Polim. Polym.* **2013**, *58*, 805–815. [CrossRef]
66. Bouza, R.; Barral, L.; Díez, F.J.; López, J.; Montero, B.; Rico, M.; Ramírez, C. Study of thermal and morphological properties of a hybrid system, iPP/POSS. Effect of flame retardance. *Compos. Part B Eng.* **2014**, *58*, 566–572. [CrossRef]
67. Chen, G.; Feng, B.; Zhu, K.; Zhao, Y.; Yuan, X. Effect of polyhedral oligomeric silsesquioxane and sorbitol on properties of isotactic polypropylene. *Chem. Res. Chin. Univ.* **2015**, *31*, 303–307. [CrossRef]
68. Zhou, Z.; Zhang, Y.; Zeng, Z.; Zhang, Y. Properties of POSS-filled polypropylene: Comparison of physical blending and reactive blending. *J. Appl. Polym. Sci.* **2008**, *110*, 3745–3751. [CrossRef]
69. Camino, G.; Lomakin, S.M.; Lageard, M. Thermal polydimethylsiloxane degradation. Part 2. The degradation mechanisms. *Polymer* **2002**, *43*, 2011–2015. [CrossRef]
70. Blazsó, M. *Pyrolysis for Recycling Waste Composites*; Goodship, V., Ed.; Woodhead Publishing Series in Composites Science and Engineering, Management, Recycling and Reuse of Waste Composites; Woodhead Publishing: Cambridge, UK, 2010; pp. 102–121.
71. Kundie, F.; Azhari, C.H.; Muchtar, A.; Ahmad, Z.A. Effects of Filler Size on the Mechanical Properties of Polymer-filled Dental Composites: A Review of Recent Developments. *J. Phys. Sci.* **2018**, *29*, 141–165. [CrossRef]
72. Omar, M.F.; Akil, H.M.; Ahmad, Z.A. Particle size—Dependent on the static and dynamic compression properties of polypropylene/silica composites. *Mater. Des.* **2013**, *45*, 539–547. [CrossRef]
73. Mansha, M.; Gauthier, C.; Gérard, P.; Schirrer, R. The effect of plasticization by fatty acid amides on the scratch resistance of PMMA. *Wear* **2011**, *271*, 671–679. [CrossRef]
74. Sivakumar, G.; Jackson, J.; Ceylan, H.; Sundararajan, S. Effect of plasticizer on the wear behavior and ice adhesion of elastomeric coatings. *Wear* **2019**, *426-427*, 212–218. [CrossRef]
75. Kitano, T.; Kataoka, T.; Shirota, T. An empirical equation of the relative viscosity of polymer melts filled with various inorganic fillers. *Rheol. Acta* **1981**, *20*, 207–209. [CrossRef]
76. Swapna, V.P.; Kaliyathan, A.V.; Abhisha, V.S.; Maria, H.J.; Nambissan, P.M.G.; Thomas, S.; Stephen, R. Changes in free volume and gas permeation properties of poly(vinyl alcohol) nanocomposite membranes modified using cage-structured polyhedral oligomeric silsesquioxane. *J. Appl. Polym. Sci.* **2021**, *138*. [CrossRef]
77. Perilla, J.E.; Lee, B.-J.; Jana, S. Rheological investigation of interactions between sorbitol and polyhedral oligomeric silsesquioxane in development of nanocomposites of isotactic polypropylene. *J. Rheol.* **2010**, *54*, 761. [CrossRef]

Supplementary Materials for

Why POSS-type compounds should be considered nanomodifiers, not nanofillers - a polypropylene blends case study

Dariusz Brząkalski[1], Robert E. Przekop[2]*, Bogna Sztorch[2], Miłosz Frydrych[1], Daria Pakuła[1], Marek Jałbrzykowski[3], Grzegorz Markiewicz[3], Bogdan Marciniec[1,2]*

[1] Faculty of Chemistry, Adam Mickiewicz University in Poznan, Poznan, Poland
[2] Centre for Advanced Technologies, Adam Mickiewicz University in Poznan, Poznan, Poland
[3] Bialystok University of Technology, Faculty of Mechanical Engineering, Wiejska 45 C, 15-351 Bialystok, Poland
* Correspondence: robert.przekop@amu.edu.pl (R.P.); bogdan.marciniec@amu.edu.pl (B.M.)

Table of contents:

1. Table of isolated compounds:

Structure	Compound #	Code
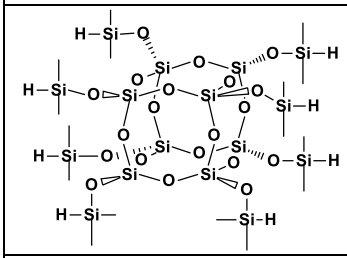	**1**	SS-H
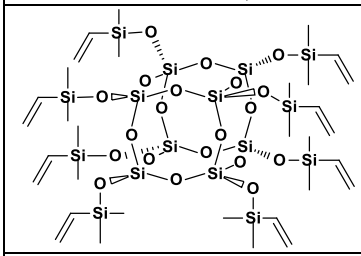	**2**	SS-Vi
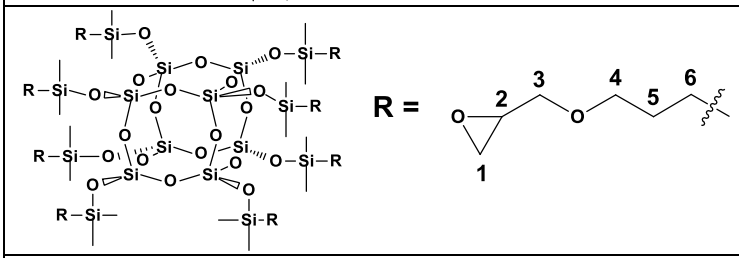	**3**	SS-Glycidyl
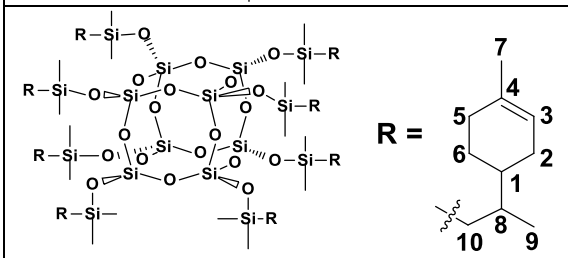	**4**	SS-Limonene
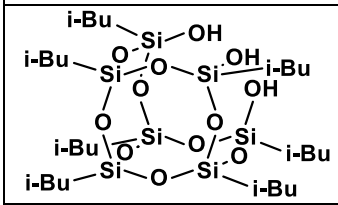	**5**	iBu$_7$SSQ-3OH
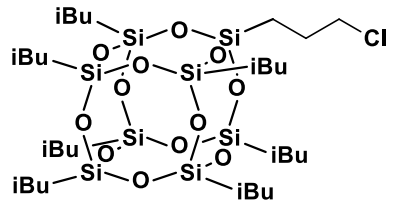	**6**	iBu$_7$SSQ-Cl
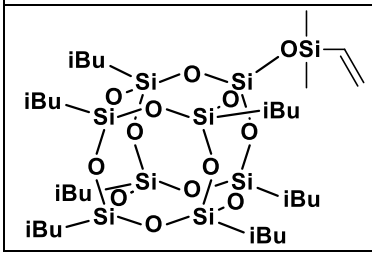	**7**	iBu$_7$SS-Vi

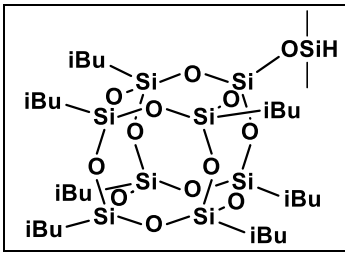	**8**	iBu_7SS-H

2. Additional Figures

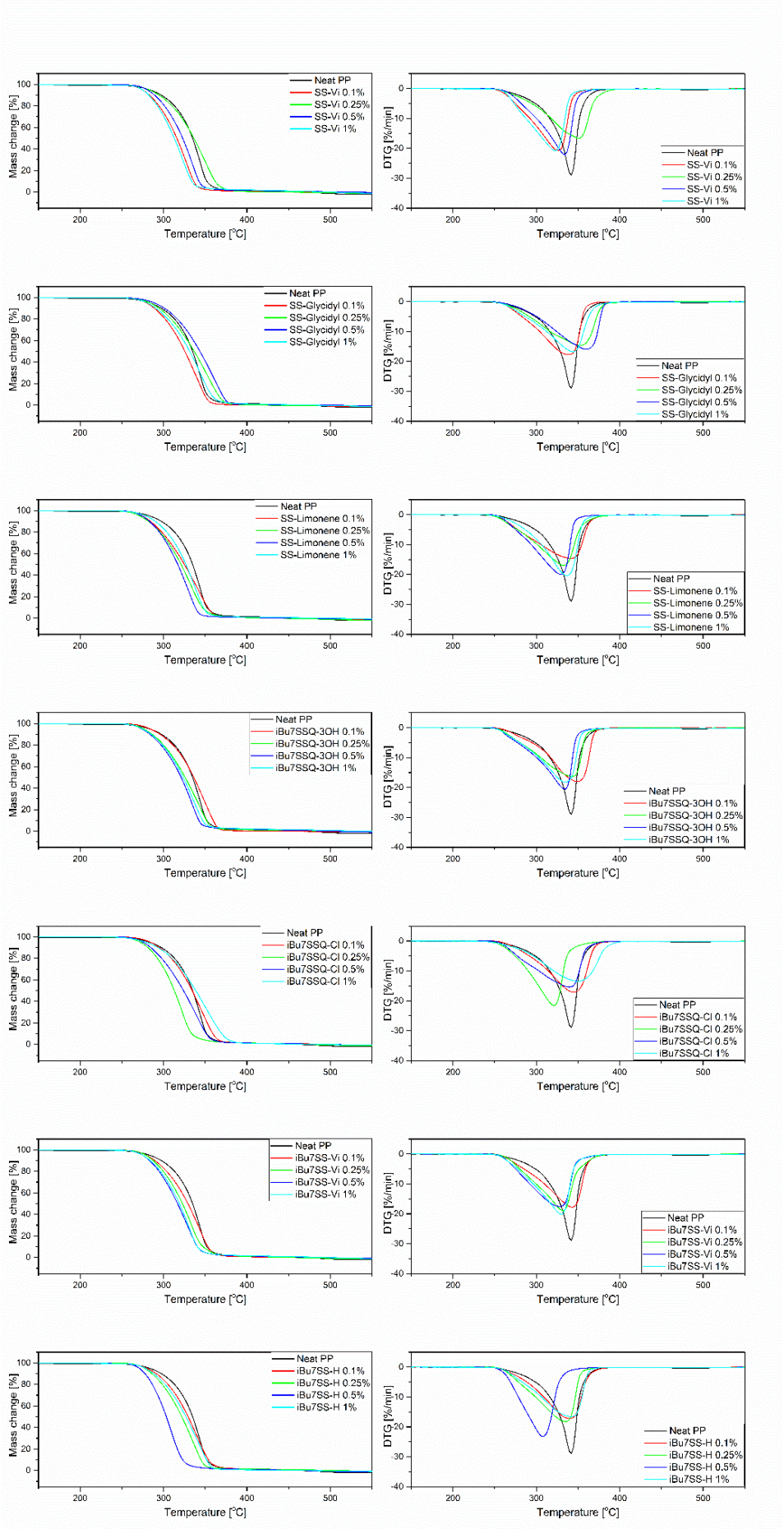

Figure S1: TGA thermograms of CS/iPP compositions.

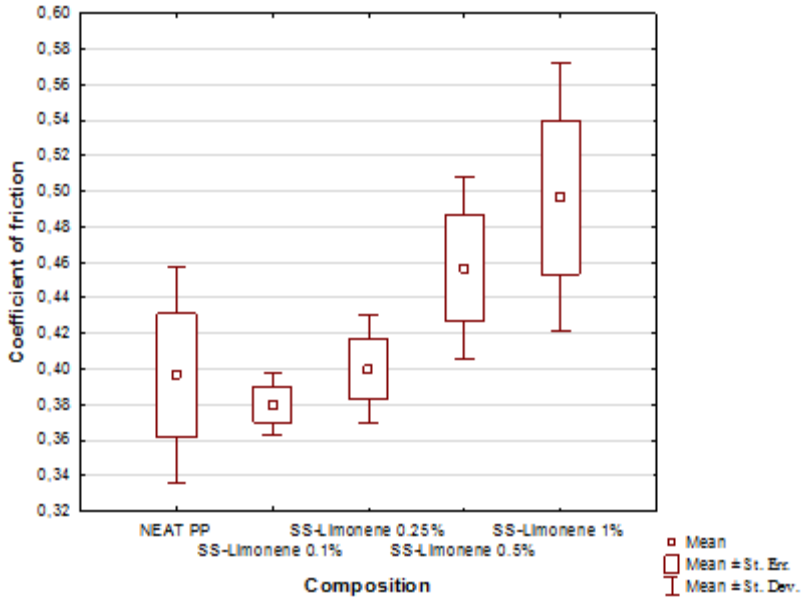

Figure S2. Coefficients of friction for SS-Limonene/iPP composites.

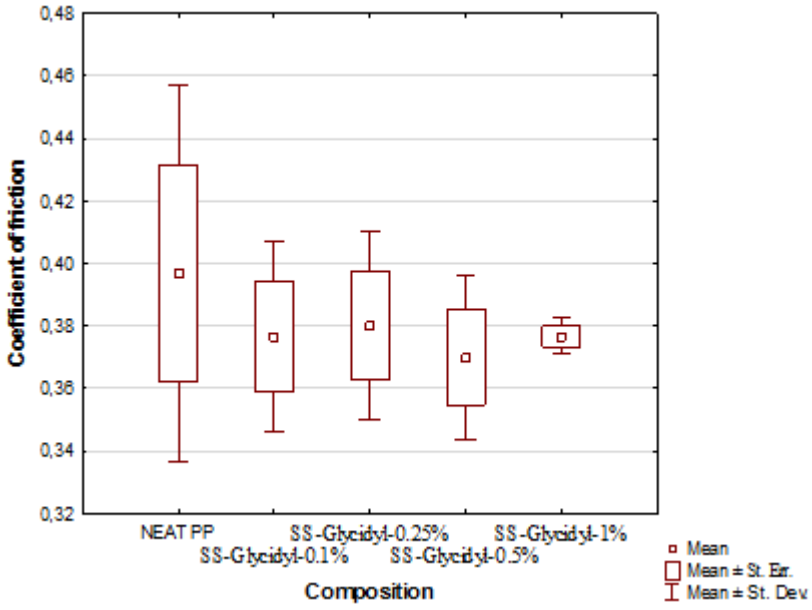

Figure S3. Coefficients of friction for SS-Glycidyl/iPP composites.

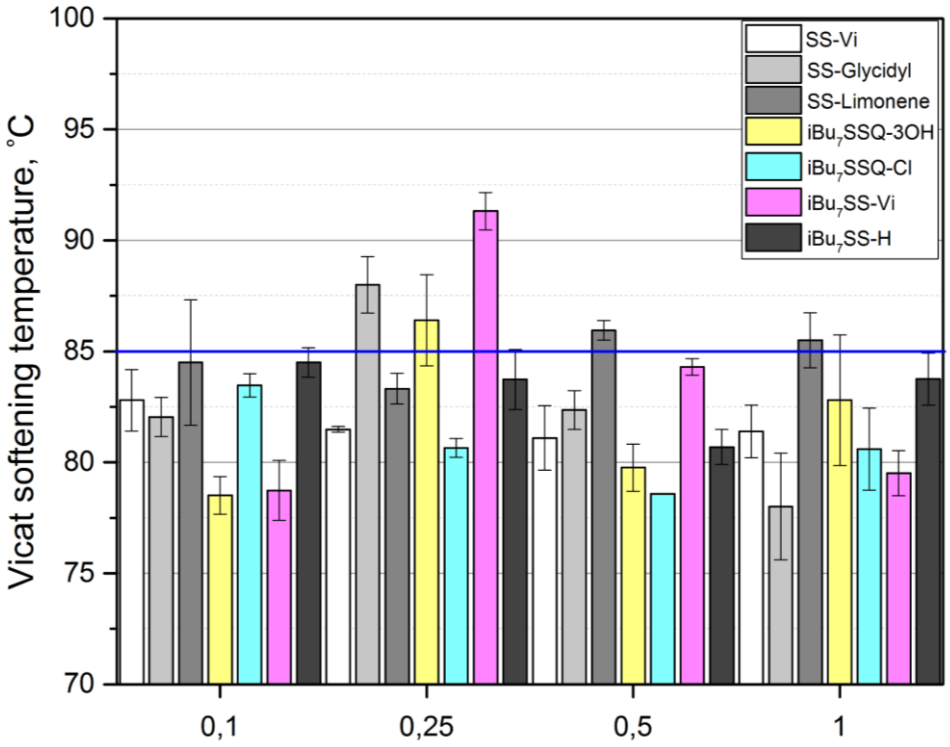

Figure S4. Vicat softening temperatures of the obtained CS/iPP composites.

3. Spectroscopic characterization of the products:

1,3,5,7,9,11,13,15-hepta(dimethylsiloxy)-pentacyclo[9.5.1.1^{3,9}.1^{5,15}.1^{7,13}]octasiloxane (1)

^{1}H NMR (400 MHz, $CDCl_3$): δ (ppm) = 4.73 (sep, J=2.8Hz, 8H, SiH), 0.26 (d, J=2.8Hz, 48H, $SiMe_2$);

^{13}C NMR (101 MHz, $CDCl_3$): δ (ppm) = 0.23 ($SiMe_2$);

^{29}Si NMR (79,5 MHz, $CDCl_3$): δ (ppm) = -1.41 ($SiMe_2$), -108.68 (core).

FT-IR (ATR): 2965, 2905, 2141, 1254, 1069, 889, 834, 769-726, 650, 628, 541.

^{1}H NMR *($CDCl_3$, 400MHz):*

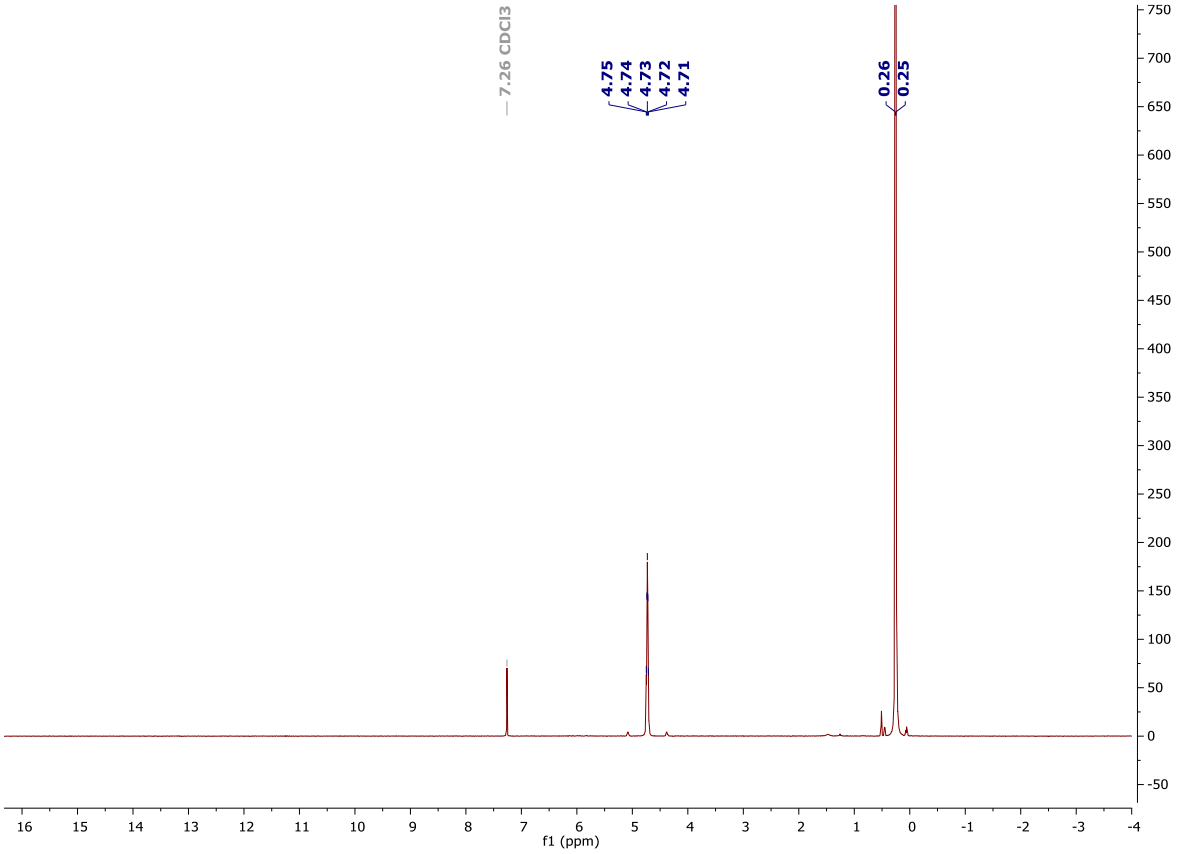

^{13}C NMR (101 MHz, $CDCl_3$)

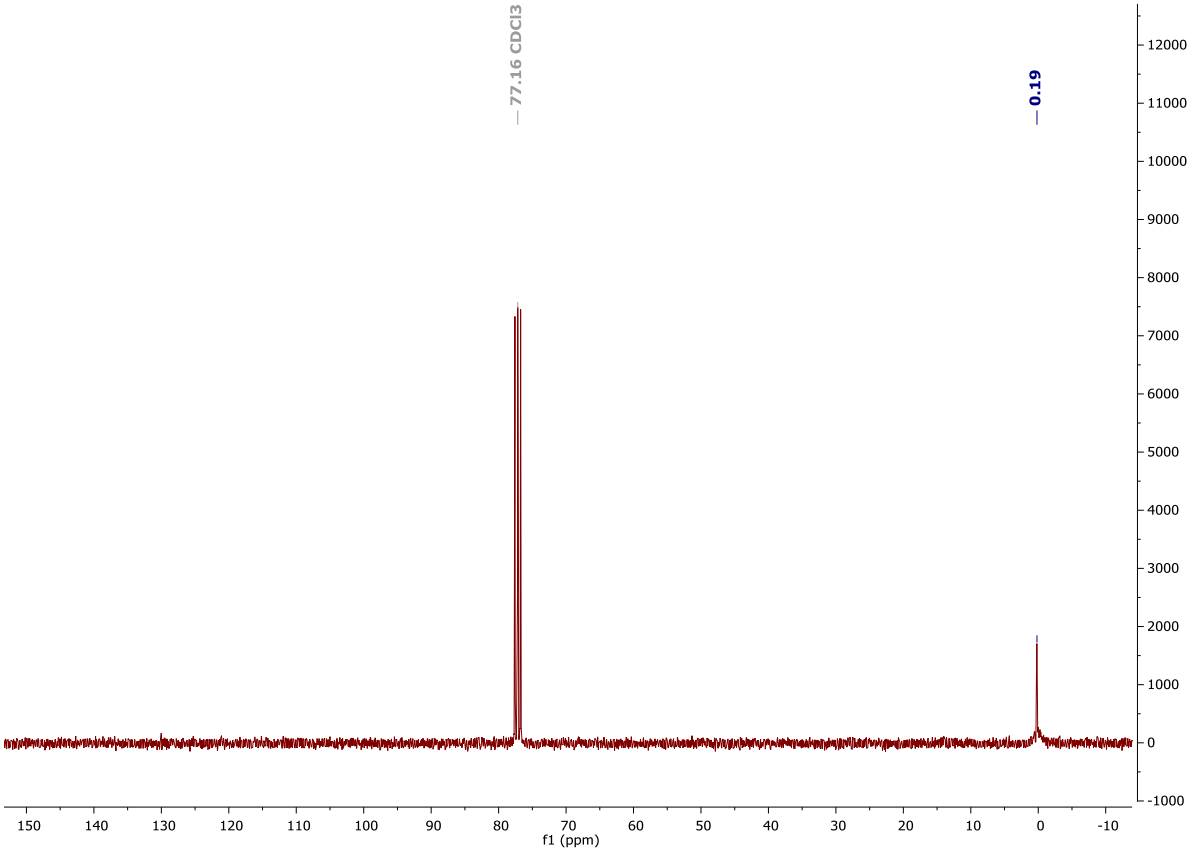

^{29}Si NMR (79,5 MHz, $CDCl_3$)

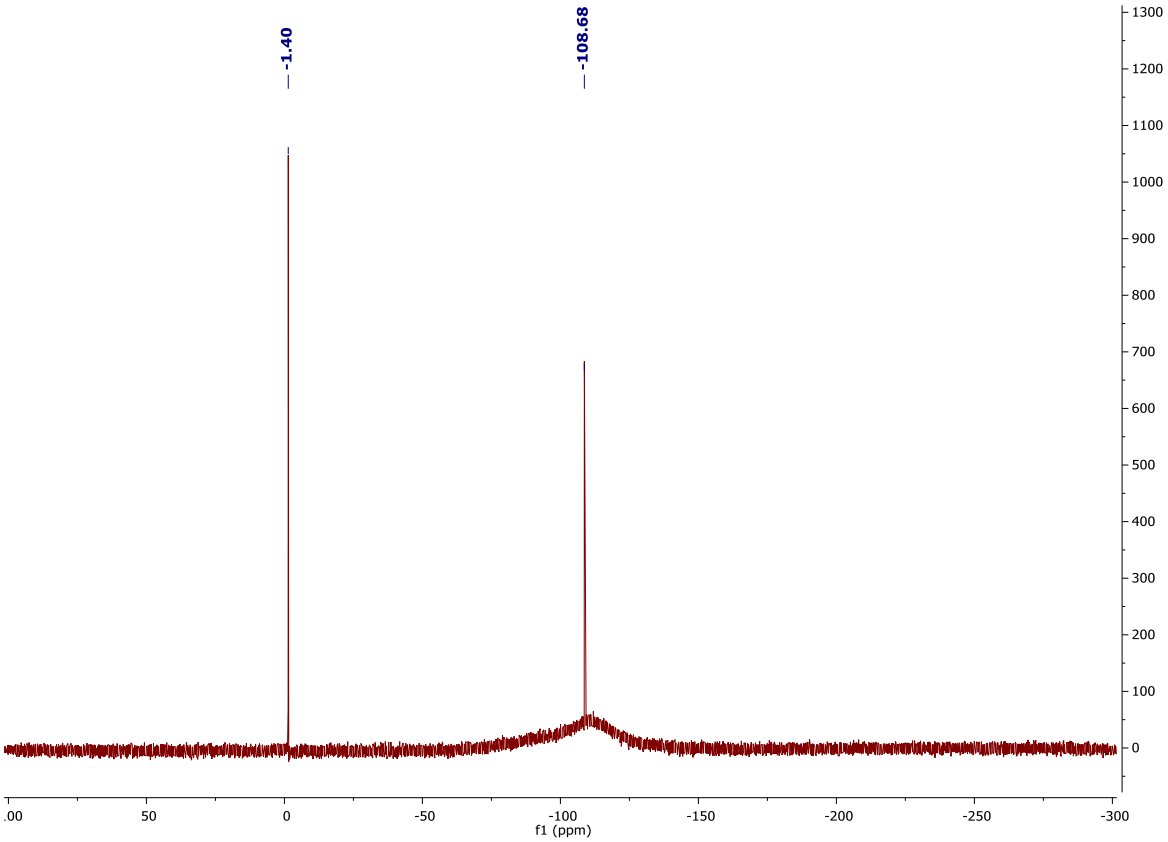

1,3,5,7,9,11,13,15-octa(dimethylvinylsiloxy)-pentacyclo[9.5.1.1^{3,9}.1^{5,15}.1^{7,13}]octasiloxane (2)

^{1}H NMR (400 MHz, $CDCl_3$): δ (ppm) = 6.13 (dd, J_1=20.2Hz, J_2=14.9Hz, 8H, -C<u>H</u>=CH_2), 5.96 (dd, J_1=14.9Hz, J_2=4.0Hz, 8H, -CH=C<u>H$_2$</u>), 5.79 (dd, J1=20.2Hz, J2=4.0Hz, 8H, -CH=C<u>H$_2$</u>), 0.21 (s, 48H, $SiMe_2$);
^{13}C NMR (101 MHz, $CDCl_3$): δ (ppm) = 138.09, 132.61 (-CH=CH_2), -00.06 ($SiMe_2$);
^{29}Si NMR (79,5 MHz, $CDCl_3$): δ (ppm) = 0.51 ($SiMe_2$), -109.14 (core).
FT-IR (ATR): 3068, 3027, 2988, 2962, 1603, 1408, 1276, 1081, 1002, 967, 775, 568.

^{1}H NMR *($CDCl_3$, 400MHz):*

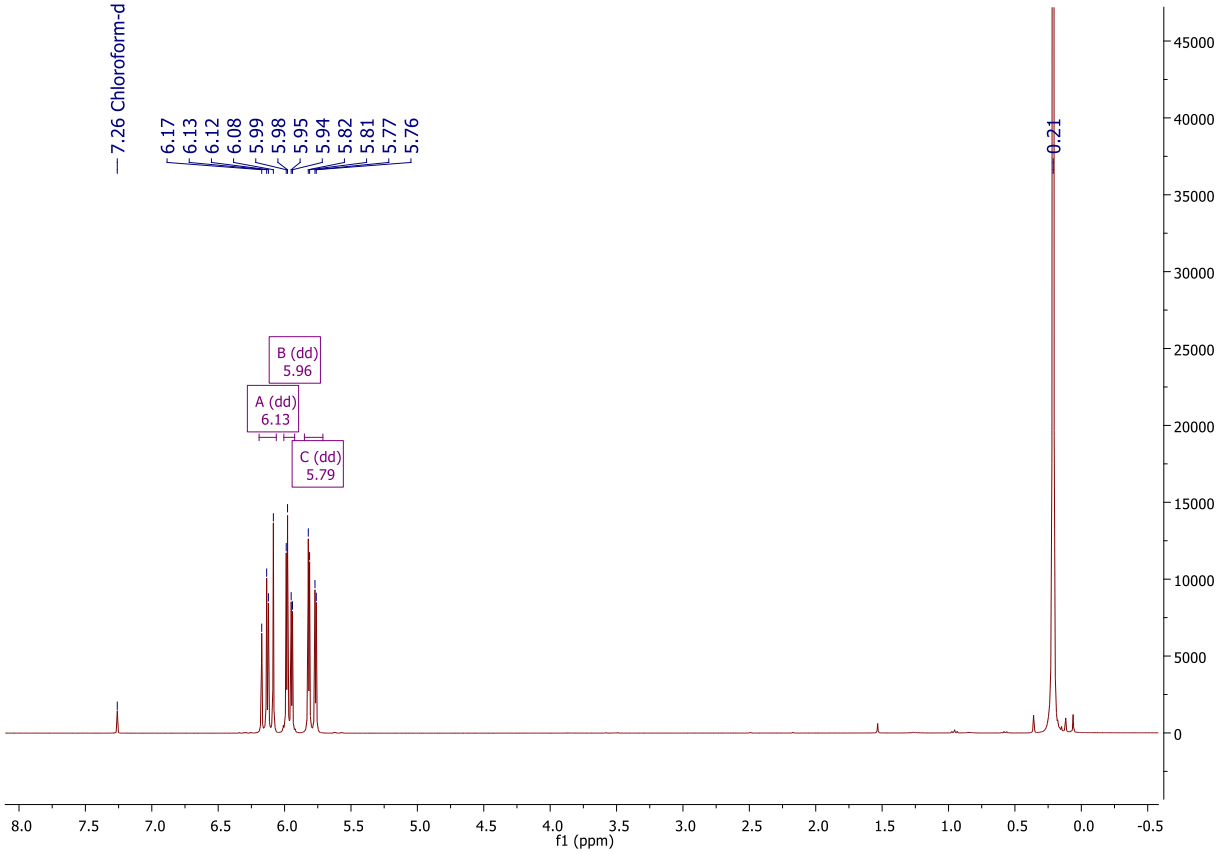

^{13}C NMR *($CDCl_3$, 101 MHz):*

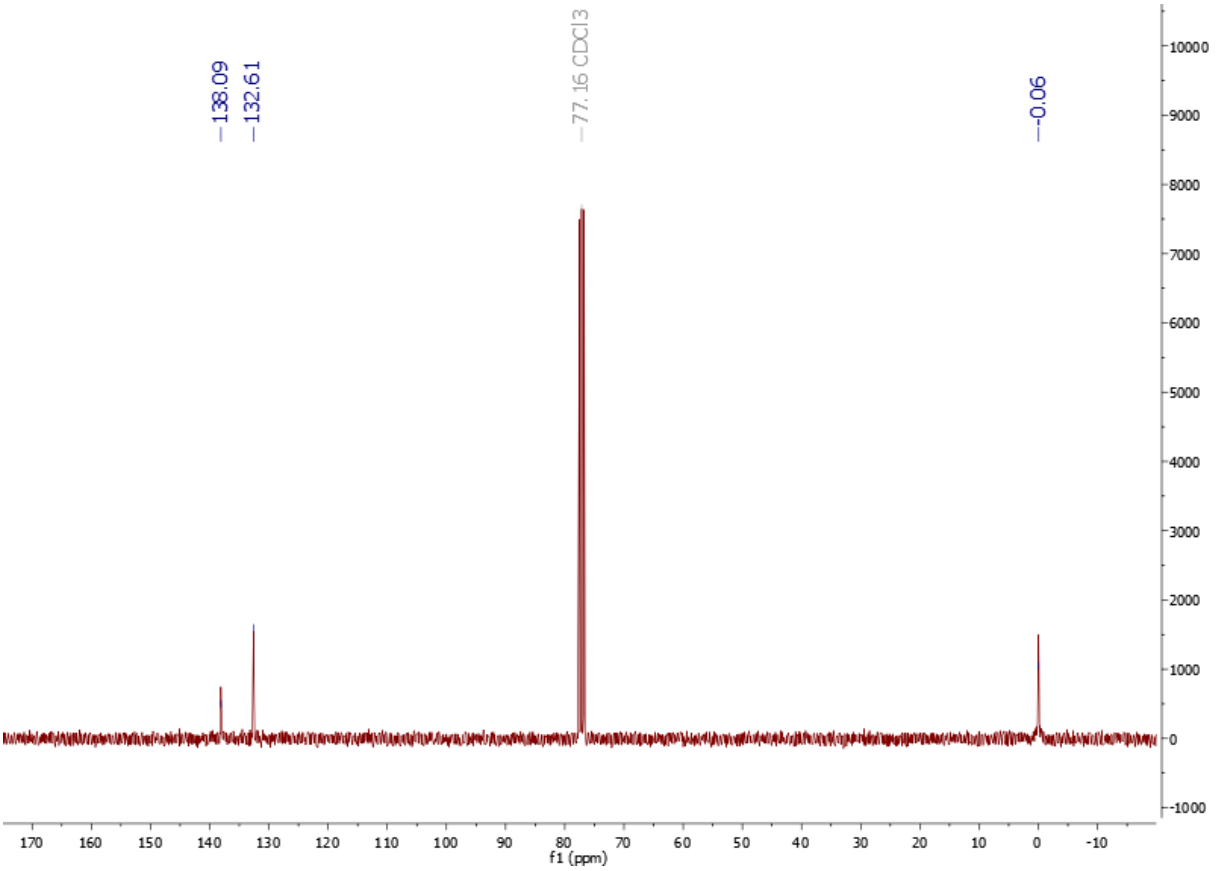

^{29}Si NMR *($CDCl_3$, 79.5 MHz):*

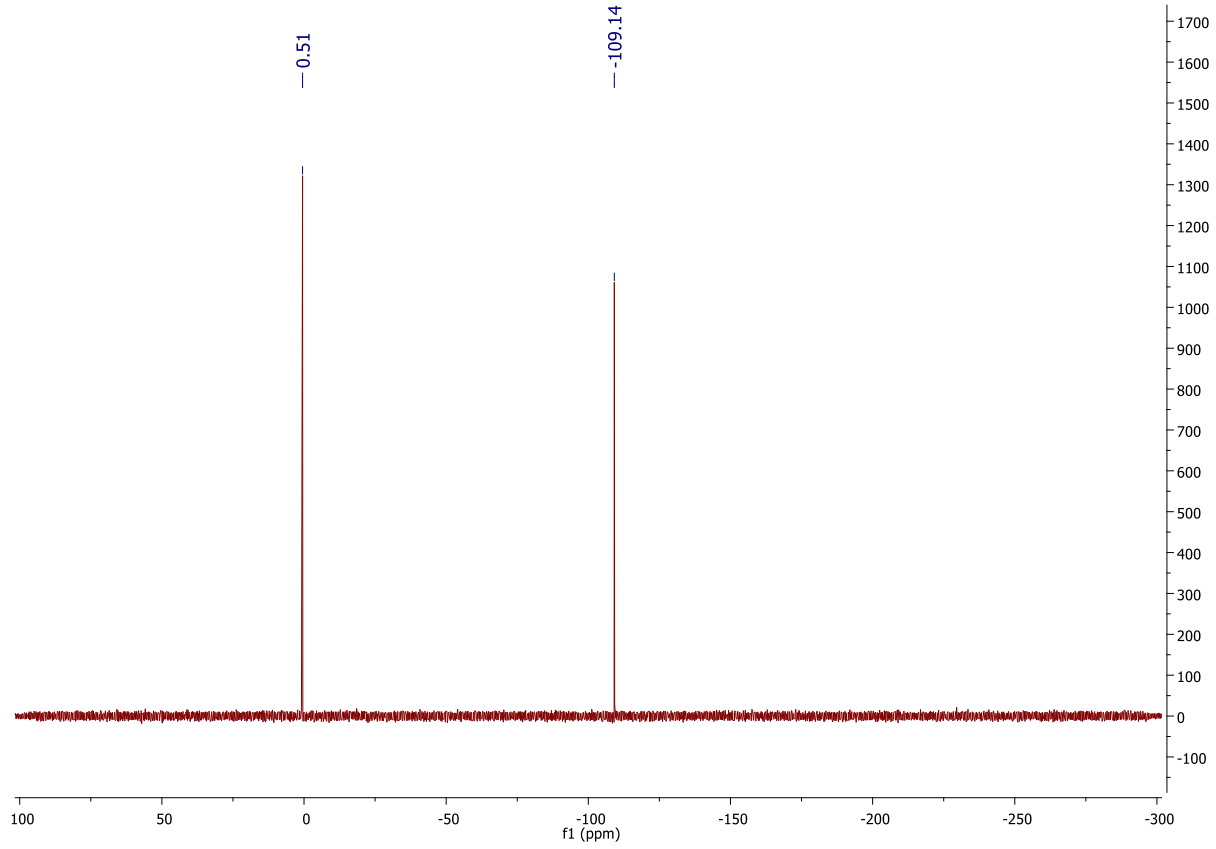

1,3,5,7,9,11,13,15-octa((3-glycidoxypropyl)dimethylsiloxy)-pentacyclo[9.5.1.1^{3,9}.1^{5,15}.1^{7,13}]octasiloxane (3)

^{1}H NMR (400 MHz, $CDCl_3$): δ (ppm) = 3.70-3.67 (m, 8H position 3), 3.48-3.40 (m, 16H, position 4), 3.39-3.36 (m, 8H, position 3), 3.14-3.11 (m, 8H, position 2), 2.79-2.77 (m, 8H, position 1), 2.60-2.59 (m, 8H, position 1), 1.65-1.60 (m, 16H, position 5), 0.62-0.58 (m, 16H, position 6), 0.14 (s, 48H, $SiMe_2$);
^{13}C NMR (101 MHz, $CDCl_3$): δ (ppm) = 74.23 (position 4), 71.58 (position 3), 50.96 (posirion 2), 44.44 (position 1), 23.31 (position 5), 13.80 (position 6)(glycidoxypropyl\1 group), -0.25 ($SiMe_2$);
^{29}Si NMR (79,5 MHz, $CDCl_3$): δ (ppm) = 12.92 ($SiMe_2$), -109.09 (core).
FT-IR (ATR): 3053, 2996-2870, 1479-1390, 1343, 1253, 1160-1070, 909-729, 631, 546.

^{1}H NMR *($CDCl_3$, 400MHz):*

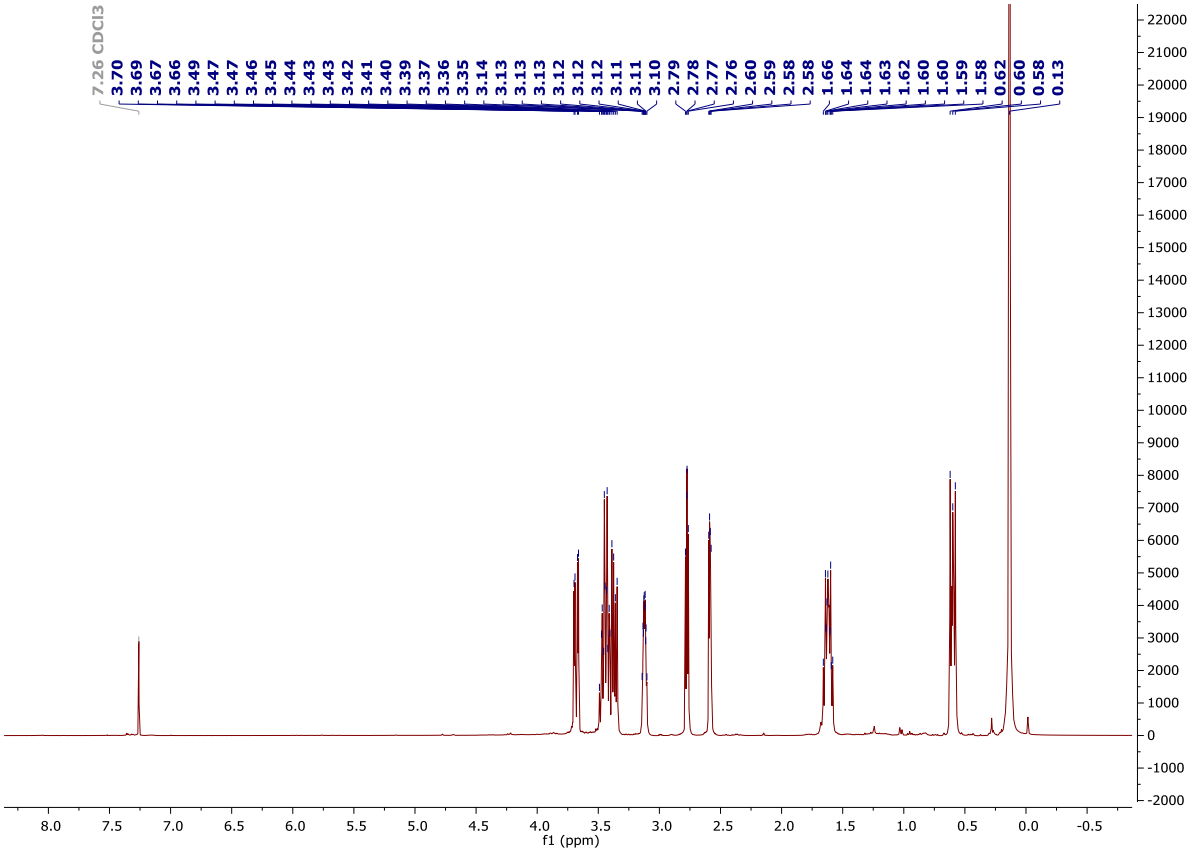

^{13}C NMR *($CDCl_3$, 101 MHz):*

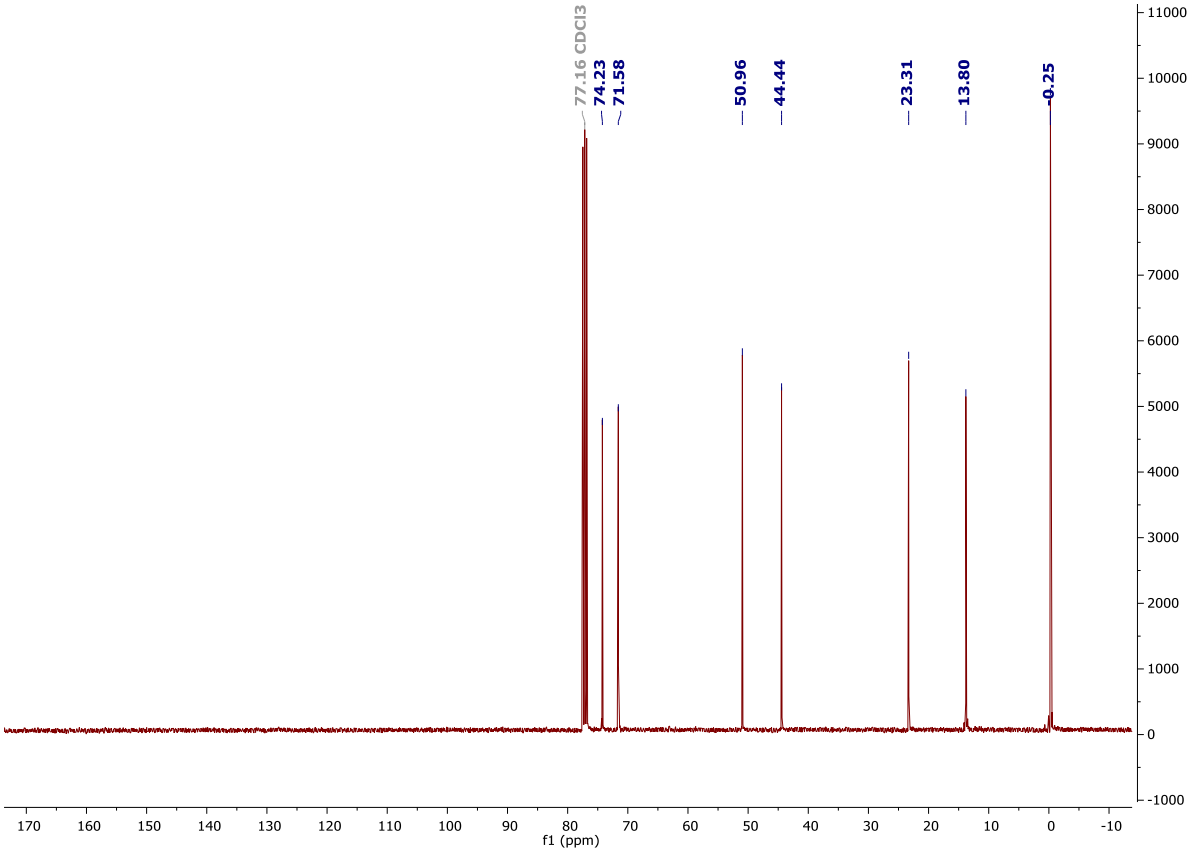

^{29}Si NMR *($CDCl_3$, 79.5 MHz):*

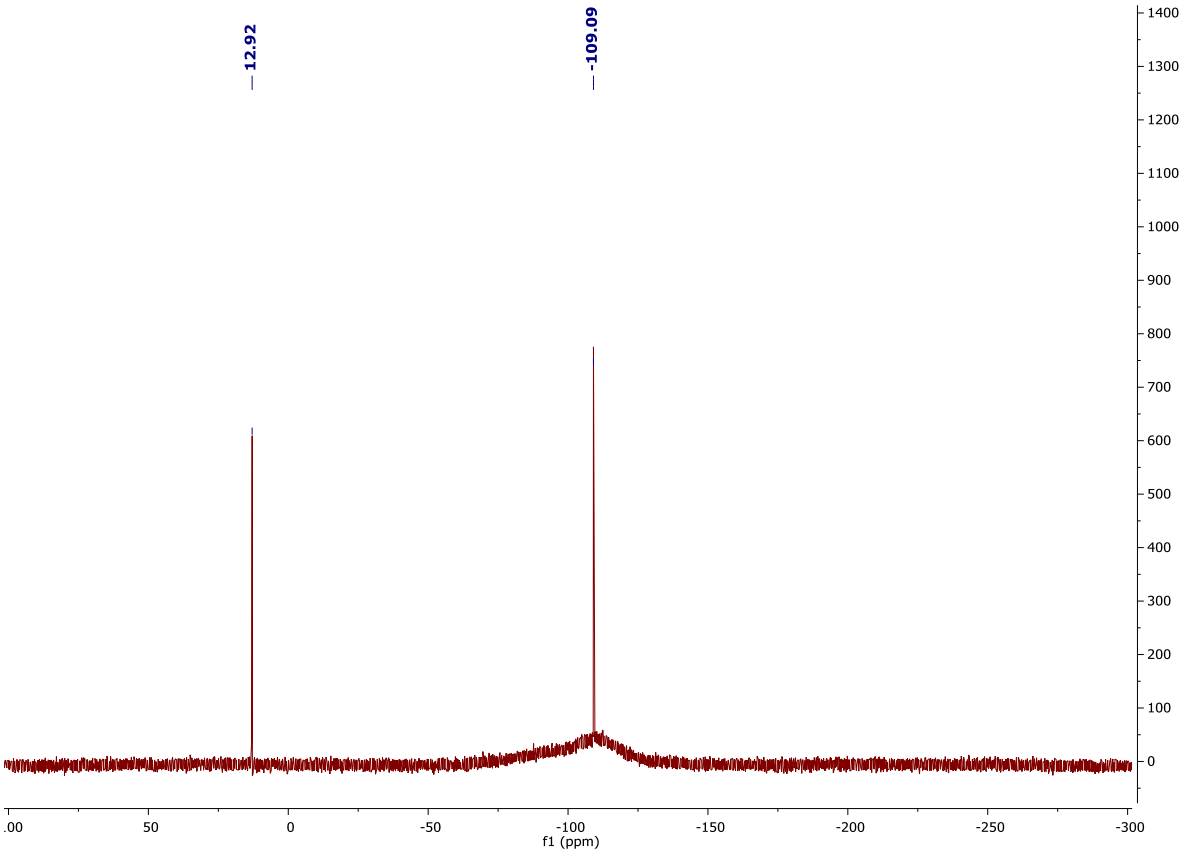

1,3,5,7,9,11,13,15-octa(dimethyl((2-(4-methylcyclohex-3-en-1-yl)propyl)silyl)-pentacyclo[9.5.1.1^{3,9}.1^{5,15}.1^{7,13}]octasiloxane (4)

^{1}H NMR (400 MHz, $CDCl_3$): δ (ppm) = 5.36 (s, 8H, position **3**), 2.00-1.87 (m, 24H, positions **1, 2, 5**), 1.78-1.56 (m, 24H, positions **2, 5, 8**), 1.63 (s, 24H, position **7**), 1.34-1.18 (m, 16H, position **6**), 0.90 (d, 24H, position **9**), 0.75-0.69 (m, 8H, position **10**), 0.52-0.44 (m, 8H, position **10**), 0.15 (s, 48H, $SiMe_2$);
^{13}C NMR (101 MHz, $CDCl_3$): δ (ppm) = 133.96, 121.28, 121.26, 41.48, 41.33, 33.08, 32.93, 31.19, 31.12, 28.80, 28.24, 26.71, 25.71, 23.64, 23.63, 22.87, 22.48, 19.52, 19.22, 0.83, 0.72, 0.66;
^{29}Si NMR (79,5 MHz, $CDCl_3$): δ (ppm) = 12.78 ($SiMe_2$), -109.10 (core).
FT-IR (ATR): 2980-2867, 1252, 1169-1069, 869-734, 549.

^{1}H NMR *($CDCl_3$, 400MHz):*

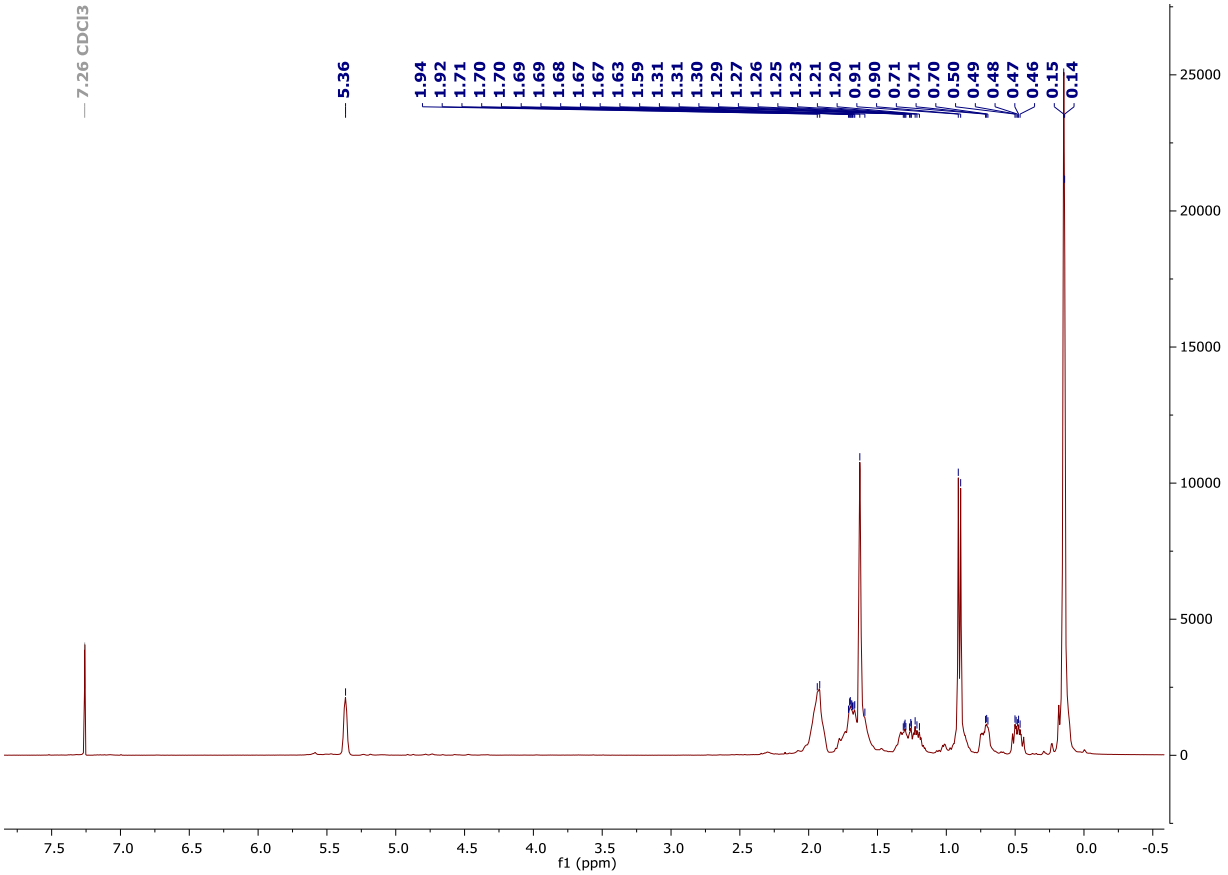

^{13}C NMR *($CDCl_3$, 101 MHz):*

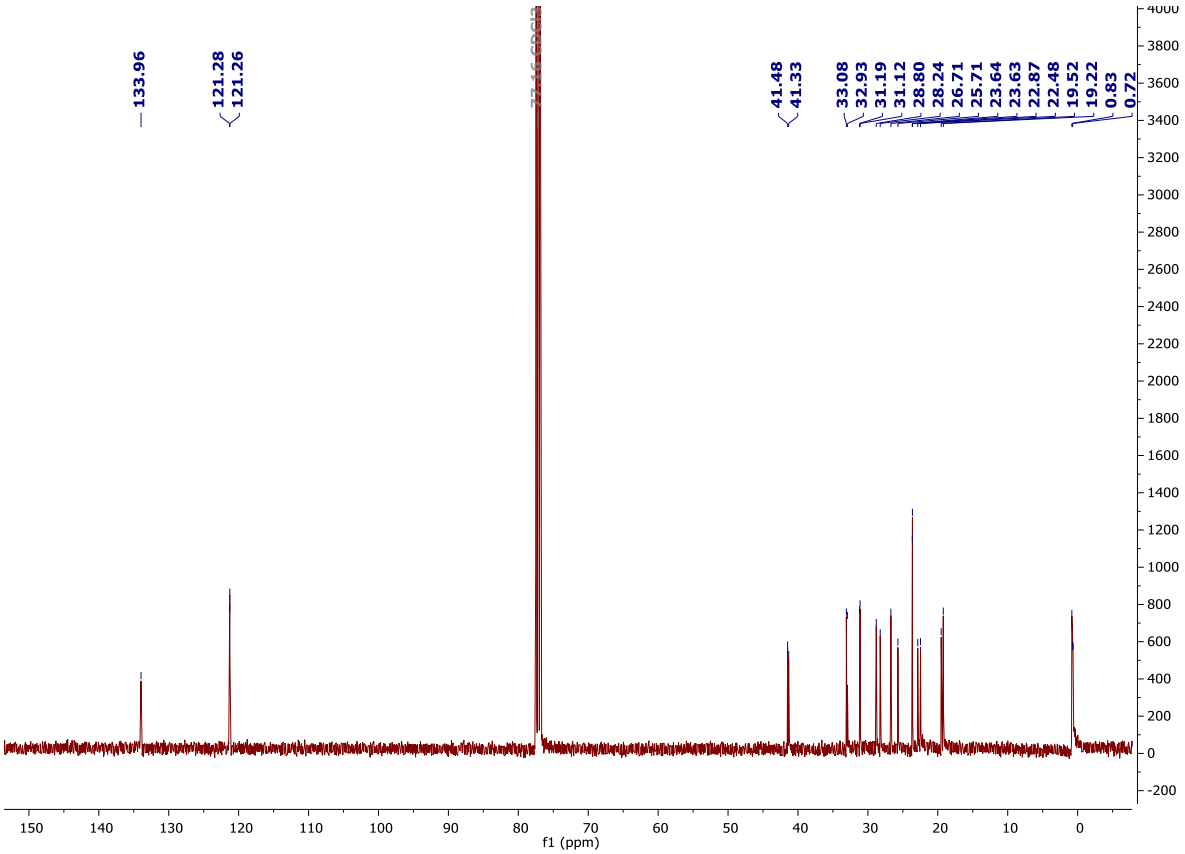

^{29}Si NMR *($CDCl_3$, 79.5 MHz):*

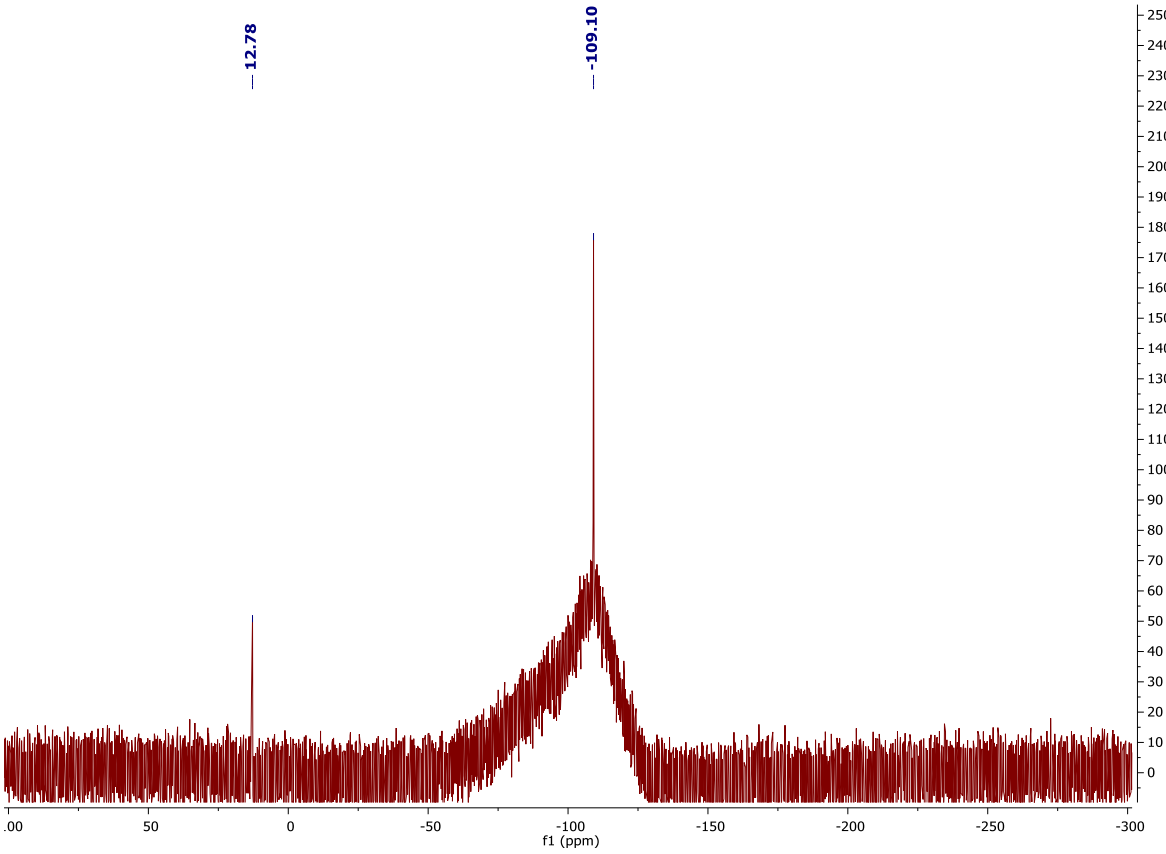

1,3,5,7,9,11,13-heptaisobutyltricyclo[5.5.1.1^{3,9}.1^{7,13}]heptasiloxane-1,5,13-triol (5)

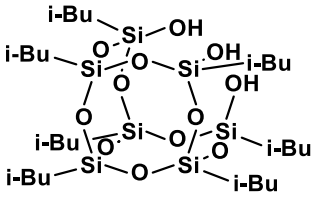

^{1}H NMR (400 MHz, $CDCl_3$): δ (ppm) = 6.83 (s, 3H, -OH), 1.92-1.77 (m, 7H, (-CH_2C<u>H</u>(CH_3)$_2$), 0.97-0.94 (m, 42H, -CH_2CH(C<u>H</u>$_3$)$_2$), 0.61-0.56 (m, 14H, -C<u>H$_2$</u>CH(CH_3)$_2$);
^{13}C NMR (101 MHz, $CDCl_3$): δ (ppm) = 25.94, 25.90, 25.80, 24.10, 24.07, 23.36, 22.98, 22.63;
^{29}Si NMR (79,5 MHz, $CDCl_3$): δ (ppm) = -58.82, -67.46, -68.66.
FT-IR (ATR) = 2953, 2928, 2906, 2871, 1464, 1398, 1383, 1366, 1332, 1228, 1168, 1085, 955, 838, 804, 746, 683, 556.

^{1}H NMR *($CDCl_3$, 400MHz):*

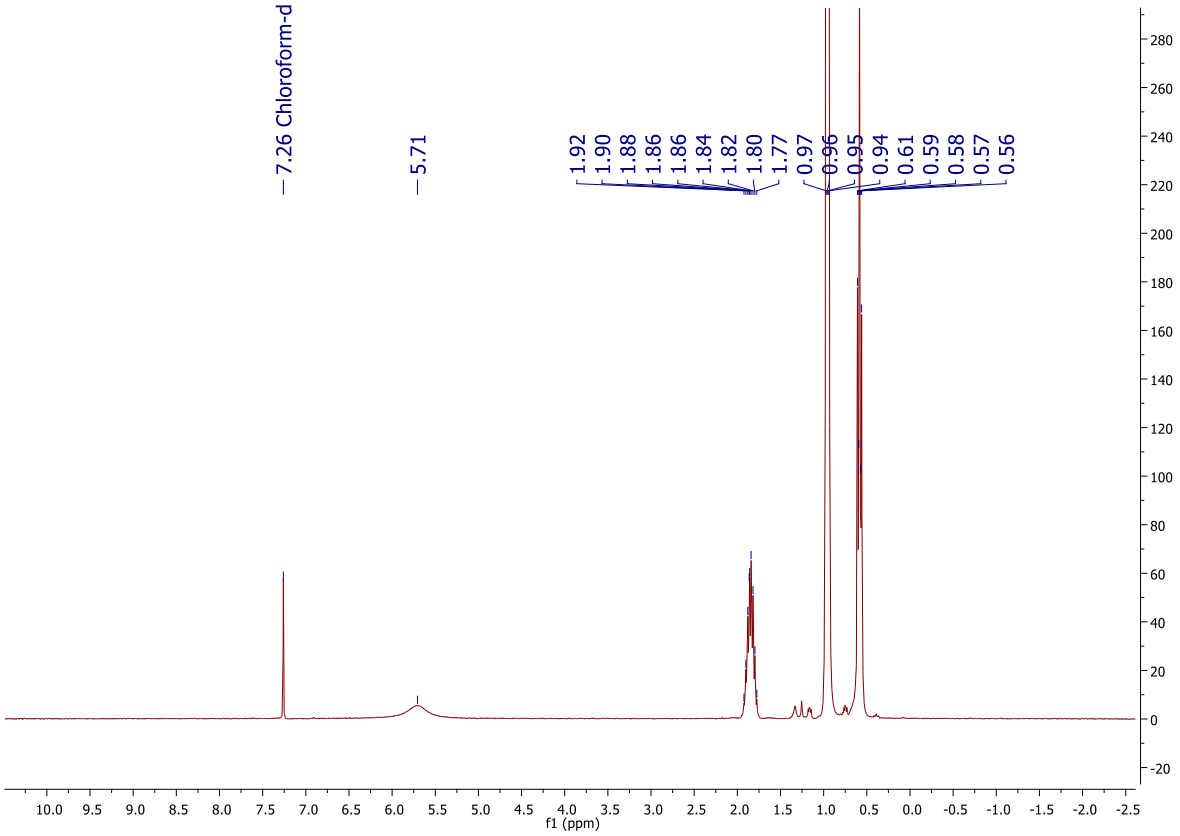

^{13}C NMR *($CDCl_3$, 101 MHz):*

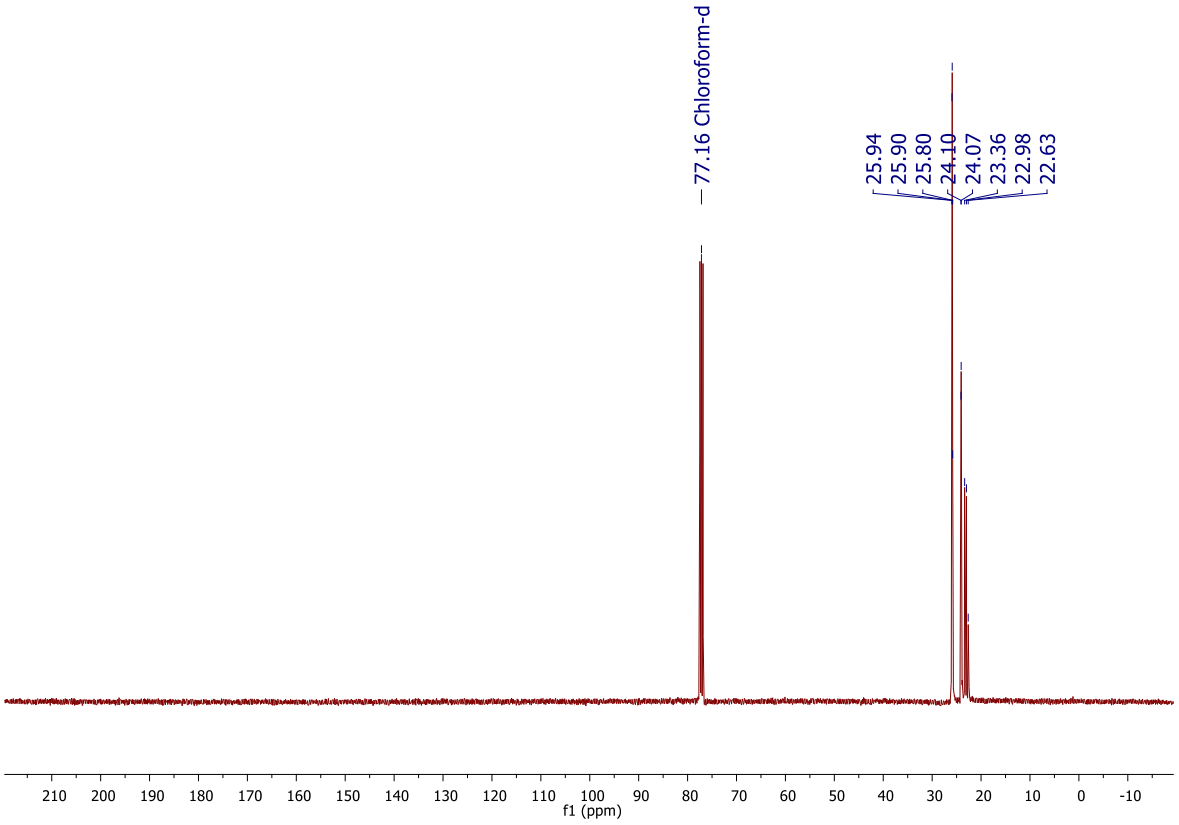

^{29}Si NMR *($CDCl_3$, 79.5 MHz):*

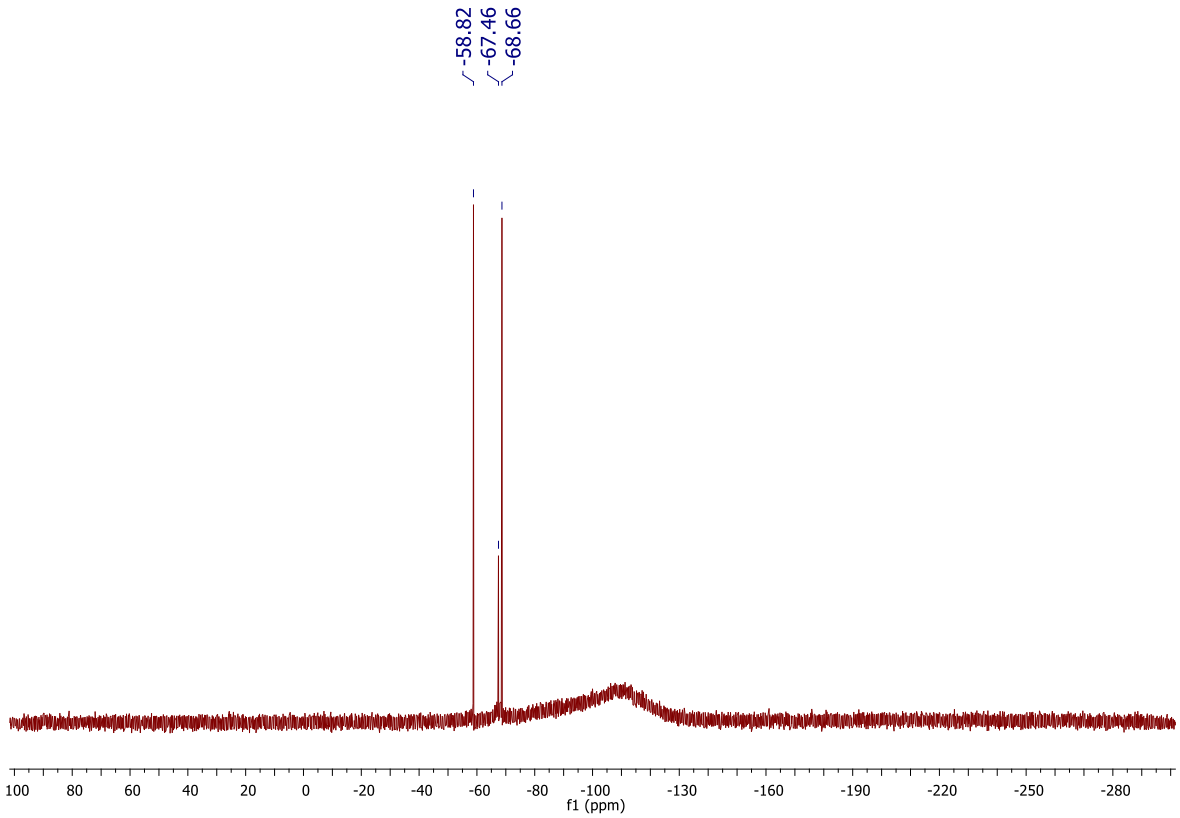

1-(3-chloropropyl)-3,5,7,9,11,13,15-heptaisobutylpentacyclo[9.5.1.1^{3,9}.1^{5,15}.1^{7,13}]octasiloxane (6)

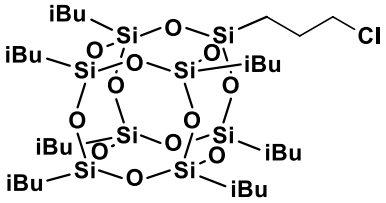

^{1}H NMR (400 MHz, $CDCl_3$): δ (ppm) = 3.52 (t, J = 8.1Hz, 2H, -$CH_2CH_2C\underline{H_2}$Cl), 1.92-1.79 (m, 9H, -$CH_2C\underline{H}(CH_3)_2$, -$CH_2C\underline{H_2}CH_2$Cl), 0.96 (d, J = 6.6Hz, 42H, -$CH_2CH(C\underline{H_3})_2$), 0.74 (t, J = 8.1Hz, 2H, -$C\underline{H_2}CH_2CH_2$Cl), 0.62-0.59 (m, 14H, -$C\underline{H_2}CH(CH_3)_2$);
^{13}C NMR (101 MHz, $CDCl_3$): δ (ppm) = 47.41 (-$CH_2CH_2\underline{CH_2}$Cl), 26.63 -$CH_2\underline{CH_2}CH_2$Cl), 25.85, 24.03, 22.65, 22.59 (iBu), 9.94 (-$C\underline{H_2}CH_2CH_2$Cl);
^{29}Si NMR (79,5 MHz, $CDCl_3$): δ (ppm) = -67.59, -67.87, -68.12.
FT-IR (ATR) = 2953, 2928, 2905, 2871, 1464, 1398, 1383, 1366, 1332, 1229, 1168, 1081, 955, 916, 838, 804, 745, 680, 556.

^{1}H NMR *($CDCl_3$, 400MHz):*

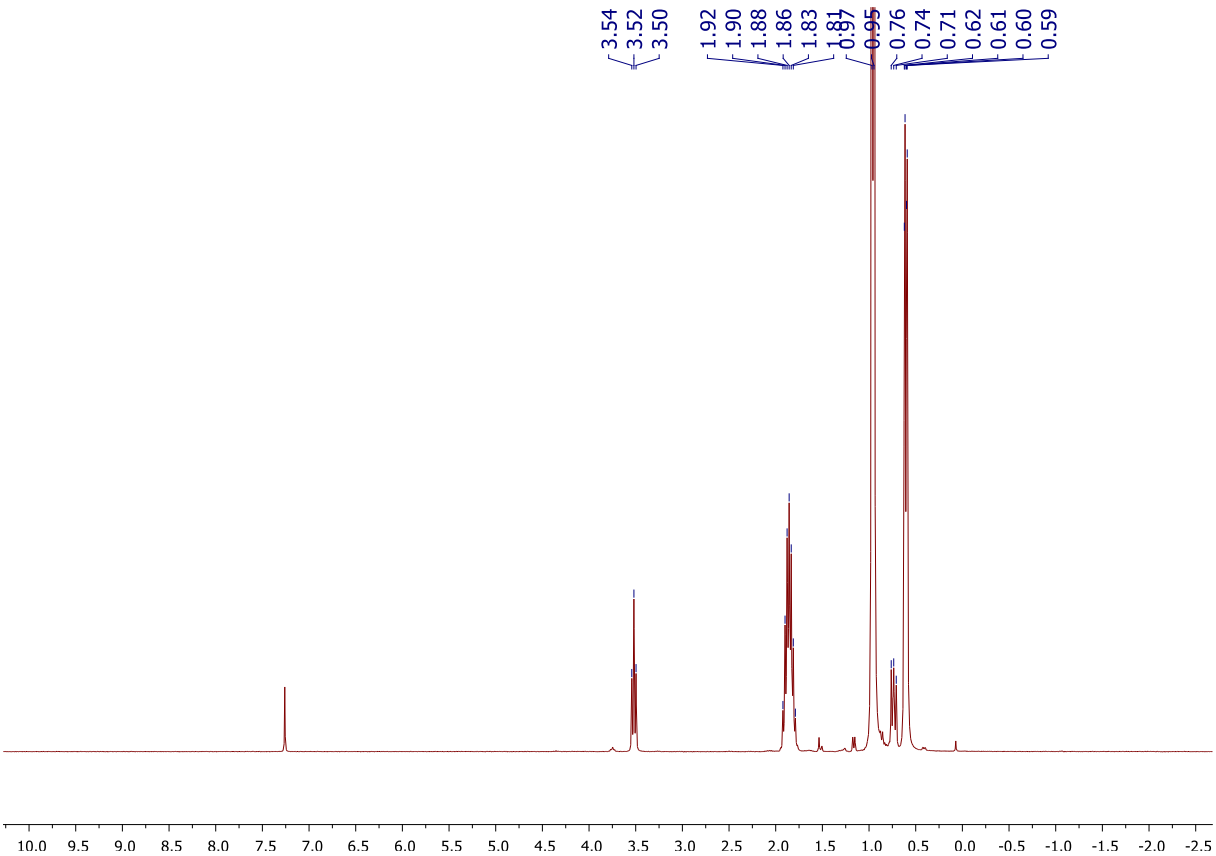

^{13}C NMR *($CDCl_3$, 101 MHz):*

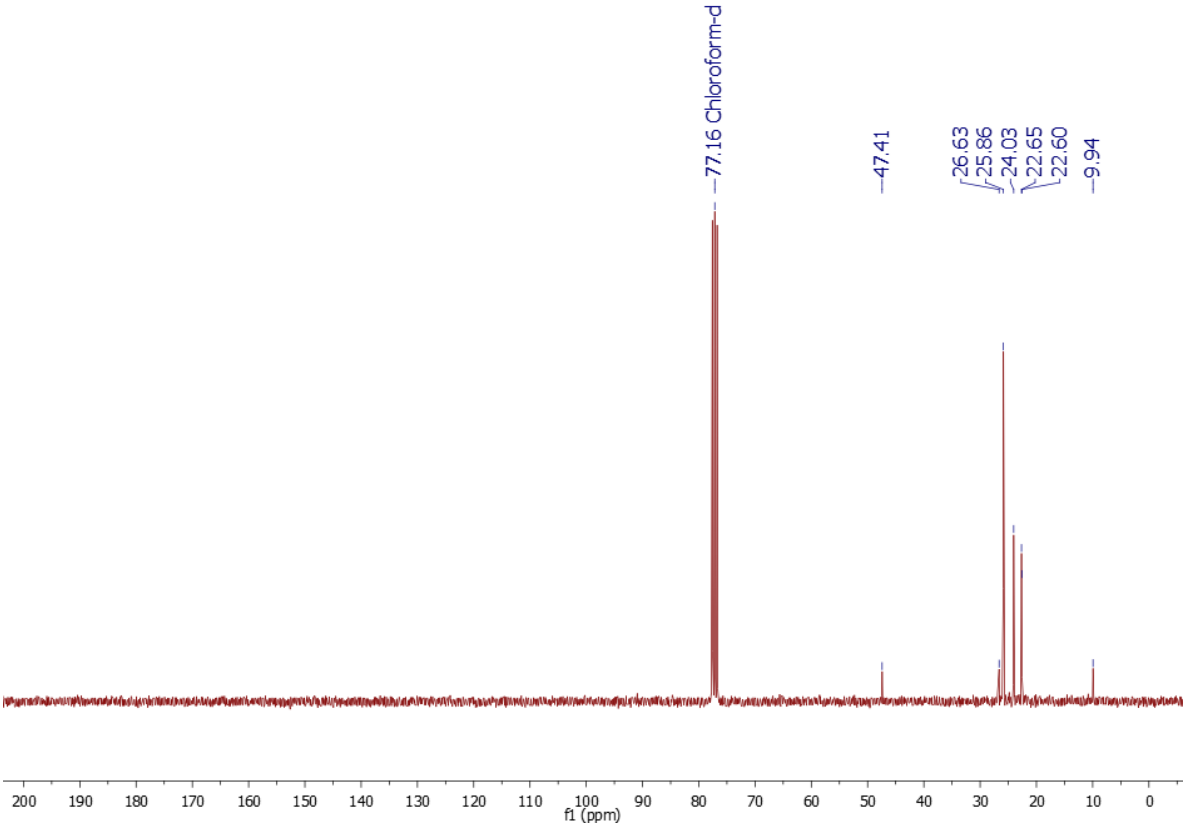

^{29}Si NMR *($CDCl_3$, 79.5 MHz):*

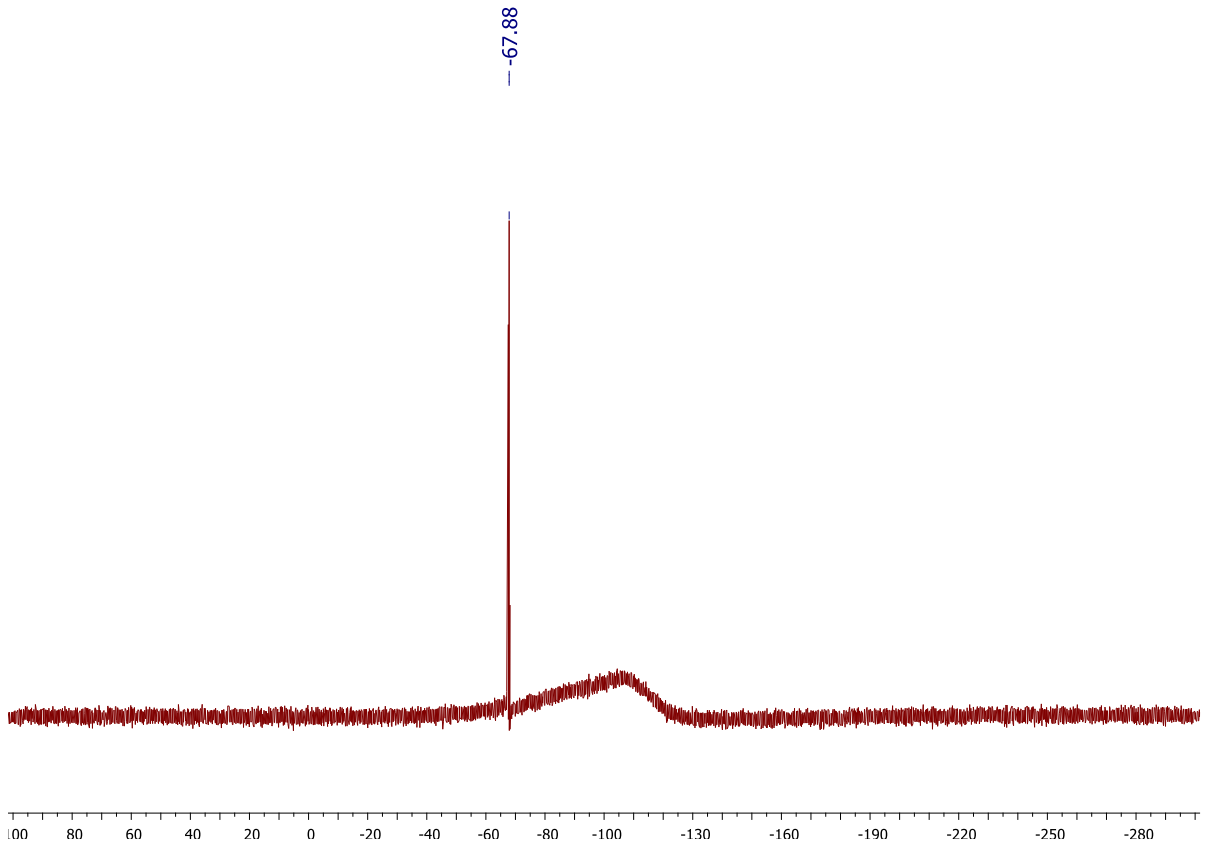

1-(dimethylvinylsiloxy)-3,5,7,9,11,13,15-heptaisobutylpentacyclo[9.5.1.1^{3,9}.1^{5,15}.1^{7,13}]octasiloxane (7)

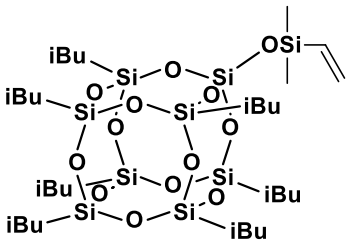

^{1}H NMR (400 MHz, $CDCl_3$): δ (ppm) = 6.12 (dd, J1 = 20.0Hz, J2 = 14.9Hz, 1H, -C<u>H</u>=CH_aH_b), 5.95 (dd, J1 = 14.9 Hz, J2 = 4.3Hz, 1H, -CH=C<u>H$_a$</u>H$_b$), 5.77 (dd, J1 = 20.0Hz, J2 = 4.3Hz, 1H, -CH=CH_a<u>H$_b$</u>), 1.93-1.79 (m, 7H, -CH_2C<u>H</u>(CH_3)$_2$), 0.96 (d, J = 6.6Hz, 42H. -CH_2CH(C<u>H$_3$</u>)$_2$), 0.62-0.59 (m, 14H, -C<u>H$_2$</u>CH(CH_3)$_2$), 0.19 (s, 6H, $SiMe_2$);
^{13}C NMR (101 MHz, $CDCl_3$): δ (ppm) = 138.50, 132.25 (Vi), 25.85, 25.82, 24.02, 23.96, 22.62, 22.57, 22.54, 22.45 (iBu), -0.03 ($SiMe_2$);
^{29}Si NMR (79,5 MHz, $CDCl_3$): δ (ppm) = -0.71 ($SiMe_2$), -67.01, -67.87, -67.89 (cage), -109.59 (SiO_4).
FT-IR (ATR) = 2953, 2926, 1905, 2869, 1465, 1401, 1383, 1366, 1332, 1253, 1229, 1208, 1074, 954, 901, 837, 787, 769, 738, 626, 561.

^{1}H NMR *($CDCl_3$, 400MHz):*

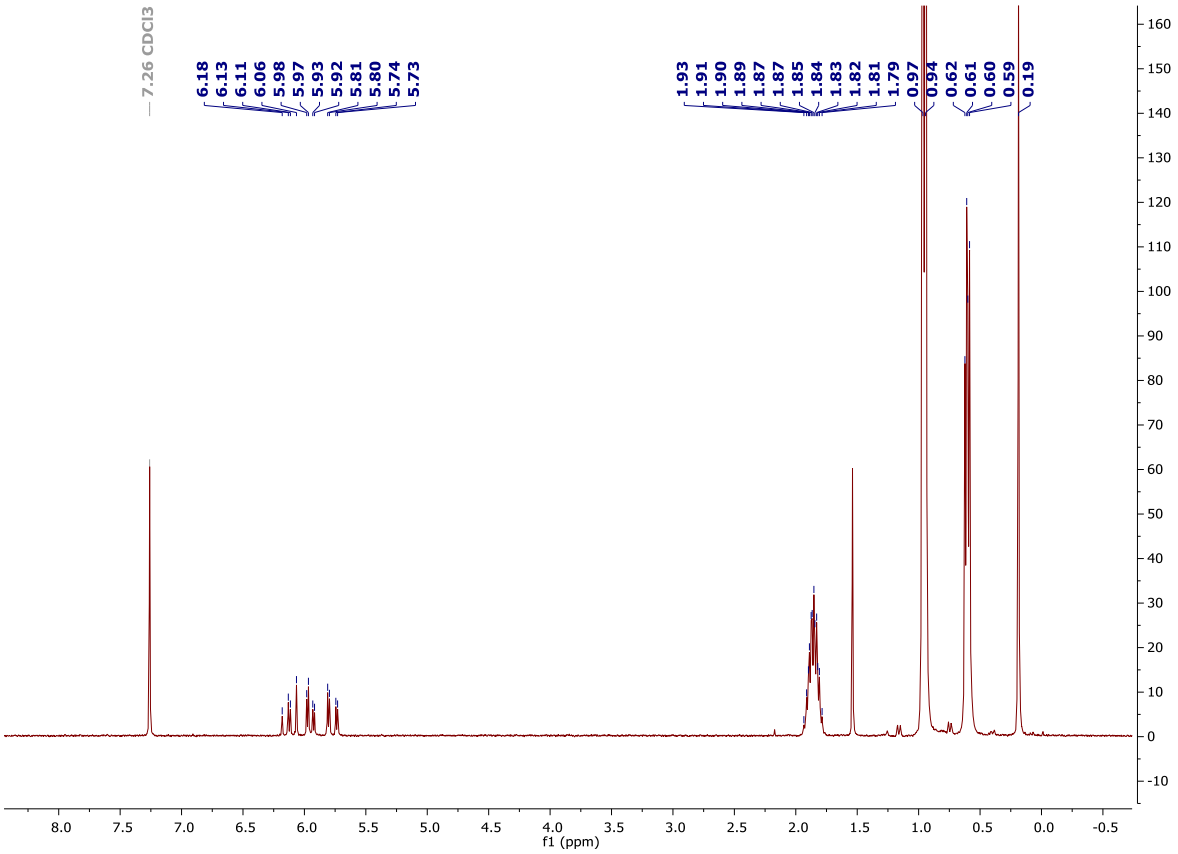

^{13}C NMR *($CDCl_3$, 101 MHz):*

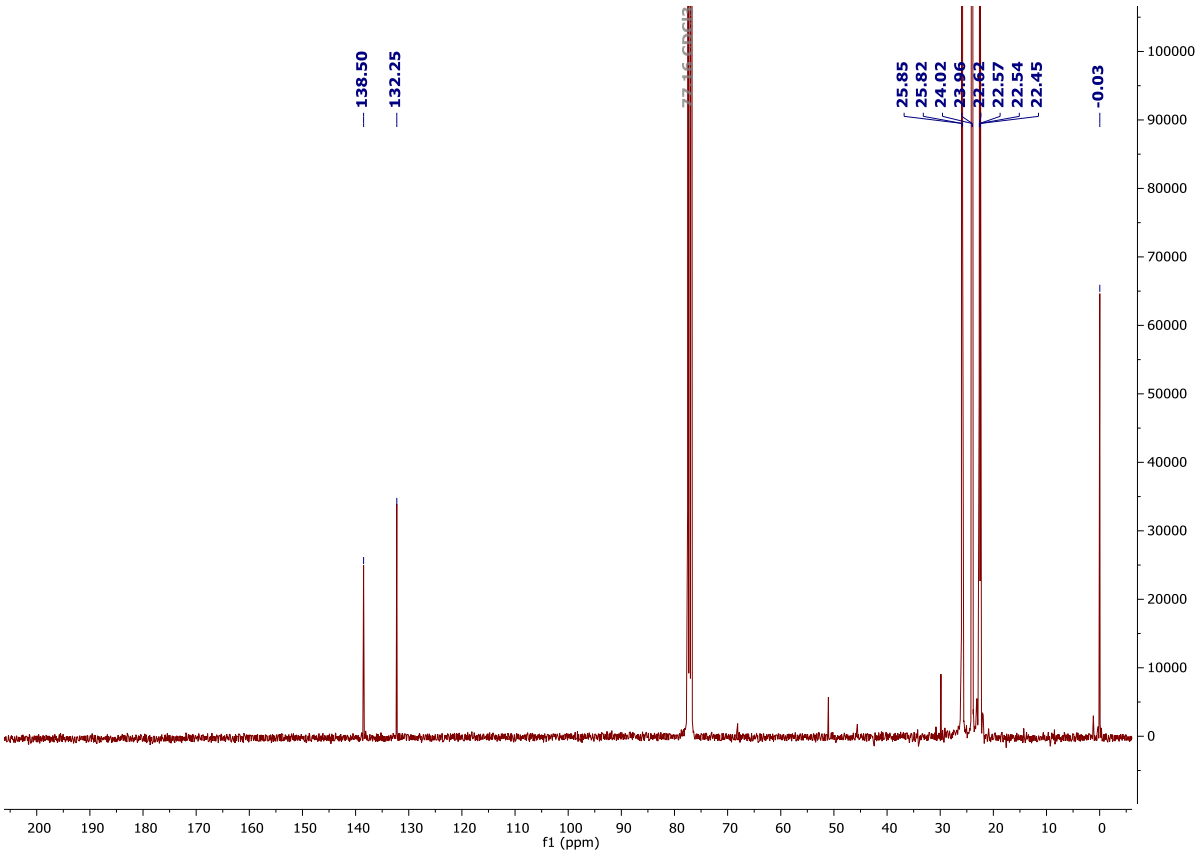

^{29}Si NMR *($CDCl_3$, 79.5 MHz):*

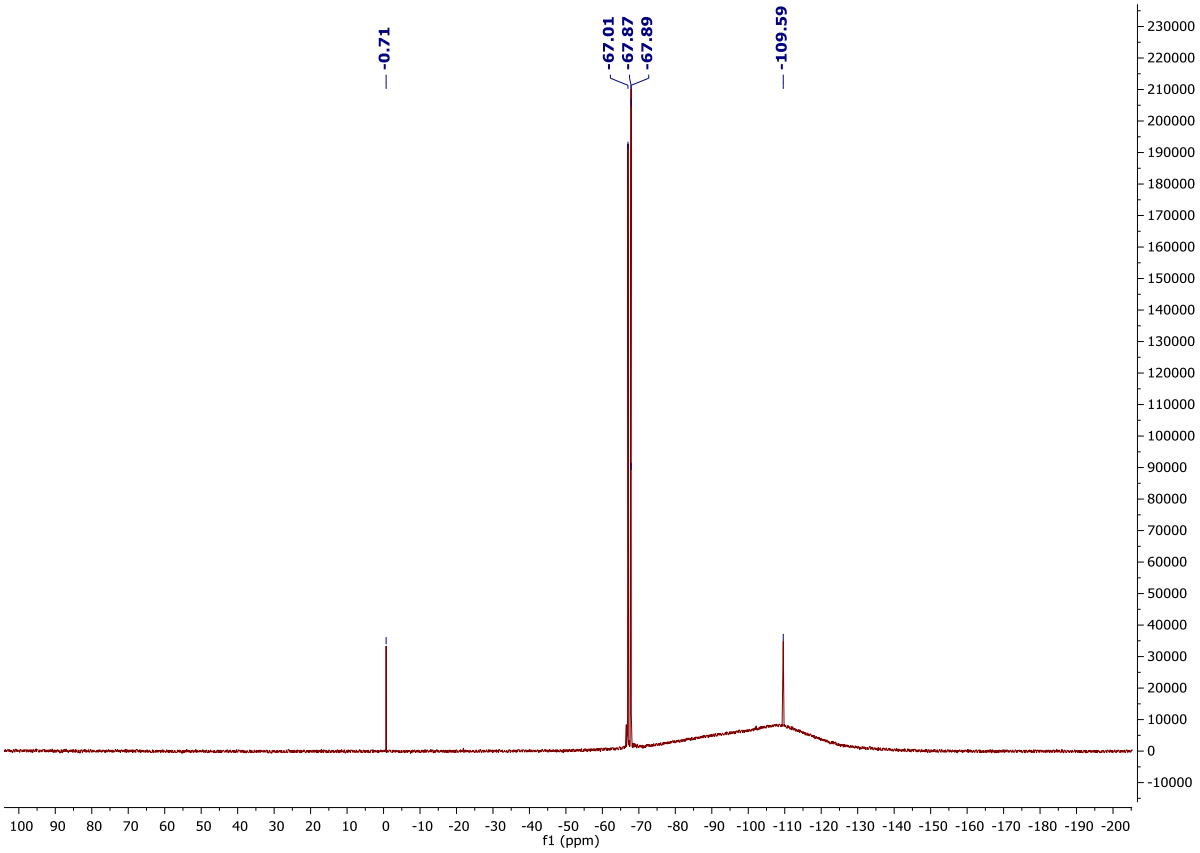

1-(dimethylsiloxy)-3,5,7,9,11,13,15-heptaisobutylpentacyclo[9.5.1.1^{3,9}.1^{5,15}.1^{7,13}]octasiloxane (8)

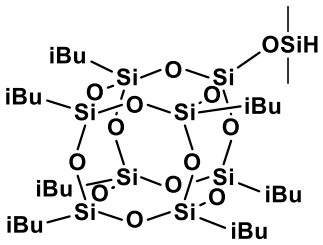

^{1}H NMR (400 MHz, $CDCl_3$): δ (ppm) = 4.72 (sept, J = 2.9Hz, 1H, SiH), 1.93-1.81 (m, 7H, -$CH_2CH(CH_3)_2$), 0.98-0.95 (m, 42H. -$CH_2CH(CH_3)_2$), 0.64-0.60 (m, 14H, -$CH_2CH(CH_3)_2$), 0.23 (d, J = 2.9Hz, 6H, $SiMe_2$);
^{13}C NMR (101 MHz, $CDCl_3$): δ (ppm) = 25.87, 25.85, 24.04, 24.00, 22.68, 22.63, 22.53 (iBu), 0.36 ($SiMe_2$);
^{29}Si NMR (79,5 MHz, $CDCl_3$): δ (ppm) = -3.00 ($SiMe_2$), -66.93, -67.86, -67.88 (cage), -109.05 (SiO_4).
FT-IR (ATR) = 2953, 2927, 2906, 2870, 2143, 1464, 1430, 1383, 1366, 1332, 1253, 1229, 1074, 955, 899, 838, 770, 740, 697, 627, 561, 529.

^{1}H NMR *($CDCl_3$, 400MHz):*

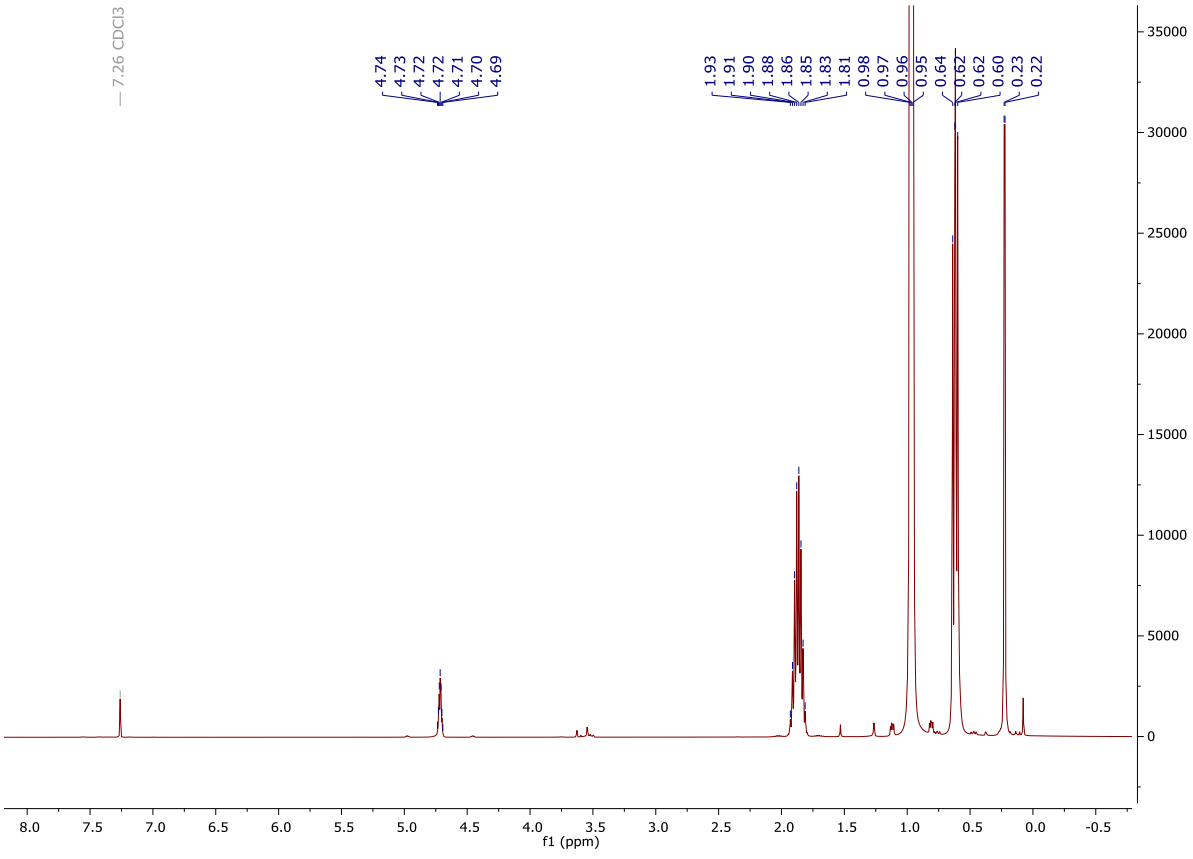

^{13}C NMR *($CDCl_3$, 101 MHz):*

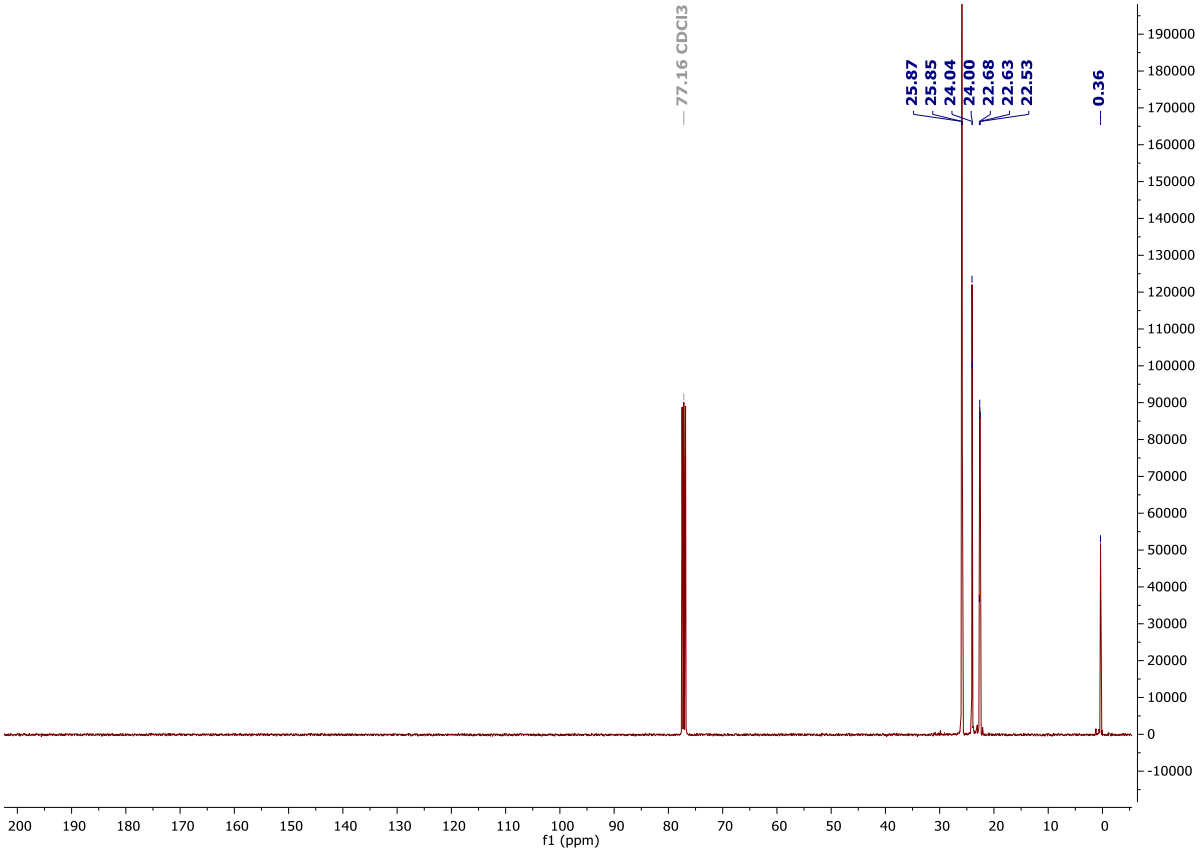

^{29}Si NMR *($CDCl_3$, 79.5 MHz):*

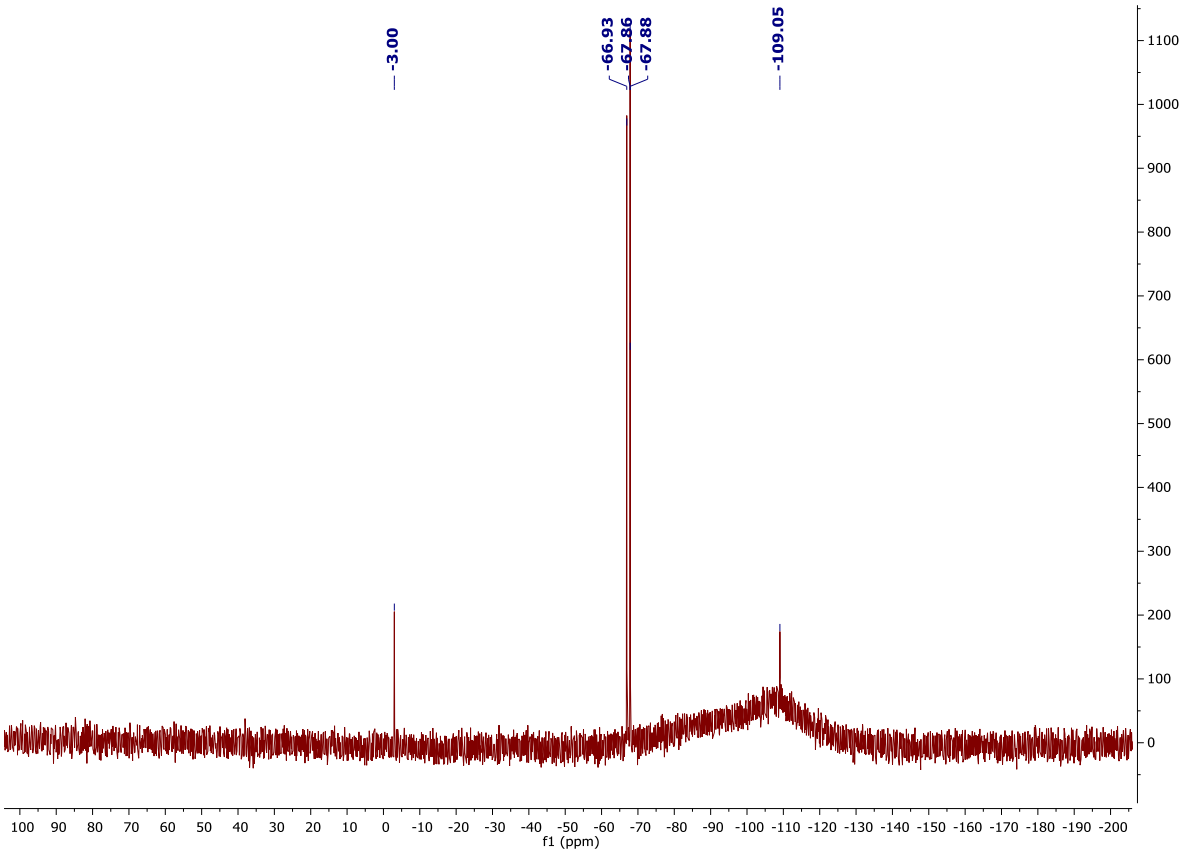

3. SEM and EDS images of the SS/PP composites

0.1% SS-Vi/PP

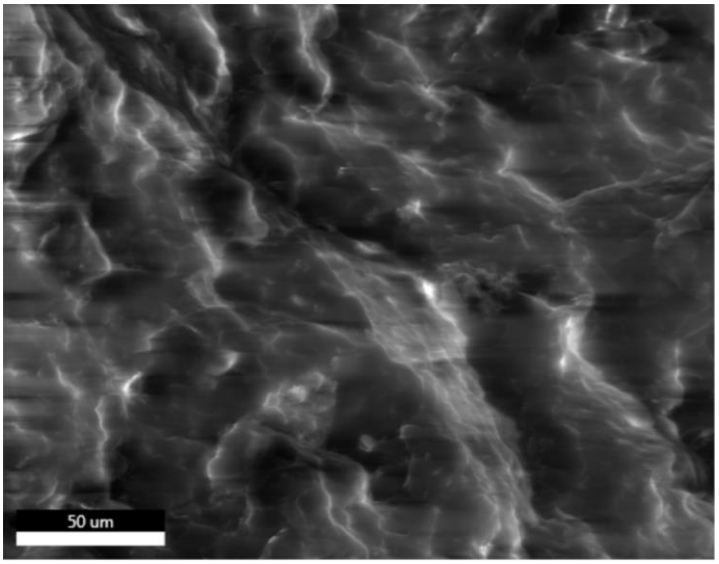

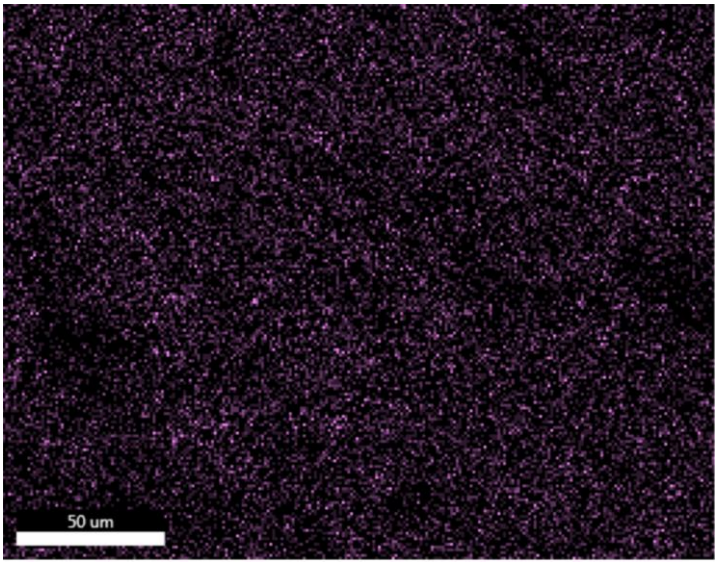

0.25% SS-Vi/PP

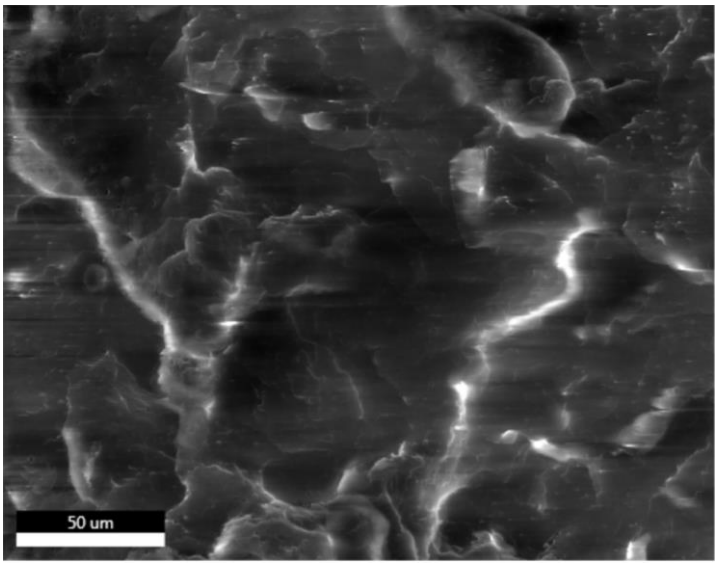

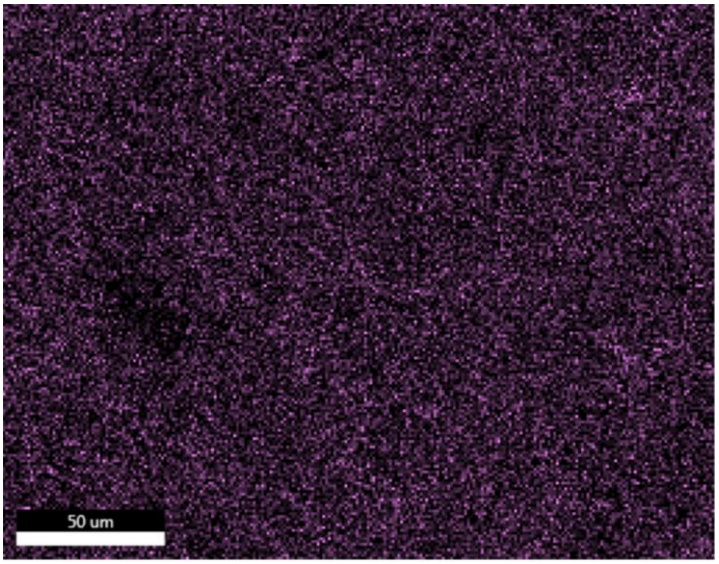

0.5% SS-Vi/PP

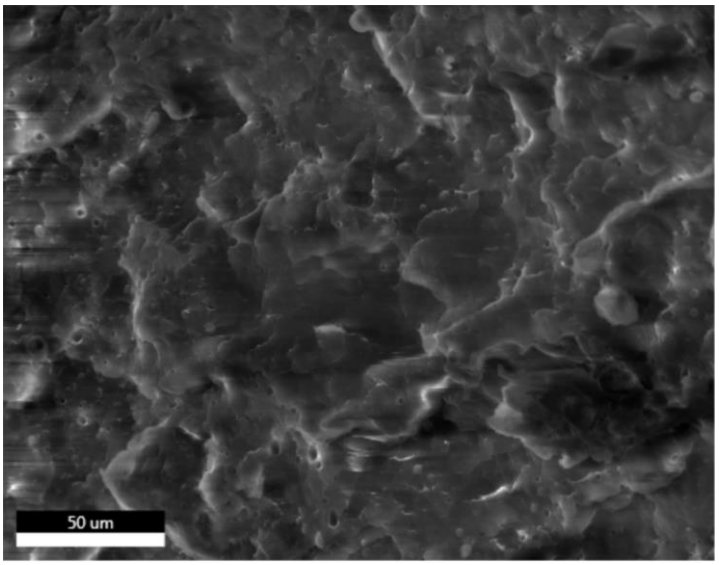

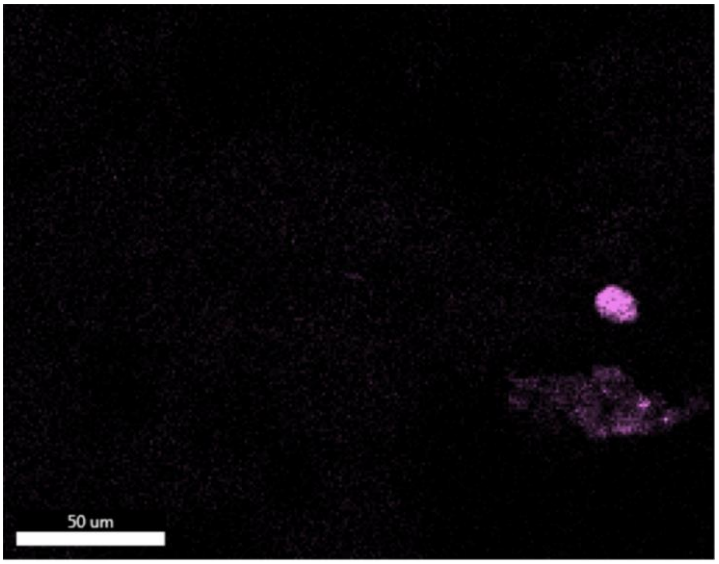

1% SS-Vi/PP

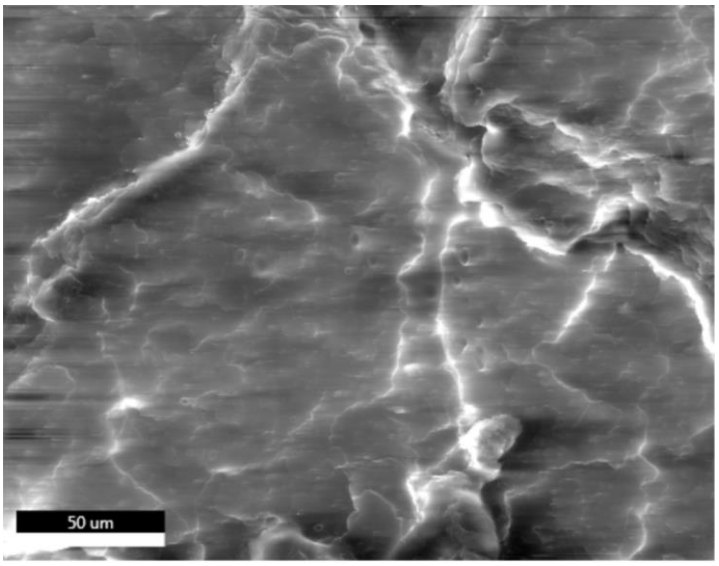

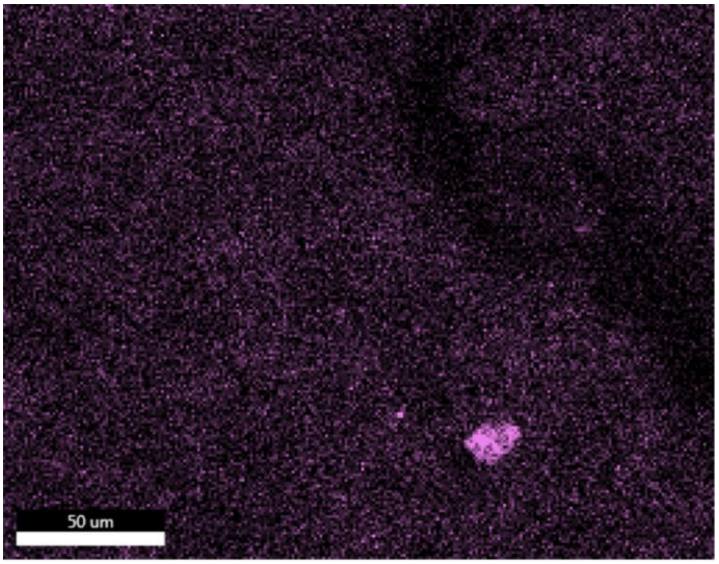

0.1% SS-Glycidyl/PP

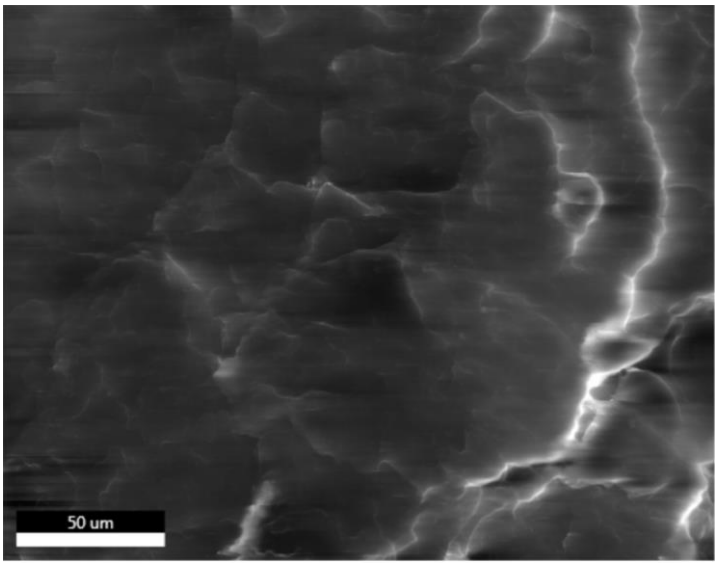

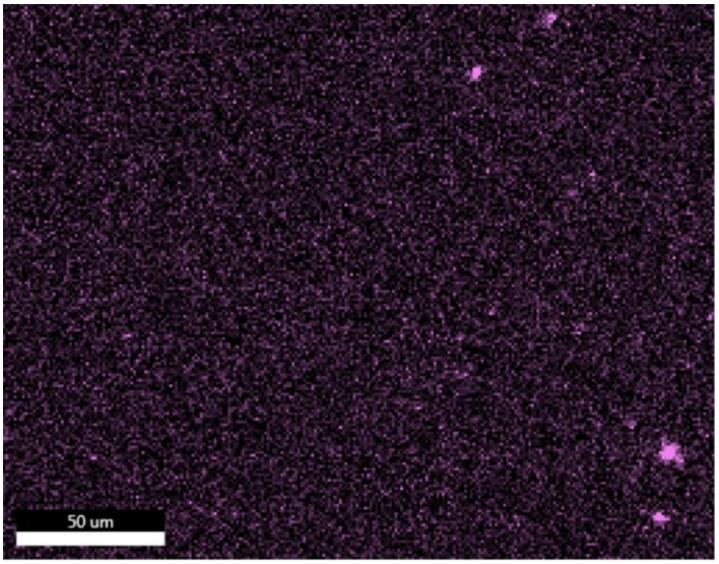

0.25% SS-Glycidyl/PP

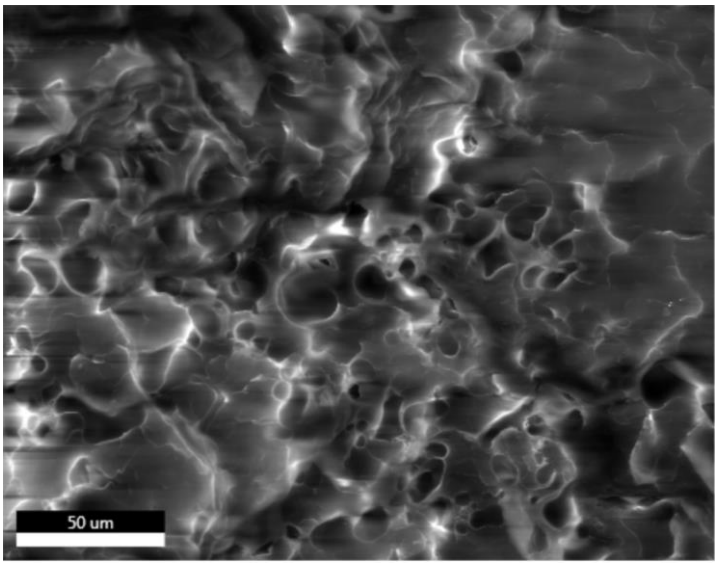

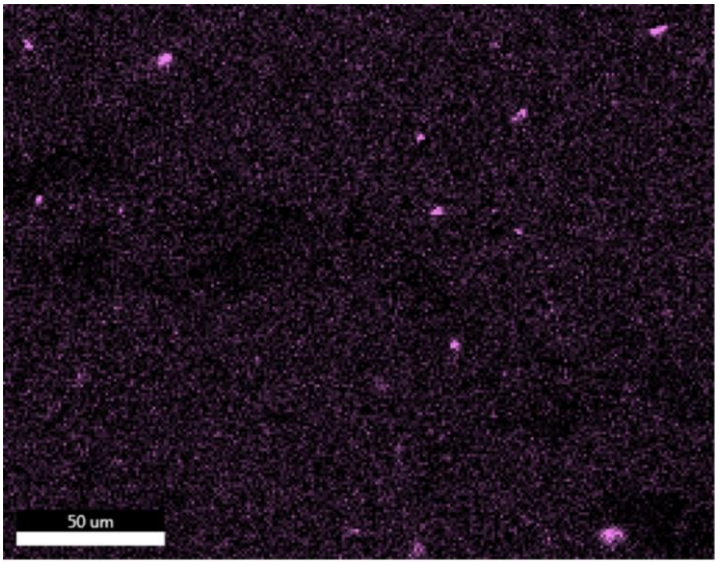

0.5% SS-Glycidyl/PP

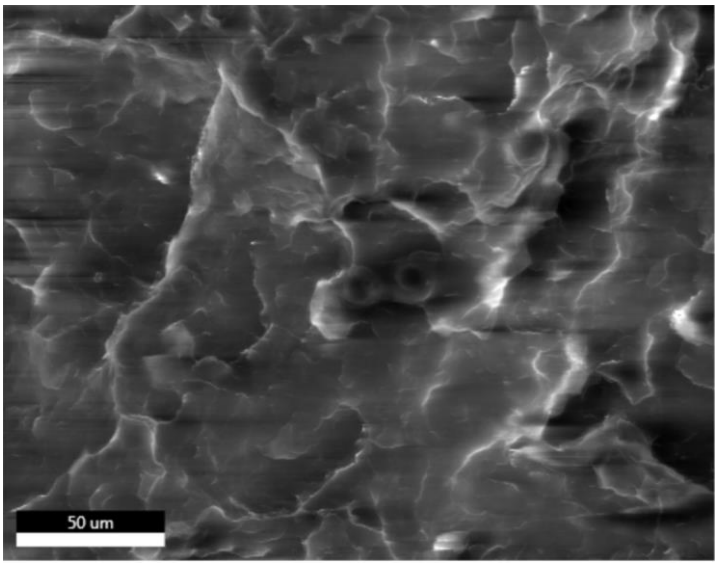

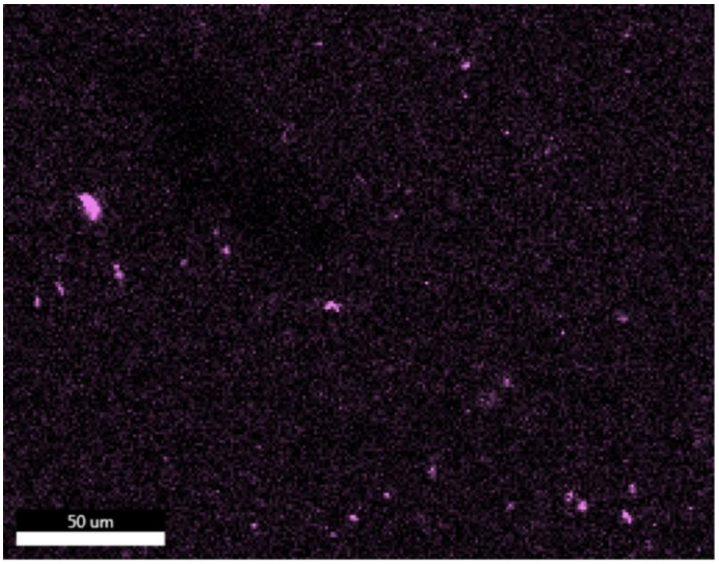

1% SS-Glycidyl/PP

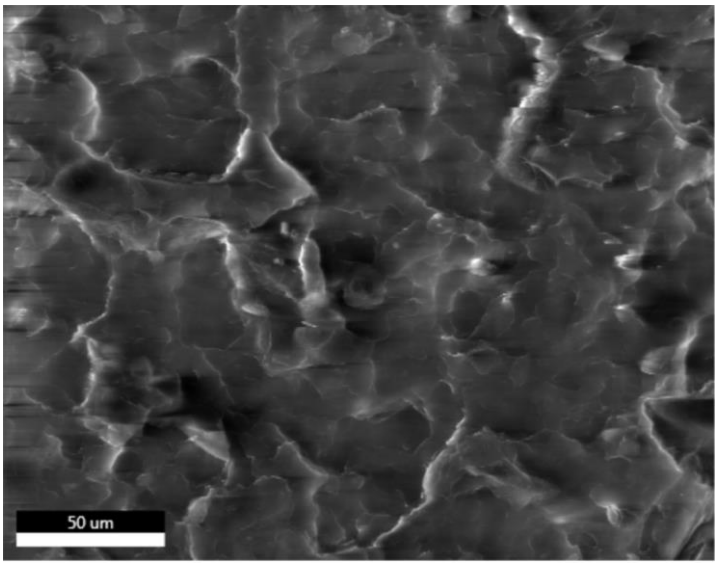

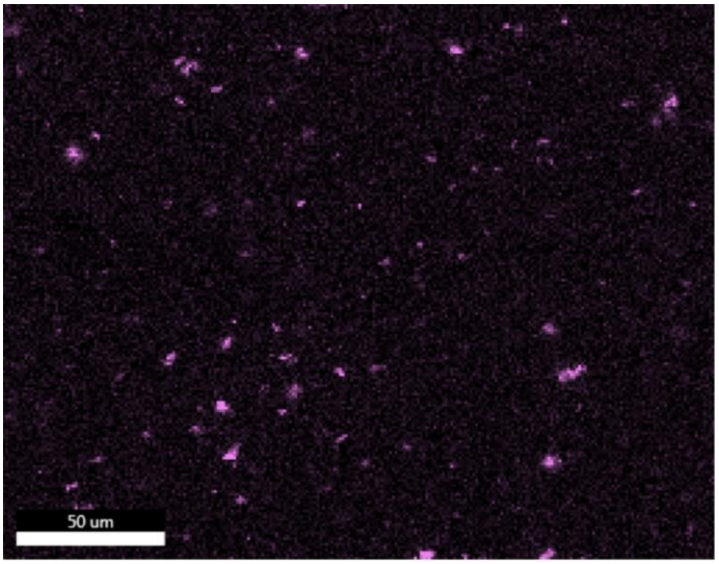

0.1% SS-Limonene/PP

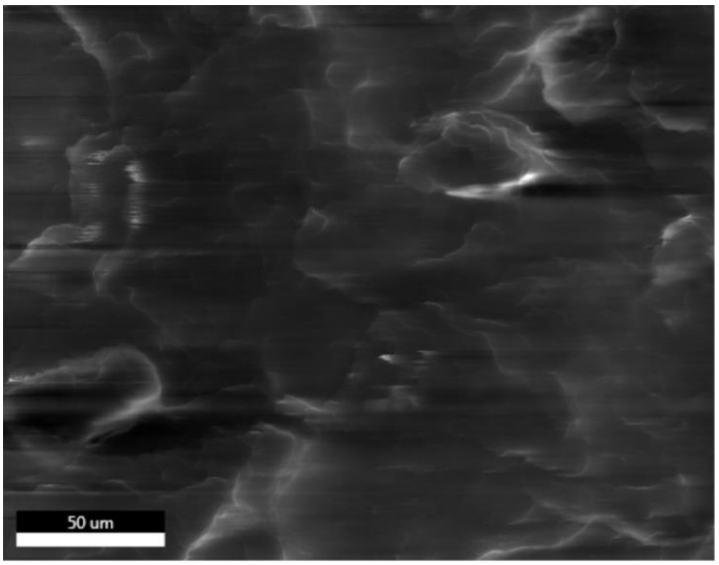

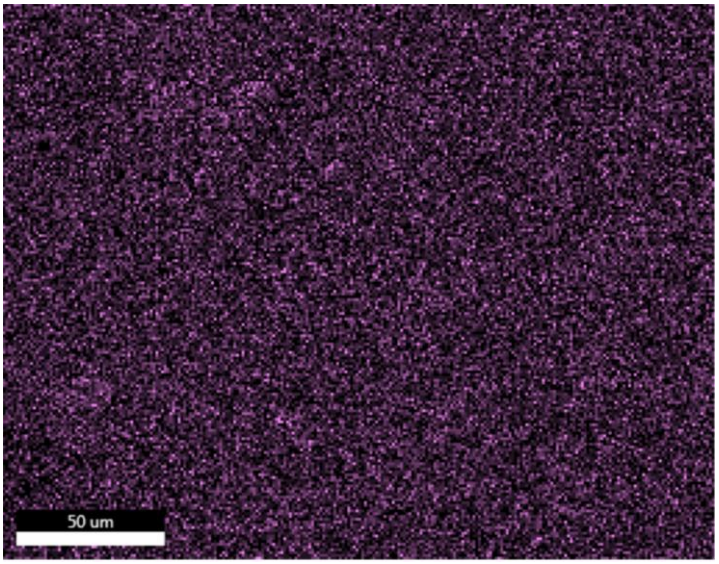

0.25% SS-Limonene/PP

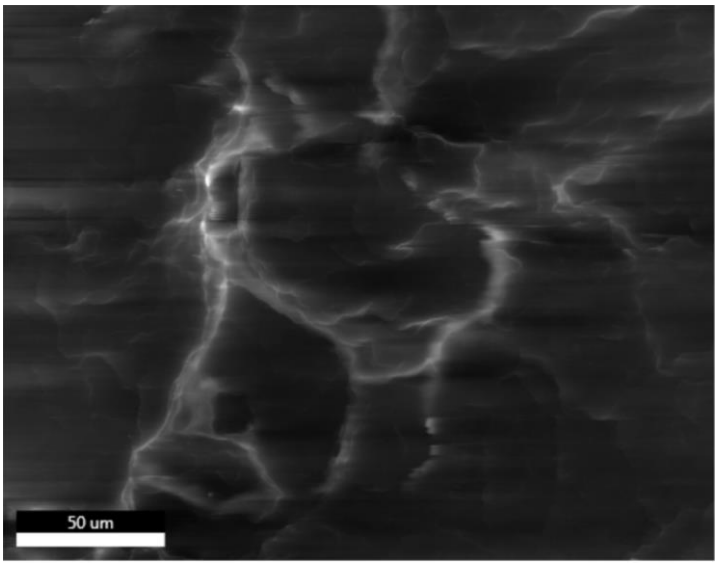

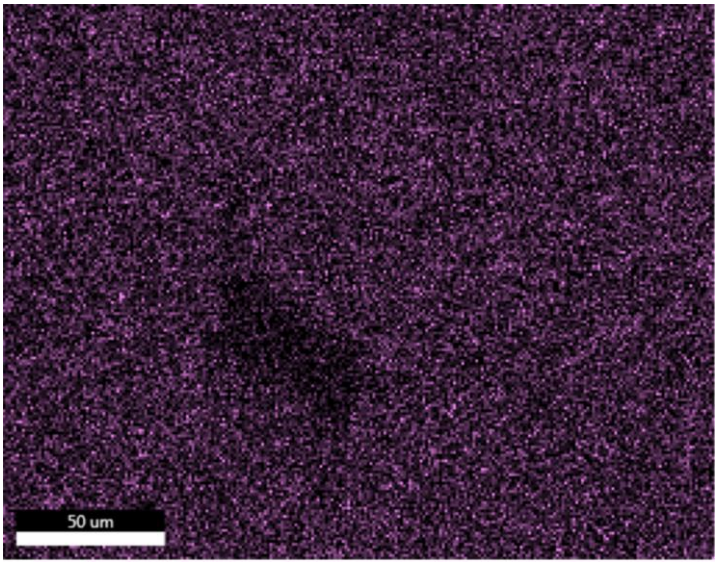

0.5% SS-Limonene/PP

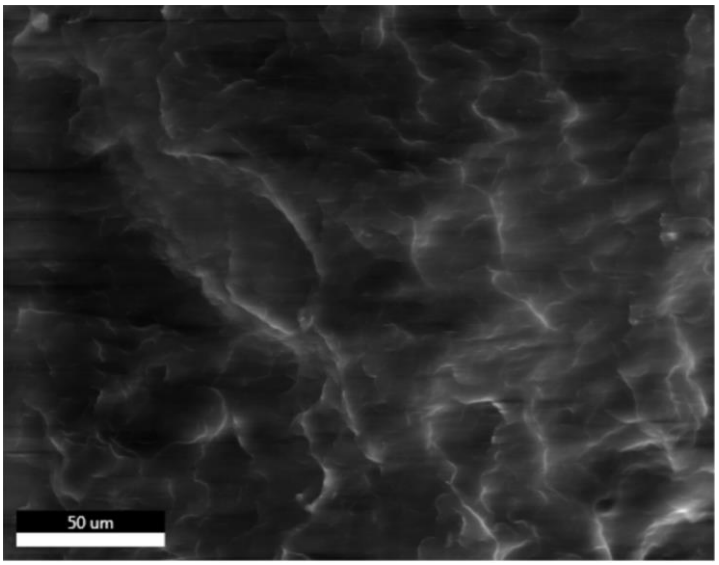

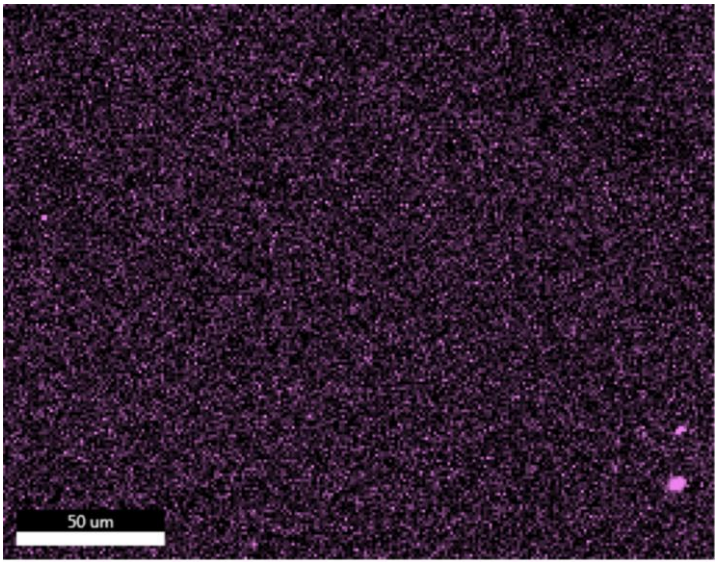

1% SS-Limonene/PP

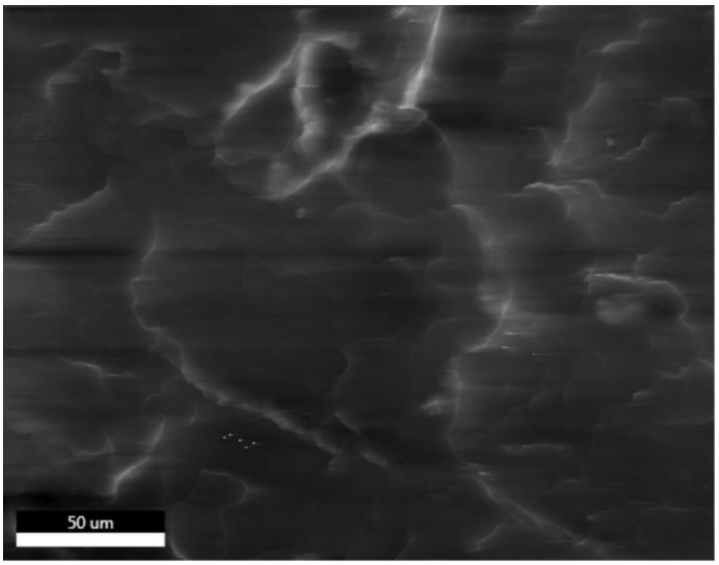

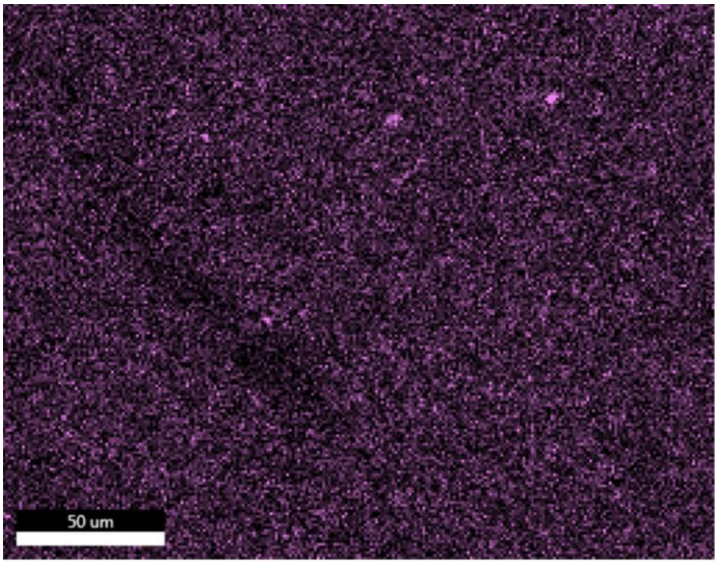

0.1% iBu$_7$SSQ-3OH/PP

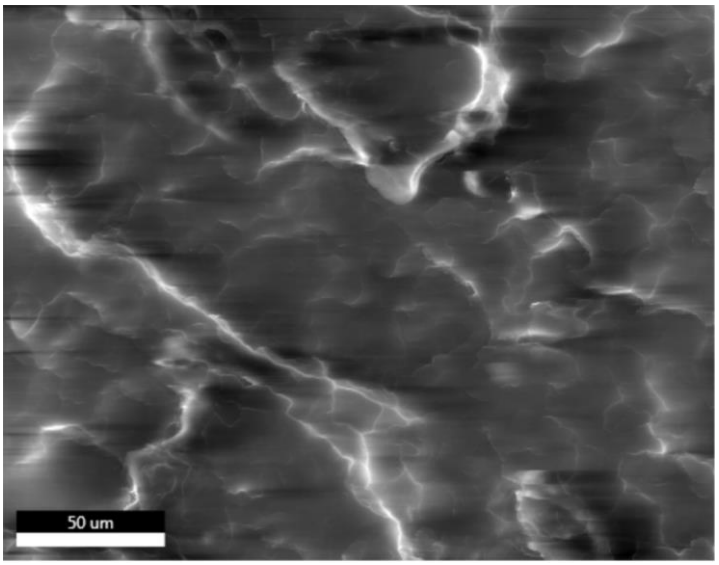

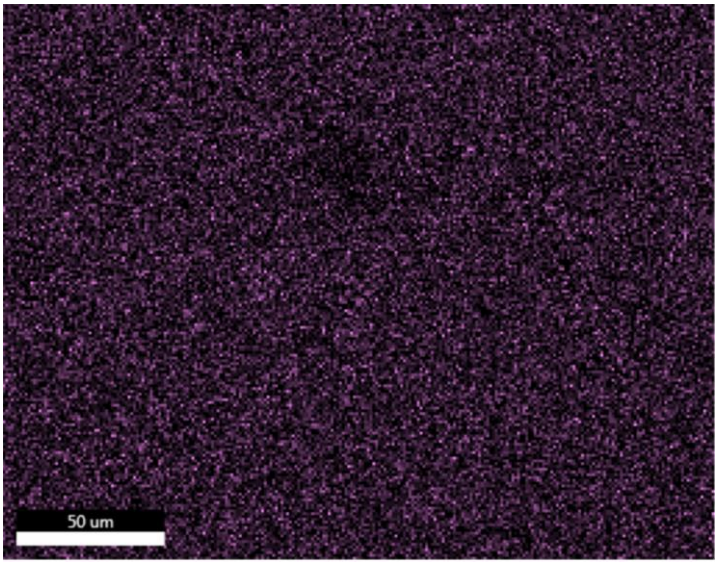

0.25% $iBu_7SSQ\text{-}3OH$/PP

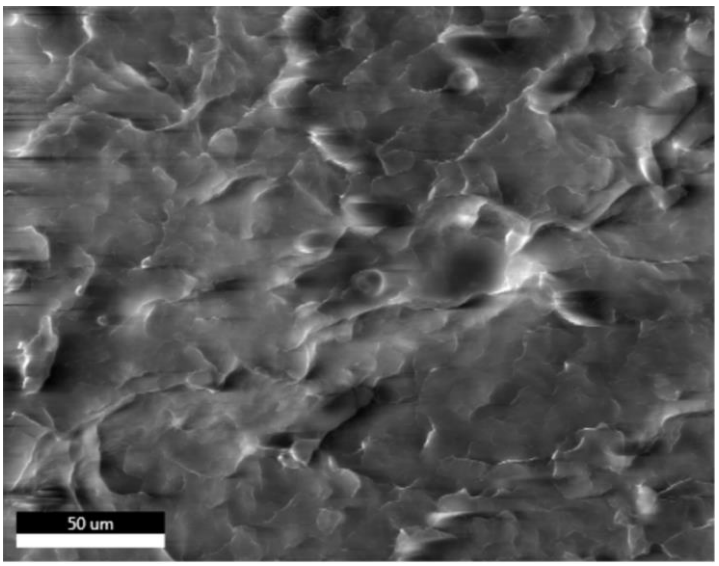

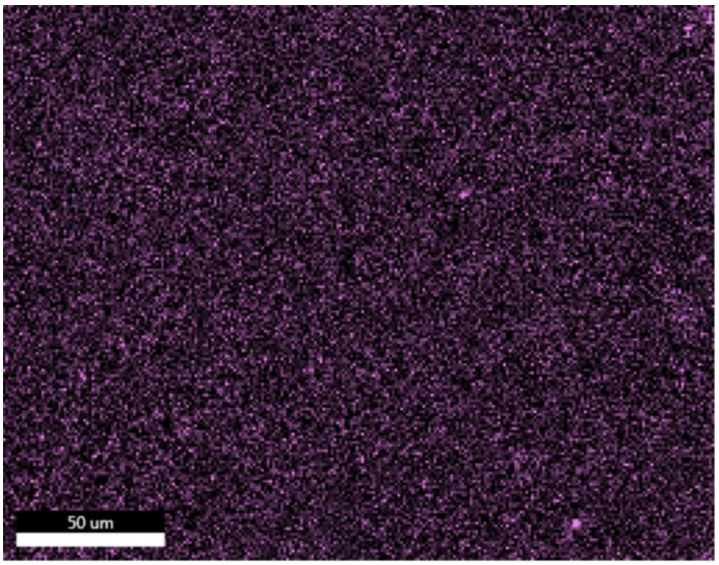

0.5% $iBu_7SSQ\text{-}3OH$/PP

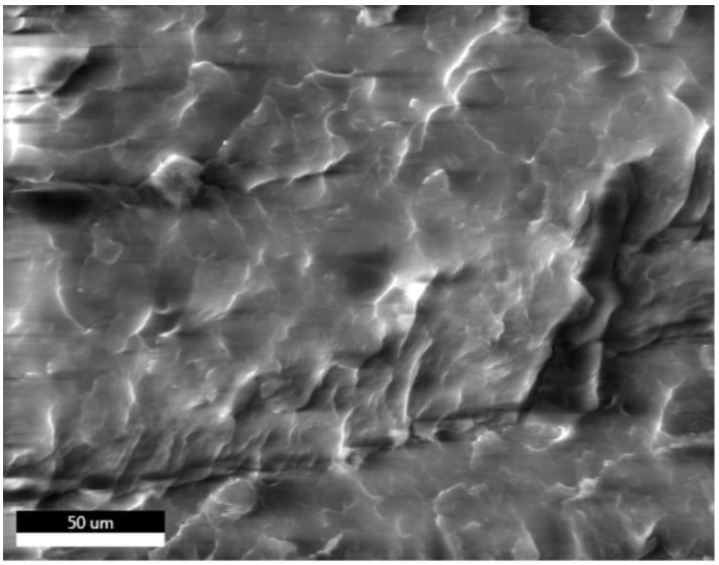

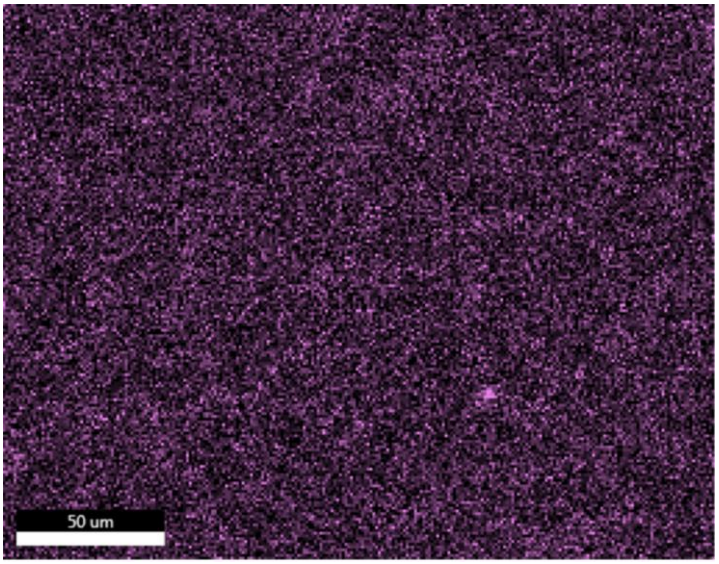

1% iBu$_7$SSQ-3OH/PP

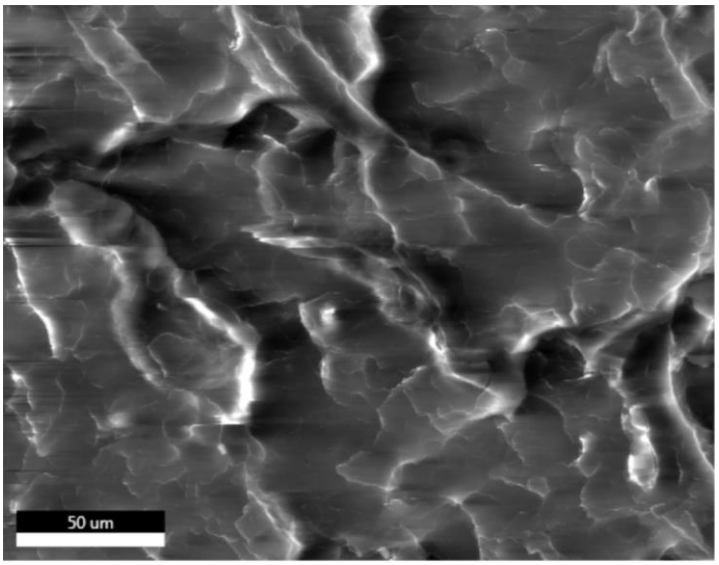

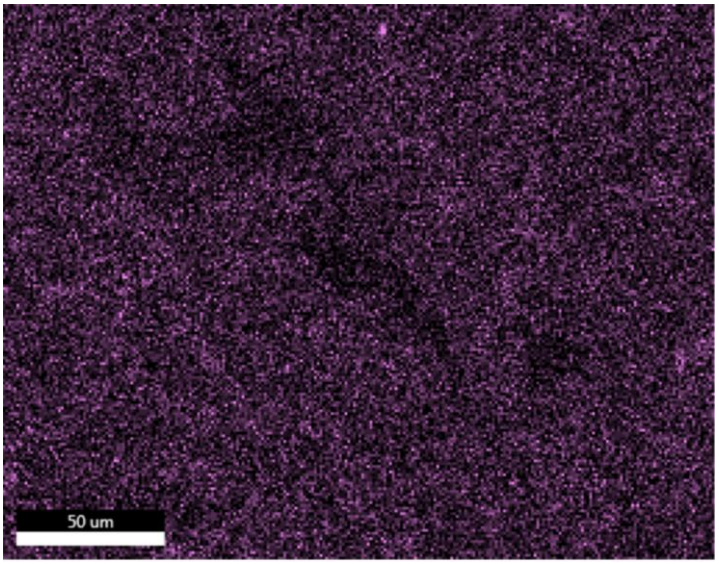

0.1% iBu$_7$SSQ-Cl/PP

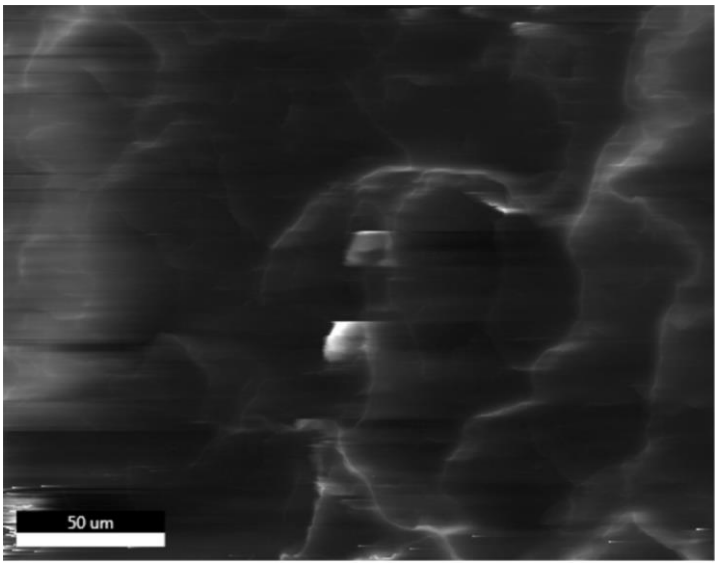

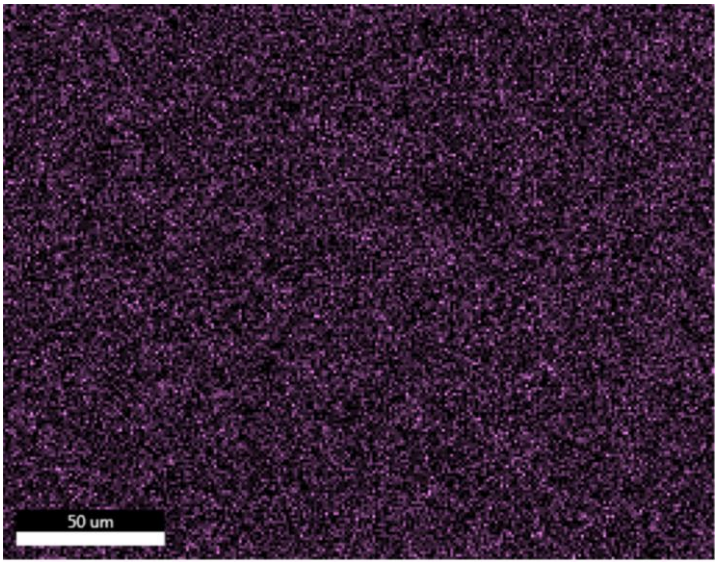

0.25% iBu_7SSQ-Cl/PP

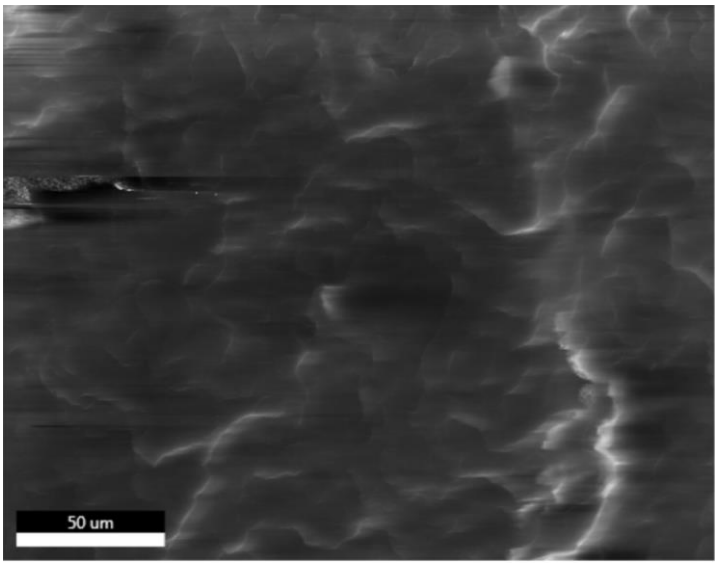

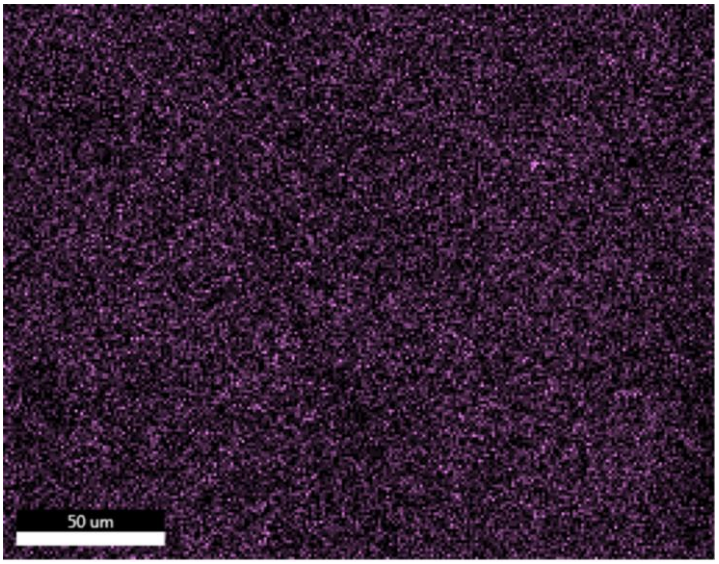

0.5% iBu_7SSQ-Cl/PP

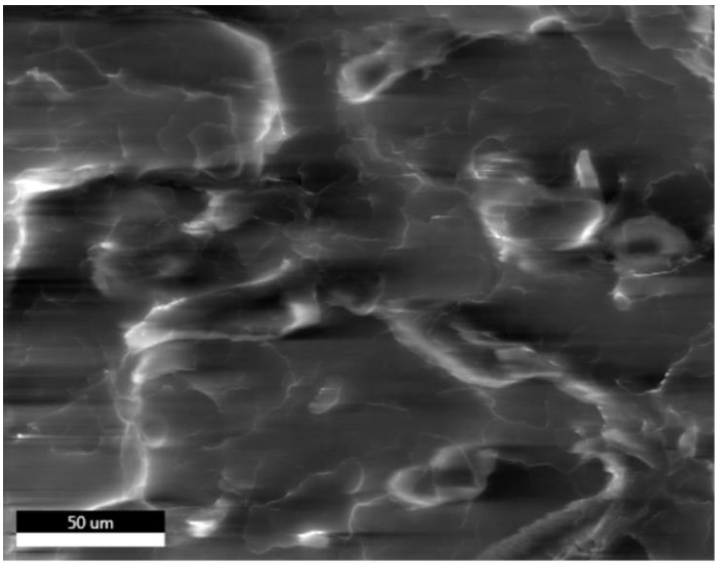

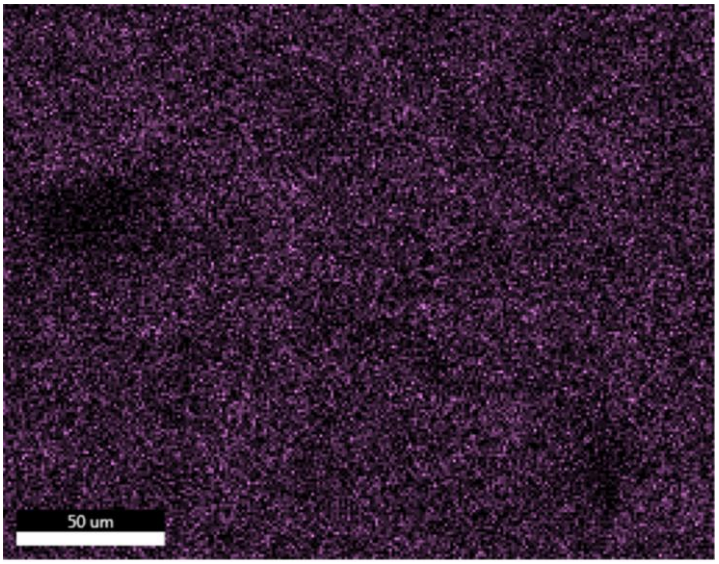

1% iBu$_7$SSQ-Cl/PP

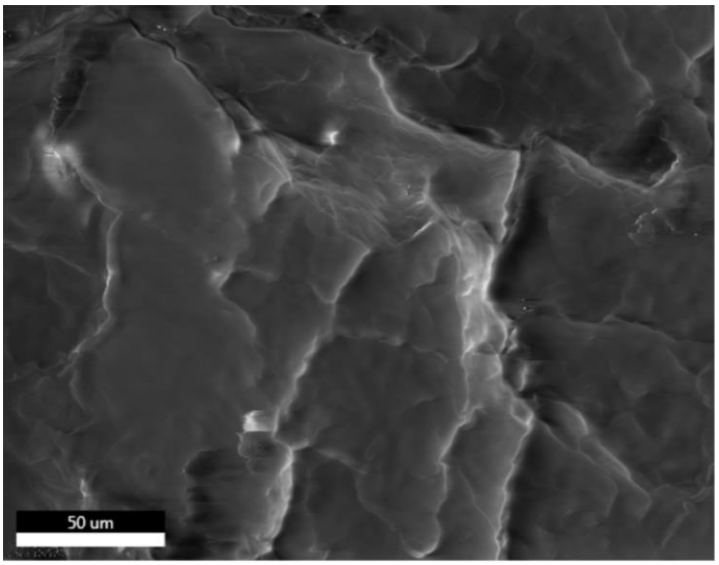

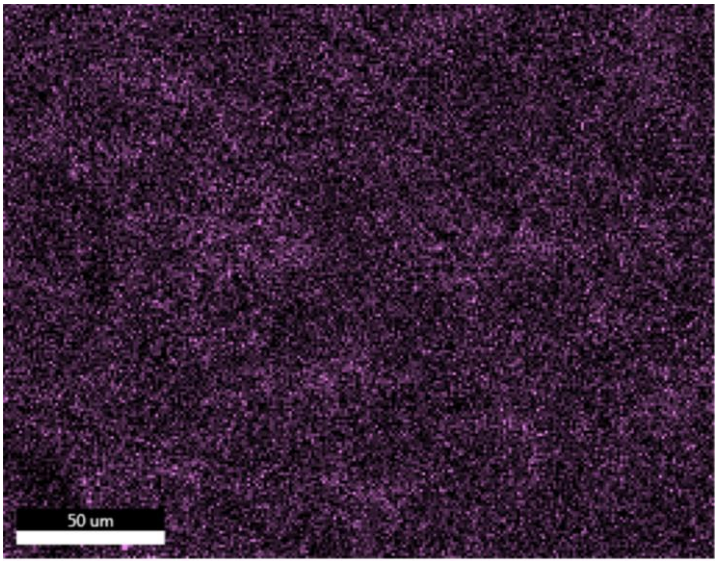

0.1% iBu$_7$SS-Vi/PP

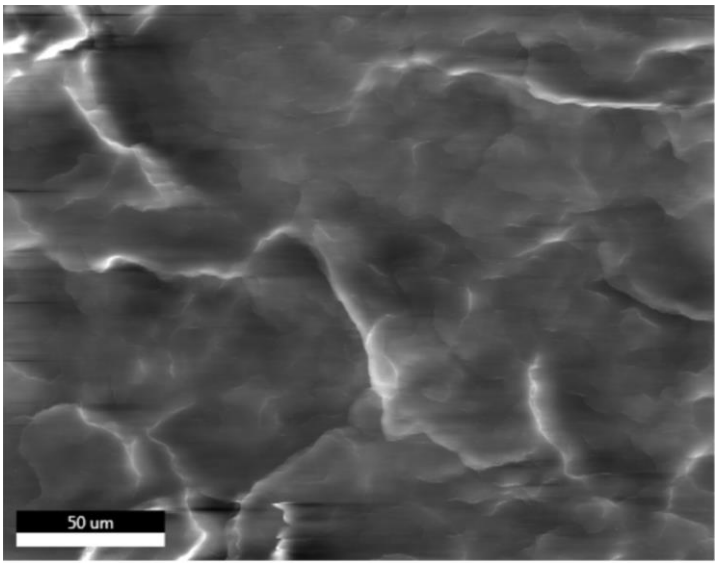

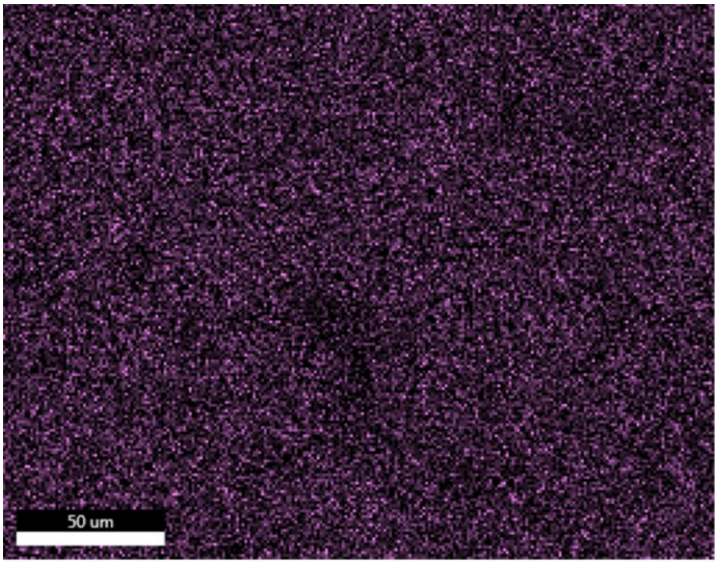

0.25% iBu$_7$SS-Vi/PP

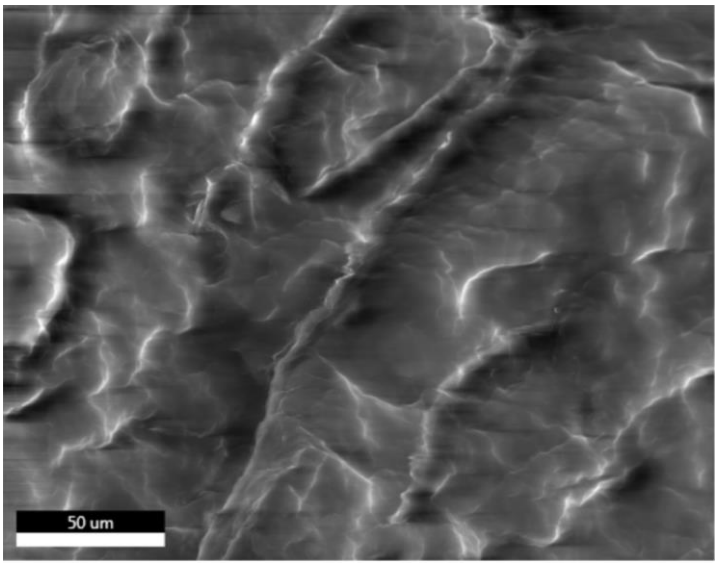

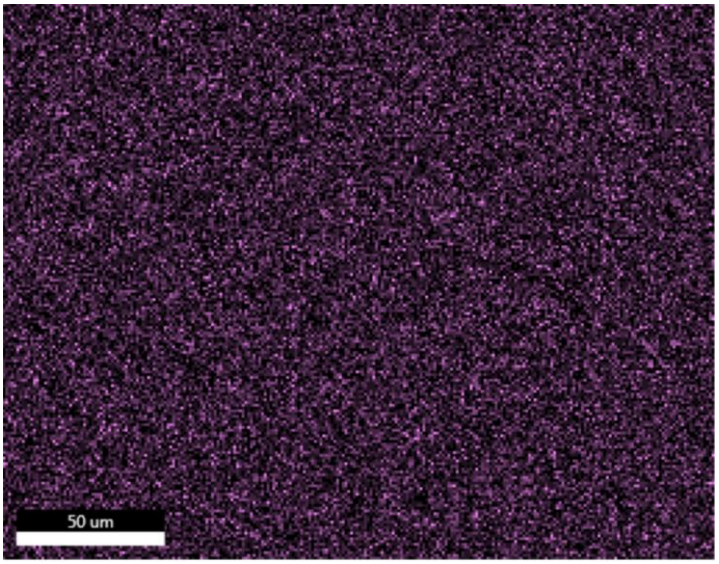

0.5% iBu$_7$SS-Vi/PP

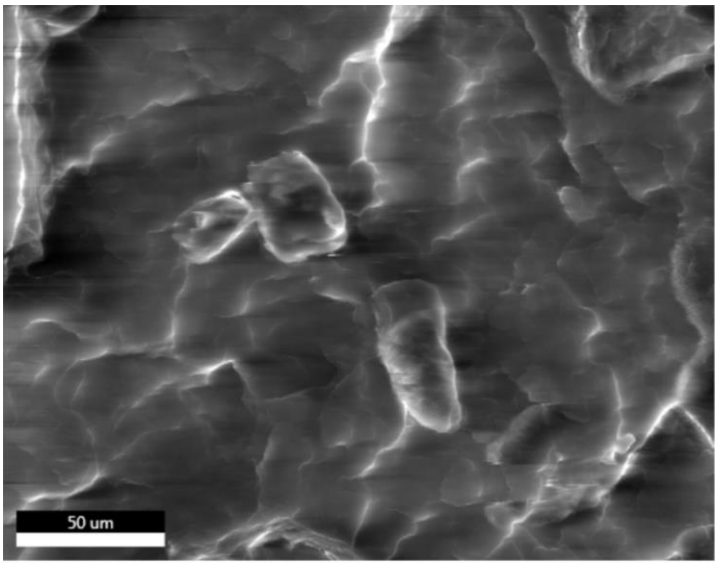

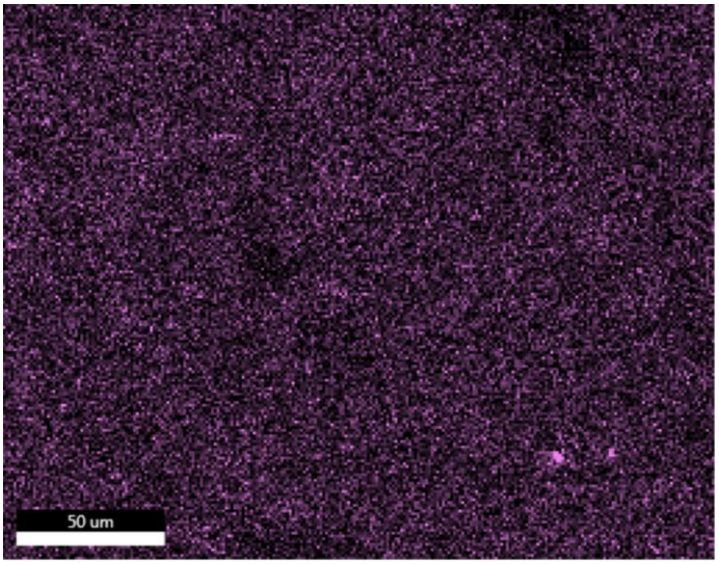

1% iBu$_7$SS-Vi/PP

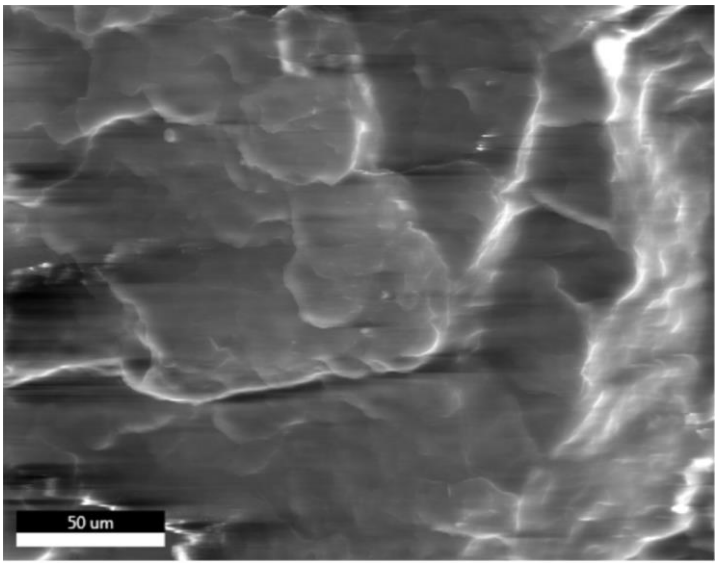

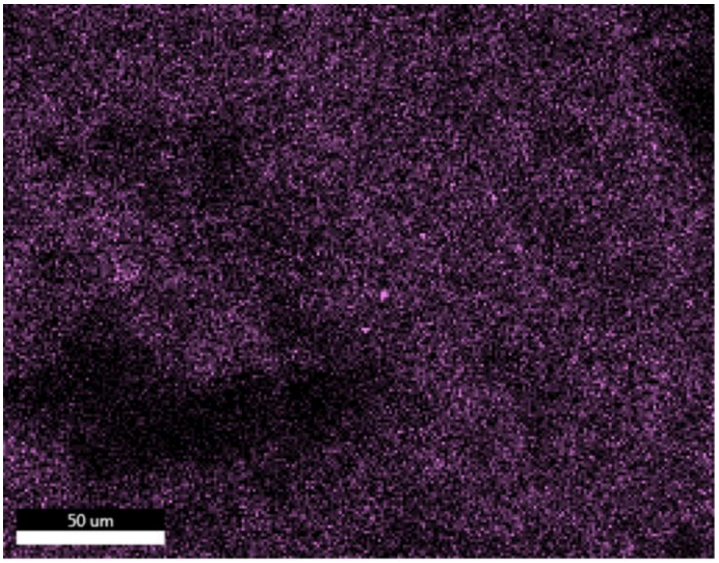

0.1% iBu$_7$SS-H/PP

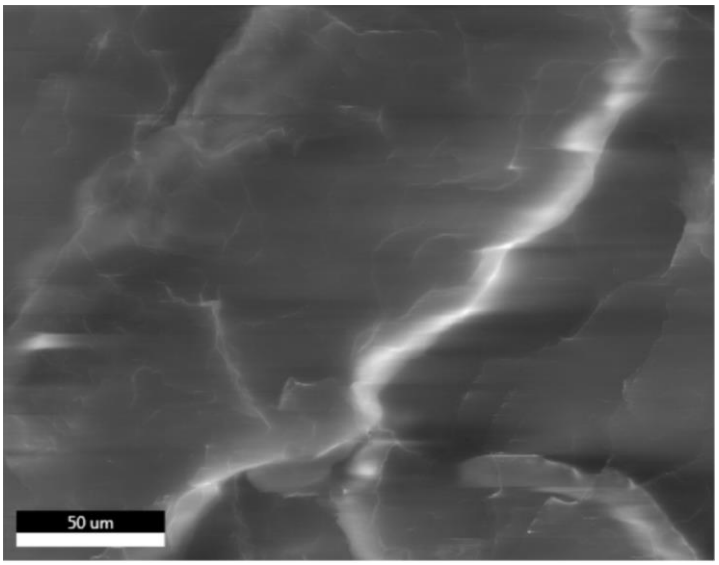

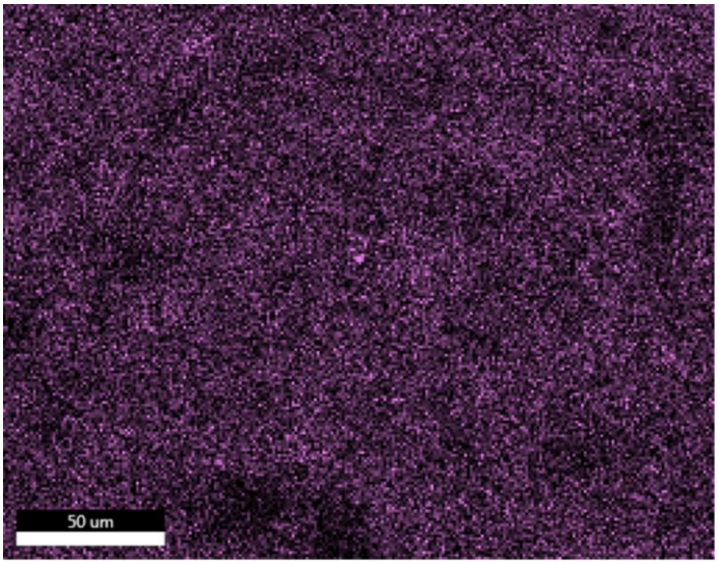

0.25% iBu$_7$SS-H/PP

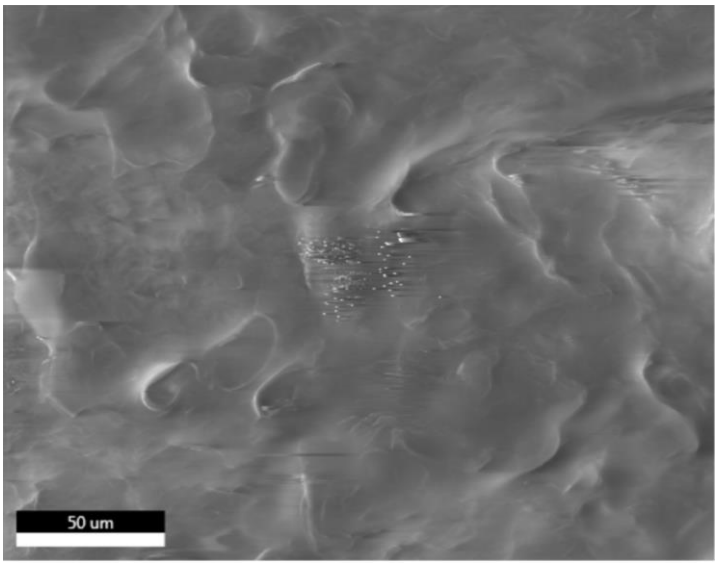

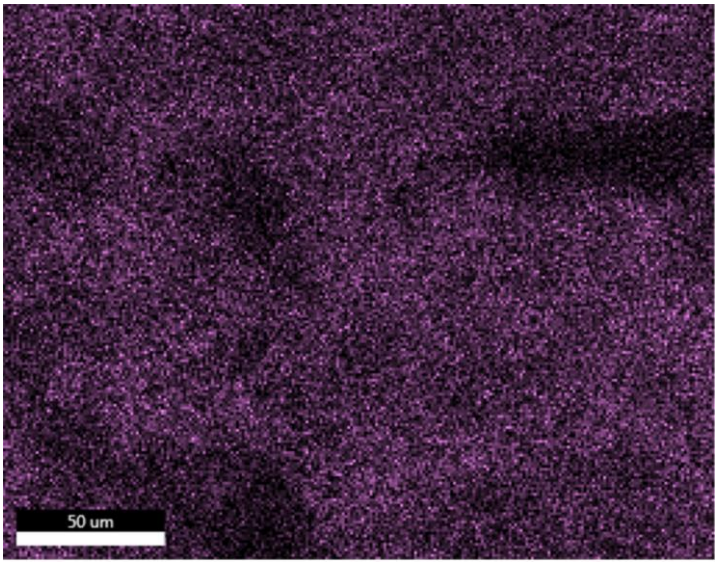

0.5% iBu$_7$SS-H/PP

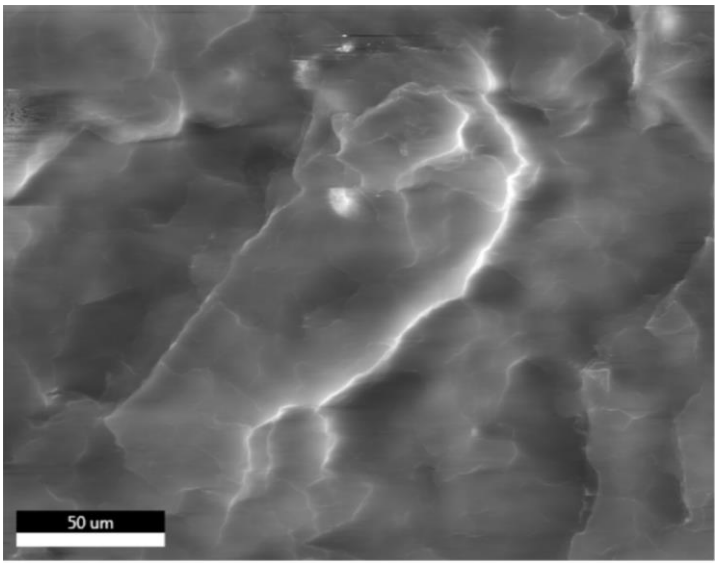

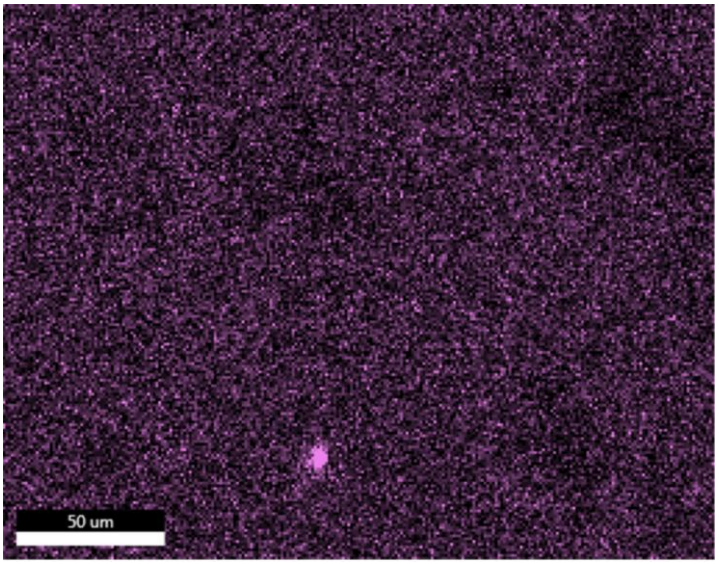

1% iBu_7SS-H/PP

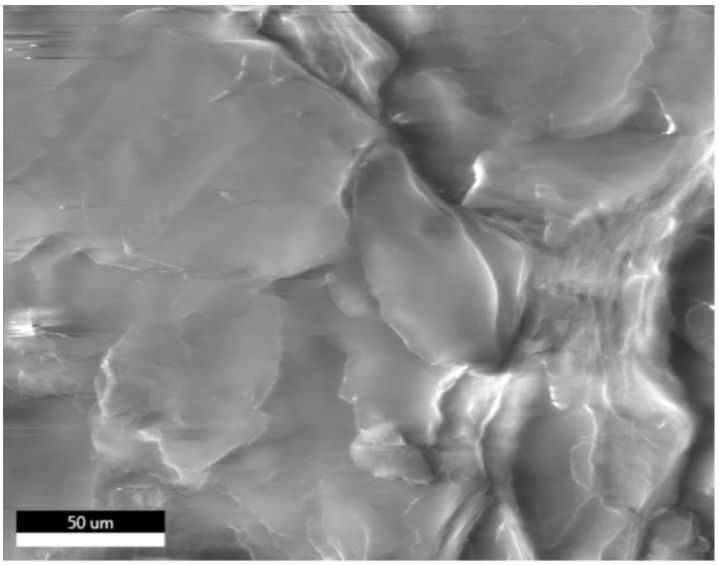

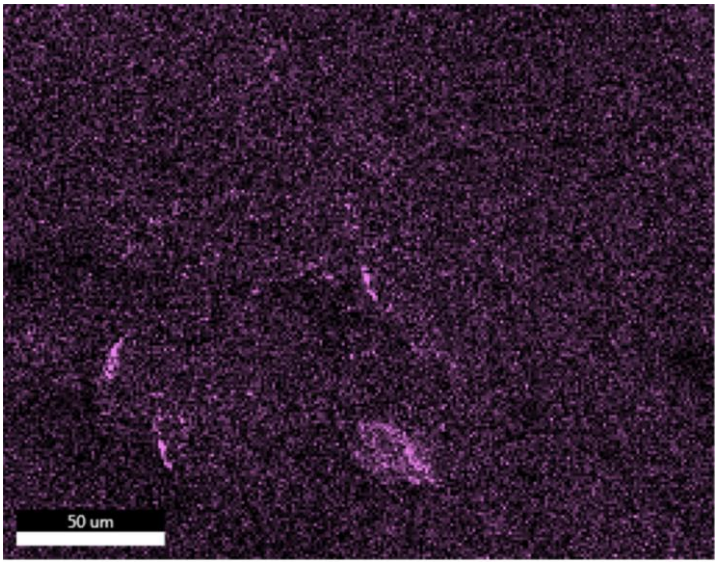

materials

MDPI

Article

Where ppm Quantities of Silsesquioxanes Make a Difference—Silanes and Cage Siloxanes as TiO_2 Dispersants and Stabilizers for Pigmented Epoxy Resins

Dariusz Brząkalski [1], Robert E. Przekop [2,*], Miłosz Frydrych [1], Daria Pakuła [1], Marta Dobrosielska [3], Bogna Sztorch [2] and Bogdan Marciniec [1,2,*]

[1] Faculty of Chemistry, Adam Mickiewicz University in Poznań, 8 Uniwersytetu Poznańskiego, 61-614 Poznań, Poland; d.brzakalski@gmail.com (D.B.); frydrych@amu.edu.pl (M.F.); darpak@amu.edu.pl (D.P.)
[2] Centre for Advanced Technologies, Adam Mickiewicz University in Poznań, 10 Uniwersytetu Poznańskiego, 61-614 Poznań, Poland; bogna.sztorch@amu.edu.pl
[3] Faculty of Materials Science and Engineering, Warsaw University of Technology, 141 Wołoska, 02-507 Warsaw, Poland; Marta.Dobrosielska@pw.edu.pl
* Correspondence: r.przekop@gmail.com or rprzekop@amu.edu.pl (R.E.P.); bogdan.marciniec@amu.edu.pl (B.M.)

Abstract: In this work, silsesquioxane and spherosilicate compounds were assessed as novel organosilicon coupling agents for surface modification of TiO_2 in a green process, and compared with their conventional silane counterparts. The surface-treated TiO_2 particles were then applied in preparation of epoxy (EP) composites and the aspects of pigment dispersion, suspension stability, hiding power, as well as the composite mechanical and thermal properties were discussed. The studied compounds loading was between 0.005–0.015% (50–150 ppm) in respect to the bulk composite mass and resulted in increase of suspension stability and hiding power by over an order of magnitude. It was found that these compounds may be an effective alternative for silane coupling agents, yet due to their low cost and simplicity of production and manipulation, silanes and siloxanes are still the most straight-forward options available. Nonetheless, the obtained findings might encourage tuning of silsesquioxane compounds structure and probably process itself if implementation of these novel organosilicon compounds as surface treatment agents is sought for special applications, e.g., high performance coating systems.

Keywords: silsesquioxane; spherosilicate; cage siloxane; silane; POSS; composite; titanium white; coating; surface treatment; coupling agent

Citation: Brząkalski, D.; Przekop, R.E.; Frydrych, M.; Pakuła, D.; Dobrosielska, M.; Sztorch, B.; Marciniec, B. Where ppm Quantities of Silsesquioxanes Make a Difference—Silanes and Cage Siloxanes as TiO_2 Dispersants and Stabilizers for Pigmented Epoxy Resins. *Materials* **2022**, *15*, 494. https://doi.org/10.3390/ma15020494

Academic Editors: Alessandro Pegoretti, Rani F El Elhajjar and Milena Pavlíková

Received: 10 November 2021
Accepted: 5 January 2022
Published: 10 January 2022

1. Introduction

In polymers industry, additives are applied to fulfil one or more of multiple tasks at once: to cut costs (extending fillers, mostly), to improve mechanical properties (plasticizers, reinforcing fillers, e.g., fibres, nanoparticles), to reduce flammability (fire retardants), to improve the processability for the given processing technology or the final surface properties (lubricants, defoamers), or to add colour to the material (pigments). For inorganic additives, their price is one of the main decisive factors behind considering a given additive both an extending filler and a special purpose additive (functional filler), or just the latter [1,2]. The more expensive additives need to be applied in reasonable quantities in order to keep the production of the desired material economically viable. In case of pigments, there are more and less economical options available, differing also in terms of pigmenting efficiency and environmental friendliness. Regarding white pigments, the most commonly used white pigment is titanium white (TiO_2), characterized by high pigmenting efficiency thanks to its nanostructure and quite good dispersibility, and comprising 69% of the worldwide market of inorganic pigments in year 2000, and together with carbon black

and iron oxides, for over 90% of the world market in 2009 [3,4]. At the same time, titanium white is relatively expensive (around 2500 EUR as of 2020 [5]). Although being an effective pigment, it naturally agglomerates in polymer matrix, which results in need for using it at higher loadings, especially in thin foils, to achieve the desired opacity/pigmentation. Therefore, achieving good dispersion of TiO_2 within polymer translates to reduction of the amount of the pigment used, while obtaining the same pigmentation level and thus reducing the production price for the given plastic material, as well as saving the natural resources used. Titanium white is not considered a high performance pigment due to its cost and agglomeration tendency, therefore treatment procedures are applied in industry and being studied in R&D [3,4].

Epoxy resins are available on the market in different colours for two main reasons. The first one is obviously the aesthetic value, as they are often used for decoration/artistic purposes. Secondly, epoxy resins are commonly slightly yellow in colour, and even more often are the curing components (hardeners) thereof, especially the most common amine type ones. Upon storage, this yellow colour becomes more intense. Therefore, colouration/pigmentation of the epoxy allows to hide this discolouration and make the resin colour more reproducible from batch to batch during production. In case of storing the resin, it is important for the pigment to form a stable mixture with the epoxy base and not to separate from it upon time. Therefore, white-pigmented epoxy resins of satisfactory shelf-life are of high demand and increasing this shelf-life is sought [4,6]. Also, improved dispersion translates into increased hiding power, understood as the coating ability of optically blocking the surface it covers [7].

Organosilicon compounds are nowadays the most common agents for surface treatment of inorganic materials, the older and discontinued agents being chromium and titanium-based [8,9]. For over 20 years now, silsesquioxane derivatives have been studied as a novel class of organosilicon compounds suitable as polymer processing additives. In comparison to traditional silane coupling agents, their polarity, melting temperatures and vapour pressures are much lower, allowing them to be directly processed with a polymer, which is strongly limited for organofunctional silanes. Also, for a couple of years now, silsesquioxanes have been studied as a new class of silane coupling agents for treatment of inorganic fillers and other particles/nanoparticles. In terms of serving as direct polymer additives for epoxy resins, silsesquioxane compounds were introduced both in a reactive and non-reactive (physical blending) manner. For reactive additives, $iOc_7SSQ\text{-}(CH_2)_3NH_2$ [10], $i Bu_7SSQ\text{-}(CH_2)_3NH_2$ [11], 3-glycidoxypropylhepta(isobutyl)octasilsesquioxane [12], 3-glycidoxypropylhepta(isooctyl) octasilsesquioxane and 3-glycidoxypropylheptaphenyloctasilsesquioxane [13] epoxycyclohexyl-hepta(isobutyl)octasilsesquioxane [14], (3-glycidoxypropyl)silsesquioxane cage mix [14,15], tris(glycidyldimethylsiloxy)hepta(isobutyl)silsesquioxane [16,17], octakis(aminophenyl) octasilsesquioxane [18], octakis(3-aminopropyl)octasilsesquioxane [19] mixed substituent hexyl/4-glycidylbutyloctaspherosilicates [13], and hybrids of DGEBA with SSQ molecules attached as a side group [13]. For non-reactive additives, $Ph_7SSQ\text{-}3OH$ (phenyltrisilanol) and $i Bu_7SSQ\text{-}3OH$ (isobutyltrisilanol) [20], 9,10-dihydro-9-oxa-10-phosphaphenanthrene-10-oxide (DOPO)-modified silsesquioxanes [21], methyl- and methyl-vinyl polysilsesqioxanes [22] were used. Additionally, in recent years, green chemical approach towards preparation of hybrid materials is sought and the examples of the first silsesquioxane-containing materials prepared in aqueous conditions were given [23]. Silsesquioxanes, as well as polysilsesquioxanes, have been studied as additives moderating dielectric properties of nanocomposites and nanocomposite films [24].

For improved dispersion and interaction with the matrix polymer, TiO_2 has been treated with $Ph_7SSQ\text{-}3OH$ [25,26] and $i Bu_7SSQ\text{-}3OH$ [27,28], for processing of polyolefin nanocomposites; $i Bu_7SSQ\text{-}(CH_2)_3NH_2$ (for preparation of hybrid graphene oxide-TiO_2 material and cyanate ester composite containing thereof [29]), as to verify these compounds as novel coupling agents for surface treatment of inorganic nanoparticles.

In this work, an approach towards application of well-defined organosilicon compounds, that is, silsesquioxane and spherosilicate derivatives, as dispersants and stabilizers

of TiO_2 nano- and microparticles is presented. More importantly, they were used at low loadings for the studied solution to be economically viable, as well as technologically feasible during standard procedures of pigment manufacturing or pigmented epoxy preparation, without no additional chemical processing steps or organic solvents involved during surface treatment. The organosilicon compounds are compared to much cheaper and readily available, conventional silane coupling agents (trialkoxysilanes) to assess any possible advantages of the former.

2. Materials and Methods

2.1. Materials and Instrumentation

The chemicals were purchased from the following sources: Tetraethoxysilane (TEOS), tetrachlorosilane, chlorodimethylsilane, tetramethylammonium hydroxide (TMAH) 25% methanol solution from ABCR, *iso*butyltrimethoxysilane, triethylamine, allyl-glycidyl ether, vinyltrimethoxysilane, chloroform-d and Karstedt's catalyst xylene solution from Aldrich, P_2O_5, tetrahydrofuran (THF), methanol, hydrochloric acid, toluene, acetonitrile, and acetone from Avantor (Poland). Toluene was degassed and dried by distilling it from P_2O_5 under argon atmosphere. TiO_2 was obtained from Grupa Azoty Z.Ch. "Police" S.A. (Poland), as a 50% *w*/*w* water slurry with no additives. Epidian 5 was obtained from Ciech Sarzyna (Poland) and according to the manufacturer's data, was characterized by density of 1.17 g/cm^3 and viscosity of 20,000–30,000 mPa·s at 25 °C, and epoxide number of 0.48–0.51 mol/100 g. Curing agent, triethylenetetramine (branded as Z-1 hardener), was also purchased from Ciech.

Octahydrospherosilicate was prepared according to a literature procedure [30]. Chlorohepta(isobutyl)octasilsesquioxane was prepared according to literature procedures [31,32].

^{1}H, ^{13}C, and ^{29}Si Nuclear Magnetic Resonance (NMR) spectra were recorded at 25 °C on a Bruker Ascend 400 and Ultra Shield 300 spectrometers using $CDCl_3$ as a solvent. Chemical shifts are reported in ppm with reference to the residual solvent ($CHCl_3$) peaks for ^{1}H and ^{13}C.

Fourier Transform-Infrared (FT-IR) spectra were recorded on a Nicolet iS 50 Fourier transform spectrophotometer (Thermo Fisher Scientific) equipped with a diamond ATR unit with a resolution of 0.09 cm^{-1}.

Differential scanning calorimetry (DSC) was performed using a NETZSCH 204 F1 Phoenix calorimeter. Samples of 6 ± 0.2 mg were placed in an aluminium crucible with a punctured lid. The measurements were performed under nitrogen in the temperature range of −30–230°C and at a 5 °C/min heating rate. T_{gu} was measured from the first heating cycle, T_g was measured from the second heating cycle.

MALDI-TOF mass spectra were recorded on a UltrafleXtreme mass spectrometer (Bruker Daltonics), equipped with a SmartBeam II laser (355 nm) in the 500–4000 m/z range. 2,5-Dihydroxybenzoic acid (DHB, Bruker Daltonics, Bremen, Germany) served as matrix. Mass spectra were measured in reflection mode. The data were analysed using the software provided with the Ultraflex instrument—FlexAnalysis (version 3.4).

SEM/EDS analyses were recorded on a Quanta FEG 250 (FEI) instrument; SEM at 5 kV and EDS at 30 kV, respectively. The samples were frozen in liquid nitrogen and fractured with pliers to reveal satisfactory surface for analysis.

Rheological measurements were performed on Anton Paar MCR302 dynamic mechanical thermal (DMTA) rheometer, working in plate-plate configuration, using 25 mm plates.

Contact angle analyses were performed by the sessile drop technique at room temperature and atmospheric pressure, with a Krüss DSA100 goniometer. Three independent measurements were performed for each sample, each with a 5 µL water drop, and the obtained results were averaged to reduce the impact of surface nonuniformity.

For tensile and flexural strength tests, a Universal testing machine Instron 5969 was used, in accordance to the norm EN ISO 527-2:1996. The speed of traverse was set to 2 mm/min for both tensile strength and flexural strength tests.

The measurements of hiding power were performed by placing the samples of prepared resin systems in the optical path between the light source (an LED)and a UV-NIR spectrophotometer, AvaSpec-Mini2048CL (Avantes, Louisville, CO, USA). The amount of light transmitted was through the sample was measured and on this basis, the relative hiding strength was determined, 1Ti(s) sample being used as a reference of the lowest value.

For mixing of base epoxy resin with TiO_2, a self-made mixing device was used (see Supplementary Information, Figure S1). The machine was based on a high-torque Internal gear (Crescent type, Figure 1) rotary positive displacement pump (Yildiz Pompa YKF 1, Turkey) powered by a 0.75 kW electrical engine (Marelli Motori D6C 90 S6 B3, Italy). The setup was characterized by 900 rpm of maximum operating speed. The pump was connected to a reservoir in a closed circuit setup, resulting in constant circulation of the resin under high shear stress, inflicting mechanical breakdown of TiO_2 particles and improved dispersion of TiO_2 within the epoxy resin. During the mixing cycle, the resin would heat up to ~45 °C due to internal friction, which resulted in a significant viscosity drop (as simulated by DMTA analysis under constant shear and temperature gradient conditions, presented in Figure 2), which additionally helped with nanoparticle dispersion.

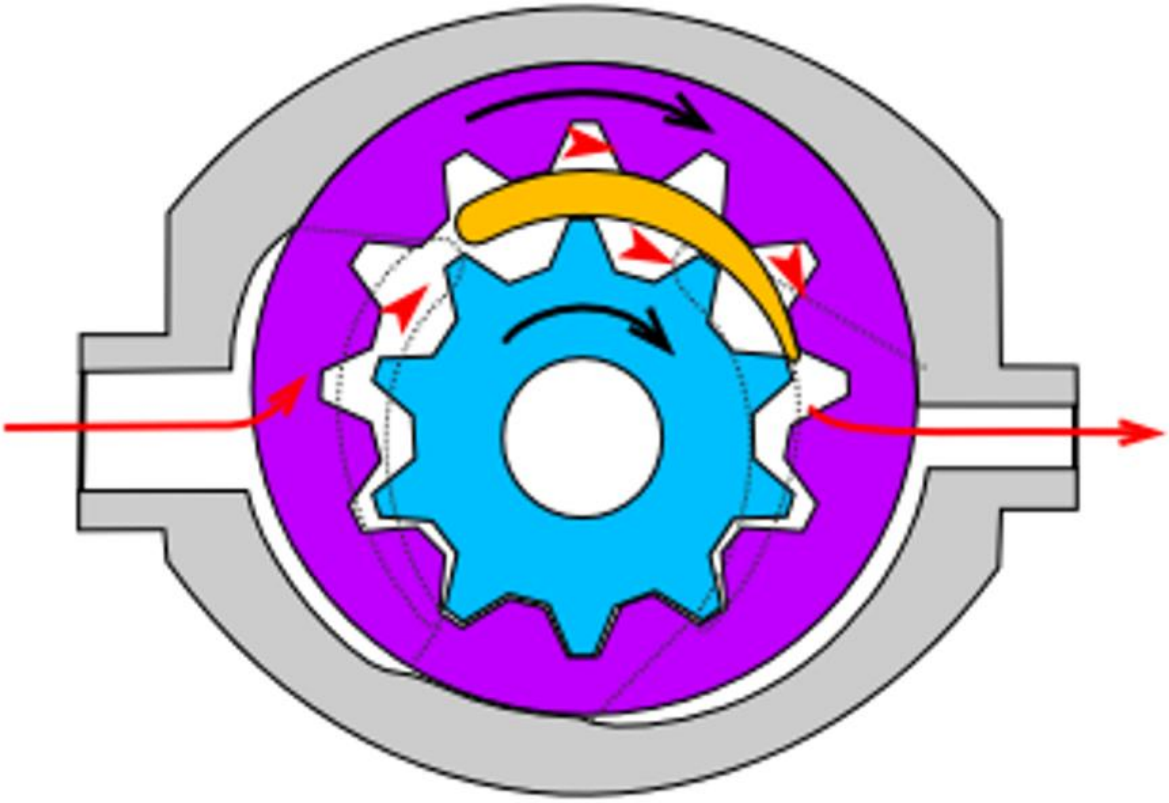

Figure 1. Internal gear pump (crescent type) design scheme. Red arrows present the pathway of the pumped medium, the black ones—the rotation direction of the gears. Source: https://commons.wikimedia.org/w/index.php?curid=38795, Creative Commons license CC BY-SA 3.0. Accessed on 2 September 2021.

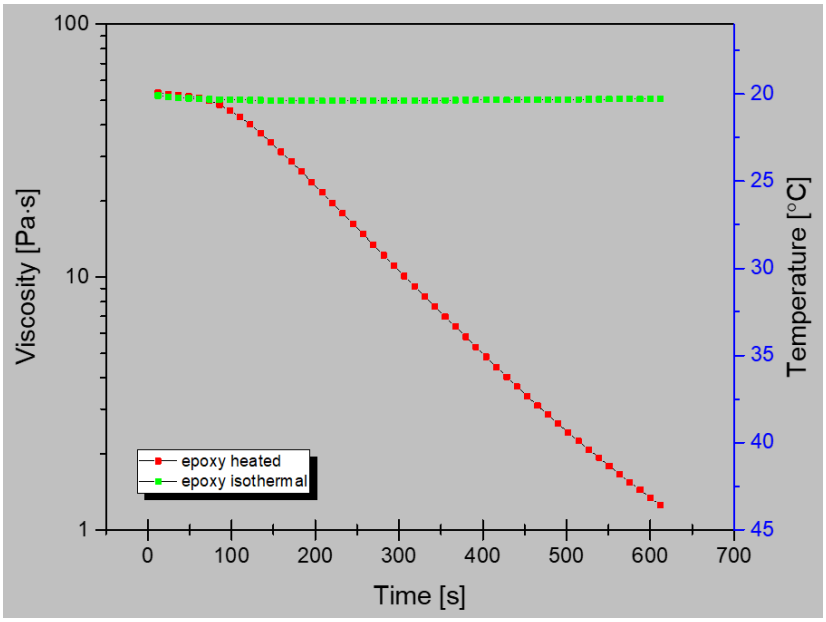

Figure 2. Dynamic viscosity curves of neat epoxy under isothermal and non-isothermal conditions under constant shear rate of 100/s.

2.2. Procedure for Hydrosilylation of Octaspherosilicates

All hydrosilylation syntheses were conducted under argon atmosphere in round-bottom flasks equipped with condensers, gas bubblers, and magnetic stirrers, the general approach being reported earlier [33]. In a typical procedure, a 500 mL three-neck, round-bottom flask was charged with 25 g of octahydrospherosilicate, 250 mL of dry toluene and a mixture of olefins (allyl-glycidyl ether and vinyltrimethoxysilane, 6:2 molar ratio for SS-6GP-2TMOS, 5:3 ratio for SS-5GP-3TMOS). A thermometer and condenser equipped with an argon inlet and oil bubbler were attached, the flask placed in a heating mantle and the system was purged with argon. The reaction mixture was set on 110 °C and before reaching boiling, Karstedt's catalyst solution (10^{-5} eq Pt/mol SiH) was added, which resulted in quick increase of temperature and the system starting to reflux. The reaction mixture was kept at the boiling temperature and samples were taken for FT-IR control until full Si-H group consumption was observed. Then, the solvent was evaporated under vacuum to dryness to obtain an analytically pure sample. The products appeared as low-viscosity oils.

2.3. Procedure for Preparation of iBu$_7$SSQ-OEt

The synthesis was conducted under argon atmosphere in a round-bottom flask equipped with a condenser, a gas bubbler, and a magnetic stirrer. A 500 mL three-neck, round-bottom flask was charged with 15 g of chlorohepta(isobutyl)octasilsesquioxane. A thermometer and condenser equipped with an argon inlet and oil bubbler were attached and the system was purged with argon. After that, the flask was further charged with 250 mL of dry THF and 4.9 mL of NEt_3 (2 eq in correspondence to Si-Cl group), the flask was placed in a heating mantle, and 50 mL of dry EtOH was slowly added. The mixture was heated to 50 °C and stirred for 3 h. Then, the reaction was transferred to a rotary evaporator, the solvent mixture removed almost to dryness, 250 mL of hexane was added to the remaining solid, and the suspension was sonicated for 30 min. The obtained mixture, comprised of the main product solution and triethylammonium hydrochloride suspension, was filtered through a sintered glass funnel to eliminate the ammonium hydrochloride solid, the flask being washed with additional 150 mL of hexane, and the obtained clear hexane solution was evaporated to dryness to obtain analytically pure sample. The product appeared as a white solid.

2.4. Procedure for Treatment of TiO_2 with Organosilicon Compounds

In a typical procedure, a 2.5 L milling jar was charged with 750 g of 50% TiO_2 water slurry, 100 mL of demineralized water (to reduce the mixture viscosity), 20 ceramic milling balls of 20 mm diameter, and either 1.875 g or 5.625 g (corresponding to either 0.5% or 1.5% *w*/*w* of dry TiO_2) of a chosen organosilicon coupling agent (see Tables 1 and 2 and Figure 2). The milling jar was closed and placed on the ball mill, and rotated at 30 rpm for 20 h. After that, the slurry was transferred to a container, dried at 105 °C to constant weight and milled again in a ball mill for 20 h. The obtained modified TiO_2 was then sampled for water contact angle measurements and used for preparation of TiO_2/EP composites. Tests for treatment of TiO_2 with 3% and 5% loadings of organosilicon coupling agents were also performed, but the resulting materials were waxy and/or sticky and difficult to handle, which was a sign of the coupling agents being used in excess. Therefore, only the samples treated with 0.5% and 1.5% of coupling agents were used for further studies.

Table 1. Silsesquioxane, spherosilicate, and silane coupling agents used in this study.

Name	Abbreviation
Isobutyltrimethoxysilane	*i*BuTMOS
3-glycidoxypropyltriethoxysilane	GPTES
ethoxyhepta(isobutyl)octasilsesquioxane	*i*Bu$_7$SSQ-OEt
hexa(3-glycidoxypropyl)di(trimethoxysilylethyl)octaspherosilicate	SS-6GP-2TMOS
penta(3-glycidoxypropyl)tri(trimethoxysilylethyl)octaspherosilicate	SS-5GP-3TMOS

Table 2. The TiO_2/epoxy resin composites prepared in this study.

Sample Name	Organosilicon Coupling Agent Type	Organosilicon Coupling Agent Amount [%] [1]	TiO_2 Amount [%]	Mixing Method	Sample Code
1	none	-	1	Mechanical stirrer	1Ti(s)
2	none	-	1	Mixing pump	1Ti(p)
3	none	-	2	Mixing pump	2Ti(p)
4	*i*BuTMOS	0.5	1	Mixing pump	1Ti05*i*BuTMOS(p)
5	*i*BuTMOS	0.5	2	Mixing pump	2Ti05*i*BuTMOS(p)
6	*i*BuTMOS	1.5	1	Mechanical stirrer	1Ti15*i*BuTMOS(s)
7	*i*BuTMOS	1.5	1	Mixing pump	1Ti15*i*BuTMOS(p)
8	*i*BuTMOS	1.5	2	Mixing pump	2Ti15*i*BuTMOS(p)
9	GPTES	0.5	1	Mixing pump	1Ti05GPTES(p)
10	GPTES	0.5	2	Mixing pump	2Ti05GPTES(p)
11	GPTES	1.5	1	Mechanical stirrer	1Ti15GPTES(s)
12	GPTES	1.5	1	Mixing pump	1Ti15GPTES(p)
13	GPTES	1.5	2	Mixing pump	2Ti15GPTE (p)
14	*i*Bu$_7$SSQ-OEt	0.5	1	Mixing pump	1Ti05*i*Bu$_7$SSQ-OEt(p)
15	*i*Bu$_7$SSQ-OEt	0.5	2	Mixing pump	2Ti05*i*Bu$_7$SSQ-OEt(p)
16	*i*Bu$_7$SSQ-OEt	1.5	1	Mechanical stirrer	1Ti15*i*Bu$_7$SSQ-OEt(s)
17	*i*Bu$_7$SSQ-OEt	1.5	1	Mixing pump	1Ti15*i*Bu$_7$SSQ-OEt(p)
18	*i*Bu$_7$SSQ-OEt	1.5	2	Mixing pump	2Ti15*i*Bu$_7$SSQ-OEt(p)
19	SS-6GP-2TMOS	0.5	1	Mixing pump	1Ti05 SS-6GP-2TMOS (p)
20	SS-6GP-2TMOS	0.5	2	Mixing pump	2Ti05 SS-6GP-2TMOS (p)
21	SS-6GP-2TMOS	1.5	1	Mechanical stirrer	1Ti15 SS-6GP-2TMOS (s)
22	SS-6GP-2TMOS	1.5	1	Mixing pump	1Ti15 SS-6GP-2TMOS (p)
23	SS-6GP-2TMOS	1.5	2	Mixing pump	2Ti15 SS-6GP-2TMOS (p)
24	SS-5GP-3TMOS	0.5	1	Mixing pump	1Ti05 SS-5GP-3TMOS (p)
25	SS-5GP-3TMOS	0.5	2	Mixing pump	2Ti05 SS-5GP-3TMOS (p)
26	SS-5GP-3TMOS	1.5	1	Mixing pump	1Ti15 SS-5GP-3TMOS (p)
27	SS-5GP-3TMOS	1.5	2	Mixing pump	2Ti15 SS-5GP-3TMOS (p)

[1] Silane coupling agent amount is given in correspondence to TiO_2, as *w*/*w* % of TiO_2.

2.5. Procedure for Preparation of TiO_2/EP Composites

In a typical procedure, the mixing pump was charged with around 1 kg of base epoxy resin and the stirring was engaged. After 5 min, TiO_2 sample of a given modification grade (see Table 2) was added in an amount corresponding to either 1 wt% or 2 wt% of the final composition and stirred for further 15 min at 800 rpm. After that, the resin mixture was transferred to a container, chilled to room temperature, and sampled for pigment stability tests. Next, the resin mixture was mixed with 12 wt% of the curing agent (Z-1) using a mechanical stirrer, degassed for 5 min in a vacuum chamber, and cast into plates of 4 mm thickness. After 16 h, the plates were removed from the moulds and set for seven days for further curing (see Supplementary Information, Figure S2). After that time, the plates were cut into standardized test specimens for mechanical analysis (dumbbells and bars) with the aid of a CNC milling plotter. The milled specimens were additionally post-cured for 17 h at 70 °C to ensure the most uniform curing state for all tested samples. Such prepared samples were used for mechanical analyses.

For the samples prepared with the mechanical stirrer (Table 2), the resin was mixed with TiO_2 for the same amount of time with the aid of the mechanical stirrer instead of the dissolver, and the rest of the procedure remained unchanged.

The composite sample codes are as follows:

$$\text{x Ti y CODE (z)} \quad (1)$$

where x—% loading of TiO_2 in the composite; y—% loading of a given silane coupling agent in correspondence to TiO_2; CODE—the type of organosilicon coupling agent used (see Table 1, Figure 3); z—mixing method: 's' for mechanical stirrer, 'p' for mixing pump

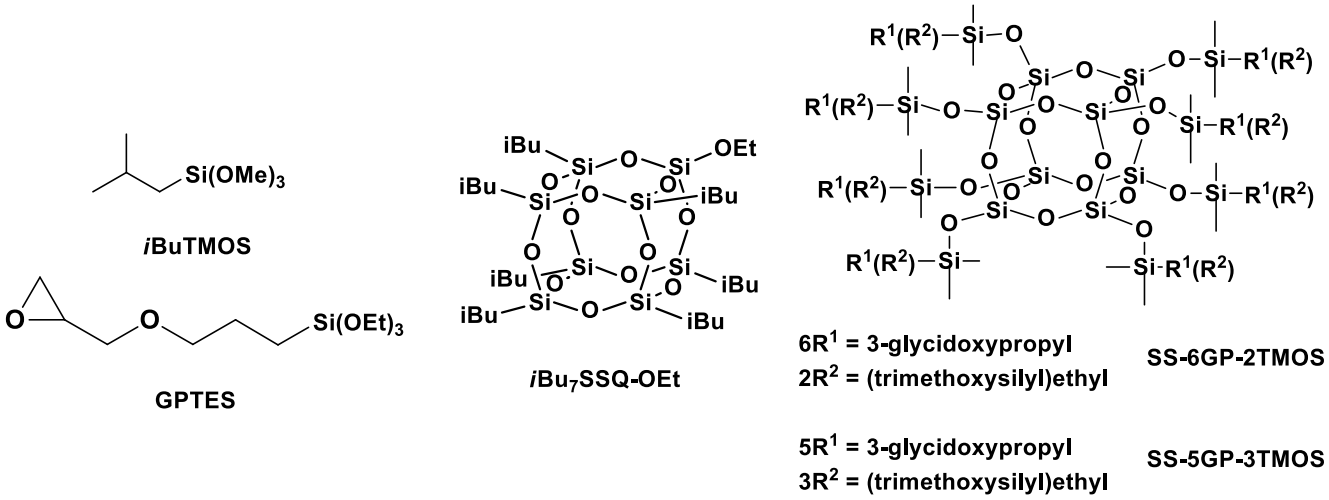

Figure 3. Structures of the silane and cage siloxane compounds studied in this work.

3. Results and Discussion

3.1. Characterization of the Obtained Products

The products were characterized by ^{1}H, ^{13}C, ^{29}Si NMR spectroscopy and MALDI-TOF mass spectrometry to verify the obtained molecular structures (see Supplementary Information). While iBu_7SSQ-OEt was obtained as a single product, for SS-6GP-2TMOS and SS-5GP-3TMOS, it was observed on MALDI-TOF spectrograms that due to random introduction of the olefin substrates into the spherosilicate cage, a mixture of products was obtained in both cases and nine molecules were formed instead of the one that a given synthesis is designated with. Although the macroscopic stoichiometry of the systems was controlled by using the proper amounts of the olefin reagents, the intramolecular stoichiometry cannot be controlled and the synthesis affords a family of nine congeners, each containing a different internal ratio of organic substituents coming from the parent olefins,

that is, vinyltrimethoxysilane and allyl-glycidyl ether. On the basis of the normalized signal intensity of the congener ions (in a form of sodium ion adducts) recorded by MS, normal distributions similar to Gaussian model were obtained, with the maximum visible near the intended system stoichiometry (Figure 4). Also, the peaks on the left side of the maximum are higher than those on the right for both systems, which can be explained on the basis of different ionization efficiency of glycidyl and alkoxysilyl groups, the glycidyl groups showing higher ionization efficiency. The effect of chemical structure on the ionization efficiency has been studied and discussed by other groups [34,35]. Therefore, this distribution should not be mistakenly considered as a direct depiction of the actual quantitative composition of the studied systems, and rather a qualitative one. It can be seen that for SS-6GP-2TMOS, the maximum is at the SS-7GP-1TMOS congener, which is likely due to the effect discussed above.

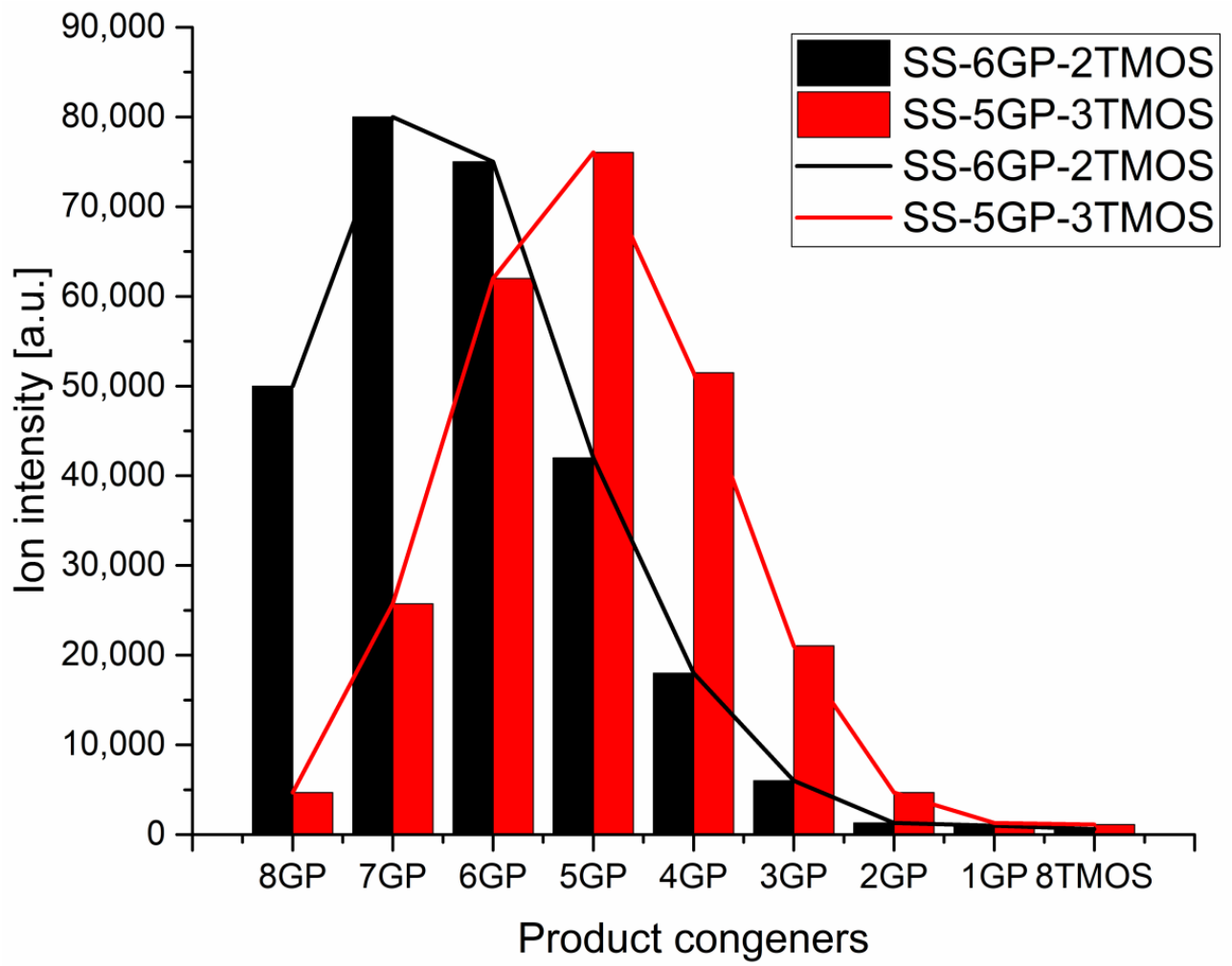

Figure 4. Distributions of congener products for SS-6GP-2TMOS and SS-5GP-3TMOS syntheses presented as MS signal intensity.

3.2. Surface Properties of the Obtained Modified TiO_2 Pigments

Modified TiO_2 pigments were analysed for their surface properties by measuring their water contact angle values (Table 3). Water contact angle is a non-direct measure of surface polarity of materials, as water is repelled by hydrophobic (non-polar) materials, thus resulting in formation of droplets with high contact angle on the surface of the measured samples. TiO_2, as an inorganic nanomaterial, shows a strongly polar surface character, which is a reason for the particles thereof to agglomerate in polymer matrices, as they are usually characterized by substantially lower polarity. Introduction of organic (or

organosilicon) groups onto the surface of TiO_2 nanoparticles allows for controlling of their surface character, that is chemistry and polarity. It then translates into better filler-matrix interaction, without which a filler (in this case the pigment) tends to agglomerate [36].

Table 3. Water contact angles of TiO_2 modified with the studied silane coupling agents.

Silane Coupling Agent Type	Silane Coupling Agent Amount [%] [1]	Water Contact Angle [°]
None	-	0
$_i$BuTMOS	0.5	0
$_i$BuTMOS	1.5	Superhydrophobic [2]
GPTES	0.5	0
GPTES	1.5	0
$_i$Bu$_7$SSQ-OEt	0.5	0
$_i$Bu$_7$SSQ-OEt	1.5	Superhydrophobic [2]
SS-6GP-2TMOS	0.5	0
SS-6GP-2TMOS	1.5	0
SS-5GP-3TMOS	0.5	0
SS-5GP-3TMOS	1.5	0

[1] Silane coupling agent amount is given in correspondence to TiO_2, as *w/w* % of TiO_2; [2] roll-off observed at each attempt at measuring the contact angle.

The samples treated with any of the glycidyl ether-derived compounds (GPTES, SS-6GP-2TMOS, SS-5GP-3TMOS) showed retainment of their hydrophilic character independently of the amount of the silane agent used, the water droplets being quickly absorbed by the material. It might be either due to polar character of glycidyl group itself, or its partial hydrolysis to even more hydrophilic diol group on the surface of TiO_2. Kochkar et al. reported that oxirane moiety hydrolyzed to diol one partially when studying epoxidation of cyclohexene on a TiO_2-SiO_2-mixed catalyst [37]. This hypothesis is supported by FT-IR spectra of the glycidyl-derived compounds used and the TiO_2 samples modified with those. The IR spectra allow to observe the effect of capping TiO_2 hydroxyl groups, as the −OH stretching band is smaller for modified pigments than for the neat titanium white (Figure 5E, the reduction of absorption intensity marked with shaded area) as well as Ti-O-Si moiety vibrations being visible as a small bulge at ~910 cm^{-1} (Figure 5F), which is in agreement with the literature reports [38,39] Additionally, C-H vibrations are visible, coming from organosilicon additives grafted on the pigment particles surface (Figure 5A,C, green lines). However, while the absorption bands at 1450–1490 cm^{-1}, characteristic for C-C oxirane ring vibrations are visible for both the organosilicon compounds and for the obtained pigments (Figure 5B,D, red lines), confirming the successful functionalization thereof, the FT-IR spectra of the latter also show additional absorption bands matching the vibration of the diol C-OH bonds (Figure 5D, blue lines, the oxirane ring opening presented on Figure 8). It is the most clear for the TiO_2–1.5%GPTES sample, with an absorption band with the maximum at ~1380 cm^{-1}, however the remaining modified TiO_2 samples also show similar absorption at ~1385 cm^{-1}.

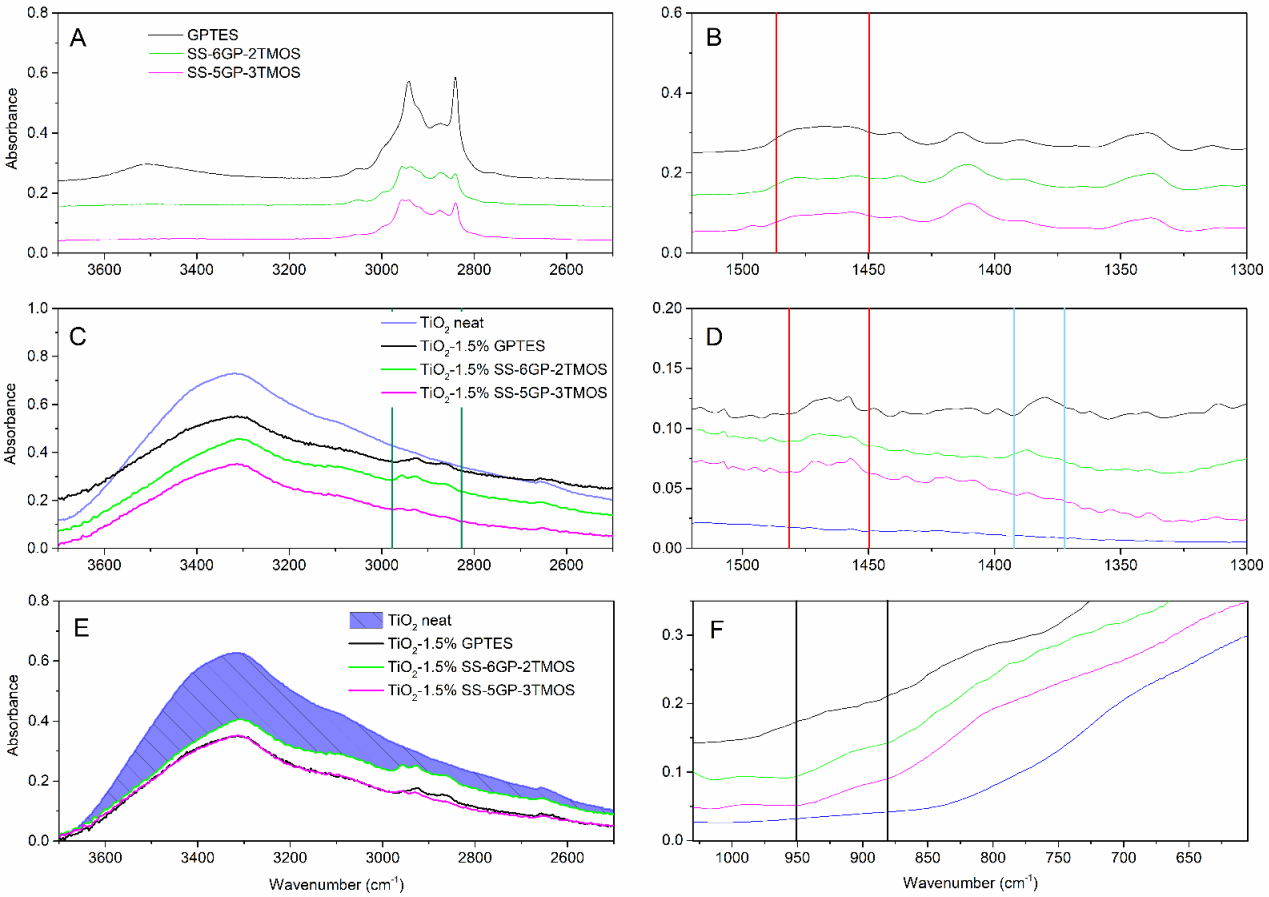

Figure 5. FT-IR of glycidyl-derived silane coupling agents (**A**,**B**), pristine TiO_2 and TiO_2 modified thereof (**C**–**F**). Red lines represent the region of oxirane ring vibrations, the blue lines—the diol vibrations, green ones—C-H vibrations, black ones—Ti-O-Si vibrations.

The last effect considered is the gelation of the silane agent, thus reducing the coating effect of the silane agent. SS-6GP-2TMOS was observed on SEM images to form microdroplets accompanying TiO_2 particles in the final composite (Figure 6A,B visualizing the microdroplets on TiO_2, Figure 6D confirming the silicon-rich area on the TiO_2 microaggregate). On the other hand, butylated agents (both *i*BuTMOS and *i*Bu_7SSQ-OEt) showed strong hydrophobicizing action, as the obtained materials were superhydrophobic. The droplets formed were completely repulsed by TiO_2, making it impossible to lay a droplet for the measurement, and when dropped from air, they would immediately roll off even at the angle of ~0° (Figure 7, particles of TiO_2 visible on the bottom surface of the water droplets after attempts of placing the droplets on the samples' surface).

Based on the FT-IR spectra and water contact angle measurements, proposed mechanisms of TiO_2 surface functionalization with the studied organosilicon coupling agents is presented on Figure 8.

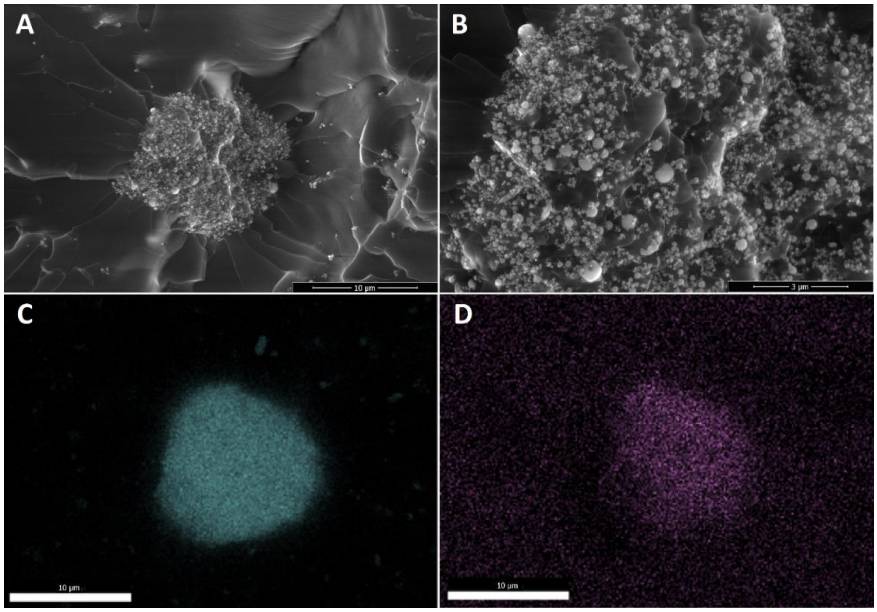

Figure 6. Microdroplets of condensed SS-6GP-2TMOS together with TiO_2 particles visible for 1Ti15SS-6GP-2TMOS. (**A**)—10,000× magnification; (**B**)—30,000× magnification; (**C**)—titanium (Ti) EDS; (**D**)—silicon (Si) EDS.

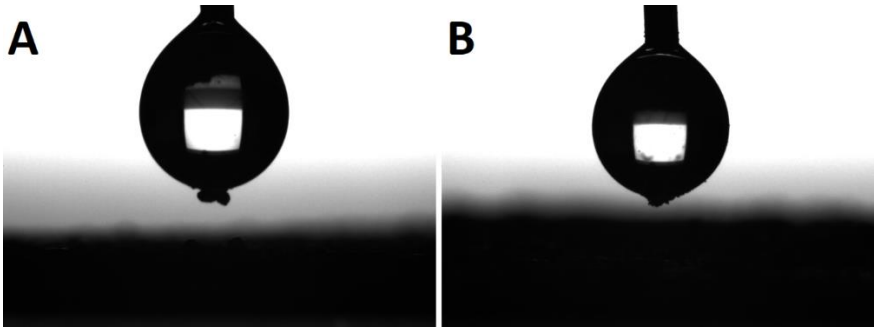

Figure 7. Water droplets during sessile drop analysis. Particles of modified TiO_2 visible on the bottom of each droplet after an attempt at placing the droplet on the pigment surface. (**A**)—TiO_2-1.5% *i*BuTMOS; (**B**)—TiO_2-1.5% *i*Bu_7SSQ-OEt.

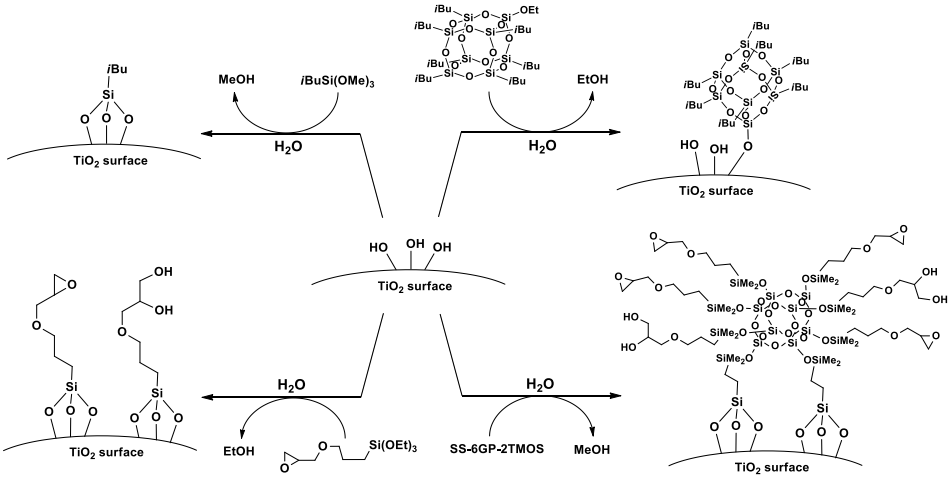

Figure 8. A proposed mechanism of TiO_2 surface silanization with *i*Bu_7SSQ-OEt, SS-6GP-2TMOS and silane coupling agents.

3.3. Microscopic Analysis and the Effect of Processing Methodology on TiO_2 Dispersion

SEM imaging was used to assess the dispersion of TiO_2 particles in the epoxy matrix (see Supplementary Information Section 4: SEM images of the TiO_2/EP composites). It was observed that the sample prepared with untreated TiO_2 by mechanical stirring showed the largest agglomeration effect, as not only the particles of TiO_2 formed multi-micron aggregates of size up to 50 μm, but also these aggregates were surrounded by barely no well-dispersed microparticles. On the other hand, both high-torque pump stirring and application of organosilicon coupling agents improved the dispersion of the pigment. It is visible on the SEM images of samples containing pristine TiO_2 that after pump mixing, the primary aggregates observed are of size up to approx. 20 μm, and that they are accompanied by a fraction of particles of <2 μm. Also, for all the sample series, the increase in TiO_2 loading from 1% to 2% resulted in a higher number of aggregates visible on the SEM images. At 0.5%, *i*BuTMOS was a highly effective dispersing agent both under mechanical stirring and pump stirring conditions, the latter resulting in almost complete elimination of TiO_2 aggregates above 2 μm, when the pigment was at the 1% loading. At 1.5%, *i*BuTMOS and 1% TiO_2 loading, all the pigment was dispersed below 1 μm after pump mixing, which proved the successful homogenization of the system components. In comparison, GPTES was slightly less effective in terms of the size of the aggregates observed, which was especially visible under mechanical stirring. $_i$Bu$_7$SSQ-OEt was highly effective at dispersing TiO_2 even when the pigment was at the 2% loading. When compared to simple silane coupling agents (trialkoxysilanes), $_i$Bu$_7$SSQ-OEt does not have the ability to form gel products (polysilsesquioxanes), which, depending on the silane: filler ratio and processing conditions, may cause secondary aggregation of TiO_2 by binding the particles together with polysilsesquioxane gel. SS-6GP-2TMOS effectively dispersed the pigment at 0.5% additive loading for both 1% and 2% of TiO_2 used, while at the higher loading of silane agent, aggregation was observed due to the agent gelation. The gelling effect was more visible for SS-5GP-3TMOS, however the additive still allowed for elimination of larger (>10 μm) primary agglomerates. In addition, the dispersing effect of a selected modifier, *i*Bu$_7$SSQ-OEt, was visualized with aid of digital optical microscopy (Figure 9), where diluted samples containing 0.0625% TiO_2 (see *Section 3.4. Pigment Stability and Hiding Power Studies*) were observed in light transmission mode. For the samples containing modified TiO_2, a significant drop in abundance of larger pigment agglomerates was observed, and in their place, even graininess effect was visible, which corresponded to the presence of finely dispersed pigment particles, as confirmed with detailed SEM imaging discussed above (for SEM images, see Supplementary Information Section 4: SEM images of the TiO_2/EP composites).

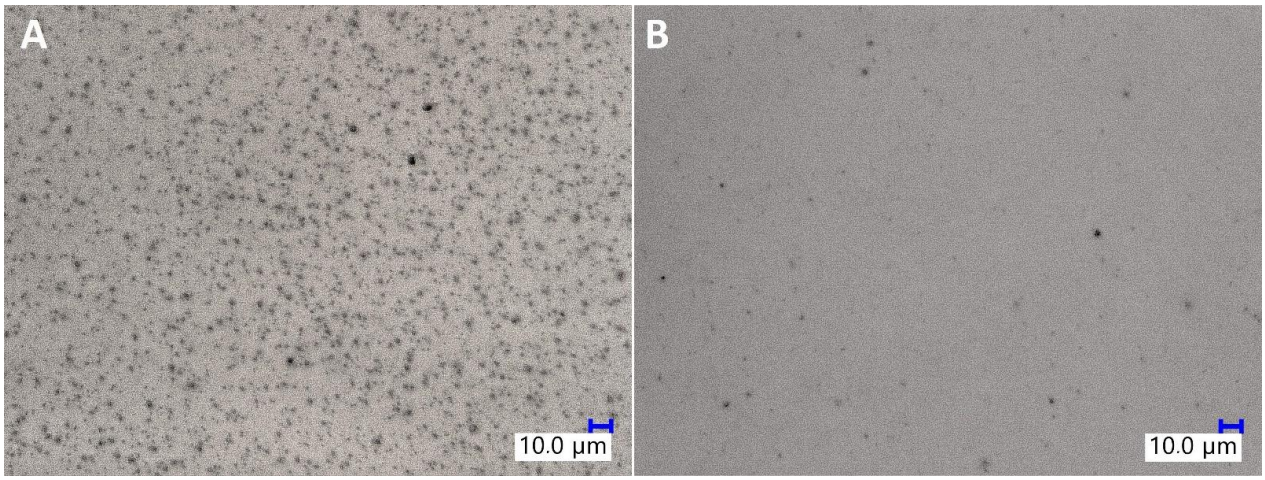

Figure 9. Digital optical microscopic images of neat TiO_2/EP (**A**) and 1.5% *i*Bu$_7$SSQ-OEt TiO_2/EP (**B**).

3.4. Pigment Stability and Hiding Power Studies

The stability of modified and pristine TiO_2/liquid epoxy resin suspensions was assessed by pouring samples of the suspensions in screw-capped centrifuge vials and leaving them on standing. Then, they were checked every couple of days for any signs of phase separation, including pigment precipitation on the vial walls or bottom, resin cloudiness, or discoloration near the surface. The samples prepared by mechanical stirring all underwent heavy phase separation within two weeks from preparation, as the larger agglomerates of TiO_2 were characterized by poor stability in the suspension. It correlates with the SEM images (Supplementary Information), as these larger agglomerates were captured. On the other hand, the samples prepared by high shear pump mixing showed much higher suspension stability, the improved dispersing method increasing the stability time by over an order of magnitude for some of the studied systems (Figure 10). The main conclusion obvious from the results obtained is that, independently of the discussed TiO_2 system used, increasing pigment loading from 1% to 2% resulted in more or less severe reduction in the suspension stability. It can be understood as higher concentration of TiO_2 particles in the epoxy suspension causing their faster aggregation over storage time; however, the SEM images of TiO_2/EP composites made from freshly prepared suspensions also revealed increased agglomeration in the composites containing 2% of TiO_2. These results suggest that for the TiO_2 pigments of limited stability, formation of primary agglomerates (<10 μm) is a fast process, after which these agglomerates grow at the rate depending on the pigment concentration in the suspension and the surface physicochemistry of the particles, up to the point of spontaneous sedimentation. This idea is further supported by the results of hiding power study (Figure 11). Interestingly, some of the studied coupling agents provided virtually no stabilization to the pigment over prolonged time, that is, SS-6GP-2TMOS at 0.5% loading and SS-5GP-3TMOS at both loadings. It may be due to the protic character of the diol groups generated during surface coupling of TiO_2, resulting in interparticle attraction, but also less effective particle coating with the coupling agent and the gelling thereof, as discussed earlier (*Section 3.2. Surface Properties of the Obtained Modified TiO_2 Pigments*). GPTES showed behaviour comparable to that of SS-6GP-2TMOS. On the other hand, $_i$Bu$_7$SSQ-OEt at 0.5% loading provided stabilization superior to all the other coupling agents studied, and at 1.5% loading, slightly higher than that of *i*BuTMOS. It is due to the apolar character of the isobutyl group, which both the SSQ and silane compounds share in common.

The studies of hiding power based on the samples' visible light transmittance revealed the effect of both processing technique and coupling agent choice on the pigmenting efficacy of the resulting epoxy systems. While application of modified TiO_2 via mechanical stirring resulted in slight improvement of hiding power (approximately two-fold on the average of the studied systems), and the implementation of pump mixing allowed for a more significant improvement (over five-fold for neat TiO_2 at 1% loading), the most impressive results were obtained when both surface treatment and pump mixing were applied. It proves that chemical modification of the pigment particles results not only in enhanced dispersability thereof in the epoxy during suspension preparation, but also stabilizes these particles in the suspension, hampering their secondary self-aggregation. For neat TiO_2, increasing the pigment loading from 1% to 2% resulted in only 17% increase of hiding power, making little change in the overall performance of the composition. On the other hand, for the systems containing TiO_2 treated with 0.5% of $_i$Bu$_7$SSQ-OEt it was 59% increase; for 0.5% and 1.5% of SS-6GP-2TMOS, 679% and 300%, respectively; for 0.5% and 1.5% of SS-5GP-3TMOS, 958% and 1490%, respectively. Interestingly, despite showing moderate to poor stability over storage time, the discussed spherosilicate-based modifiers still performed well at enhancing pigmentation efficacy of the TiO_2 treated thereof. The best performing pigment system was pump-mixed TiO_2 treated with 1.5% of *i*Bu$_7$SSQ-OEt, where at 1% TiO_2 loading, the relative hiding power was over ten times higher than that of the sample containing pump-mixed neat TiO_2; at 2% loading, the hiding power was nine times higher than that of the neat pigment counterpart.

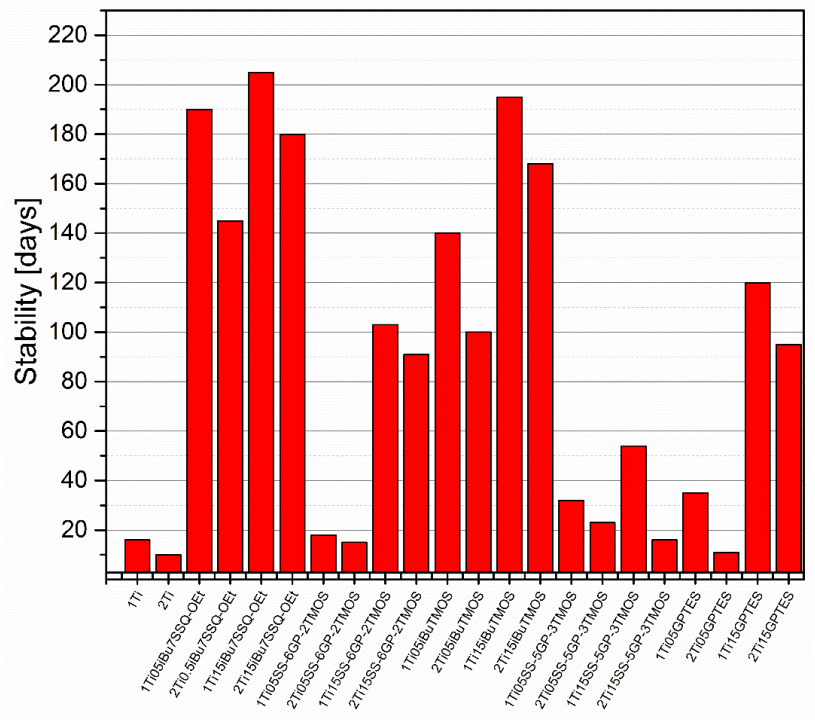

Figure 10. Time-dependent stability of TiO_2 suspensions in liquid epoxy systems prepared by pump mixing.

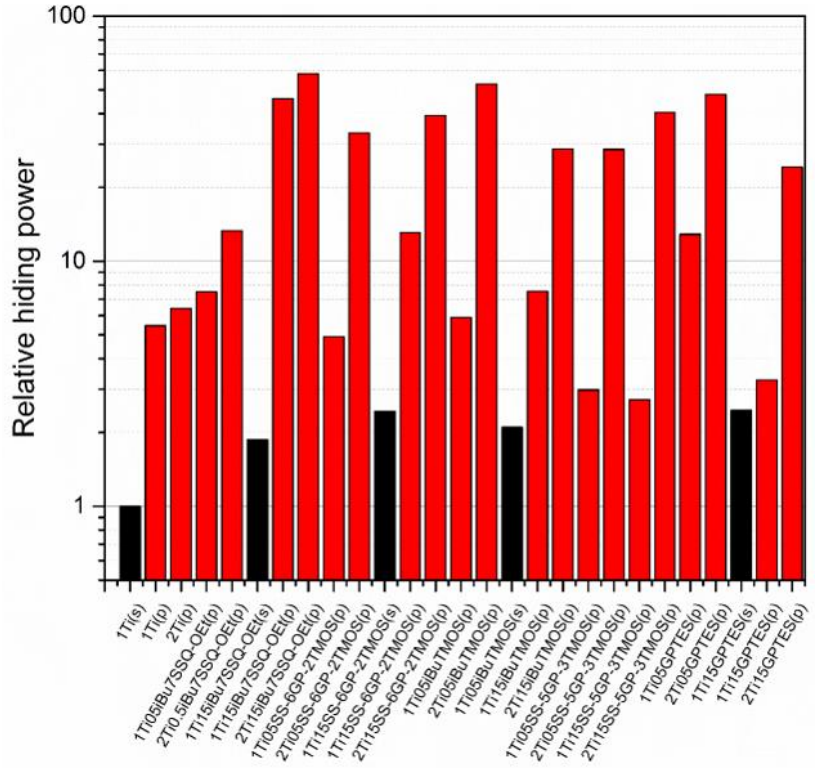

Figure 11. Relative hiding power of the pigmented epoxy systems.

To visualise the practical effect of improved TiO_2 dispersion within the epoxy base, an additional experiment was performed where a sample of a chosen epoxy containing 1% of modified TiO_2 and a series of dilutions was prepared with neat epoxy to obtain samples of 0.5%, 0.25%, 0.125%, and 0.0625% of TiO_2 (Figure 12, the last concentration omitted due to

poor pigmentation). After that, pigmentation was evaluated comparatively between the series of samples by assessing their visual opaqueness on a colourful background. While the samples containing neat TiO_2 were already visibly transparent at 0.5% loading, the samples containing 1.5% *i*Bu$_7$SSQ-OEt-modified TiO_2 provided satisfactory pigmentation up to the 0.25% dilution.

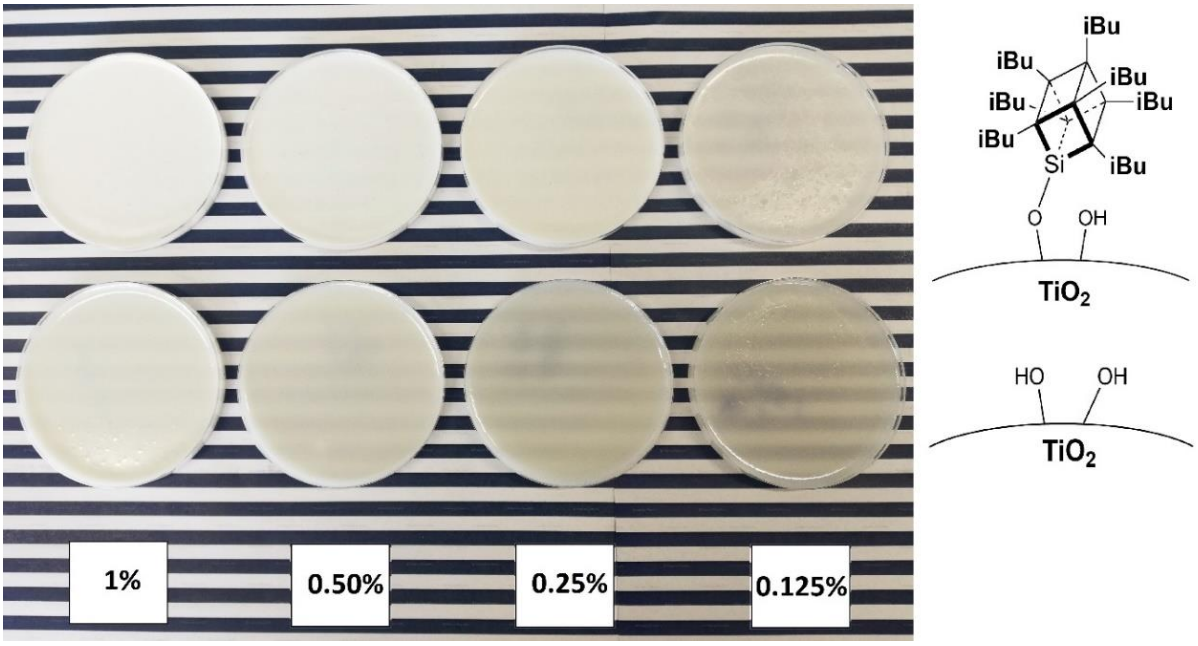

Figure 12. Serial dilution samples of mixing pump-prepared 1.5% *i*Bu$_7$SSQ-OEt TiO_2/EP (top) and neat TiO_2/EP (bottom).

3.5. Mechanical Studies

Mechanical analysis revealed subtle differences between the TiO_2/epoxy systems studied, even despite low loading of TiO_2 in the composites (Figures 13–16). For Young's modulus, it was observed that the systems present stiffness comparable to the neat epoxy within the limits of the standard deviation (Figure 14). Also, for the samples containing either 1% or 2% of the same type of prepared TiO_2 (either pristine or modified), there was a tendency towards Young's modulus increase along with the pigment concentration for well-dispersed systems (e.g., 0.5% $_i$Bu$_7$SSQ-OEt/TiO_2, 0.5% *i*BuTMOS/TiO_2), while for the agglomerating pigments, the value would drop (e.g., pristine TiO_2, 0.5% GPTES/TiO_2). Due to low loadings of the pigmenting filler used, retention of tensile properties (tensile strength and elongation at break, that is) should rather be considered instead of their improvement, as the loading of the filler is too small to provide enough reinforcement and the mechanical failure may propagate throughout the bulk polymer. For tensile strength, mechanical stirrer-prepared composites were the weakest from each series, as the agglomerated particles provided spots of structural imperfection, causing material failure. Some of the highest values of tensile strength and elongation at break were recorded for systems loaded with TiO_2 modified with 1.5% of SS-6GP-2TMOS and 0.5% of SS-5GP-3TMOS due to high dispersion and well-developed particle-polymer interphase. Also, $_i$Bu$_7$SSQ-OEt/TiO_2, performed slightly better than its silane counterpart system, iBuTMOS/TiO_2, suggesting that silsesquioxane- and spherosilicate-based coupling agents provide better surface treatment agents, likely due to less gelation side reactions.

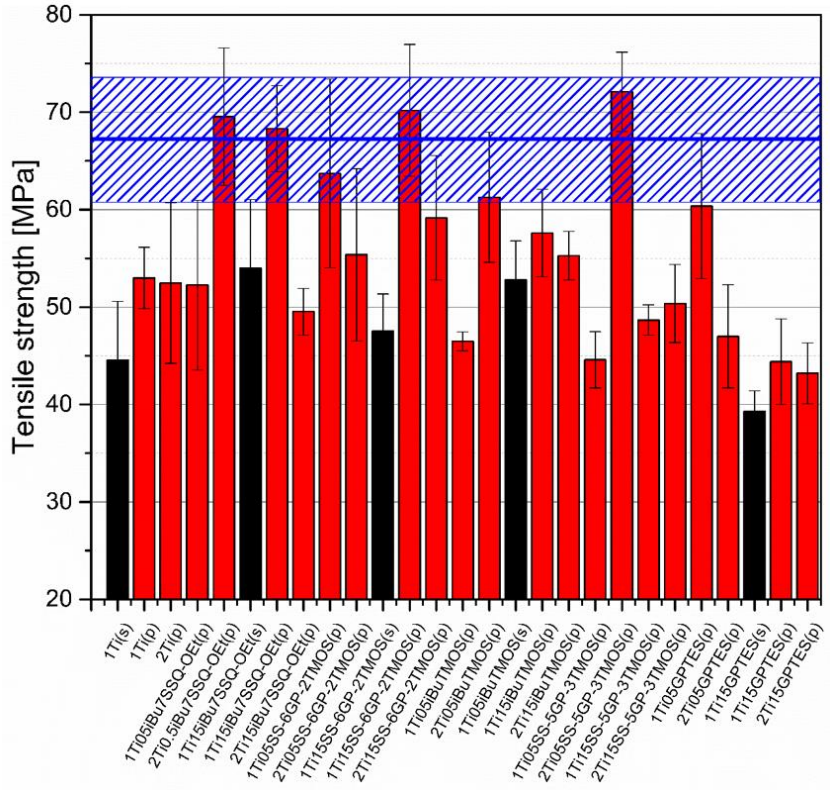

Figure 13. Tensile strength of neat and modified TiO_2/EP composites.

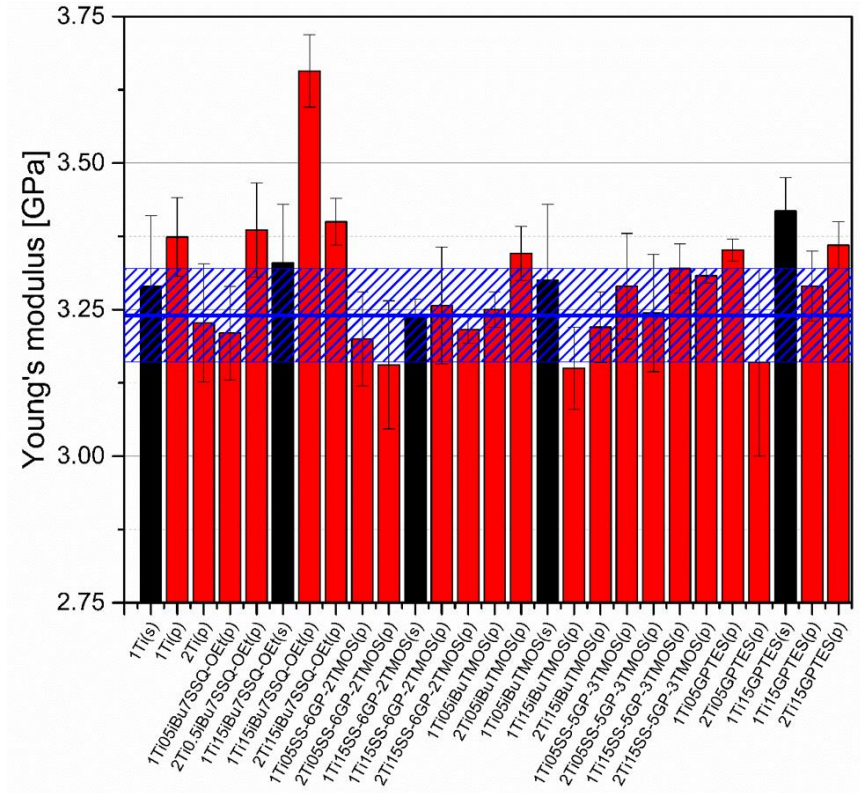

Figure 14. Young's modulus of neat and modified TiO_2/EP composites.

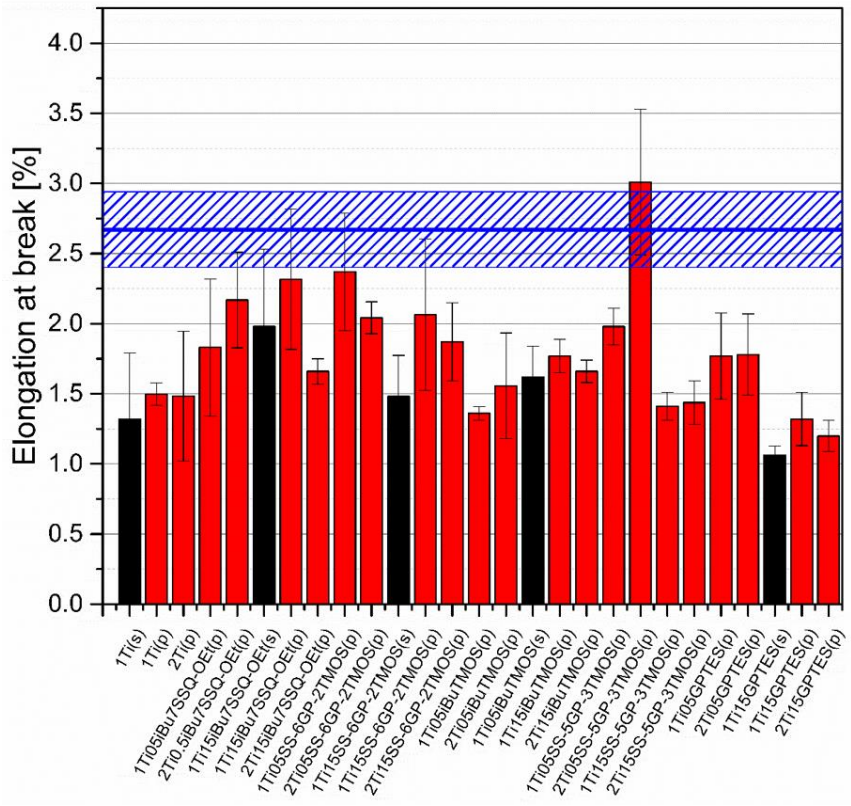

Figure 15. Elongation at break of neat and muodified TiO_2/EP composites.

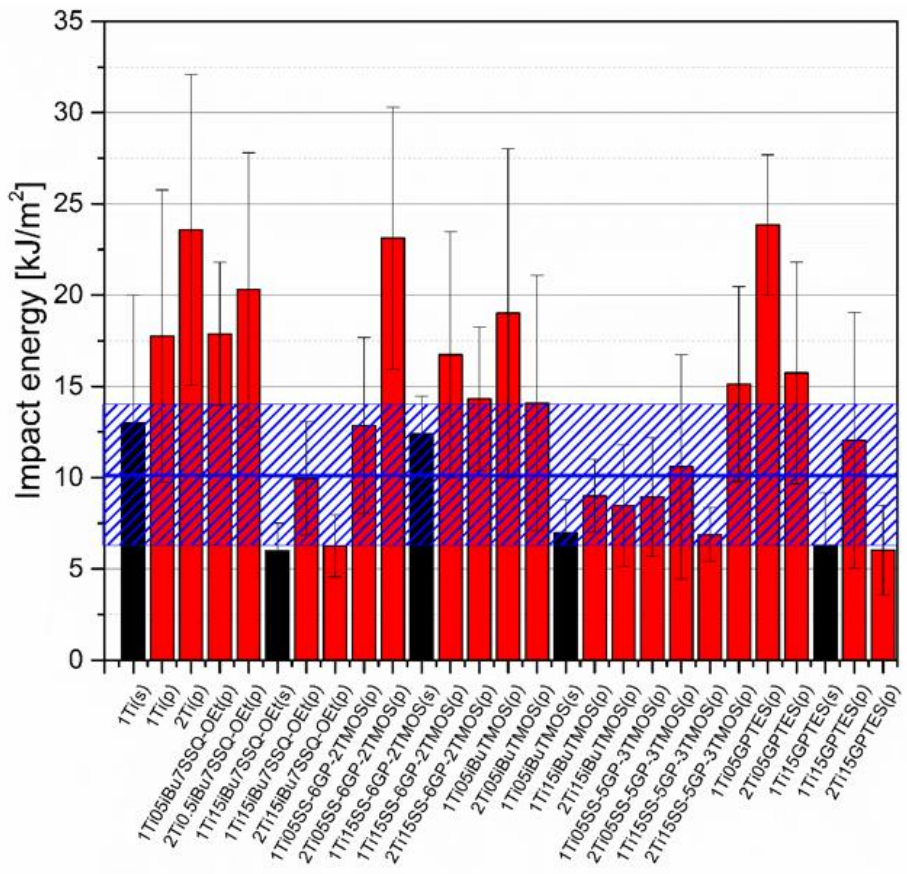

Figure 16. Impact energy of neat and modified TiO_2/EP composites.

Impact resistance tests revealed that some of the prepared systems were characterized by up to over 100% increase in durability described by the mean impact energy (Figure 16). Among those, samples containing pristine TiO_2 showed satisfactory performance and that the systems of the highest dispersion of the pigment are not the ones of the highest impact resistance. This proves that the agglomerates and particles of moderate size may work as crack propagation interrupters. Findings supporting such statement were reported earlier when studying diatomite-filled epoxy composites [40]. Triethylenetetramine-cured epoxy resins under low temperatures and high strain rates tend to undergo continuous crack propagation and such heterogeneous regions introduced in the polymer bulk may help to discontinue this propagation [41].

3.6. Thermal Studies

Although the studied materials share the same polymer matrix and the base pigmenting filler, the preparation methodology applied and the coupling agent used cause subtle structural and interfacial differences that can be elucidated with DSC (Figure 17, top). Epoxy systems of similar polymer matrix were studied earlier [40,42]. It can be seen that for the second heating cycle, the T_g of most of the samples appears at ~120 °C, being close to that of the neat epoxy (Figure 17, bottom). However, for the mechanical stirrer-prepared compositions, the T_g was observed to be slightly lowered for all examples, both compared to the mixing pump-prepared ones and the neat epoxy. It has been a subject of discussion that fillers presenting weak interaction with the polymer tend to reduce T_g by creating an interface where due to poor filler surface wetting action, a fraction of polymer is formed, characterized by more freedom than that of the bulk polymer [43–45]. By this thesis, it can be explained that the poorly dispersed TiO_2 particles create such interface due to their reduced surface/volume ratio. Another observation was made on the change of T_g over time. Two measurements were taken 21 days apart, after seven and 30 days of resin casting. By the time of the second measurement, T_g would increase by average of two degrees Celsius for most samples, as additional diffusion between the epoxy and TiO_2 occurred over time. The effect was less prominent for the samples containing GPTES-treated TiO_2, suggesting stronger and less elastic grafting of the epoxy chains on the modified particles in the first place. Similar behaviour of nanocomposites containing fillers with reactive group-containing coupling agents was described by Ash, Schadler et al. [45]. Additionally, the glass transition of epoxy composites with no thermal treatment was studied (glass transition of residually uncured resin, T_{gu}, Figure 17, middle). In this case, the phenomenon of low-temperature glass transition is caused mostly by the bulk resin, with polymer domains containing highly flexible chains containing either unreacted oxirane or amine groups. These chains undergo further partial cross-linking upon sample aging, but for more complete curing, samples need to be heated above that T_{gu} temperature for the unreacted chains to regain mobility and undergo further cross-linking. As was mentioned, this phenomenon is caused by the bulk material and by so, the filler has a very small and unclear effect on the T_{gu} values. For the studied systems, T_{gu} was in a 52–54 °C range for all the samples after seven days from casting, and after 30 days the value would increase by average of 6 °C. The highest ΔT_{gu} were observed for the samples containing TiO_2 treated with 1.5% of GPTES and spherosilicate agents, and prepared by mixing pump, supporting the abovementioned hypothesis that the well-dispersed, modified nanoparticles undergo grafting of epoxy chains on their surface, which introduces regions of decreased chain mobility within the matrix. The effect was less prominent for the remaining modifiers, suggesting more mobile nanoparticle-matrix interphase caused by the non-covalent interactions.

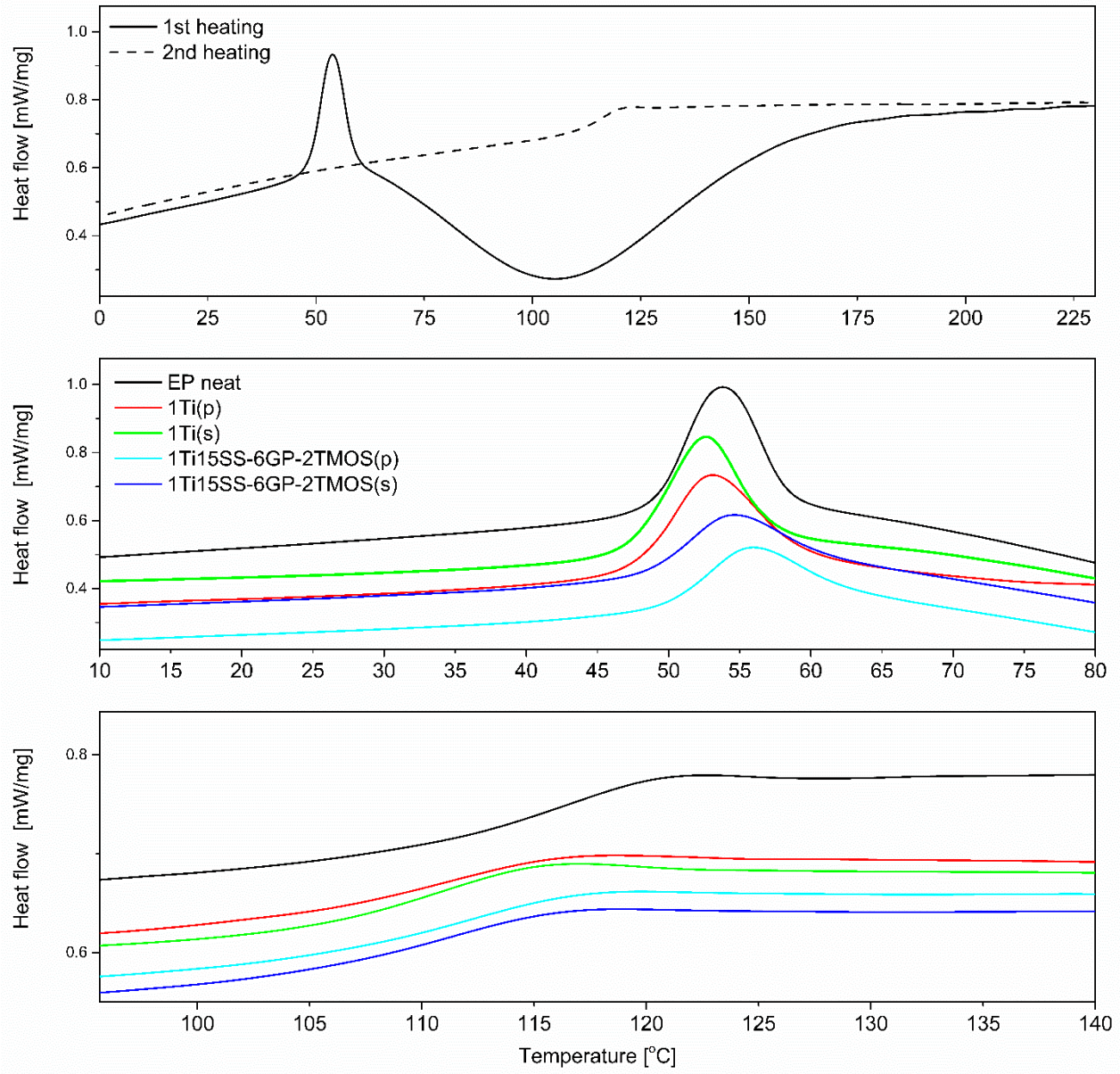

Figure 17. DSC plots of selected epoxy systems; neat EP (**top**); T_{gu} region (**middle**), T_g region (**bottom**).

4. Conclusions

The conclusions to be drawn from this study, are:

(1) A novel method for preparation of highly dispersed TiO_2/epoxy systems with the aid of a custom high-shear gear pump was presented. The impact of the pigment dispersing method on the properties of epoxy systems has been discussed in detail, including suspension stability and composite hiding power. It was shown that physical means of dispersing the nanoparticles are as much important as the chemical ones for their surface treatment, and together, a synergistic effect is obtained.

(2) An effective and green method for TiO_2 surface treatment in aqueous media was described. Herein the method may be introduced into the production line of TiO_2 pigments for coating/paint industry, if professional application of such systems was to be considered.

(3) Improved mechanical properties were observed in terms of impact resistance and Young's modulus, when silsesquioxane coupling agent was used, due to good dispersion of the nanoparticles within the epoxy matrix.

(4) High hiding power was obtained with the described methodology including both chemical surface treatment of the TiO_2 pigment and high-shear dispersing procedure

thereof, proving the synergistic effect of the two. The proposed methodology may serve for preparation of novel, high-performance coating systems. Additionally, improved dispersion and particle stability may allow for reduction of pigment loading for the epoxy base to obtain the satisfactory hiding power.

(5) TiO_2 dispersions of long shelf life were obtained, the selected cage siloxane additives showing superior stabilizing effect over silane coupling agents.

(6) Superhydrophobic effect for TiO_2 surface was obtained for two coupling agents—$_i$BuTMOS and $_i$Bu$_7$SSQ-OEt, showing the great possibilities in terms of modification of the surface properties of TiO_2 with the application of silsesquioxane agents.

(7) The chemical reactions occurring during TiO_2 surface modification were proposed and confirmed with FT-IR. The hydrolytic opening of oxirane ring to the corresponding diol has been confirmed, possibly catalysed by TiO_2 itself, which is an important finding concerning surface treatment of similar materials in water-based media.

The obtained findings show that the silsesquioxane- and spherosilicate-based coupling agents are somehow similar to their silane counterparts, but have their advantages over simple silanes. It might encourage tuning of silsesquioxane compounds structure and the process of their application, if their use as surface treatment agents is sought for special applications, e.g., high performance coating systems.

Supplementary Materials: The following are available online at https://www.mdpi.com/article/10.3390/ma15020494/s1, Figure S1. Internal gear pump setup used for preparation of TiO2/epoxy dispersions; Figure S2. A sample of cured TiO_2/epoxy composite prepared; NMR spectroscopy of the obtained compounds; MALDI-TOF mass spectra of obtained spherosilicate compounds; SEM images of the TiO_2/EP composites.

Author Contributions: Conceptualization, D.B. and R.E.P.; Data curation, D.B., M.F., D.P., M.D. and B.S.; Formal analysis, D.B., M.F., D.P., M.D. and B.S.; Funding acquisition, D.B. and B.M.; Investigation, D.B. and R.E.P.; Methodology, R.E.P.; Project administration, D.B. and R.E.P.; Resources, D.B.; Software, D.B., M.F., D.P. and M.D.; Supervision, R.E.P. and B.M.; Validation, R.E.P.; Visualization, D.B., M.F., D.P., M.D. and B.S.; Writing—original draft, D.B., R.E.P., M.F. and D.P. All authors have read and agreed to the published version of the manuscript.

Funding: This research was funded by the National Science Centre, Poland, grant number UMO-2018/29/N/ST5/00868 and UMO/2017/27/B/ST5/00149.

Institutional Review Board Statement: Not applicable.

Informed Consent Statement: Not applicable.

Data Availability Statement: All the data were collected and provided either in the main manuscript file or in the Supplementary Materials File.

Conflicts of Interest: The authors declare no conflict of interest.

References

1. Chanda, M.; Roy, S.K. *Industrial Polymers, Specialty Polymers, and Their Applications*; CRC Press: Boca Raton, FL, USA, 2009.
2. Xanthos, M. *Functional Fillers for Plastics*, 2nd ed.; Wiley-VCH: Weinheim, Germany, 2010.
3. Faulkner, E.B.; Schwartz, R.J. *High Performance Pigments*, 2nd ed.; Wiley-VCH: Weinheim, Germany, 2009.
4. Buxbaum, G.; Pfaff, G. *Industrial Inroganic Pigments*, 3rd ed.; Wiley-VCH: Weinheim, Germany, 2005.
5. Available online: https://www.icis.com/explore/resources/news/2020/04/17/10497512/europe-tio2-demand-buffeted-by-coronavirus-headwinds-loom (accessed on 8 November 2021).
6. Dong, X.; Zhang, X.; Yu, X.; Jiang, Z.; Liu, X.; Li, C.; Sun, Z.; Zheng, S.; Dionysiou, D.D. A novel rutile TiO2/AlPO4 core-shell pigment with substantially suppressed photoactivity and enhanced dispersion stability. *Powder Technol.* **2020**, *366*, 537–545. [CrossRef]
7. Xue, B.; Yan, R.; Wang, C.; Zhang, H.; Yue, Y.; Luo, J. Study on the characterization technology of hiding power of powder coating. *J. Phys. Conf. Ser.* **2021**, *1965*, 012046. [CrossRef]
8. Plueddeman, E.P. *Silane Coupling Agents*, 2nd ed.; Springer Science + Business Media: New York, NY, USA, 1991.
9. Kokszul, J. *Materiały Polimerowe*; Wydawnictwo Politechniki Częstochowskiej: Częstochowa, Poland, 1999.
10. Misasi, J.M.; Jin, Q.; Knauer, K.M.; Morgan, S.E.; Wiggins, J.S. Hybrid POSS-Hyperbranched polymer additives for simultaneous reinforcement and toughness improvements in epoxy networks. *Polymer* **2017**, *117*, 54–63. [CrossRef]

11. Liu, Y.-L.; Chang, G.-P. Novel approach to preparing epoxy/polyhedral oligometric silsesquioxane hybrid materials possessing high mass fractions of polyhedral oligometric silsesquioxane and good homogeneity. *J. Polym. Sci. Part A Polym. Chem.* **2006**, *44*, 1869–1876. [CrossRef]
12. Strachota, A.; Whelan, P.; Kříž, J.; Brus, J.; Urbanová, M.; Šlouf, M.; Matějka, L. Formation of nanostructured epoxy networks containing polyhedral oligomeric silsesquioxane (POSS) blocks. *Polymer* **2007**, *48*, 3041–3058. [CrossRef]
13. Brus, J.; Urbanová, M.; Strachota, A. Epoxy Networks Reinforced with Polyhedral Oligomeric Silsesquioxanes: Structure and Segmental Dynamics as Studied by Solid-State NMR. *Macromolecules* **2008**, *41*, 372–386. [CrossRef]
14. Suliga, A.; Hamerton, I.; Viquerat, A. Cycloaliphatic epoxy-based hybrid nanocomposites reinforced with POSS or nanosilica for improved environmental stability in low Earth orbit. *Compos. Part B Eng.* **2018**, *138*, 66–76. [CrossRef]
15. Frechette, M.F.; Anh, T.T.; Heid, T.; Vanga-Bouanga, C.; Ghafarizadeh, S.B.; David, E.; El-Khoury, D.; Castellon, J. Dielectric properties of epoxy composites containing both molecular and nanoparticulate silica. In Proceedings of the 2016 IEEE Conference on Electrical Insulation and Dielectric Phenomena (CEIDP), Toronto, ON, Canada, 16–19 October 2016. [CrossRef]
16. Longhi, M.; Pistor, V.; Zini, L.P.; Kunst, S.R.; Zattera, A.J. Influence of Functionality of Polyhedral Oligomeric Silsesquioxane (POSS) Dispersed in Epoxy Resin for Application in Hybrid Coating. *Mater. Sci. Forum* **2017**, *899*, 278–282. [CrossRef]
17. Heid, T.; Frechette, M.; David, E. Dielectric properties of epoxy/POSS composites. In Proceedings of the 2013 Annual Report Conference on Electrical Insulation and Dielectric Phenomena, Shenzhen, China, 20–23 October 2013. [CrossRef]
18. Huang, X.; Li, Y.; Liu, F.; Jiang, P.; Iizuka, T.; Tatsumi, K.; Tanaka, T. Electrical properties of epoxy/POSS composites with homogeneous nanostructure. *IEEE Trans. Dielectr. Electr. Insul.* **2014**, *21*, 1516–1528. [CrossRef]
19. Jahren, S.; Männle, F.; Graff, J.M.; Olafsen, K. The effect of hybrid nanoparticle additives on epoxy-nanocomposite behavior and morphology. *J. Appl. Polym. Sci.* **2011**, *120*, 3212–3216. [CrossRef]
20. Fu, B.X.; Namani, M.; Lee, A. Influence of phenyl-trisilanol polyhedral silsesquioxane on properties of epoxy network glasses. *Polymer* **2003**, *44*, 7739–7747. [CrossRef]
21. Zhang, W.; Li, X.; Yang, R. Blowing-out effect and temperature profile in condensed phase in flame retarding epoxy resins by phosphorus-containing oligomeric silsesquioxane. *Polym. Adv. Technol.* **2013**, *24*, 951–961. [CrossRef]
22. Anoop, V.; Sankaraiah, S.; Jaisankar, S.N.; Chakraborty, S.; Mary, N.L. Enhanced mechanical, thermal and adhesion properties of polysilsesquioxane spheres reinforced epoxy nanocomposite adhesives. *J. Adhes.* **2019**, *97*, 1–18. [CrossRef]
23. Bahrami, Z.; Akbari, A.; Eftekhari-Sis, B. Double network hydrogel of sodium alginate/polyacrylamide cross-linked with POSS: Swelling, dye removal and mechanical properties. *Int. J. Biol. Macromol.* **2019**, *129*, 187–197. [CrossRef]
24. Wahab, M.A.; Kim, I.; Ha, C.-S. Microstructure and properties of polyimide/poly(vinylsilsesquioxane) hybrid composite films. *Polymer* **2003**, *44*, 4705–4713. [CrossRef]
25. Anh, T.T.; Fréchette, M.; David, É.; Veillette, R.; Moraille, P. Effect of POSS-grafted titanium dioxide on the electrical and thermal properties of LDPE/TiO2 polymer nanocomposite. *J. Appl. Polym. Sci.* **2017**, *135*, 46095. [CrossRef]
26. Zazoum, B.; Frechette, M.; David, E. Effect of POSS as compatibilizing agent on structure and dielectric response of LDPE/TiO2 nanocomposites. In Proceedings of the 2015 IEEE Conference on Electrical Insulation and Dielectric Phenomena (CEIDP), Ann Arbor, MI, USA, 18–21 October 2015. [CrossRef]
27. Li, X.; Mao, H.; Liu, Y.; Nie, M.; Wang, Q. Compatibilization of polyhedral oligomeric silsesquioxane for polypropylene-titanium dioxide composites and effect of the processing temperature. *J. Appl. Polym. Sci.* **2017**, *134*, 44766. [CrossRef]
28. Wheeler, P.A.; Misra, R.; Cook, R.D.; Morgan, S.E. Polyhedral oligomeric silsesquioxane trisilanols as dispersants for titanium oxide nanopowder. *J. Appl. Polym. Sci.* **2008**, *108*, 2503–2508. [CrossRef]
29. Peng, D.; Qin, W.; Wu, X. Improvement of the atomic oxygen resistance of carbon fiber-reinforced cyanate ester composites modified by POSS-graphene-TiO2. *Polym. Degrad. Stab.* **2016**, *133*, 211–218. [CrossRef]
30. Dias Filho, N.L.; De Aquino, H.A.; Pires, G.; Caetano, L. Relationship between the Dielectric and Mechanical Properties and the Ratio of Epoxy Resin to Hardener of the Hybrid Thermosetting Polymers. *J. Braz. Chem. Soc.* **2006**, *17*, 533–541. [CrossRef]
31. Ye, M.; Wu, Y.; Zhang, W.; Yang, R. Synthesis of incompletely caged silsesquioxane (T7-POSS) compounds via a versatile three-step approach. *Res. Chem. Intermed.* **2018**, *44*, 4277–4294. [CrossRef]
32. Xu, Y.; Ma, Y.; Deng, Y.; Yang, C.; Chen, J.; Dai, L. Morphology and thermal properties of organic–inorganic hybrid material involving monofunctional-anhydride POSS and epoxy resin. *Mater. Chem. Phys.* **2011**, *125*, 174–183. [CrossRef]
33. Brząkalski, D.; Przekop, R.E.; Dobrosielska, M.; Sztorch, B.; Marciniak, P.; Marciniec, B. Highly bulky spherosilicates as functional additives for polyethylene processing—Influence on mechanical and thermal properties. *Polym. Compos.* **2020**, *41*, 3389–3402. [CrossRef]
34. Leito, I.; Herodes, K.; Huopolainen, M.; Virro, K.; Künnapas, A.; Kruve, A.; Tanner, R. Towards the electrospray ionization mass spectrometry ionization efficiency scale of organic compounds. *Rapid Commun. Mass Spectrom.* **2008**, *22*, 379–384. [CrossRef] [PubMed]
35. Cech, N.B.; Enke, C.G. Practical implications of some recent studies in electrospray ionization fundamentals. *Mass Spectrom. Rev.* **2001**, *20*, 362–387. [CrossRef] [PubMed]
36. Przekop, R.E.; Jakubowska, P.; Sztorch, B.; Kozera, R.; Dydek, K.; Jałbrzykowski, M.; Osiecki, T.; Marciniak, P.; Martyła, A.; Kloziński, A.; et al. Opoka—Sediment Rock as New Type of Hybrid Mineral Filler for Polymer Composites. *AppliedChem* **2021**, *1*, 90–110. [CrossRef]

37. Kochkar, H.; Figueras, F. Synthesis of Hydrophobic TiO_2–SiO_2 Mixed Oxides for the Epoxidation of Cyclohexene. *J. Catal.* **1997**, *171*, 420–430. [CrossRef]
38. Nguyen, V.G.; Thai, H.; Mai, D.H.; Tran, H.T.; Tran, D.L.; Vu, M.T. Effect of titanium dioxide on the properties of polyethylene/TiO2 nanocomposites. *Compos. Part B Eng.* **2013**, *45*, 1192–1198. [CrossRef]
39. Tuan, V.M.; Jeong, D.W.; Yoon, H.J.; Kang, S.; Vu Giang, N.; Hoang, T.; Thinh, T.I.; Kim, M.Y. Using Rutile TiO2Nanoparticles Reinforcing High Density Polyethylene Resin. *Int. J. Polym. Sci.* **2014**, *2014*, 758351. [CrossRef]
40. Dobrosielska, M.; Dobrucka, R.; Gloc, M.; Brząkalski, D.; Szymański, M.; Kurzydłowski, K.J.; Przekop, R.E. A New Method of Diatomaceous Earth Fractionation—A Bio-Raw Material Source for Epoxy-Based Composites. *Materials* **2021**, *14*, 1663. [CrossRef]
41. Yamini, S.; Young, R.J. Stability of crack propagation in epoxy resins. *Polymer* **1977**, *18*, 1075–1080. [CrossRef]
42. Dobrosielska, M.; Dobrucka, R.; Brząkalski, D.; Gloc, M.; Rębiś, J.; Głowacka, J.; Kurzydłowski, K.J.; Przekop, R.E. Methodological Aspects of Obtaining and Characterizing Composites Based on Biogenic Diatomaceous Silica and Epoxy Resins. *Materials* **2021**, *14*, 4607. [CrossRef] [PubMed]
43. Mayes, A.M. Softer at the boundary. *Nat. Mater.* **2005**, *4*, 651–652. [CrossRef]
44. Bansal, A.; Yang, H.; Li, C.; Cho, K.; Benicewicz, B.C.; Kumar, S.K.; Schadler, L.S. Quantitative equivalence between polymer nanocomposites and thin polymer films. *Nat. Mater.* **2005**, *4*, 693–698. [CrossRef] [PubMed]
45. Ash, B.J.; Schadler, L.S.; Siegel, R.W. Glass transition behavior of alumina/polymethylmethacrylate nanocomposites. *Mater. Lett.* **2002**, *55*, 83–87. [CrossRef]

materials

MDPI

Supplementary Information

Where ppm Quantities of Silsesquioxanes Make a Difference—Silanes and Cage Siloxanes as TiO_2 Dispersants and Stabilizers for Pigmented Epoxy Resins

Dariusz Brząkalski [1], Robert E. Przekop [2,*], Miłosz Frydrych [1], Daria Pakuła [1], Marta Dobrosielska [3], Bogna Sztorch [2], Bogdan Marciniec [1,2,*]

[1] Faculty of Chemistry, Adam Mickiewicz University in Poznań, 8 Uniwersytetu Poznańskiego, 61−614 Poznań, Poland; d.brzakalski@gmail.com (D.B.), frydrych@amu.edu.pl (M.F.); darpak@amu.edu.pl (D.P.), bogdan.marciniec@amu.edu.pl (B.M.)

[2] Centre for Advanced Technologies, Adam Mickiewicz University in Poznań, 10 Uniwersytetu Poznańskiego, 61-614 Poznań, Poland; rprzekop@amu.edu.pl (R.E.P.), bogna.sztorch@amu.edu.pl, bogdan.marciniec@amu.edu.pl (B.M.)

[3] Faculty of Materials Science and Engineering, Warsaw University of Technology, 141 Wołoska, 02-507 Warsaw, Poland; Marta.Dobrosielska@pw.edu.pl (M.D.);

* Correspondence: r.przekop@gmail.com, rprzekop@amu.edu.pl (R.E.P.), bogdan.marciniec@amu.edu.pl (B.M.)

Table of contents

1. Pictures of the equipment and samples

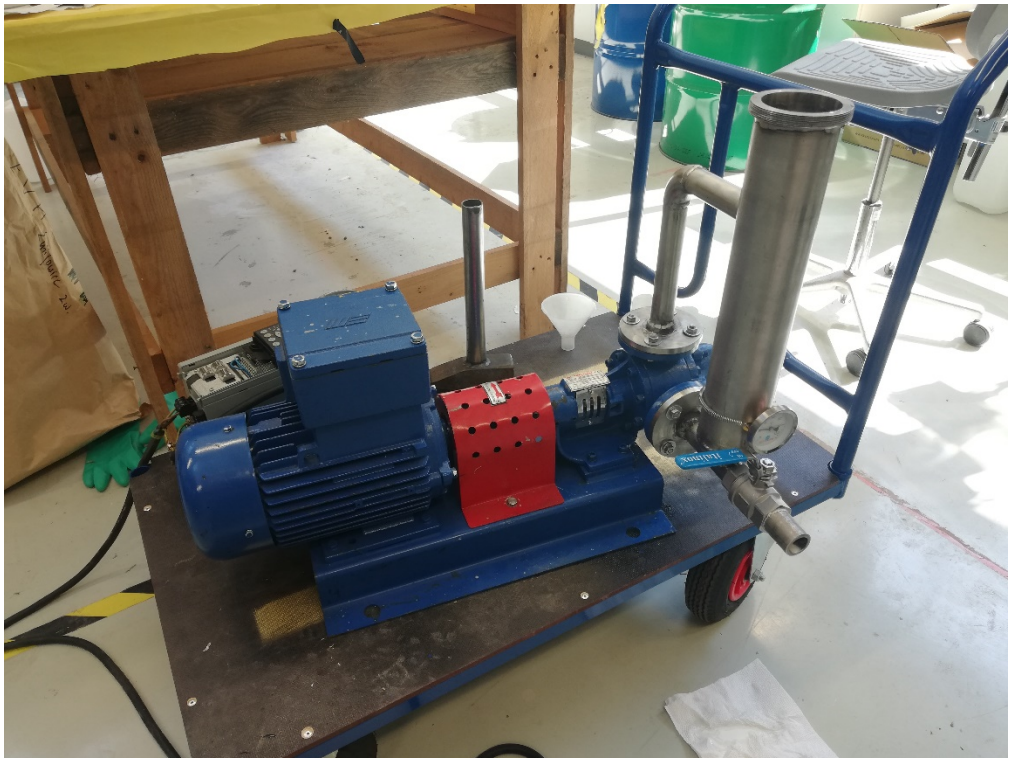

Figure S1. Internal gear pump setup used for preparation of TiO_2/epoxy dispersions

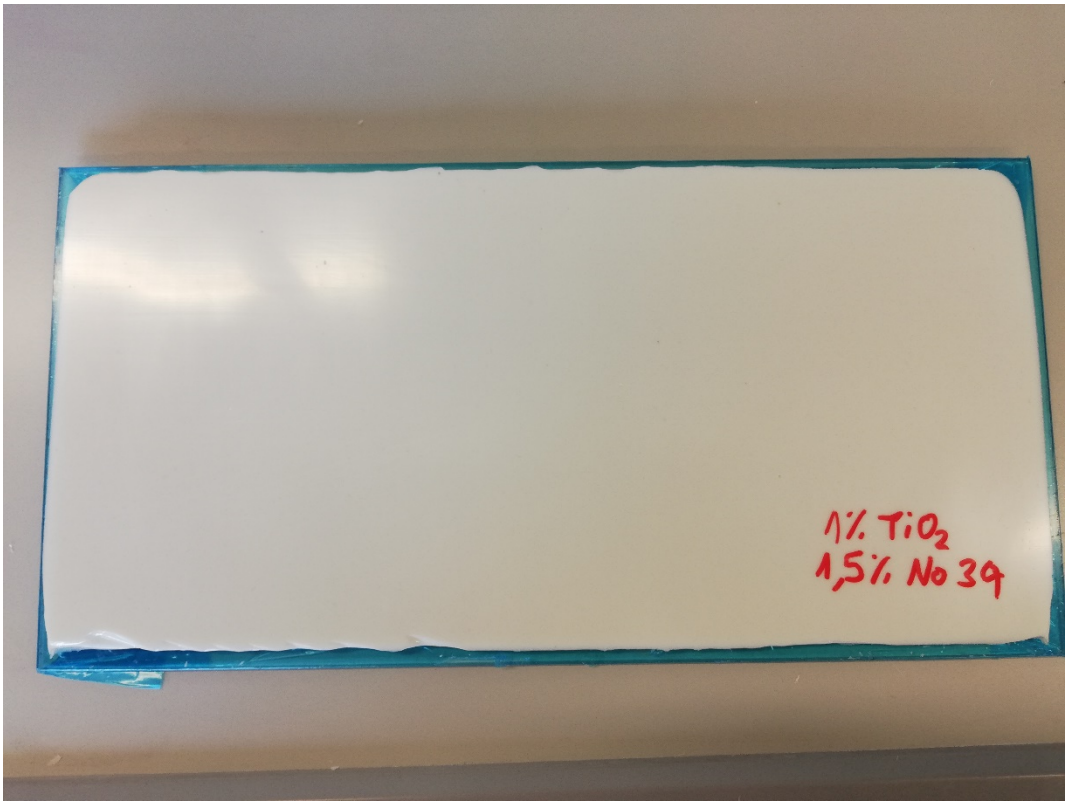

Figure S2. A sample of cured TiO_2/epoxy composite prepared

2. NMR spectroscopy of the obtained compounds

1,3,5,7,9,11,13,15-hexa((3-glycidoxypropyl)dimethylsiloxy)-di((trimethoxysilyl)dimethylsilloxy) pentacyclo[9.5.1.1^{3,9}.1^{5,15}.1^{7,13}]octasiloxane (SS-6GP-2TMOS)

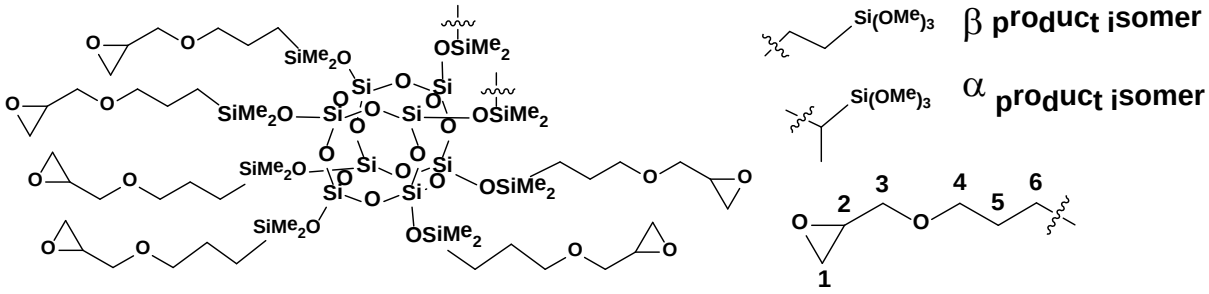

^{1}H NMR (400 MHz, $CDCl_3$): δ (ppm) = 3.70-3.67 (m, 6H position 3), 3.55 (s, 18H, OMe), 3.48-3.40 (m, 12H, position 4), 3.39-3.36 (m, 6H, position 3), 3.14-3.11 (m, 6H, position 2), 2.79-2.77 (m, 6H, position 1), 2.60-2.59 (m, 6H, position 1), 1.65-1.60 (m, 12H, position 5), 1.11 (d, alpha product -CH_3), 0.62-0.59 (m, 20H, SiCH_2CH_2Si, position 6), 0.14 (s, 48H, $SiMe_2$); ***α*** and **β** isomers were obseved in 8 : 92 ratio;

^{13}C NMR (101 MHz, $CDCl_3$): δ (ppm) = 74.25, 71.59, 71.58 (glycidoxy group), 50.97, 50.78, 50.69 (OMe), 44.46 (propyl-3-CH_2), 23.32, 13.81, 13.80 (propyl-1 and propyl-2-CH_2), 8.62, 8.60 (Si-CH_2CH_2-Si), 7.41, 5.29 (Si$CH(CH_3)$Si), 0.44 (Si-CH_2CH_2-Si), -0.25, -0.28, -0.31 (glycidoxypropyl $SiMe_2$), -0.95, -0.98, -1.01 (trimethoxysilylethyl $SiMe_2$);

^{29}Si NMR (79,5 MHz, $CDCl_3$): δ (ppm) = 13.23-13.18 (Si-trimethoxysilylethyl), 12.97-12.91 (Si-glycidyloxypropyl), -41.67 ($Si(OMe)_3$), -109.09 (core).

^{1}H NMR

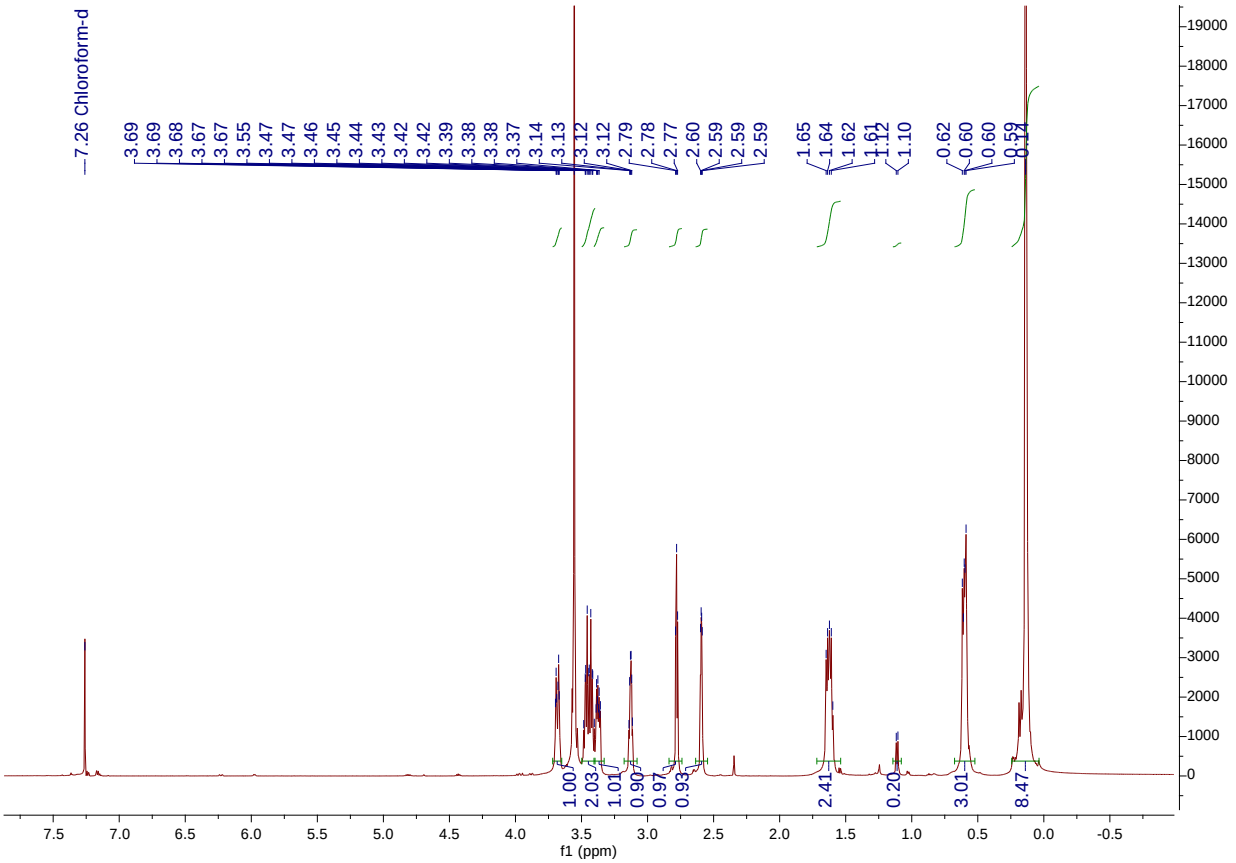

^{13}C NMR

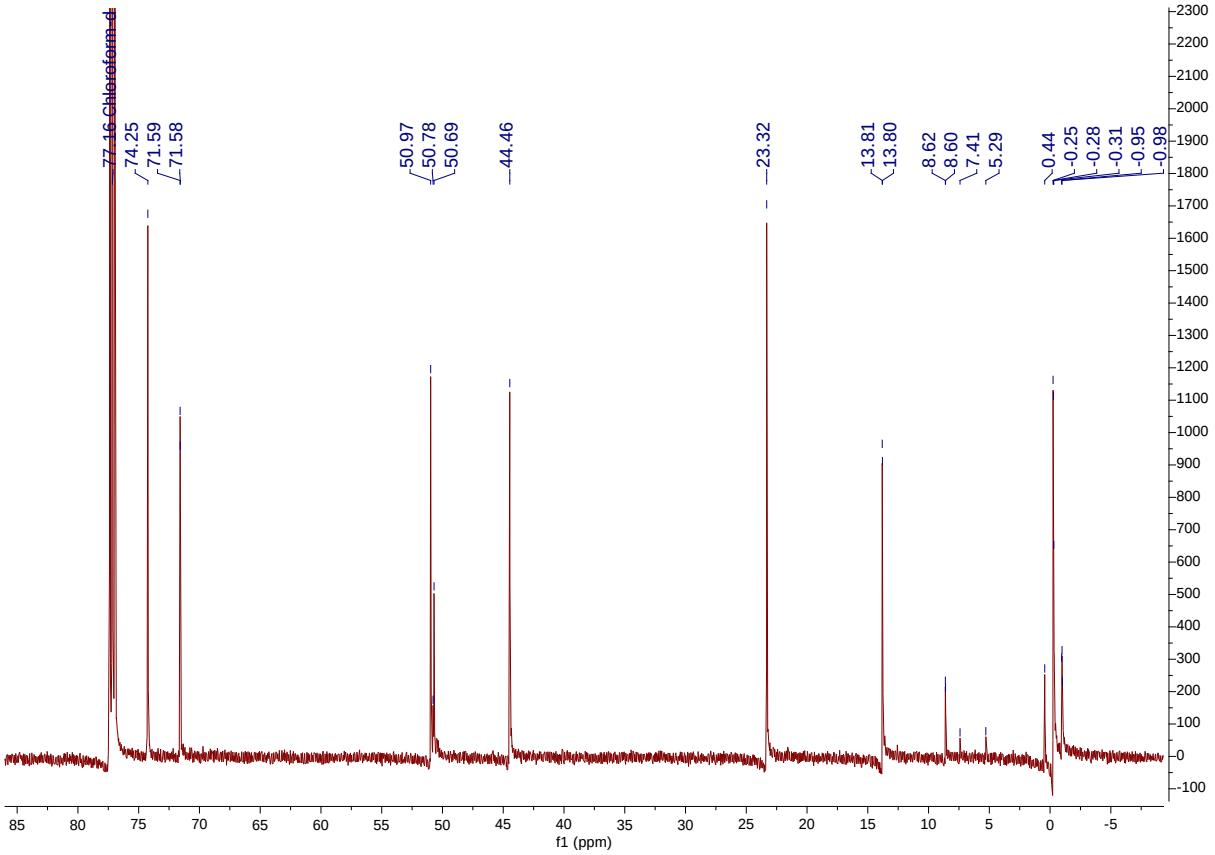

^{29}Si NMR

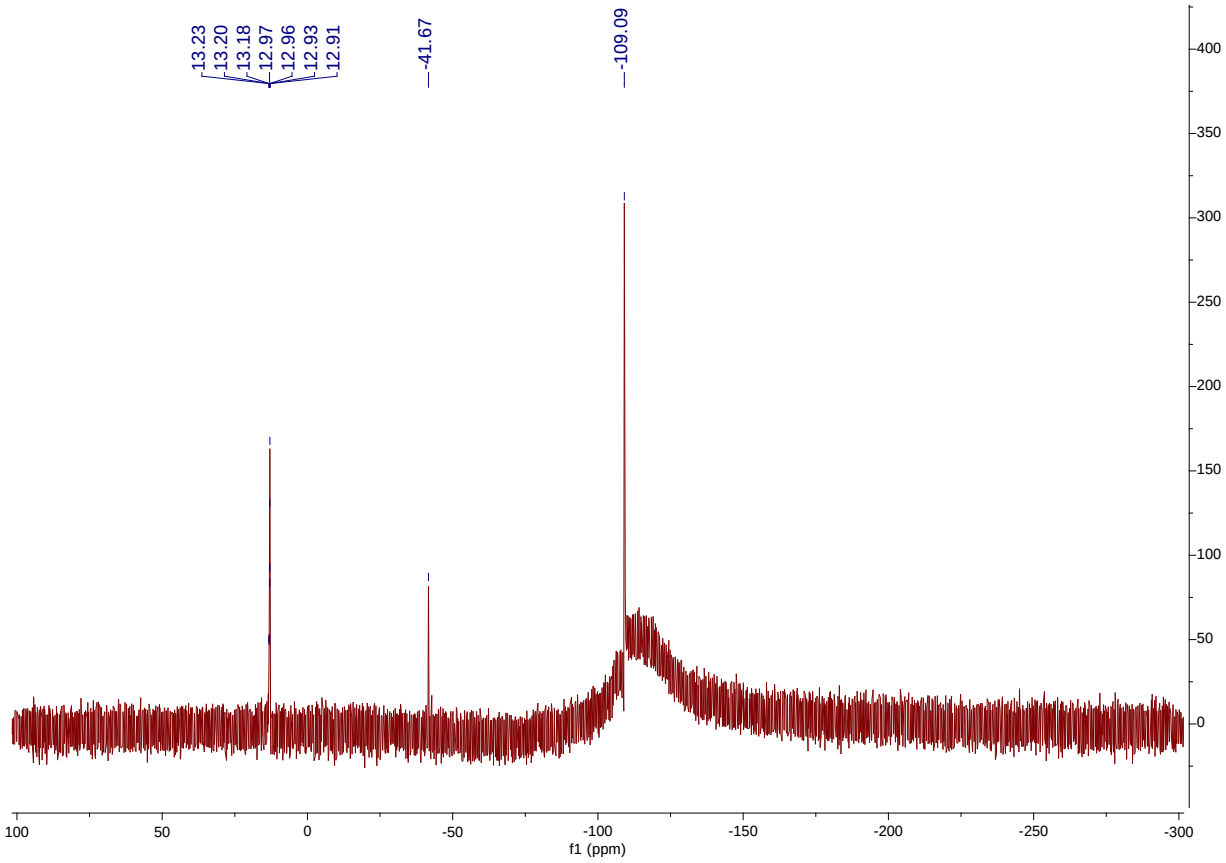

1,3,5,7,9,11,13,15-penta((3-glycidoxypropyl)dimethylsiloxy)-tri((trimethoxysilyl)dimethylsilloxy) pentacyclo[9.5.1.1^{3,9}.1^{5,15}.1^{7,13}]octasiloxane (SS-5GP-3TMOS)

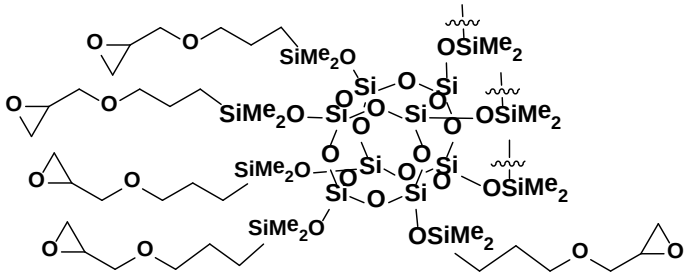

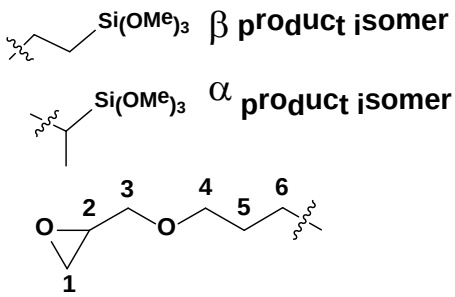

^{1}H NMR (400 MHz, $CDCl_3$): δ (ppm) = 3.70-3.66 (m, 5H position 3), 3.54 (s, 27H, OMe), 3.47-3.43 (m, 10H, position 4), 3.39-3.33 (m, 5H, position 3), 3.14-3.09 (m, 5H, position 2), 2.77-2.74 (m, 5H, position 1), 2.59-2.55 (m, 5H, position 1), 1.64-1.63 (m, 10H, position 5), 1.12 (d, alpha product -CH_3), 0.61-0.59 (m, 22H, Si$\underline{CH_2CH_2}$Si, position 6), 0.14 (s, 48H, $SiMe_2$); ***α*** and **β** isomers were obseved in 10 : 90 ratio;

^{13}C NMR (101 MHz, $CDCl_3$): δ (ppm) = 73.87, 71.31 (glycidoxy group), 50.61, 50.32 (OMe), 43.99 (propyl-3-CH_2), 23.06, 13.55 (propyl-1 and propyl-2-CH_2), 8.36 (Si-$\underline{CH_2CH_2}$-Si), 7.14, 5.01 (Si$\underline{CH(CH_3)}$Si), 0.17 (Si-$\underline{CH_2CH_2}$-Si), -0.54, -0.57, -0.61 (glycidoxypropyl $SiMe_2$), -1.24, -1.27 (trimethoxysilylethyl $SiMe_2$);

^{29}Si NMR (79,5 MHz, $CDCl_3$): δ (ppm) = 13.17-13.13 (Si-trimethoxysilylethyl), 12.92-12.87 (Si-glycidyloxypropyl), -41.87 ($Si(OMe)_3$), -109.12 (core).

^{1}H NMR

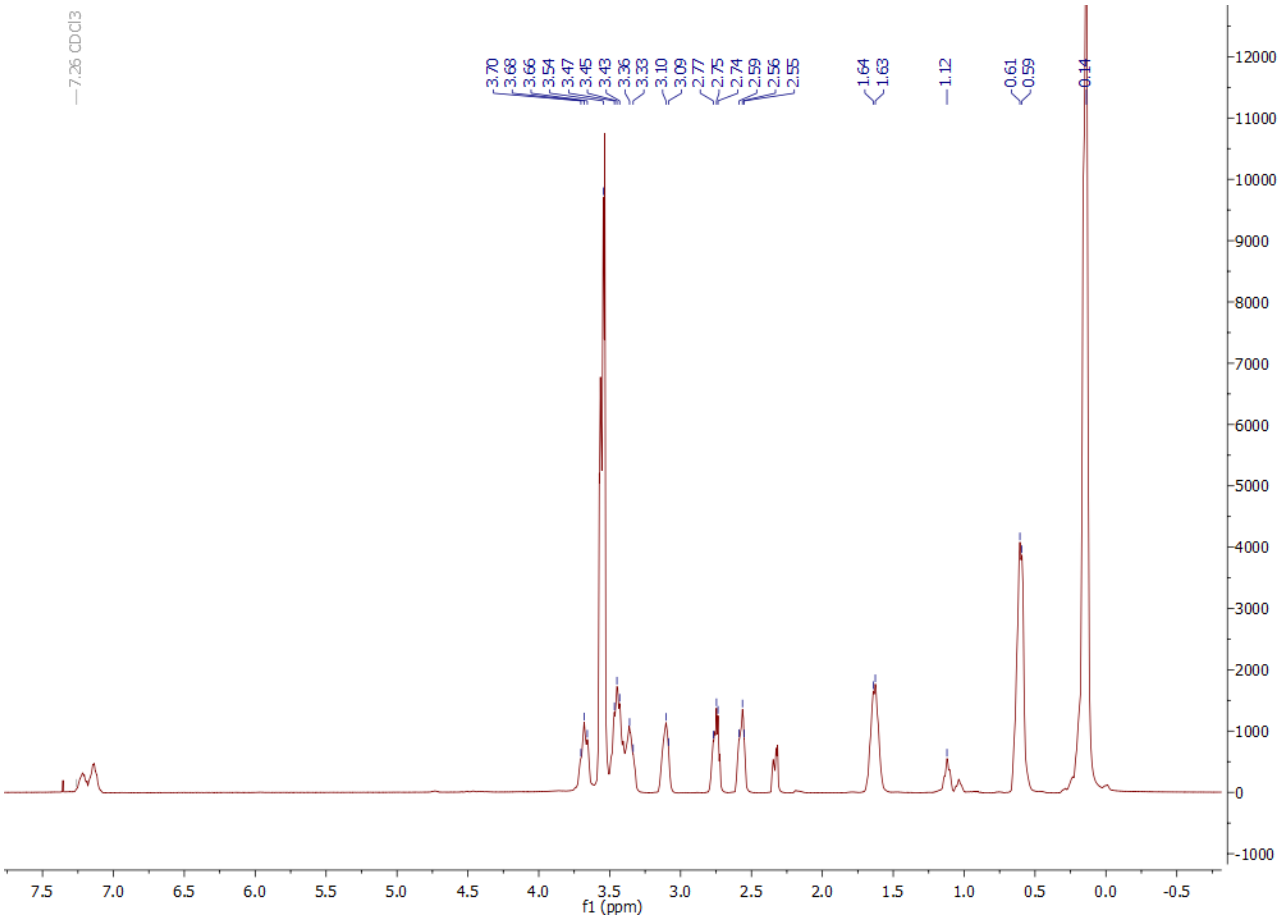
7.26 CDCl3
3.70
3.68
3.66
3.54
3.47
3.45
3.43
3.36
3.33
3.10
3.09
2.77
2.75
2.74
2.59
2.56
2.55
1.64
1.63
1.12
0.61
0.59
0.14
12000
11000
10000
9000
8000
7000
6000
5000
4000
3000
2000
1000
0
-1000
7.5
7.0
6.5
6.0
5.5
5.0
4.5
4.0
3.5
3.0
2.5
2.0
1.5
1.0
0.5
0.0
-0.5
f1 (ppm)

^{13}C NMR

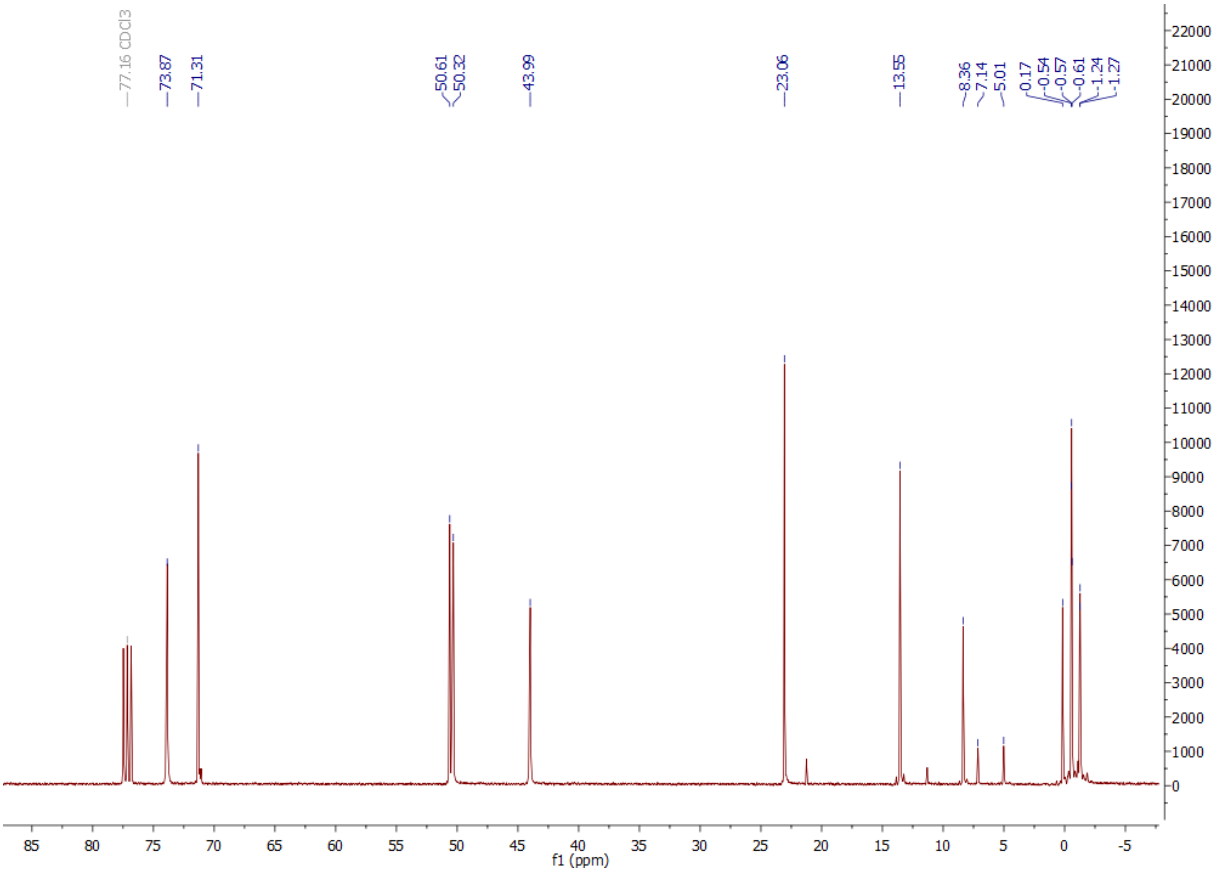
77.16 CDCl3
73.87
71.31
50.61
50.32
43.99
23.06
13.55
8.36
7.14
5.01
0.17
-0.54
-0.57
-0.61
-1.24
-1.27
f1 (ppm)

^{29}Si NMR

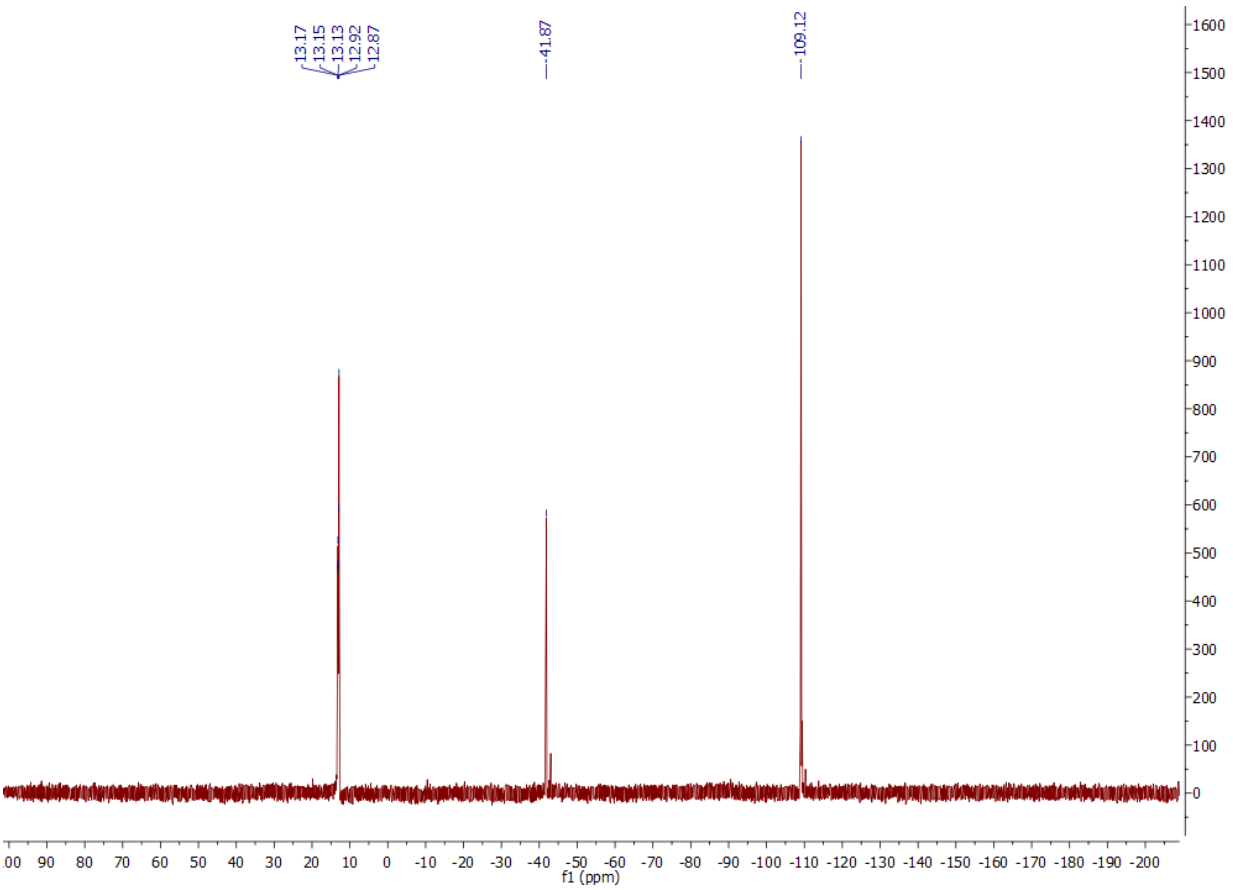
13.17
13.15
13.13
12.92
12.87
41.87
-109.12
f1 (ppm)

1-ethoxy-3,5,7,9,11,13,15-heptaisobutylpentacyclo[9.5.1.1^{3,9}.1^{5,15}.1^{7,13}]octasiloxane (iBu$_7$SSQ-OEt)

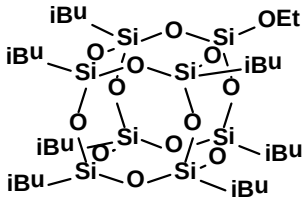

^{1}H NMR (400 MHz, $CDCl_3$): δ (ppm) = 3.84 (q, J = 7.0 Hz, 2H, $OC\underline{H}_2CH_3$), 1.92-1.80 (m, 7H, iBu), 1.23 (t, J = 7.0 Hz, 3H, $OCH_2C\underline{H}_3$), 0.97-0.95 (m, 42H, iBu), 0.64-0.59 (m, 14H, iBu);

^{13}C NMR (101 MHz, $CDCl_3$): δ (ppm) = 59.48 ($O\underline{C}H_2CH_3$), 25.85, 25.83, 24.02, 23.98, 22.64, 22.59, 22.51, 22.49 (iBu), 18.03 ($OCH_2\underline{C}H_3$);

^{29}Si NMR (79,5 MHz, $CDCl_3$): δ (ppm) = -66.71, -66.94, -67.87 (cage), -103.22 (SiOEt).

^{1}H NMR

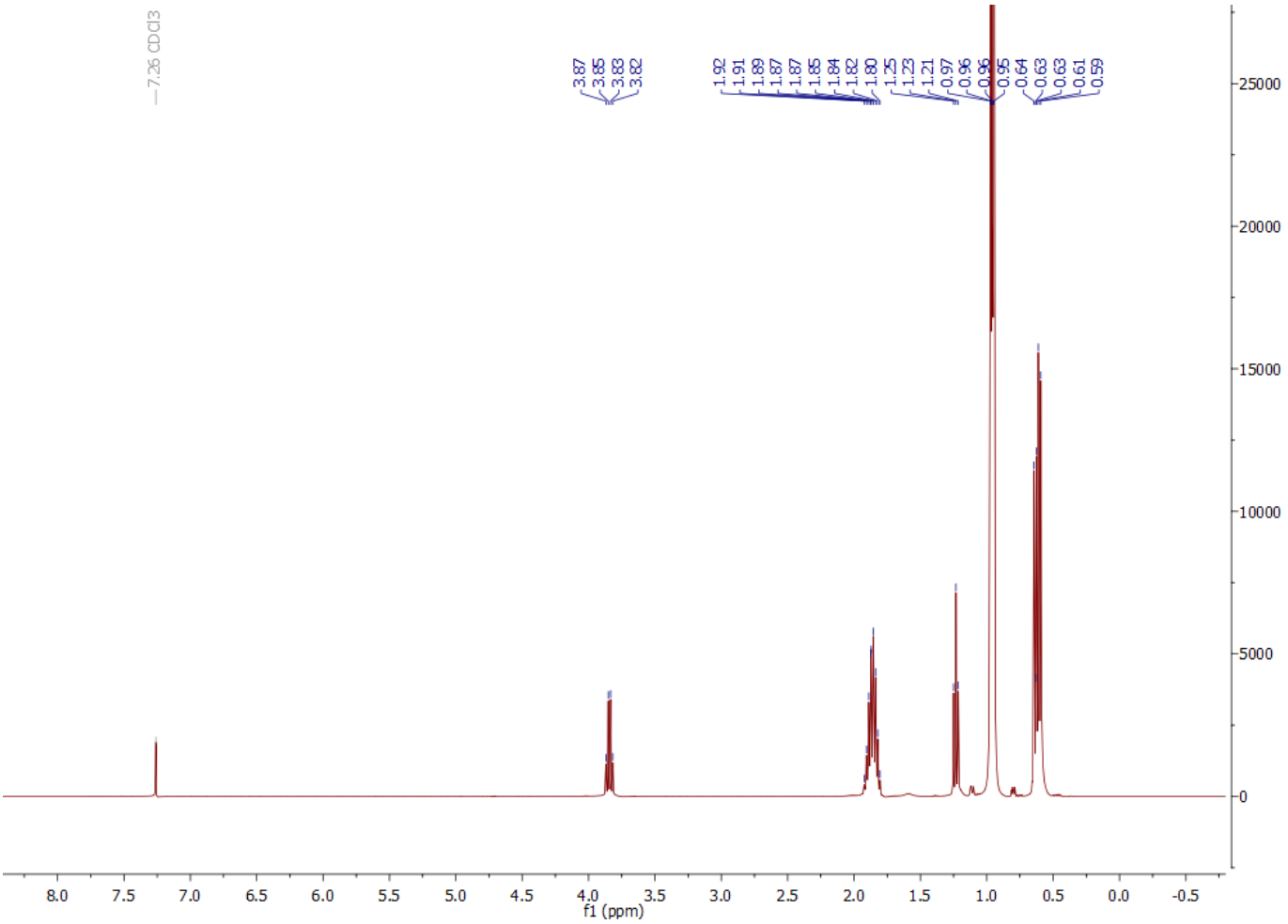

^{13}C NMR

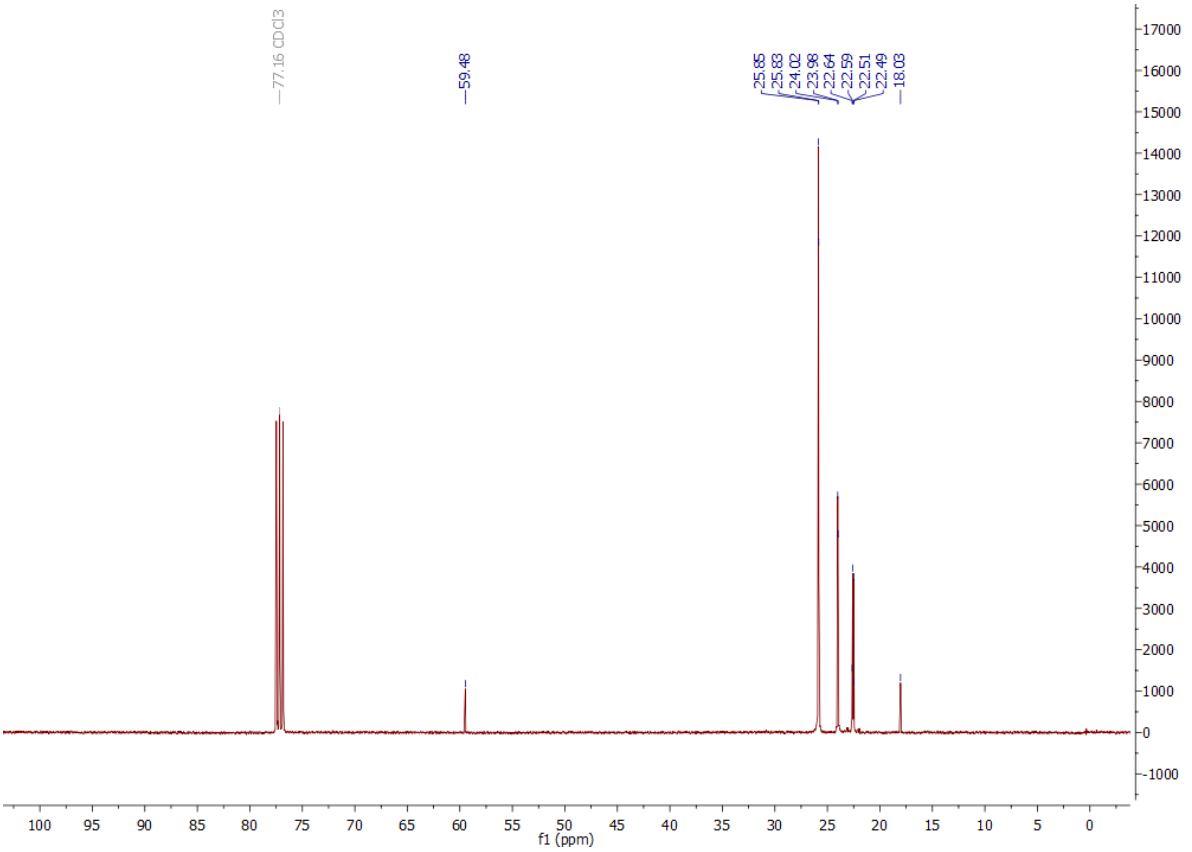

^{29}Si NMR

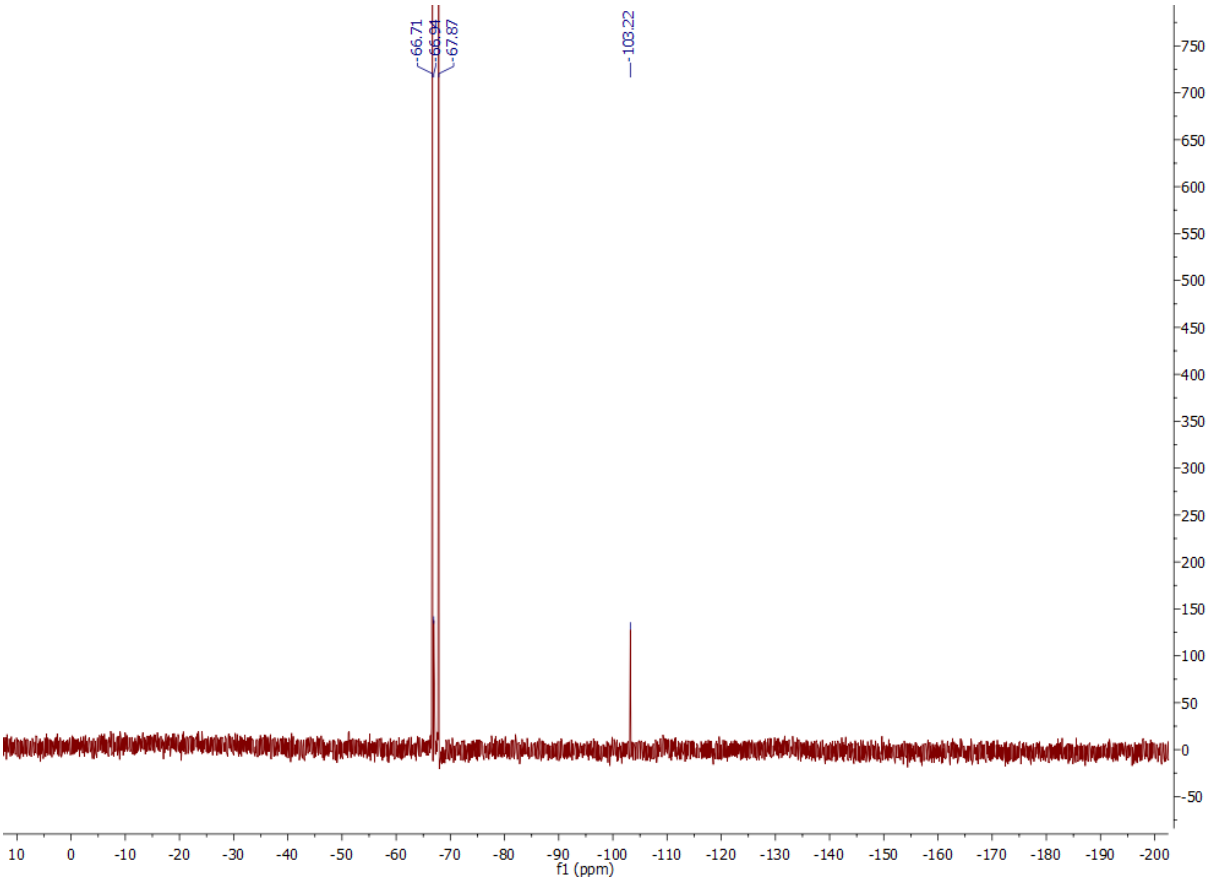

3. MALDI-TOF mass spectra of obtained spherosilicate compounds

SS-6GP-2TMOS

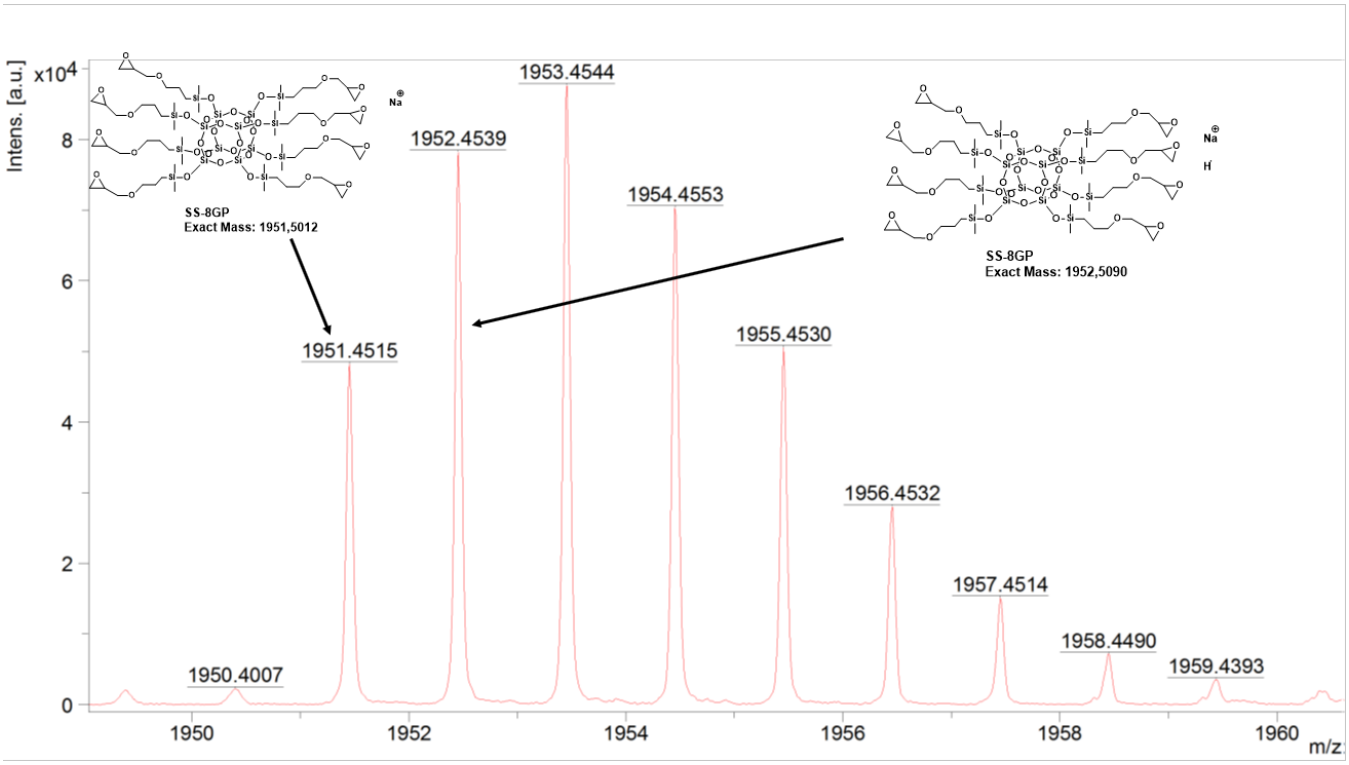

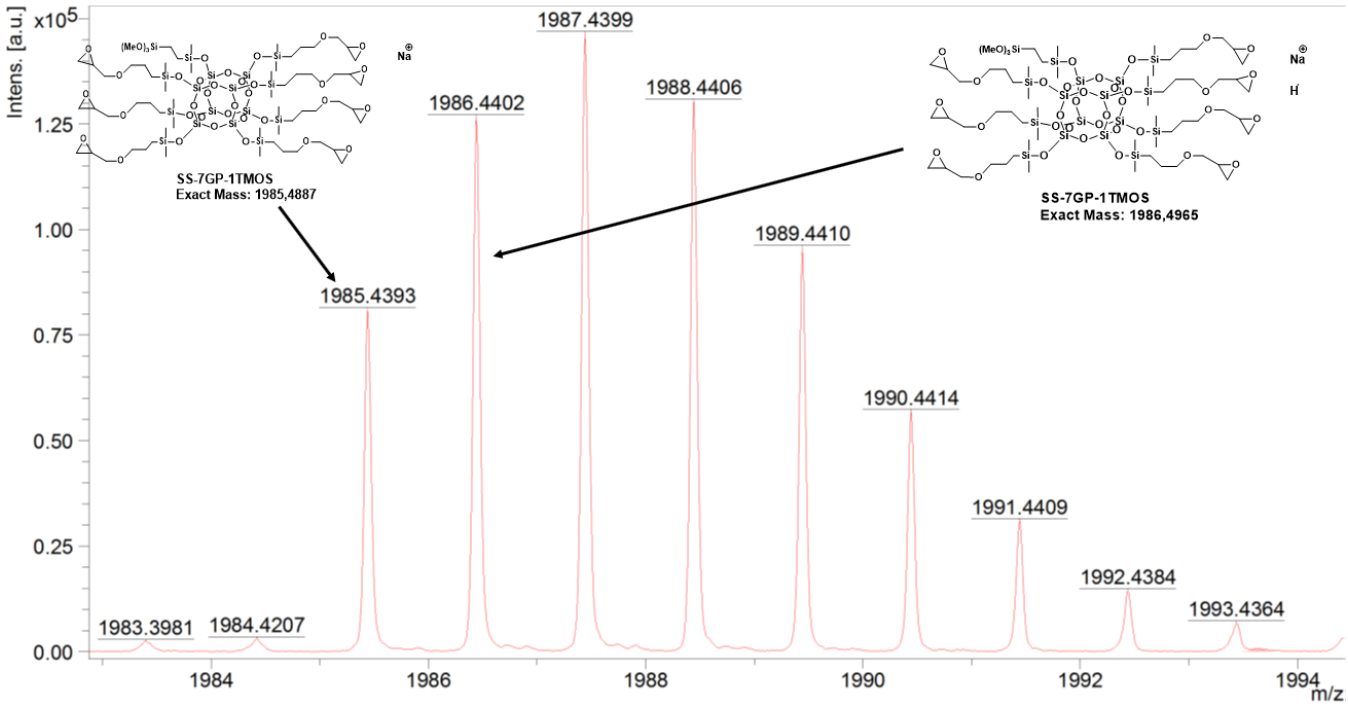

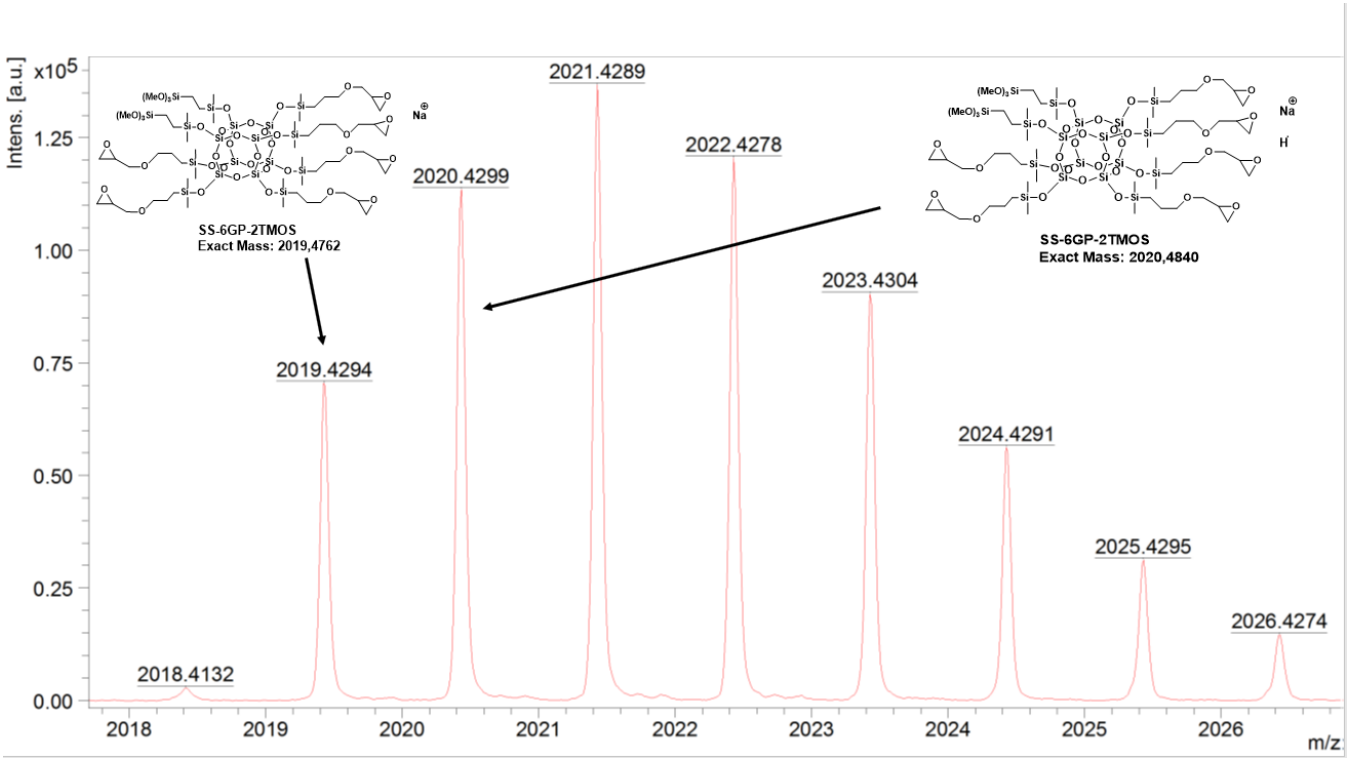
Intens. [a.u.]
x10^5
1.25
1.00
0.75
0.50
0.25
0.00
2018.4132
2019.4294
2020.4299
2021.4289
2022.4278
2023.4304
2024.4291
2025.4295
2026.4274
2018
2019
2020
2021
2022
2023
2024
2025
2026
m/z
SS-6GP-2TMOS
Exact Mass: 2019,4762
SS-6GP-2TMOS
Exact Mass: 2020,4840
Na
H

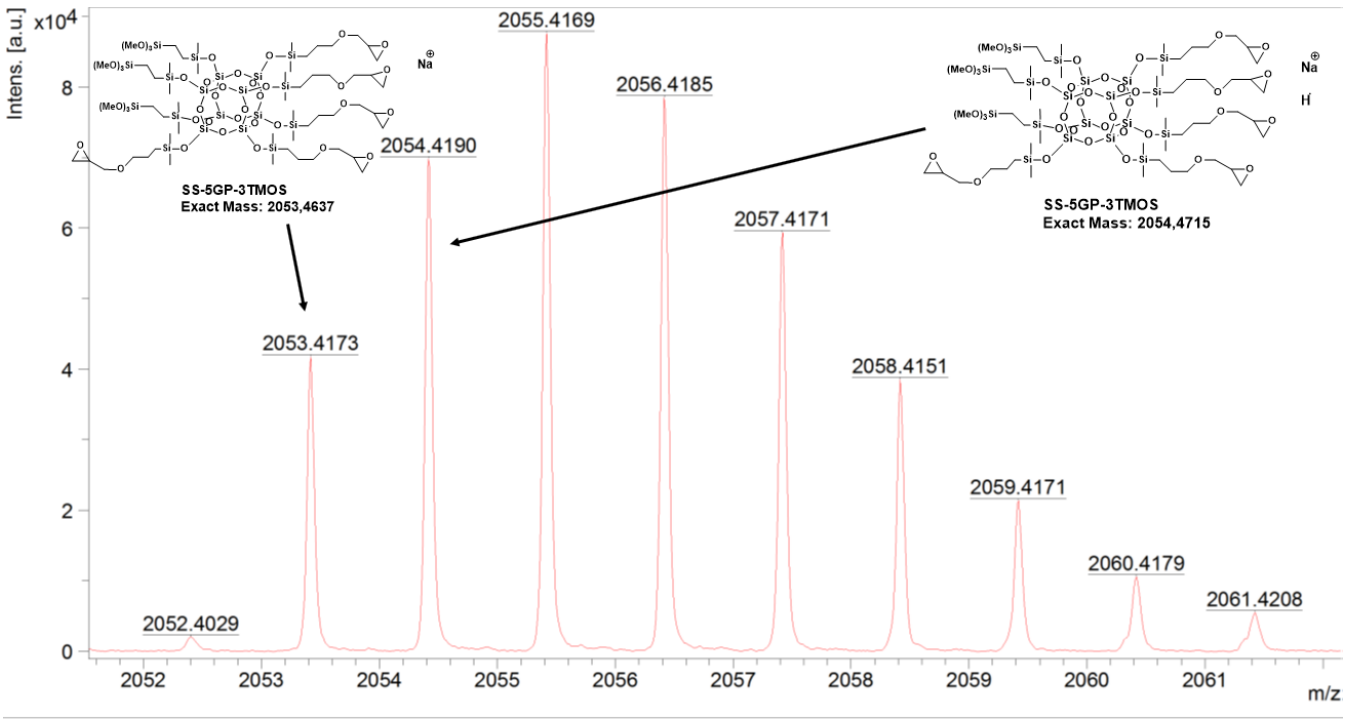
Intens. [a.u.]
x10^4
8
6
4
2
0
2052.4029
2053.4173
2054.4190
2055.4169
2056.4185
2057.4171
2058.4151
2059.4171
2060.4179
2061.4208
2052
2053
2054
2055
2056
2057
2058
2059
2060
2061
m/z
SS-5GP-3TMOS
Exact Mass: 2053,4637
SS-5GP-3TMOS
Exact Mass: 2054,4715
Na
H

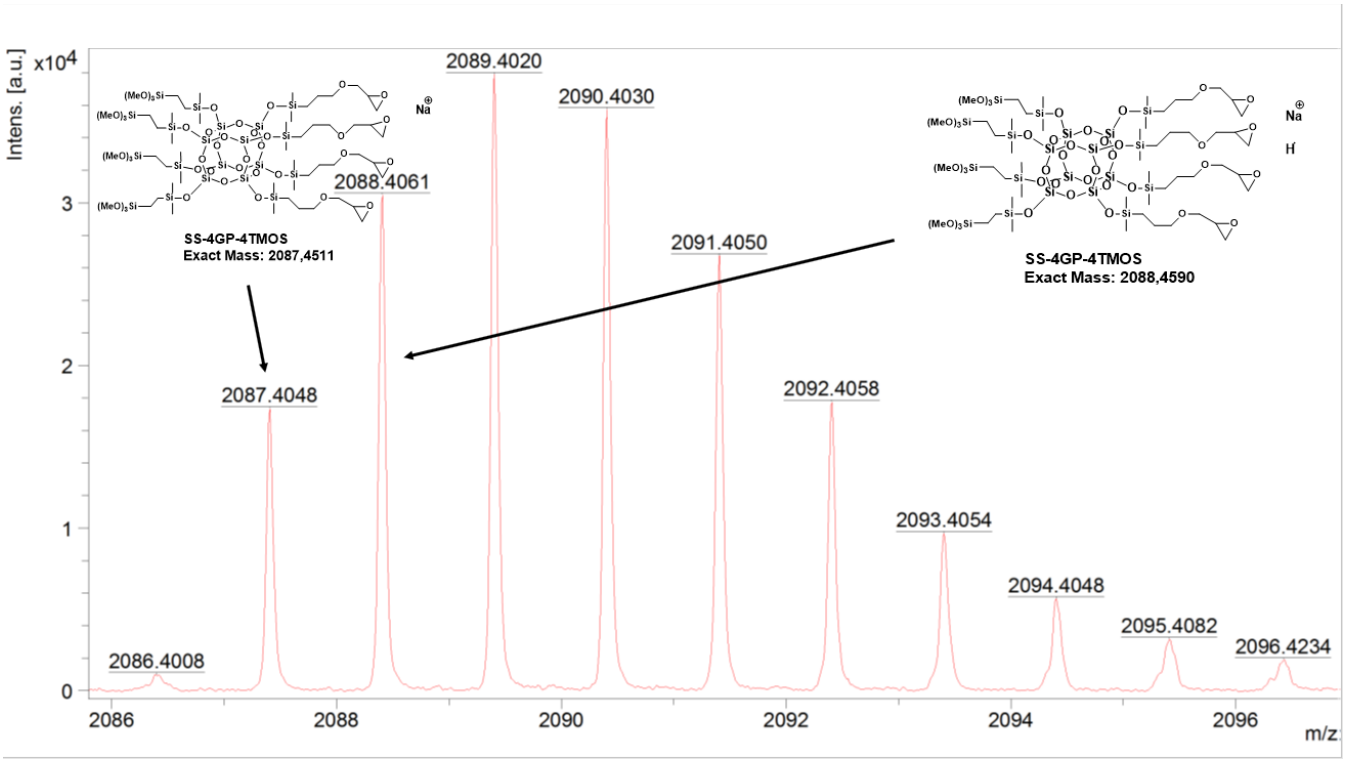
Intens. [a.u.]
x10^4
3
2
1
0
2089.4020
2090.4030
2088.4061
2091.4050
2087.4048
2092.4058
2093.4054
2094.4048
2095.4082
2096.4234
2086.4008
2086
2088
2090
2092
2094
2096
m/z
SS-4GP-4TMOS
Exact Mass: 2087,4511
SS-4GP-4TMOS
Exact Mass: 2088,4590
Na
H

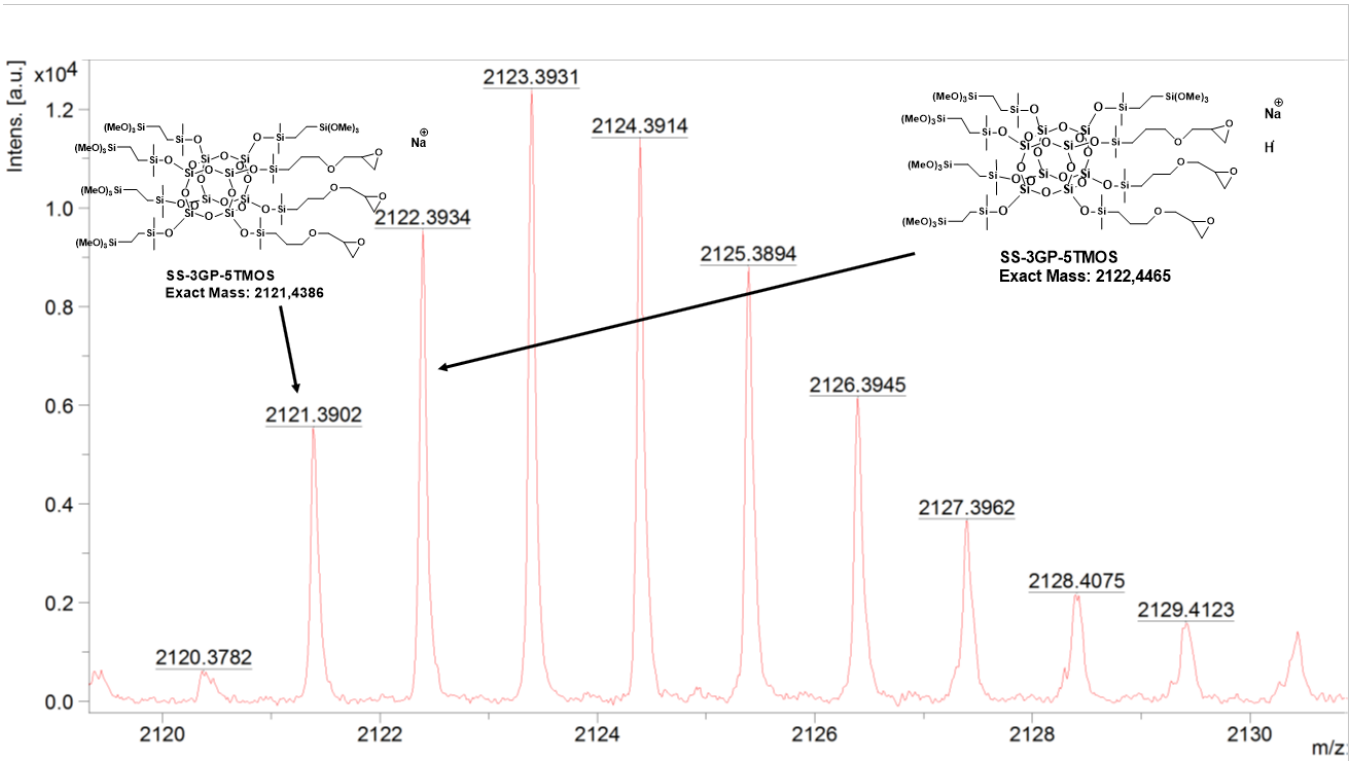
Intens. [a.u.]
x10^4
1.2
1.0
0.8
0.6
0.4
0.2
0.0
2123.3931
2124.3914
2122.3934
2125.3894
2126.3945
2121.3902
2127.3962
2128.4075
2129.4123
2120.3782
2120
2122
2124
2126
2128
2130
m/z
SS-3GP-5TMOS
Exact Mass: 2121,4386
SS-3GP-5TMOS
Exact Mass: 2122,4465
Na
H

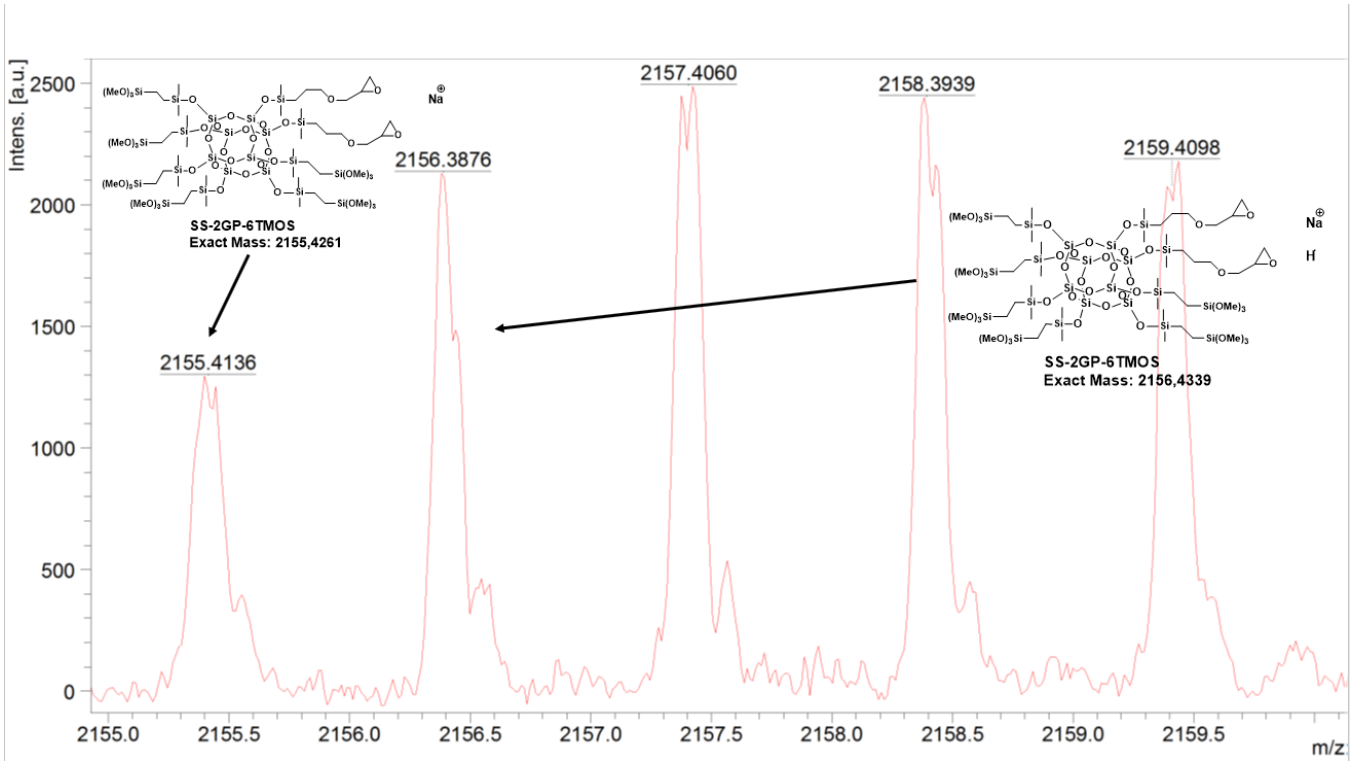
Intens. [a.u.]
2500
2000
1500
1000
500
0
2155.0
2155.5
2156.0
2156.5
2157.0
2157.5
2158.0
2158.5
2159.0
2159.5
m/z
2155.4136
2156.3876
2157.4060
2158.3939
2159.4098
SS-2GP-6TMOS
Exact Mass: 2155,4261
SS-2GP-6TMOS
Exact Mass: 2156,4339
Na
H

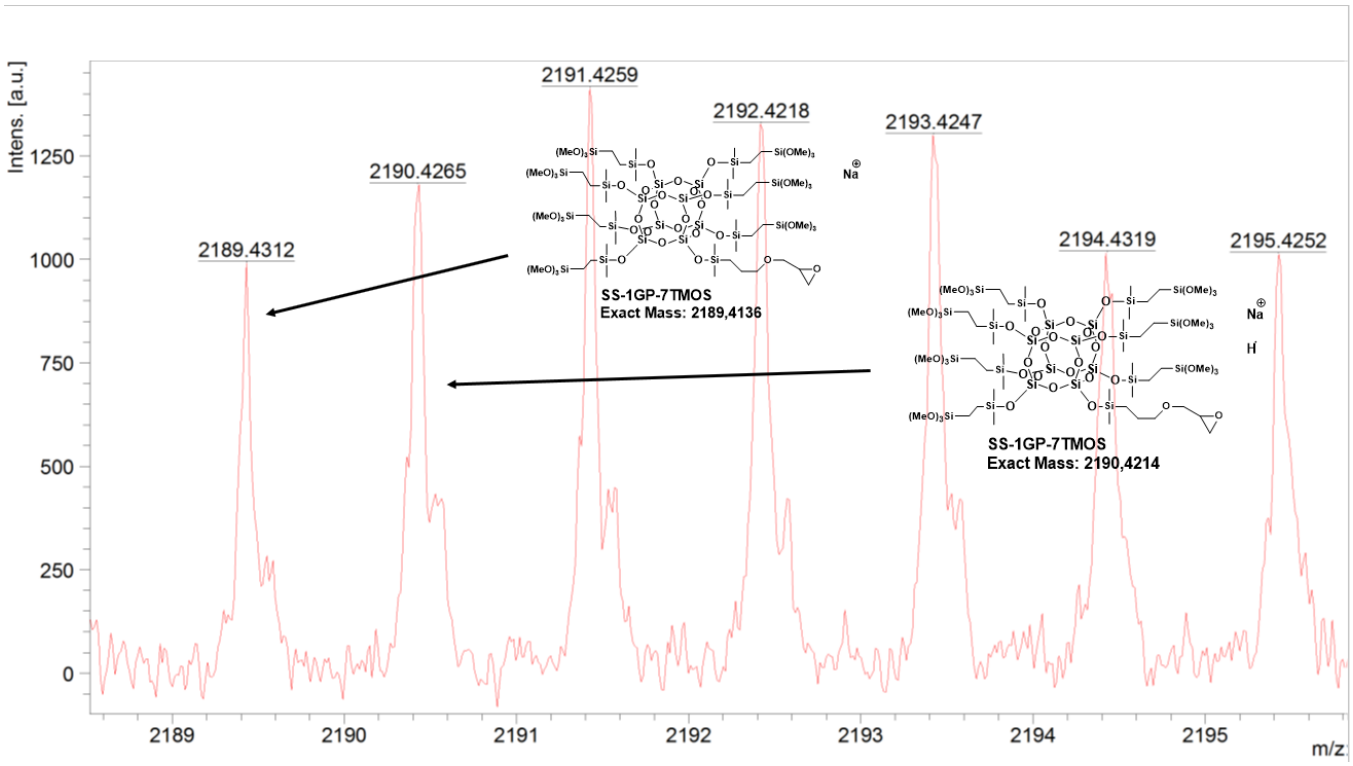
Intens. [a.u.]
1250
1000
750
500
250
0
2189
2190
2191
2192
2193
2194
2195
m/z
2189.4312
2190.4265
2191.4259
2192.4218
2193.4247
2194.4319
2195.4252
SS-1GP-7TMOS
Exact Mass: 2189,4136
SS-1GP-7TMOS
Exact Mass: 2190,4214
Na
H

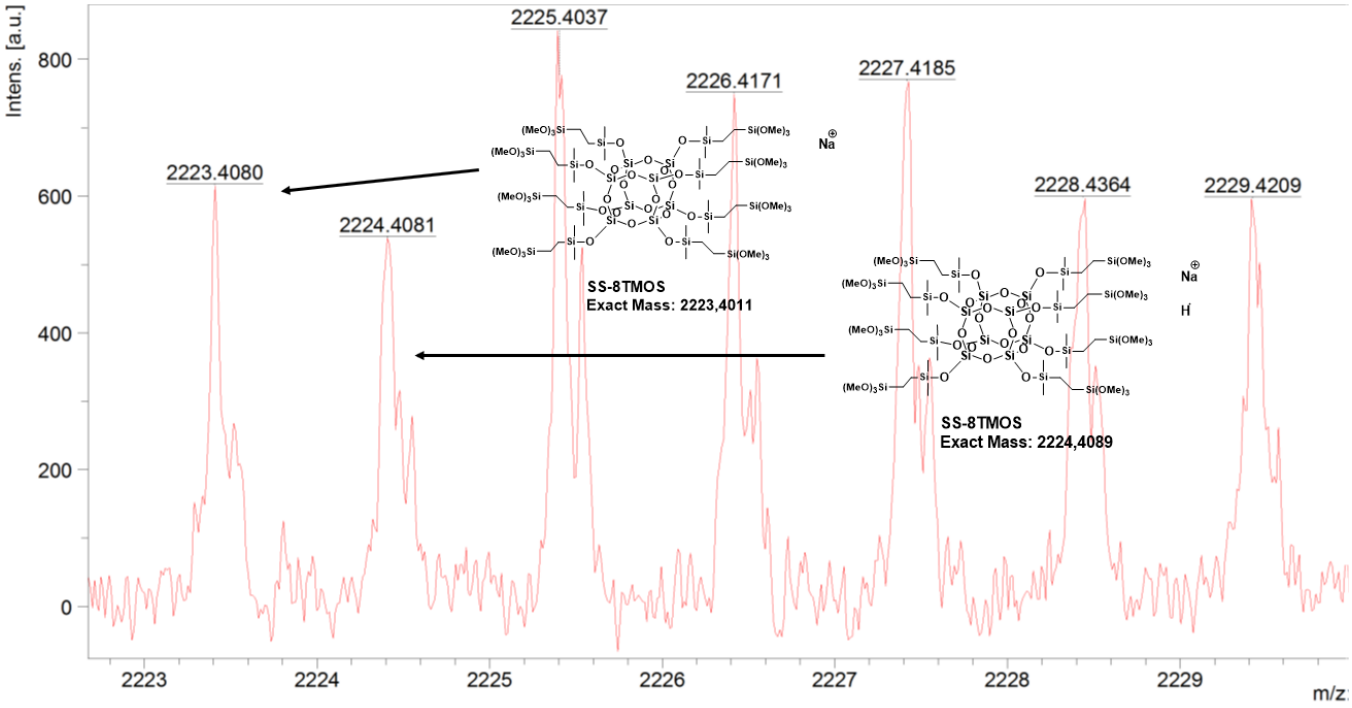
Intens. [a.u.]
800
600
400
200
0
2223.4080
2224.4081
2225.4037
2226.4171
2227.4185
2228.4364
2229.4209
SS-8TMOS
Exact Mass: 2223,4011
SS-8TMOS
Exact Mass: 2224,4089
Na
H
2223
2224
2225
2226
2227
2228
2229
m/z

SS-5GP-3TMOS

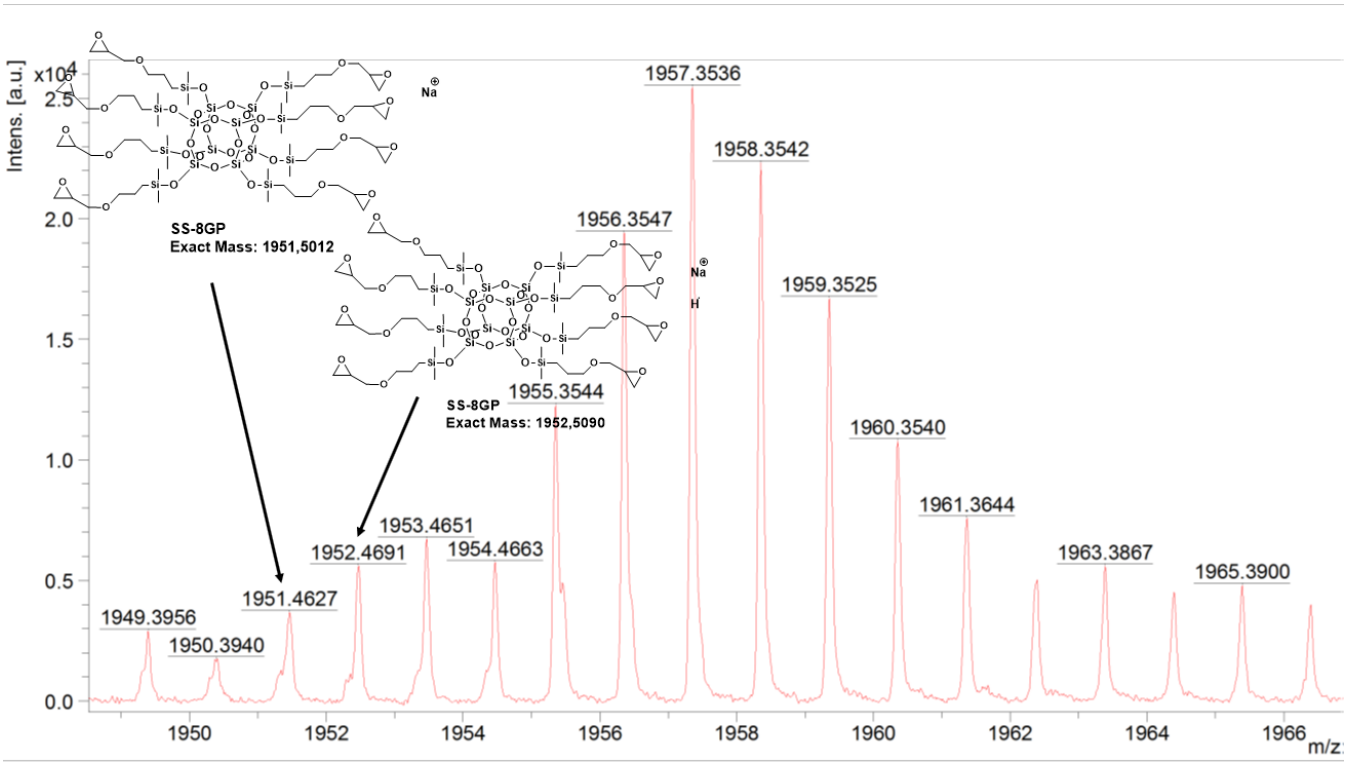
Intens. [a.u.]
x10^4
2.5
2.0
1.5
1.0
0.5
0.0
SS-8GP
Exact Mass: 1951,5012
SS-8GP
Exact Mass: 1952,5090
1957.3536
1958.3542
1956.3547
1959.3525
1955.3544
1960.3540
1961.3644
1953.4651
1952.4691
1954.4663
1963.3867
1965.3900
1951.4627
1949.3956
1950.3940
1950
1952
1954
1956
1958
1960
1962
1964
1966
m/z

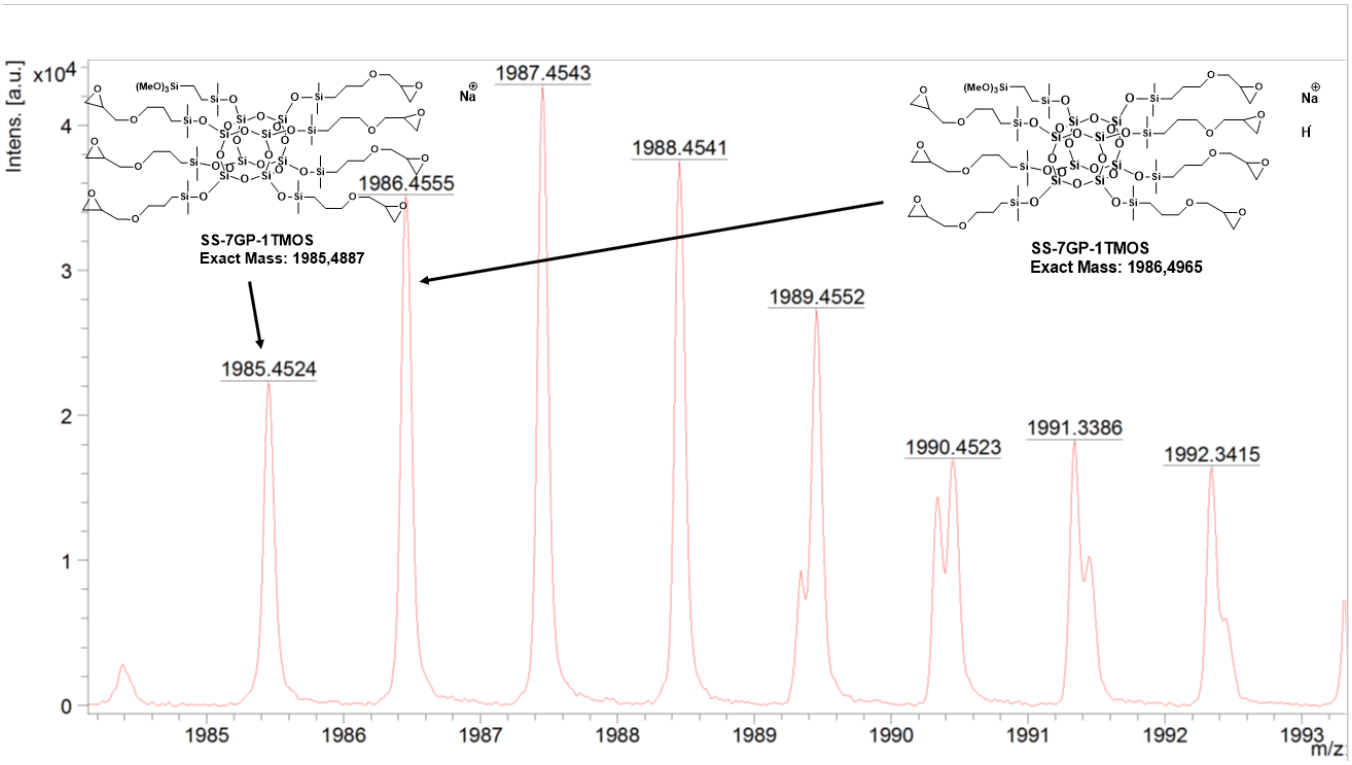
Intens. [a.u.]
x10^4
4
3
2
1
0
SS-7GP-1TMOS
Exact Mass: 1985,4887
SS-7GP-1TMOS
Exact Mass: 1986,4965
1987.4543
1988.4541
1986.4555
1989.4552
1985.4524
1990.4523
1991.3386
1992.3415
1985
1986
1987
1988
1989
1990
1991
1992
1993
m/z

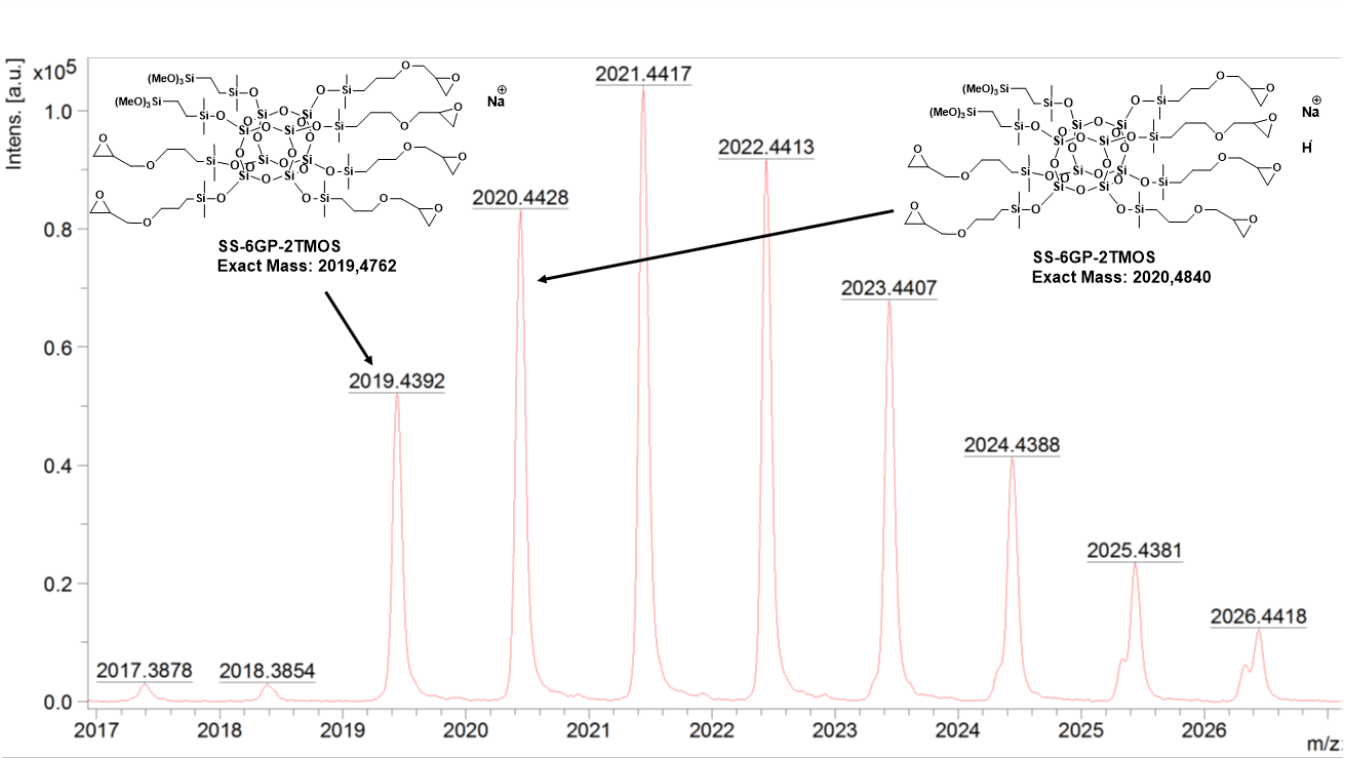
Intens. [a.u.]
x10^5
1.0
0.8
0.6
0.4
0.2
0.0
2017.3878
2018.3854
2019.4392
2020.4428
2021.4417
2022.4413
2023.4407
2024.4388
2025.4381
2026.4418
2017
2018
2019
2020
2021
2022
2023
2024
2025
2026
m/z
SS-6GP-2TMOS
Exact Mass: 2019,4762
SS-6GP-2TMOS
Exact Mass: 2020,4840
Na
H

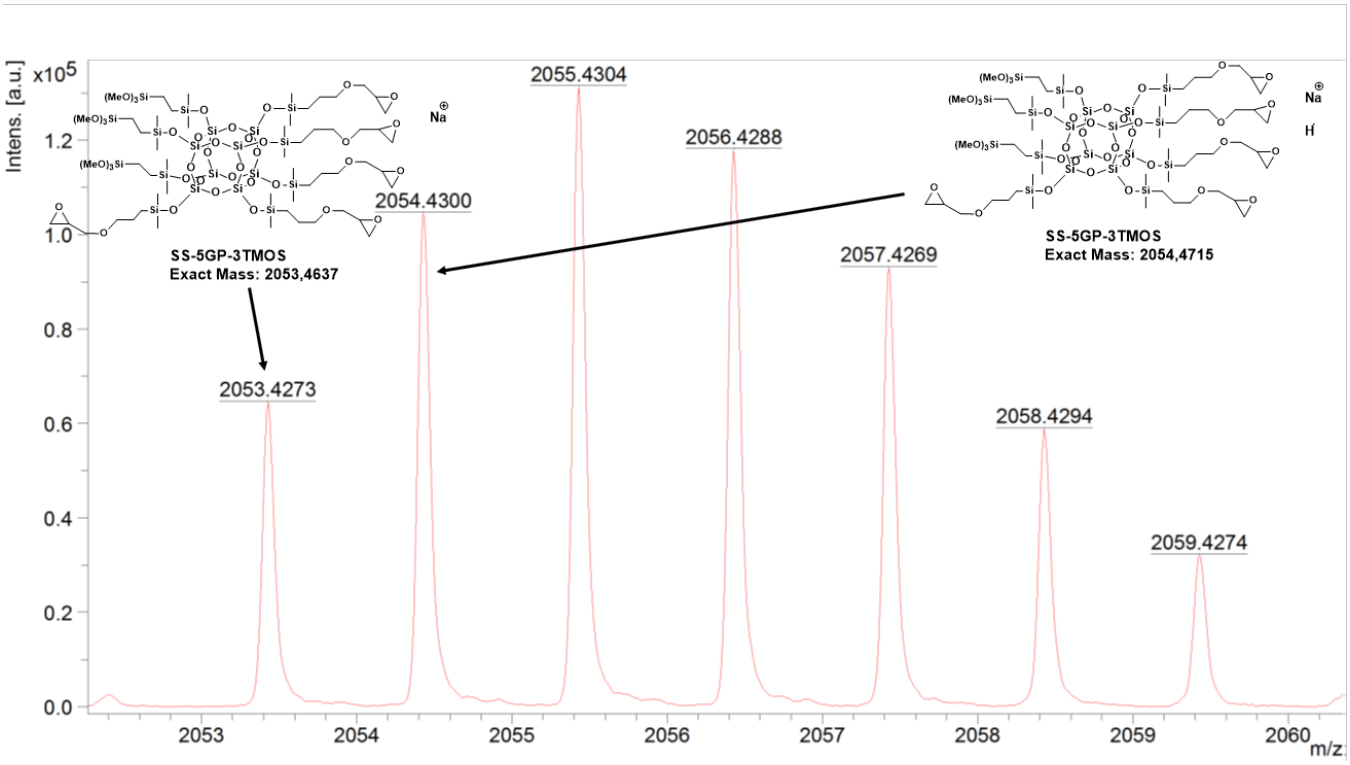
Intens. [a.u.]
x10^5
1.2
1.0
0.8
0.6
0.4
0.2
0.0
2053.4273
2054.4300
2055.4304
2056.4288
2057.4269
2058.4294
2059.4274
2053
2054
2055
2056
2057
2058
2059
2060
m/z
SS-5GP-3TMOS
Exact Mass: 2053,4637
SS-5GP-3TMOS
Exact Mass: 2054,4715
Na
H

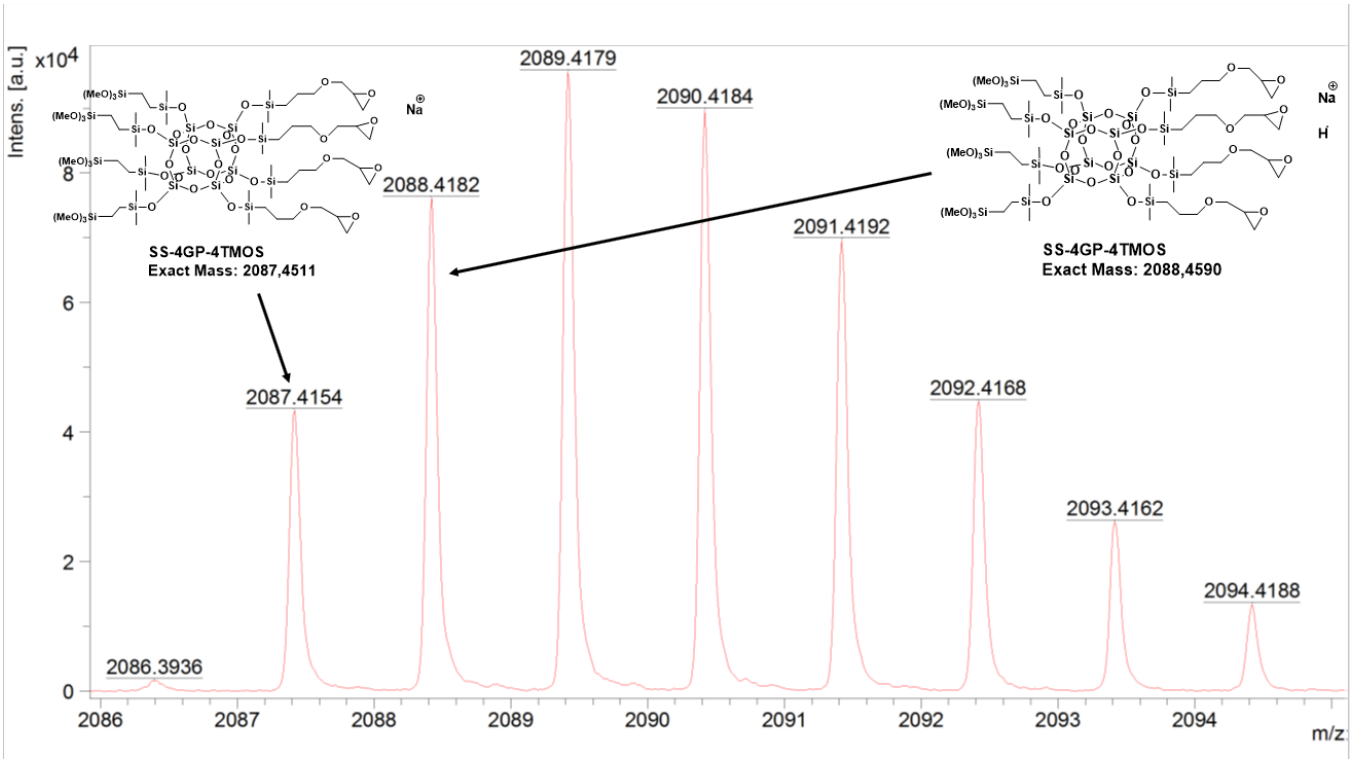
Intens. [a.u.]
x10^4
2089.4179
2090.4184
2088.4182
2091.4192
2087.4154
2092.4168
2093.4162
2094.4188
2086.3936
SS-4GP-4TMOS
Exact Mass: 2087,4511
SS-4GP-4TMOS
Exact Mass: 2088,4590
m/z

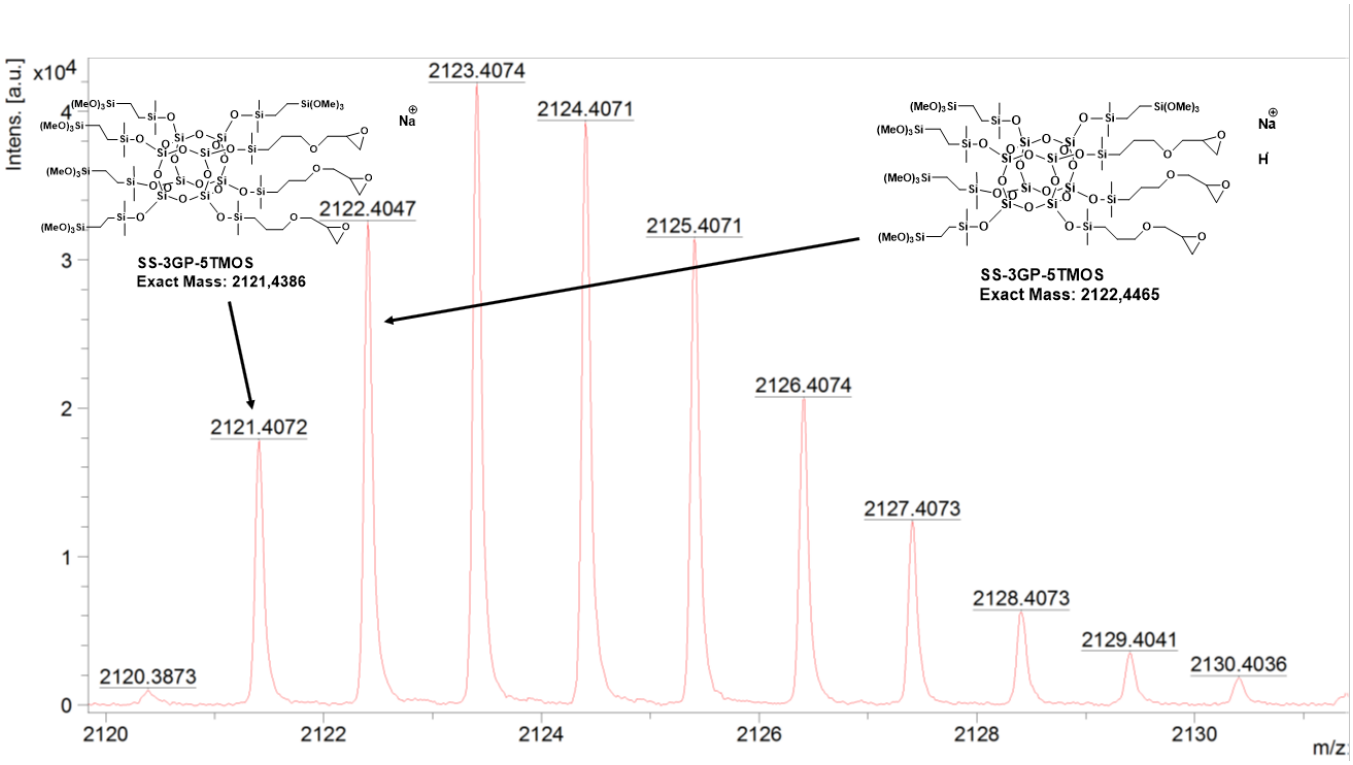
Intens. [a.u.]
x10^4
2123.4074
2124.4071
2122.4047
2125.4071
2121.4072
2126.4074
2127.4073
2128.4073
2129.4041
2130.4036
2120.3873
SS-3GP-5TMOS
Exact Mass: 2121,4386
SS-3GP-5TMOS
Exact Mass: 2122,4465
m/z

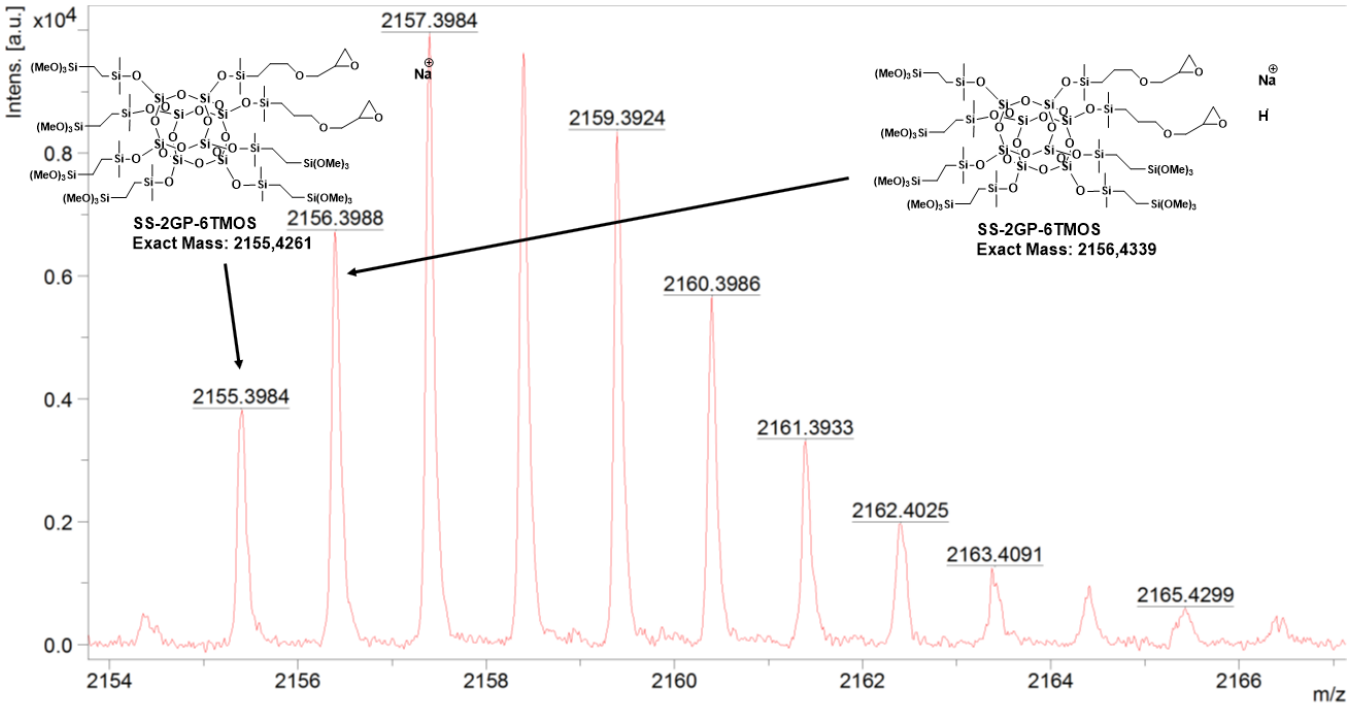
x10^4
Intens. [a.u.]
2157.3984
Na
2159.3924
2156.3988
2160.3986
2155.3984
2161.3933
2162.4025
2163.4091
2165.4299
SS-2GP-6TMOS
Exact Mass: 2155,4261
SS-2GP-6TMOS
Exact Mass: 2156,4339
Na
H
0.0
0.2
0.4
0.6
0.8
2154
2156
2158
2160
2162
2164
2166
m/z

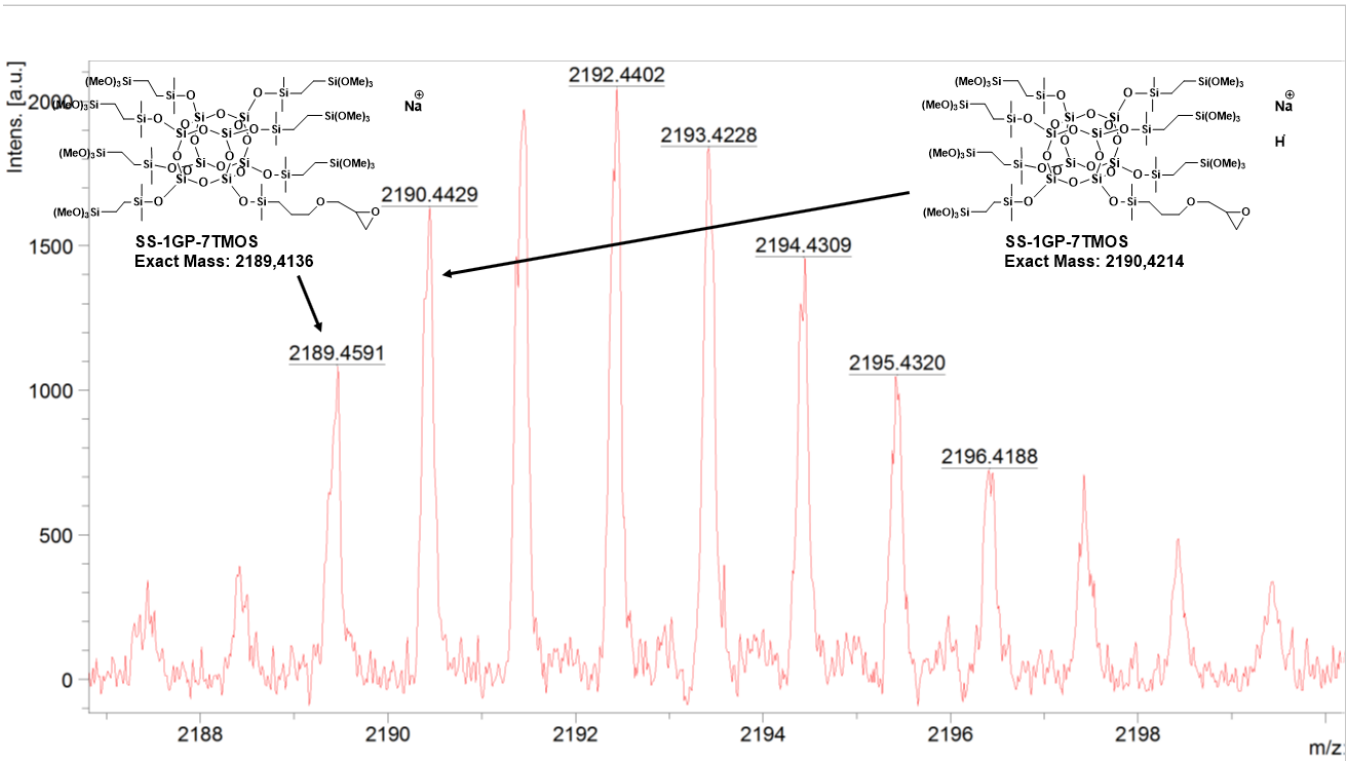
Intens. [a.u.]
2192.4402
2193.4228
Na
2190.4429
2194.4309
2189.4591
2195.4320
2196.4188
SS-1GP-7TMOS
Exact Mass: 2189,4136
SS-1GP-7TMOS
Exact Mass: 2190,4214
Na
H
0
500
1000
1500
2000
2188
2190
2192
2194
2196
2198
m/z

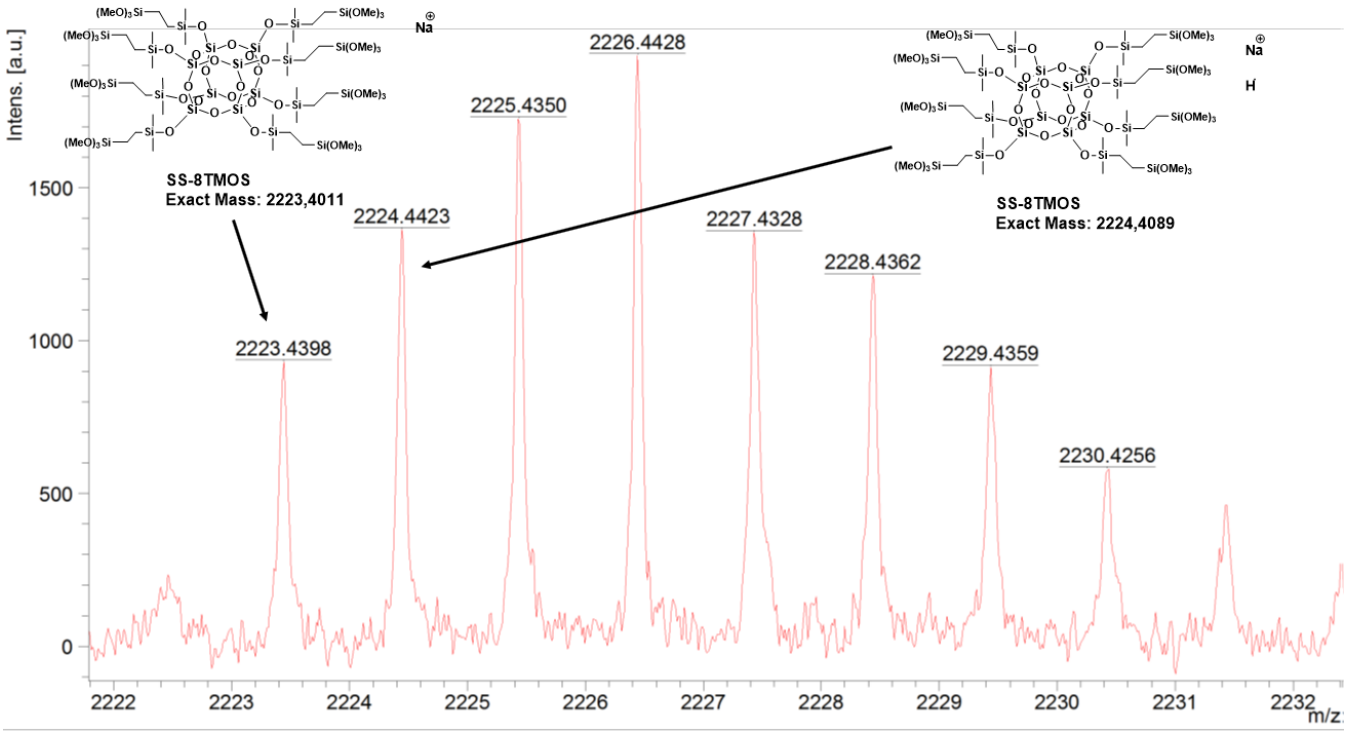
Intens. [a.u.]
1500
1000
500
0
2222
2223
2224
2225
2226
2227
2228
2229
2230
2231
2232
m/z
2223.4398
2224.4423
2225.4350
2226.4428
2227.4328
2228.4362
2229.4359
2230.4256
SS-8TMOS
Exact Mass: 2223,4011
SS-8TMOS
Exact Mass: 2224,4089
Na
H

4. SEM images of the TiO_2/EP composites

1% TiO_2, unmodified, mechanical stirrer

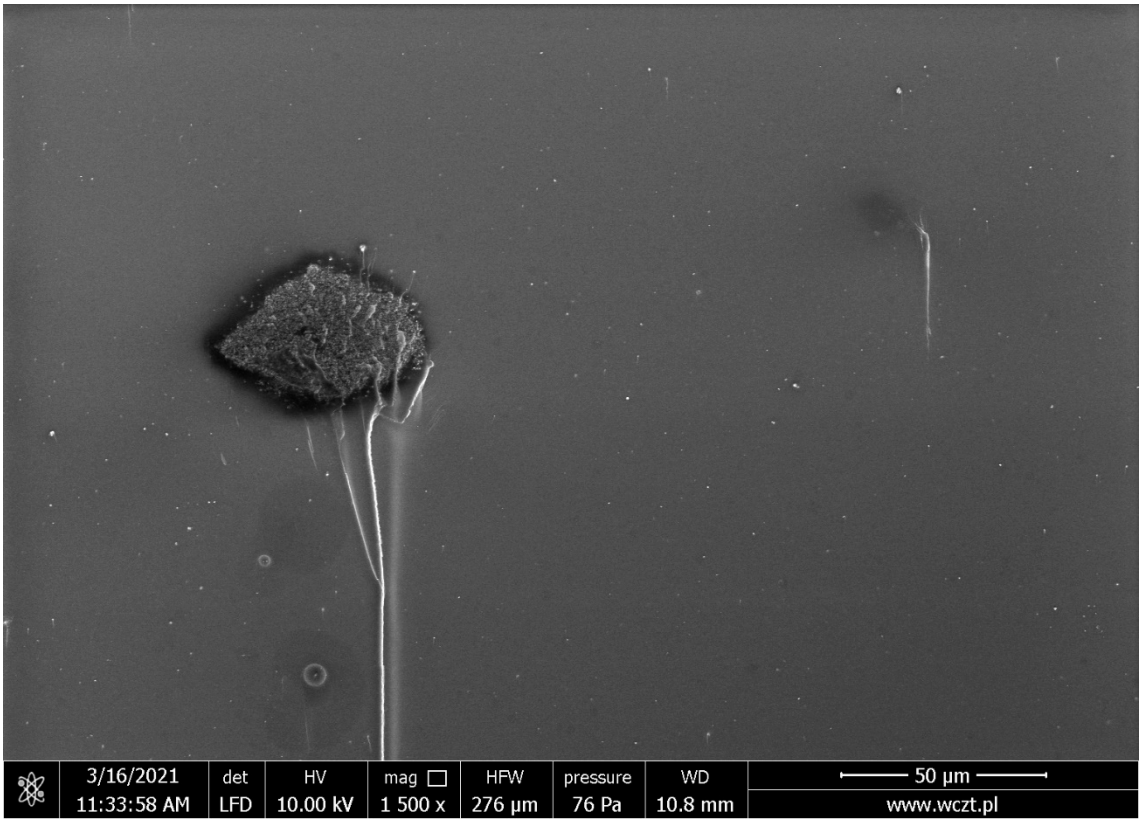

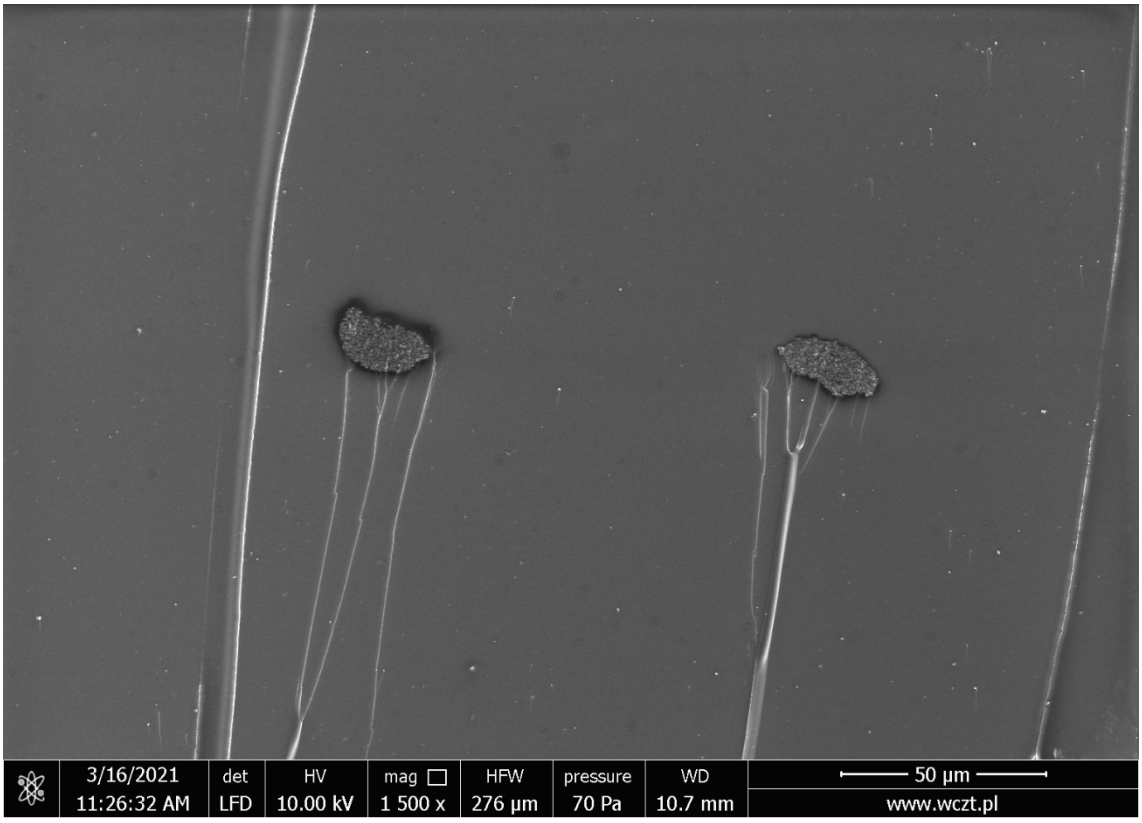

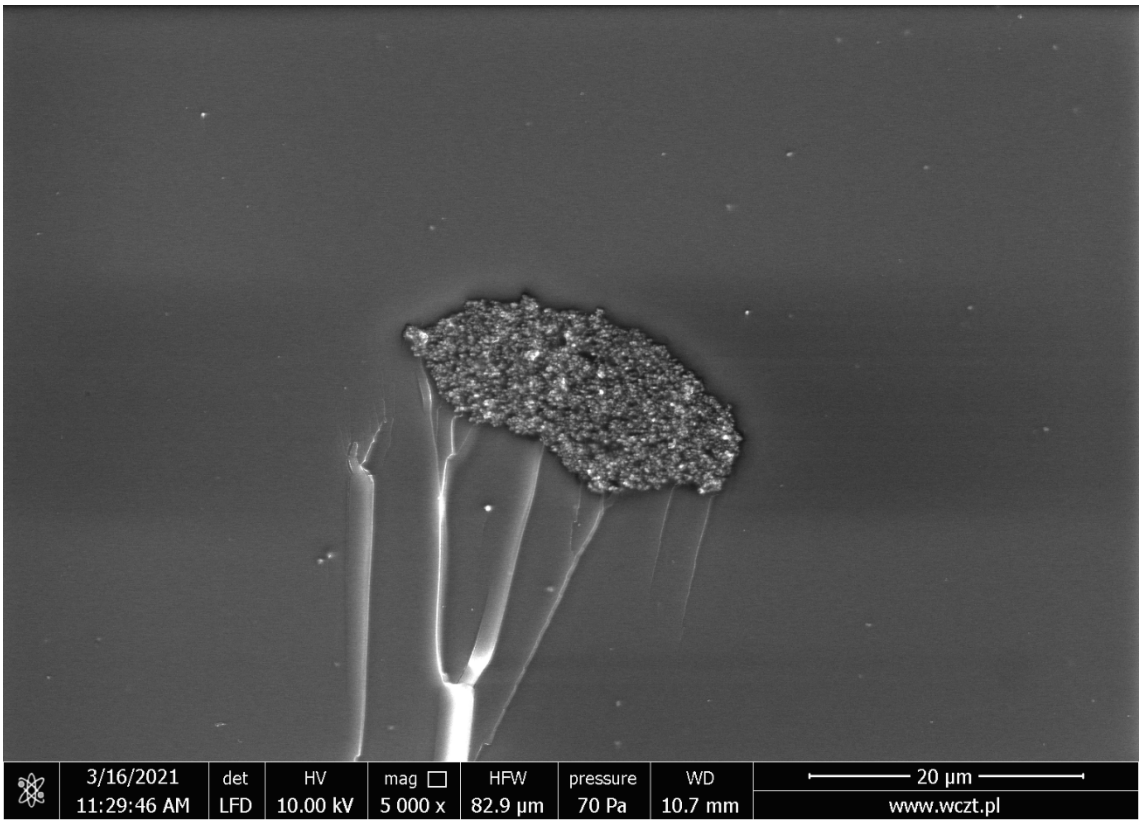
3/16/2021
11:29:46 AM
det
LFD
HV
10.00 kV
mag
5 000 x
HFW
82.9 µm
pressure
70 Pa
WD
10.7 mm
20 µm
www.wczt.pl

1% TiO_2, unmodified, mixing pump

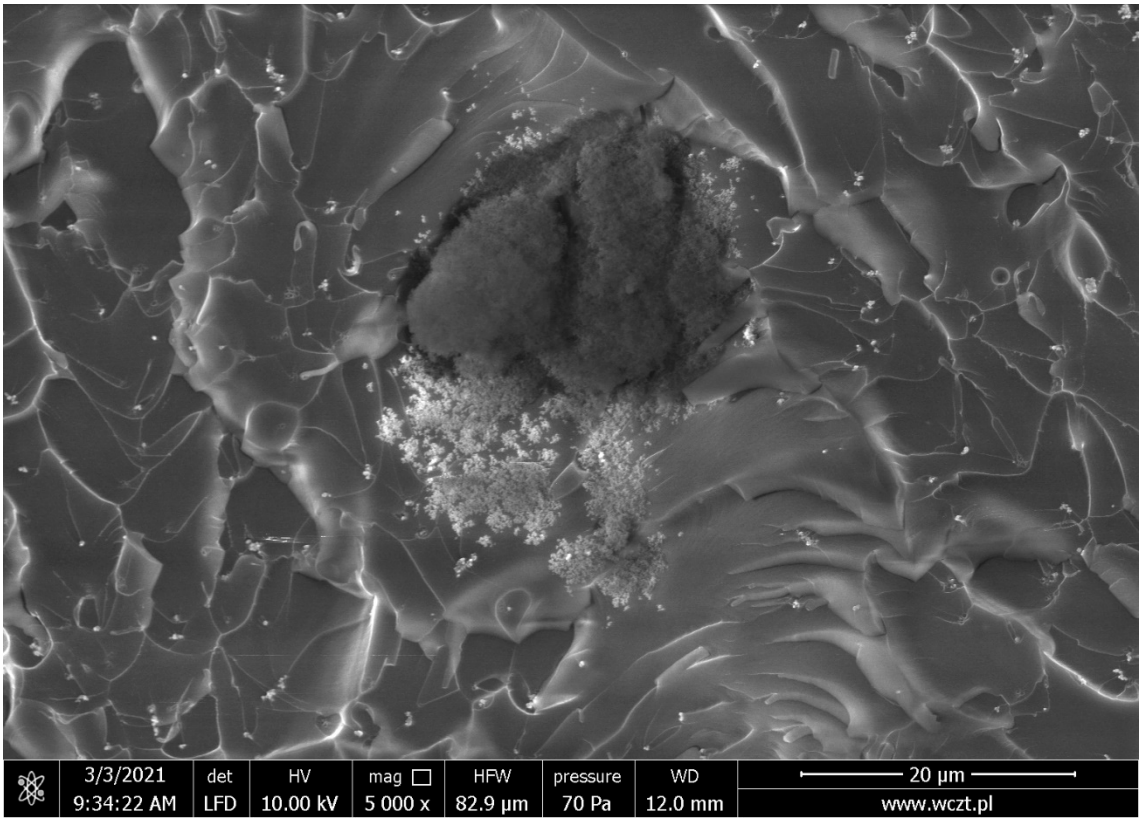

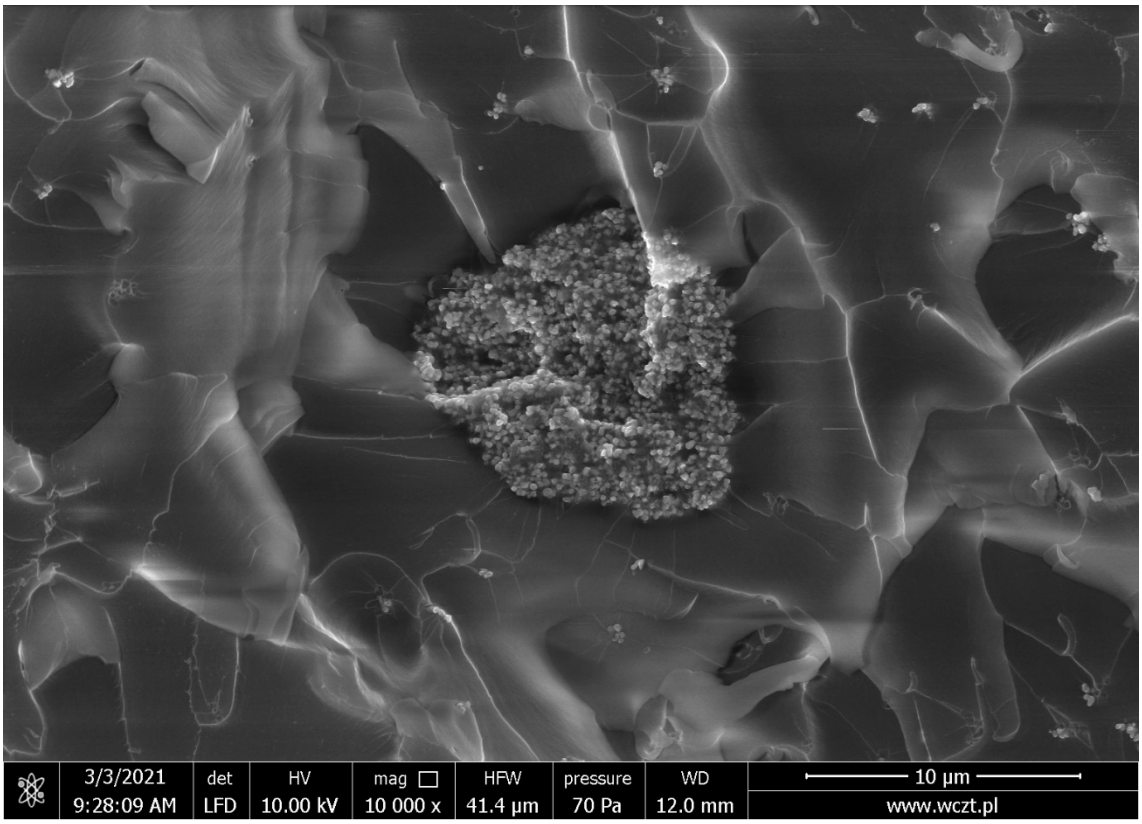

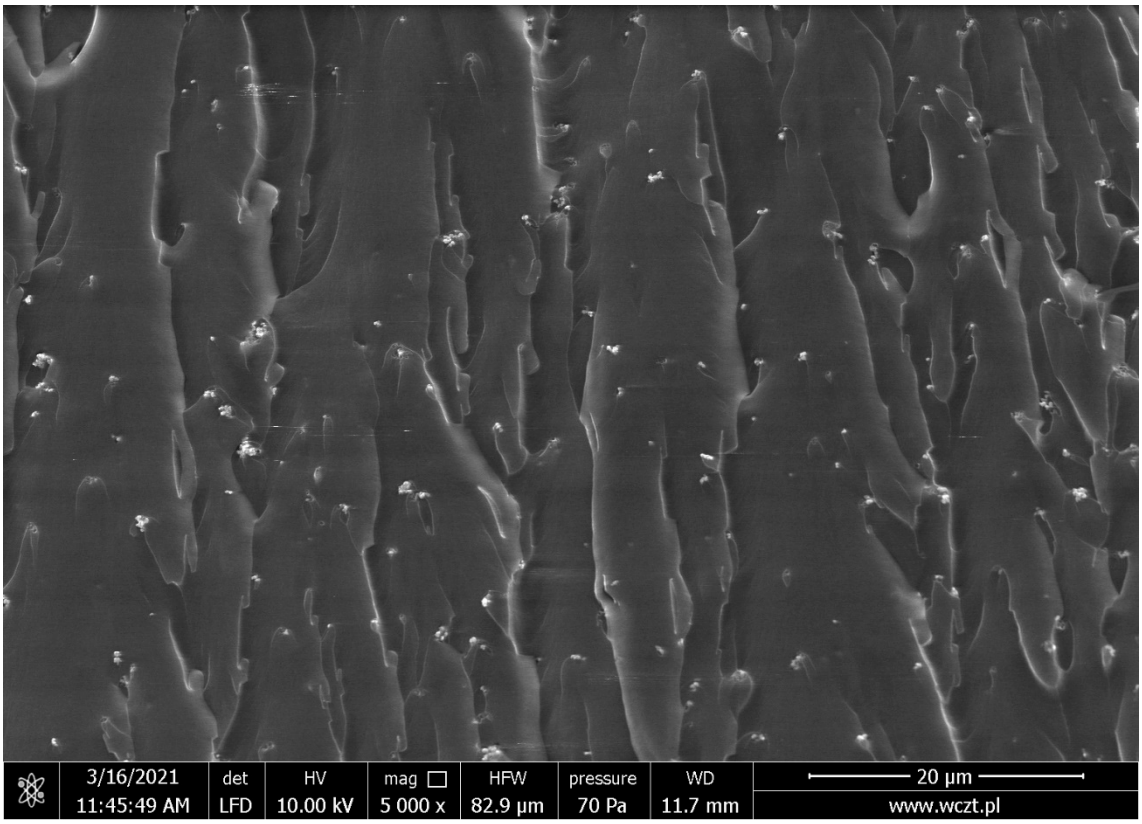
3/16/2021
11:45:49 AM
det
LFD
HV
10.00 kV
mag
5 000 x
HFW
82.9 µm
pressure
70 Pa
WD
11.7 mm
20 µm
www.wczt.pl

2% TiO_2, unmodified, mixing pump

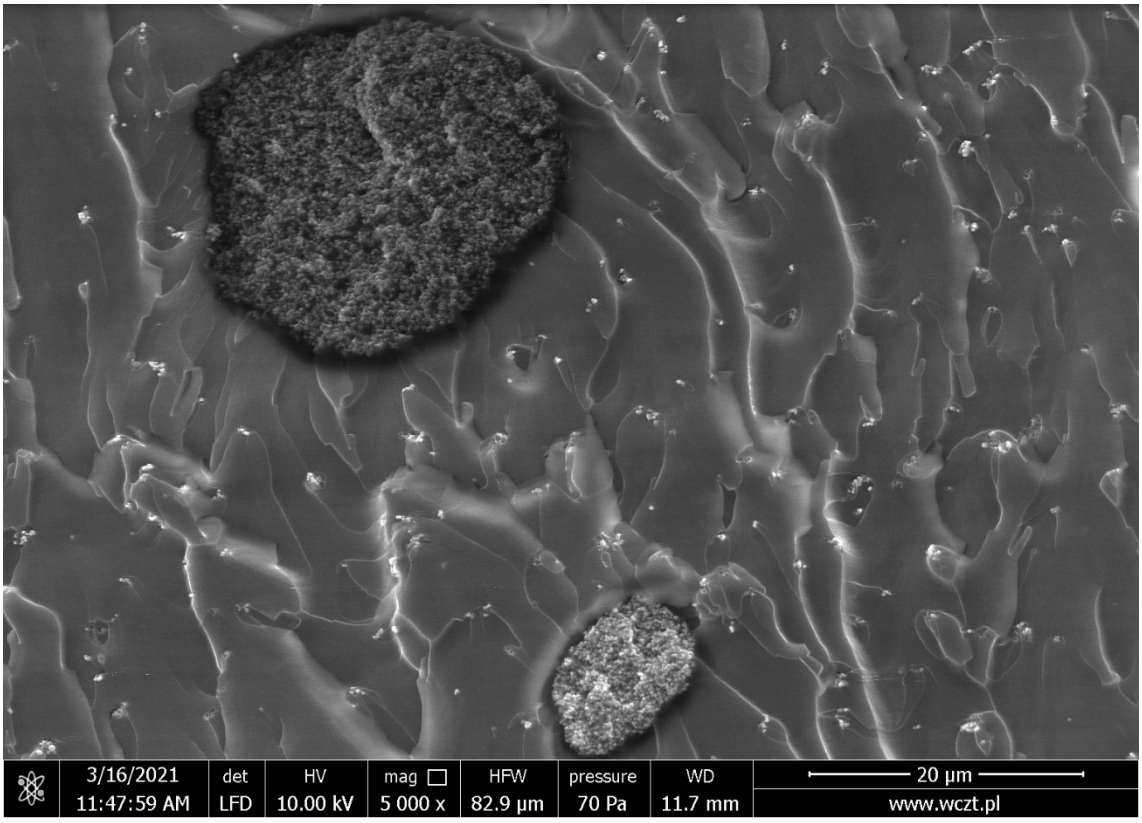

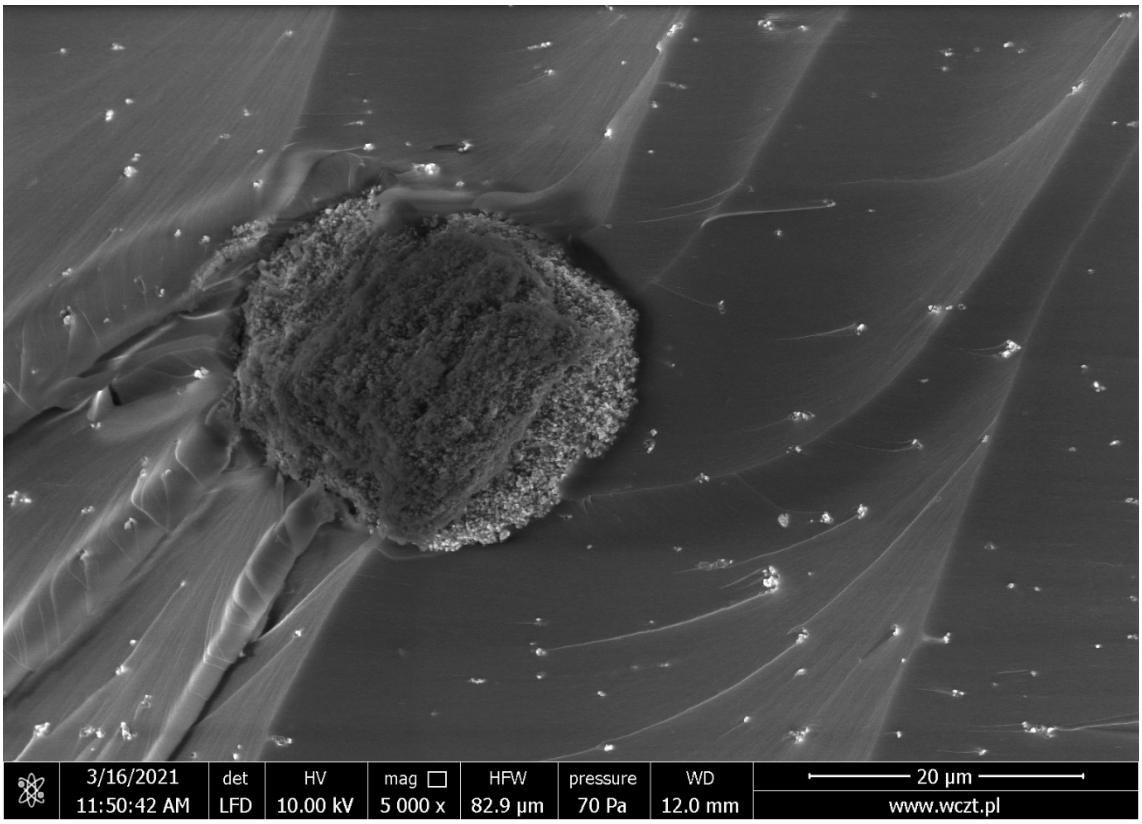

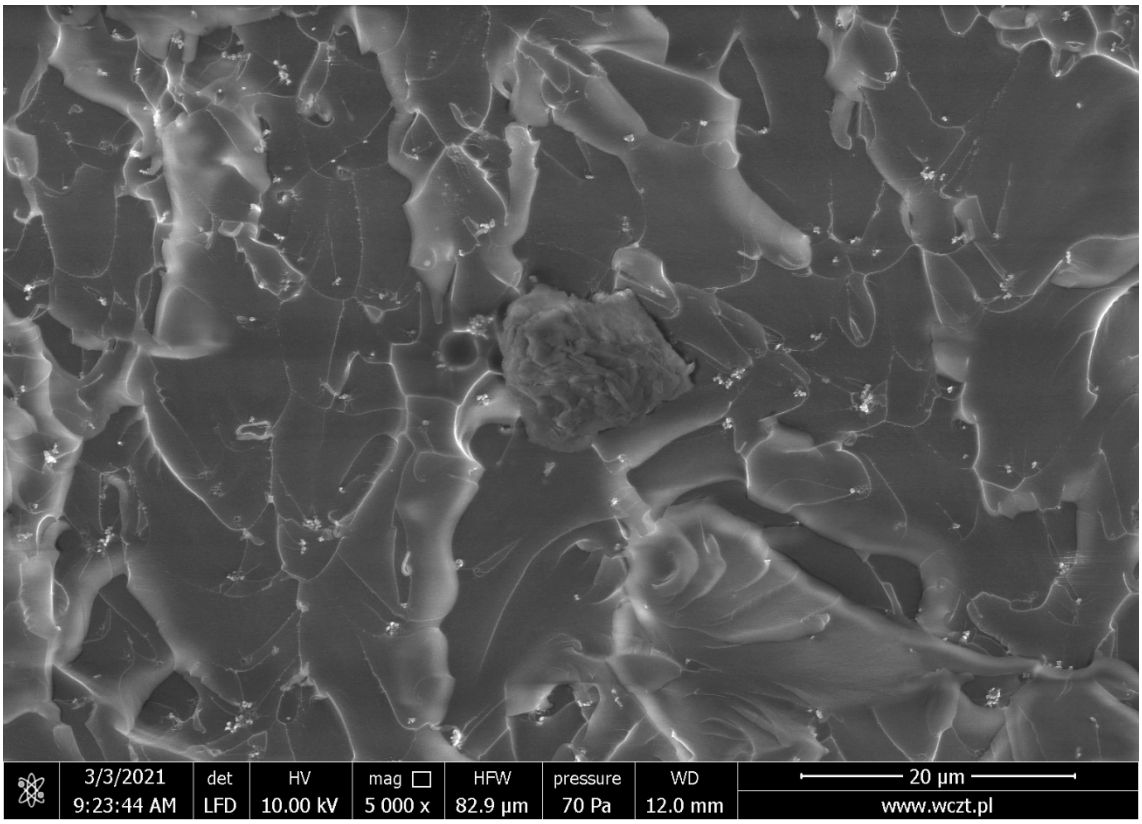
3/3/2021
9:23:44 AM
det
LFD
HV
10.00 kV
mag
5 000 x
HFW
82.9 µm
pressure
70 Pa
WD
12.0 mm
20 µm
www.wczt.pl

1%TiO_2, 0.5% iBuTMOS, mixing pump

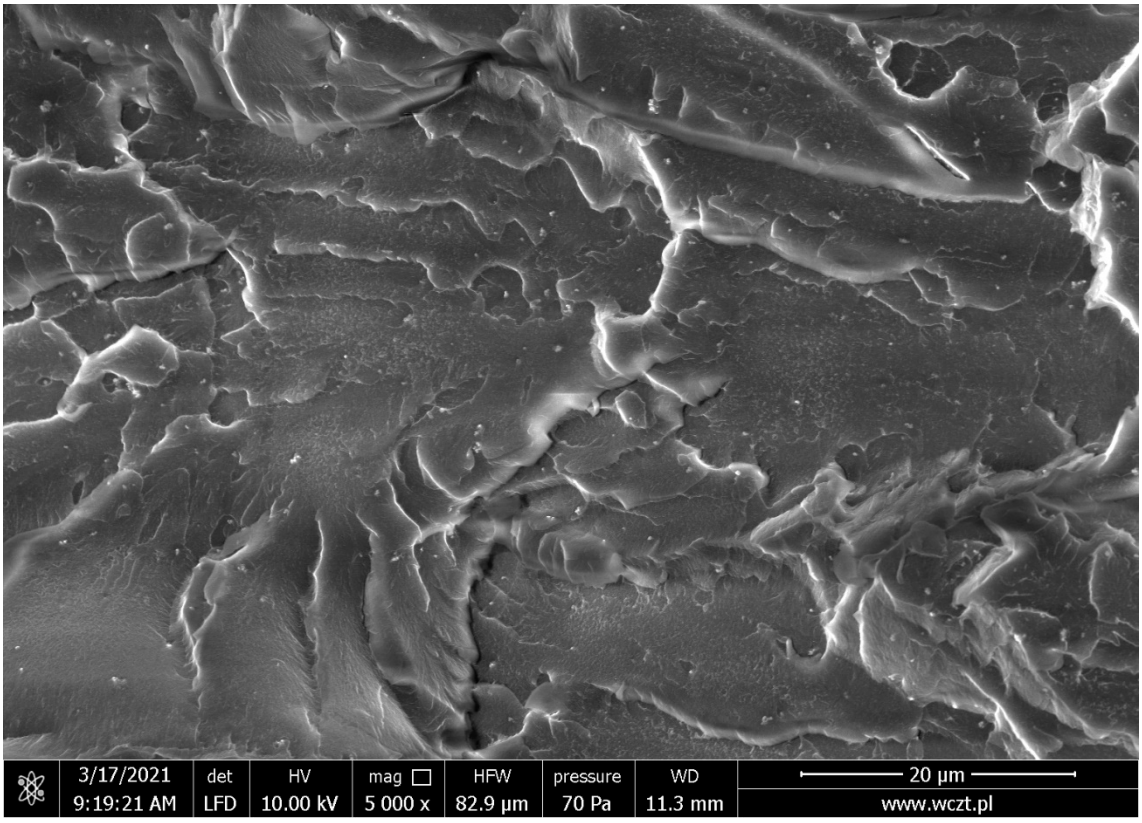

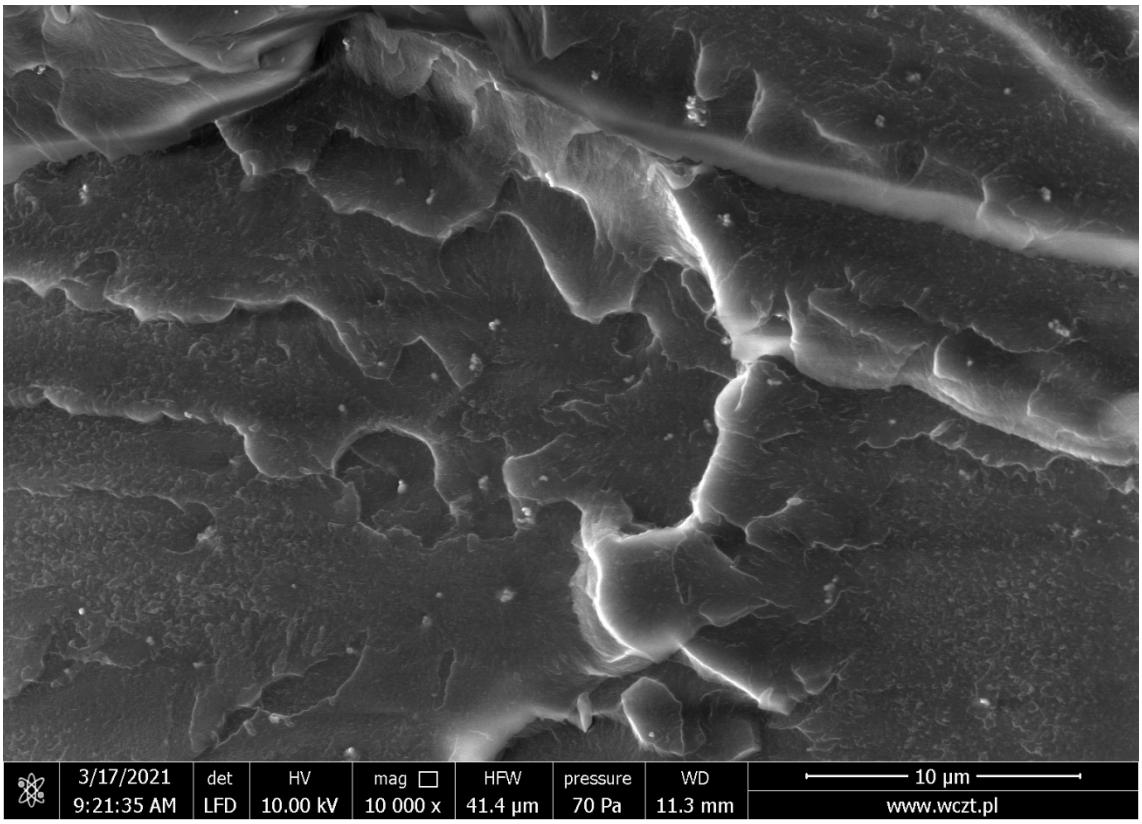

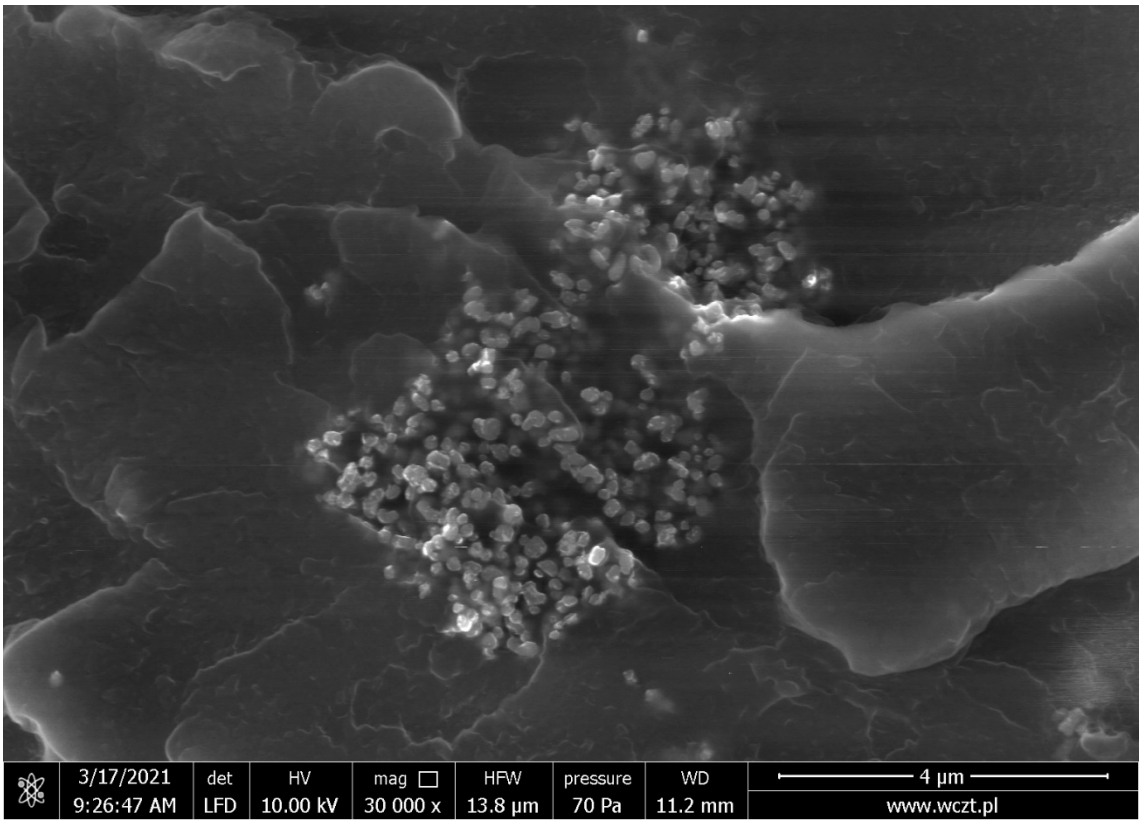
3/17/2021
9:26:47 AM
det
LFD
HV
10.00 kV
mag
30 000 x
HFW
13.8 µm
pressure
70 Pa
WD
11.2 mm
4 µm
www.wczt.pl

2%TiO_2, 0.5% iBuTMOS, mixing pump

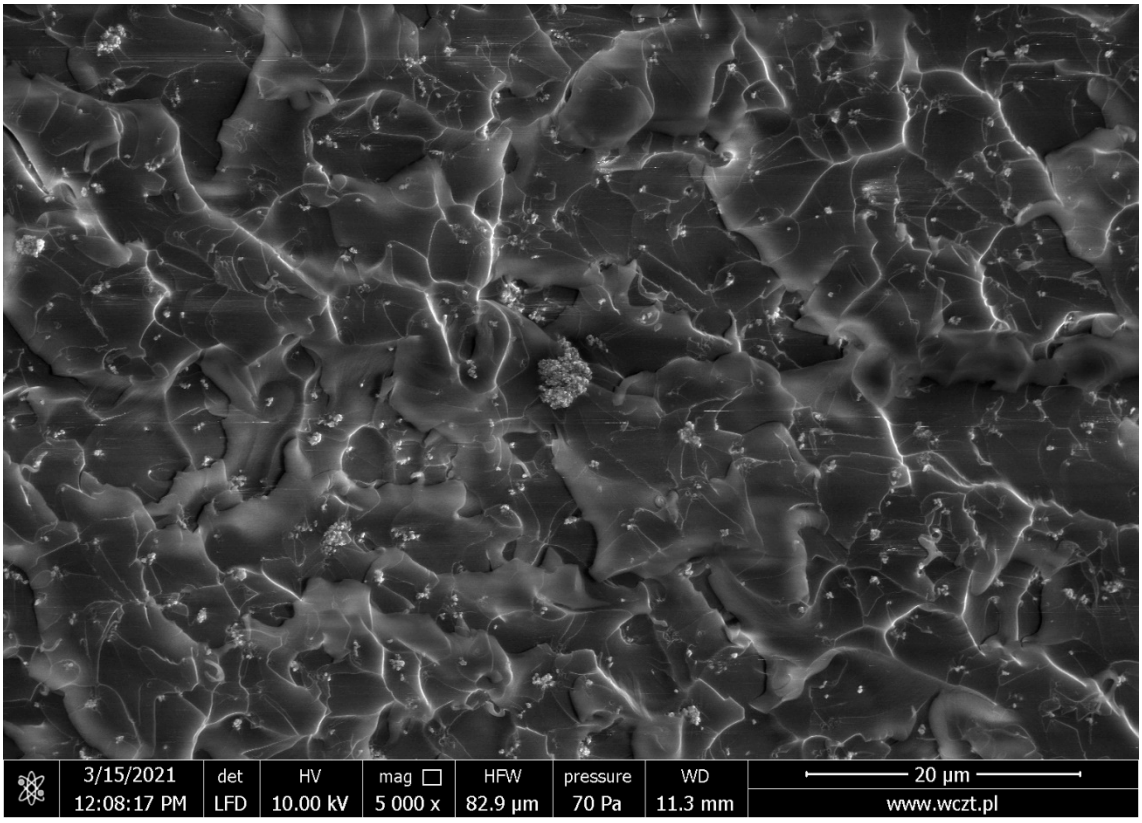

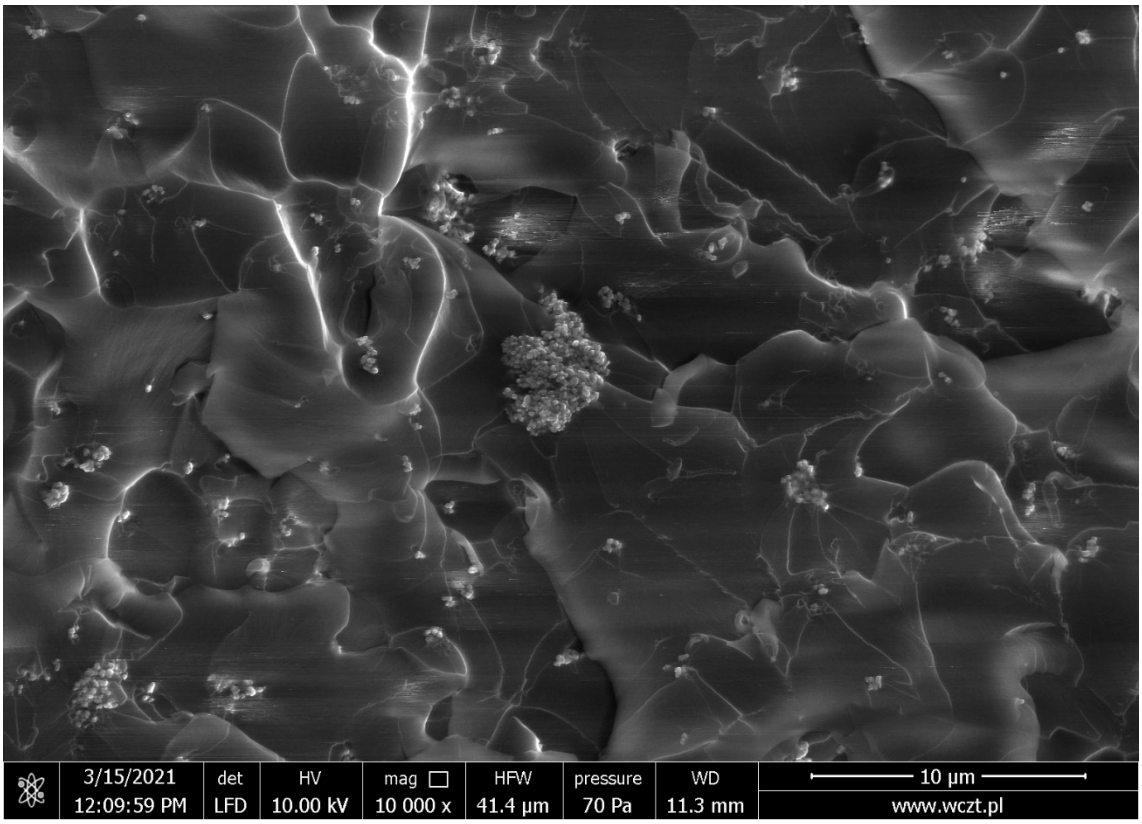

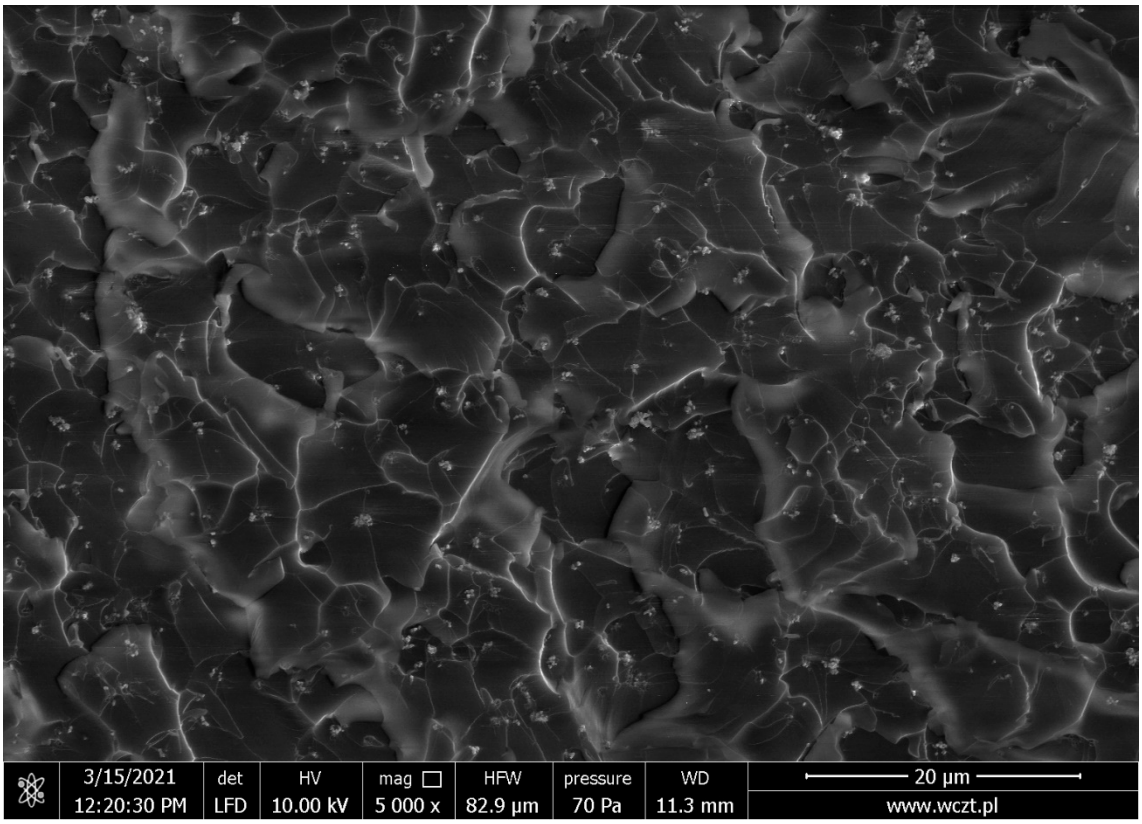
3/15/2021
12:20:30 PM
det
LFD
HV
10.00 kV
mag
5 000 x
HFW
82.9 µm
pressure
70 Pa
WD
11.3 mm
20 µm
www.wczt.pl

1%TiO_2, 1.5% iBuTMOS, mechanical stirrer

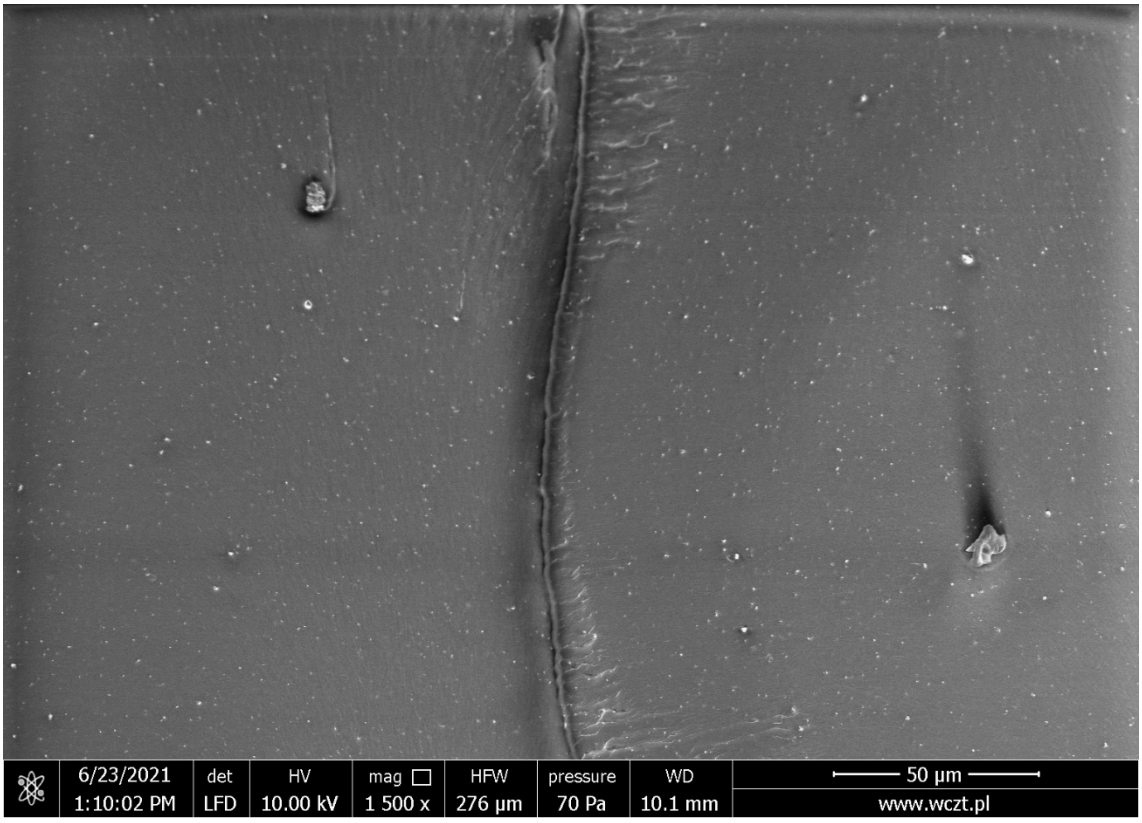

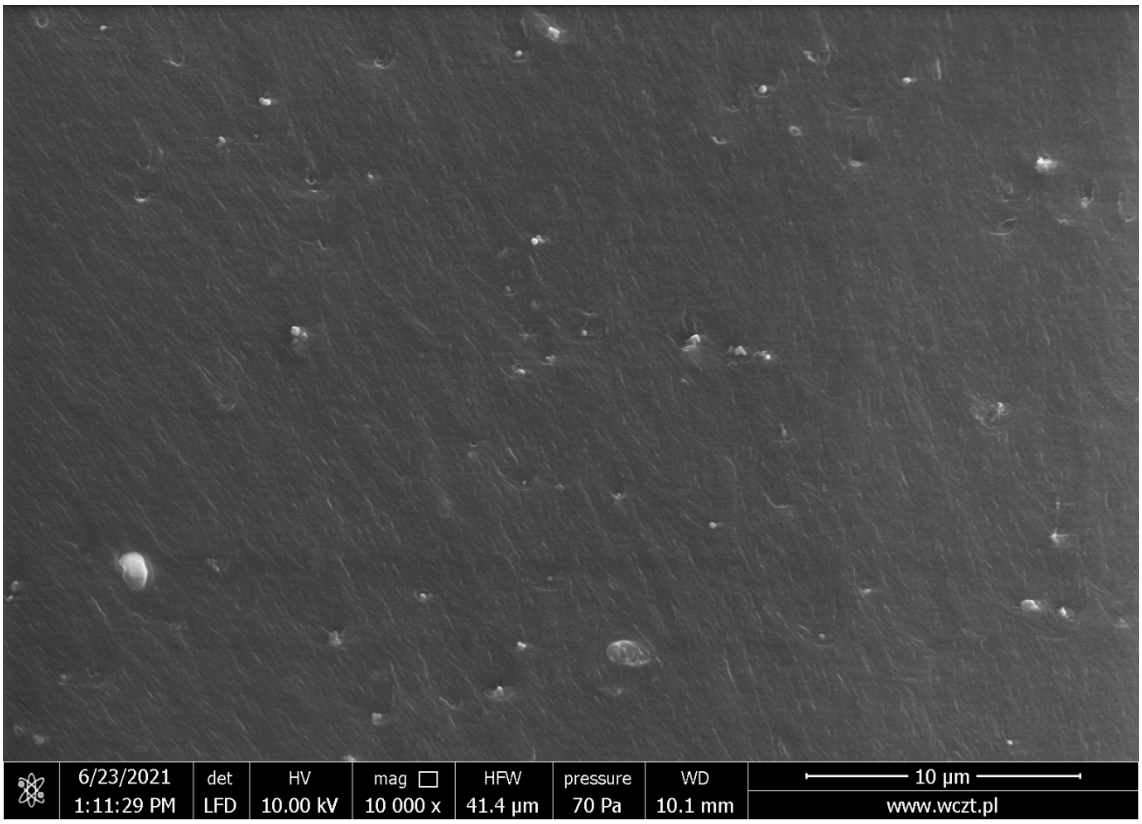

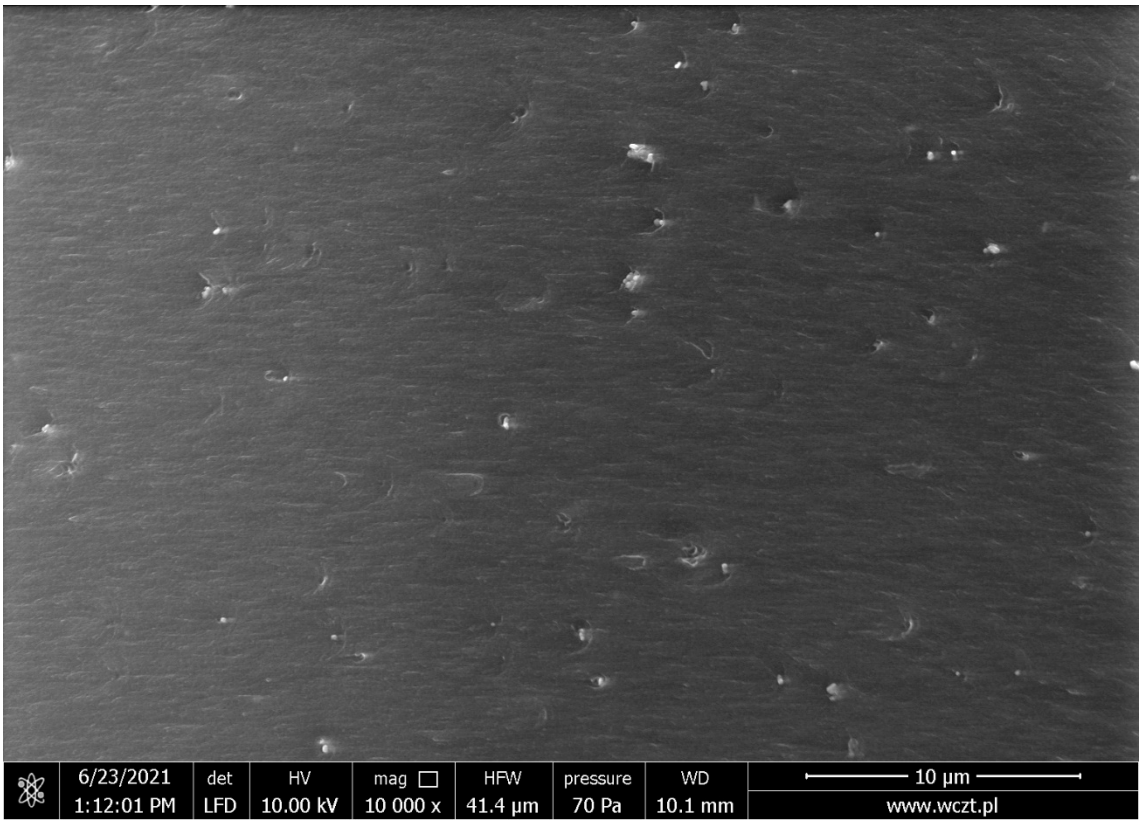
6/23/2021
1:12:01 PM
det
LFD
HV
10.00 kV
mag
10 000 x
HFW
41.4 µm
pressure
70 Pa
WD
10.1 mm
10 µm
www.wczt.pl

1%TiO_2, 1.5% iBuTMOS, mixing pump

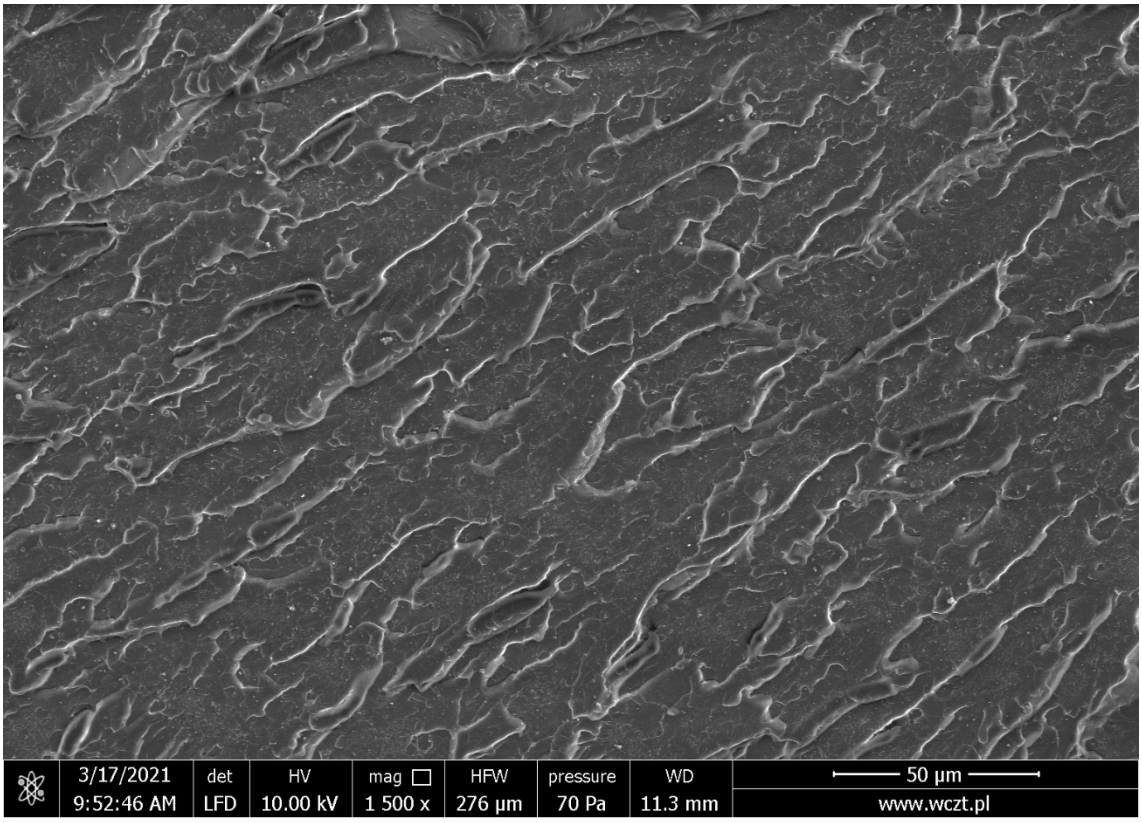

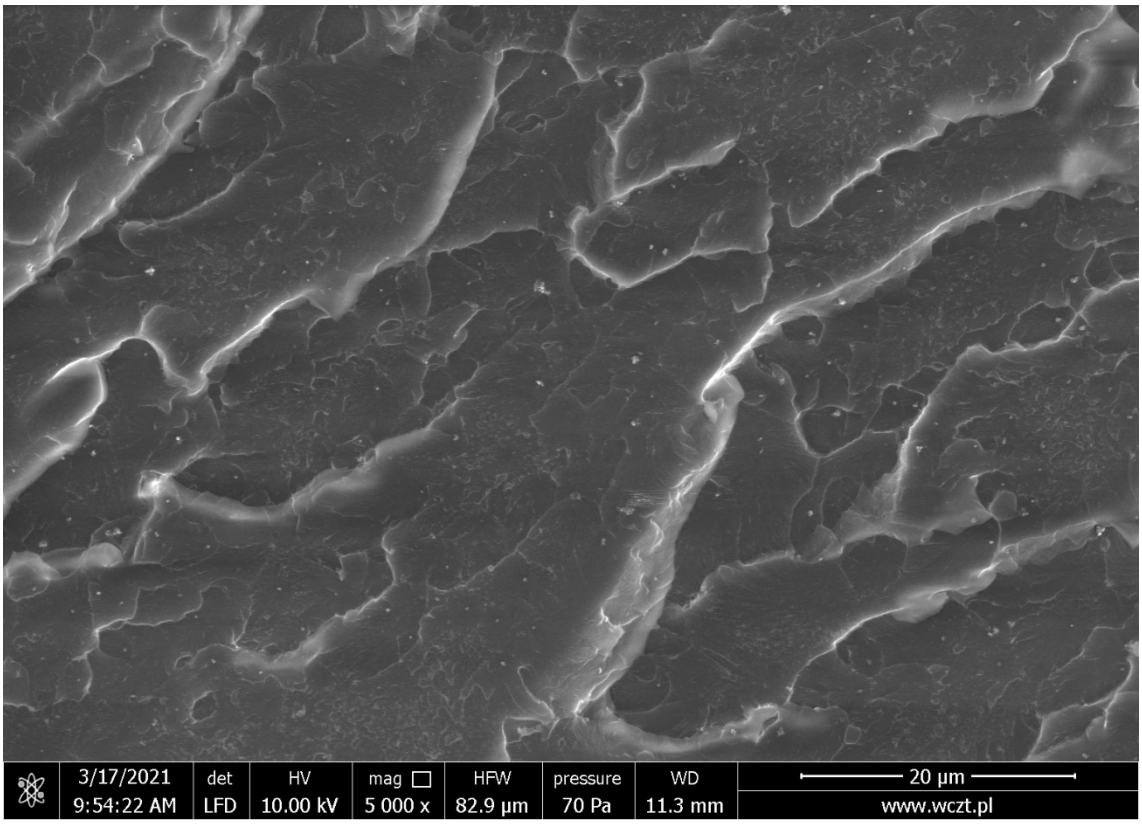

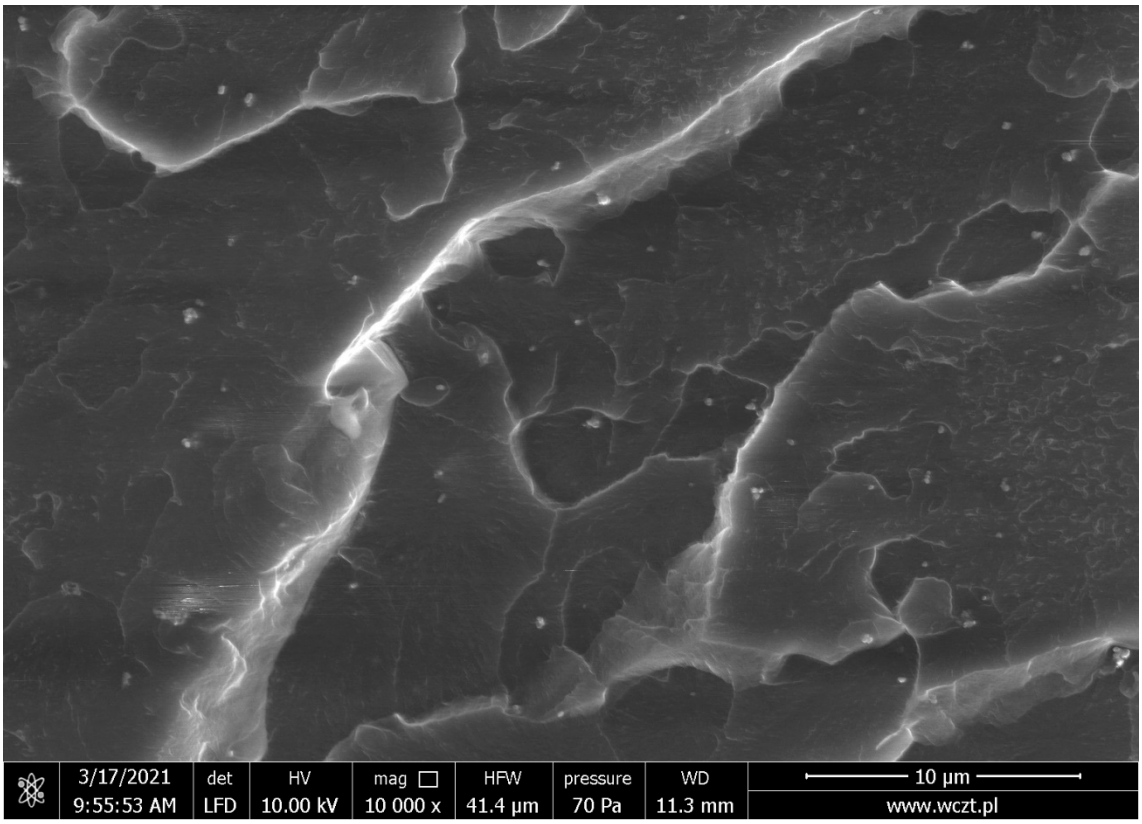
3/17/2021
9:55:53 AM
det
LFD
HV
10.00 kV
mag
10 000 x
HFW
41.4 µm
pressure
70 Pa
WD
11.3 mm
10 µm
www.wczt.pl

2%TiO_2, 1.5% iBuTMOS, mixing pump

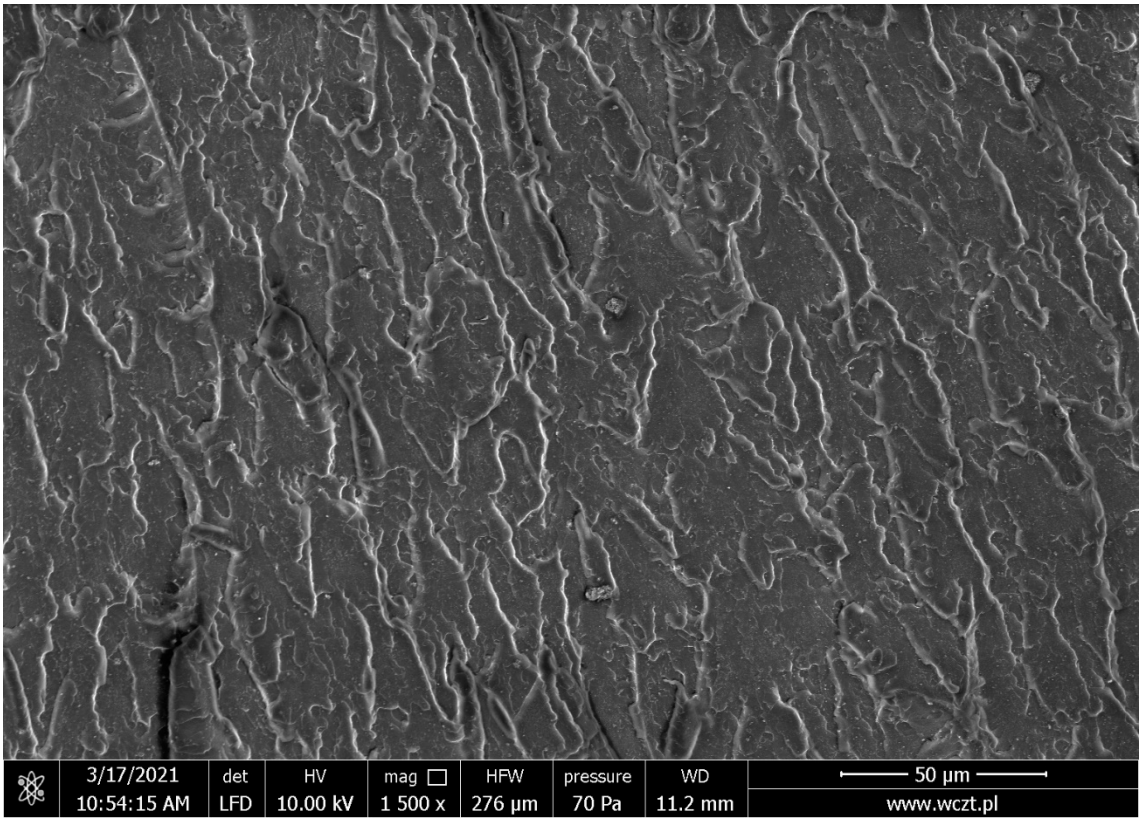

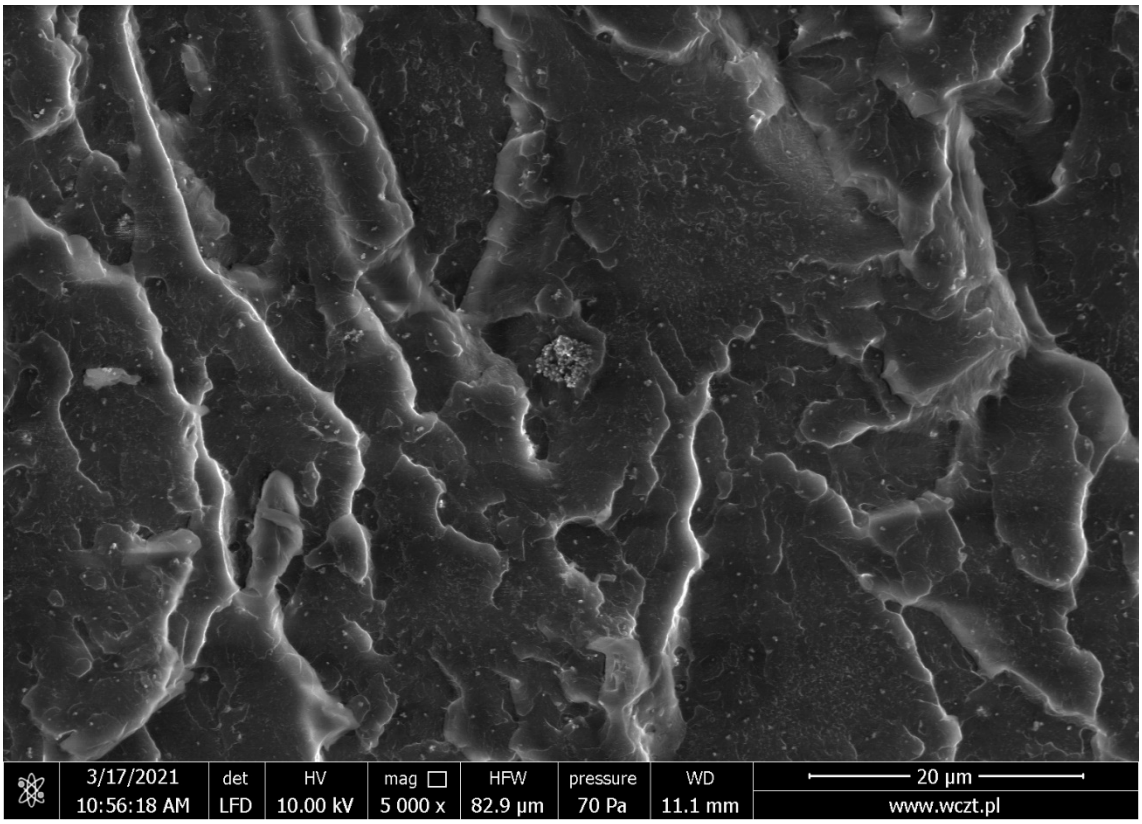

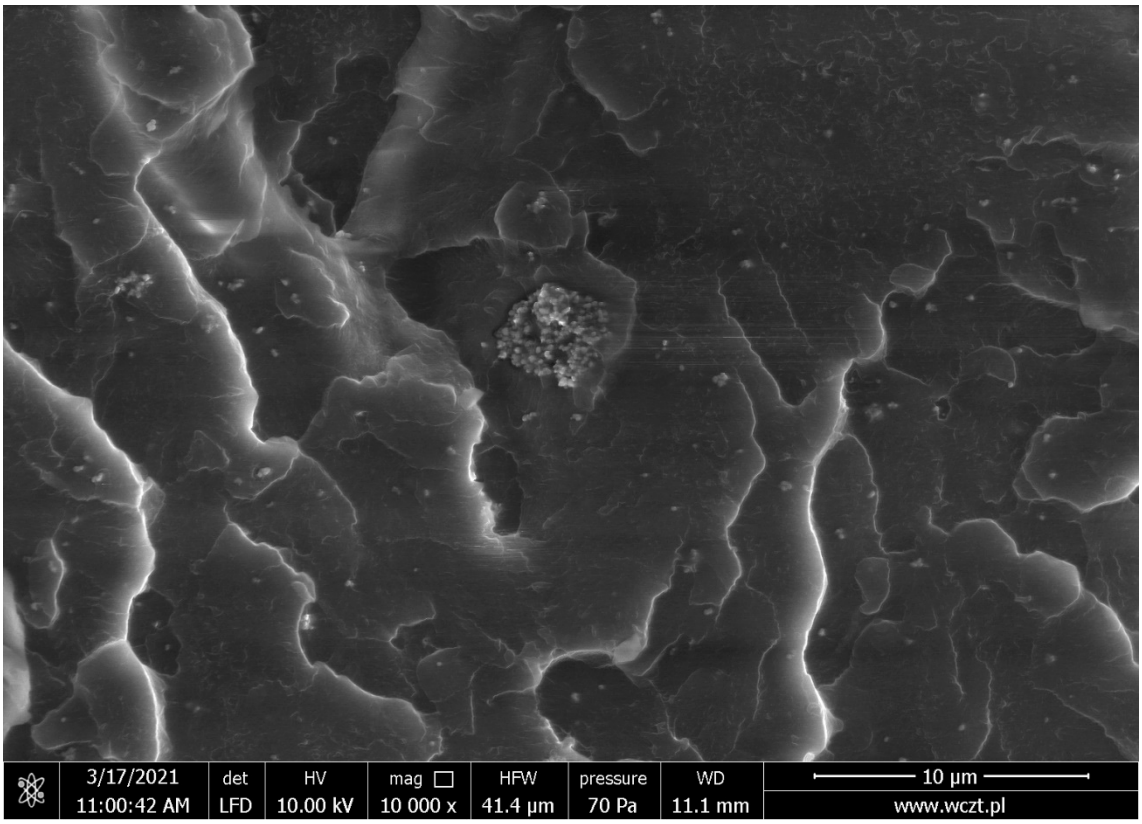
3/17/2021
11:00:42 AM
det
LFD
HV
10.00 kV
mag
10 000 x
HFW
41.4 µm
pressure
70 Pa
WD
11.1 mm
10 µm
www.wczt.pl

1%TiO_2, 0.5% GPTES, mixing pump

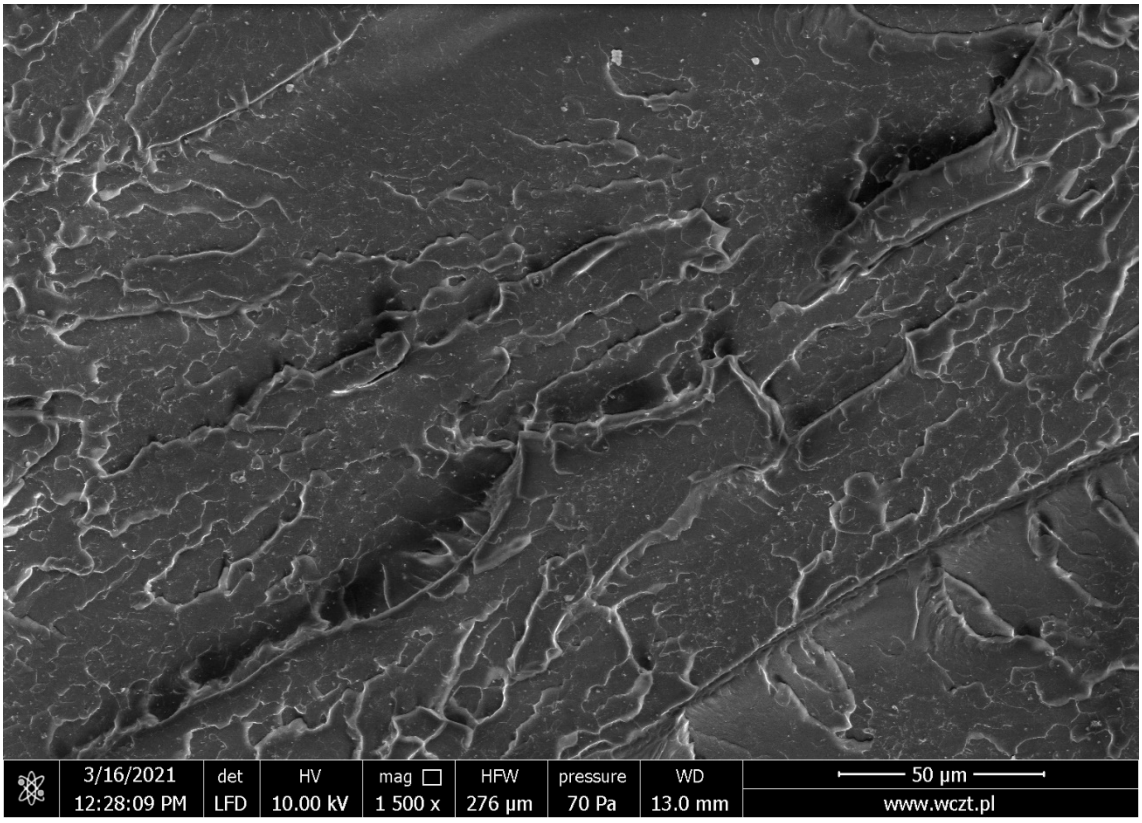

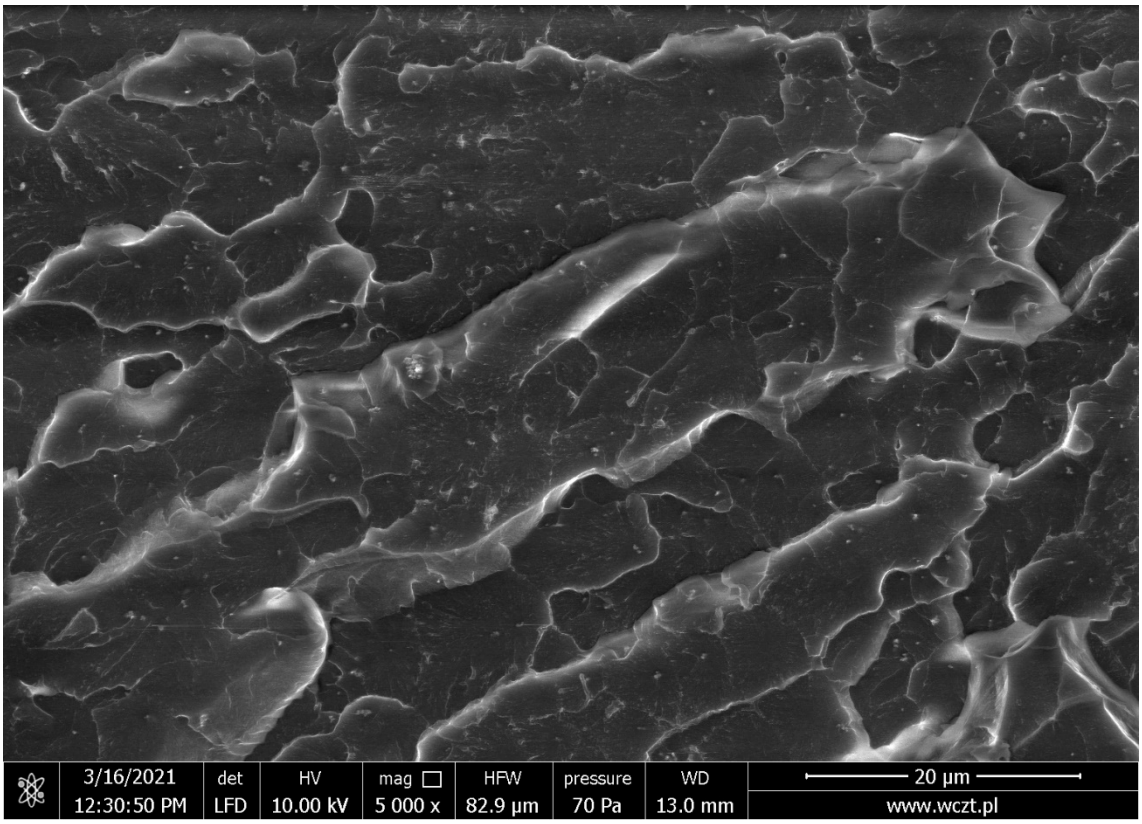

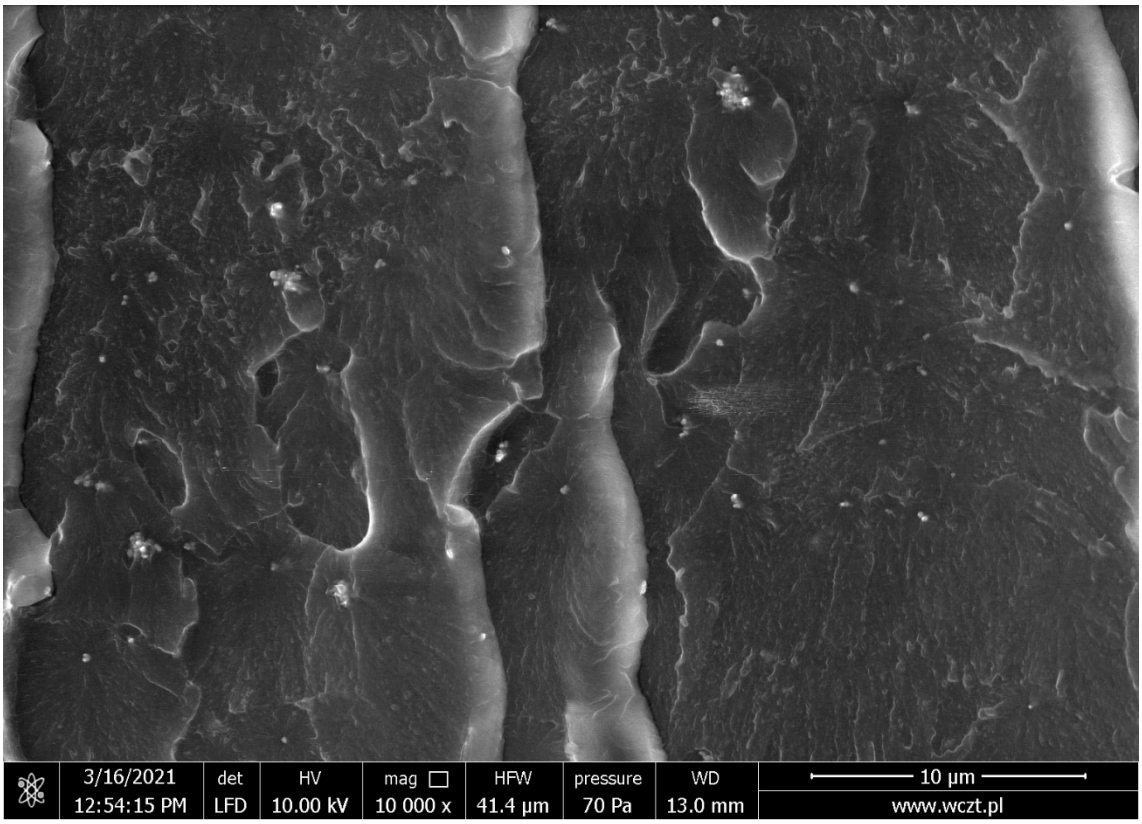
3/16/2021
12:54:15 PM
det
LFD
HV
10.00 kV
mag
10 000 x
HFW
41.4 µm
pressure
70 Pa
WD
13.0 mm
10 µm
www.wczt.pl

2%TiO_2, 0.5% GPTES, mixing pump

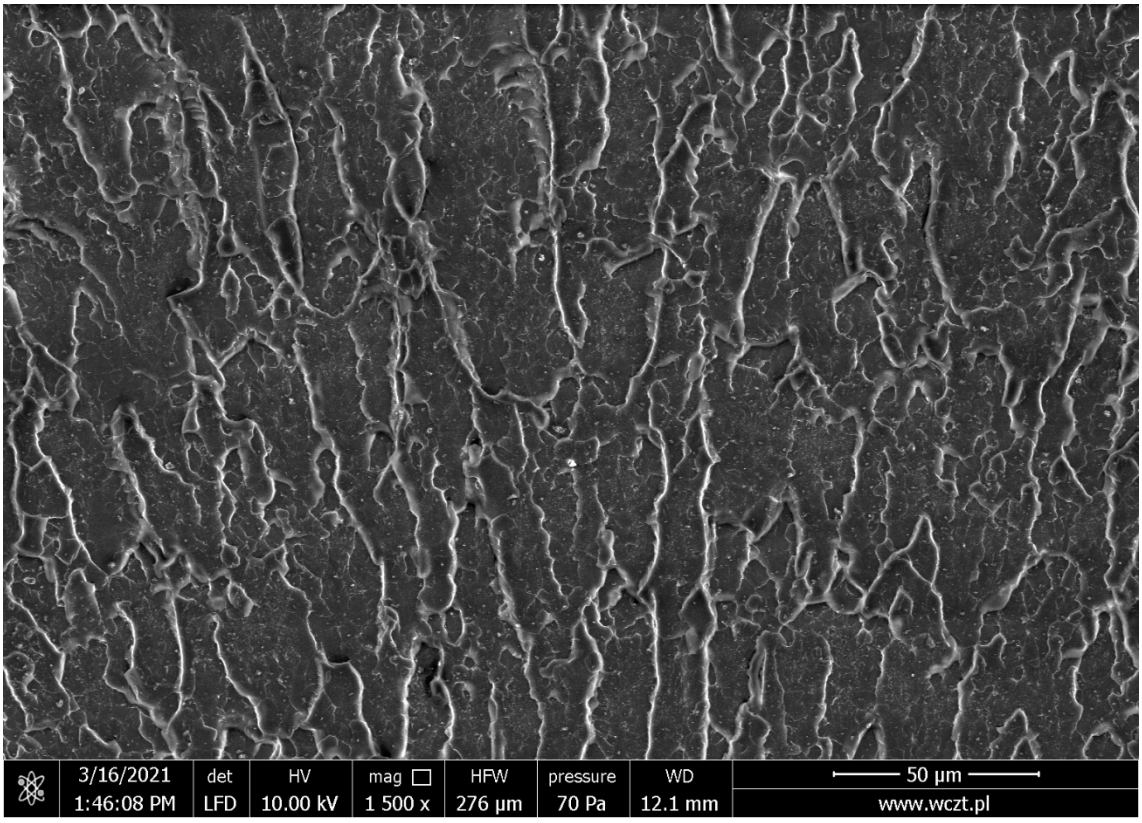

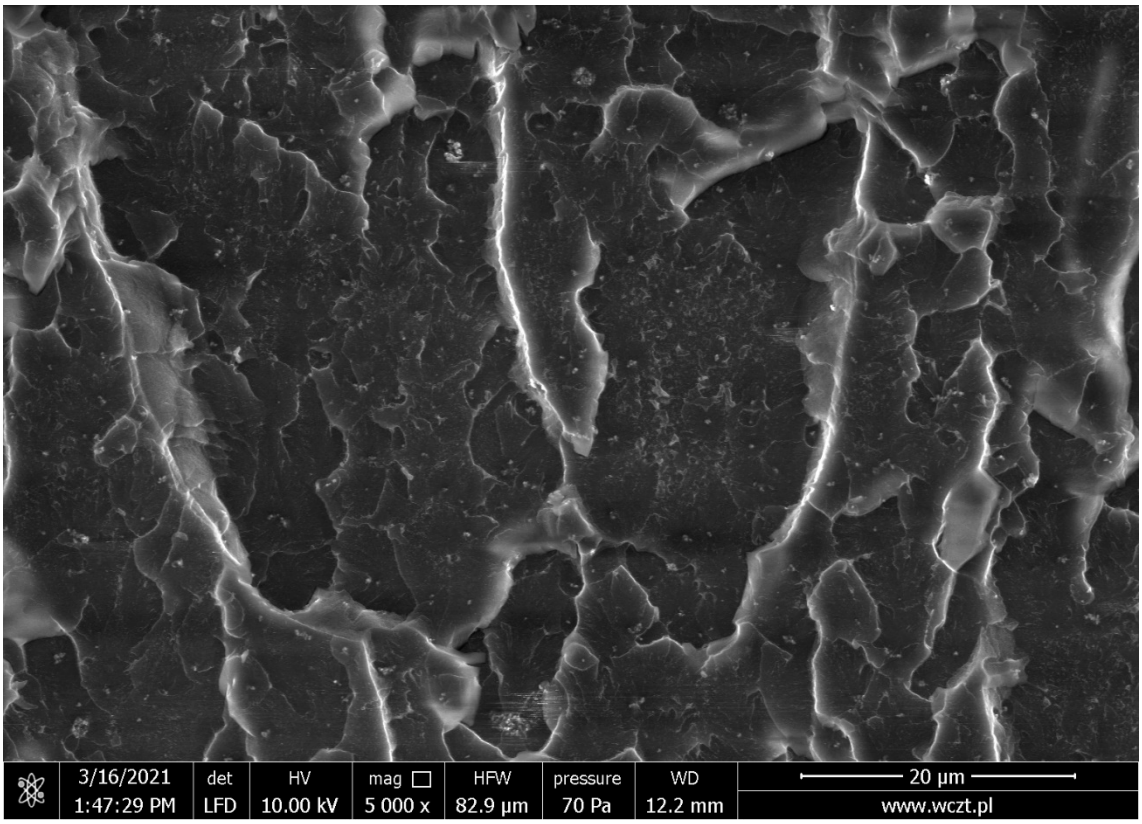

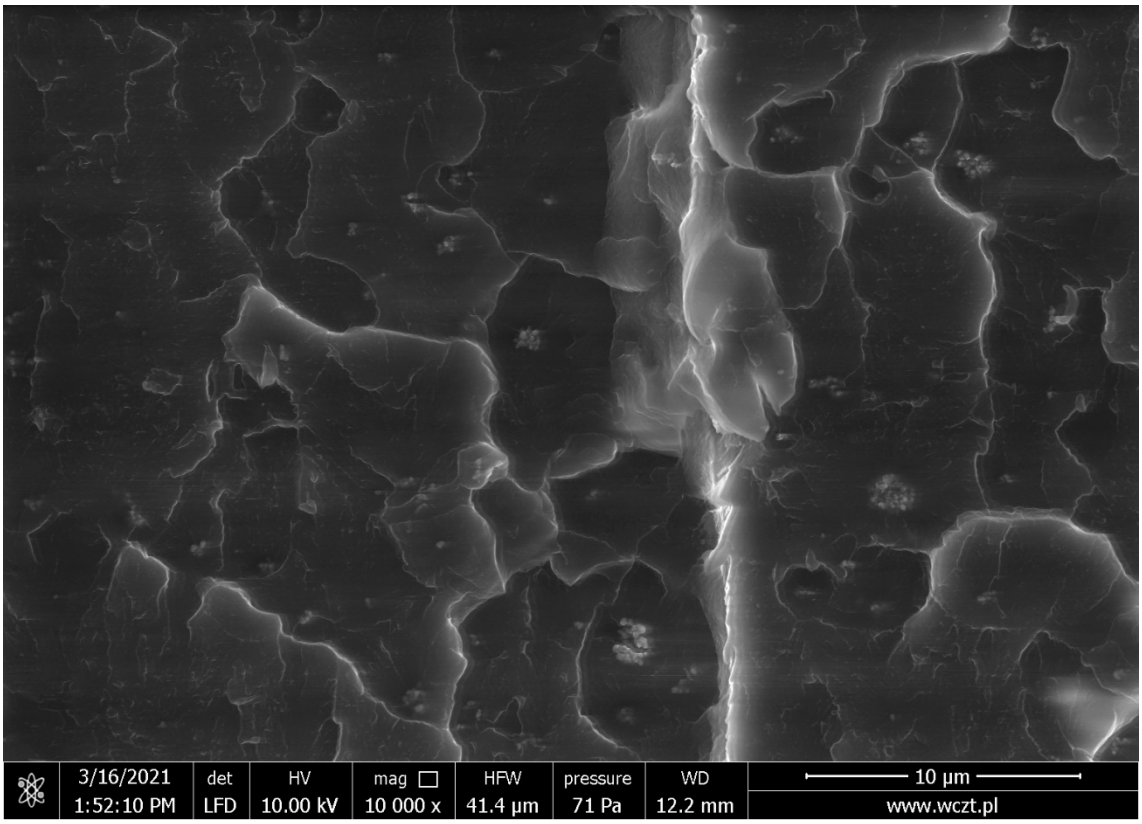
3/16/2021
1:52:10 PM
det
LFD
HV
10.00 kV
mag
10 000 x
HFW
41.4 µm
pressure
71 Pa
WD
12.2 mm
10 µm
www.wczt.pl

1%TiO_2, 1.5% GPTES, mechanical stirrer

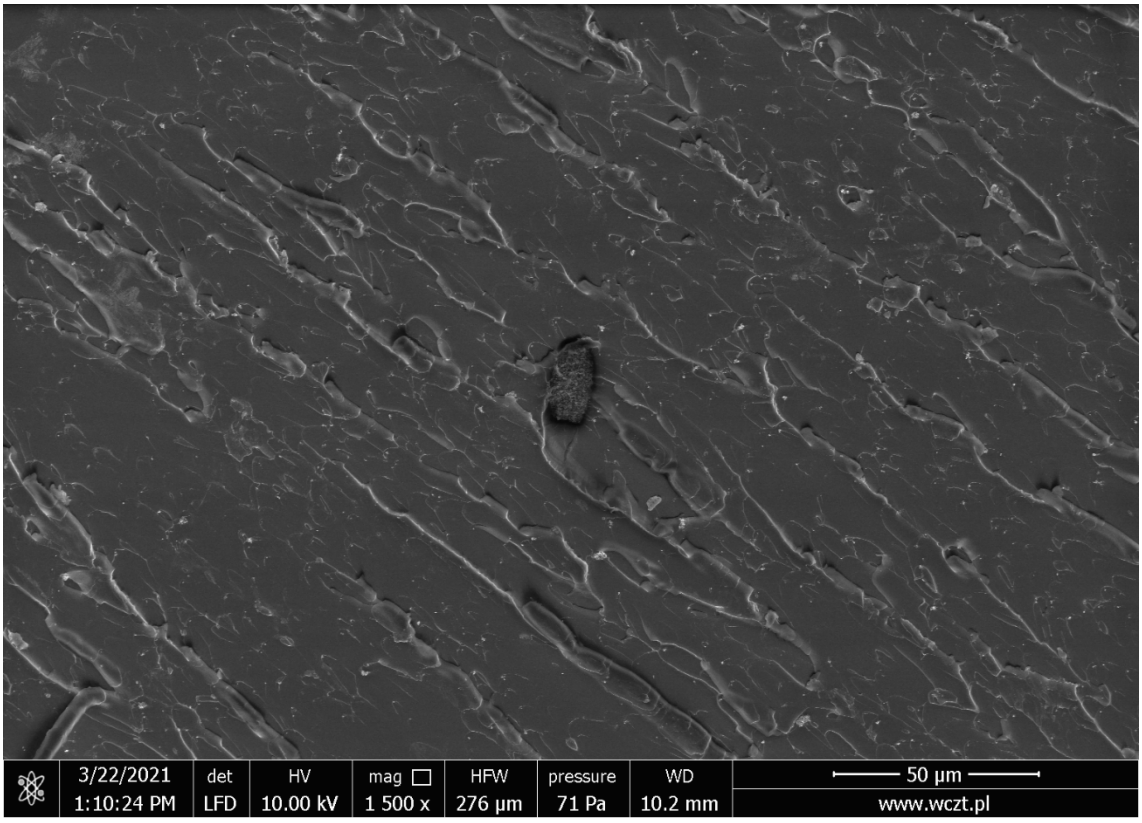

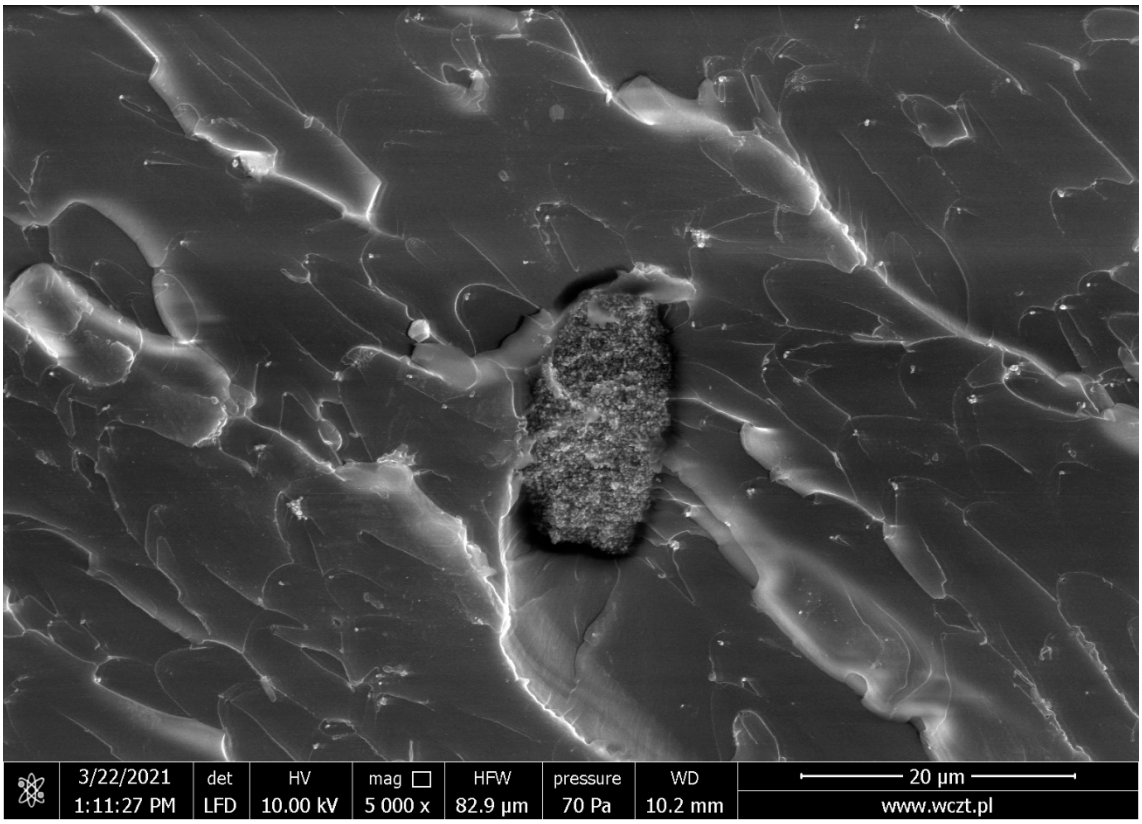

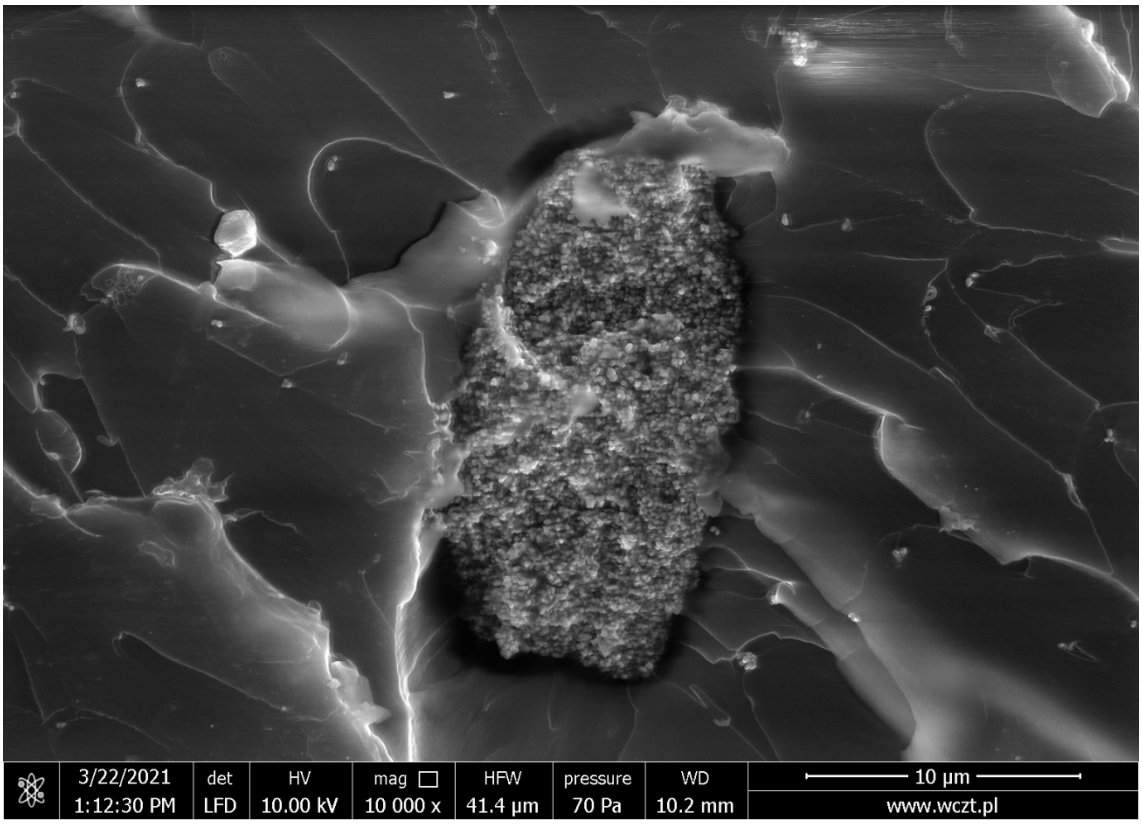
3/22/2021
1:12:30 PM
det
LFD
HV
10.00 kV
mag
10 000 x
HFW
41.4 µm
pressure
70 Pa
WD
10.2 mm
10 µm
www.wczt.pl

1%TiO_2, 1.5% GPTES, mixing pump

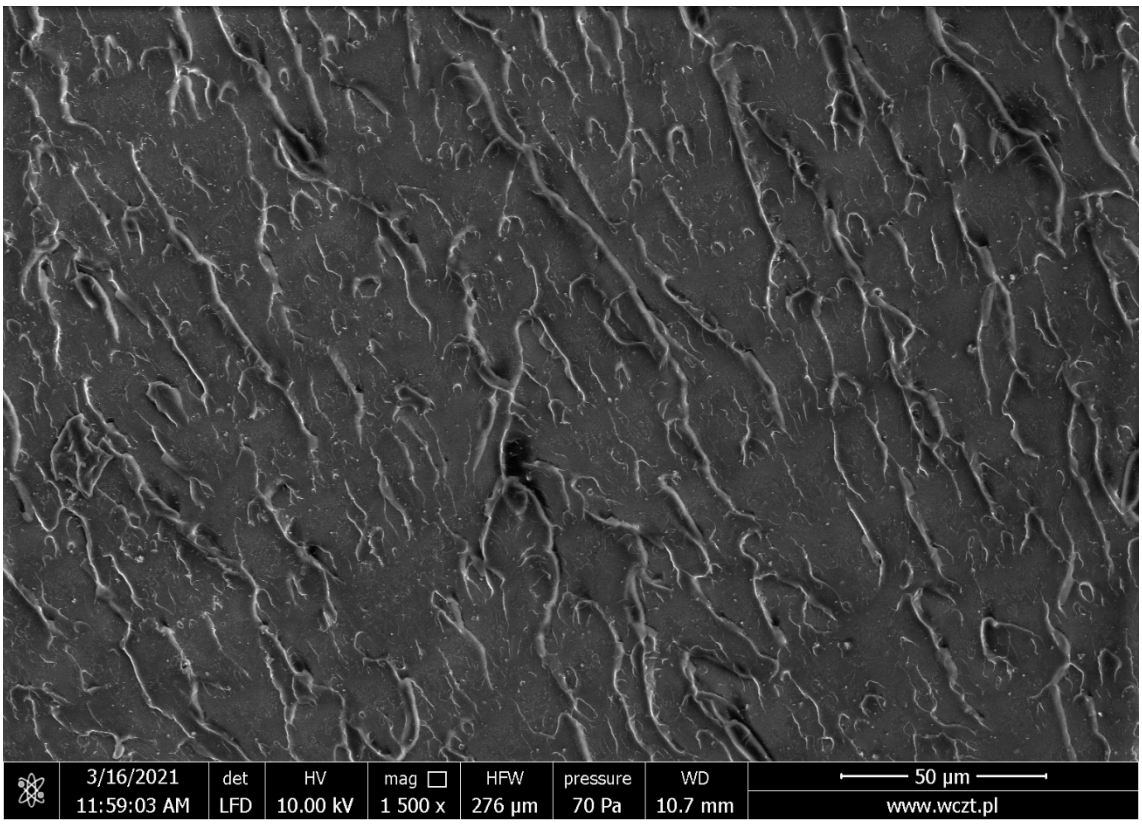

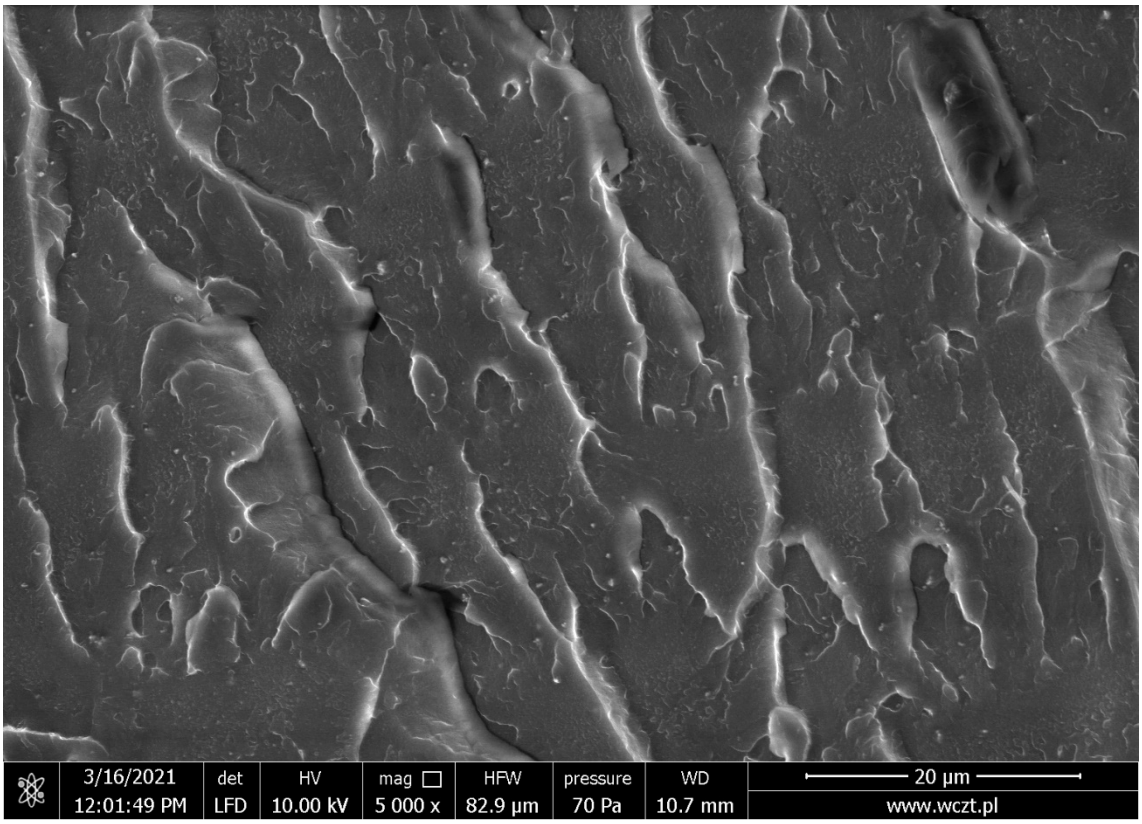

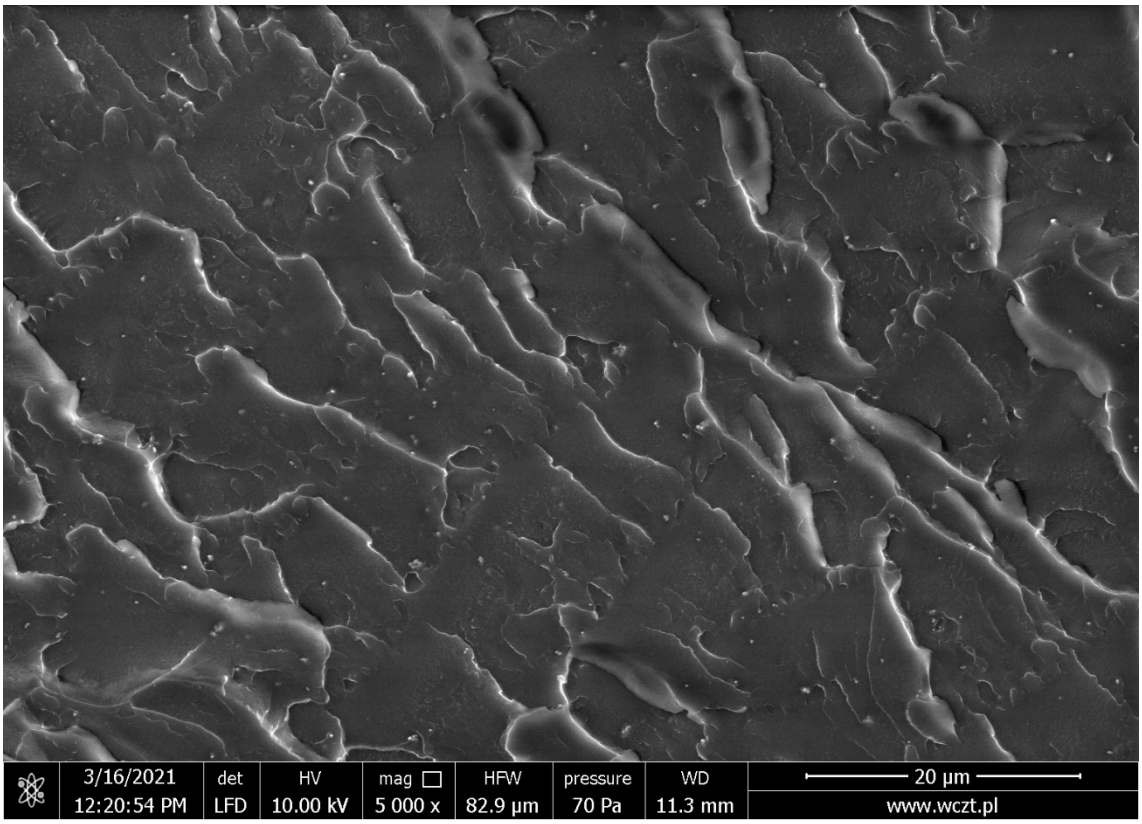
3/16/2021
12:20:54 PM
det
LFD
HV
10.00 kV
mag
5 000 x
HFW
82.9 µm
pressure
70 Pa
WD
11.3 mm
20 µm
www.wczt.pl

2%TiO_2, 1.5% GPTES, mixing pump

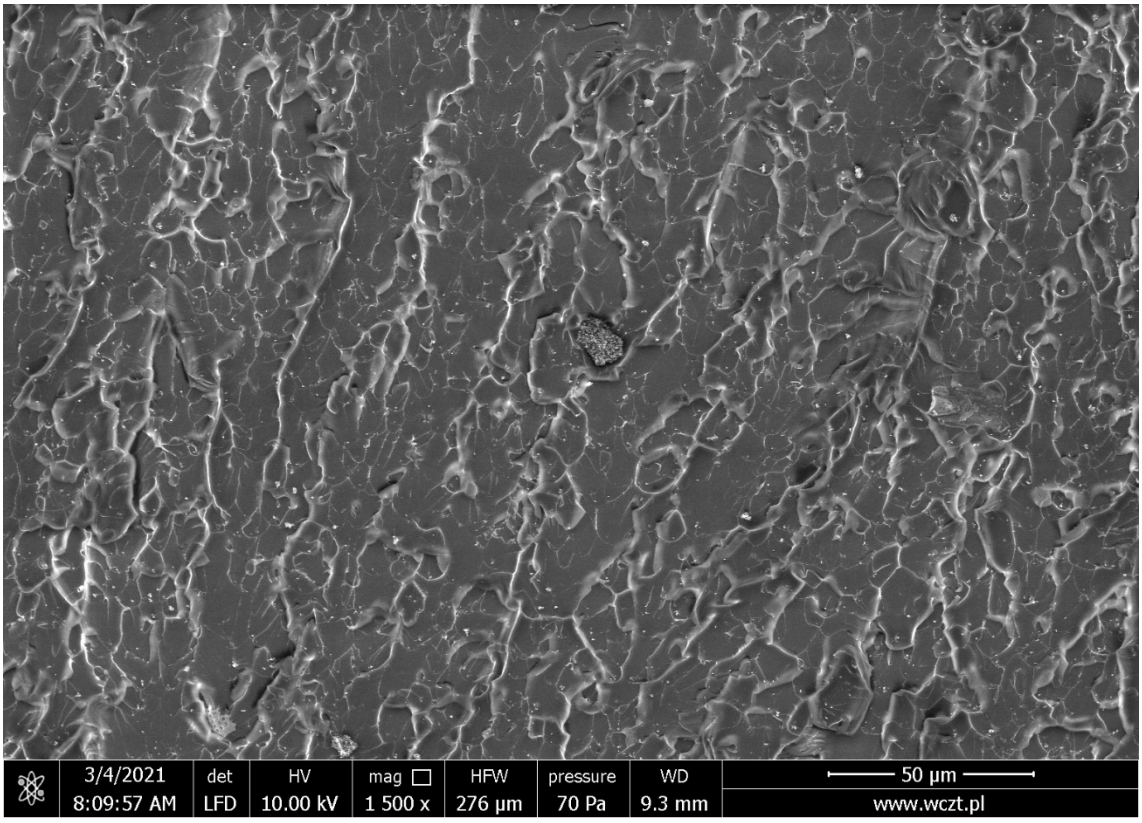

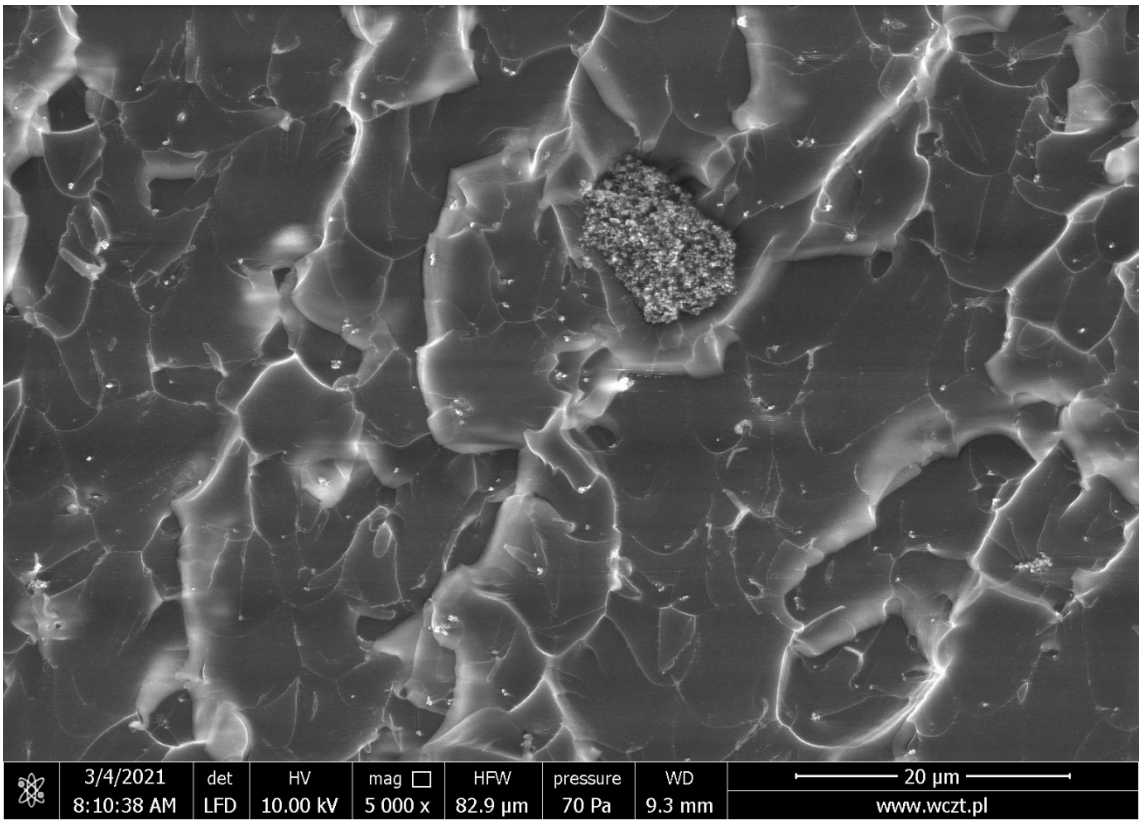

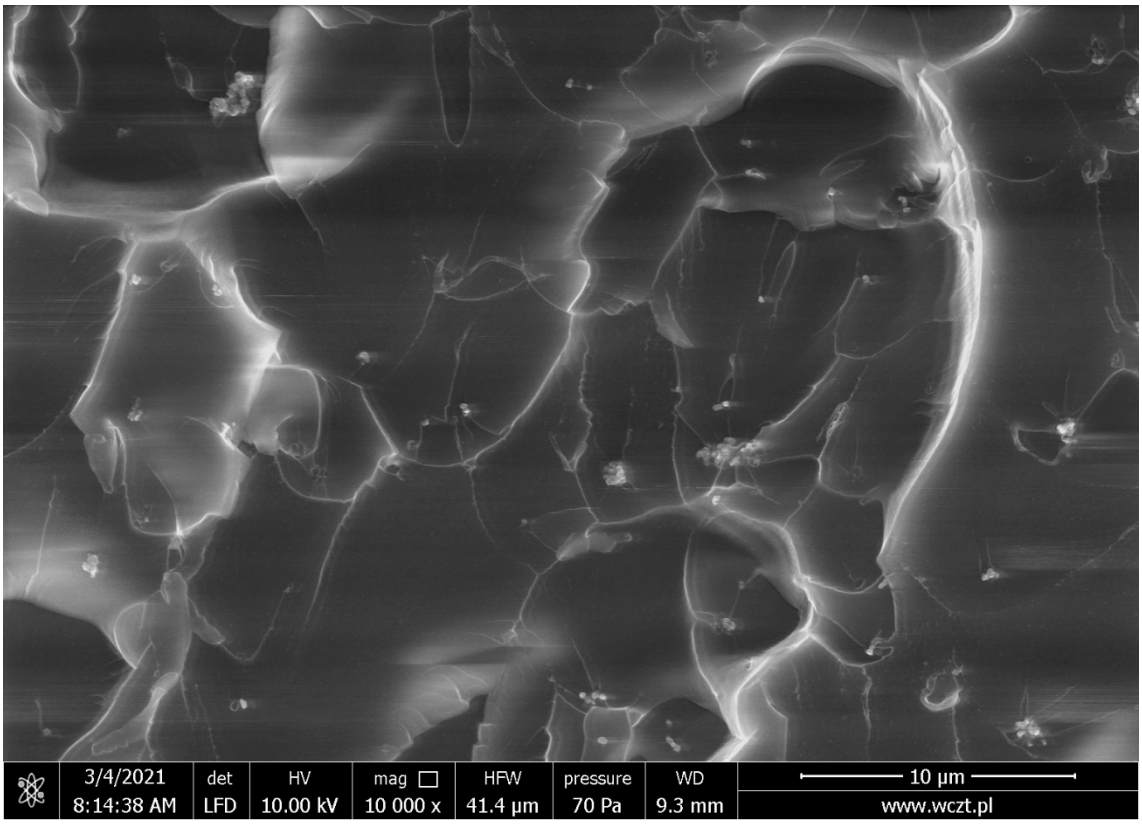
3/4/2021
8:14:38 AM
det
LFD
HV
10.00 kV
mag
10 000 x
HFW
41.4 µm
pressure
70 Pa
WD
9.3 mm
10 µm
www.wczt.pl

1%TiO_2, 0.5% iBu_7SSQ-OEt, mixing pump

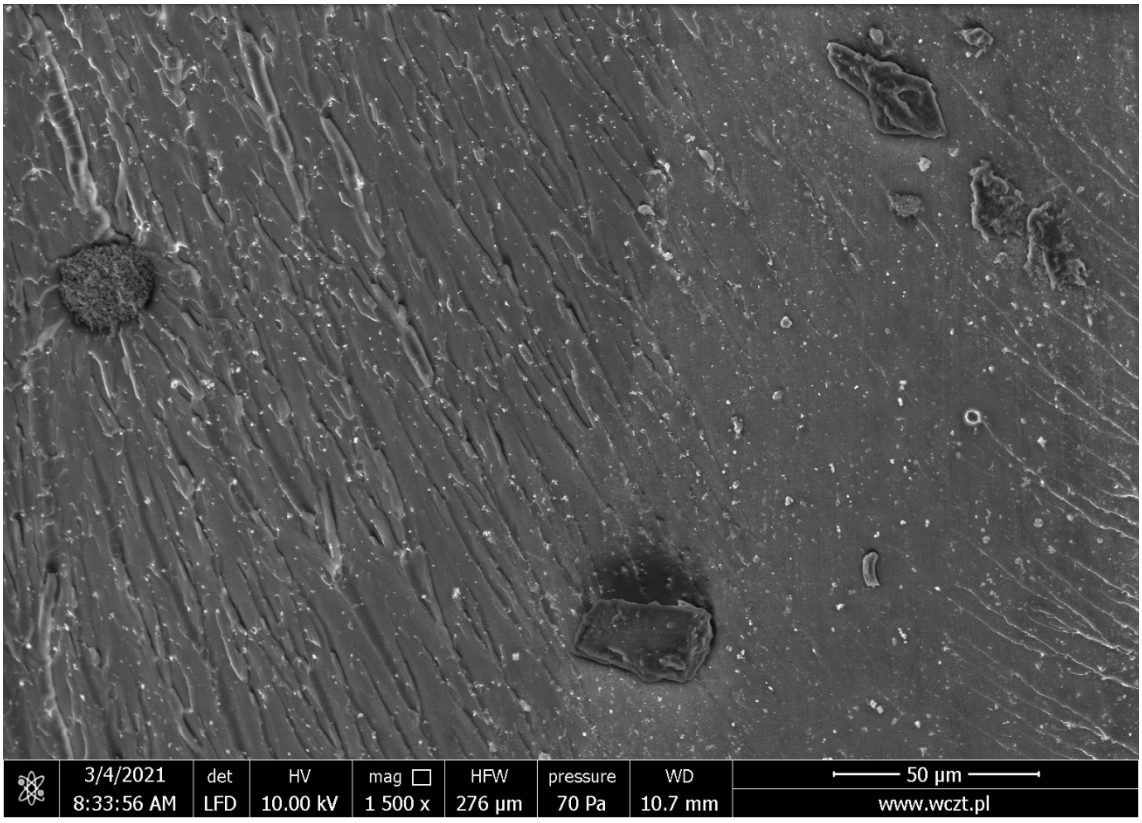

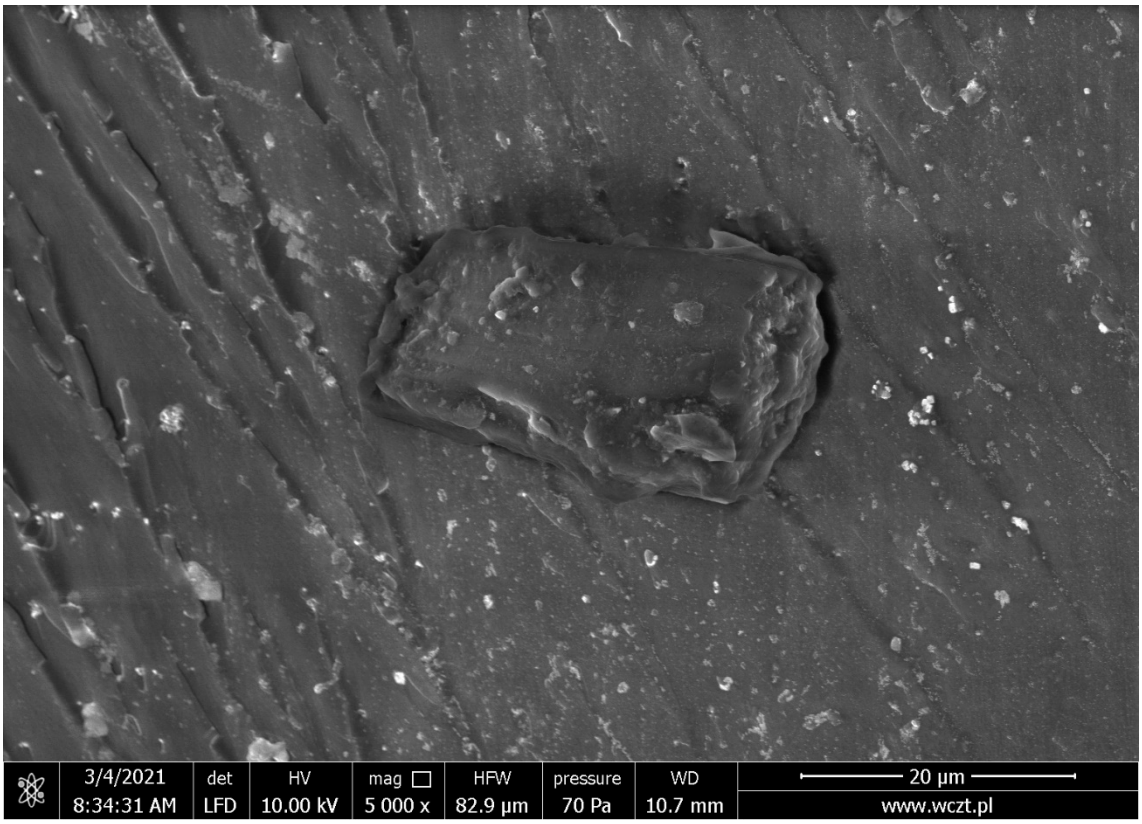

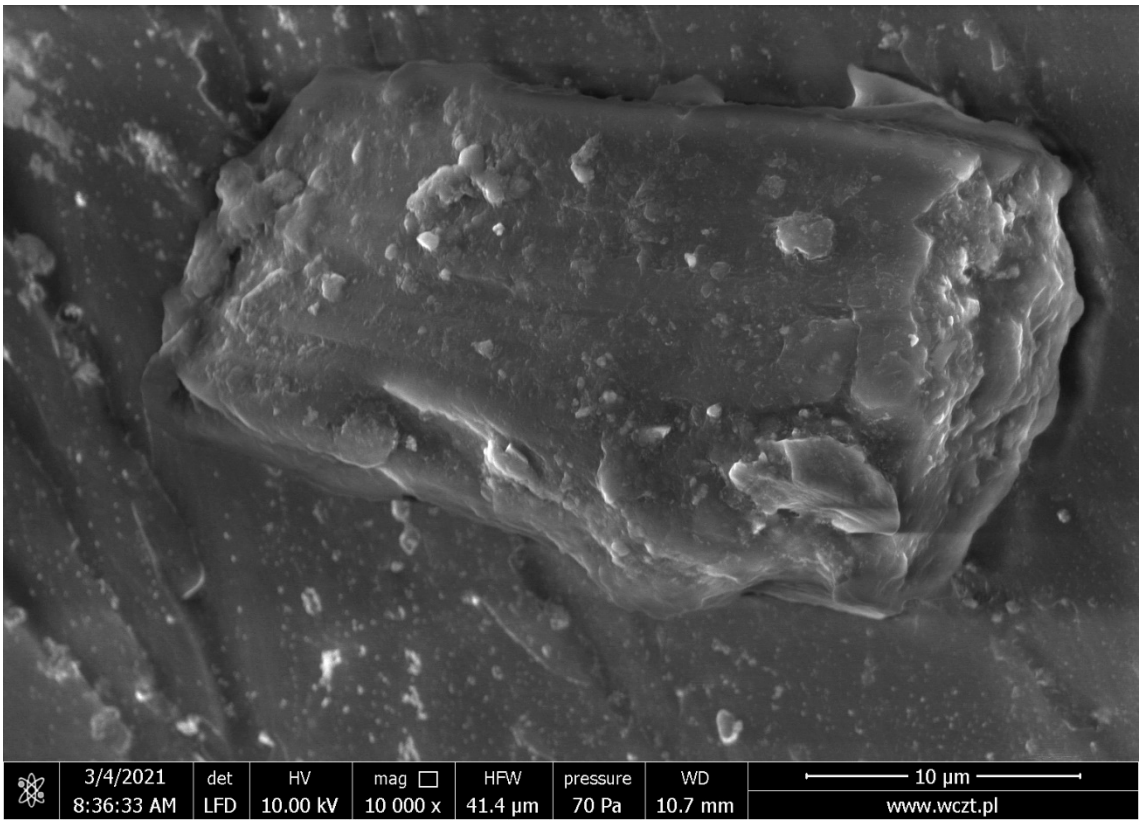
3/4/2021
8:36:33 AM
det
LFD
HV
10.00 kV
mag
10 000 x
HFW
41.4 µm
pressure
70 Pa
WD
10.7 mm
10 µm
www.wczt.pl

2%TiO_2, 0.5% iBu_7SSQ-OEt, mixing pump

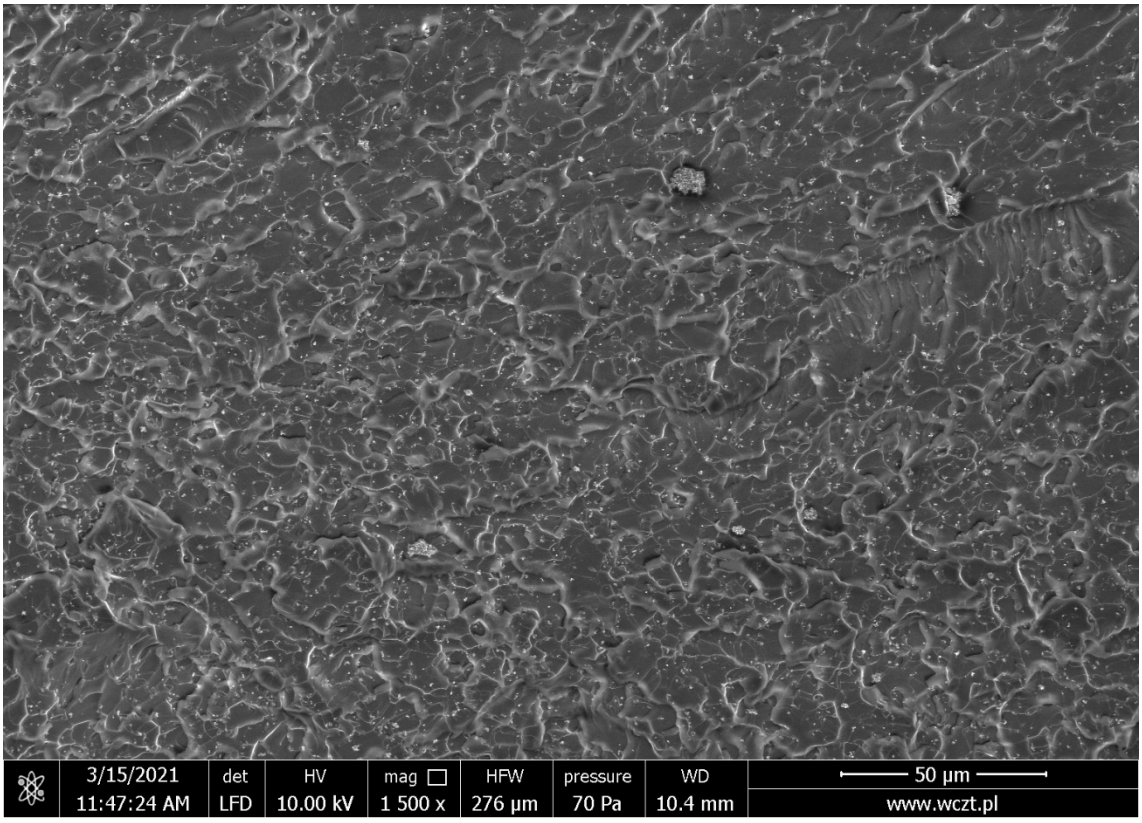

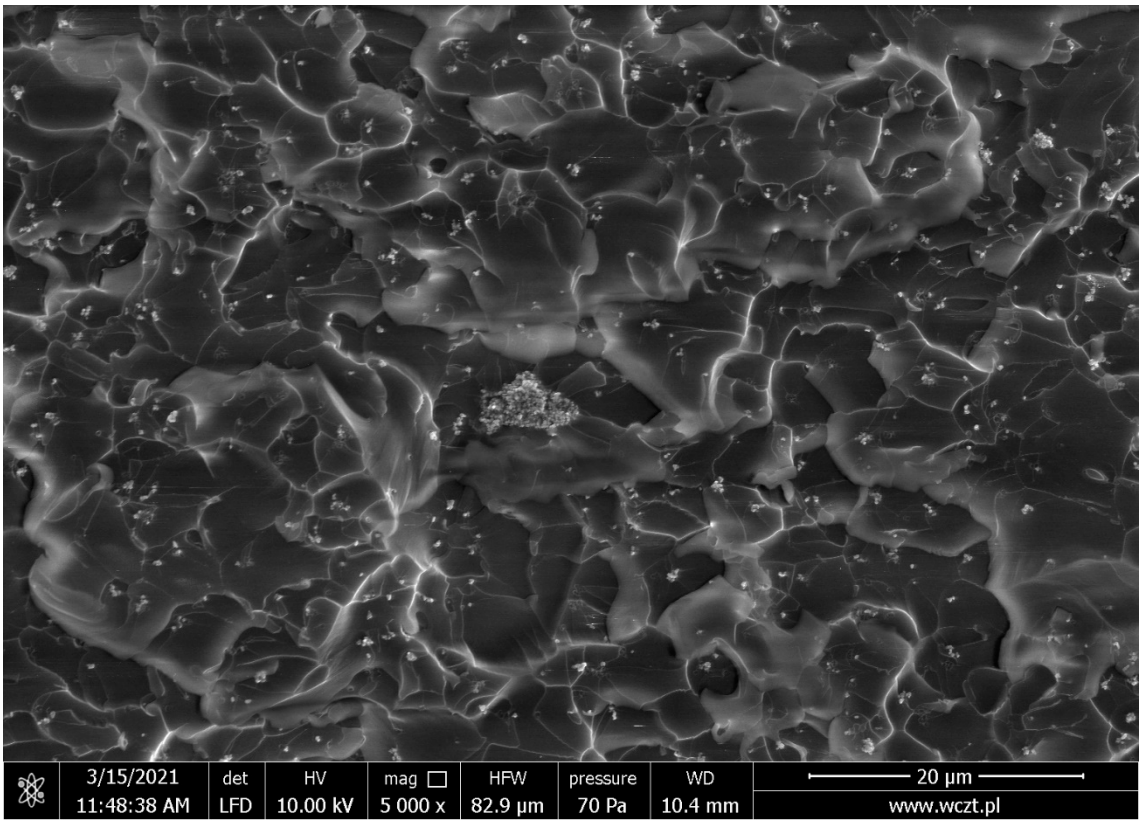

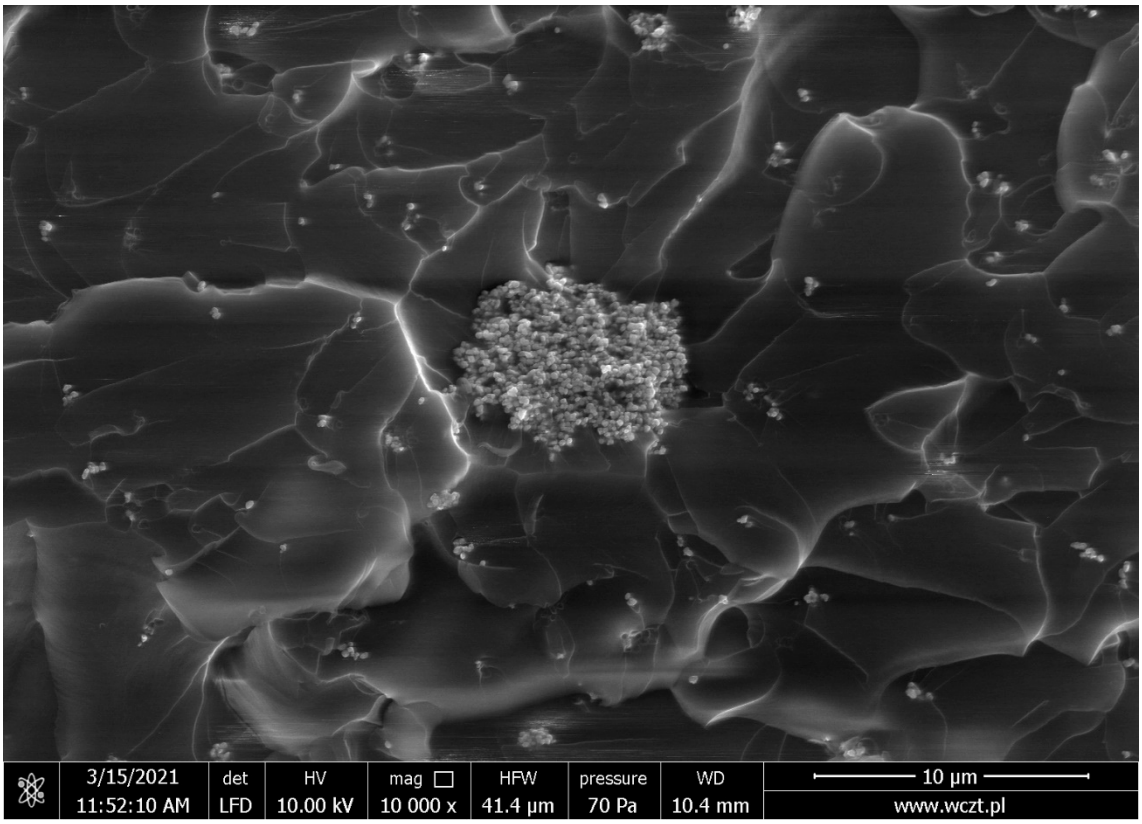
3/15/2021
11:52:10 AM
det
LFD
HV
10.00 kV
mag
10 000 x
HFW
41.4 µm
pressure
70 Pa
WD
10.4 mm
10 µm
www.wczt.pl

1%TiO_2, 1.5% iBu_7SSQ-OEt, mechanical stirrer

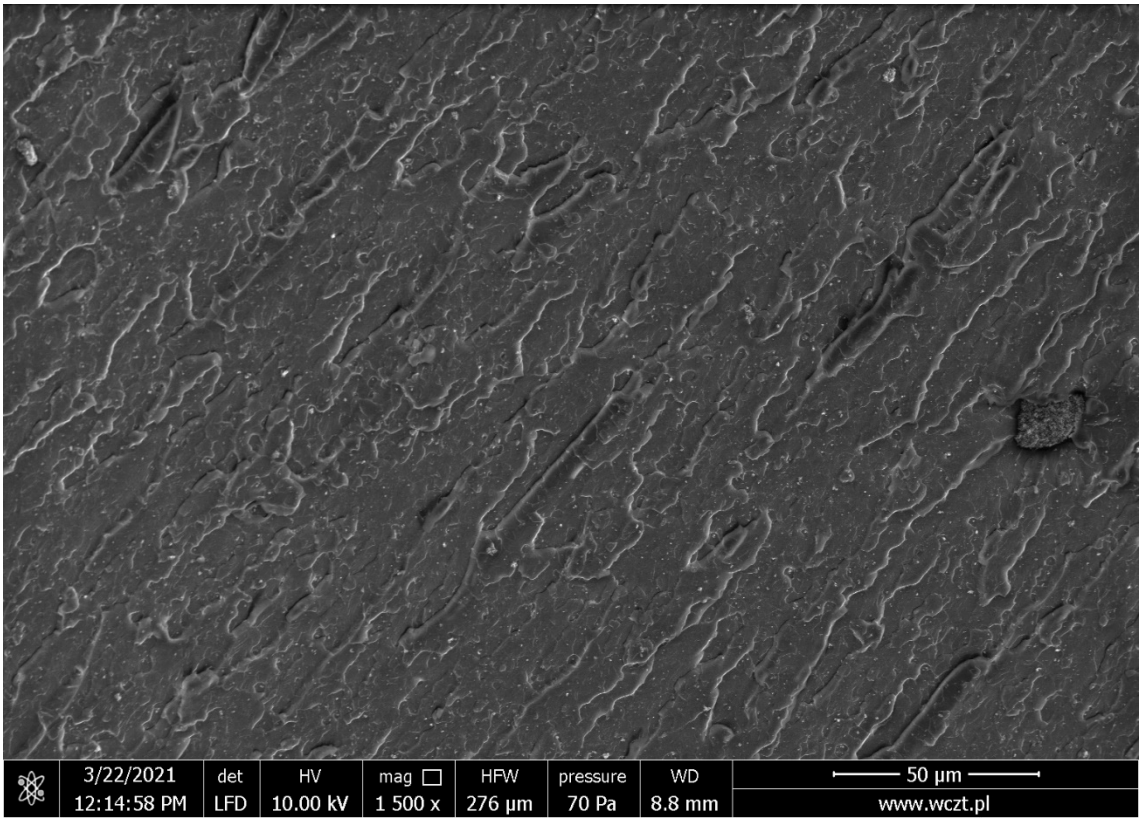

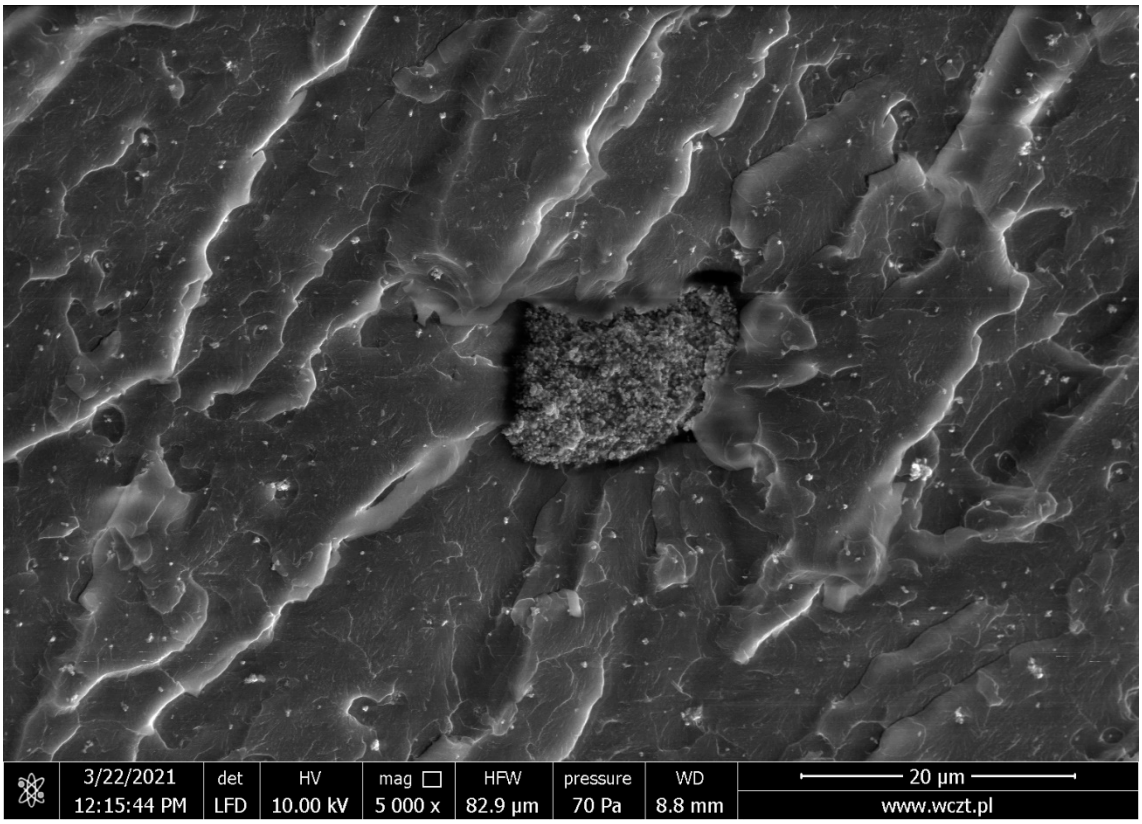

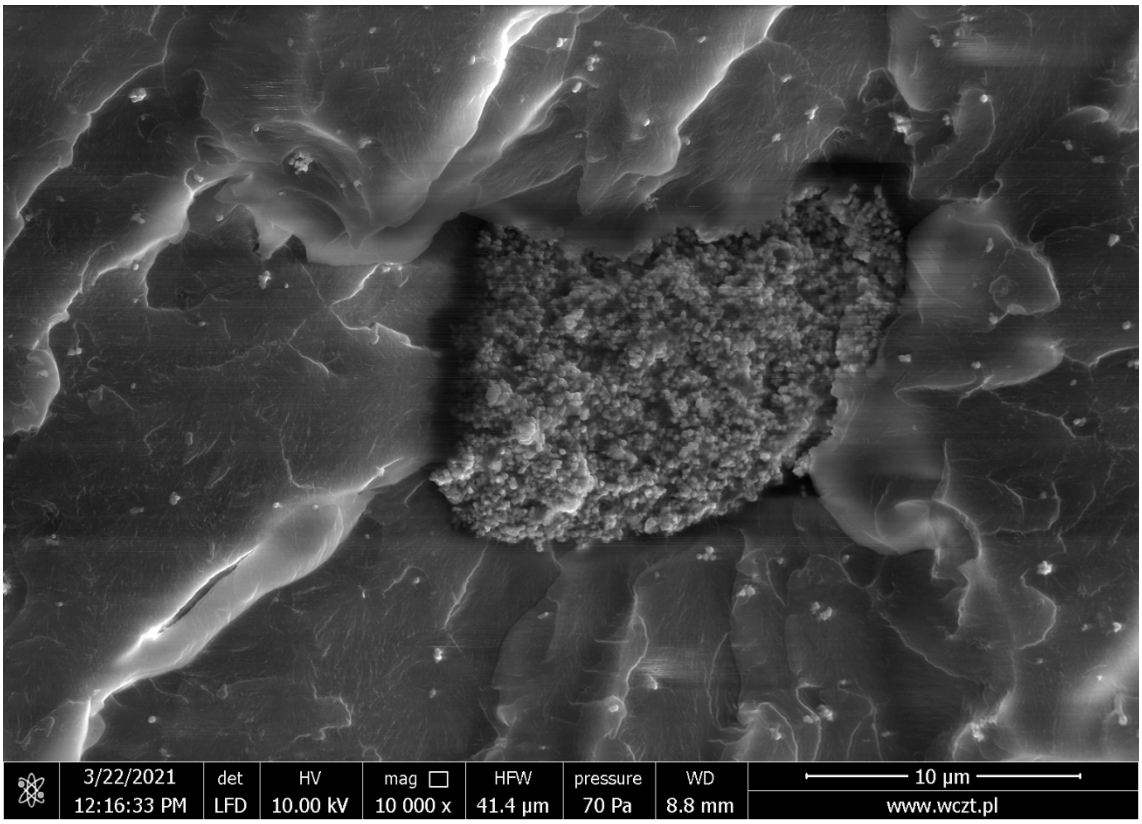
3/22/2021
12:16:33 PM
det
LFD
HV
10.00 kV
mag
10 000 x
HFW
41.4 µm
pressure
70 Pa
WD
8.8 mm
10 µm
www.wczt.pl

1%TiO_2, 1.5% iBu_7SSQ-OEt, mixing pump

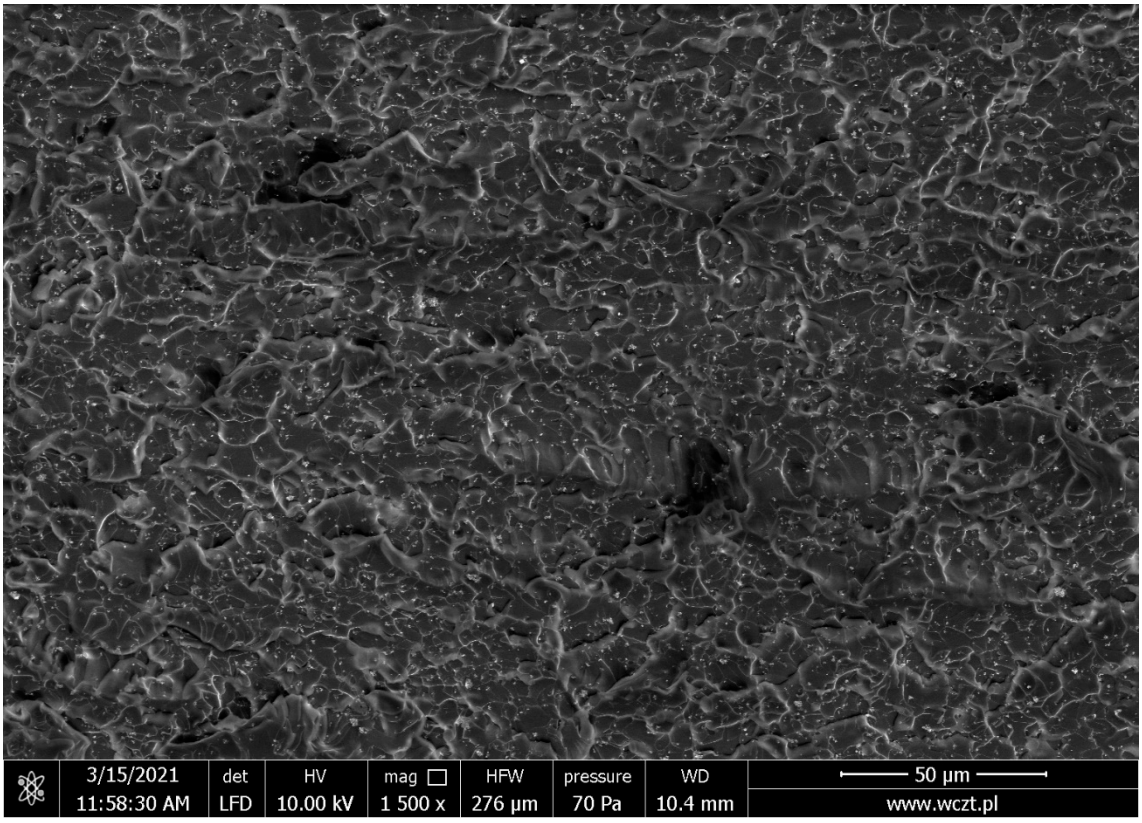

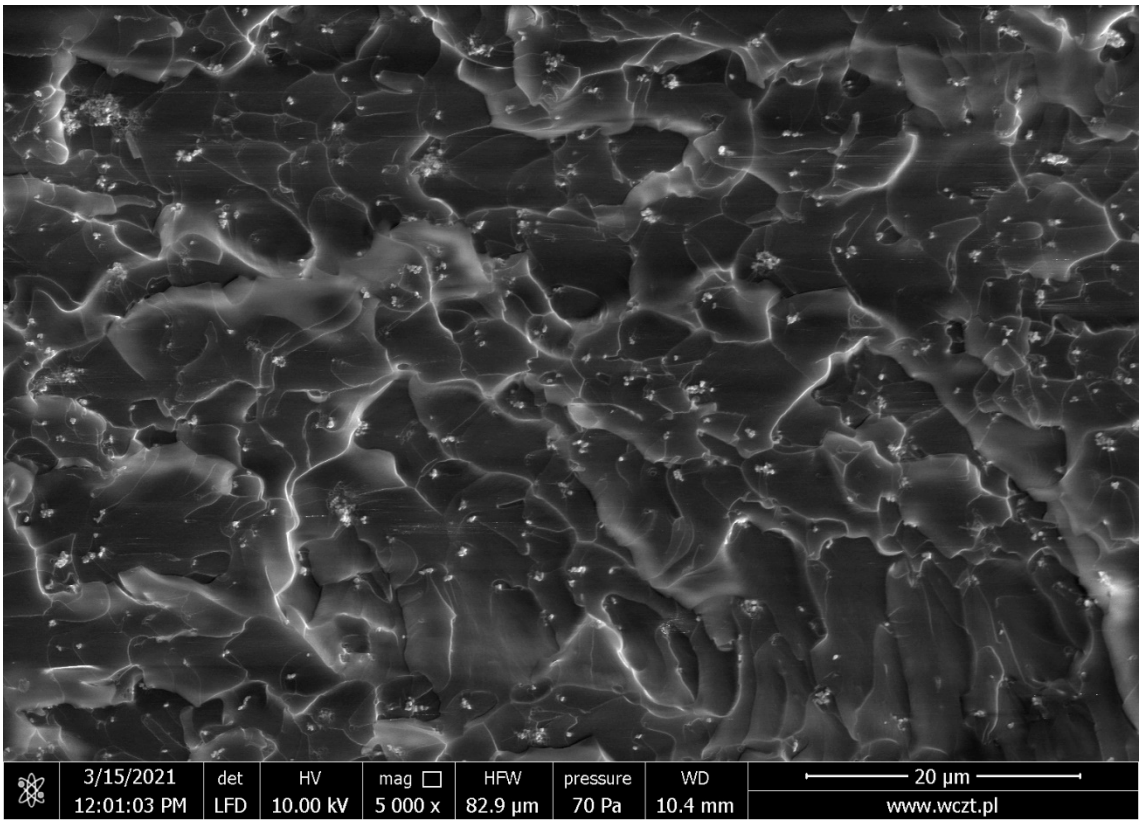

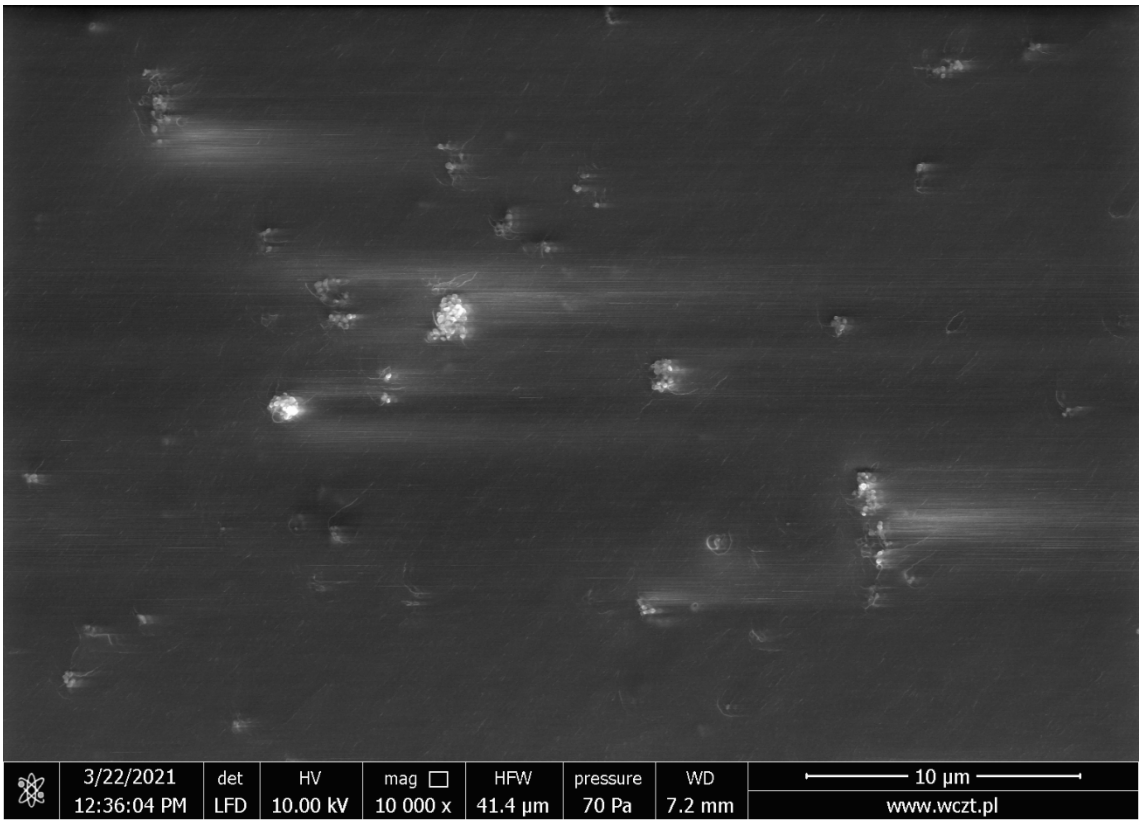
3/22/2021
12:36:04 PM
det
LFD
HV
10.00 kV
mag
10 000 x
HFW
41.4 µm
pressure
70 Pa
WD
7.2 mm
10 µm
www.wczt.pl

2%TiO_2, 1.5% iBu_7SSQ-OEt, mixing pump

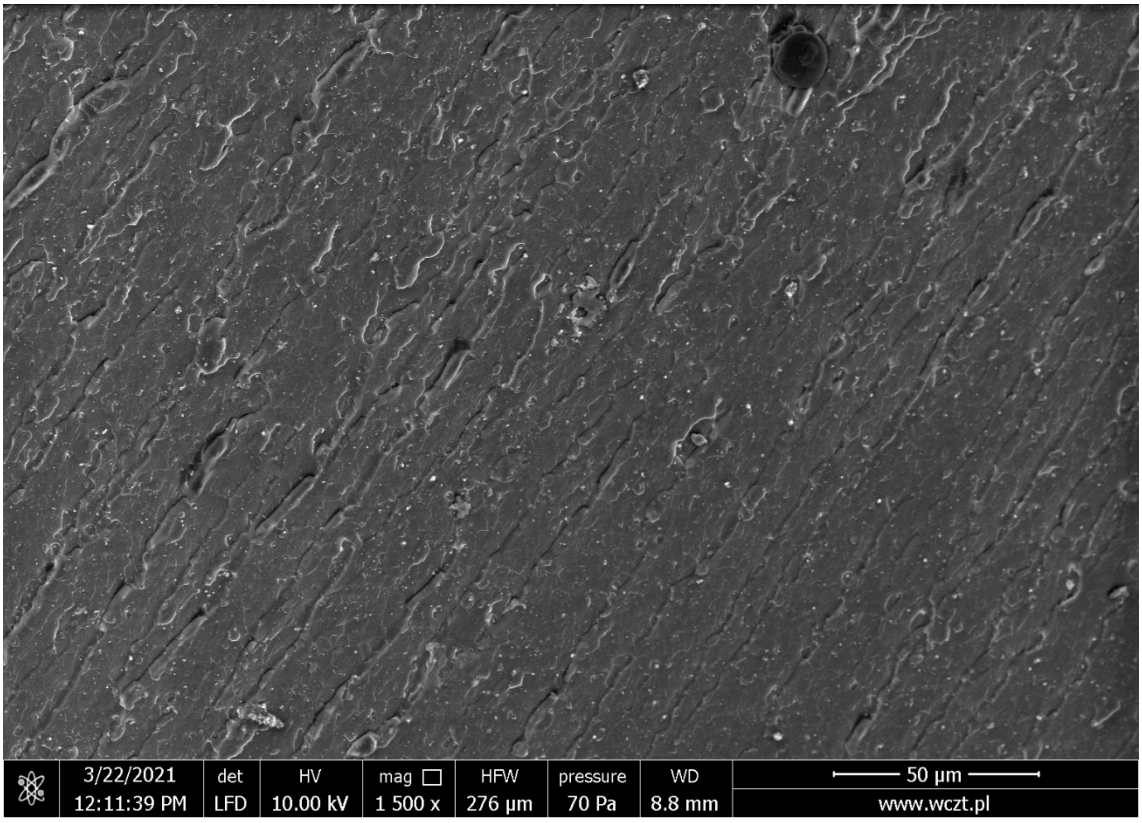

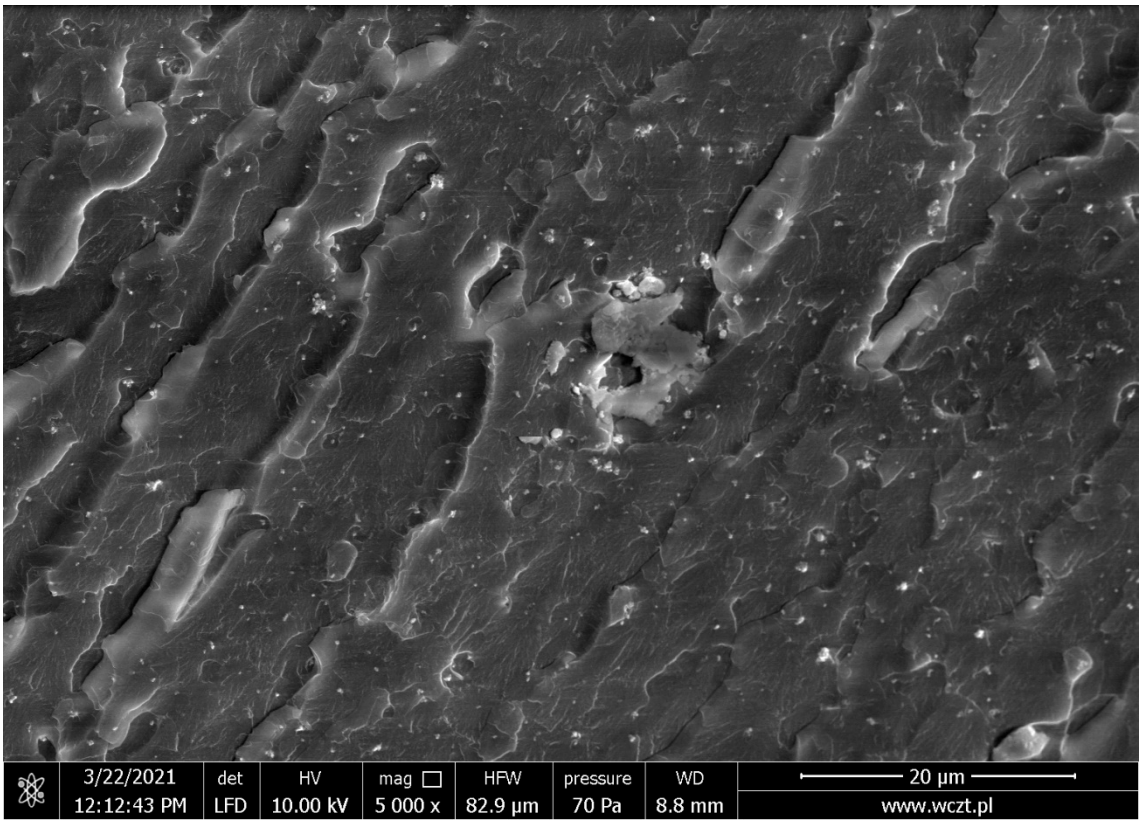

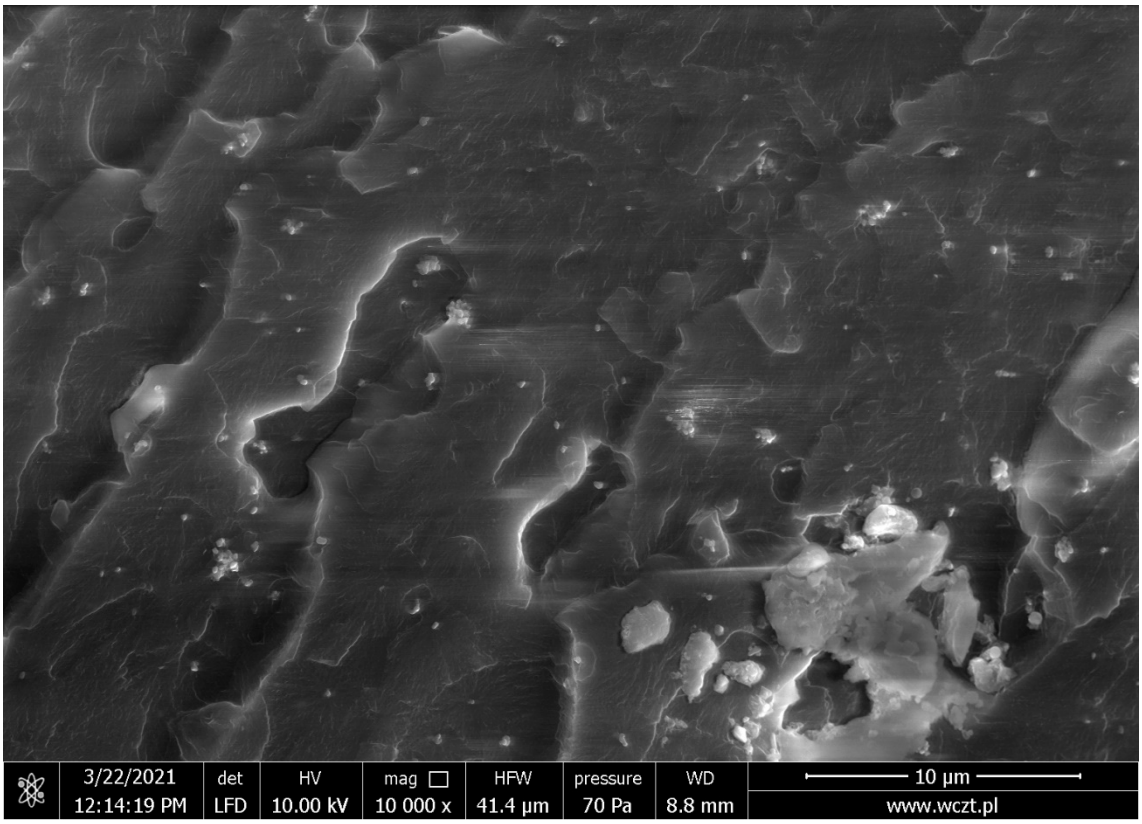
3/22/2021
12:14:19 PM
det
LFD
HV
10.00 kV
mag
10 000 x
HFW
41.4 µm
pressure
70 Pa
WD
8.8 mm
10 µm
www.wczt.pl

1%TiO_2, 0.5% SS-6GP-2TMOS, mixing pump

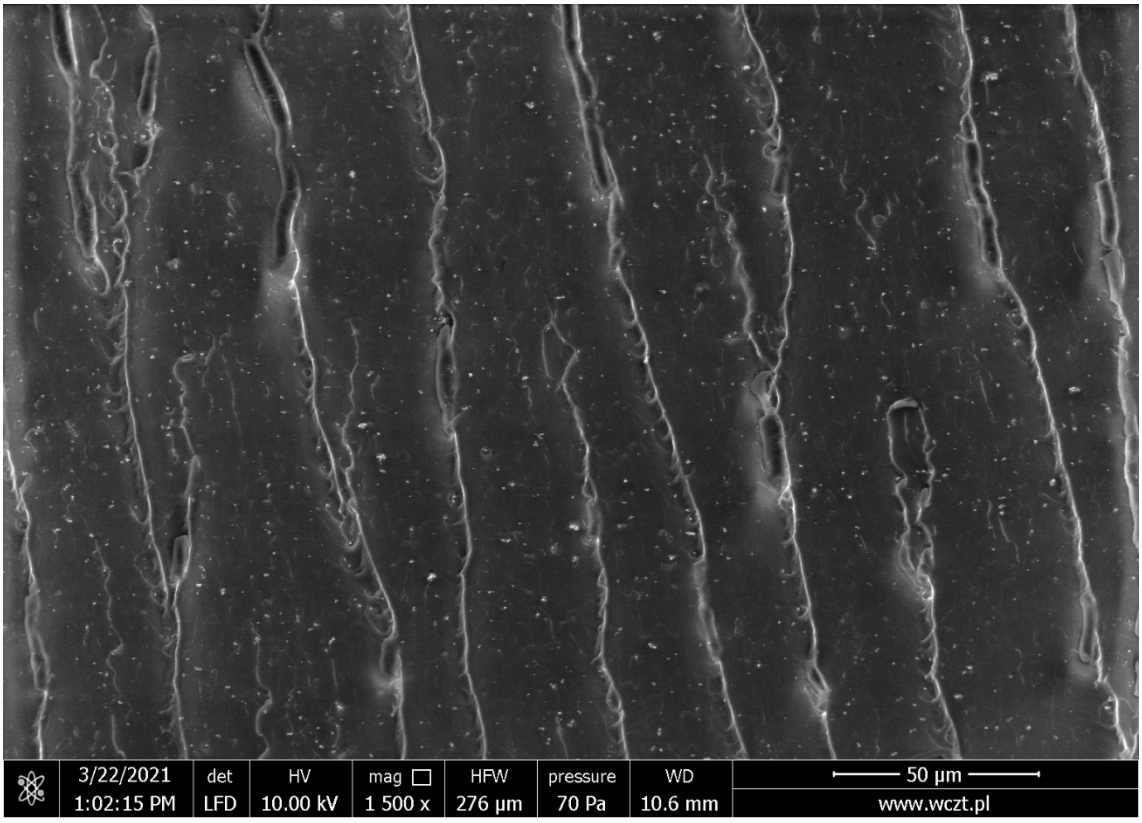

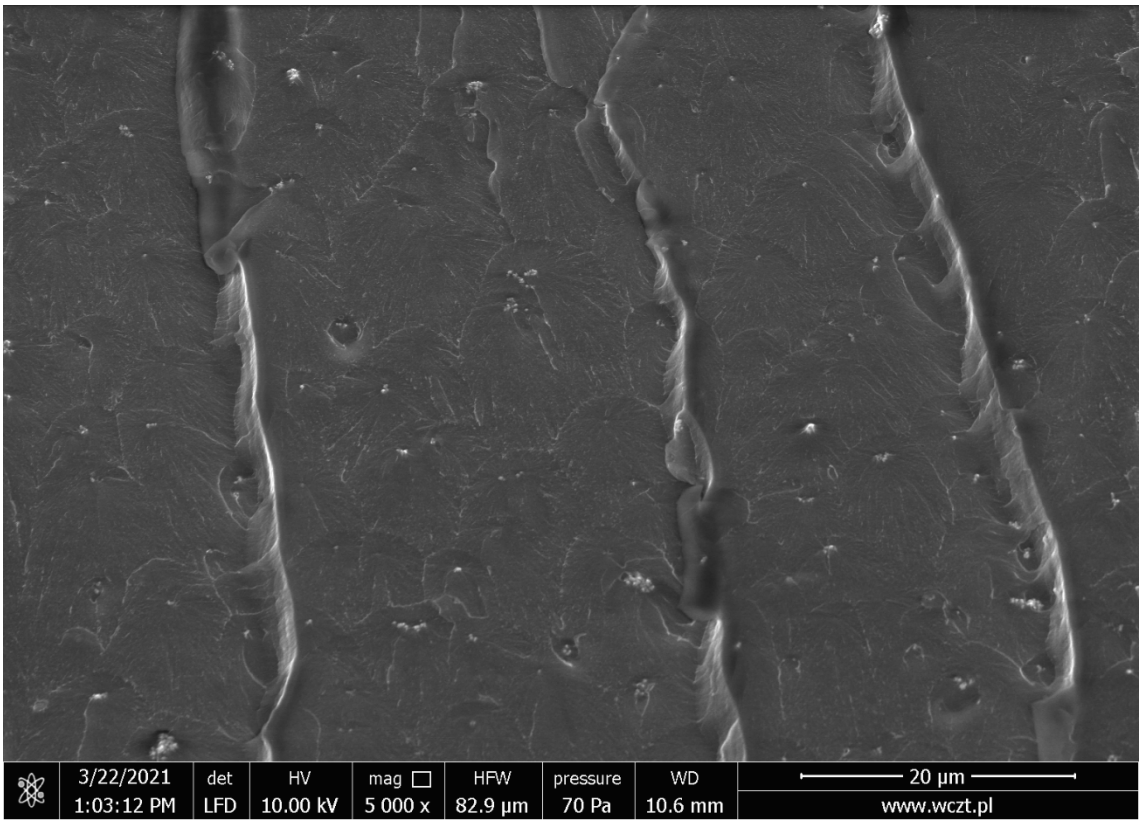

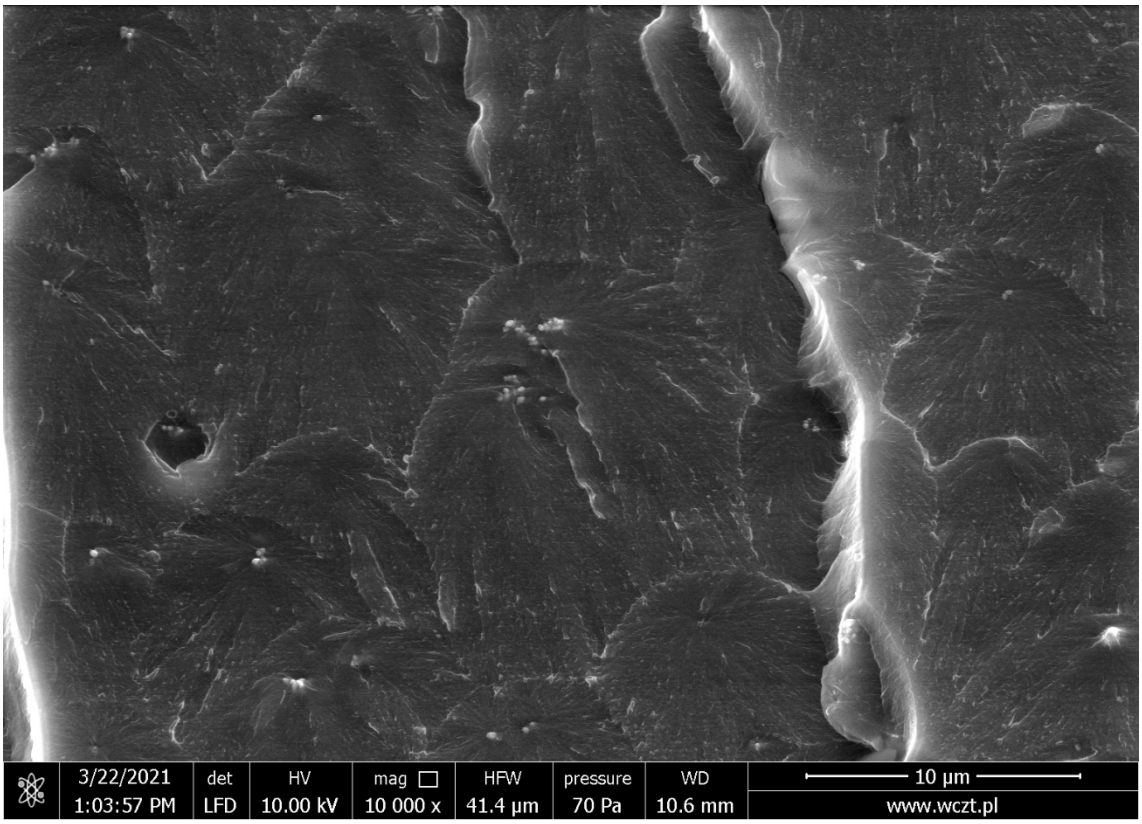
3/22/2021
1:03:57 PM
det
LFD
HV
10.00 kV
mag
10 000 x
HFW
41.4 µm
pressure
70 Pa
WD
10.6 mm
10 µm
www.wczt.pl

2%TiO_2, 0.5% SS-6GP-2TMOS, mixing pump

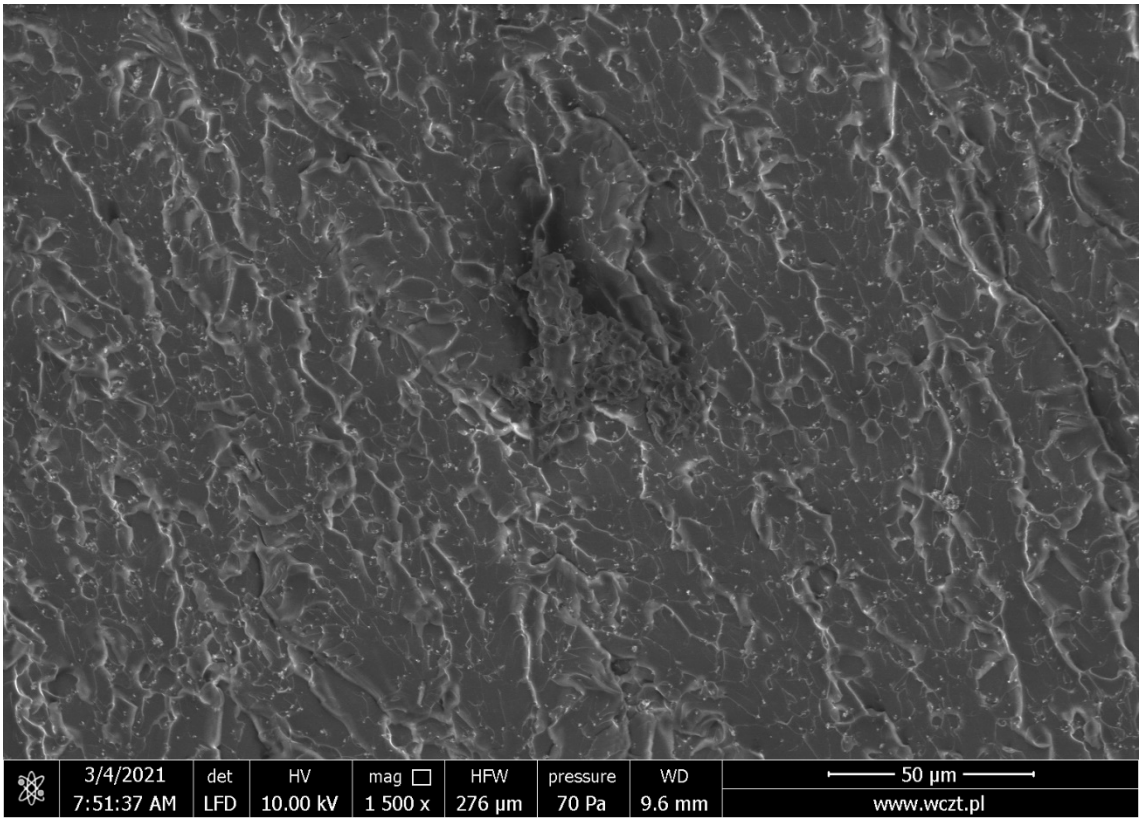

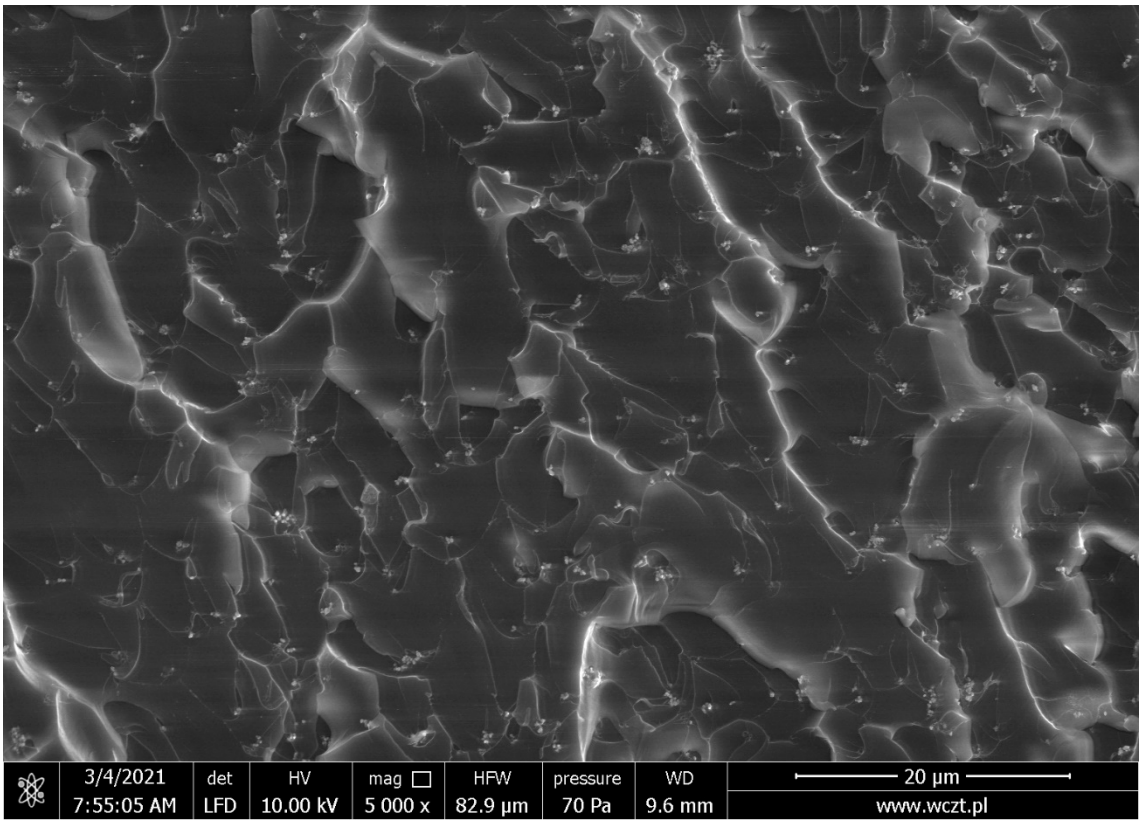

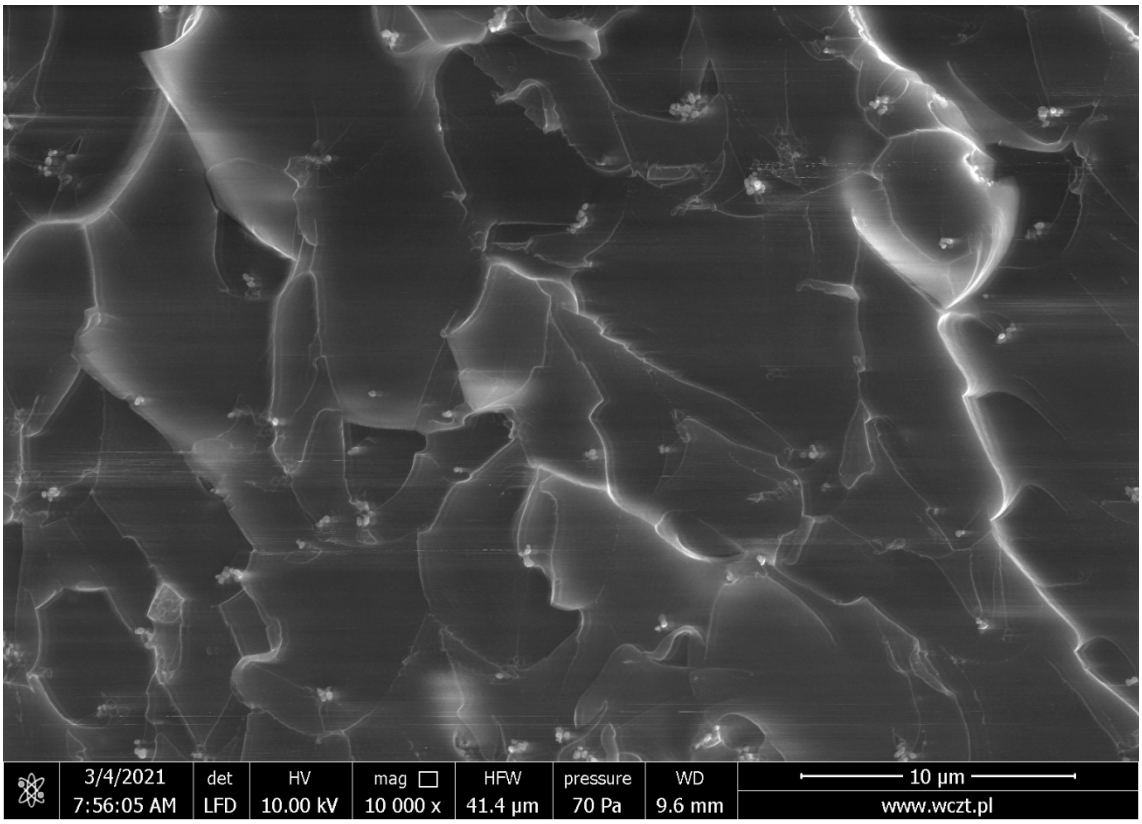
3/4/2021
7:56:05 AM
det
LFD
HV
10.00 kV
mag
10 000 x
HFW
41.4 µm
pressure
70 Pa
WD
9.6 mm
10 µm
www.wczt.pl

1%TiO_2, 1.5% SS-6GP-2TMOS, mechanical stirrer

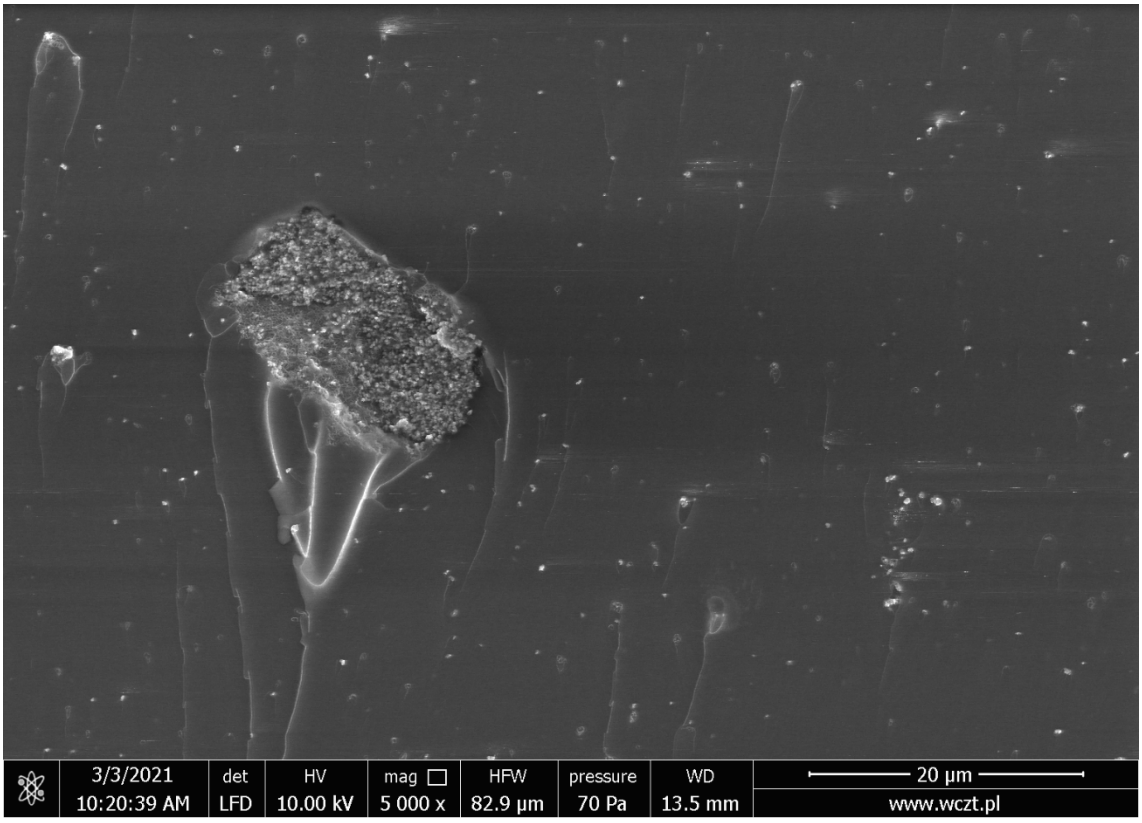

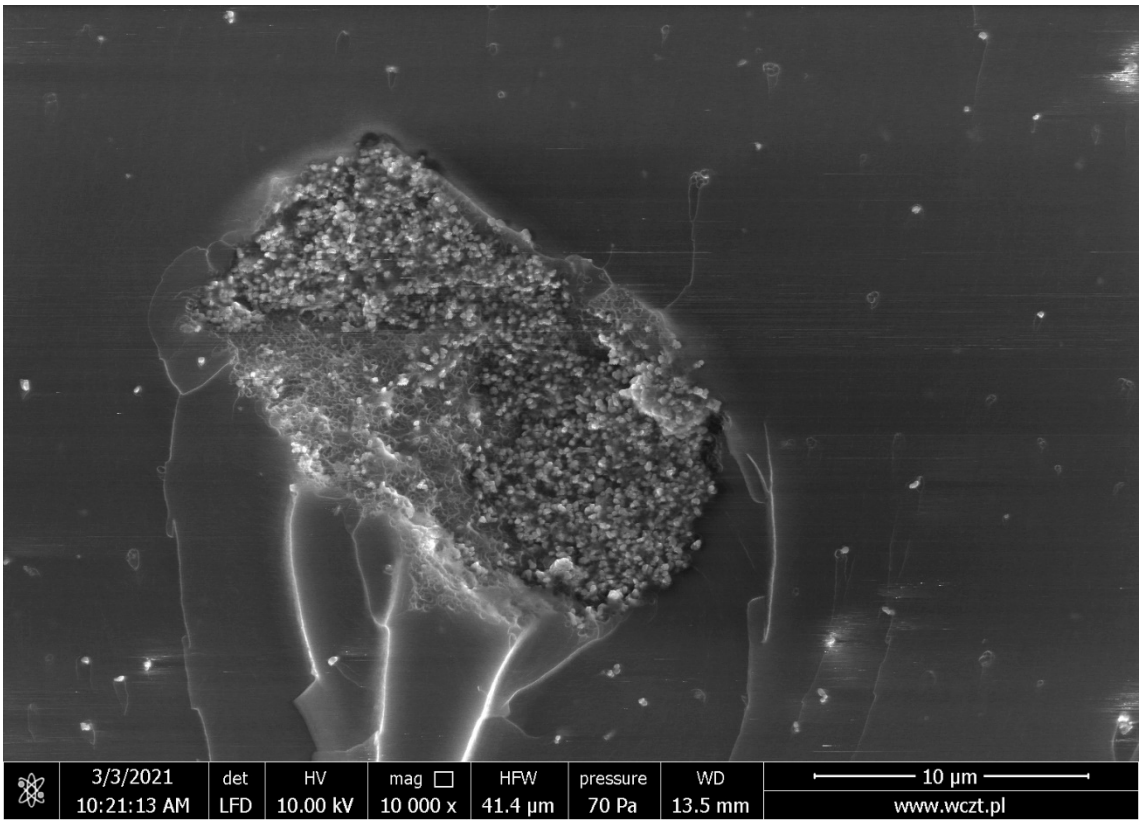

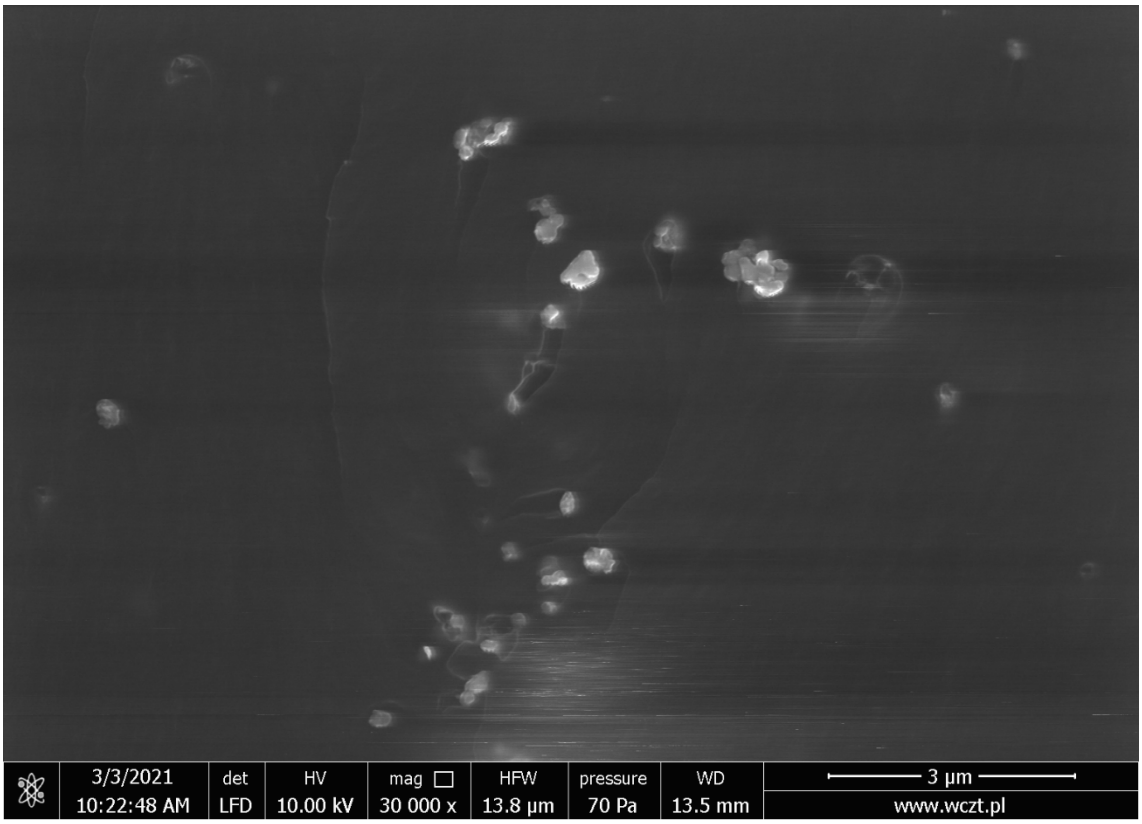
3/3/2021
10:22:48 AM
det
LFD
HV
10.00 kV
mag
30 000 x
HFW
13.8 µm
pressure
70 Pa
WD
13.5 mm
3 µm
www.wczt.pl

1%TiO_2, 1.5% SS-6GP-2TMOS, mixing pump

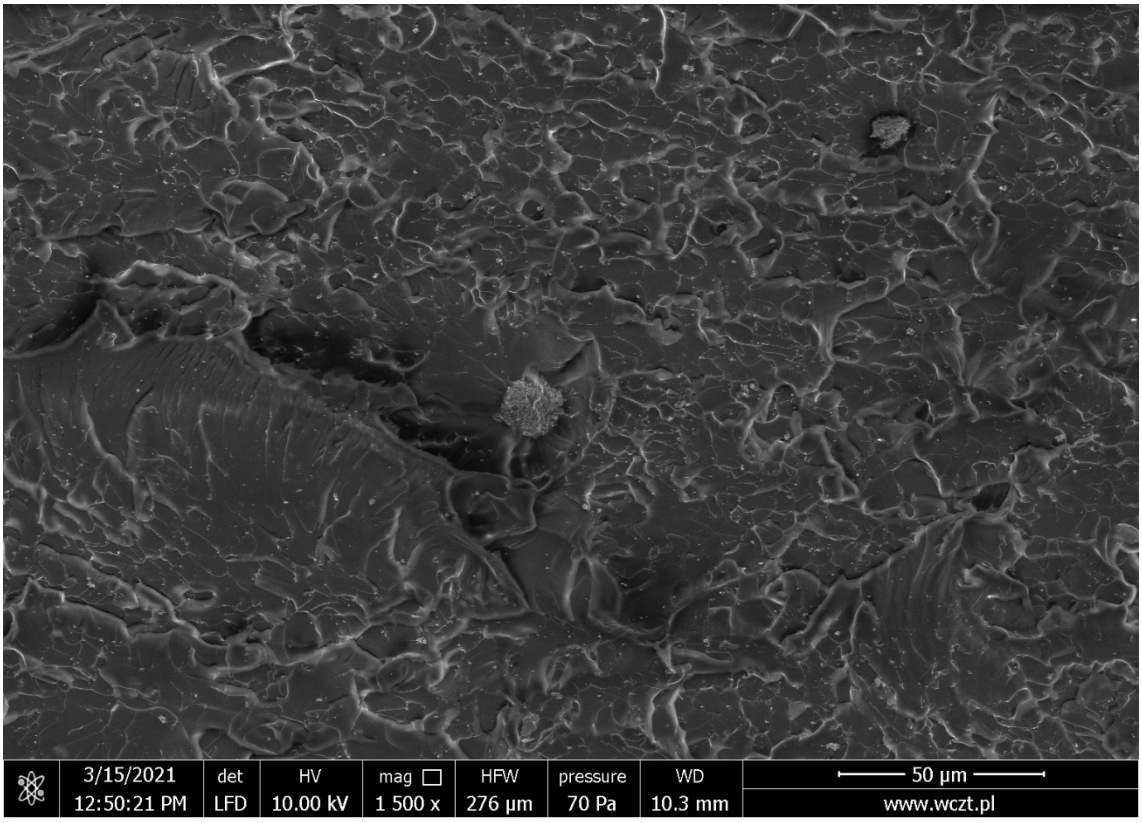

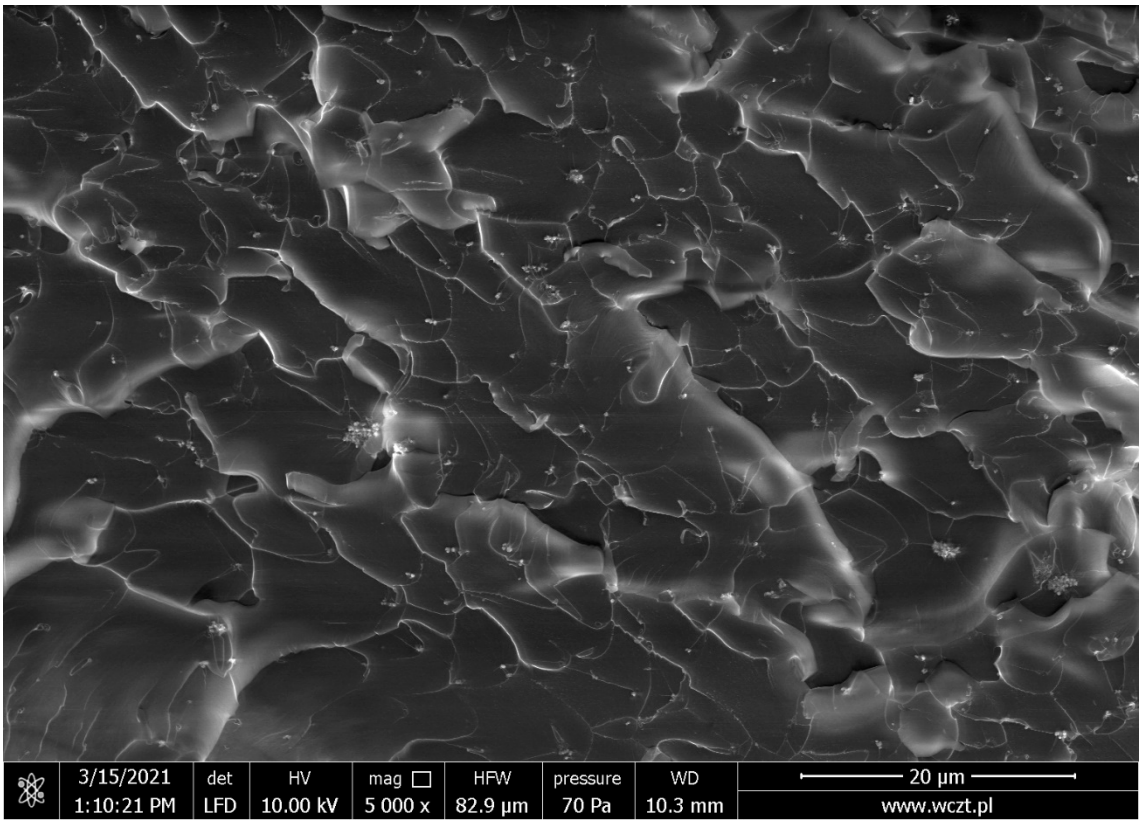

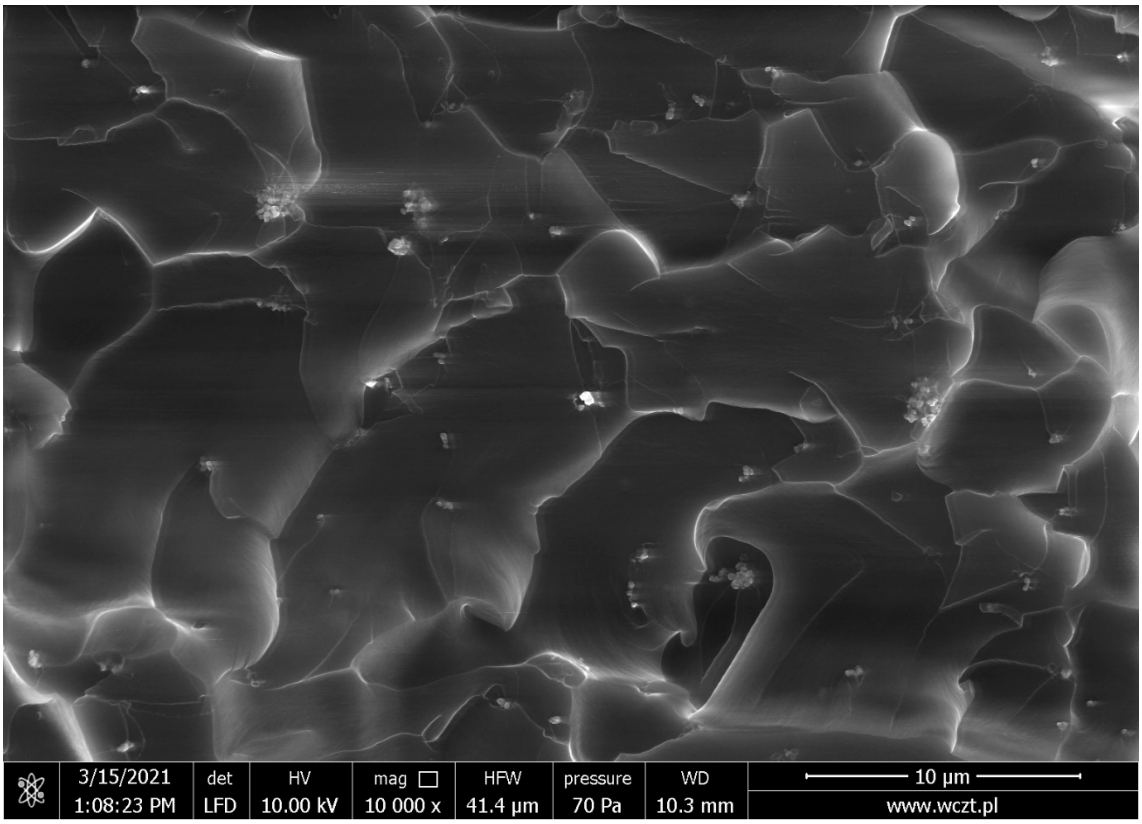
3/15/2021
1:08:23 PM
det
LFD
HV
10.00 kV
mag
10 000 x
HFW
41.4 µm
pressure
70 Pa
WD
10.3 mm
10 µm
www.wczt.pl

2%TiO_2, 1.5% SS-6GP-2TMOS, mixing pump

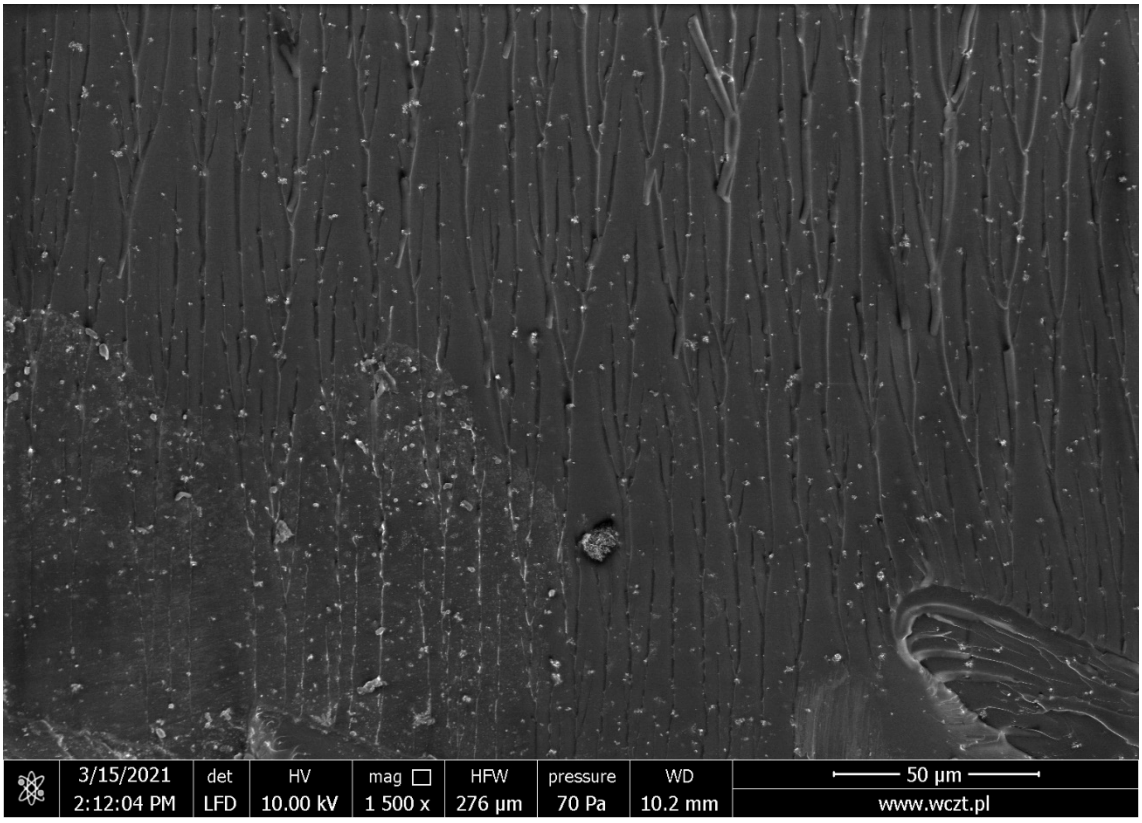

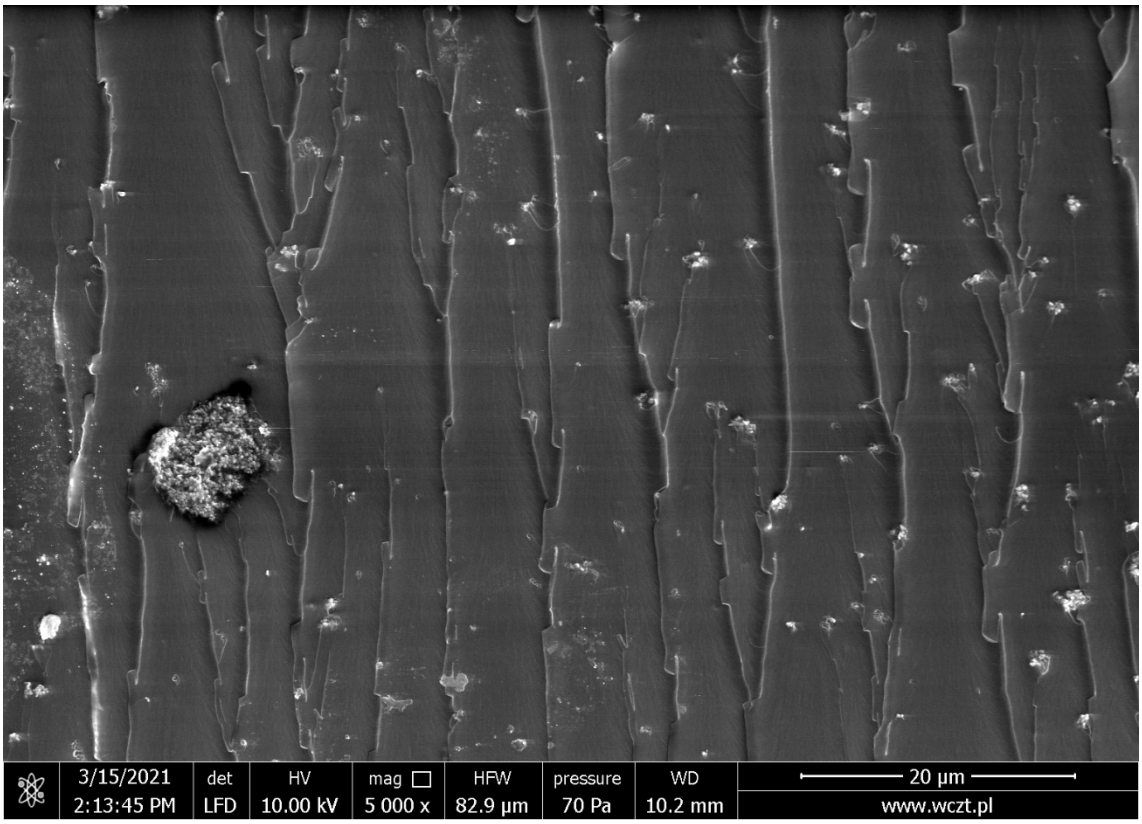

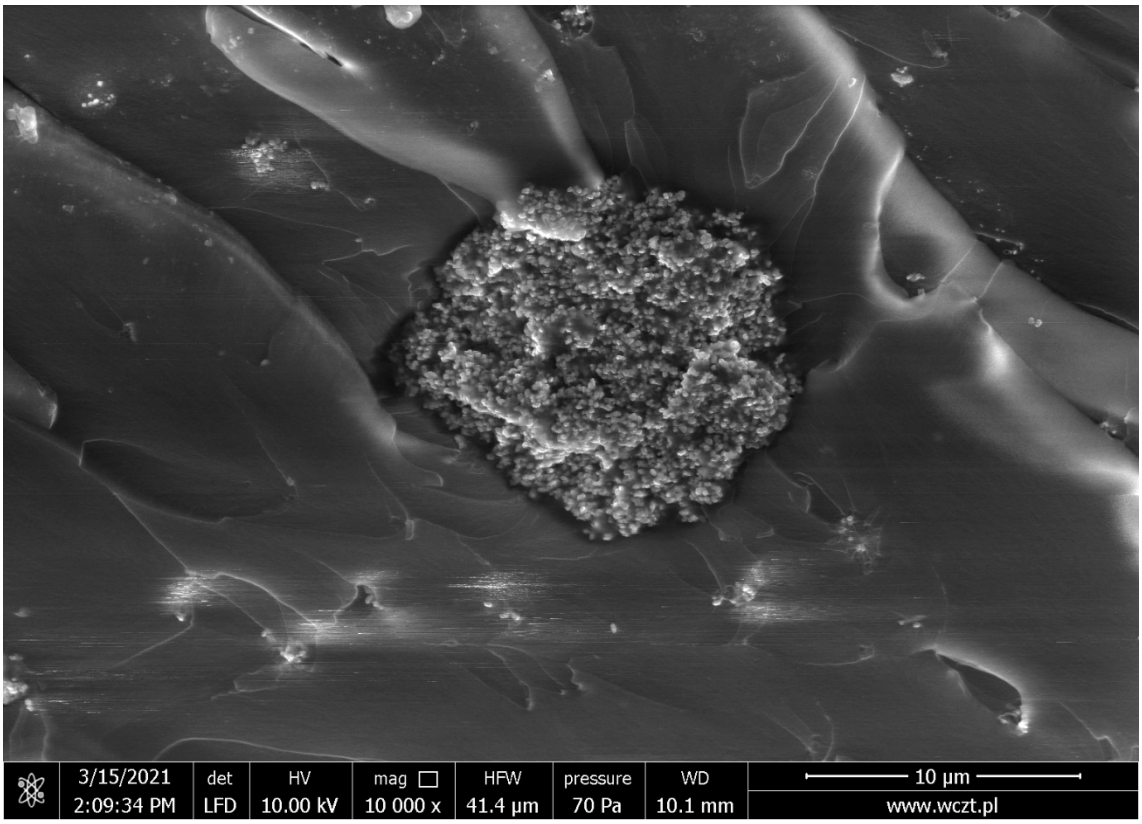
3/15/2021
2:09:34 PM
det
LFD
HV
10.00 kV
mag
10 000 x
HFW
41.4 µm
pressure
70 Pa
WD
10.1 mm
10 µm
www.wczt.pl

1%TiO_2, 0.5% SS-5GP-3TMOS, mixing pump

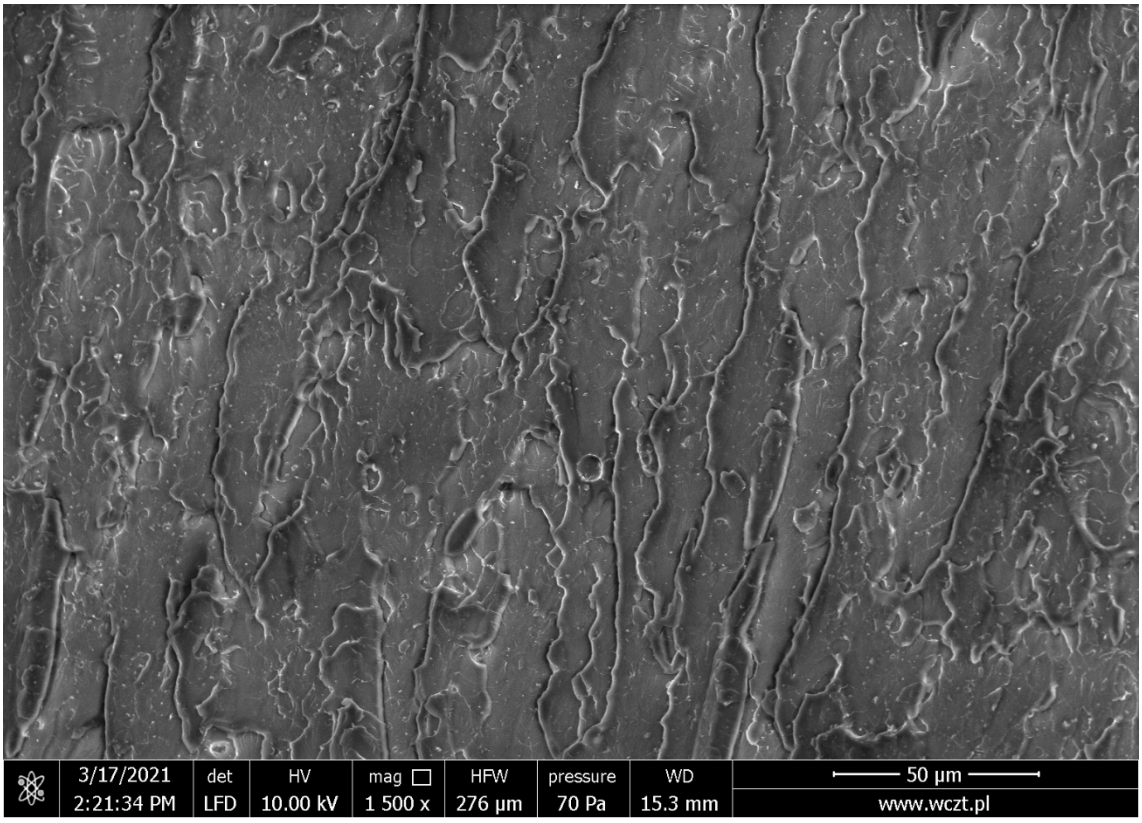

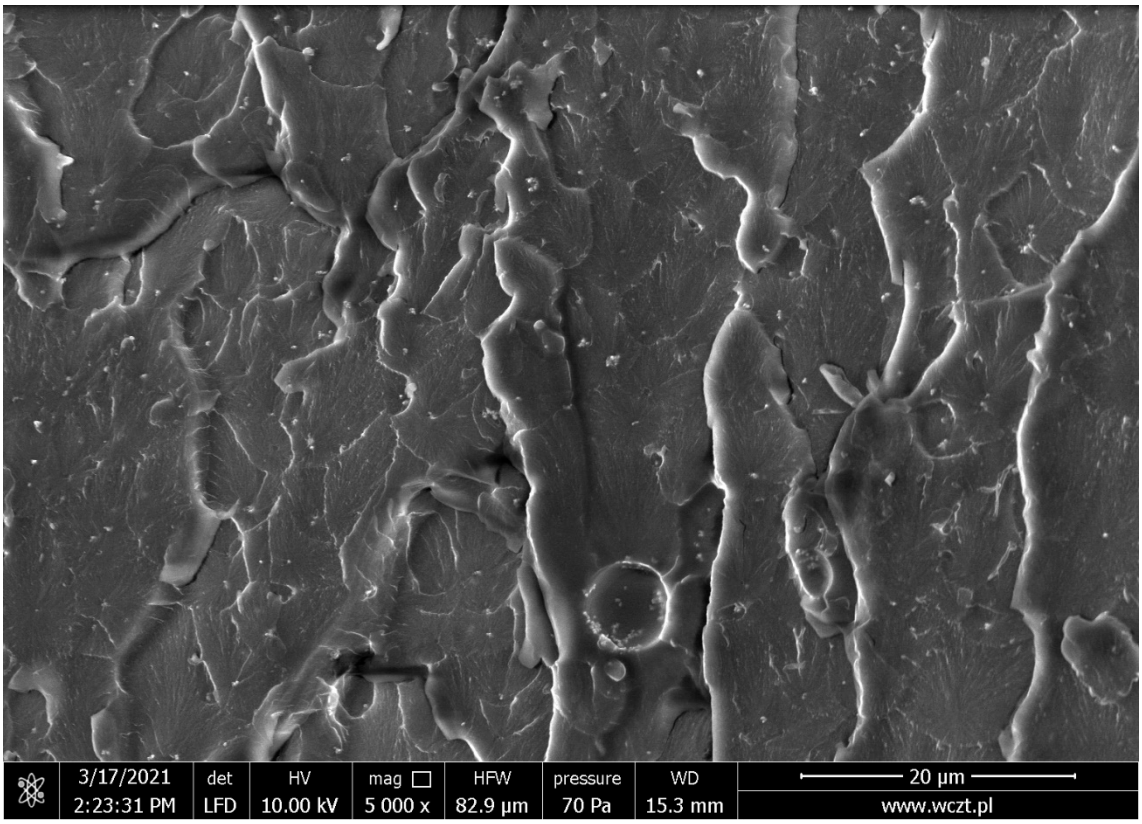

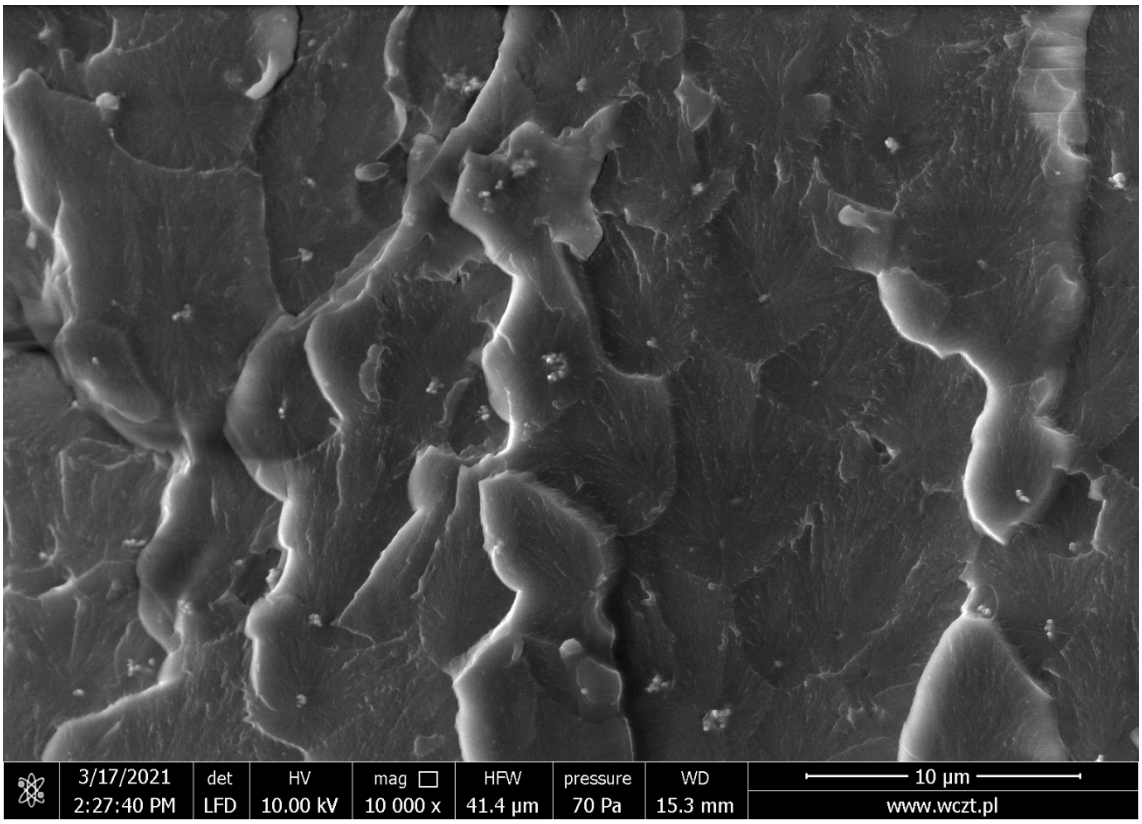
3/17/2021
2:27:40 PM
det
LFD
HV
10.00 kV
mag
10 000 x
HFW
41.4 µm
pressure
70 Pa
WD
15.3 mm
10 µm
www.wczt.pl

2%TiO_2, 0.5% SS-5GP-3TMOS, mixing pump

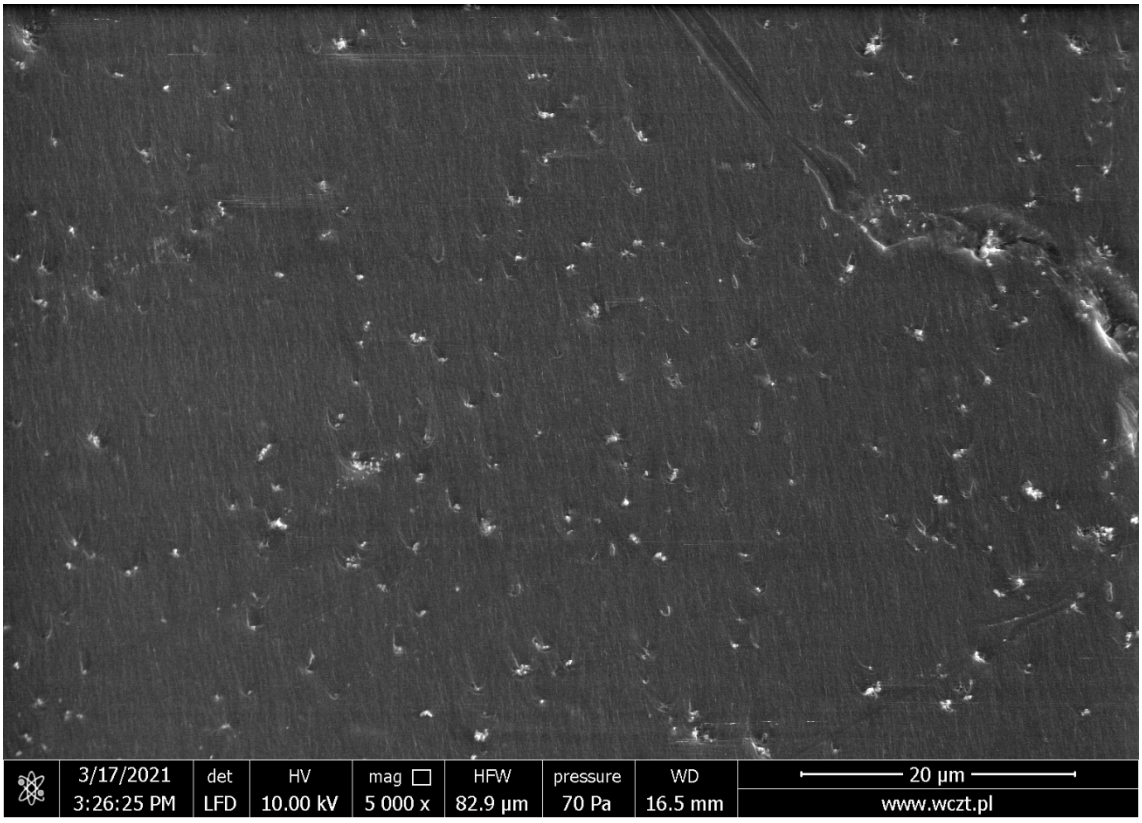

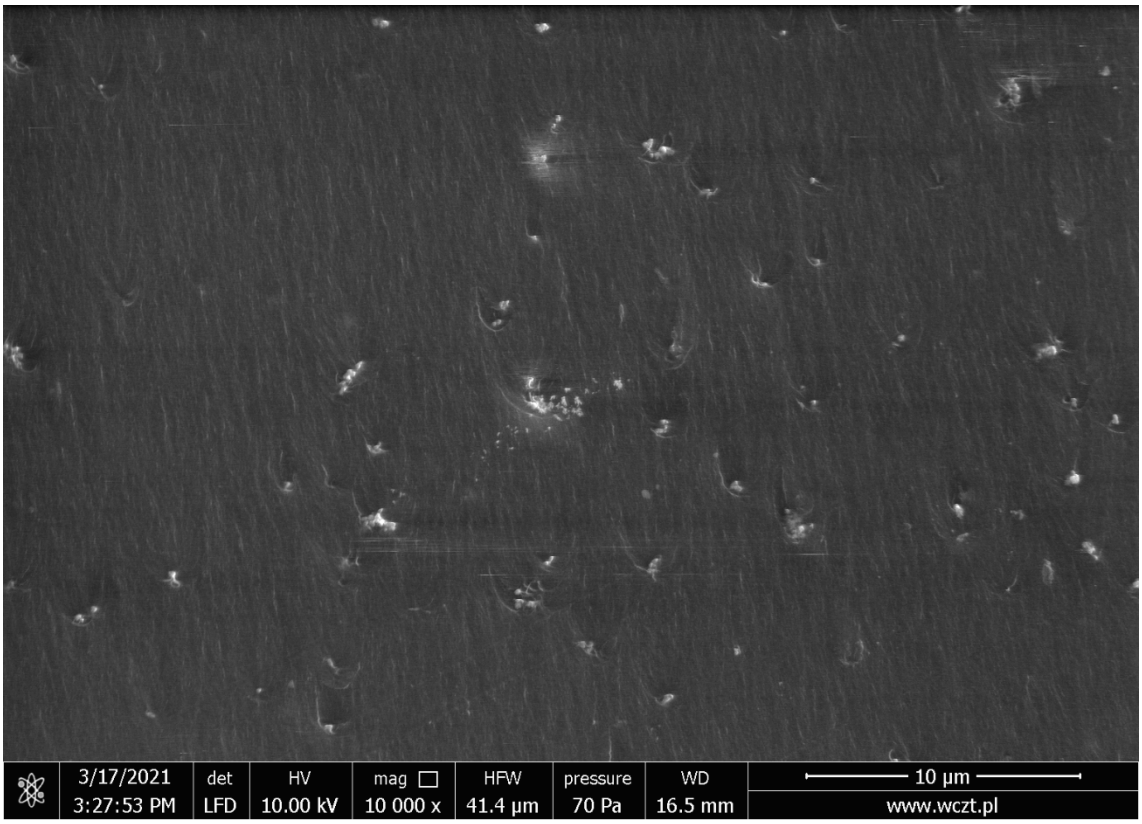

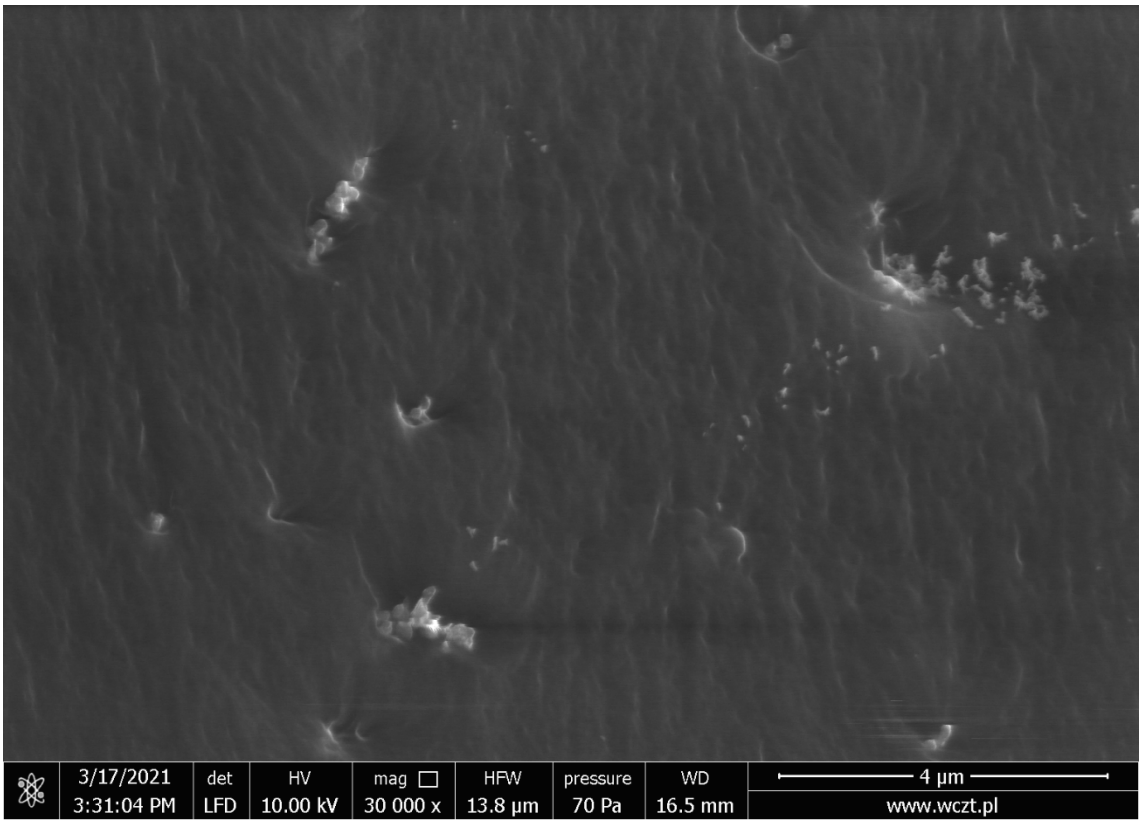
3/17/2021
3:31:04 PM
det
LFD
HV
10.00 kV
mag
30 000 x
HFW
13.8 µm
pressure
70 Pa
WD
16.5 mm
4 µm
www.wczt.pl

1%TiO_2, 1.5% SS-5GP-3TMOS, mixing pump

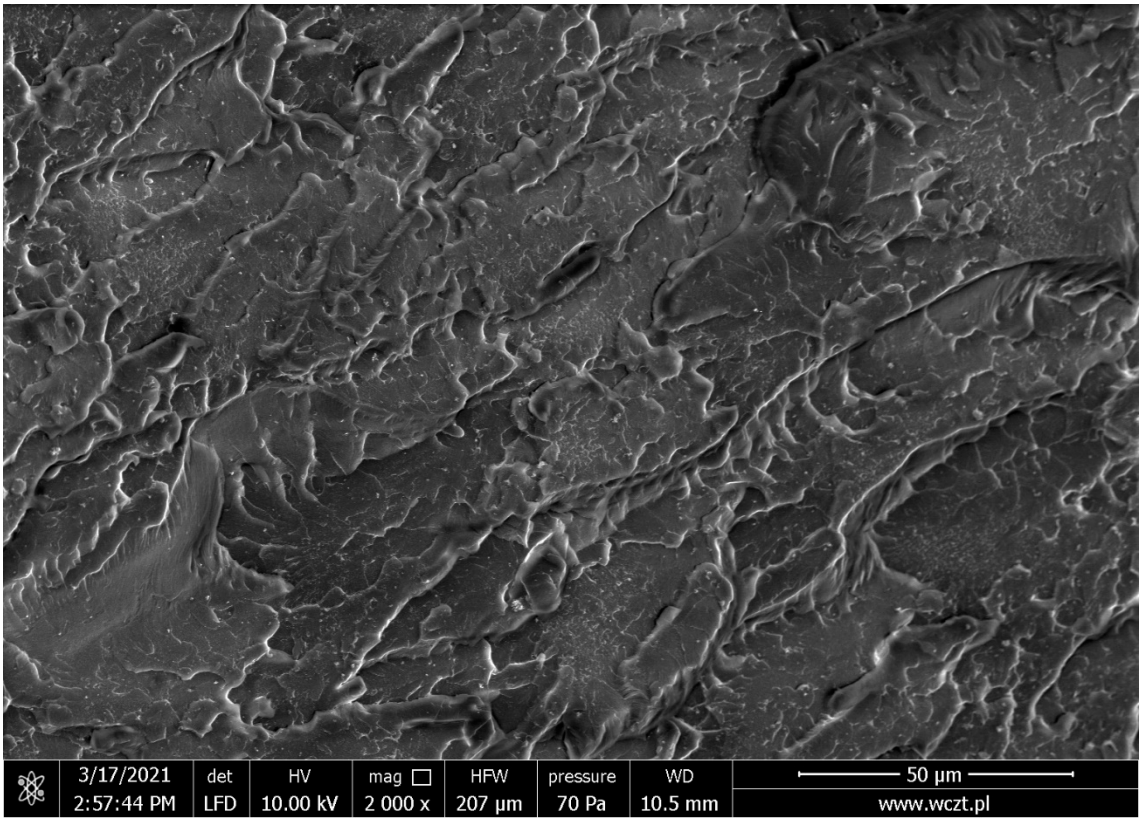

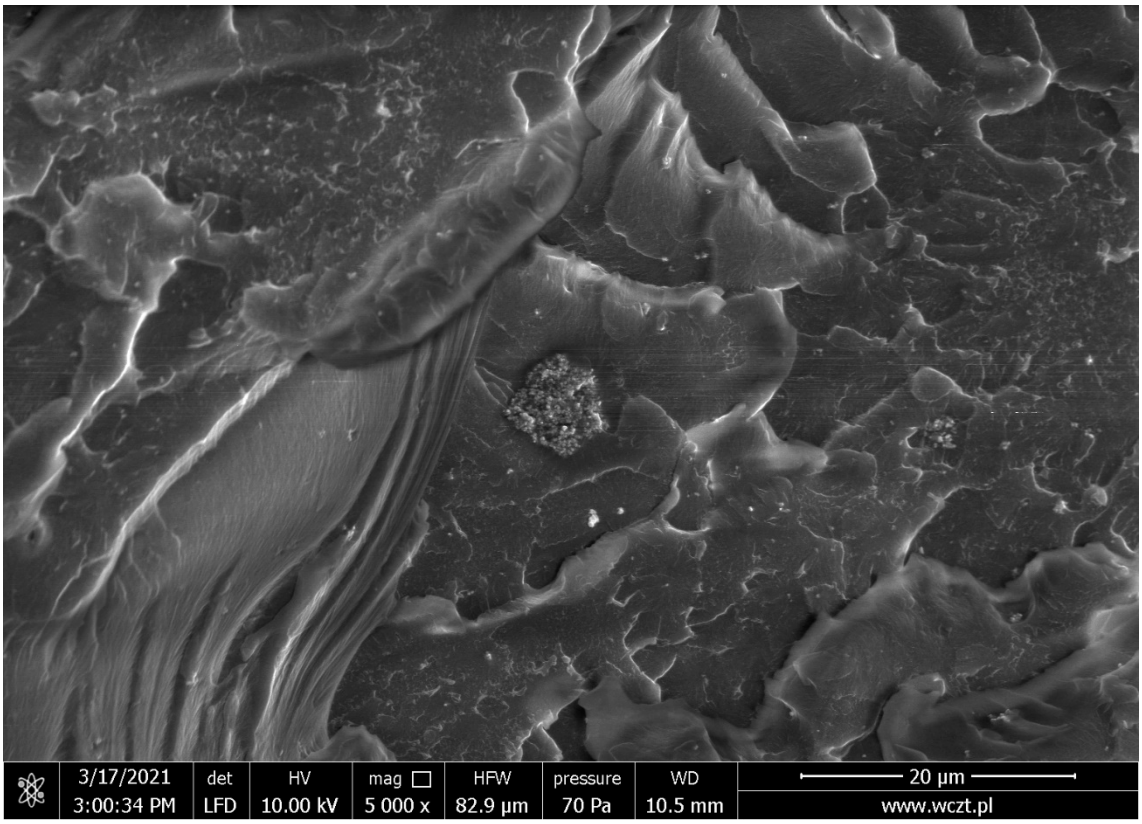

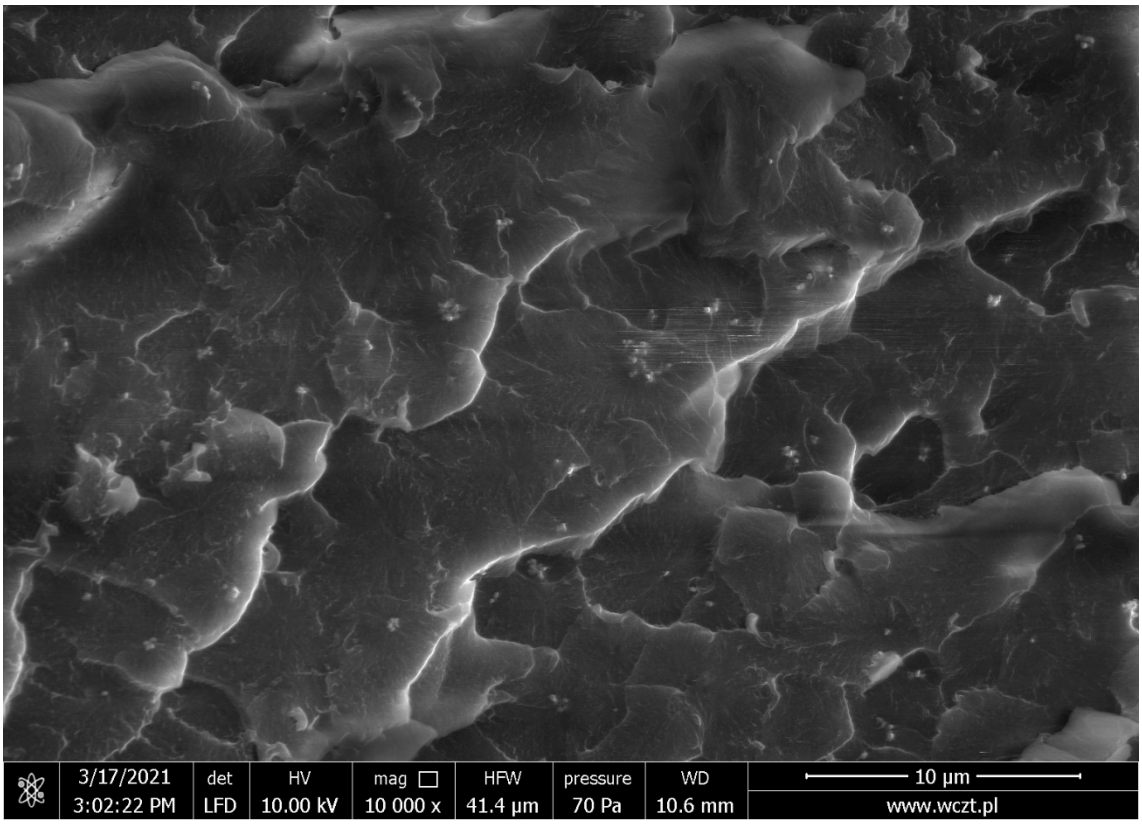
3/17/2021
3:02:22 PM
det
LFD
HV
10.00 kV
mag
10 000 x
HFW
41.4 µm
pressure
70 Pa
WD
10.6 mm
10 µm
www.wczt.pl

2%TiO_2, 1.5% SS-5GP-3TMOS, mixing pump

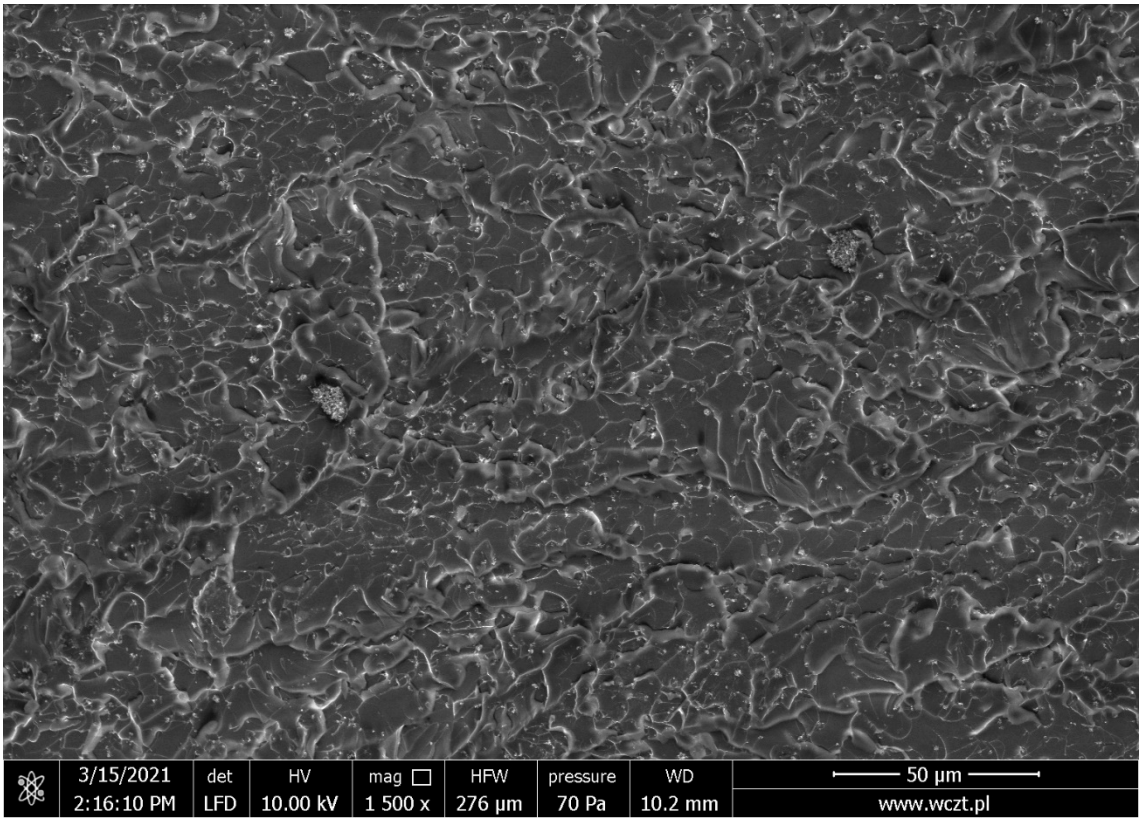

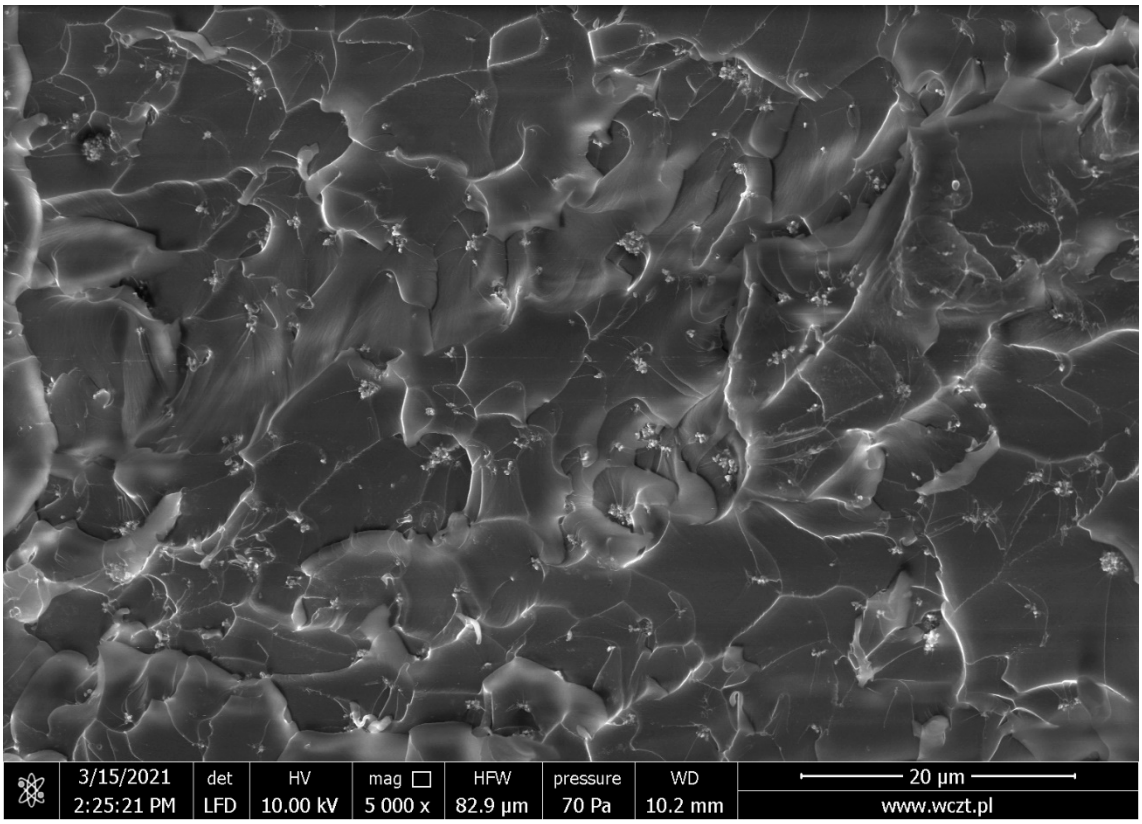

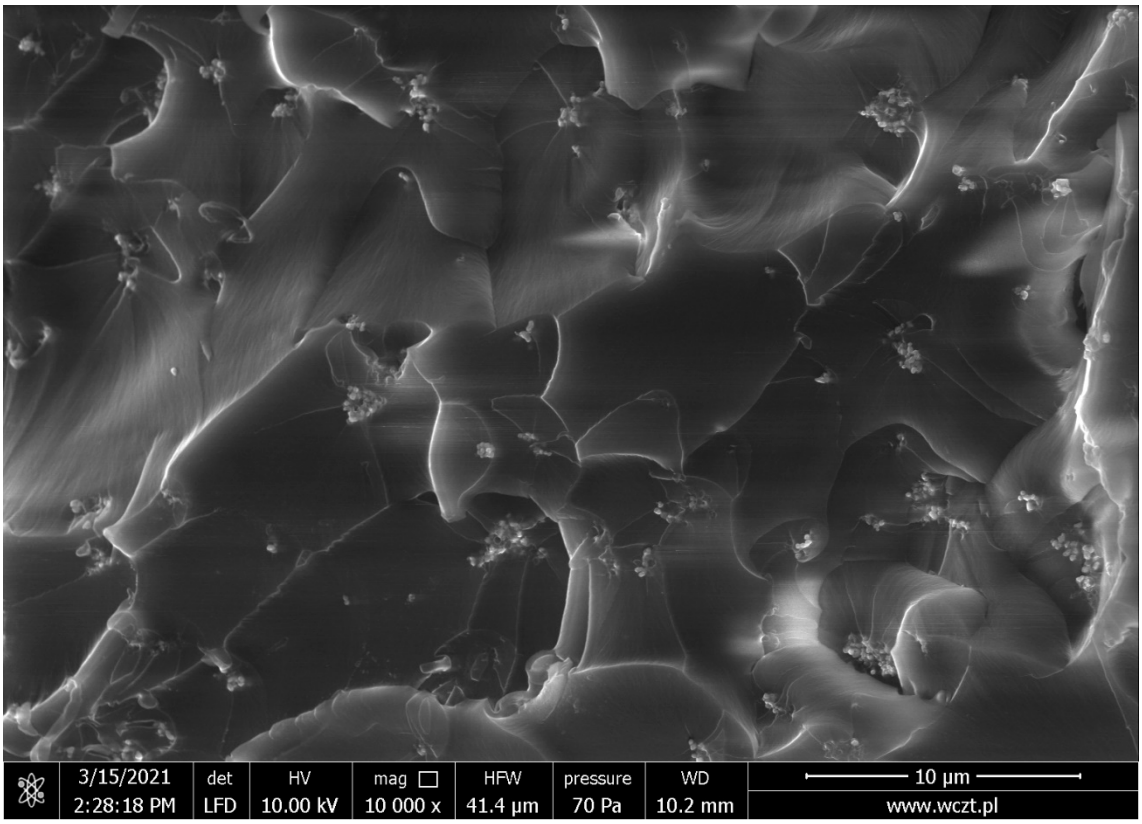
3/15/2021
2:28:18 PM
det
LFD
HV
10.00 kV
mag
10 000 x
HFW
41.4 µm
pressure
70 Pa
WD
10.2 mm
10 µm
www.wczt.pl